QUANTIFYING THE SEISMIC SITE AMPLIFICATION CHARACTERISTICS OF ADELAIDE'S REGOLITH

by

Bambang Setiawan

Thesis submitted for the degree of

Doctor of Philosophy

The University of Adelaide

School of Civil, Environmental and Mining Engineering

December 2018

INTENTIONALLY BLANK

To my father Ahmad Tony Alm. & father in law Said Mustafa,
my mother Kustinah & mother in law Syarifah Nadirah,
my wife Syarifah Mastura,
my son Di Raja Qusayyi Rabbani,
and
my daughter Wan Lubnayya Nabigha.

INTENTIONALLY BLANK

PREFACE

The work described in this thesis was undertaken from July 2013 to June 2018, in the School of Civil, Environmental, and Mining Engineering at the University of Adelaide. Throughout the thesis, all materials, techniques, concepts and conclusions attained from other external resources have been duly referenced and appropriately acknowledged in the text.

Listed below are the sections of the thesis that designate the work, to the best of his knowledge and belief, the author claims originality.

In **Chapter 2**:

- Three historical seismic events, that have damaged the Old Exchange Building in Pirie St, Adelaide, South Australia which, are investigated for local site effects that contributed to considerable damage to the Britannia statue on top of the Old Exchange Building.

- Synthetic ground motion time histories of three past seismic events (1897 Beachport, 1902 Warooka and 1954 Adelaide) are generated and validated.

- The significance of local site effects by an amplification factor of up to 3.4 that led to considerable damage to the Britannia statue at the Old Exchange Building in Pirie St, Adelaide, Australia is revealed.

In **Chapter 3**:

- Seismic site classification, which is the most widely accepted practical method in the design of seismic resistant infrastructure, for regolith sites by means of the horizontal to vertical spectral ratio (HVSR) technique for analysing ambient noise data is successfully applied.

- Seismic site classification of classes D to C (NEHRP classification system), classes D to B (Australian Standard classification system) or classes D/DE to C (regolith case classification system) for the city of Adelaide, South Australia are justified.

In **Chapter 4**:

- An application of array ambient seismic noise analysis by means of the spatial autocorrelation (SPAC) method with a slight modification to the adopted parameters is proposed to estimate bedrock depth at a regolith site which is underdeveloped and requires further attention.

- Validation of the superiority of the SPAC method by comparing the bedrock depth predictions from the SPAC method with boreholes drilled in close proximity.

In **Chapter 5**:

- Investigation of the robustness of shear wave velocity profiles by means of array ambient noise analysis of the SPAC method for regolith sites.

- New constraints by means of shear wave velocity for the study case site are established and validated.

A list of publications that have been prepared as a result of this research is presented below.

Refereed Conference Posters/Papers:

Setiawan, B., Jaksa, M. B., Griffith, M., and Love, D. (2015). Application of the single microtremor method to the Adelaide's regolith. *AFAC 15 Conference*, 1-3 September 2015, Adelaide, South Australia, Poster paper.

Setiawan, B., Jaksa, M. B., Griffith, M., and Love, D. (2015). HVSR recording duration for regolith sites: an experimental approach. *Proceedings of the Tenth Pacific Conference on Earthquake Engineering*, 6-8 November 2015, Sydney, Australia, Paper No. 171. (Included in Appendix A).

Refereed Journal Papers:

Setiawan, B., Jaksa, M. B., Griffith, M. C., and Love, D. (2018). An investigation of local site effects in Adelaide-South Australia: learning from the past. *Bollettino di Geofisica Teorica ed Applicata*, 59(1): 27–46, DOI: 10.4430/bgta0218. (Included in Appendix B).

Setiawan, B., Jaksa, M. B., Griffith, M. C., and Love, D. (2018). Seismic site classification based on constrained modeling of measured HVSR curve in regolith sites. *Soil Dynamics and Earthquake Engineering*, 110: 244–261, DOI: 10.1016/j.soildyn.2017.08.006. (Included in Appendix C).

Setiawan, B., Jaksa, M. B., Griffith, M. C., and Love, D. (2018). Estimating bedrock depth in the case of regolith sites using ambient noise analysis. *Engineering Geology,* 243: 145 – 159, DOI: 10.1016/j.enggeo.2018.06.022. (Included in Appendix D).

Setiawan, B., Jaksa, M. B., Griffith, M. C., and Love, D. (2018). Passive noise datasets at regolith sites. *Data in Brief,* 20:735 - 747, DOI: 10.1016/j.dib.2018.08.055.

Setiawan, B., Jaksa, M. B., Griffith, M. C., and Love, D. (2018). Estimating near surface shear wave velocity using the SPAC method at regolith sites. *Soil Dynamics and Earthquake Engineering,* Submitted for review on 12 June 2018.

Reports:

Setiawan, B., Jaksa, M. B., Griffith, M. C., and Love, D. (2016). Analysis of microtremor array measurement using the spatial autocorrelation (SPAC) method across the Adelaide City. *Report No. 196,* School of Civil, Environmental and Mining Engineering, the University of Adelaide.

INTENTIONALLY BLANK

ABSTRACT

The historical seismic events have clearly indicated that site amplification has played a principal role in defining the damage to structures founded on the regolith in the city of Adelaide, South Australia. An amplification factor of up to 3.7 is suggested. Thus, a seismic site amplification study in Adelaide city is needed. The use of the ambient noise method for quantifying seismic site amplification of Adelaide's regolith was selected because of its advantages (non-destructive and affordable). The application of ambient noise analysis for the study of site effects at regolith locations was carried out as it is underdeveloped and requires further attention. A case study is examined which explores Adelaide's regolith and incorporates 10 in situ ambient noise measurements carried out across the city of Adelaide for seismically classifying the site, estimating bedrock depth and obtaining the shear wave velocity profile.

Seismic site classification was investigated using the horizontal vertical spectral ratio (HVSR) technique. The results show that Adelaide's regolith varies from classes D to C (NEHRP classification system), classes D to B (Australian Standard classification system) or classes D/DE to C (regolith case classification system) and are in a good agreement with several previous studies.

The depth of bedrock is crucial in seismic hazard studies because the basin geometry has been shown to play an important role in the altering of seismic waves. Both the generic function (GF) of the classic HVSR method and the spatial autocorrelation (SPAC) technique were used to estimate the depth to bedrock. The bedrock depth predictions from the seismic methods were validated against boreholes drilled in close proximity to the measured sites. The comparison demonstrates that the SPAC method provides better estimates, especially to those obtained from another approach.

In the general framework of seismic hazard analysis for quantifying site amplification, the knowledge of near surface shear wave velocity profile is crucial. New constraints by means of shear wave velocities for the study case site were developed and proposed. The

proposed shear wave velocity models were compared and validated against previous studies and forward modelling techniques. On the basis of these validation results, the applicability of the array SPAC method at regolith sites is justified.

STATEMENT OF ORIGINALITY

I certify that this work contains no material which has been accepted for the award of any other degree or diploma in my name in any university or other tertiary institution and, to the best of my knowledge and belief, contains no material previously published or written by another person, except where due reference has been made in the text. In addition, I certify that no part of this work will, in future, be used in a submission in my name for any other degree or diploma in any university or other tertiary institution without the prior approval of the University of Adelaide and where applicable, any partner institution responsible for the joint award of this degree.

I give consent to this copy of my thesis, when deposited in the University Library, being made available for loan and photocopying, subject to the provisions of the Copyright Act 1968.

The author acknowledges that copyright of published works contained within this thesis resides with the copyright holder(s) of those works.

I also give permission for the digital version of my thesis to be made available on the web, via the University's digital research repository, the Library Search and also through web search engines, unless permission has been granted by the University to restrict access for a period of time.

Signed: Date: 07 December 2018

INTENTIONALLY BLANK

ACKNOWLEDGMENTS

In the name of Allah, the Most Gracious, the Most Merciful. All praise is due to Allah, Lord of all that exists and may His peace and blessing be upon His Prophet and Final Messenger Muhammad (pbuh). I am indebted to Allah Subhanahu Wata'ala for the strength, nourishment, and opportunities which I have been blessed with during this period of study.

This document encapsulates the last four years of research I have undertaken at the University of Adelaide, Australia. This period has been a special part of my life that I have thoroughly enjoyed and will always look back on with fond memories. This is the direct result of the support, friendship, and direction that many people have afforded me.

First and foremost, I owe a great deal to my principal supervisor, Professor Mark Jaksa from the University of Adelaide. He has provided a great source of direction and support throughout this research. For this, I am forever indebted to him. I would also like to share my appreciation for the support of my co-supervisor, Professor Michael Griffith, also from the University of Adelaide. He has provided invaluable direction regarding the laboratory testing and its application. I would also like to share my appreciation for the support of my co-supervisor, Mr. David Love, also from the Department of State Development, Government of South Australia. He has provided invaluable direction regarding the use of the seismometer set, a huddle test, and field testing.

I would also like to acknowledge additional people who have all been involved in this project: Mr. Brendan Scott, Mr. Gary Bowman, and Mr. Dale Hodson, from the University of Adelaide. Mr. Brendan Scott has given me an opportunity to share his project site for an additional comparison test. Mr Gary Bowman and Mr. Dale Hodson have assisted me with some equipment supports. I also acknowledge the editorial assistance of Leticia Mooney.

I wish to thank fellow postgraduate students in Room N233 Engineering North Building of the North Terrace Campus of the University of Adelaide for their friendship,

encouragement, and advice. I would also like to thank the Graduate Centre of the University of Adelaide for financial support given to me during my candidature scholarship.

I will always be indebted to my family, particularly my wife, Syarifah Mastura, my son, Di Raja Qusayyi Rabbani, and my daughter, Wan Lubnayya Nabigha, for their constant love, sacrifice, and support throughout the period of my candidature. In addition, I am indebted to my father and father in law, Alm. Ahmad Tony and Said Mustafa, and my mother and mother in law, Kustinah and Syarifah Nadirah, for the considerable sacrifices which they have made for me throughout my life.

TABLE OF CONTENTS

LIST OF FIGURES

LIST OF TABLES

ABBREVIATIONS AND NOTATIONS

σ_i	uncertainty of the frequency samples considered
AS	Australian Standard
BGS	Below Ground Surface
BH	Borehole
BSSC	Building Seismic Safety Council
c	phase velocity
CBD	Central Business District
CPT	Cone Penetration Test
DAF	Dynamic Amplification Factor
DC	Dispersion Curve
d_j	desired (actual) output, $d_j = d_1, d_2, d_3, ..., d_n$
D_{max}	maximum spacing sensor distance
D_{min}	minimum spacing sensor distance
DMITRE	Department for Manufacturing, Innovation, Trade, Resources and Energy
EERA	Equivalent-linear Earthquake Response Analysis
EXSIM	Extended Finite Fault Simulation
f_0	fundamental frequency
F_{EW}	Fourier amplitude spectra in east-west direction
FINSIM	Finite Fault Simulation
F_{NS}	Fourier amplitude spectra in north-south direction
f_o	resonance frequency;
F_{UD}	Fourier amplitude of vertical component
G	gravity unit

GF	Generic Function
GHS	Government House, Adelaide
h	thickness of the layer
HVSR	Horizontal to Vertical Spectral Ratio
INST.	Instrument
J_0	zero-order Bessel function of first kind
k_{max}	aliasing limit
k_{min}	resolution limit
MAE	Mean Absolute Error
MAM	Microtremor Array Measurement
MASW	Multi-channel Analysis of Surface Waves
ML	Magnitude of Local
MM	Modified Mercalli
MMI	Modified Mercalli Intensity
MS	Magnitude Scale
n	a total number of layers
n	number of pairs of data
NA	Neighborhood Algorithm
NCST	National Committee on Soil and Terrain
NEHRP	National Earthquake Hazards Reduction Program
n_F	number of frequency samples
NZ	New Zealand
PGA	Peak horizontal Ground Acceleration
PGV	Peak Ground Velocity
Q_p	Quality factor of compression wave velocity
Q_s	Quality factor of shear wave velocity
r	coefficient of correlation

r	distance
R	earthquake distance
RMSE	Root Mean Squared Error
S	power spectral density
SA	Spectral Acceleration
SAC	Seismic Analysis Code
SASW	Spectral Analysis of Surface Waves
SCR	Stable Continent Region.
SD	Standard Deviation
SESAME	Seismic EffectS assessment using AMbient Excitations
SPAC	Spatial Autocorrelation
SPT	Standard Penetration Test
SV	Spectral Velocity
t	time
T_0	fundamental site period
u	wave forms velocity
V_p	compression wave velocity
V_s	shear wave velocity
$V_{s,10}$	mean shear wave velocity of the uppermost 10 m of the subsurface layers
$V_{s,20}$	mean shear wave velocity of the uppermost 20 m of the subsurface layers
$V_{s,30}$	mean shear wave velocity of the uppermost 30 m of the subsurface layers
V_{si}	shear wave velocity of *i*th layer
x_{ci}	theoretical velocity at the frequency f_i
x_{di}	experimental velocity at the frequency f_i
y_j	model (estimated) output, $y_j = y_1, y_2, y_3, ..., y_n$

Z	depth/thickness
ρ	density
θ	angle
λ_{max}	maximum wavelength
λ_{min}	minimum wavelength
ρ	spatial autocorrelation coefficient
ϕ	directions
ω	angular frequency

Chapter One

INTRODUCTION

1.1 INTRODUCTION

The increasing numbers of high rise buildings and specific installations that have been constructed recently in Adelaide require a heightened sensitivity towards the threat presented by earthquakes with their potential impact on human safety and infrastructure. Adelaide has the highest earthquake risk of any Australian capital city (AS 1170.4-2007). In the latter half of the 1900s, the city experienced more medium-sized earthquakes than any other city. This included the 1954 Adelaide earthquake, (McCue, 1990), which is the strongest and closest seismic event experienced in Adelaide in recorded history.

The Adelaide region's underlying upper mantle is being compressed at an estimated rate of 0.1 millimetres annually, which over time results in stress build-up in the rock. At a certain level of stress, rocks slip and cause earthquakes.

Quantifying the seismic characteristics is key to assessing and mitigating the risk associated with earthquakes. This quantification involves two factors that control the impact of seismic events for any specific site: Seismic source and site effects. Quantifying the seismic source characteristics in low-to-moderate seismic regions such as Adelaide is very demanding due to an incomplete seismic catalogue and a paucity of historical strong seismic records (Love, 2013). Earthquakes cannot be predicted, but quantifying such events in the context of Adelaide's regolith helps researchers and practitioners to predict the likelihood of earthquakes in the Adelaide region. Discussing the seismic source and the likelihood of seismicity in the Adelaide region is however beyond the scope of this study.

The latter factor of site effects is the main focus of this study as, empirically, the damage caused by moderate to large earthquakes is significantly influenced by the relationship

between the seismic waves and the near surface geology setting. This is called the *site effect*.

The site effect has, in many earthquake situations, played a principal role in defining the damage to structures. Good examples are Mexico (Booth *et al.*, 1986) and Los Angeles (Somerville & Graves, 1996). In the Michoacan earthquake, the peak ground acceleration (PGA) of the incoming motions in the rock [generally less than 0.04*g* (gravity)] was amplified about five times (Finn & Wightman, 2003). The quake caused severe damage to structures founded on the 30 million-year-old lakebed deposits. In the 1989 Loma Prieta earthquake, major damage occurred at soft soil sites in the San Francisco–Oakland region. In this case, the spectral accelerations were amplified by two to four times over adjacent rock sites (Housner 1989 cited by Finn & Wightman 2003).

The site amplification phenomenon also occurs in Adelaide. The earthquake ground acceleration recording in Adelaide's regolith is very much stronger than that recorded on a rock just outside the city during the 1997 Burra earthquake (DMITRE Minerals, 2013). Site response analysis in the present study also found the amplification phenomenon in the Adelaide City (see Chapter 2).

Generally, studies of the site effects are based on measurement of three aspects: (i) strong and weak earthquakes; (ii) the near-surface geological parameters, e.g. seismic wave/near-surface geophysical testing; and (iii) the seismic noise or ambient vibration. The first method is not feasible for a stable continental region (SCR) such as Australia. The second one, active seismic testing in boreholes, complemented by in situ and laboratory tests, provides a rich source of high quality subsurface data. However, this is not practical within densely populated urban environments because the cost of such testing is prohibitive. The present study employs the last method of measurement, as outlined in Chapters 3, 4 and 5. The selected method adopted in the present study, which involves ambient noise measurement (a passive method), offers several advantages, such as being non-destructive, low cost, and feasible for urban environments.

1.2 AIMS AND SCOPE OF STUDY

This study focuses on the evaluation of seismic site amplification using ambient noise data analysis. It seeks to add to the body of knowledge associated with various impedance contrast sites. The technique developed in this study will enable researchers to estimate bedrock depth in regolith environment sites.

The results of this study will provide a better understanding of the application of the ambient noise data analysis at regolith sites that are subjected to various (low-high) impedance contrasts for seismic site amplification assessment. The techniques for analysing ambient noise data have been successfully applied to the estimation of seismic site classes associated with seismic hazards, to quantify site effects. This has mainly been carried out in relatively homogenous, uniform and high impedance contrast sites. However, the application of the technique in complex subsurface regions for site seismic classification, with various impedance contrasts between the upper layer and bedrock (such as in regolith sites), is uncertain and requires attention.

Knowledge of subsurface geometry, particularly the depth of bedrock, is crucial in seismic hazard studies because the basin geometry has been shown to play an important role in the altering of seismic waves. This study proposes an improved resolution of seismic site classification and seismic hazard parameters for Adelaide, South Australia, gained through subsurface shear wave velocity profiles.

This new constraint is crucial for reliable site response analysis at the study site, which results in improved seismic resilience infrastructure and emergency action plans.

The scope of this study involves:

1. A huddle test of all the deployed equipment sets to investigate the repeatability of all the deployed seismometers, to examine the temporal variability at the study site and to justify the appropriate duration of site ambient noise measurement. The study recorded more than two days of continuous ambient noise. The results of this huddle test were presented at an international conference (see Appendix A).

2. Site microtremor measurements across the Adelaide city. Ten locations were examined, 5 to the north and 5 to the south of the city. Array sets of equipment were

deployed at 4 sites (#01, #02, #04 and #05) to the north of Adelaide, and one site (#03) was measured using a single device. Similarly, to the south of the city, array sets of equipment were deployed at 4 sites (#06, #07, #09 and #10) and location #08 was measured using a single device. Detailed locations of the microtremor measurement sites are provided in Chapter 3.

3. An investigation of seismic site amplification based on the historical seismic events at a particular location. This site was founded on a regolith. This investigation is to justify the existence of site effects at regolith sites that are subjected to various impedance contrasts between bedrock and overlying materials.

4. Analysis of the recorded ambient noise for various purposes related to the seismic site amplification study. This included: enhancing single microtremor measurements for obtaining the shear wave velocity profile and site predominant frequency; proposing a simple method of ambient noise array analysis for estimating bedrock depth; and developing a new constraint for the subsurface dynamic parameters for seismic hazard studies.

1.3 ORGANISATION OF THE THESIS

This thesis adopts the format of a thesis by publication. As such, the thesis is, in the main, a compilation of 4 journal papers, as presented in Chapters 2 to 5. The general content of each chapter is outlined below.

In **Chapter 2**, the justification of seismic site effects, i.e. site amplification for regolith sites is investigated. In this chapter, historical seismic events that damage a particular structure founded on a regolith are outlined. Synthetic time histories of such historical seismic events need to be generated and confirmed. The suitability of the generation of the time histories method using an instrumental seismometer network has yet to be established and representative 1D soil profiles need to be developed and validated. Site response analysis at the building site is carried out to obtain the seismic parameters at the investigated site. The results are compared with the historical intensity maps of the events which are assumed to be the actual spectral accelerations during the events. This paper

was submitted to the journal of *Bollettino di Geofisica Teorica ed Applicata* in June 2018 and has been published (see Appendix B).

Chapter 3 focuses on the application of the HVSR (horizontal to vertical spectral ratio) technique to regolith sites. First, seismic site classification is defined, which is the most widely accepted practical method in the design of seismic resistant infrastructure. The application of ambient noise data analysis using the HVSR technique for estimating seismic site classes associated with seismic hazards is then outlined. The results of a case study in the central business district of Adelaide, South Australia are examined using 10 in situ ambient noise measurements carried out across the city. The results and comparisons with several previous studies are presented and discussed. This paper was submitted to the journal of *Soil Dynamics and Earthquake Engineering* in November 2016 and was published in March 2018 (see Appendix C).

Chapter 4 proposes the application of the ambient noise analyses for estimating the depth of bedrock at regolith sites. This bedrock depth, which represents the basin geometry, is crucial in seismic hazard studies because the basin geometry has been shown to play an important role in the altering of seismic waves. Analyses of ambient noise data are carried out using the generic function (GF) of the classical HVSR method and the spatial autocorrelation (SPAC) techniques. The chapter presents a comparison of the bedrock depth predictions. This paper was submitted to the journal of *Engineering Geology* in December 2016 and has been published (see Appendix D).

Chapter 5 presents an investigation into the quantification of near surface shear wave velocity profiles. This is crucial for assessing site amplification in the general framework of seismic hazard analysis. The investigation uses an array ambient noise analysis in the form of the spatial autocorrelation (SPAC) method. This investigation explores the robustness of shear wave velocity profiles by means of array ambient noise analysis for regolith sites and proposes new constraints for shear wave velocities for the investigated sites. A rigorous validation of the proposed shear wave models is carried out using previous studies, geological data and forward modelling techniques. This paper was submitted to the journal of *Soil Dynamics and Earthquake Engineering* in June 2018 and is currently under review.

Finally, **Chapter 6** concludes the thesis. The limitations of this study are presented, and future studies to enhance some findings of this study are proposed.

Chapter Two

AN INVESTIGATION OF LOCAL SITE EFFECTS IN ADELAIDE-SOUTH AUSTRALIA: LEARNING FROM THE PAST

INTENTIONALLY BLANK

Statement of Authorship

Title of Paper	An investigation of local site effects in Adelaide – South Australia: learning from the past
Publication Status	☑ Published ☐ Accepted for Publication ☐ Submitted for Publication ☐ Unpublished and Unsubmitted work written in manuscript style
Publication Details	Setiawan, B., Jaksa, M., Griffith, M., and Love, D., 2018. An investigation of local site effects in Adelaide – South Australia: learning from the past. Bollettino di Geofisica Teorica ed Applicata, 59(1): 27-46, DOI: 10.4430/bgta0218.

Principal Author

Name of Principal Author (Candidate)	Bambang Setiawan		
Contribution to the Paper	Performed data collection, carried out analysis, interpreted the results, wrote the manuscript and acted as corresponding author.		
Overall percentage (%)	80%		
Certification:	This paper reports on original research I conducted during the period of my Higher Degree by Research candidature and is not subject to any obligations or contractual agreements with a third party that would constrain its inclusion in this thesis. I am the primary author of this paper.		
Signature		Date	14 June 2017

Co-Author Contributions

By signing the Statement of Authorship, each author certifies that:

i. the candidate's stated contribution to the publication is accurate (as detailed above);

ii. permission is granted for the candidate in include the publication in the thesis; and

iii. the sum of all co-author contributions is equal to 100% less the candidate's stated contribution.

Name of Co-Author	Mark Jaksa		
Contribution to the Paper	Overall percentage – 10% Supervised the development of work, helped in data interpretation and manuscript preparation. He also reviewed this manuscript rigorously.		
Signature		Date	14/6/17

Name of Co-Author	Michael Griffith		
Contribution to the Paper	Overall percentage – 5% Provided some valuable comments on the manuscript contents.		
Signature		Date	14/6/17

Name of Co-Author	David Love		
Contribution to the Paper	Overall percentage - 5% Provided some valuable comments on the manuscript contents. Evaluated and edited the manuscript.		
Signature		Date	14 June 2017

Please cut and paste additional co-author panels here as required.

2.1 INTRODUCTION

Of all Australia's cities, Adelaide is most at risk of a severe earthquake (Standard Australia, 2007). In the last 150 years, the city has experienced more medium-sized earthquakes than any other Australian city. Three significant events include the 1897 Beachport earthquake, the 1902 Warooka earthquake, and the 1954 Adelaide earthquake (the 'three historical seismic events'), (McCue, 1990; Malpas, 1991; Dyster, 1996; Love, 1996). These three historical seismic events caused damage to the Old Exchange Building at Pirie St, Adelaide, southern Australia (Figure 2.1). The damage was manifested in the Britannia statue located on the parapet of the building. The statue lost its arm during the 1897 Beachport earthquake [Modified Mercalli Intensity (MMI) IV–V], and its helmeted head was bent over in the 1902 Warooka seismic event (MMI V–VI). Due to heavy damage, the statue was finally removed after the 1954 Adelaide earthquake (MMI VI-VII) (Malpas, 1991; Dyster, 1996). Local site effects for the particular case of the Old Exchange Building have never been investigated.

Figure 2.1. The Old Exchange Building with the Britannia Statue on parapet.

This study investigates the local site effects with respect to the Old Exchange Building, which is situated on a regolith site. The investigation is based on past seismic events.

Synthetic bedrock time histories of the three historic seismic events have been generated using EXSIM (Motazedian & Atkinson, 2005). The time histories are used in the 1D site response analyses to estimate the peak ground acceleration (PGA), and other seismic parameters (i.e. response spectral acceleration, velocity and displacement) at the Old Exchange Building site. The results are examined alongside the historical experiences and

the intensity maps associated with the seismic events that are assumed to be the actual spectral accelerations during these events. The MMIs of the 1897 Beachport, 1902 Warooka, and 1954 Adelaide earthquakes were MMI of IV–V, V–VI, and VI-VII, respectively (Malpas, 1991; Dyster, 1996). The comparison reveals the significance of local site effects in the damage manifested in the building. The findings from this study may form a basis for further comprehensive and systematic analyses of site effects and seismic-related studies in Adelaide, southern Australia.

2.2 THE CHARACTERISTICS OF THE PAST SEISMIC AND GEOLOGICAL SETTING OF THE INVESTIGATED SITE (THE OLD EXCHANGE BUILDING SITE) AND SURROUNDING AREAS

As mentioned above, this study examines the impact of just three historical seismic events. These seismic events were estimated at 6.5, 6.0 and 5.3 on the Richter local magnitude scale (M_L) for the 1897 Beachport, 1902 Warooka and 1954 Adelaide earthquakes, respectively (Everingham *et al*. 1982). Both the 1897 Beachport and 1902 Warooka events caused extensive damage (MMI IX–VII) in the areas near the epicentre. These events were also felt at distances of hundreds of kilometres from the epicentres, including the city of Adelaide (Malpas, 1991). After about a half century, Kerr-Grant (1956) and McCue (1975) reported that Adelaide was shaken on March 1, 1954. This seismic event is the strongest earthquake in Adelaide's recorded history. Due to this event, at least 30,000 insurance claims were made. Each of these three past seismic events testify to the need for estimating ground surface motion in the city, which includes site effects. The location of Adelaide, as well as the epicentres of the three major historical earthquakes (after Everingham *et al*., 1982), are shown in Figure 2.2. The Old Exchange Building is located in the middle of the central business district (CBD) of Adelaide, as shown in Figure 2.3.

The major geological structures of the Adelaide city and its surrounding region are fault segments that develop in a NE to SW direction. Most of the faults can be characterised by lithological disposition. There were several past seismic events associated with these faults as documented and presented by Selby (1984). The most significant event was associated with intra-plate activity along the Burnside-Eden Fault zone. This occurred on March 1, 1954, and is known as the 'Adelaide earthquake'. This seismic event was estimated at a magnitude of 5.3 (Selby, 1984; Love, 1996). Two main faults delimit the

city of Adelaide to the west (Para Fault) and east (Eden-Burnside Fault). Both the Para and Eden-Burnside Faults predominantly control the ground surface morphology of the city and its adjacent areas.

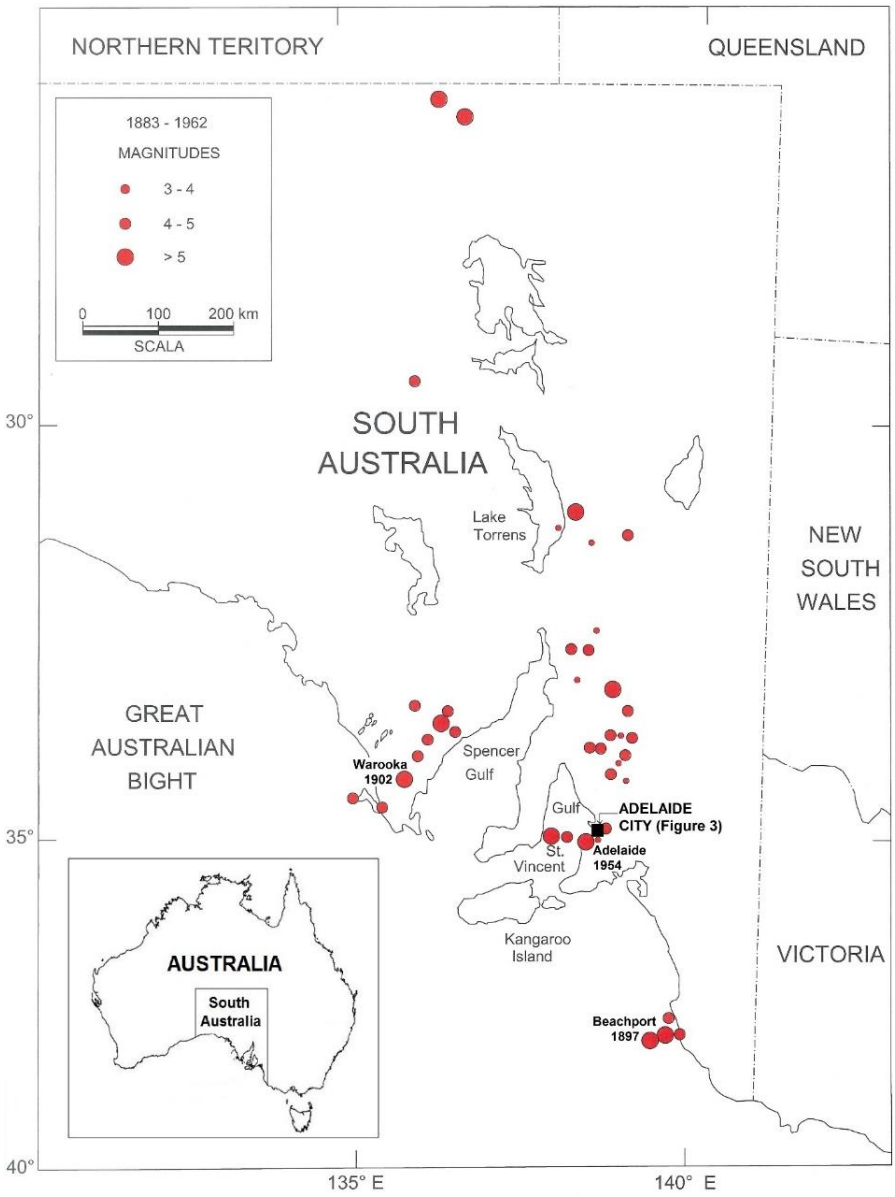

Figure 2.2 Locations of the epicentres of the South Australian historical seismic events, including the three events that damaged the Old Exchange Building (after Malpas, 1991).

Most of the upper ground layer of Adelaide is made up of fill material and other surficial covers. Below the top fill and surficial cover, the subsurface profile is composed of Holocene deposits of Callabonna Clay and the Pooraka Formation. Beneath these Holocene deposits is the Hindmarsh Clay. Sheard & Bowman (1987a; 1987b) separated Keswick Clay from the Hindmarsh Clay formation below the Holocene deposits. Below these Quaternary deposits there is an unconformity beneath which are the Burnham

Limestone and Hallett Cove Sandstone Formation. Below this lies another unconformity followed by the sand unit of the Port Willunga Formation and the Tandanya Sand Member of the Chinaman Gully Formation. These units were deposited between the Pleistocene and Eocene (Selby & Lindsay, 1982). They are followed by the Undifferentiated Basal Blanche Point Formation and Tortachilla Limestone, South Maslin Sand and Clinton Formation, prior to the Precambrian bedrock. The reduced level of the bedrock is believed to be approximately 88.5 m or less to the north of the city, and can be up to 94.3 m or more below ground to the south of the city (Selby & Lindsay, 1982).

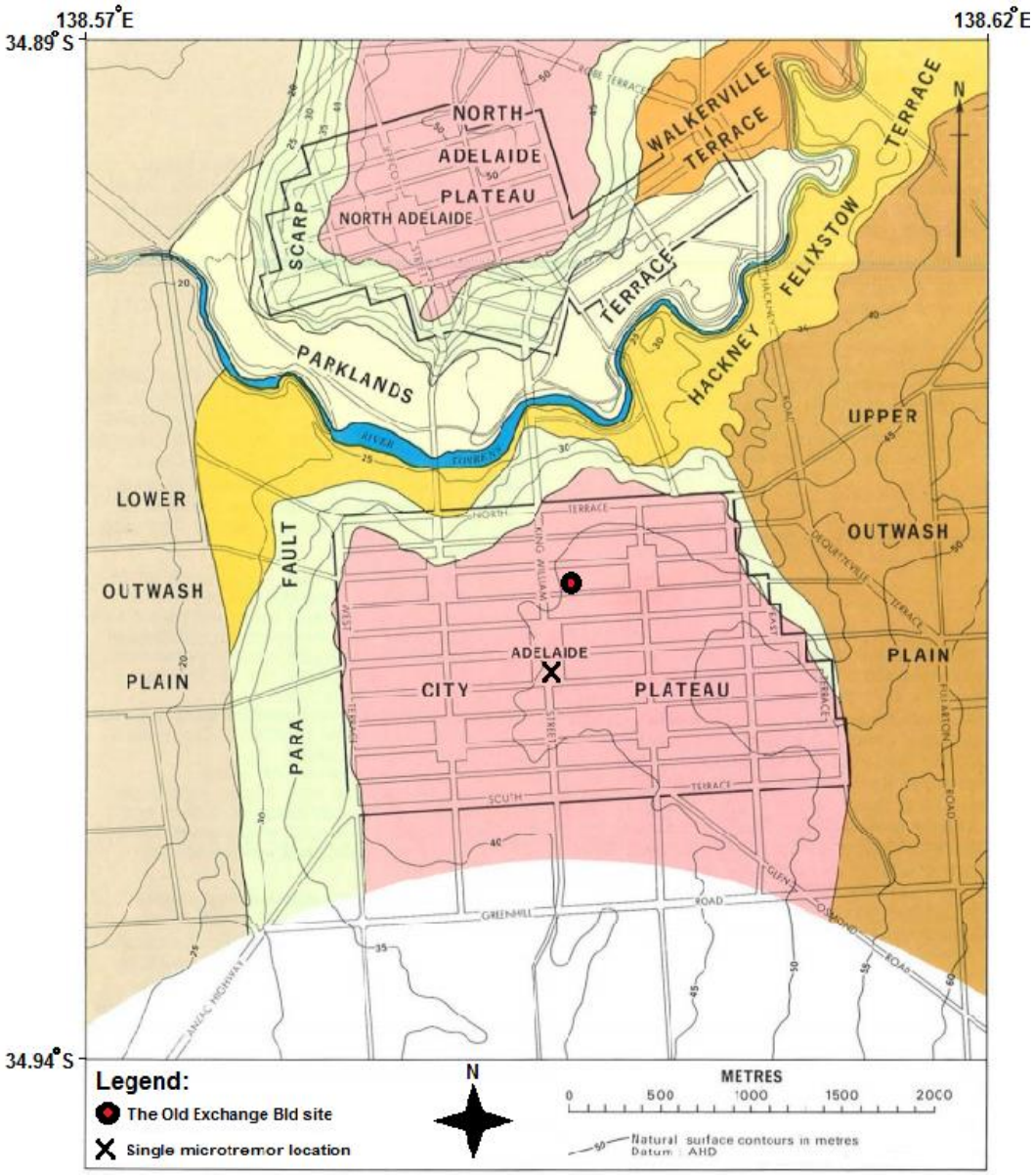

Figure 2.3 Morphology of the Adelaide city, with the location of the Old Exchange Building site.

As shown in Figure 2.3, much of the commercial development of the Adelaide city is founded on two morphological plateaus; one to the north and the other to the south of the city. The remaining morphologies, i.e. the upper outwash plain, lower outwash plain, terrace and fault scarps, are associated with either parklands or residential developments. Selby & Lindsay (1982) suggested that faults predominantly control the morphology of the city in the present day.

2.3 METHODOLOGY OF THIS STUDY

In this study, as there were no actual ground motions recorded for the three major historical seismic events, synthetic seismic motions are considered to represent the ground motions of these earthquakes. The generation of the synthetic seismic motions, as well as other parameters and site response analysis adopted in this study, are described below.

2.3.1 Generating input seismic motions

Table 2.1 details the main data associated with the seismic events of the 1987 Beachport, 1902 Warooka and 1954 Adelaide earthquakes that were used to generate the seismic motions. This study uses a stochastic finite-fault model, EXSIM (Motazedian & Atkinson, 2005), to simulate the time histories of the 1897 Beachport, 1902 Warooka, and 1954 Adelaide earthquakes. There are some salient features of the adopted approach (EXSIM). Firstly, the model has been validated using a minimum of 300 strong motion stations at distances of 40 to 500 km (Motazedian & Atkinson, 2005; Atkinson & Macias, 2009). For the case of the close distance seismic event (i.e. 1954 Adelaide earthquake), an analytical model proposed by Mavroeidis & Papageorgiou (2003) is included in EXSIM. Secondly, the model was based on FINSIM (Beresnez & Atkinson, 1998) with ground motions generated by ruptures along faults. Thirdly, this finite-source model is appropriate for large earthquakes at relatively close distances (Hartzell, 1978; Joyner & Boore, 1986). Santulin *et al*. (2012) employed EXSIM for generating two historical earthquakes (the 1936 Cansiglio and 1976 Friuli earthquakes) in Italy. In the present study, additional parameters are needed to produce the synthetic ground motions as shown in Table 2.2. Most of the input parameters are adopted from Allen (2012). Additional parameters for analytical modelling proposed by Mavroeidis & Papageorgiou (2003) were employed in the case of the close distance seismic event. These additional

parameters, shown in Table 2.2, have been validated by Motazedian & Moinfar (2006) against the 2003 Bam earthquake in SE Iran.

Table 2.1 Three historical seismic events contributed to the damage of the Old Exchange Building.

Event	Magnitude (M_L)	Depth (km)	Estimated distance (km)	Intensity at the investigated site	
				MMI	Reference
1897 Beachport earthquake	6.5	14	260	IV–V	McCue (1975)
1902 Warooka earthquake	6.0	4	60	V	McCue (1975)
				VI	Malpas (1991)
1954 Adelaide earthquake	5.3	4	12	VI–VII	After Malpas (1991)

Four different input motions are considered. The first is a synthetic seismic motion generated for the 1897 Beachport event (earthquake of M_L 6.5 at a distance, R, of 260 km from the city of Adelaide). The second is a synthetic seismic motion produced for the 1902 Warooka event (earthquake of M_L 6.0 at R = 60 km from Adelaide). The third is a synthetic seismic motion calculated for the 1954 Adelaide event, considered the worst near-field seismic scenario for the city (earthquake of M_L 5.3 at R = 12 km from Adelaide). The fourth is a synthetic seismic motion calculated for the 1997 Burra event (earthquake of M_L 5.1 at R = 130 km from Adelaide). The first three synthetic ground motion time histories are shown in Figure 2.4. These synthetic time histories are used for a site-specific ground response analysis of the site of interest, to estimate the PGA and validate site amplification during the 1897 Beachport, 1902 Warooka and 1954 Adelaide earthquakes. The fourth synthetic seismic motion for the 1997 Burra earthquake is generated to examine the suitability of the stochastic finite-fault model in this study. The application of this 1997 Burra synthetic seismic motion into the site response analysis of the investigated site is compared to the application of the actual recorded seismic motions at the Government House site (GHS) Adelaide, which is a similar model (Figure 2.5). The GHS is a soil site and is located approximately 0.5 km from the Old Exchange Building. A deconvolution of the generated time histories at bedrock level using EXSIM was carried out. This deconvolution of the time histories was compared to the actual time histories at the GHS site.

Table 2.2 Parameters for ground motion simulations using EXSIM (after Allen, 2012).

Input Parameter	**Value**	**Remarks**
Shear-wave velocity, β	3,600 m/s (Wesson, 1988)	Beta
Density, ρ	2,800 kg/m^3	Rho
Rupture propagation speed	0.8 β	Vrup
Brune stress drop, $\Delta\sigma$	23 MPa	Stress
Pulsing percentage	25%	Pulsing Percent
Geometrical attenuation R^b, b	–1.33 (0–90 km) +0.32 (90–150 km) –1.66 (> 150 km)	Gsprd
κ_0	0.006 s	Kappa
Distance-dependent duration	0.00 (0–10 km) +0.14 (10–70 km) –0.04 (70–160 km) +0.07 (> 160 km)	Trilinier duration and properties
Fault dip	35°	Dip
Earthquake magnitude (M)	6.5, 6.0 and 5.3	1898 Beachport, 1902 Warooka & 1954 Adelaide earthquakes
Earthquake distance	260 km, 60 km and 12 km	Distance from the epicentre of each earthquake to Adelaide CBD
Prevailing frequency ($f_P = 1/T_P$)	Log T_P = -2.2+0.4M	Parameters for the 1954 Adelaide earthquake only.
Phase angle	10 degrees	
Oscillatory character	1.5	

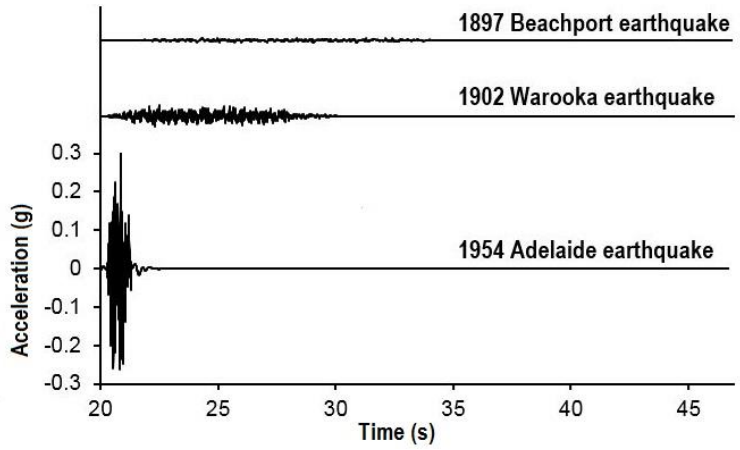

Figure 2.4 Synthetic acceleration time histories of the three past earthquakes.

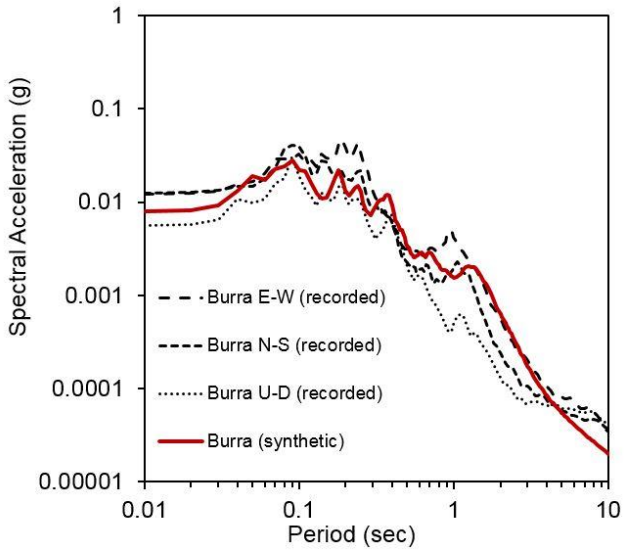

Figure 2.5 Response spectral acceleration validation of the synthetic time histories generated using the 1997 Burra seismic event.

2.3.2 Developing a one-dimensional (1D) profile

Detailed knowledge of the subsurface characteristics of the investigated site contributed to generating a 1D profile for the investigated site. The subsurface lithology profiles of the investigated site are developed based on the work of Selby & Lindsay (1982). They examined an extensive amount of geotechnical borehole, groundwater and deep excavation data from which stratigraphic profiles and cross-sections of Adelaide were

developed. Two boreholes (BH 42 and BH 83) were drilled by Selby & Lindsay (1982) near to the Old Exchange Building site, and two sections (C-C and G-G) were developed by Selby & Lindsay (1982) from these boreholes.

From these two sections, two subsurface models are established in this study. The first model is based mainly on Section C-C, hereafter referred to as Model A. The second is established primarily from Section G-G, hereafter referred to as Model B. The total depth of both Models A and B is up to the Pre-Cambrian bedrock. Both Models A and B share similar geological formations from the ground surface down to the Pre-Cambrian bedrock. Slight differences in the thicknesses of the formations are observed due to the modest lateral heterogeneity of the geological formations.

In addition to the stratigraphic profile, in situ, ambient-noise single station and array measurements were conducted in order to quantify the shear wave velocity profiles in the Adelaide city (Setiawan *et al*., 2016).

A shear wave velocity profile at a location of approximately 200 m from the investigated site was developed by the authors (Setiawan *et al*., 2016). This shear wave velocity profile is incorporated into the 1D profile for the site response analysis at the investigated site. To validate the appropriateness of the shear wave velocity model deduced by Setiawan *et al*. (2016), a forward-computation of the model proposed by Garcia-Jerez *et al*. (2016) is employed to obtain a spectral ratio between the horizontal and vertical components (HVSR). The computed HVSR for the inverted 1D soil profiles is compared with the observed HVSR of the measured microtremor. The comparison of the mean HVSR observed by McCue & Love (1997), the mean HVSR observed by Setiawan *et al*. (2016) and the computed HVSR of this study, is presented in Figure 2.6. Generally, the comparison between the observed and calculated HVSR curves show comparable results. Both the observed and calculated HVSRs suggest two-peak frequency characteristics at frequencies of about 0.8–0.9 and 4.0–5.0 Hz. The subsequent developed 1D profiles for the Old Exchange Building site are presented in Table 2.3.

Table 2.3 Developed 1D profiles for the investigated site.

Formation	Description	Thickness or (Depth)		Estimated mean shear wave (m/s)
		Model A	Model B	
Quaternary alluvium, Pooraka Formation [HOLOCENE]	Red brown silty CLAY (CH), grades downwards to SAND and GRAVEL (SP-GP)	2.4	2.3	137
Keswick CLAY [PLEISTOCENE]	Grey-green CLAY (CH) with red and brown mottling, stiff to hard, fissured	6.1	6.3	159
Hindmarsh CLAY [PLEISTOCENE]	Grey-green CLAY (CH) with yellow and red mottling with overlying SAND (SC)	6.1	6.3	354
Bunham Limestone and Hallet Cove Sandstone [PLEISTOCENE TO PLIOCENE]	White clayey, sandy and rubbly LIMESTONE; Pale grey to yellow brown calcareous SANDSTONE with layers of sand (SP)	7.9	9.1	433
Sand unit of Port Willunga Formation [EOCENE]	Fine silty SAND (SM)	5.5	4.0	330
Tandanya Sand Member of Chinaman Gully Formation [EOCENE]	Gravelly, clayey SAND (SC-GW)	9.7	12.6	333
Gull Rock Member of Blanche point Formation [EOCENE]	Alternating bands of cherty siltstone and grey SILT (ML)	21.8	22.9	317
Undifferentiated basal Blanche Point Formation and Tortachilla Limestone [EOCENE]	Green to dark grey clayey SAND (SC) with LIMESTONE	4.8	5.1	283
South Maslin Sand [EOCENE]	Dark grey, brown at depth, but weathering to red brown or yellow, silty SAND (SM) with pyrite lumps	10.3	11.4	261
Clinton Formation [EOCENE]	Dark grey CLAY (CL) with LIGNITE; irregular clayey SAND zones (SC)	13.9	14.3	269
Precambrian bedrock	White, pink, brown, purple, blue-grey and greenish grey with thin sandy bands, decomposed quartzite or quarts veins, high plasticity SILT slightly sandy, very stiff to hard with a moisture content well below the plastic limit > 480 kPa	(88.5)	(94.3)	926

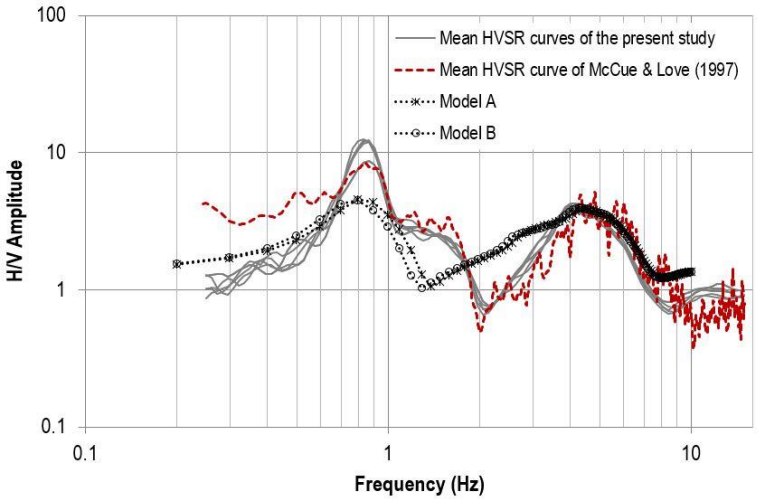

Figure 2.6 Comparison between the mean of the observed and calculated HVSR curves from the best fit models.

2.3.3 Modulus reduction and damping curves

Ideally, for a site-specific ground response analysis, the modulus reduction and damping curves are developed in accordance with the samples obtained from the soil profile. However, as the default curves provided by SHAKE91 (Idriss & Sun, 1992) or EERA (Equivalent-linear Earthquake Response Analysis) (Bardet *et al.*, 2000) have proven to work well in most applications for site response analysis (Sykora & Davis, 1993; Uthayakumar & Naesgaard, 2004), this study has also adopted these curves (Figure 2.7). Each curve represents a unique, typical material behaviour during strain. The shear modulus reduction and damping ratio curves (Figure 2.7a) were proposed by Seed & Sun (1989). The curves were developed from the upper bound shear modulus curve for clay (Seed & Sun, 1989). The shear modulus curve for sand (Figure 2.7a) was by Seed & Idriss (1970), which was developed from the upper bound shear modulus curve of sand. The damping curves for clay and sand were proposed by Idriss (1990) cited by Bardet *et al.*, (2000) (Figure 2.7a), and for rocks by Schnabel *et al.* (1972) (Figure 2.7b). In the present site response analysis, these curves are accordingly assigned to each layer of the subsurface model.

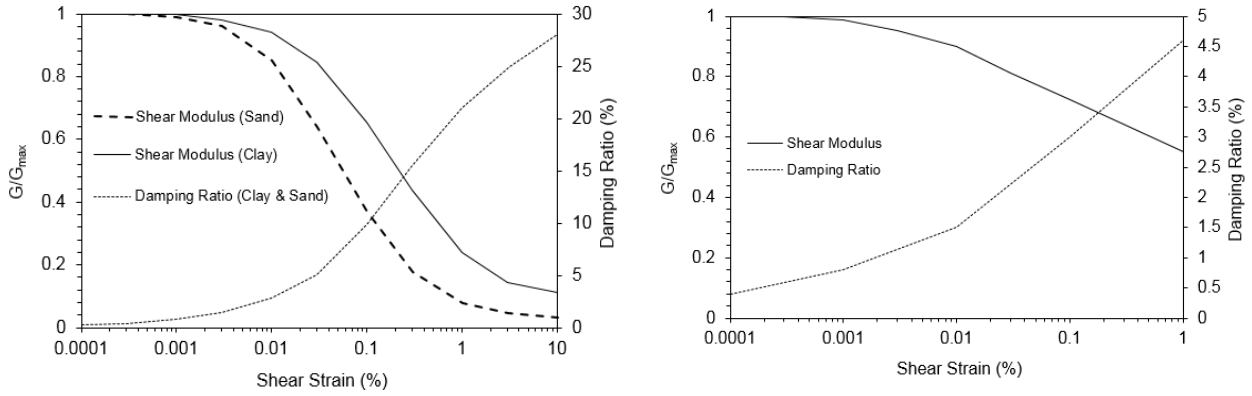

(a) (b)

Figure 2.7 Shear modulus, shear strain and damping ratios for: (a) clay (upper range) [Seed & Sun, 1989], sand [Seed & Idriss, 1970] and clay & sand damping ratio [Idriss, 1990 cited by Bardet *et al*., 2000]; (b) rock [Schnabel *et al*., 1972 cited by Bardet *et al*., 2000].

2.3.4 Conducting equivalent-linear site response analysis

Standard practice for the dynamic analysis of soils in geotechnical earthquake engineering is the equivalent-linear site response analysis (Borja *et al.*, 2000). This method assumes that soil stiffness and damping are consistent for a certain level of maximum shear-strain. It has been demonstrated that this analysis is reliably able to simulate soil behaviour due to dynamic loading (Priolo *et al*., 2008). This equivalent-linear site response analysis has been implemented in the SHAKE (Schnabel *et al*., 1972) computer program, which has been one of the most widely used tools for site response analysis for decades. The advantages of SHAKE are that it is simple and compact. Another equivalent-linear site response analysis program, EERA, was developed by taking advantage of the most recent developments of FORTRAN 90 and the Windows operating system at the time. The EERA program was developed from the basic principles of SHAKE (Bardet *et al*., 2000). Unlike SHAKE, EERA is an add-on program embedded in Microsoft Excel. Good agreement is obtained between the results of SHAKE and those of EERA for use in site-specific ground response analysis, as demonstrated by Bardet *et al*. (2000). As a result, EERA has been adopted here.

2.4 RESULTS AND DISCUSSIONS

Several outputs of the site-response analysis at the Old Exchange Building site, using the synthetic ground motions, are presented in Figures 2.8 (a) to 2.9 (c), for Model A, and in

Figures 2.9 (d) to 2.10 (f), for Model B. The results are summarised in Tables 2.4 and 2.5 for Models A and B, respectively.

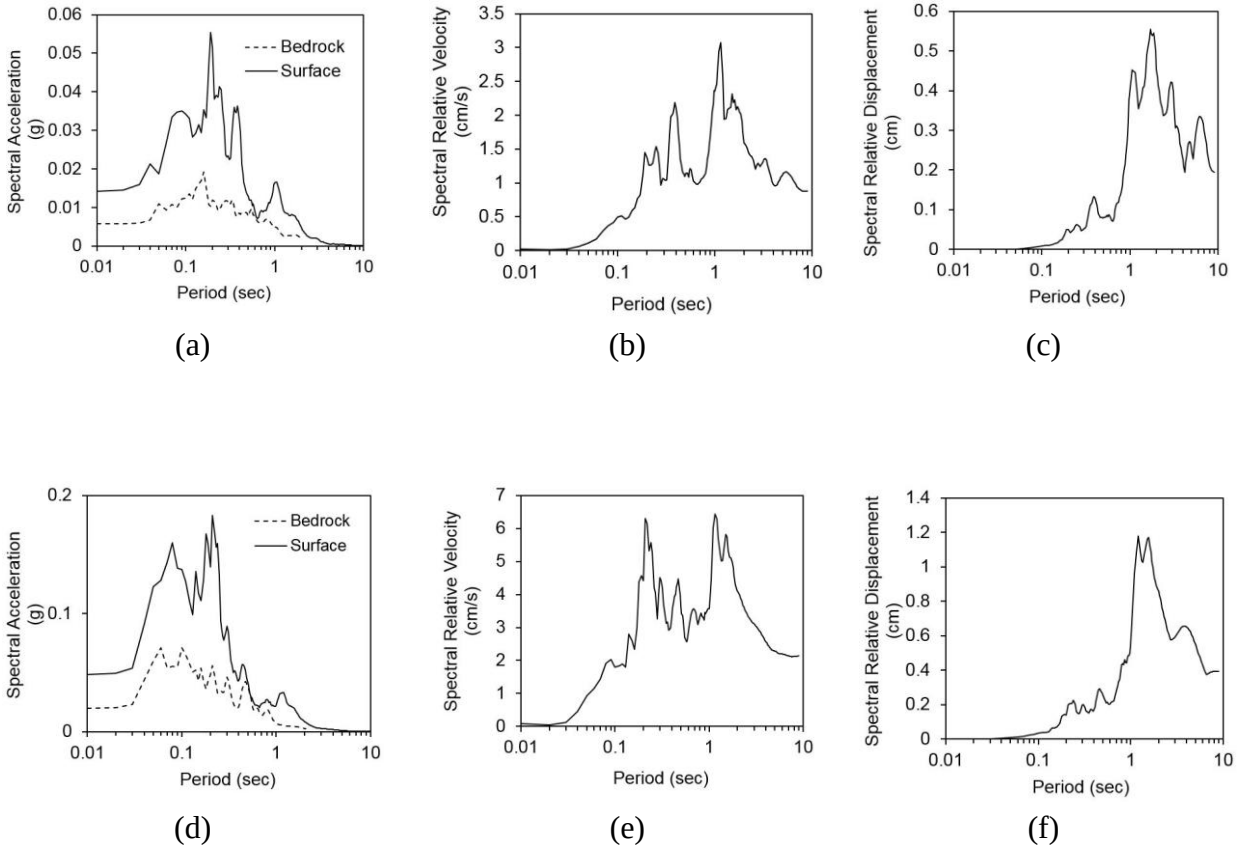

Figure 2.8 Model A input motion of 1897 Beachport earthquake: (a) response spectral acceleration, (b) velocity, and (c) displacement outputs; and Model A input motion of 1902 Warooka earthquake: (d) response spectral acceleration, (e) velocity, and (f) displacement outputs.

Table 2.4 Results of site-specific ground response analysis using EERA for Model A.

Parameters	1897 Beachport	1902 Warooka	1954 Adelaide
PGA (g)	0.014	0.049	0.321
Fundamental frequency (Hz)	0.8	0.8	0.8
Max spectral relative acceleration (g)	0.06	0.18	0.92
Max spectral relative velocity (cm/s)	3.08	6.43	36.80
Max spectral relative displacement (cm)	0.55	1.17	2.68

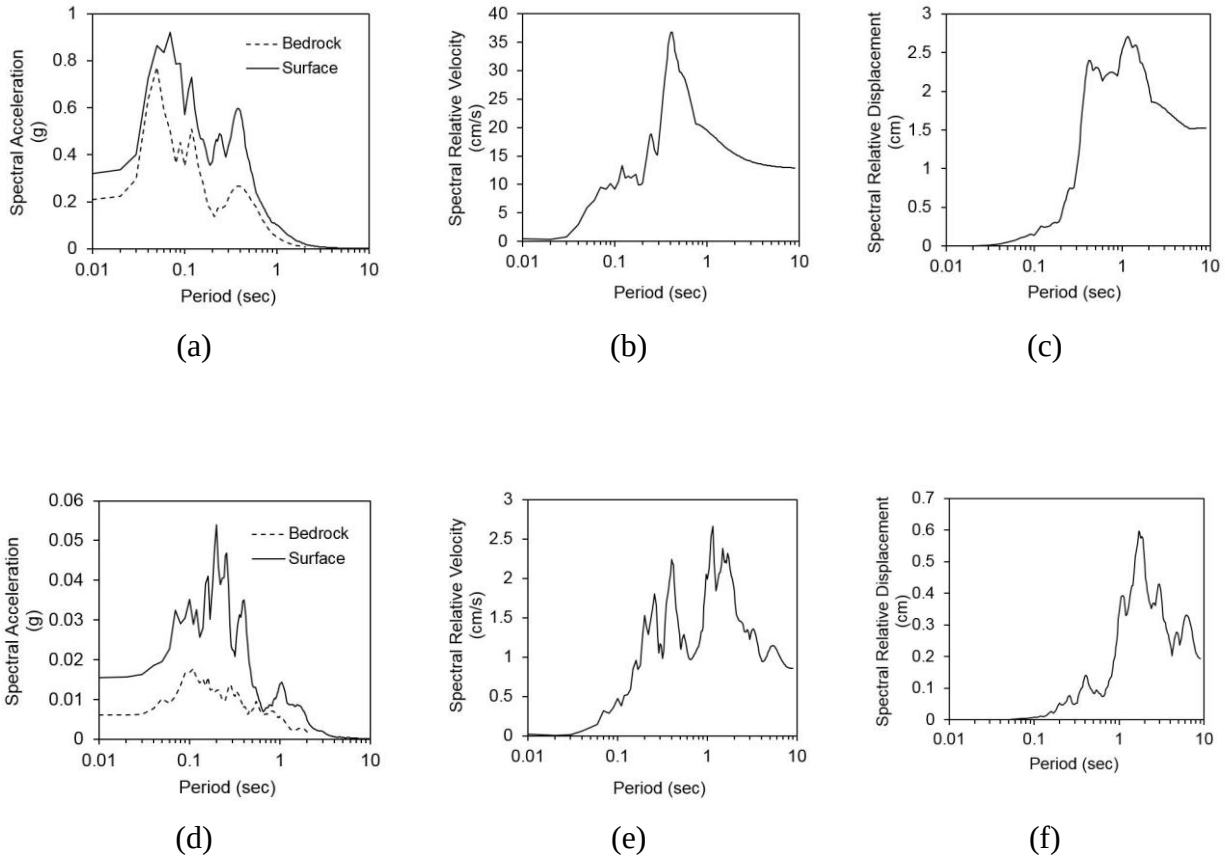

Figure 2.9 Model A input motion of 1954 Adelaide earthquake: (a) response spectral acceleration, (b) velocity, and (c) displacement outputs; and Model B input motion of 1897 Beachport earthquake: (d) response spectral acceleration, (e) velocity, and (f) displacement outputs.

Table 2.5 Results of site-specific ground response analysis using EERA for Model B.

Parameters	1897 Beachport	1902 Warooka	1954 Adelaide
PGA (g)	0.016	0.056	0.322
Fundamental frequency (Hz)	0.8	0.8	0.8
Max spectral relative acceleration (g)	0.05	0.18	0.96
Max spectral relative velocity (cm/s)	2.66	6.10	37.36
Max spectral relative displacement (cm)	0.58	1.21	2.56

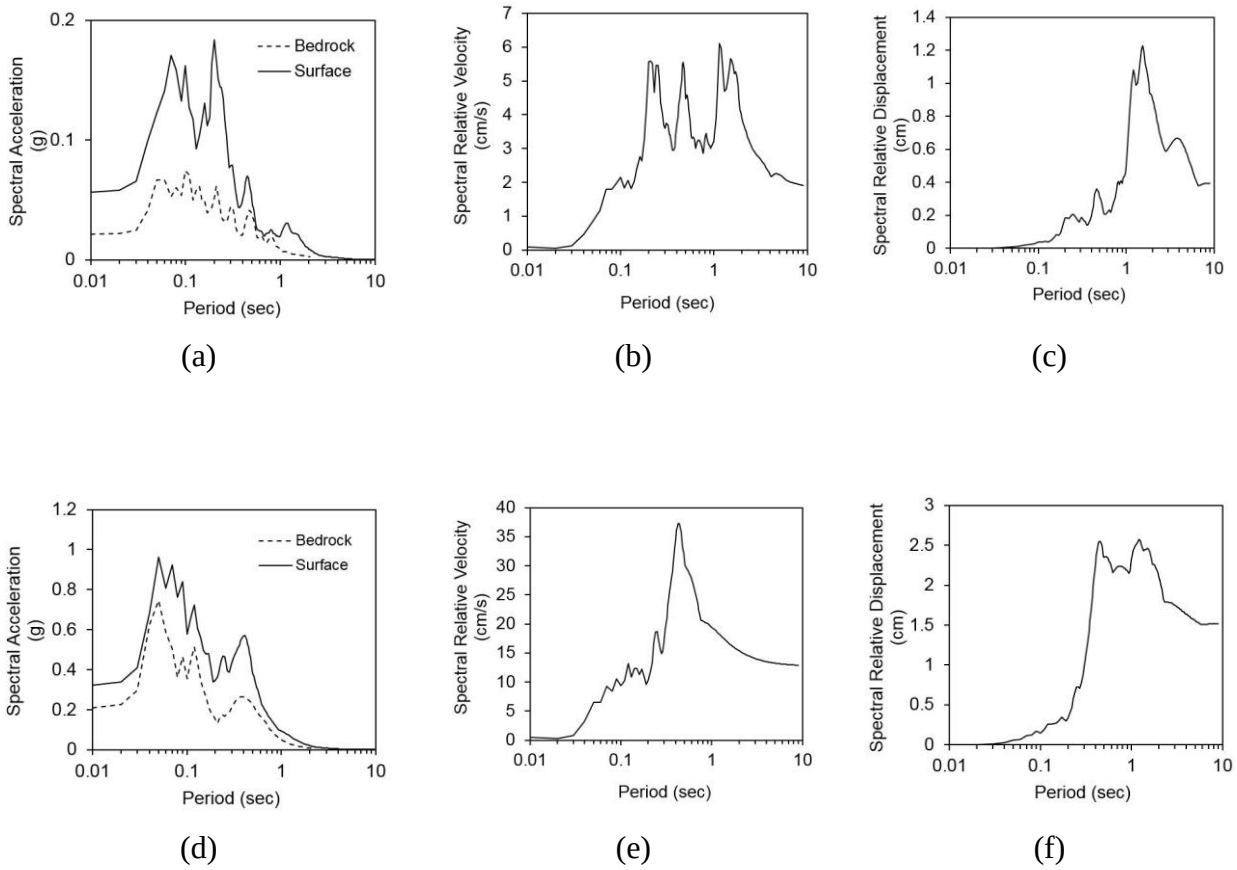

Figure 2.10 Model B input motion of 1902 Warooka earthquake: (a) response spectral acceleration, (b) velocity, and (c) displacement outputs; and Model B input motion of 1954 Adelaide earthquake: (d) response spectral acceleration, (e) velocity, and (f) displacement outputs.

For Model A, the PGA results are 0.01*g*, 0.06*g* and 0.3*g* for the 1897 Beachport, 1902 Warooka and 1954 Adelaide seismic events, respectively. The estimated fundamental frequency of the site is estimated about 0.8 Hz. The response spectrum analysis, with a critical damping ratio of 5%, shows maximum spectral accelerations (SAs) for these events to be 0.06*g*, 0.18*g* and 0.92*g* for the 1987 Beachport, 1902 Warooka and 1954 Adelaide earthquakes, respectively. The maximum spectral relative velocities (SVs) are estimated to equal 3.1 cm/s for the 1897 Beachport event, 6.4 cm/s for 1902 Warooka event, and 36.8 cm/s for the 1954 Adelaide event. By considering the PGA, SA, and SV, the analysis here determines that the 1954 Adelaide earthquake presented the highest threat of all three to damage the Old Exchange Building. As expected, in terms of spectral displacement (SD), the highest displacement of the Old Exchange Building appears to have also resulted from the 1954 Adelaide earthquake. That earthquake generated a

displacement of approximately 2.7 cm. The 1897 Beachport earthquake caused a displacement of 0.55 cm, and the 1902 Warooka earthquake was estimated to cause a displacement of about 1.2 cm.

For Model B, the PGA results are 0.02*g*, 0.06*g* and 0.32*g* for the 1897 Beachport, 1902 Warooka and 1954 Adelaide seismic events, respectively. Model B results in an estimated fundamental frequency at the Old Exchange Building site of 0.8 Hz. The maximum amplification amplitude for this model occurs at a frequency of 2.4 or 4.0 Hz. The response spectrum analysis, using a critical damping ratio of 5%, produces a maximum SA of 0.05*g*, 0.18*g* and 0.96*g* for the 1987 Beachport, 1902 Warooka and 1954 Adelaide earthquakes, respectively. The maximum SV is 2.66 cm/s for the 1897 Beachport event, 6.1 cm/s for the 1902 Warooka event and 37.4 cm/s for the 1954 Adelaide event. Among these three historical seismic events, Model B, again by considering the PGA, SA and SV, indicates that the 1954 Adelaide earthquake presented the highest threat of the three events. As with Model A, in terms of SD of the Old Exchange Building, the most critical value resulted from the 1954 Adelaide earthquake. This event again produced a displacement approximately 2.6 cm. The 1897 Beachport and 1902 Warooka earthquakes are estimated to cause displacements of approximately 0.58 and 1.2 cm, respectively.

The use of the analytical approach by Mavroeidis & Papageorgiou (2003) in the generation of the near source seismic event (i.e. Adelaide earthquake) in this study has several consequences on the results of the site response analysis. It estimates the PGA of up to 0.3*g*, which generally provides better estimation than without using the Mavroeidis & Papageorgiou (2003) analytical approach. This 0.3*g* PGA for the 1954 Adelaide seismic event slightly overestimates the actual damage for this MMI of VI-VII event (see the later discussion). Furthermore, the analytical approach by Mavroeidis & Papageorgiou (2003) in the Adelaide earthquake case allows EXSIM to generate the long-period velocity pulses (Motazedian & Atkinson, 2005). This extension will simulate low frequency or long period ground motion components. An amplification of the long period of the ground motion coherent components (i.e. velocity and displacement) is unavoidable in such near-source seismic events (Mimoglou *et al.*, 2017). The application of the analytical approach by Mavroeidis & Papageorgiou (2003) has increased the maximum SV up to 36.8 cm/s in Model A and up to 37.4 cm/s in Model B. The maximum spectral displacement of the Adelaide earthquake has also increased up to 2.7

cm in Model A and up to 2.6 cm in Model B. In contrast, the site response analyses without the application of the Mavroeidis & Papageorgiou (2003) analytical approach suggest the maximum spectral velocity of 20.9 cm/s for Model A, 23.4 cm/s for Model B and the maximum SD of 0.9 cm for both Models A and B (not shown in this paper). The effect of the seismic duration on the velocity component of ground motion was also suggested by Hamedi & Tehranizadeh (2000). The SV and displacement amplification on the inelastic response of structures due to near seismic sources is also reported by Panagiotou (2008), Iervolino and Cornell (2008), and Taflampas & Psycharis (2008). Therefore, the site response analysis results of the spectral relative velocity and displacement of the Adelaide earthquake must be carefully examined.

The PGA outputs from our study are compared with the empirical attenuation function by Wald *et al*. (1999) and Linkimer (2008), as shown in Table 6. The PGA calculations, using the empirical attenuation functions, are based on the seismic MMIs of IV–V, V–VI, and VI-VII for the 1897 Beachport, 1902 Warooka, and 1954 Adelaide earthquakes, respectively. The comparison suggests good agreement with the results of both the 1897 Beachport and 1902 Warooka earthquakes. However, this study suggests a slightly higher seismic intensity resulting from the 1954 Adelaide earthquake.

Table 2.6 Comparison PGA estimation at the Old Exchange Building site.

Seismic event	**Estimated MMI at Old Exchange Building site**	**Estimated PGA (*g*)**		
		Wald *et al*. (1999)	**Linkimer (2008)**	**Present study**
1897 Beachport	IV-V (see: McCue, 1975)	0.02 to 0.07	0.02 to 0.06	0.014 to 0.016
1902 Warooka	V-VI (see: McCue, 1975 & Malpas, 1991)	0.07 to 0.13	0.06 to 0.11	0.049 to 0.056
1954 Adelaide	VI - VII (see: Malpas, 1991)	0.13 to 0.24	0.11 to 0.20	0.32

2.4.1 Hazard spectra

Log-log plots of the spectral accelerations for both Models A and B for the three historical seismic events are shown in Figure 2.11. As mentioned above, the 1954 Adelaide earthquake is estimated to result in higher spectral accelerations than others, particularly below a period of 0.4 s.

The spectral acceleration outputs are compared with the results of Love (1996) and Leonard *et al*. (2013). The maximum SA obtained is 0.92*g*, which is associated with the 1954 Adelaide earthquake. Love (1996) suggested a maximum SA of 0.76*g* and Leonard *et al*. (2013) estimated a value of approximately 0.3*g* for a 2,500-year return period. Hence, our study has obtained slightly larger estimated SAs than those proposed by Love (1993). Furthermore, this work suggests a maximum SA three times larger than that suggested by Leonard *et al.* (2013). This large discrepancy is likely to be caused by the adopted shear wave velocity profile, modulus reduction and damping curves, and input ground motion. Our study adopts shear wave velocity profiles based on forward modelling of the measured HVSR curves with an average of the top 30 m shear wave velocity (V_{s30}) between 315 and 320 m/s, whereas Leonard *et al.* (2013) most likely employed an empirical shear wave profile with V_{s30} between 315 and 460 m/s. The study here employs the generic modulus reduction and damping curves, whereas Leonard *et al.* (2013) likely used different modulus reduction and damping curves. In terms of input ground motions, we selected the ground motions based on past seismic events (i.e. 1897 Beachport, 1902 Warooka, and 1954 Adelaide earthquakes), whereas the seismic event adopted by Leonard *et al.* (2013) is based on a probabilistic analysis. The paucity of strong motion events in the low-moderate seismic region of southern Australia, influences the results of such probabilistic analysis, as the seismic source zone is difficult to define.

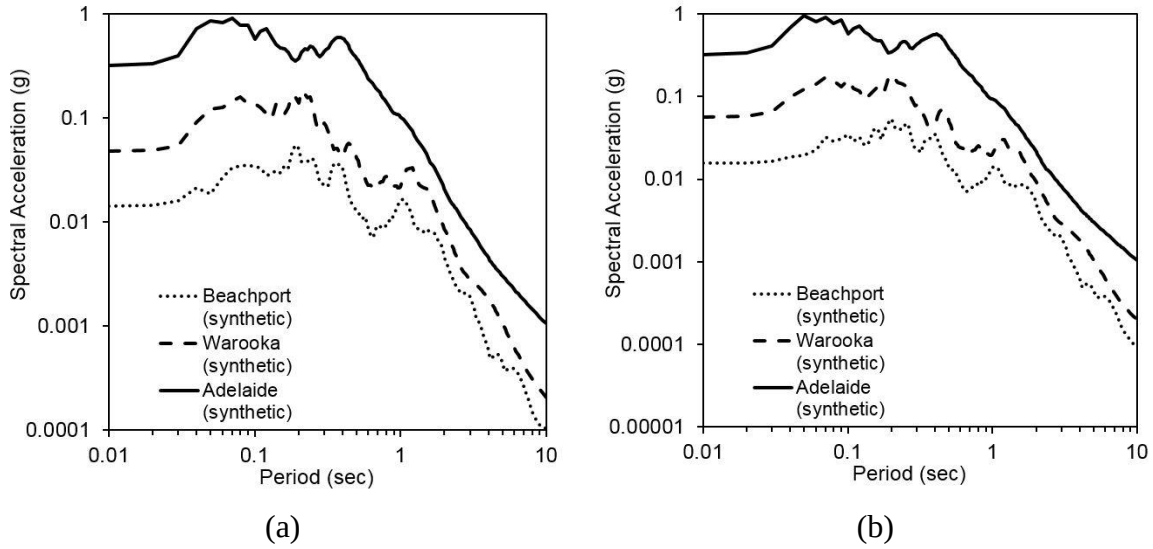

Figure 2.11 Response spectral accelerations of site response analysis for (a) Model A and (b) Model B.

2.4.2 Site amplification

Site amplification can be estimated using a comparison between the maximum acceleration of the ground surface layer and the maximum acceleration at bedrock level. Site response analysis results of the maximum acceleration profile at the Old Exchange Building site for Models A and B are shown in Figures 2.12 (a) and (b). These maximum acceleration profiles are used to deduce the amplification factor at the investigated site. The results are shown in Figures 2.12 (c) and (d), which indicate an amplification factor at the ground surface level for Model A of between 1.5 to 2.5 and Model B of 1.5 to 2.6.

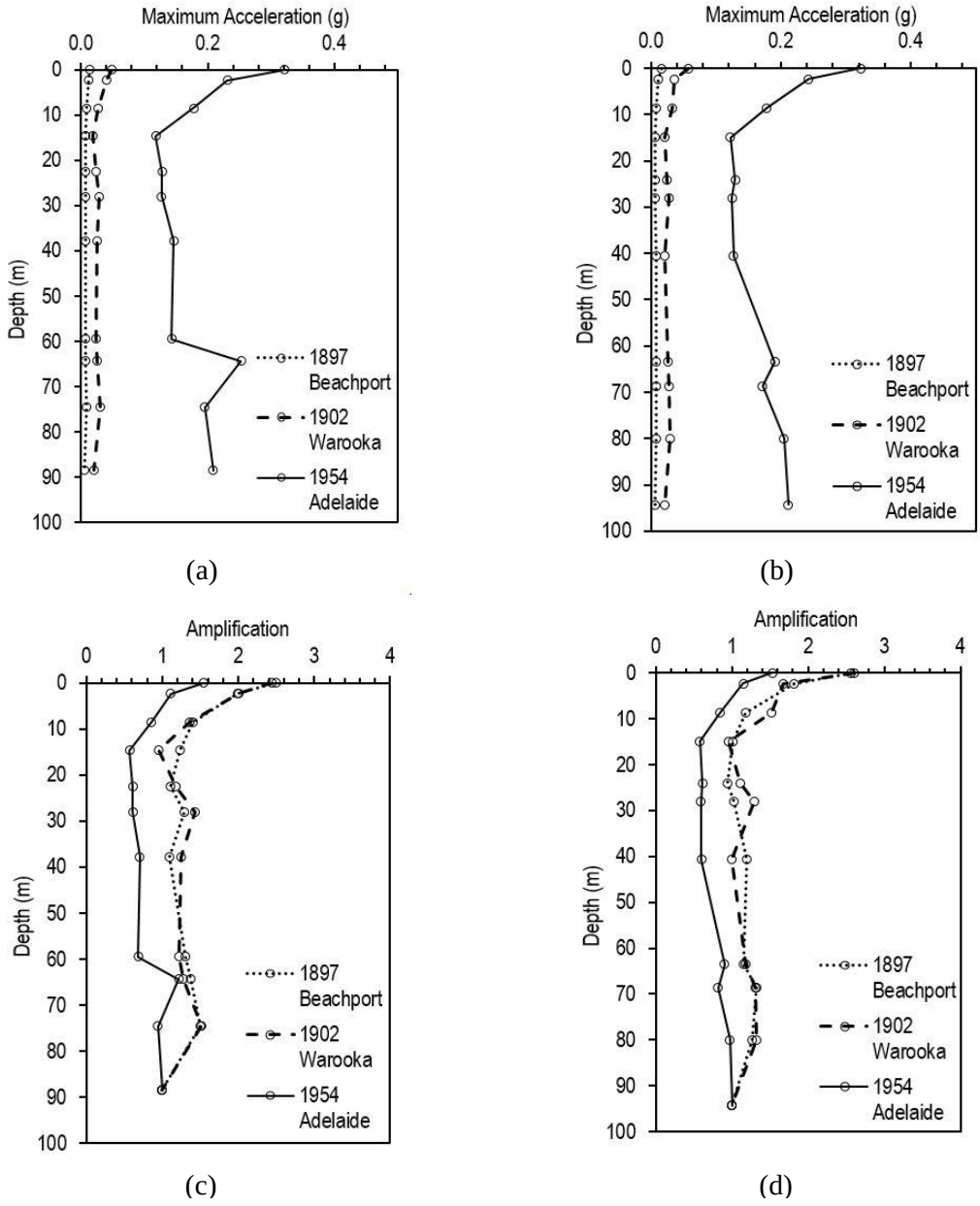

Figure 2.12 Site response analysis results: Maximum acceleration profiles for: (a) Model A, and (b) Model B; and Amplification profiles for: (c) Model A and (d) Model B.

Site amplification factors are used to understand the seismic motion behavior in the study area by means of the method proposed by Herak (2008), which has been has been shown to yield reliable results (Herak *et al.*, 2010; Lunedei & Albarello, 2015). The mean compression wave, shear wave and density models obtained here are used to quantify the amplification factors. The quality factors of Q_p and Q_s, for the compression and shear waves, respectively, are estimated using the approaches suggested by Olsen *et al*. (2003) and Zhang & Stewart (2007), respectively, which represent a linear estimate of amplification.

The results of the site amplification factors (Amp-HVSR) are presented in Figure 2.13. Generally, a site amplification of up to 3.4 is suggested. Averaging the amplification from 0.4 to 10 Hz at each site suggests that the amplification factor is only 1.2. By using identical subsurface models, a dynamic amplification factor (DAF) for the investigated site is also calculated. The method proposed by Herak (2008) is employed to calculate DAF. Unlike the Amp-HVSR, the DAF uses the most likely seismic event in the calculation. Generally, the result of this study shows that the estimated DAF slightly overestimates the amplification analysis using the Amp-HVSR method. As shown in Figure 2.14, the obtained value of DAF is 1.9.

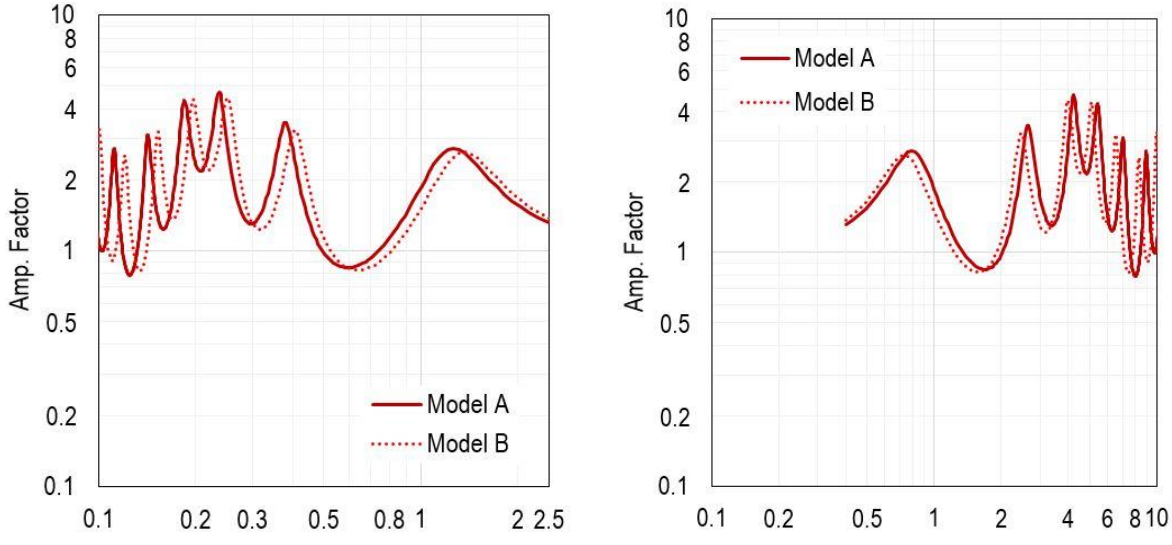

Figure 2.13 Amplification factor plotted against: (a) periods and (b) frequency at the Old Exchange Building site.

As stated by Herak (2008), the amplification factors of both Amp-HVSR and DAF do not consider the non-linear behavior of the subsurface material. Therefore, these estimates

need to be judiciously applied in practice. Whilst a non-linear site response analysis could potentially yield more reliable estimates, this is beyond the scope of the work here.

Additional evidence of site amplification in Adelaide is obtained from the recorded ground motions that occurred during the 1997 Burra earthquake. The recorded earthquake ground accelerations in Adelaide's regolith have been shown to be very much stronger than those recorded on bedrock just outside the city during this seismic event (DMITRE Minerals, 2013). Ground response analyses using historical ground motions also confirms site amplification. Thus, site amplification contributed to the damage experienced by the Old Exchange Building, as has been demonstrated to occur to similar buildings, such as in Mexico (Booth *et al*., 1986; Finn & Wightman, 2003), Kobe (Brebbia, 1996), and Umbria-Marche-Italy (Bindi *et al*., 2004; Castro *et al*., 2004; Luzi *et al*., 2005).

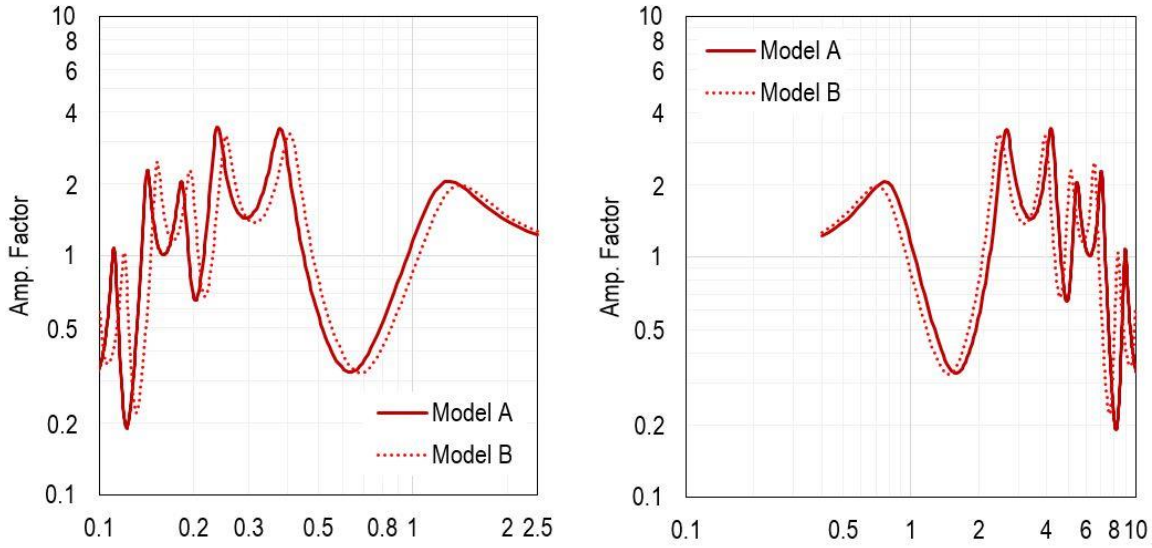

(a) (b)

Figure 2.14 DAFs plotted against: (a) periods and (b) frequency at the Old Exchange Building site.

2.4.3 Site fundamental frequency

For the Old Exchange Building site, observed HVSR curves by McCue & Love (1997) and Setiawan *et al*. (2016), have indicated a site fundamental frequency of 0.7–0.8 Hz (as shown in Figure 6) and first mode frequency of 4.0–4.5 Hz. Good agreement between both the observed HVSR curves of McCue & Love (1997) and Setiawan *et al*. (2016) highlight the consistency of the HVSR method with respect to time, as the measurement of the first reference was carried out in 1997, whereas the HVSR data of the later reference were obtained in 2015. This temporal stability of the HVSR analysis was also

suggested by Okada (2003). The obtained site frequencies are also correlated to the Old Exchange Building frequency to analyze the possibility of resonance effects which will occur when the ground frequency is equal or close to the natural frequency of the building. In terms of the number of stories (N), the Old Exchange Building was a low-rise (3 story) building. By adopting the building fundamental frequency approximation of Kramer (1996), which is approximated by 10/N (Hz), the Old Exchange Building frequency is estimated to be between 3.0 and 3.5 Hz. As mentioned above, the observed site fundamental frequency at the Old Exchange Building site is 0.8-0.9 Hz, which is three times lower than the Old Exchange Building's natural frequency. However, the first mode site frequency (4.0–4.5 Hz) is relatively close to the Old Exchange Building's natural frequency. This implies that the first mode of site frequency is likely to have increased the Old Exchange Building's vibration and enhanced the prospect of structural collapse.

2.4.4 Study limitations and future work

While this study has provided useful information relating to site effects, the analysis is limited. Firstly, the study is confined to a specific case at a single site (i.e. the Old Exchange Building case). Clearly, extending the study to incorporate several sites across the city of Adelaide is desirable to obtain a more reliable predictions of the dynamic characteristics of Adelaide's sub-surface. However, given the limited data currently available, such additional analyses are not possible at this time. Secondly, the sub-surface shear wave velocity models were developed from forward modelling of a measurement obtained at a distance of approximately 200 m from the site. Again, it is preferable the direct shear wave velocity measurement to be obtained at the site of interest. However, this was not possible due to access constraints. Finally, soil-structure interaction effects were not considered here and are beyond the scope of this study. Future improvements include extending the use of ambient vibration measurements for site characterisation in regolith environments and enhancing geophysical methods to investigate the basin structure of the investigated site.

2.5 CONCLUSION

Three historical seismic events, the 1897 Beachport (MMI IV–V), 1902 Warooka (MMI V–VI), 1954 Adelaide (MMI VI–VII) earthquakes, caused damage to the Old Exchange Building located in Pirie St, Adelaide. As there were no recorded time histories of the

three events, generated time histories are required. Time histories of the three events have been generated using a method that was validated using recorded ground motions of the 1997 Burra earthquake. Two representative models for the Old Exchange Building site were developed and validated using a single microtremor measurement at the nearby site.

The results of both the synthetic time histories of historical seismic events and the development of 1D profiles of the Old Exchange Building site, were used for investigating site effects. Analytical models used in this study for a site-specific ground response analysis proved to simulate the ground behaviour reasonably well. The results of the ground response analyses clearly indicate that, for the case of Old Exchange Building site, the input parameters are influenced by local site effects by an amplification factor of up to 3.4.

INTENTIONALLY BLANK

Chapter Three

SEISMIC SITE CLASSIFICATION BASED ON CONSTRAINED MODELING OF MEASURED HVSR CURVE IN REGOLITH SITES

INTENTIONALLY BLANK

Statement of Authorship

Title of Paper	Seismic site classification based on constrained modeling of measured HVSR curve in regolith sites
Publication Status	☑ Published ☐ Accepted for Publication ☐ Submitted for Publication ☐ Unpublished and Unsubmitted w ork w ritten in manuscript style
Publication Details	Setiawan, B., Jaksa, M., Griffith, M., and Love, D., 2018. Seismic site classification based on constrained modeling of measured HVSR curve in regolith sites. Soil Dynamics & Earthquake Engineering, 110: 244-261, DOI: 10.1016/j.soildyn.2017.08.006

Principal Author

Name of Principal Author (Candidate)	Bambang Setiawan		
Contribution to the Paper	Performed field data collection, carried out analysis on all field data, interpreted the results, wrote the manuscript and acted as corresponding author.		
Overall percentage (%)	80%		
Certification:	This paper reports on original research I conducted during the period of my Higher Degree by Research candidature and is not subject to any obligations or contractual agreements with a third party that would constrain its inclusion in this thesis. I am the primary author of this paper.		
Signature		Date	14 June 2017

Co-Author Contributions

By signing the Statement of Authorship, each author certifies that:

i. the candidate's stated contribution to the publication is accurate (as detailed above);

ii. permission is granted for the candidate in include the publication in the thesis; and

iii. the sum of all co-author contributions is equal to 100% less the candidate's stated contribution.

Name of Co-Author	Mark Jaksa		
Contribution to the Paper	Overall percentage - 10% Supervised the development of work, helped in data interpretation and manuscript preparation. He also reviewed this manuscript rigorously.		
Signature		Date	14/6/17

Name of Co-Author	Michael Griffith		
Contribution to the Paper	Overall percentage - 5% Provided some valuable comments on the manuscript contents.		
Signature		Date	14/6/17

Name of Co-Author	David Love		
Contribution to the Paper	Overall percentage - 5% Helped the field data collection, evaluated and edit the manuscript. Provided some valuable comments on the manuscript contents.		
Signature		Date	14 June 2017

Please cut and paste additional co-author panels here as required.

3.1 INTRODUCTION

Seismic site classification is widely accepted in the design of seismic resistant infrastructure. Currently, the majority of seismic site classifications are carried out based on recommendations provided by the National Earthquake Hazards Reduction Program [NEHRP] (BSSC, 2001). However, the application of the NEHRP classification system in regolith sites is the subject significant research effort (e.g. McPherson & Hall, 2007 and Anbazhagan *et al*., 2013), including in Adelaide, South Australia. The National Committee on Soil and Terrain [NCST] (2009) characterized regolith as unique geological materials which generally have low impedance contrast comparable to that of bedrock. Regoliths are formed or altered by land surface processes, whereas bedrock is formed or altered by deep-seated crustal processes. The characterization of regoliths and bedrock is by their formation processes, rather than by their material type (Wilford & Thomas, 2013). These different formation processes result in distinctive characteristics of regolith masses when compared to bedrock. Generally, the density, strength, and cohesion of regolith masses are lower than bedrock masses (NCST, 2009). Anbazhagan *et al*. (2013) addressed the difficulties in the application of NEHRP seismic site classification in such sites, including ones in Australia. McPherson & Hall (2007) suggested a modification to the NEHRP seismic classification system for the application to regolith sites.

The horizontal vertical spectral ratio (HVSR) technique (Nakamura, 1989) has been widely used in seismic hazard assessment since it is relatively straightforward, convenient and reliable in urban areas. Separate studies by Picozzi *et al*. (2009) and Mokhberi *et al*. (2010) successfully implemented the HVSR technique in Turkey and Iran, respectively, to calculate the site predominant frequency and Fah *et al*. (2003), Harutoonian *et al*. (2003) and Di Stefano *et al*. (2014) enhanced the HVSR technique to infer the subsurface shear wave profile. To date, the application of the HVSR technique in regolith regions for site seismic classification is still under development (McPherson & Hall, 2007). Regardless of some limitations of this method, Di Stefano *et al*. (2014) and Wotherspoon *et al*. (2015) observed that the HVSR method is reasonably robust in seismic hazard assessment, provided the geological setting at the target location is well defined.

The present study aims to investigate the HVSR method for seismic site classification at regolith and Adelaide, the capital and largest city in South Australia, which is founded on

a regolith, is selected as a case study in the present work. Previous investigations (*cf* Collins *et al*., 2006 and Leonard, 2015) suggested low impedance contrast of the regolith of Adelaide (assuming that large impedance contrast is > 4–5 as suggested by SESAME (2004). Shear wave velocity measurement at the Government House Site (GHS), using the spectral analysis of surface waves (SASW) method Collins *et al*. (2006), suggested an average of about 420 m/s and 810 m/s for Adelaide's overlying layer and bedrock shear wave velocities, respectively. By assuming densities of 1,900 kg/m^3 and 2,100 kg/m^3 for the top layer and the bedrock, respectively, measurements by Collins *et al*. (2006) suggested an impedance contrast of only 2.1 (i.e. a low impedance contrast). Preliminary results from a site investigation by Leonard (2015) suggested a shear wave velocity of at least 315 m/s for the upper 30 m for most of the Adelaide city. Only the areas along the River Torrens were expected to have a shear wave velocity of at least 225 m/s. Thus, a raw estimation of the impedance contrast of most of the Adelaide city sites, based on the recommendations of Leonard (2015), will be approximately 3.5 by assuming the shear wave velocity of the top layer and bedrock are 315 m/s and 1,000 m/s, respectively. Densities of 1,900 kg/m^3 and 2,100 kg/m^3 for the top layer and the bedrock, respectively, are used for this raw impedance contrast calculation. This impedance contrast of 3.5 is also below that suggested by SESAME (2004), where values > 4–5 are considered as large impedance contrast.

Adelaide is within the most seismically active region on the Australian continent (Sandiford, 2003; Quigley *et al*., 2006; and Quigley *et al*., 2007). Although this continent is classified as a stable continent region [SCR] (Johnston, 1996a; Celerier, *et al*., 2005; and Hillis *et al*., 2008) with low to moderate (Veevers, 1984) seismic activity, the Australian continent deformation rate is higher than other stable intraplate regions (Hillis *et al*., 2008). The continent experiences a magnitude ≥ 6.0 earthquake approximately every 5 years (McCue, 1990) and historically, the continent has experienced some major devastating earthquakes, such as those that occurred at Meeberrie (1941; ML 6.8), Meckering (1986; MS 6.8), Cadoux (1979; MS 6.4) and Tennant Creek (1988; MS 6.3) [Johnston, 1996b; Crone, *et al*., 1997; Sandiford *et al*., 2004]. The seismic activity of the Adelaide region was also investigated by Greenhalgh & Parham (1986) and Greenhalgh *et al*. (1986). Greenhalgh *et al*. (1986) found at least 300 earthquakes are recorded by instruments each year in South Australia and in the last 150 years, 15 events were of magnitude 5 or greater. McCue (1990) found that the Adelaide city experienced more

medium-sized earthquakes than any other capital city in Australia in the past half of the last century. Furthermore, the site amplification phenomenon also occurs in Adelaide, which is observed by comparing the ground motion recording on Adelaide's regolith to that on a rock site just outside the city during the 1997 Burra earthquake. The recorded motions on the regolith are very much stronger than those recorded on rock (DMITRE Minerals, 2013). Thus, an in-depth seismic hazard study of the Adelaide region is highly desirable.

A group of seismometer sets has been deployed across the Adelaide city to measure the ambient noise at a range of regolith sites. The data are used to obtain the seismic hazard parameters, such as site periods and shear wave profiles, from which the seismic site classification of Adelaide is quantified. The results of the present study are valuable, not only to the seismic site classification of Adelaide, but also to the seismic assessment of regolith sites with a similar geological context.

2.2 SEISMIC SITE CLASSIFICATION IN AUSTRALIA

The most widely used seismic site classification system is based on the mean shear wave velocity of the uppermost 30 m of the subsurface layers, $V_{s,30}$, which was proposed by the National Earthquake Hazards Reduction Program [NEHRP] (Collins *et al*., 2006; and Anbazhagan *et al*., 2010; and Anbazhagan *et al*., 2013) and can be calculated by:

$$V_{s,30} = \frac{\sum_{i=1}^{n} Z_i}{\sum_{i=1}^{n} \left(\frac{Z_i}{V_{si}} \right)} \quad \text{..... (3.1)}$$

where, Z is thickness (in meters), V_{si} is shear wave velocity of ith layer, and n is a total number of layers in the top 30 m.

This classification system categorizes the subsoil into 5 subsoil classes from hard rock (subsoil class A) to thick medium-soft soils (subsoil class E). Standards Australia (Standards Australia, 2007) (AS 1170.4–2007) modified the NEHRP seismic classification system in the following manner: (1) rock (subsoil class B) applies to $V_{s,30}$ above 360 m/s instead of 760 m/s in the NEHRP system; (2) a site fundamental period is introduced to separate subsoil Class D from Class C; and (3) subsoil Class E applies to

sites with greater than 10 m thickness of soil with a shear wave velocity less than 150 m/s. The amendment to AS 1170.4 Standards Australia followed Standards New Zealand (Standards New Zealand, 2004) at a stage when the two countries were attempting to produce a unified earthquake code. The work, principally performed by McVerry *et al*. (2000) and McVerry *et al*. (2006), showed that deep stiff soils produced amplification similar to soft shallow soils, thus producing a departure from the standard NEHRP method. An alternative and applicable classification system was suggested by McPherson & Hall (2007), which clusters the system into 7 classes and includes a physical description and age associated with each. Details of the seismic site classification in accordance with NEHRP, AS 1170.4 and McPherson & Hall (2007) are summarized in Table 3.1.

Table 3.1 Seismic site classification in Australia.

Site class	**Generalized soil description**	**NEHRP (BSSC, 2001)**	**AS 1170.4 (Standards Australia, 2007)**	**Australian National Regolith Site Classification Map (McPherson & Hall, 2007)**	
		$V_{s,30}$ **(m/s)**			**Description**
A	Hard rock	> 1500	> 1500	–	–
B	Rock	760 – 1500	> 360	> 760	Fresh to moderately weathered hard rock units (plutonic & metamorphic rocks, most volcanic rocks, coarse-grained sedimentary rocks, Cretaceous & older)
BC		–	–	555 – 1000	Highly weathered hard rock; some Tertiary volcanics
C	Very dense soil & soft rock	360 – 760	≤ 0.6 s (surface to rock)	360 – 760	Sedimentary rocks of Oligocene age; coarse-grained sedimentary rocks of younger age; extremely weathered hard rock units
CD	–	–	–	270 – 555	Sedimentary rocks of Miocene and younger age, unless formation is notably coarse-grained; Plio-Pleistocene alluvial units; older (Pleistocene) alluvium; some areas of coarse younger alluvium
D	Dense to medium soils	180 – 360	> 0.6 s (surface to rock)	180 – 360	Young (Holocene to Late Pleistocene) alluvium
DE	–	–	–	90 – 270	Fine-grained alluvial, deltaic, lacustrine and estuarine deposits
E	Medium to soft soils	< 180	Greater than 10 m soil depth with $V_s \leq 150$	< 180	Intertidal and back-barrier swamp deposits

2.3 GEOLOGICAL SETTING OF ADELAIDE

The structural geology of the Adelaide city is characterized by faults oriented in the north-east to south-west directions. Earthquakes related to the faults in Adelaide were documented and presented by Selby, (1984). The most significant seismic event in Adelaide was the 1954 Adelaide Earthquake which was associated with intra-plate activity along the Burnside-Eden Fault to the east of the city (Selby, 1984 and Love, 1996).

Adelaide is situated in the eastern part of the St. Vincent Basin and the morphology of the city is predominantly controlled by the bounding faults to the west (Para Fault) and east (Eden-Burnside Fault) of the city (Selby & Lindsay, 1982). Below the fill and surficial layer, most of the natural immediate surface consists of Holocene stratigraphic units of either red brown clay (Callabonna Clay) or light brown silty clay with calcareous with layers of calcrete gravel (Pooraka Formation). In addition, a relatively narrow channel along the River Torrens, crossing from east to west within the Adelaide city, has eroded these layers and deposited alluvium. The combined thickness of these Holocene units may up to 21 m thick (Selby & Lindsay, 1982 and Sheard & Bowman, 1996). Below the Holocene units is a layer of Keswick Clay, Hindmarsh Clay, or a combination of both, for the majority of the southern part of the city (Jaksa, 1995). These layers are highly plastic, over-consolidated clays which exhibit properties remarkably similar to those of the London Clay (Cox, 1970). These layers are underlain by either the Carisbrooke Sand, Burnham Limestone and Hallett Cove Sandstone or the Gull Rock member of the Blanche Point Formation. In some areas these are underlain by a sand unit of the Port Willunga Formation or the Tandanya Sand Member of the Chinaman Gully Formation. The age of these stratigraphic units varies from Pleistocene to Eocene (Selby & Lindsay, 1982). Most areas in the city of Adelaide are further underlain by the South Maslin Sand and Clinton Formation, before Precambrian bedrock is encountered at about 64 m or less to the north of the city and up to 118 m or more to the south (Selby & Lindsay, 1982). Moreover, Selby & Lindsay (1982) suggested a higher stratigraphic variability to the south of the city than to the north. A detailed summary of the geological units in the Adelaide City is given in Table 3.2.

Table 3.2 Summary of the formations included in the constrained model (after Selby & Lindsay, 1982).

Formation	Description	Formation Code
Quaternary alluvium, Pooraka Formation [HOLOCENE]	Red brown silty CLAY (CH), grades downwards to SAND and GRAVEL (SP-GP)	A
Keswick CLAY [PLEISTOCENE]	Grey-green CLAY (CH) with red and brown mottling, stiff to hard, fissured	A1
Hindmarsh CLAY [PLEISTOCENE]	Grey-green CLAY (CH) with yellow and red mottling with overlying SAND (SC)	A2
Carisbrooke Sand [PLEISTOCENE]	Yellow, orange brown and grey, fine to medium clayey and silty SAND (SC-SM)	B
Bunham Limestone and Hallett Cove Sandstone [PLEISTOCENE TO PLIOCENE]	White clayey, sandy and rubbly LIMESTONE; Pale grey to yellow brown calcareous SANDSTONE with layers of sand (SP)	C
Sand unit of Port Willunga Formation [EOCENE]	Fine silty SAND (SM)	D
Tandanya Sand Member of Chinaman Gully Formation [EOCENE]	Gravelly, clayey SAND (SC-GW)	E
Gull Rock Member of Blanche point Formation [EOCENE]	Alternating bands of cherty siltstone and grey SILT (ML)	F
Undifferentiated basal Blanche Point Formation and Tortachilla Limestone [EOCENE]	Green to dark grey clayey SAND (SC) with LIMESTONE	G
South Maslin Sand [EOCENE]	Dark grey, brown at depth, but weathering to red brown or yellow, silty SAND (SM) with pyrite lumps	H
Clinton Formation [EOCENE]	Dark grey CLAY (CL) with LIGNITE; irregular clayey SAND zones (SC)	J
Precambrian bedrock	White, pink, brown, purple, blue-grey and greenish grey with thin sandy bands, decomposed quartzite or quarts veins, high plasticity SILT slightly sandy, very stiff to hard with a moisture content well below the plastic limit > 480 kPa	K

2.4 ADELAIDE SEISMIC HAZARD STUDY

Adelaide, with a population in excess of 1.3 million people, is the only capital city in Australia that has recorded a medium or higher seismic event with an epicenter in very close proximity to the city, with an earthquake of a magnitude of 5.4 ML which struck the city on 1 March 1954. This has been responsible for the city being assigned the highest seismic exposure of all capital cities in Australia. Despite several changes in seismic hazard exposure among Australian capital cities in 2012, the seismic hazard for Adelaide remains under development. To date, several studies examining local site effects related

to Adelaide have been undertaken (McPherson & Hall, 2007; Collins *et al*., 2006; Leonard, 2015 and McCue & Love, 1997). McPherson & Hall (2007) undertook a further seismic assessment which resulted in a general seismic site classification for South Australia at low resolution. McCue & Love (1997) identified a fundamental site frequency of 1 Hz for most of the Adelaide city. A study by Collins *et al*. (2006), using the NEHRP seismic site classification system, assigned Adelaide a Class D, which corresponds to a $V_{s,30}$ of 257 m/s. However, their measurement was limited to only a single location, namely the Government House site. These studies combined, suggest that the applicable soil model for Adelaide lies in the subsoil range between Classes C and D.

This broad seismic classification has a number of ramifications from an earthquake structural design perspective and McBean (2010) investigated the consequences of these two different seismic classes and concluded that the Adelaide CBD can be represented as Class D. However, it is widely appreciated that the subsurface of the City of Adelaide is highly variable (Selby & Lindsay, 1982 and Jaksa, 1995).

2.5 SITE LOCATION, DATA ACQUISITION AND PROCESSING

In order to undertake the HVSR technique, microtremor measurements were carried out across the Adelaide city. Ten locations were examined, 5 to the north and 5 to the south of the city, as indicated by the red circles in Figure 3.1. Three sets of equipment were deployed at 4 sites (#01, #02, #04 and #05) to the north of Adelaide and one site (#03) was measured using a single device. Field survey data sheets are provided in Appendix E. Similarly, to the south of the city, 3 sets of equipment were deployed at 4 sites (#06, #07, #09 and #10) and location #08 was measured using a single device. The recorded noise data were separated into 30-minute duration datasets using the Eqwave application (ES&S, 2013) as suggested by Setiawan *et al*. (2015). A typical example of the acquired data is shown in Figure 3.2. Each dataset includes noise measurement in 3 orthogonal directions (two horizontal and one vertical). Figure 3.1 also shows (with red squares) the locations of selected tests undertaken by McCue & Love (1997), which will be discussed in a later section. A typical subset of the acquired 30 minute waveform data, saved as standard ASCII (*.SAF) files, as recommended by the Site Effects Assessment using Ambient Excitation [SESAME] (SESAME, 2004).

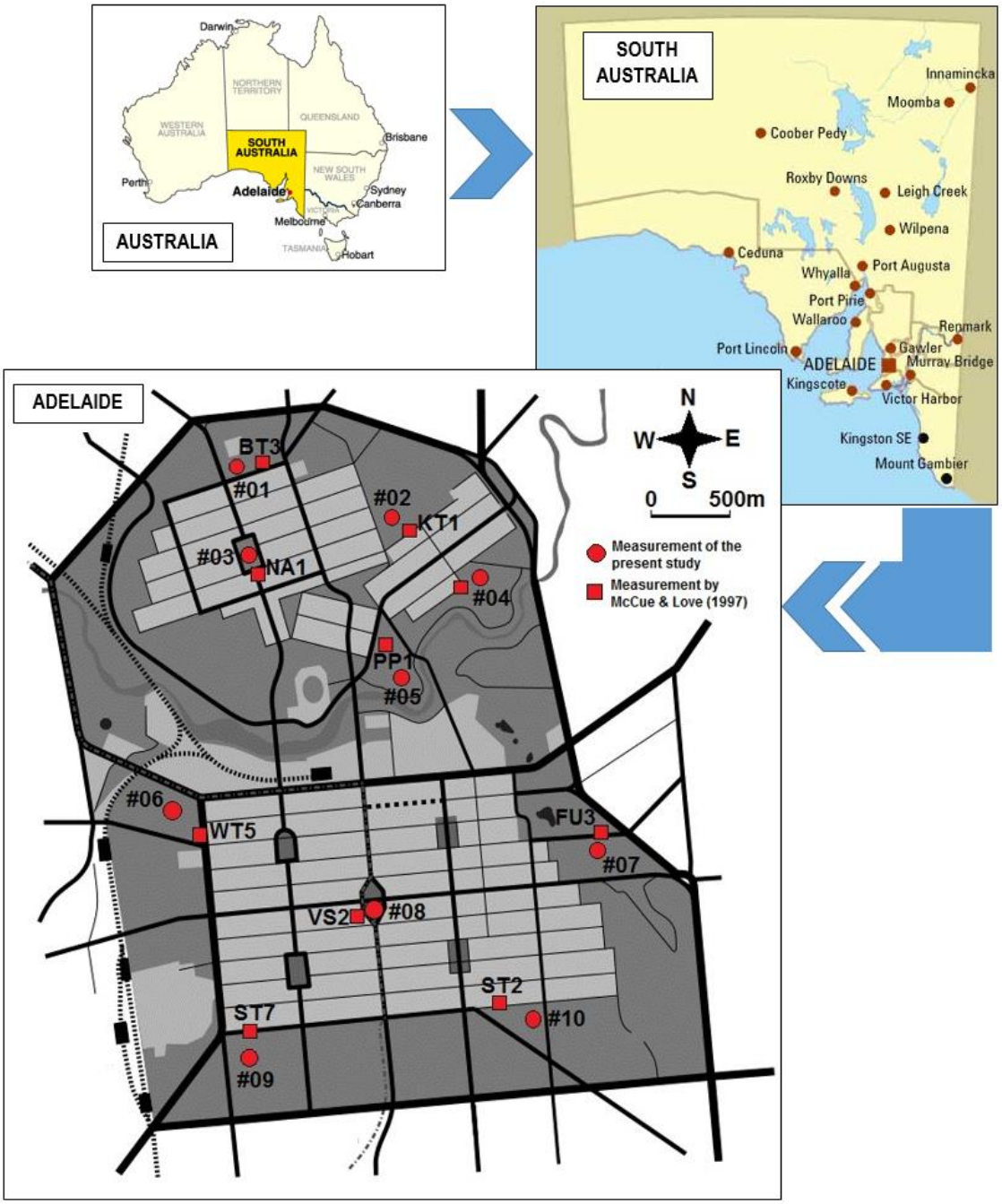

Figure 3.1 Site locations of microtremor measurements of the present study (red circles) and McCue & Love (1997) (red squares).

The equipment used to acquire the data consisted of a seismometer with two horizontal and one vertical sensor, an analog-to-digital recorder, a GPS antenna and a laptop computer which was used for initial setup and checking. A battery was used to power the system. Ambient noise data were acquired continuously for at least two hours using a LE-3Dlite Lennartz seismometer and Kelunji digital data recorder. The seismometer was set

on top of a 20 mm thick circular concrete slab over a generally firm to stiff ground surface. The location, where the seismometer was fixed, was cleared of any tall grass and leveled so as to minimize any instability to the seismometer during recording. The seismometer was oriented to North and protected from the wind with a plastic bucket and stabilized with a masonry brick.

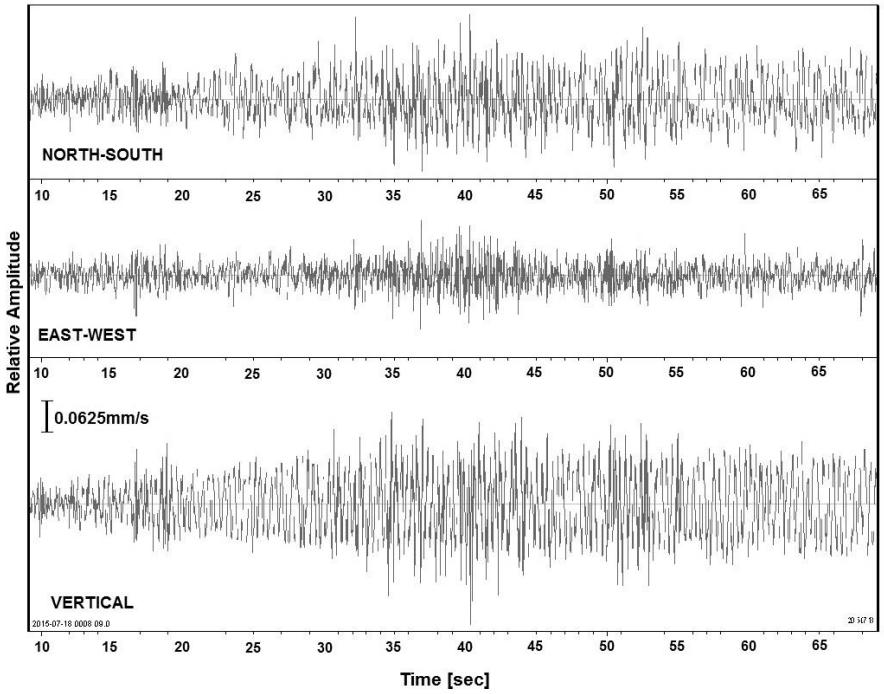

Figure 3.2 Typical example of the measured ambient noise data.

In the present study, two hours of noise data are considered sufficient for appropriately representing the measured site, as temporal variability has been examined by recording more than two days of continuous ambient noise data in the Adelaide city. After examining the reliability of the recorded noise data, as well as exploring whether any of the data originated from an industrial source over 96 datasets [each set involves a 30 minute noise record, as suggested by Setiawan *et al*. (2015)], an HVSR analysis using Geopsy (Geopsy, 2015) is carried out and the results are shown in Figure 3.3. The HVSR analysis using Geopsy is explained in detail later. As shown in Figure 3.3, the results of the HVSR analysis demonstrate similar curve patterns, particularly from about 0.8 Hz to 10.0 Hz. A high curve pattern dispersion, from a frequency of 0.8 Hz downward to 0.25 Hz, suggests a low noise source intensity over this frequency interval, as shown later in the paper. Further investigation is undertaken to validate whether or not two hours of

noise data are sufficient by arranging the fundamental frequency of all the HVSR analyses, with respect to the time and date of the measurement, the results of which are shown in Figure 3.4. This is undertaken because 4 consecutive fundamental frequencies, beyond the mean fundamental frequency ± one standard deviation, are unavailable. The analysis also suggests a fundamental frequency of 1.0 Hz with a discrepancy of approximately 0.025 Hz. In other words, the analysis confirms that two hours of continuously recorded data are sufficient to detect any spurious measurements. Moreover, Figure 3.4 also demonstrates that the time of measurement has no appreciable effect on the results. Furthermore, all of the equipment sets deployed in the present study are examined for their repeatability. Whilst conducting the testing described above, all other deployed equipment sets were also run at the same location, with a separation distance of approximately 0.5 m from one another. The HVSR analysis curves of all deployed equipment sets are presented in Figure 3.5. These results confirm the repeatability of the equipment.

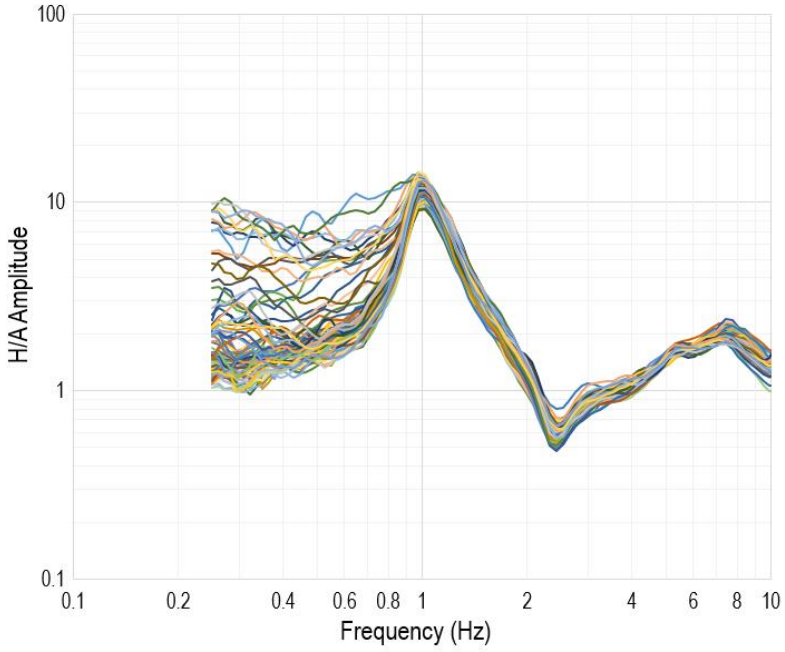

Figure 3.3 HVSR test results of continous 2 days of data in lengths of 30 minutes for one of equipment sets used in the present study.

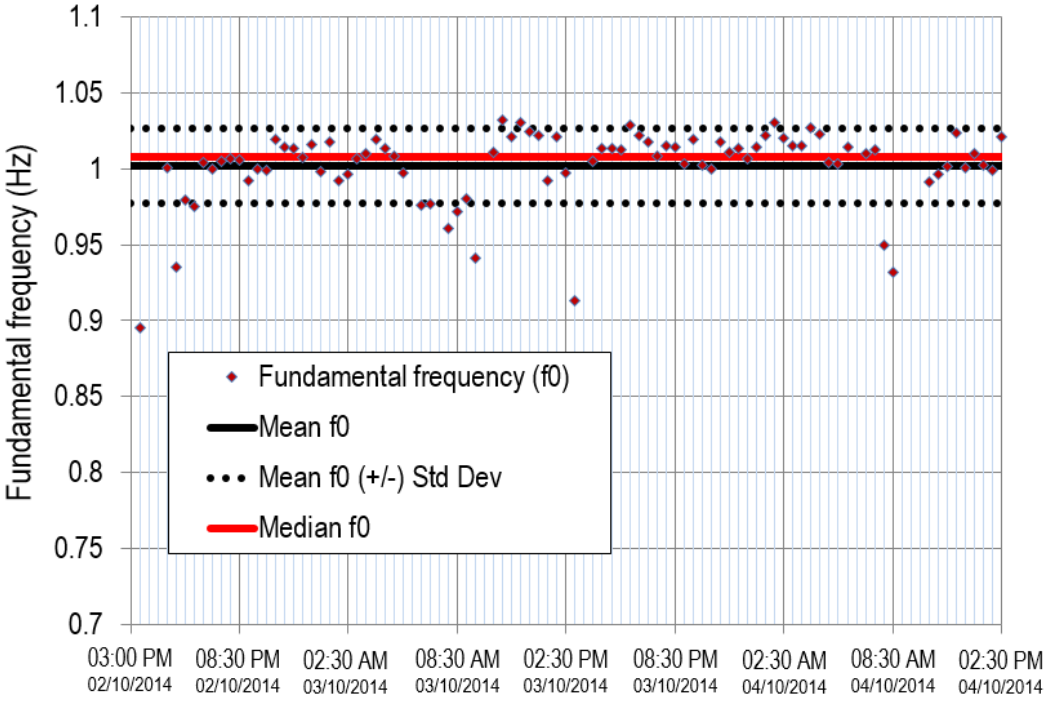

Figure 3.4 Fundamental frequency of HVSR test results of continous 2 days of data in lengths of 30 minutes for one of equipment sets used in the present study.

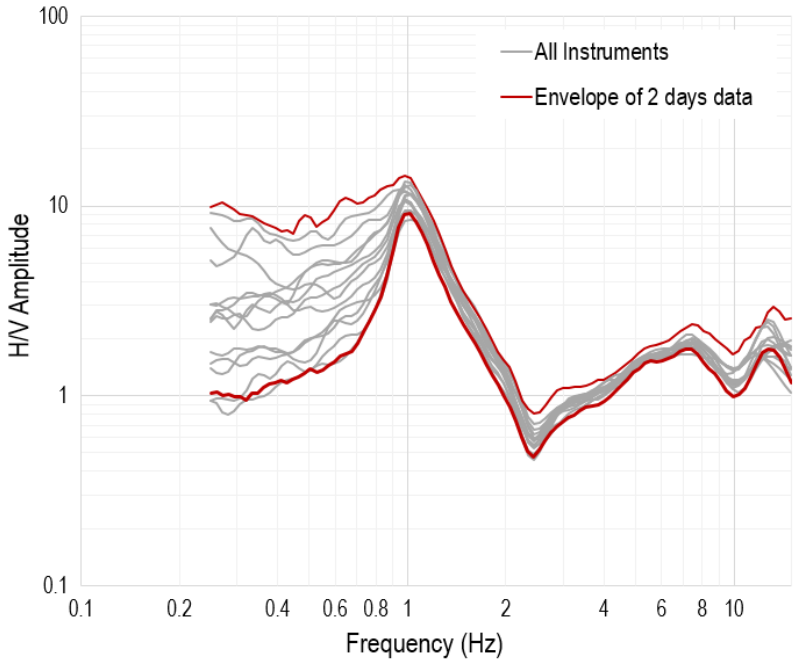

Figure 3.5 HVSR test results for all used equipment sets used in the present study incorporating the envelope of the HVSR analysis of 2 days of continously recorded data subdivided into sets of 30 minute lengths.

As mentioned above, 30-minute datasets were post-processed to obtain the horizontal vertical spectral ratio (HVSR), which is necessary to determine the site periods and to infer the shear wave velocity profile. HVSR processing was carried out using the Geopsy software (Geopsy, 2015) developed within the framework of the Site Effects Assessment using Ambient Excitation (SESAME) Project. In the present study, the default parameters and auto window selection were adopted. Prior to conducting the HVSR analysis, the Geopsy damping toolbox is adopted to detect the presence of any data originating from an industrial source. An industrial origin is concluded if the damping is much lower than 1% and the frequency is sustained. This detection is important to justify the validity of the recorded ambient noise data used in the HVSR analysis. Some typical results from the detection of any data originating from an industrial source are shown in Figure 3.6. Industrial origin detection results are attached in Appendix F.

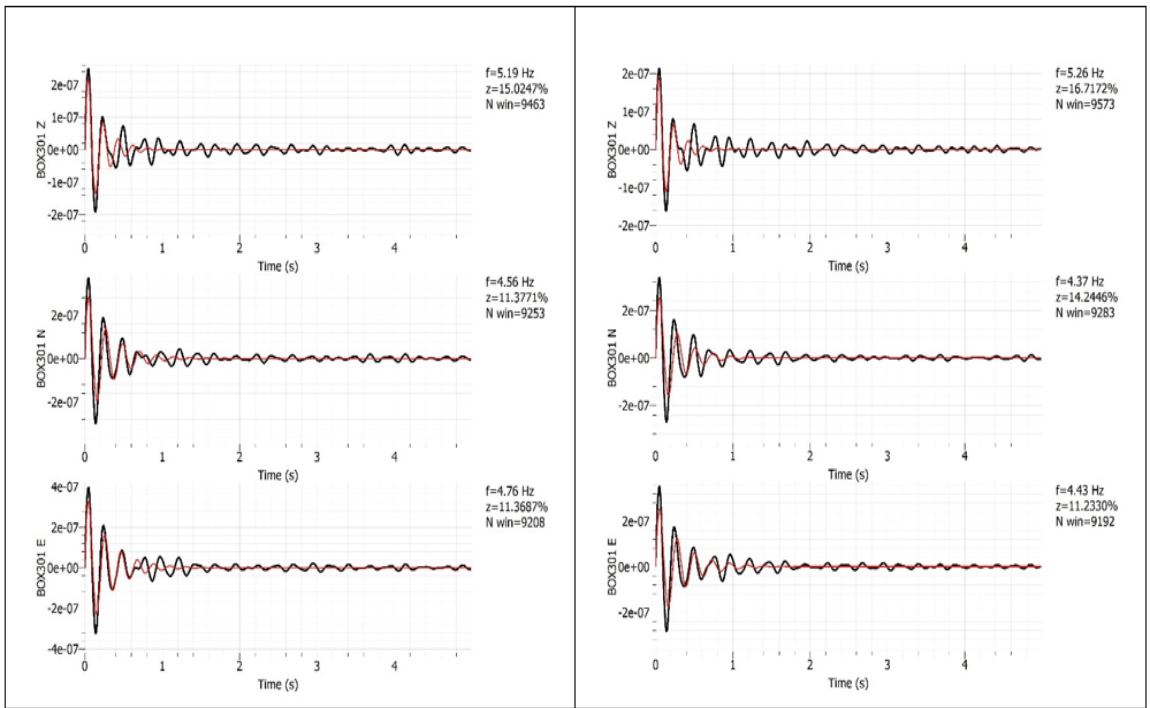

Estimated damping	Up-Down	15%	Estimated damping	Up-Down	16%
	North-South	11%		North-South	14%
	East-West	11%		East-West	11%
Sustained frequency?		No	Sustained frequency?		No

Figure 3.6 Typical results of identification of data from an industrial source.

3.5.1 Sources of recorded ambient noise data

In the investigation of the subsurface structure the frequency of the ambient noise sources is found to range between 0.005 to 10 Hz. A threshold of 1 Hz is widely accepted to delineate natural sources of noise from anthropogenic sources (SESAME, 2004). The frequency range of the natural noise, known as microseisms and triggered by natural processes such as ocean waves, tides and wind, is between 0.005 Hz and 1 Hz, whereas the frequency range of anthropogenic noise, known as microtremor and is associated with human activities, ranges between 1 and 10 Hz (SESAME, 2004). In the present study, ambient noise data sources, recorded at all the measured sites, ranged between 0.4 and 15 Hz. However, greater intensity is captured from at least 0.8 Hz. Spectral analysis of the ambient noise data recorded in the present study suggests the highest intensity, manifested by strong amplitude, occurs at a range of 2 to 6 Hz, a typical example of which is shown in Figure 3.7. These observations suggest that the sources of the recorded ambient noise data are related mainly to human activities. This frequency range has been found to be useful in investigating the near-surface geology, which is mainly concerned with site effects for seismic hazard assessment (Bard, 1998; Shapiro & Campillo, 2004; and Bonnefoy-Claudet *et al*., 2006). Figure 3.7 also shows that the anthropogenic noise sources in the present study originate from all directions. This suggests that noise originating from industrial sources is not present in any of the recorded data used in this study.

3.5.2 Calculation of the HVSR curve

The HVSR method is based on the spectral ratio analysis between the Fourier amplitude spectrum of the horizontal (H) and vertical (V) components of the recorded ambient vibration. Initially, selecting the most stationary parts of the ambient vibration to exclude transient waves, such as footsteps and close distance traffic, was carried out by dividing the time series of each component into windows. Several parameters i.e. window length, a threshold of the short-time average/long-time average (STA/LTA) and the lengths of STA/LTA were employed in this process. Each selected window is then smoothed using a filter. The present study adopts the Konno & Ohmachi (1998) smoothing approach with a smoothing constant of 40. Subsequently, the HVSR is computed with the merged horizontal (H) components for each selected time window using the geometric mean. Finally, evaluation and averaging of the HVSR are carried out. The Geopsy software

implemented within the SESAME project (SESAME, 2004) is used to carry out the HVSR analysis. The HVSR method is undertaken at three stations at each of the sites. This method allows the generation of an HVSR ellipticity curve for each site from which the fundamental resonance frequency is identified. The HVSR ellipticity curve is also used to obtain the shear wave velocity profile for each site.

3.5.3 Inversion of the HVSR ellipticity curve

As discussed above, the HVSR ellipticity curves are inverted to a 1D shear wave velocity profile. A stratigraphic constraint is also incorporated in the inversion process by fixing the layer depths, including the level of the bedrock, in the inversion code. A comprehensive subsurface analysis of the study site, developed by (Selby & Lindsay, 1982) and shown in Table 3.2, is adopted in the present study to establish the stratigraphic parameters at the measurement sites. Additional data by McPherson & Hall (2007), Sheard & Bowman (1996), Jaksa (1995) and McBean (2010) are also incorporated in the development of the parametric limit search. Generally, the parameterization models, in terms of compression wave velocity, shear wave inversion, Poisson ratio and density for the inversion process, are summarized in Table 3.3.

Table 3.3. Search limits for the case sites of the present paper.

Parameter	Limit search	Formation Code	Remarks
Compression wave velocity of V_p (m/s)	200 – 1,000	Formations A to H	Ref. (McPherson & Hall, 2007), (Love, 1996), (Selby & Lindsay, 1982), (Sheard & Bowman, 1996) and (McBean, 2010) The formations vary from one site to another.
	200 – 2,000	Formation J	
	700 – 5,000	Pre-Cambrian bedrock	
Shear wave velocity of V_s (m/s)	150 – 500	Formations A to H	
	150 – 1,000	Formation J	
	500 – 3,500	Pre-Cambrian bedrock	
Poisson ratio	0.3 – 0.5	Formations A to A2	
	0.2 – 0.4	Formations B to J	
	0.2 – 0.25	Pre-Cambrian bedrock	
Density (kg/m^3)	1,800 – 2,000	Formations A to J	
	2,000 – 2,400	Pre-Cambrian bedrock	

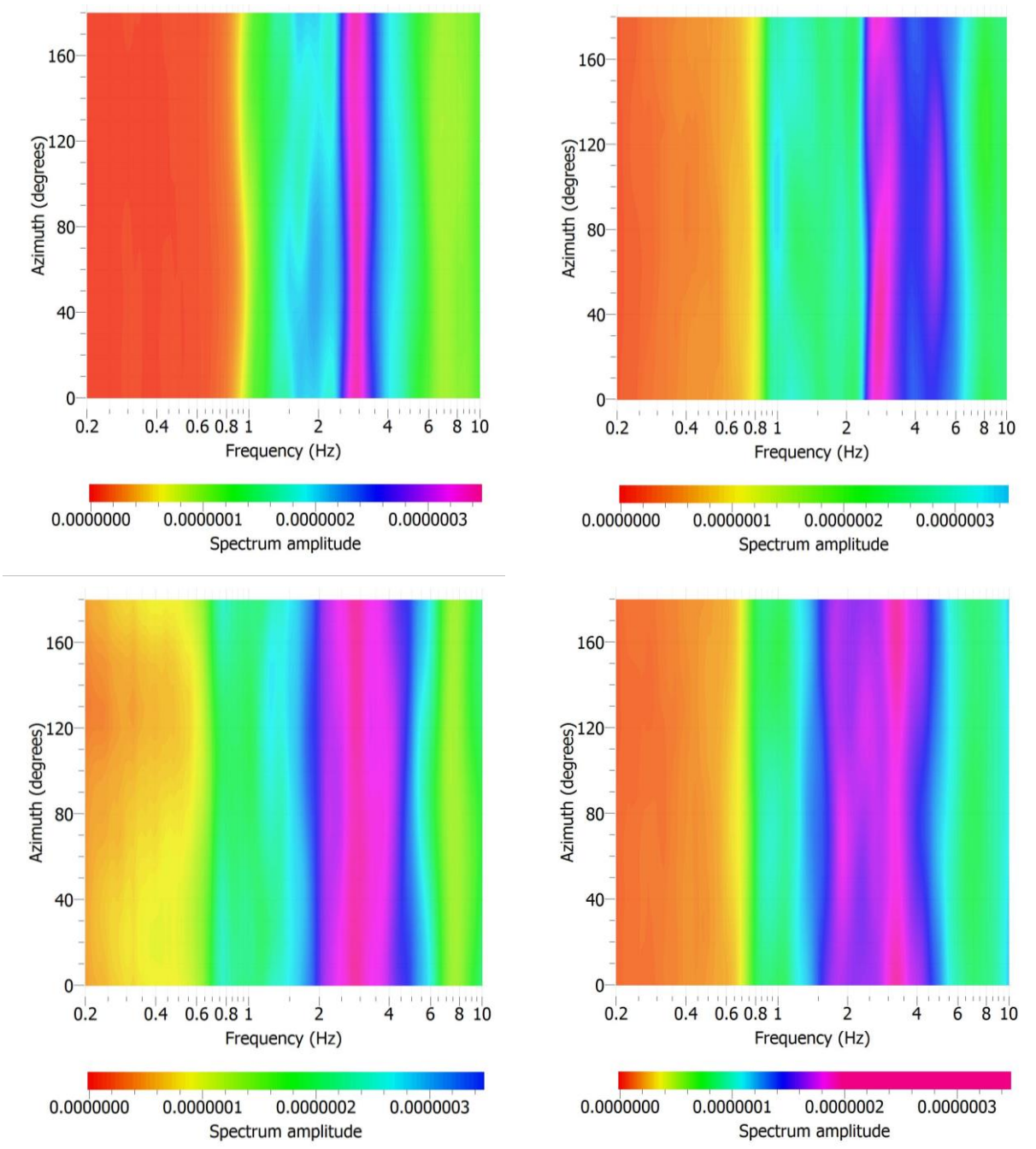

Figure 3.7 Typical results of frequency of noise sources in the recorded ambient noise data.

The inversion of the HVSR ellipticity curves is carried out using the Dinver inversion code in the Geopsy software ((Wathelet *et al*., 2004; Wathelet *et al*., 2008 and Wathelet *et al*., 2005). The neighborhood algorithm of Sambridge, (1999) was implemented by Wathelet *et al*. (2004) in the Dinver inversion code. The neighborhood algorithm offers a simple interpolation of an irregular distribution of points in space by using Voronoi geometry to detect the most promising parts of the parameter space. Hence, Wathelet *et al*. (2004) suggested checking the robustness of the final results by running the same

inversion several times using different random seeds. As such, in the present study, at least three runs using different seeds (i.e. starting models) were carried out in the inversion process. At least 28,050 models for each run were generated, from which the best 20 models are extracted. The best 20 shear wave profiles represent the lowest 20 misfit inversions from the measured HVSR ellipticity curves. Finally, the ground shear wave velocity models are developed from each run of each ellipticity curve inversion and the mean and median shear wave velocities are subsequently evaluated.

3.6 HVSR TECHNIQUE RESULTS

This section presents the results of the HVSR technique and examines the site fundamental frequency and shear wave velocity profiles.

3.6.1 Site fundamental frequency

The site fundamental frequencies obtained from the HVSR analyses are shown in Table 3.4. All HVSR analysis curves of the present study are attached in Appendix G. Typical examples of these are shown in Figure 3.8. Most of the sites in Adelaide are estimated to yield a fundamental frequency of approximately 1 Hz. Only 3 sites (#07, #8, #10) exhibit fundamental frequencies below 1 Hz. A clear fundamental frequency peak can be observed at Locations #01, #02, #03, #04, #07, #08 and #09, whereas #05, #06 and #10 indicate otherwise. At Location #05 and #06, Instrument #A was unable to capture a distinct and reliable peak. Two instruments at Location #10 (Instruments #A and #B), were unable to obtain a clear and reliable HVSR peak curve. This suggests a high lateral variability of the subsurface conditions at Locations #05, #06 and #10. Location #05 is adjacent to the River Torrens, which is underlain by recent fluvial deposits (Selby & Lindsay, 1982 and Sheard & Bowman, 1996). On the other hand, Location #06 is adjacent to the Para Fault zone (Aitchison *et al*., 1954) which is also expected to exhibit high lateral variability due to sediment tilting. Furthermore, stresses along the faults also may contribute to the complexity of the dynamic parameter, i.e. the shear wave velocity of the subsurface profile at this site. At Location #10 the deepest bedrock level was encountered. Another factor which contributes to the unclear and unreliable nature of the HVSR curve is the source of the ambient noise during the measurement. The amplitude of the noise sources was not strong enough to be captured during site measurement.

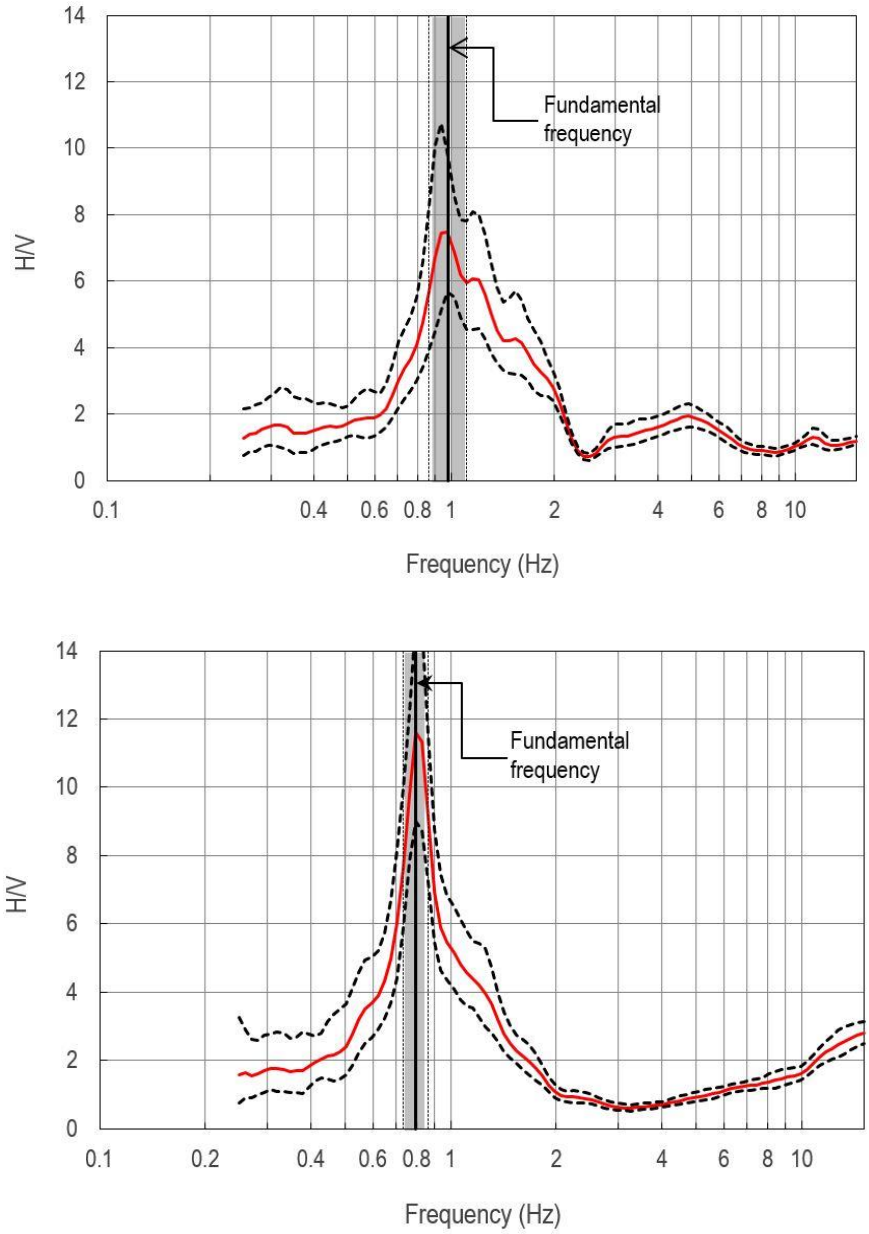

Figure 3.8 Examples of HVSR curves.

Another interesting observation associated with the HVSR curves is the presence of secondary peaks, even at low amplitudes (less than 4), at Locations #01, #02, #03, #08 and #09. The secondary peak frequency is between 4 and 6 Hz. The two-peak HVSR curves suggest that there are two different impedance contrasts at two different scales: the first peak relates to a deep structure and the second a shallow structure (SESAME, 2004; Toshinawa *et al*., 1997 and Gueguen *et al*., 1998).

The primary fundamental frequencies of all sites in Table 3.4 are plotted in Figure 3.9 and the mean and median of the fundamental frequencies are summarized in Table 3.5. The mean and median fundamental site periods are evaluated from the reciprocal of the fundamental frequencies. As shown in Figure 3.9, generally the amount of data variation, expressed by the standard deviation (SD), is low. The highest SD of the fundamental frequency in the present study is 0.06 Hz at Location #02. The remaining SDs from the measured sites vary between 0.004 to 0.004 Hz. Furthermore, the mean and the median of the fundamental frequency at the measured sites are generally similar, with only a discrepancy of as little as 0.013 Hz.

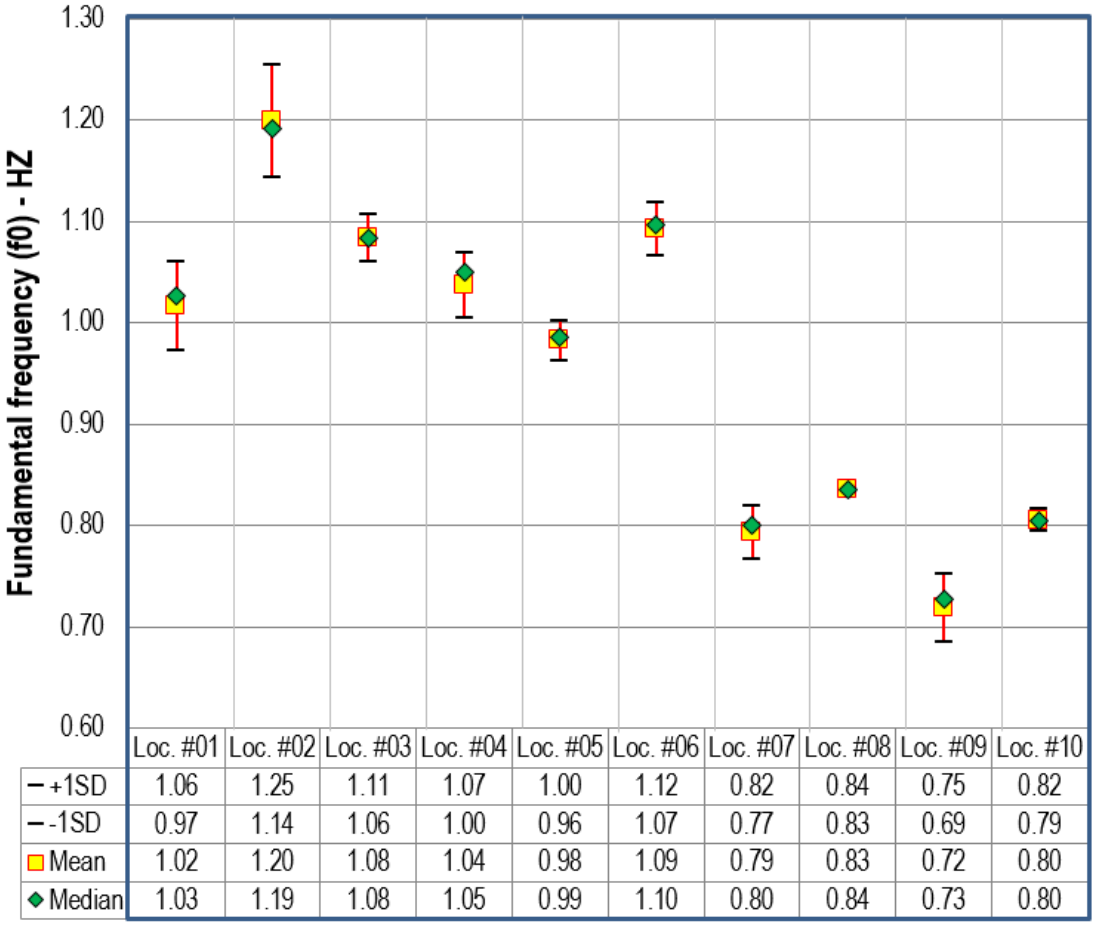

	Loc. #01	Loc. #02	Loc. #03	Loc. #04	Loc. #05	Loc. #06	Loc. #07	Loc. #08	Loc. #09	Loc. #10
+1SD	1.06	1.25	1.11	1.07	1.00	1.12	0.82	0.84	0.75	0.82
-1SD	0.97	1.14	1.06	1.00	0.96	1.07	0.77	0.83	0.69	0.79
Mean	1.02	1.20	1.08	1.04	0.98	1.09	0.79	0.83	0.72	0.80
Median	1.03	1.19	1.08	1.05	0.99	1.10	0.80	0.84	0.73	0.80

Figure 3.9 Fundamental frequencies of each site location from the ambient noise measurements.

Table 3.4 Site fundamental frequencies of all instruments.

Location	Fundamental frequency (Hz)														
	Instrument #A					Instrument #B					Instrument #C				
	a	b	c	d	e	a	b	c	d	e	a	b	c	d	a
#01	1.01	0.98	1.04	1.03	1.04	F	0.91	F	0.98	F	1.02	1.07	F	1.05	1.04
	1.02					0.95					1.05				
#02	1.19	1.22	1.22	1.18	1.19	1.33	1.12	1.25	1.20	1.25	1.19	1.12	1.18	1.15	NA
	1.2					1.23					1.16				
#03	1.11	1.08	1.09	1.06	NA										
	1.09														
#04	F	1.00	F	0.97	NA	1.02	1.05	1.06	1.06	1.01	1.04	1.08	1.07	1.05	NA
	0.99					1.04					1.06				
#05	F	F	F	F	F	1.02	1.00	0.99	0.99	1.00	0.96	0.99	0.96	0.96	0.96
	F					1					0.97				
#06	F	F	F	F	F	1.10	1.09	1.10	1.10	1.14	1.05	1.11	1.08	1.07	NA
	F					1.11					1.08				
#07	0.82	0.81	0.81	0.80	0.82	0.80	0.80	0.80	0.79	NA	0.77	0.74	0.75	F	NA
	0.81					0.80					0.75				
#08	0.84	0.84	0.84	0.83	0.84										
	0.84														
#09	F	F	0.65	F	0.67	0.72	0.72	F	0.74	NA	0.74	0.72	0.73	0.76	0.73
	0.66					0.73					0.74				
#10	F	F	F	F	NA	F	F	F	F	NA	0.79	0.80	0.81	0.82	NA
	F					F					0.81				

Note:
#01 is near Barton Terrace West.
#02 is near Lefevre Terrace.
#03 is inside Wellington Square.
#04 is near Finniss Street.
#05 is corner of Frome Road/ War Mem. Drive.
#06 is corner of West Terrace/ Port Road.
#07 is near Bartels Road.
#08 is inside Victoria Square.
#09 is corner of South Terrace/ West Terrace.
#10 is corner of South Terrace/ Hutt Road.
NA is ambient noise no data available.
F is FAIL to comply SESAME (2004) criteria.

Table 3.5 Mean and median fundamental frequencies and periods for all locations.

Location	Fundamental frequency (Hz)		Fundamental period (s)		Remarks
	Mean	**Median**	**Mean**	**Median**	
#01 (Barton Tce W)	1.02 & 5.6	1.03 & 5.1	0.98 & 0.18	0.97 & 0.20	Two-peaks
#02 (Lefevre Tce)	1.20 & 5.8	1.19 & 5.8	0.83 & 0.17	0.84 & 0.17	Two-peaks
#03 (Wellington Sq)	1.08 & 5.3	1.08 & 5.2	0.92 & 0.19	0.92 & 0.19	Two-peaks
#04 (Finniss St)	1.04	1.05	0.96	0.95	
#05 (Frome Rd/ War Mem. Dr)	0.98	0.99	1.02	1.01	
#06 (West Tce/ Port Rd)	1.09	1.10	0.92	0.91	
#07 (Bartels Rd)	0.79	0.80	1.26	1.25	
#08 (Victoria Sq)	0.83 & 4.1	0.84 & 4.0	1.20 & 0.25	1.19 & 0.25	Two-peaks
#09 (South Tce/ West Tce)	0.72 & 4.5	0.73 & 4.5	1.40 & 0.22	1.39 & 0.22	Two-peaks
#10 (Hutt Rd/ South Tce)	0.80	0.80	1.24	1.24	

3.6.2 Shear wave velocity profiles

In the present study, the shear wave profiles were obtained by using constrained modeling of the measured HVSR curves. This method has been successfully applied by Harutoonian *et al*. (2003) and Di Stefano *et al*. (2014). A slight adjustment is introduced in the present study by using a group of 3 seismometers to measure the identical noise source. The distance between each seismometer is approximately 50 m. The reason for using 3 seismometers in the present study is to ensure the consistency of the microtremor data.

As discussed above, input parameters for the constrained modeling adopted in the present study are shown in Table 3.3. The site specific parameters are developed and estimated based on studies by McPherson & Hall (2007), Selby & Lindsay (1982), Sheard & Bowman (1996), Jaksa (1995) and McBean (2010). The number of layers in the parameterization models is determined from the nearest subsurface data available (i.e. boreholes and cross sections). The main data are provided by Selby & Lindsay (1982). Additional subsurface data associated with the study sites have also been incorporated from other references (Sheard & Bowman, 1996; Jaksa, 1995 and McBean, 2010). The main reason for adopting the available stratigraphic data is to simplify the inversion process and to minimize subjectivity. These site specific input parameters are used to generate at least 28,050 shear wave profile models based on the elliptical nature of the HVSR curves in each 30-minute dataset. The best 20 models are extracted and selected from the generated profiles of each HVSR curve. In the present study, only the HVSR curve, which satisfies the reliability criteria of SESAME (2004), is used in estimating the

shear wave profile; the remainder is discarded. Generally, each set of instruments is expected to obtain 5 HVSR curves. The following sections present the results which are divided into two main sections. The first section elaborates the results of all locations to the north of the River Torrens (North Adelaide) and another presents the results of all locations to the south of the River Torrens (South Adelaide).

Shear wave velocity at North Adelaide

Five locations were measured in North Adelaide: #01 (Barton West Terrace); #02 (Lefevre Terrace); #03 (Wellington Square); #04 (Finniss Street) and #05 (Frome Road/War Memorial Drive). The ground surface profiles at the North Adelaide sites consist of 5 to 6 formations above bedrock (Selby & Lindsay, 1982). These upper layer formations suggest mean shear wave velocities varying between 152 and 703 m/s. The bedrock levels at these locations are estimated to vary between 50 and 64 meters below ground level, which suggests shear wave velocity of at least 1,610 m/s. The detailed mean and median shear wave velocity profiles for these North Adelaide locations are shown in Figures 3.10(a) to 3.12(a). For Location #05, which is situated near the River Torrens the HVSR analysis of instrument #A at this location is unable to satisfy the reliability criteria as outlined in (SESAME, 2004). Therefore, the present study excludes the inversion of the ellipticity curve for this instrument from further analysis, as indicated by "FAIL".

Shear wave velocity at South Adelaide

In South Adelaide ambient noise was measured at 5 sites: #06 (West Terrace/Port Road), #07 (Bartels Road), #08 (Victoria Square), #09 (South Terrace/West Terrace) and #10 (Hutt Road/South Terrace). Despite some difficulties to justify the bedrock level at the south-eastern of Adelaide City, the South Adelaide, generally, are founded on 8 to 10 formations overlying Precambrian bedrock (Selby & Lindsay, 1982). Mean shear wave velocities of these formations vary between 153 and 711 m/s. The South Adelaide sites suggest gradually deeper bedrock levels toward the southeast, which is estimated to be encountered between 88 to 118 meters below ground level (Selby & Lindsay, 1982). The estimated shear wave velocity of this bedrock is at least 1,191 m/s (as shown in inverted shear wave velocity profile at Location #07 in Figure 13a). Detailed estimated mean and median shear wave velocity profiles associated with these sites are shown in Figures 3.12(b) to 3.14(b). The HVSR analyses that were unable to satisfy the reliability criteria, as outlined in SESAME (2004), are excluded from further analysis and are indicated by

"FAIL". For Location #06, the discarded shear wave profile is the inferred profile from HVSR analyses of instrument #A and for Location #10 is instruments #A and #B.

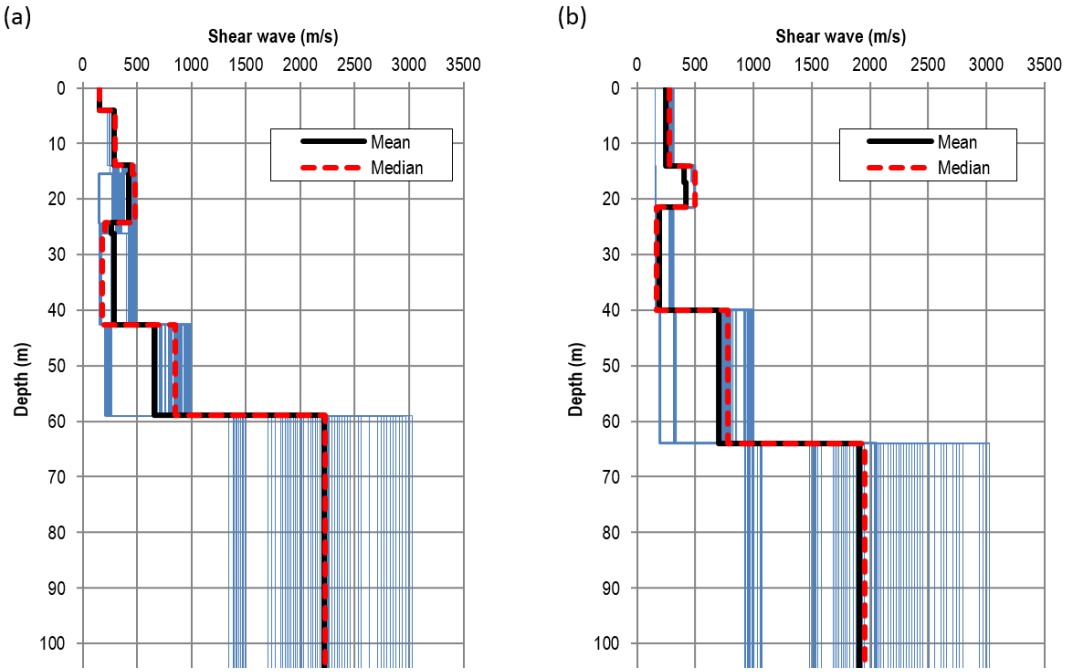

Figure 3.10 Shear wave velocity profiles at (a) Location #01 and (b) Location #02.

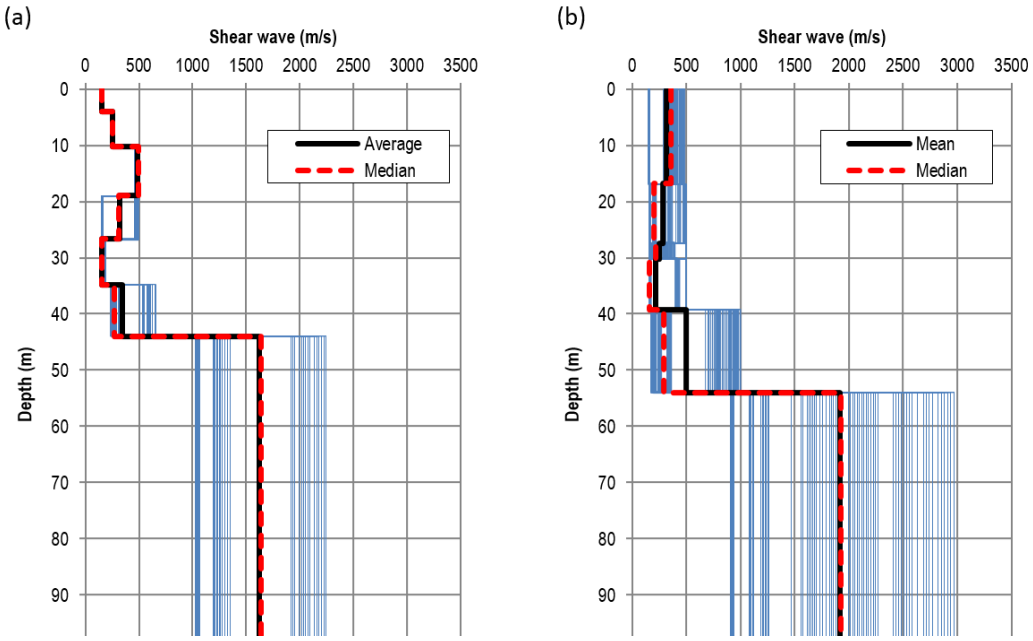

Figure 3.11 Shear wave velocity profiles at (a) Location #03 and (b) Location #04.

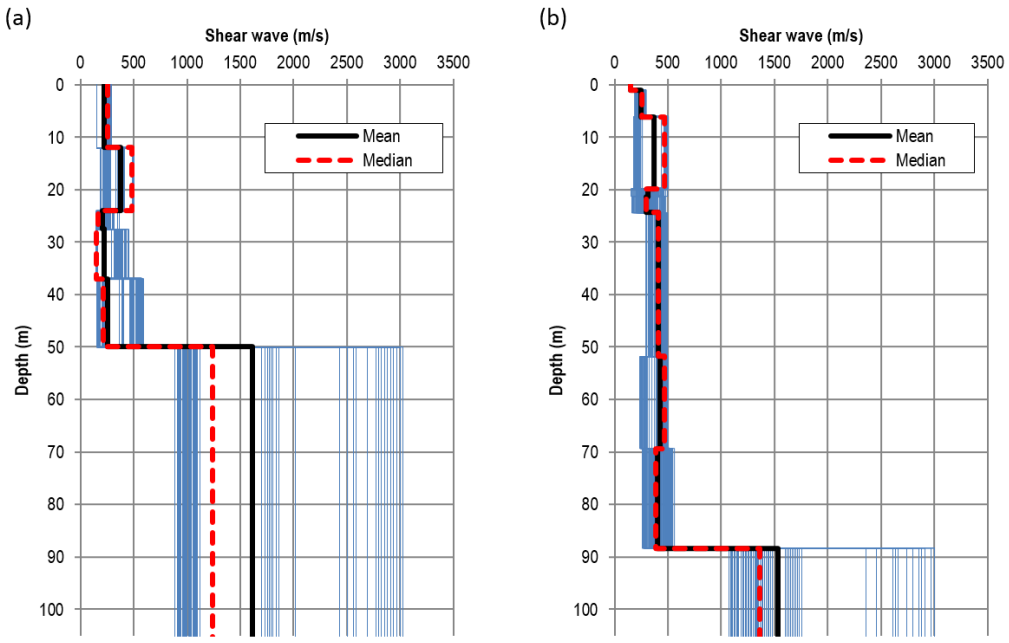

Figure 3.12 Shear wave velocity profiles at (a) Location #05 and (b) Location #06.

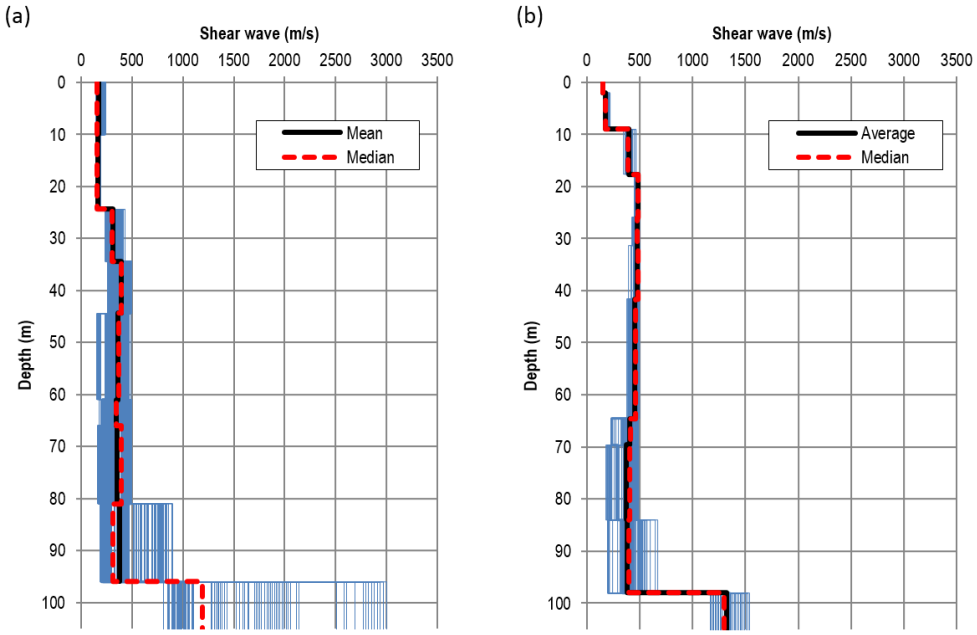

Figure 3.13 Shear wave velocity profile at (a) Location #07 and (b) Location #08.

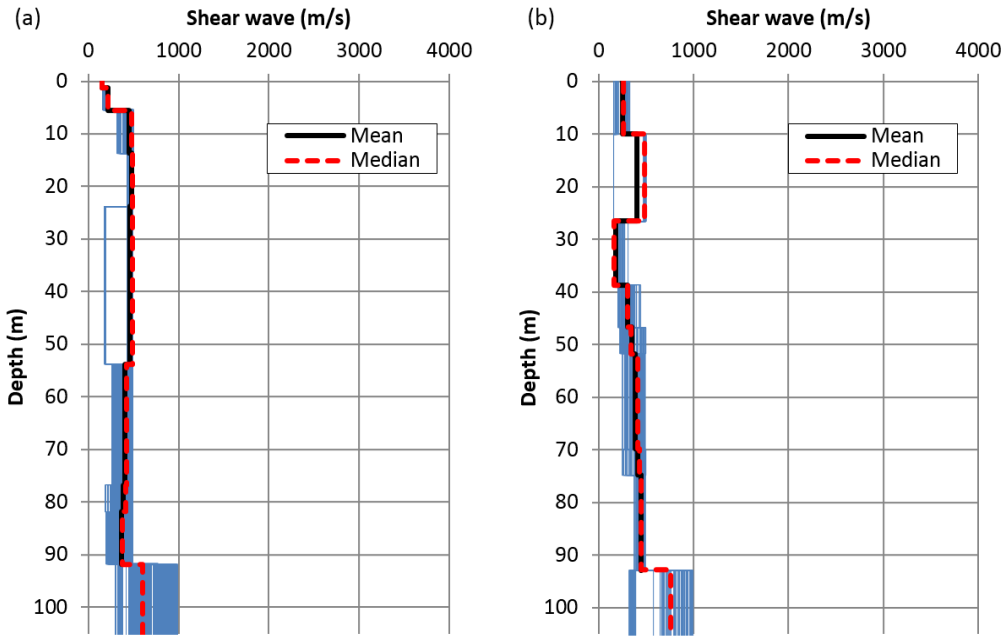

Figure 3.14 Shear wave velocity profile at (a) Location #09 and (b) Location #10.

3.7 VALIDATION OF THE OBTAINED SHEAR WAVE VELOCITY PROFILES

In order to validate the results of shear wave velocity profiles obtained in the present study and the appropriateness of the inversion results the spectral analysis of surface waves (SASW) method is adopted in addition to forward computation. These are discussed below.

3.7.1 Shear wave velocity validation using a comparison with SASW method

As discussed above, Collins *et al*. (2006) obtained shear wave measurements using the SASW method at Government House (GHS) in Adelaide (34°55’142.2”S, 138°36’00.6”E). The results of this study are compared with those from the present study using the method discussed above. More than 12 hours of single microtremor measurement was recorded at the location 34°55’08.4”S, 138°36’03.6”E. Unfortunately, it is approximately 200 m from the location where the SASW measurements were obtained due to unforeseen factors. After assessing the possibility of noise originating from an industrial source, generating the HVSR ellipticity curve, checking the reliability of the HVSR ellipticity curve using the SESAME (2004) criteria, inverting the “passed”

curve using the Dinver code, extracting and averaging the best 20 models and combining all the shear wave velocity models from 24 datasets with 30 minutes of noise record in each, the results of the analysis are shown in Figure 3.15. In general, as can be seen, the results of the present study are comparable with the results using the SASW method by Collins *et al*. (2006). The lateral and vertical variability of the site could be the main reason for the discrepancies in the results due to the 200 m separation distance as mentioned earlier. The results show that the present model is in good agreement for the top 5 m depth and from 15 to 40 m depth.

A forward computation of the fundamental Raleigh wave of the measured site (Garcia-Jerez *et al*., 2016) is also carried out to explore the appropriateness of the shear wave velocity model by comparing it to the observed HVSR. Forward computation modeling is also carried out for the SASW model. The comparison of the observed HVSR and the calculated HVSR is shown in Figure 3.16. The calculated HVSR from the present study and the observed HVSR is in good agreement. Furthermore, Figure 3.16 suggests better agreement between the calculated HVSR from the present study to the observed than the calculated HVSR from the SASW measurements. Again, the lateral and vertical variability of the shear wave velocity profiles are likely to be the main for the disparity.

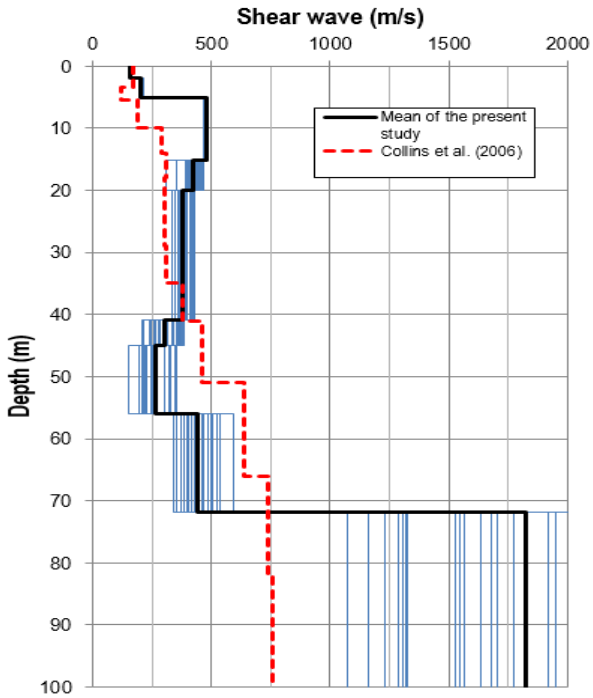

Figure 3.15 A comparison of the shear wave velocity profile of the present study to the shear wave velocity profile using the SASW method by Collins *et al*. (2006) at Government House.

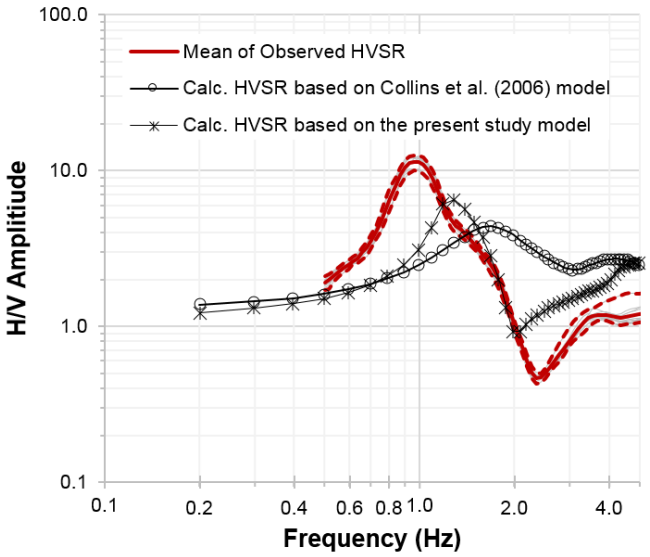

Figure 3.16 The observed mean HVSR of the microtremor data (solid red line) ± one standard deviation (dashed red line) with the computed HVSR of the fundamental-mode Raleigh waves of the present study (black line with circle) and the present study (black line with crossline) at Government House.

3.7.2 Shear wave velocity validation using forward computation

The shear wave velocity model validation using forward computation into the fundamental Raleigh wave, herein termed 'calculated HVSR', is carried out for all developed models of the present study to explore the appropriateness of the developed model. Forward modelling proposed by (Garcia-Jerez *et al.*, 2016) is employed in the present study. The horizontal to vertical spectral ratios of the calculated HVSR is compared to the observed HVSR. The comparison of the mean observed and calculated HVSR, plotted as logarithmic graphs, are given in Figures 3.17 and 3.18. As expected, the fundamental frequency using the HVSR method rises with increasing $V_{s,30}$. The observed and calculated HVSR peak frequency lies between 0.7 and 1.3 Hz. Overall, all measured sites exhibit comparable HVSR curves.

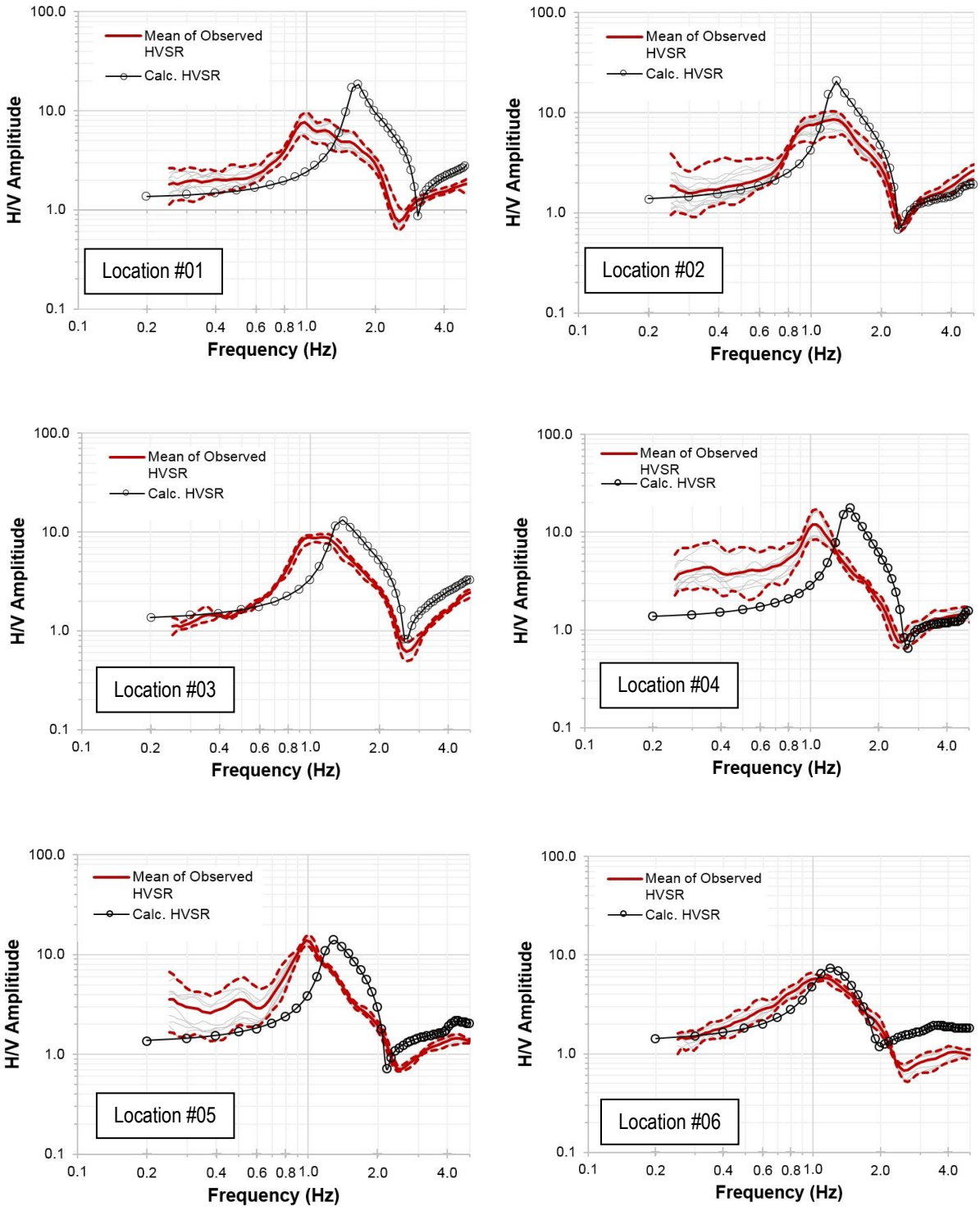

Figure 3.17 Comparison of the observed mean HVSR of the microtremor data (solid red line) ± one standard deviation (dashed red line) with the computed HVSR of the fundamental-mode Raleigh waves (black line with circle) for Locations #01 to #06.

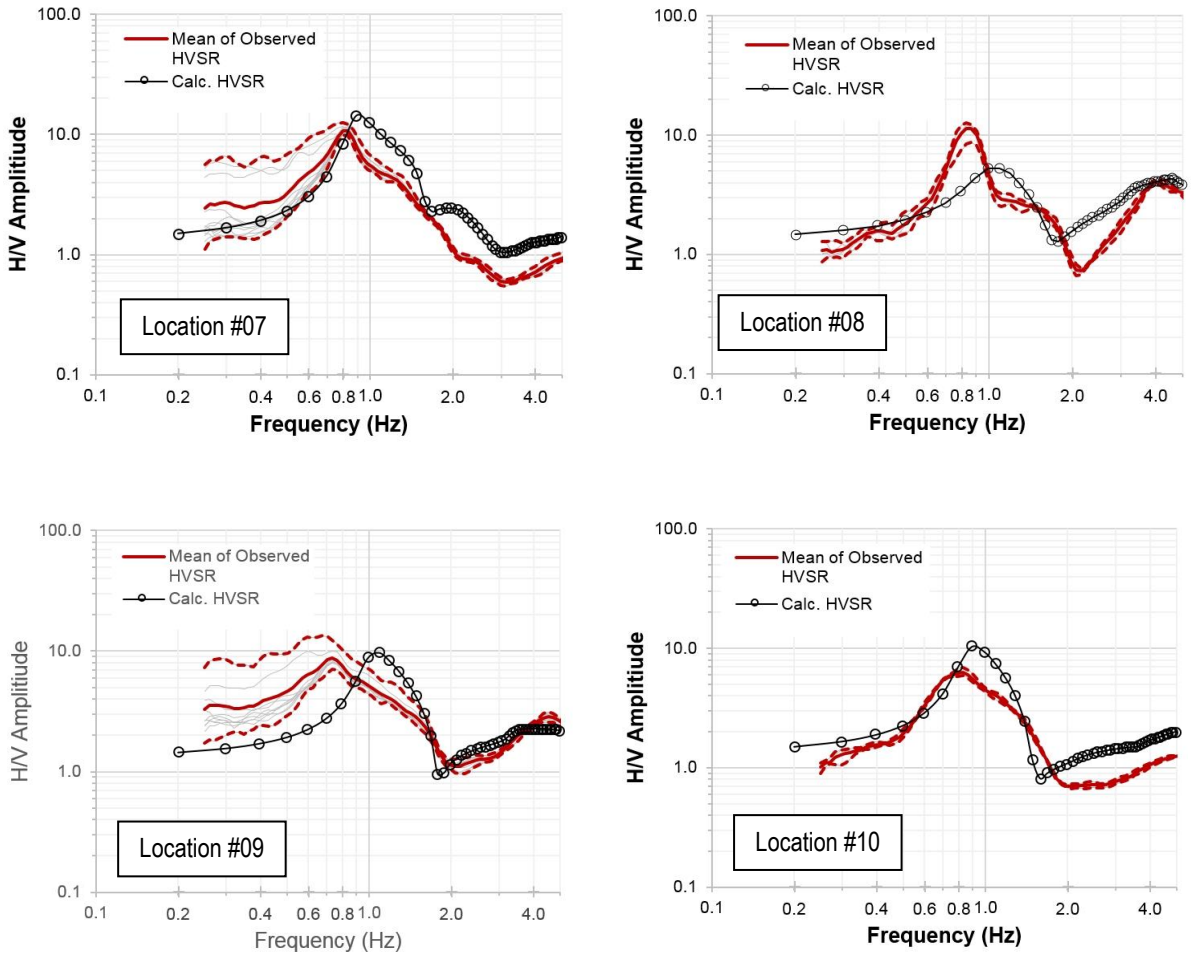

Figure 3.18 Comparison of the observed mean HVSR of the microtremor data (solid red line) ± one standard deviation (dashed red line) with the computed HVSR of the fundamental-mode Raleigh waves (black line with circle) for Locations #07 to #10.

3.8 DISCUSSION OF THE RESULTS

This section examines and discusses the results of the HVSR measurements with respect to the site fundamental frequency and seismicity site classes.

3.8.1 Site fundamental frequency

In order to provide context to the present study, this section compares the HVSR results from the present study with the extensive HVSR measurements obtained across Adelaide by McCue & Love (1997). The comparison is undertaken using the nearest locations adopted by (McCue & Love, 1997), as shown in Figure 3.1 above. The results of the comparison are presented in Figures 3.19 to 3.23. As can be observed, the mean HVSR

curves of McCue & Love (1997) fluctuate sharply, as indicated by the dashed red line, and hence a smoothing algorithm is applied to these curves and the outcomes are presented by the thick black line in the comparison figures.

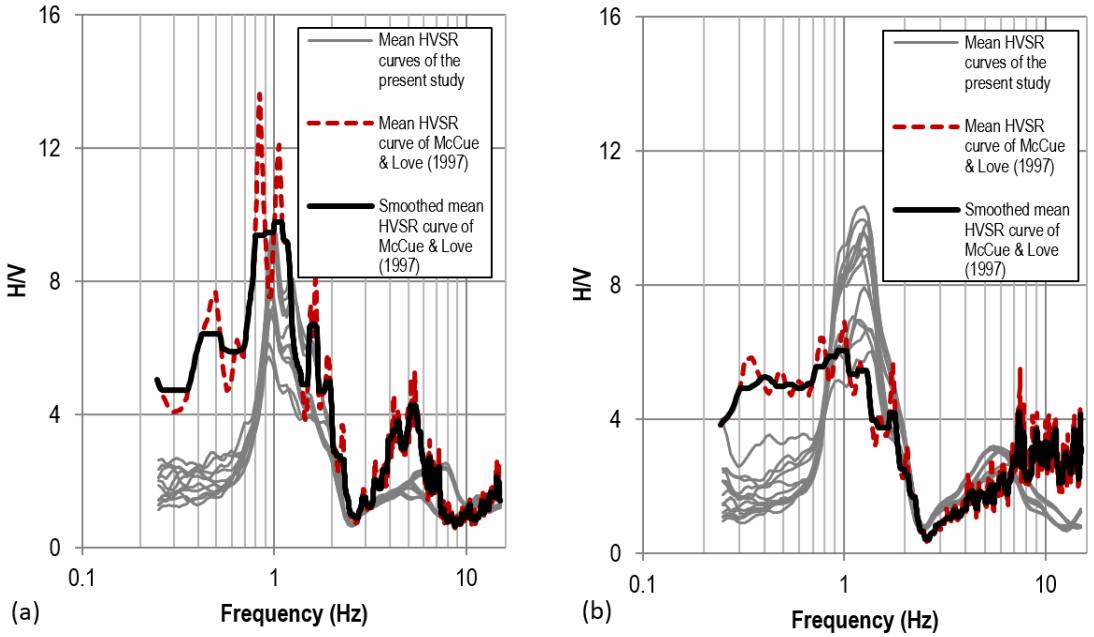

Figure 3.19 HVSR curve comparison at (a) Location #01 and (b) Location #02.

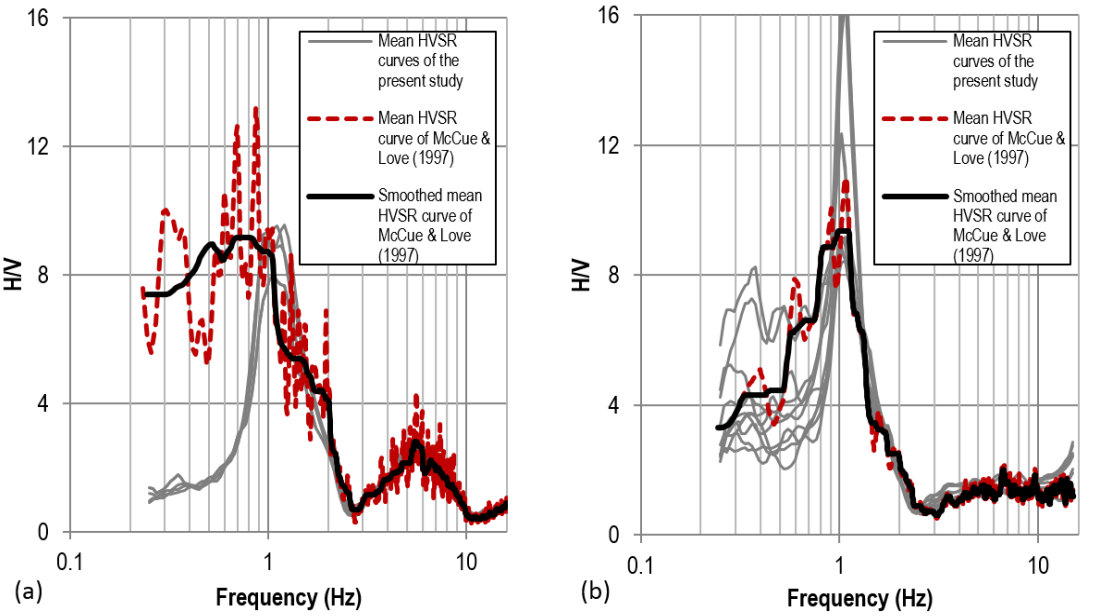

Figure 3.20 HVSR curve comparison at (a) Location #03 and (b) Location #04.

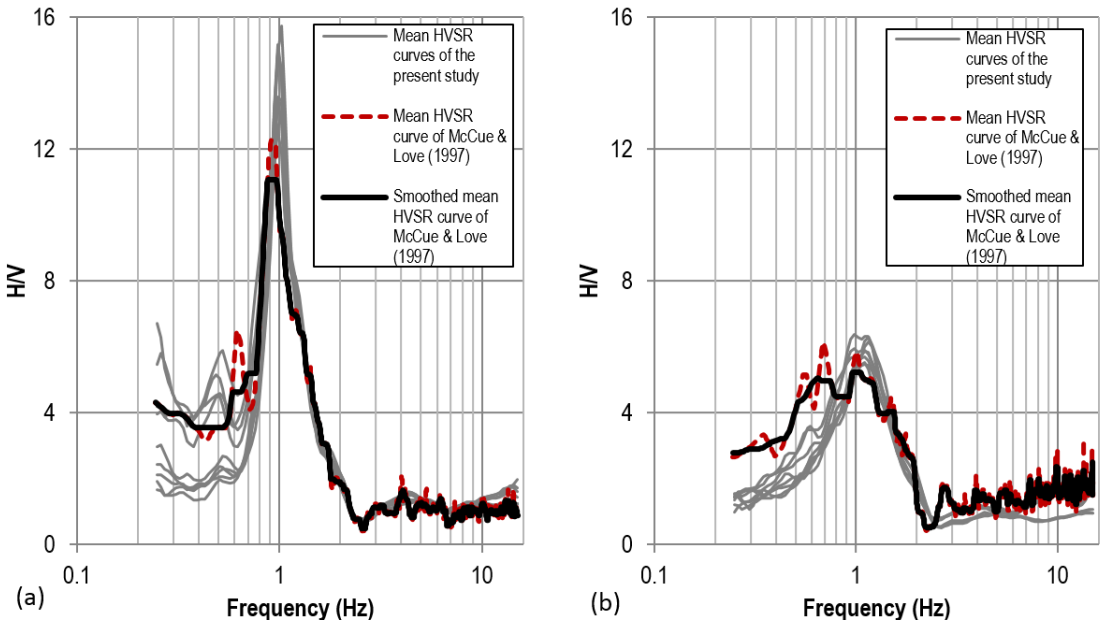

Figure 3.21 HVSR curve comparison at (a) Location #05 and (b) Location #06.

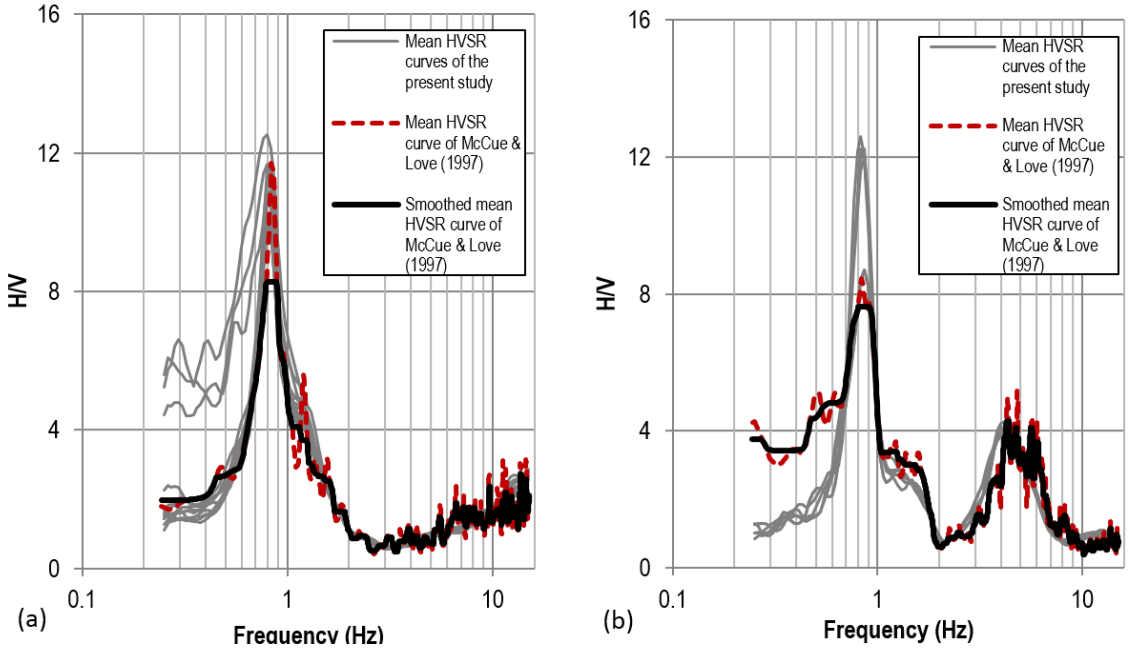

Figure 3.22 HVSR curve comparison at (a) Location #07 and (b) Location #08.

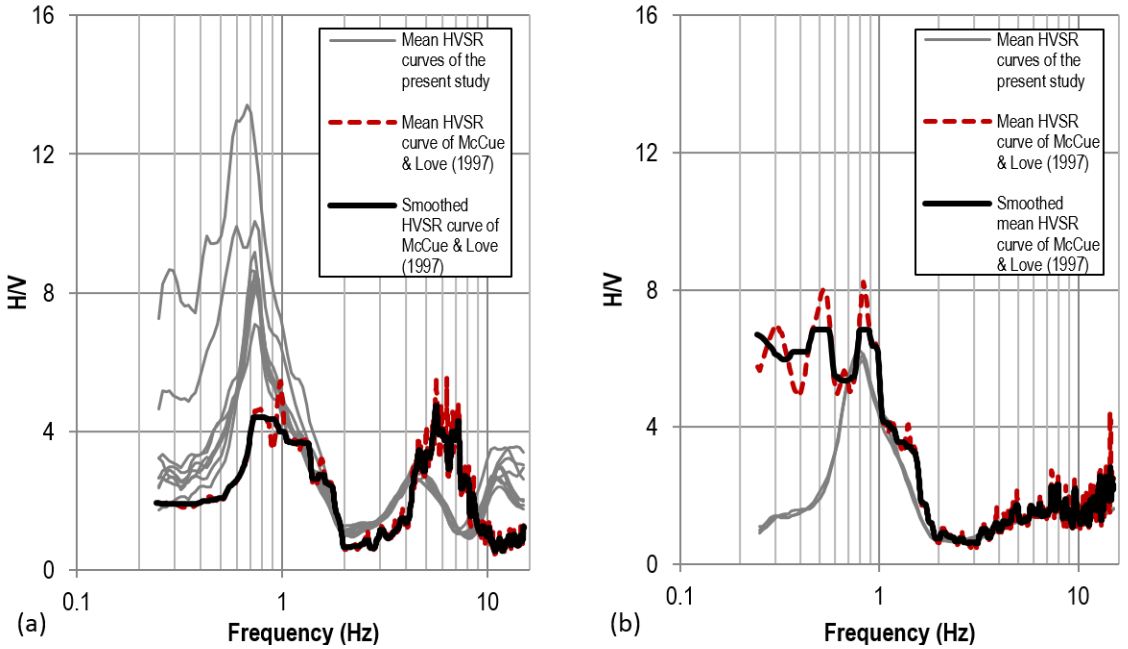

Figure 3.23 HVSR curve comparison at (a) Location #09 and (b) Location #10.

As shown in the figures, most of the mean HVSR curves of the present study are in very good agreement with those obtained by McCue & Love (1997), including all of the frequencies of the HVSR curve-peaks, except for Location #03. Furthermore, there is a clear, large-amplitude, HVSR peak at Locations #04, #05 and #07, which is likely to be the resulting of relatively high impedance contrast between the upper layers and the underlying bedrock, with estimated site frequencies ranging from 0.7 to 1.0 Hz. As mentioned above, Locations #04 and #05 are near the River Torrens, and Location #07 is close to a small creek leading to the River Torrens. Double HVSR curve peaks are encountered at Locations #01, #02, #03, #08 and #09, which highlight more complex sub-surface dynamic characteristics.

The good agreement between the mean HVSR curves of the present study and those obtained by (McCue & Love, 1997), as shown in Figures 3.19 to 3.23, suggest the consistency of the HVSR method with respect to time, as McCue & Love (1997) carried out their measurement in 1997, whereas the present study data were obtained in 2015. In particular, this temporal reliability of the HVSR analysis in the present study is also corroborated by the continuous 96 sets of ambient noise analysis from 3:00 pm on 02/10/2014 to 2:30 pm on 04/10/2014 (see Figures 3.3 and 3.4). This temporal stability of the analysis of microtremor data was also demonstrated by (Okada, 2003).

The Adelaide CBD incorporates a variety of building types and building materials. In terms of the number of stories (N), most of the north and southeast of Adelaide consists of low-rise (1-5 story) buildings. Only the city center includes medium-rise (6-10 stories) to high-rise (>10 story) buildings. By adopting the building fundamental frequency approximation suggested by Kramer (1996), which is approximated by 10/N (Hz), the Adelaide building frequency in the north and southeast of Adelaide is between 2 and 10 Hz, whereas in the city center, it is between 1 (or below) and 1.7 Hz. Resonance effects will occur when the building frequency is equal to or close to the ground frequency. This will lead to enhanced building vibration and increase the prospect of structural collapse and hence human injury and fatalities.

Overall, the results suggest a fundamental frequency of 1 Hz for much of the Adelaide City, which suggests significant seismic amplification for medium-rise buildings throughout the city. The fundamental frequency at several locations (#07, #08, #09 and #10) is expected to be about 0.7 to 0.8 Hz, which suggests high vibration of high-rise structures around these locations during a seismic event. Furthermore, an additional second fundamental frequency of between 4 and 6 Hz is suggested for Locations #01, #02, #03, #08 and #09, which also indicates resonance of low-rise structures at these locations.

3.8.2 Adelaide seismic site classes

The seismic site class across all of North Adelaide sites is consistent for all classification systems adopted in the present study. All locations in this area can be classified as subsoil Class D by NEHRP, AS 1170.4 and McPherson & Hall (2007), as shown in Tables 3.6 and 3.7. The estimated uppermost 30 m shear wave velocity ranges between 274 and 318 m/s. This uniform seismic site classification is likely the result of a relatively consistent and shallow bedrock level in this area, which is 64 m below ground or less. In the north of Adelaide a high shear wave velocity, which is typically close to that of bedrock (>760m/s), is suggested at both Locations #01 and #02 (see Figures 3.10(a) and 3.10(b)), at depths shallower than those indicated by the borehole data. The nearest borehole to Locations #01 and #02 indicates respective bedrock depths of 59 m and 64 m, whereas the present study suggests the bedrock surface is at 43 m and 40 m, respectively. This discrepancy highlights the difficulty estimating bedrock level utilizing HVSR analysis in low impedance contrast sites, such as regolith.

Table 3.6 Adelaide CBD seismic site classes for all instruments at Locations #01 – #05 (North Adelaide).

Site/Location												
#01			**#02**			**#03**	**#04**			**#05**		
INST. S#A	INST. #B	INST. #C	INST. #A	INST. #B	INST. #C	INST. #A	INST. #A	INST. #B	INST. #C	INST. #A	INT. S#B	INST. #C
304 m/s	305 m/s	342 m/s	305 m/s	259 m/s	254 m/s	315 m/s	297 m/s	340 m/s	280 m/s	NA	278 m/s	289 m/s
D	D	D	D	D	D	D	D	D	D	NA	D	D
NEHRP (BSSC, 2001)												
D	D	D	D	D	D	D	D	D	D	NA	D	D
AS 1170.4 (Standards Australia, 2007)												
D	D	D	D	CD/D	CD/D	CD/D	CD/D	CD	CD/D	NA	CD/D	CD/D
McPherson & Hall 2007)												
318 m/s			274 m/s			315 m/s	299 m/s			284 m/s		
D			D			D	D			D		
NEHRP (BSSC, 2001)												
D			D			D	D			D		
AS 1170.4 (Standards Australia, 2007)												
D			D			D	D			D		
McPherson & Hall (2007)												

Note:
#01 is near Barton Terrace West.
#02 is near Lefevre Terrace.
#03 is inside Wellington Square.
#04 is near Finniss Street.
#05 is corner of Frome Road/ War Mem. Drive.
#06 is corner of West Terrace/ Port Road.
#07 is near Bartels Road.
#08 is inside Victoria Square.
#09 is corner of South Terrace/ West Terrace.
#10 is corner of South Terrace/ Hutt Road.
INST.#A is Instrument #A
INST.#B is Instrument #B
INST.#C is Instrument #C

Table 3.7 Adelaide CBD seismic site classes for all instruments at Locations #06 – #10 (South Adelaide).

Site/Location												
#06			**#07**			**#08**	**#09**			**#10**		
INST. #A	INST. #B	INST. #C	INST. #A	INST. #B	INST. #C	INST. #A	INST. #A	INST. #B	INST. #C	INST. #A	INST. #B	INST. #C
NA	412 m/s	243 m/s	194 m/s	203 m/s	184 m/s	361 m/s	384 m/s	427 m/s	425 m/s	NA	NA	326 m/s
NA	C	C	D	D	D	C	C	C	C	NA	NA	D
NEHRP (BSSC, 2001)												
NA	B	B	D	D	D	B	B	B	B	NA	NA	D
AS 1170.4 (Standards Australia, 2007)												
NA	C	CD/D	DE	D	DE	C	C	C	C	NA	NA	CD/D
McPherson & Hall (2007)												
337 m/s			194 m/s			361 m/s	418 m/s			326 m/s		
C			D			C	C			D		
NEHRP (BSSC, 2001)												
B			D			B	B			D		
AS 1170.4 (Standards Australia, 2007)												
D			D/DE			C	C			D		
McPherson & Hall (2007)												

Note:
#01 is near Barton Terrace West.
#02 is near Lefevre Terrace.
#03 is inside Wellington Square.
#04 is near Finniss Street.
#05 is corner of Frome Road/ War Mem. Drive.
#06 is corner of West Terrace/ Port Road.
#07 is near Bartels Road.
#08 is inside Victoria Square.
#09 is corner of South Terrace/ West Terrace.
#10 is corner of South Terrace/ Hutt Road.
INST.#A is Instrument #A
INST.#B is Instrument #B
INST.#C is Instrument #C

In contrast, the area to the south of the Adelaide CBD suggests much more variable subsoil classification. In this study, the south of Adelaide is estimated to relate to an upper 30 m shear wave velocity between 194 m/s and 418 m/s. This suggests a complex subsoil classification ranging from subsoil Class C to D, in the NEHRP classification system, or subsoil Class B to D in the AS 1170.4 classification system, or subsoil Class C to DE in the classification system by McPherson & Hall (2007). Generally, the AS 1170.4 classification system is more conservative than the others, as shown at Locations #06, #08 and #09. The AS 1170.4 method classifies subsoil class B for all Locations #06, #08 and #09, whereas the others classify these as subsoil classes C or D. This variable subsoil classification in the southern part of Adelaide is likely the result of highly variable stratigraphy and the increasing bedrock depth, which is approximately 100 m below ground level. Summary of Adelaide seismic site classes of the present study is shown in Table 3.8.

Table 3.8 Summary of Adelaide seismic site classes.

Location	**Seismic site classes based on Vs,30**			Remarks
	NEHRP (BSSC, 2001)	**AS 1170.4 (Standards Australia, 2007)**	**McPherson & Hall (2007)**	
#01 (Barton Tce W)	D	D	D	North Adelaide
#02 (Lefevre Tce)	D	D	D	
#03 (Wellington Sq)	D	D	D	
#04 (Finniss St)	D	D	D	
#05 (Frome Rd/ War Memorial Dr)	D	D	D	
#06 (West Tce/ Port Rd)	C	B	D	South Adelaide
#07 (Bartels Rd)	D	D	D/DE	
#08 (Victoria Sq)	C	B	C	
#09 (South Tce/ West Tce)	C	B	C	
#10 (Hutt Rd/ South Tce)	D	D	D	

Another ambient noise analysis by means of spatial autocorrelation (SPAC) method to infer the shear profile is also carried out by (Setiawan *et al*., 2016) for 8 of the 10 locations in the present study. A comparison by means of the SPAC method with respect to the $V_{s,30}$ results is included to confirm the reliability of the inversion from the HVSR curve incorporating the stratigraphic constraints at regolith sites. The resulting values of $V_{s,30}$ from this study are in good agreement with the present study for Locations #01, #04, #05, #06, #09 and #10, as shown in Table 3.9 and Figure 3.24. By adjusting the $V_{s,30}$ at Locations #02 and #07 to follow the SPAC results, and constraining the areas along the

Torrens River, the $V_{s,30}$ of the present study is plotted and compared against the most recent $V_{s,30}$ mapping by Leonard (2015), as shown in Figure 3.25. Generally, the region corresponding to $V_{s,30}$ values less than 315 m/s is wider in the present study than that proposed by Leonard (2015). The preliminary result of the present study suggests that at least half of the Adelaide CBD areas to the north and south of the River Torrens has a $V_{s,30}$ value less than 315 m/s.

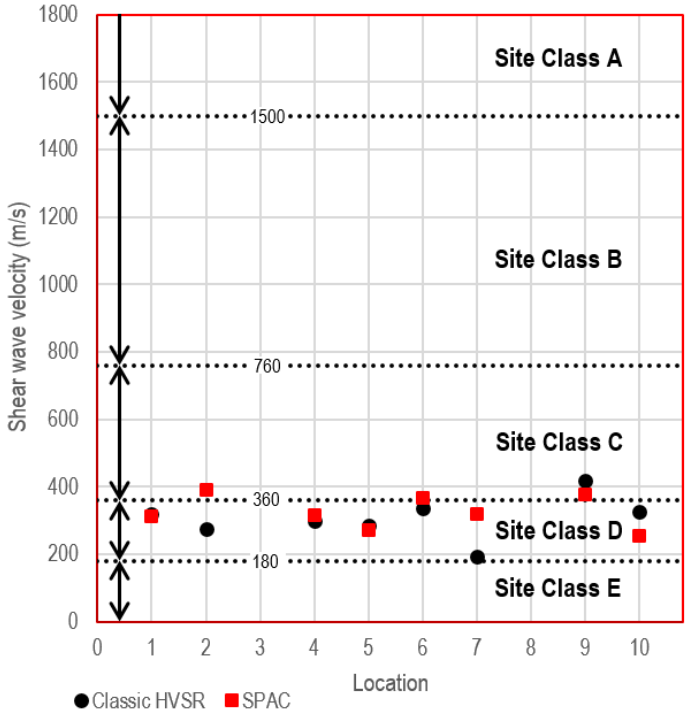

Figure 3.24 Results of shear wave velocity of the top 30 m constrained by the ellipticity of the classic HVSR and SPAC curves plotted relative to NEHRP seismic site classifications.

Table 3.9 Comparison of $V_{s,30}$ constrained using the ellipticity of the HVSR and SPAC curves.

Location	Vs,30 (m/s)		Remarks
	Classic HVSR	SPAC	
#01 (Barton Tce W)	318	340	North Adelaide
#02 (Lefevre Tce)	274	390	
#04 (Finniss St)	299	317	
#05 (Frome Rd/ War Memorial Dr)	284	272	
#06 (West Tce/ Port Rd)	337	366	South Adelaide
#07 (Bartels Rd)	194	319	
#09 (South Tce/ West Tce)	418	378	
#10 (Hutt Rd/ South Tce)	326	245	

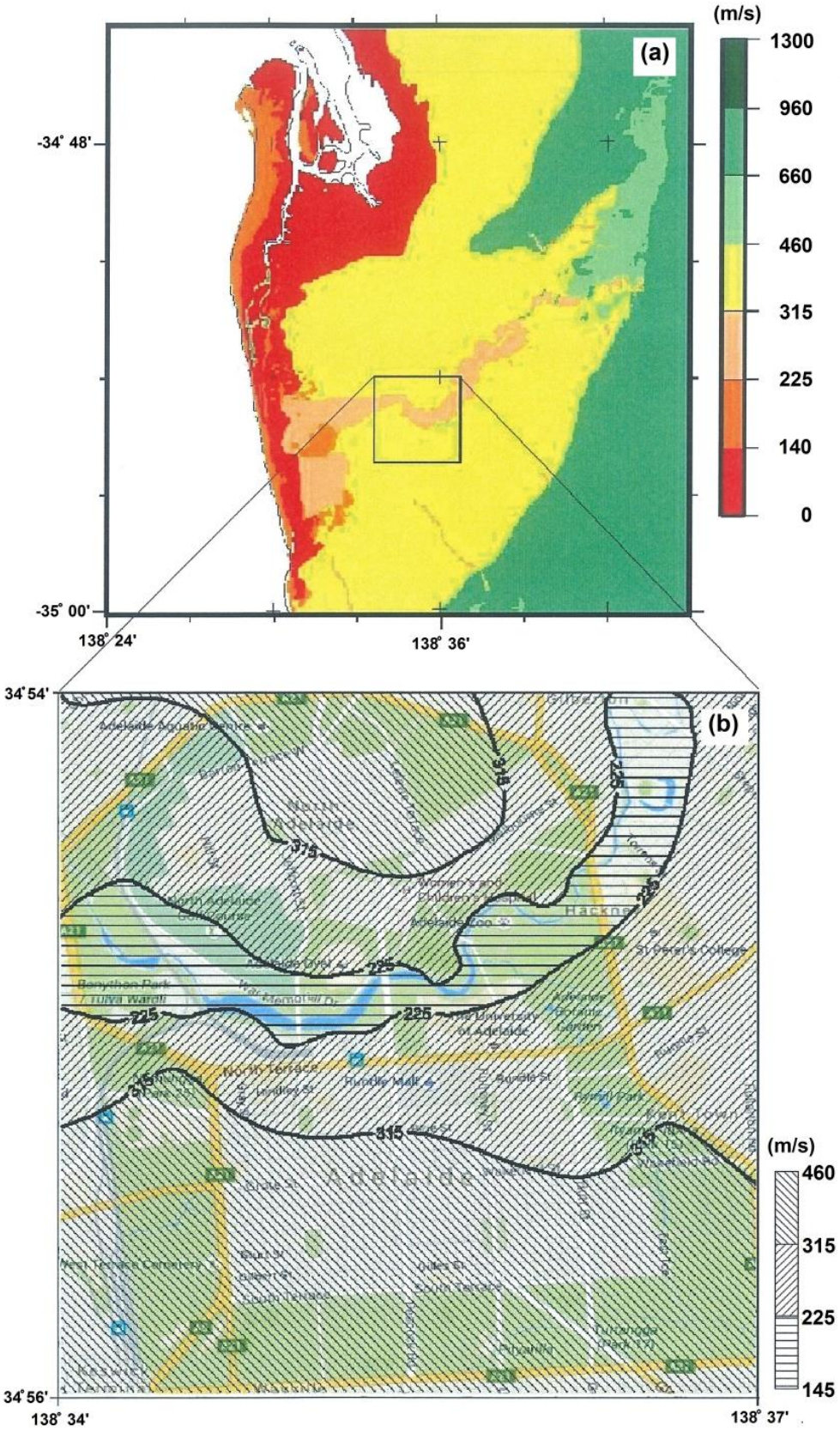

Figure 3.25 (a) Preliminary map of $V_{S,30}$ of the Adelaide CBD and the surrounding areas by Leonard (Leonard, 2015) and (b) map of $V_{S,30}$ of the Adelaide CBD based on constrained modeling of the measured HVSR curve of the present study.

3.9 CONCLUSIONS

Currently, seismic site classification is widely accepted in the design of seismic resilient infrastructure. Many researchers have successfully implemented the HVSR technique for seismic site classification because it is relatively straightforward, convenient and reliable in urban areas. However, the application of the HVSR technique in regions with various impedance contrast between the upper layer and bedrock, such as regoliths, for site seismic classification is uncertain and requires attention. The present study seeks to add to the body of knowledge associated with various impedance contrasts sites. Adelaide, the capital of and largest city in South Australia, is founded on a regolith site and is selected for the study case area. Ambient noise across the study case site is measured from which the seismic hazard parameters, i.e. site periods and shear wave profiles, are quantified using HVSR analysis and constrained modeling of measured HVSR ellipticity curves.

In the case of the Adelaide regolith, the majority of the locations are likely to have a site period greater than 0.8 seconds, and hence the site subsoil class D (NEHRP and Australian Standard) or class CD/D (McPherson & Hall, 2007) is the appropriate classification for seismic design purposes for locations in the northern part of the Adelaide CBD, whereas more complex seismic site classes from subsoil classes B to DE are identified in southern part of the CBD. Based on the 3 classification systems mentioned above, this southern part of the city can be classified as follows: subclasses D to C (NEHRP) or subclasses D to B (AS 1170.4) or DE to C (McPherson & Hall, 2007). These results are in reasonably good agreement with several previous studies.

A preliminary upper 30 m shear wave map of the study case site is proposed. A slightly wider area of shear wave velocities below 315 m/s is identified. This result can be used to increase the resolution of map proposed by Leonard (2015).

Finally, this study presents a promising application of HVSR analysis for seismic assessment of regolith sites. In this case, the ambient noise analysis is relatively straightforward, convenient and reliable.

Chapter Four

ESTIMATING BEDROCK DEPTH IN THE CASE OF REGOLITH SITES USING AMBIENT NOISE ANALYSIS

INTENTIONALLY BLANK

Statement of Authorship

Title of Paper	Estimating bedrock depth in the case of regolith sites using ambient noise analysis
Publication Status	☑ Published ☐ Accepted for Publication ☐ Submitted for Publication ☐ Unpublished and Unsubmitted work written in manuscript style
Publication Details	Setiawan, B., Jaksa, M., Griffith, M., and Love, D., 2018. Estimating bedrock depth in the case of regolith sites using ambient noise analysis. Engineering Geology, 243: 145 – 159, DOI: 10.1016/j.enggeo.2018.06.022.

Principal Author

Name of Principal Author (Candidate)	Bambang Setiawan		
Contribution to the Paper	Performed field data collection, carried out analysis on all field data, interpreted the results, wrote the manuscript and acted as corresponding author.		
Overall percentage (%)	80%		
Certification:	This paper reports on original research I conducted during the period of my Higher Degree by Research candidature and is not subject to any obligations or contractual agreements with a third party that would constrain its inclusion in this thesis. I am the primary author of this paper.		
Signature		Date	14 June 2017

Co-Author Contributions

By signing the Statement of Authorship, each author certifies that:

i. the candidate's stated contribution to the publication is accurate (as detailed above);

ii. permission is granted for the candidate in include the publication in the thesis; and

iii. the sum of all co-author contributions is equal to 100% less the candidate's stated contribution.

Name of Co-Author	Mark Jaksa		
Contribution to the Paper	Overall percentage - 10% Supervised the development of work, helped in data interpretation and manuscript preparation. He also reviewed this manuscript rigorously.		
Signature		Date	14/6/17

Name of Co-Author	Michael Griffith		
Contribution to the Paper	Overall percentage - 5% Provided some valuable comments on the manuscript contents.		
Signature		Date	14/6/17

Name of Co-Author	David Love		
Contribution to the Paper	Overall percentage - 5% Helped the field data collection, evaluated and edit the manuscript.		
Signature		Date	14 June 2017

Please cut and paste additional co-author panels here as required.

4.1 INTRODUCTION

Local site effects need to be considered when conducting seismic hazard assessments (Booth *et al*., 1986; Brebbia *et al*., 1996; Street *et al*., 2001) as earthquake motion can be significantly amplified at vulnerable soil sites and cause severe structural damage, such as that which occurred in the 1985 Mexico, 1988 Armenian, 1989 Loma Prieta, 1989 Newcastle, and 1995 Kobe earthquakes. The bedrock profile and overburden sedimentary deposits contribute to site amplification effects (Graves *et al*., 1998; Bakir *et al*., 2002; Narayan & Rao, 2003; Narayan, 2005). Irregular sub-surface profiles, subjected to incident body waves, can result in focusing and defocusing of the seismic wave field manifested at ground level. The basin interface may change the velocity and direction of the waves. In certain circumstances, the focusing and defocusing phenomenon may cause amplification and de-amplification at the ground surface. The effect of the basin bedrock profile is revealed by the damage patterns of the Northridge, Sherman Oaks, and Santa Monica, California earthquakes (Somerville & Graves, 1996; Graves *et al*., 1998).

Single station ambient noise measurements are useful for investigating the depth of bedrock. Ibs-von Seht and Wohlenberg (1999) developed an empirical relationship between fundamental resonance frequencies and overburden thickness for the Lower Rhine Embayment in Germany and suggested good agreement between the horizontal to vertical spectral ratio (HVSR) peak frequency with the overall overburden thickness, ranging from tens to more than 1,000 meters (m). These developments have provided a practical means of estimating overburden thickness using ambient noise data. Subsequently, many studies have used similar approaches for estimating the thickness of sediments overlying bedrock (e.g. Bodin *et al*., 2001; Parolai *et al.*, 2002; Gosar, 2004; D'Amico *et al*., 2004; Hinzen *et al*., 2004; Lane *et al*., 2008; Dinesh *et al*., 2010; Paudyal *et al*., 2012a & b; and Guo *et al*., 2014; Guo & Aydin, 2016). All of these studies were carried out essentially in relatively thick, homogenous and uniformly layered systems and in high impedance contrast sites. Estimating the bedrock surface using ambient noise analysis at regolith sites subjected to a complex layered system and various (low to high) impedance contrasts is the subject of ongoing research.

The present study is focused on bedrock depth estimation in presence of a complex subsurface profile and various impedance contrast sites, which is manifested in Adelaide's regolith. Regoliths include all weathered materials in the zone between the

ground surface and the underlying bedrock (Wilford & Thomas, 2013). The Australian National Committee on Soil and Terrain (NCST) (2009) characterizes the regolith as the mantle of earth and rock altered or formed by land surface processes, whereas bedrock is the zone formed or altered by deep-seated crustal processes. The NCST characterized regolith and bedrock by different processes, rather than grouping them into different classes of material. Thus, characterizing earth layers as either regolith or bedrock is a task which involves many parameters including mineralogy and structure; climate, particularly rainfall and temperature; aeolian inputs; topography; biota, including vegetation and organisms; age, and soil-landscape history (Wilford & Thomas, 2013). The unique processes and parameters that control the development of a regolith when compared to bedrock result in different characteristics of masses within the regolith zone to those within the bedrock zone. Generally, the regolith tends to have lower density, strength, and cohesion than bedrock (NCST, 2009). Two previous investigations, namely Leonard (2015) and Collins *et al*. (2006), suggested various (~2.1 to ~3.5) impedance contrasts for the regolith at the investigated sites. Collins *et al*. (2006) measured the shear wave velocity at the Government House Site (GHS) in Adelaide, South Australia, using the spectral analysis of surface waves (SASW) method. Collins *et al*. (2006) suggested an average shear wave velocity of about 420 m/s for Adelaide's overlying layer and 810 m/s for Adelaide's bedrock. By assuming densities of 1,900 kg/m^3 for the overlying layer and 2,100 kg/m^3 for the bedrock, the SASW measurements by Collins *et al*. (2006) suggested an impedance contrast of ~2.1. A near surface seismic site classification by Leonard (2015) suggested a shear wave velocity of 315 m/s for the upper 30 m for most of the Adelaide city. Thus, the impedance contrast raw estimation for much of the city is ~3.5, by assuming the shear wave velocities of the overlying layer and bedrock are 315 and 1,000 m/s, respectively, assuming respective densities of 1,900 and 2,100 kg/m^3. This study, also, suggested various impedance contrasts for the regolith at the study sites, as shown by the shear wave velocity profiles presented later in the paper. The uniqueness of the regolith in Australia has been highlighted by McPherson & Hall (2007) who suggested a modification to the seismic classification system in the widely adopted National Earthquake Hazard Reduction Program (NEHRP) for Australian National Regolith Site Classification Map. The main objective of this paper is to investigate the reliability of various ambient noise data analysis methods for engineering assessment of bedrock depth for such sites.

Adelaide, South Australia, the case study area of this paper, is considered the most seismically active of the Australian capital cities. Adelaide has suffered great losses from earthquakes (Dyster, 1992, McCue, 1975). Observations of seismic recordings obtained during the 1997 Burra earthquake suggest significant ground amplification at Adelaide (McCue *et al*., 2001). Therefore, this study is relevant for enhancing understanding of the seismic hazards of Adelaide.

4.2 SEISMICITY AND GEOLOGY OF THE CASE STUDY AREA

The Australian continent is classified as a stable continent region (SCR) (Johnston, 1996a; Celerier *et al*., 2005; Hillis *et al*., 2008). Seismic activity in this region is categorized as low to moderate (Veevers, 1984). However, the deformation rate of the Australian continent is faster than other stable intraplate regions (Hillis *et al*., 2008). The continent experiences magnitude $\geq$ 6.0 earthquake every 5 years (McCue, 1990). Furthermore, several major devastating earthquakes have occurred in such 'stable' continents such as at Meeberrie (1941; M_L 6.8), Meckering (1986; MS 6.8), Cadoux (1979; MS 6.4) and Tennant Creek (1988; MS 6.3) (*cf*. Johnston, 1996b; Crone *et al*., 1997; Sandiford *et al*., 2004; Boominathan *et al*., 2008).

Adelaide lies within the most seismically active region in the Australian continent (Sandiford, 2003; Quigley *et al*., 2006; Quigley *et al*., 2007). A comprehensive study of the historical seismicity in the Adelaide region was conducted by Malpas (1991). This author extended the seismic data by exploring historical records, local newspapers, meteorological records and other reports and at least 42 significant events ranging from 4 to 7 on the modified Mercalli intensity scale (MM) earthquakes were identified in the Adelaide region since 1837. In this pre-instrumental period, two moderate seismic events occurred at Beachport in 1897, with Richter local magnitude (M_L) of 6.3, and at Warooka in 1902 (M_L 5.9) (Malpas, 1991). Both the 1897 and 1902 events caused extensive damage in the epicenter area and were felt strongly hundreds of kilometers (Malpas, 1991) from the epicenters. The epicenters of these historical earthquakes are shown in Figure 4.1. The Malpas (1991) study suggests the importance of seismic hazard investigations in the case study area. The findings of Malpas (1991) are supported by Greenhalgh *et al*. (1994), who concluded that at least 300 earthquakes are recorded by

seismic instruments each year in South Australia, with 15 events of magnitude 5 or greater in the last 150 years.

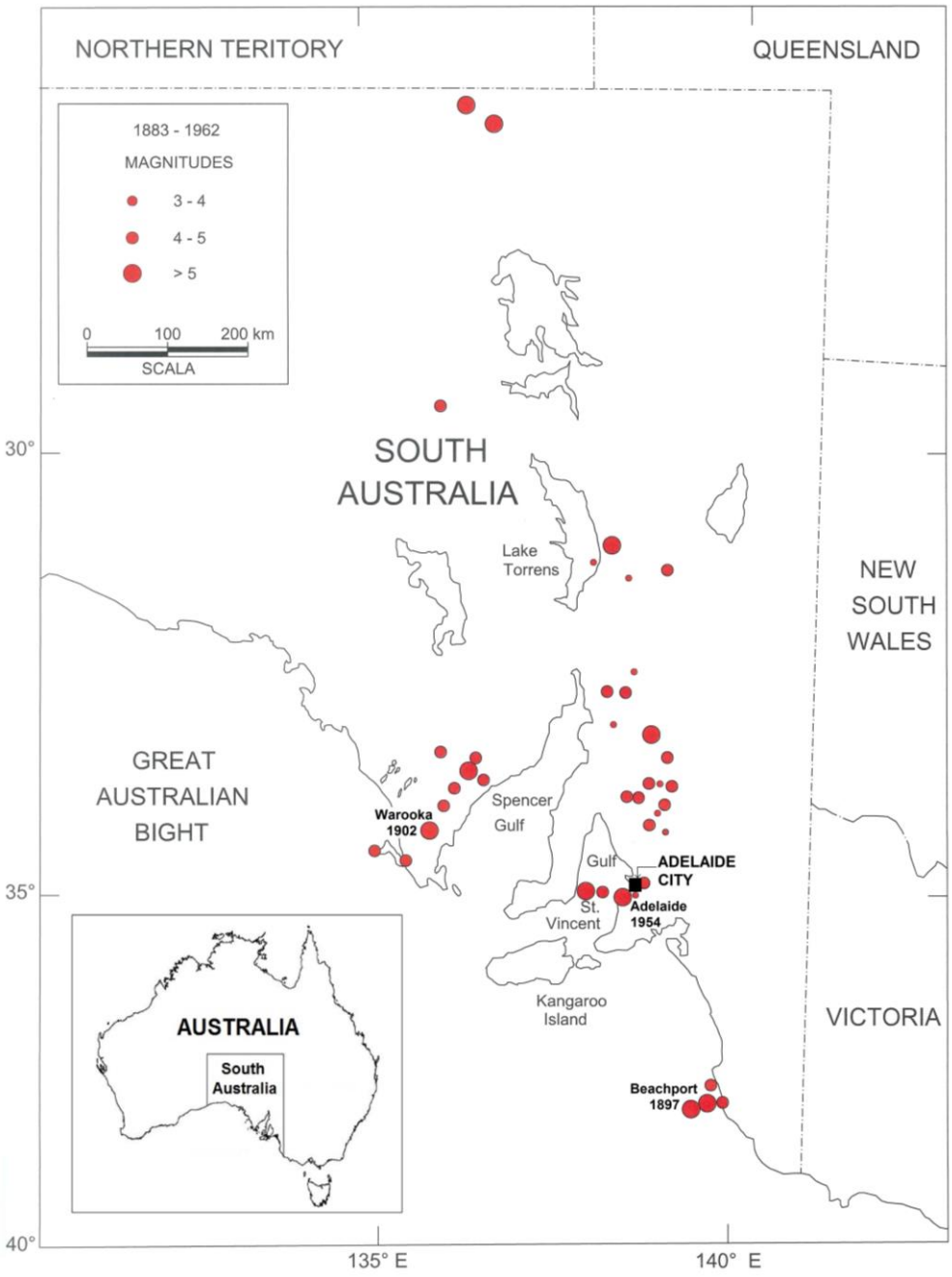

Figure 4.1 Epicentres of the historical earthquakes (Malpas, 1991) including location of Adelaide city study area.

The Adelaide case study area lies within the Adelaide Plains (Selby & Lindsay, 1982). The field sites are separated into two main plateaus, on the north and south sides of the Torrens River. In the north plateau area, geological profiles consist of 5 to 6 formations above the bedrock, which are predominantly Quaternary alluvium-Pooraka Formation,

Gull Rock Member of the Blanche Point Formation, Undifferentiated basal Blanche Point Formation and Tortachilla Limestone, South Maslin Sand, and Clinton Formation (see Table 4.1). The bedrock depth of the north plateau area is estimated to range from 50 to 64 m below ground surface (BGS) (Selby & Lindsay, 1982). The situation is more complex in the south plateau area. In this area, 8 to 10 formations (most of the formations indicated in Table 4.1) overlie Precambrian bedrock. Available information on the South Adelaide site suggests bedrock deepens towards the southeast, ranging from 88 to 118 m BGS, as shown in Figure 4.2 (Selby & Lindsay, 1982). General descriptions of the formations are given in Table 4.1. A typical high variability sub surface setting beneath the Adelaide city center is suggested by Selby & Lindsay (1982). Furthermore, the Keswick and Hindmarsh Clays underlying Adelaide have attracted some research attention. Both the Keswick and Hindmarsh clays are very similar in nature, characterized as stiff to hard, fissured, overconsolidated clays of high plasticity. Cox (1970) studied the physical properties of these clays and concluded that their geotechnical characteristics are remarkably similar to those of the London Clay. Sheard and Bowman (1996) indicated that a disconformable erosion surface exists between the Keswick and Hindmarsh clays.

4.3 METHODOLOGY

4.3.1 Field noise measurements

Ambient noise field measurements were conducted at 8 sites in the parklands that surround the Adelaide city area (Figure 4.2) using 7 sets of 3-component seismometers and at two sites using a single 3-component seismometer. Sites #01, #02, #04, #05, #06, #07, #09 and #10 used 7 sets, whereas the remainder of the sites (#03 and #08) used a single seismometer. These seismometers record the 3 orthogonal components of vibration: two horizontals (i.e. east–west and north–south) and one vertical. The data were recorded and saved to internal memory storage in each instrument. At each survey location, noise measurements were conducted for at least 2 hours at a sampling frequency of 100 Hz. Field data were filtered with a cutoff frequency of 50 Hz. A hexagonal array with a radius of 50 m (R = 50 m) was used for the array field noise measurement. Only recordings on 3 instruments (in a triangular arrangement) were used for the horizontal to vertical spectral ratio (HVSR) analysis and the vertical seismometer readings from all

instruments were used to analyse the spatial autocorrelation (SPAC). At each of the 8 sites, four tests with a duration of 30 minutes were conducted at a different time using all instruments.

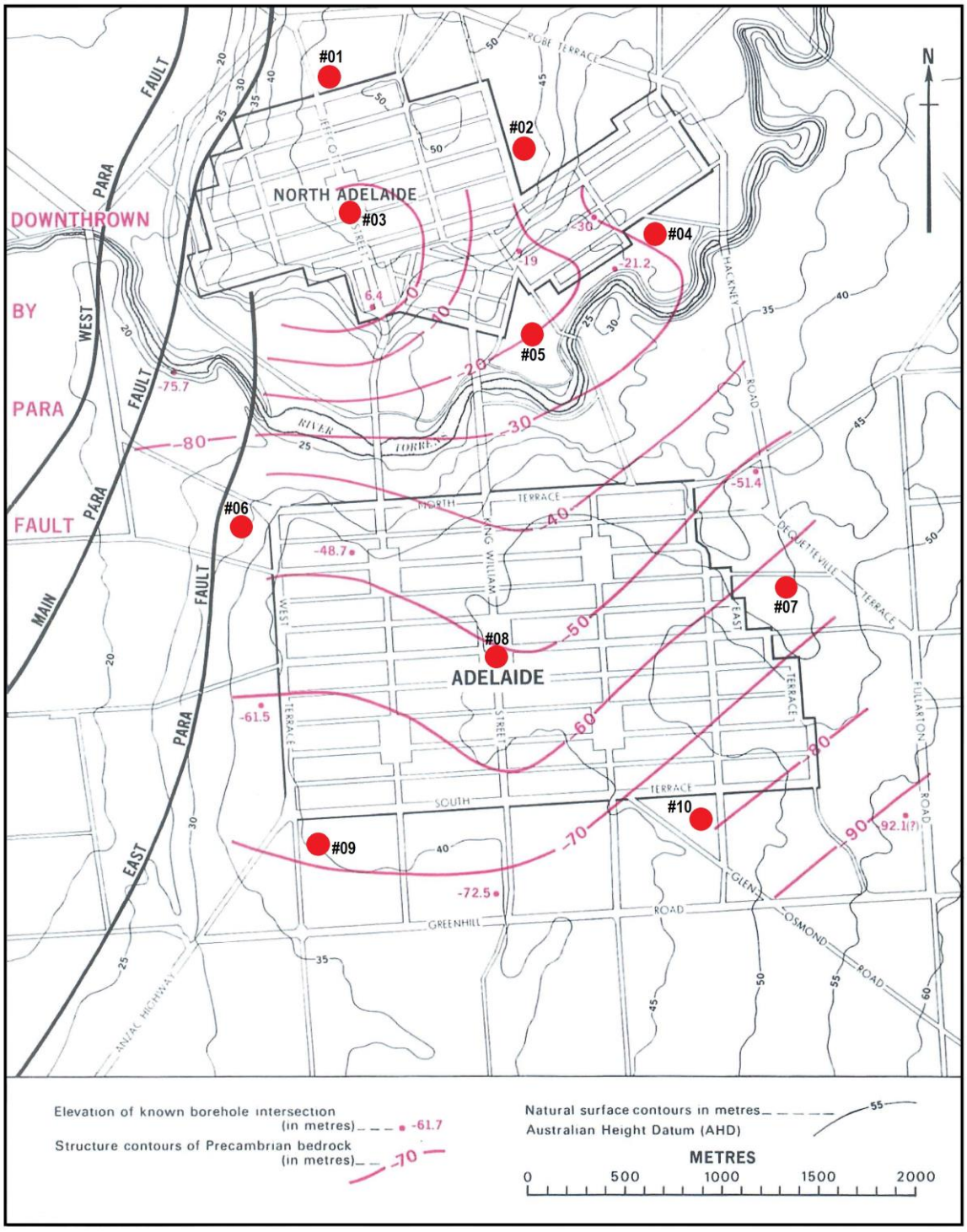

Figure 4.2 Map of the study area showing isobaths of the Precambrian bedrock (Selby & Lindsay, 1982) including locations of microtremor measurements (red circles).

Table 4.1 Descriptions of the formations of the Adelaide City (Selby & Lindsay, 1982).

Code	Formation	Description
A	Quaternary alluvium, Pooraka Formation [HOLOCENE]	Red brown silty CLAY (CH), grades downwards to SAND and GRAVEL (SP-GP)
A1	Keswick CLAY [PLEISTOCENE]	Grey-green CLAY (CH) with red and brown mottling, stiff to hard, fissured
A2	Hindmarsh CLAY [PLEISTOCENE]	Grey-green CLAY (CH) with yellow and red mottling with overlying SAND (SC)
B	Carisbrooke Sand [PLEISTOCENE]	Yellow, orange brown and grey, fine to medium clayey and silty SAND (SC-SM)
C	Bunham Limestone and Hallet Cove Sandstone [PLEISTOCENE TO PLIOCENE]	White clayey, sandy and rubbly LIMESTONE; Pale grey to yellow brown calcareous SANDSTONE with layers of sand (SP)
D	Sand unit of Port Willunga Formation [EOCENE]	Fine silty SAND (SM)
E	Tandanya Sand Member of Chinaman Gully Formation [EOCENE]	Gravelly, clayey SAND (SC-GW)
F	Gull Rock Member of Blanche point Formation [EOCENE]	Alternating bands of cherty siltstone and grey SILT (ML)
G	Undifferentiated basal Blanche Point Formation and Tortachilla Limestone [EOCENE]	Green to dark grey clayey SAND (SC) with LIMESTONE
H	South Maslin Sand [EOCENE]	Dark grey, brown at depth, but weathering to red brown or yellow, silty SAND (SM) with pyrite lumps
J	Clinton Formation [EOCENE]	Dark grey CLAY (CL) with LIGNITE; irregular clayey SAND zones (SC)
K	Precambrian bedrock	White, pink, brown, purple, blue-grey and greenish grey with thin sandy bands, decomposed quartzite or quartz veins, high plasticity SILT slightly sandy, very stiff to hard with a moisture content well below the plastic limit > 480 kPa

All the equipment used for the noise data acquisition consisted of 3 component (3C) LE-3Dlite Lennartz seismometers with an eigenfrequency of 1 Hz. These 3C seismometers were equipped with an analog-to-digital recorder (Kelunji digital data recorder), a global positioning system (GPS), antenna and a battery. A laptop computer was used for initial setup and checking. The seismometers were placed on a 20 mm thick circular concrete slab over a generally firm to a stiff ground surface, which was previously cleared of vegetation. The seismometers were leveled so as to minimize any instability during recording. The seismometers were also oriented to magnetic North and protected from

wind-induced vibrations by means of a plastic container and stabilized with a masonry brick on top. All of the equipment sets deployed in this study were examined for their repeatability. All equipment sets were run simultaneously at the same location, with a separation distance of approximately 0.5 m from one another. The HVSR analysis was carried out on all recorded data from all deployed equipment sets. The HVSR analysis curves for all equipment sets are presented in Figure 4.3, which suggests similar curve patterns, particularly between about 0.8 and 10.0 Hz. This result confirms the repeatability of the equipment. The details of the HVSR and SPAC methods are presented below.

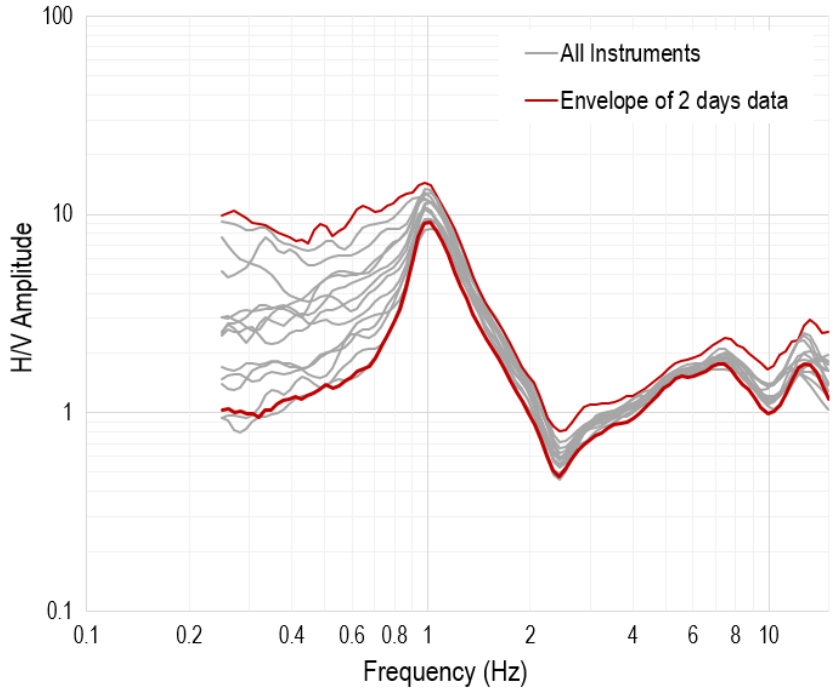

Figure 4.3 HVSR test results for all deployed equipment sets in this study incorporating the envelope of the HVSR analysis of 2 days of continuously recorded data at a station outsite the investigated sites (~3 km at the north-east of Adelaide city.

4.3.2 Horizontal to vertical spectral ratio (HVSR) analysis

The horizontal to vertical spectral ratio (HVSR) ambient noise method, herein referred to as HVSR, was introduced by Nogoshi and Igarashi (1971) based on the work of Kanay and Tanaka (1961). HVSR was popularized by Nakamura (1989) and has been used extensively since. Analysis of the spectral ratio between the Fourier amplitude spectrum of the horizontal (H) and vertical (V) components of the recorded ambient noise record is the key to HVSR. In accordance with the recommendations of the project “Site Effects

Assessment Using Ambient Excitation" (SESAME, 2004), the selection of the windows with the most stationary wave forms to exclude the transient noises is a crucial initial step in computing HVSR spectral ratios. The Fourier spectra of each HVSR component are smoothed in each selected window and then merged by adopting the geometric mean. Finally, the obtained HVSR is computed and averaged.

The HVSR is calculated by taking the root mean square of the Fourier amplitude spectra of the horizontal components (F_{NS} for the Fourier amplitude spectra in the north-south and F_{EW} for the Fourier amplitude spectra in the east-west directions) divided by the vertical component frequency spectrum (F_{UD}), as shown in Equation (4.1) (Delgado *et al*., 2000):

$$\frac{H}{V} = \sqrt{\frac{\left(F_{NS}^2 + F_{EW}^2\right)}{\left(2F_{UD}^2\right)}} \quad \text{(4.1)}$$

The ellipticity curve indicated by HVSR analysis has been used to constrain successfully the generation of the shear wave velocity model by Arai & Tokimatsu (2004), Castellaro & Mulargia (2009), Di Stefano *et al*. (2014) and Del Gaudio *et al*. (2014). In this study, the HVSR approach is used to estimate the shear wave velocities of layers above bedrock at the instrumented sites.

The frequency corresponding to the first dominant peak of the HVSR spectrum plot is referred to as the site fundamental resonance frequency (SESAME, 2004). Once the fundamental resonance frequency of the site is obtained, it can be used to estimate bedrock depth, as suggested by Kramer (1996), provided the shear wave velocity of the overlying layer is known. This approach is herein referred to as the generic function (GF). Further explanation of this approach is provided later.

4.3.3 Spatial autocorrelation (SPAC) analysis

The spatial autocorrelation (SPAC) method (Aki, 1957) requires simultaneous recording of ambient noise at a minimum of 3 microtremor stations to conform to an appropriate instrumental array (Claprood, 2012). In the present study, 7 instruments were deployed in a hexagonal array. Following the process described below, the Rayleigh wave dispersion curve is obtained and used to determine the shear wave velocity profile.

In the SPAC method, Aki (1957) considered a circular array of stations for the noise field observation. Given, for harmonic waves of frequency ω, the time series of ground velocity $u(0,0,\omega,t)$ and $u(r,\theta,\omega,t)$, recorded at the center $C(0,0)$ and at a point $X(r,\theta)$ of the array, respectively, the spatial autocorrelation function can be defined as:

$$\phi(r,\theta,\omega) = \overline{u(0,0,\omega,t)\cdot u(r,\theta,\omega,t)} \quad \text{(4.2)}$$

where the right-hand-side of Equation (4.2) represents the average of the products of simultaneous samples of the two time series. The spatial autocorrelation coefficient ρ is defined as the average of the normalized autocorrelation function in all directions over the circular array:

$$\rho(r,\omega) = \frac{1}{2\pi\cdot\phi(0,\omega)}\int_0^{2\pi}\phi(r,\theta,\omega)d\theta \quad \text{(4.3)}$$

where $\phi(0,\omega)$ is the SPAC function at the center, $C(0,0)$, of the circular array. Assuming that waves are stochastic and stationary in space and time, the integration of Equation (4.3) yields:

$$\rho(r,\omega) = J_0\left(\frac{\omega r}{c(\omega)}\right) \quad \text{(4.4)}$$

where $J_0(x)$ is the zero-order Bessel function of the first kind of x, and $c(\omega)$ is the phase velocity at the frequency ω. Using the Fourier Transform of the observed noise recording, the SPAC coefficient $\rho(r,\omega)$ can be obtained in the frequency domain as follows:

$$\rho(r,\omega) = \frac{1}{2\pi}\int_0^{2\pi}\frac{\mathrm{Re}[S_{CX}(\omega,r,\theta)]}{\sqrt{S_C(\omega)\cdot S_X(\omega,r,\theta)}}d\theta \quad \text{(4.5)}$$

where $S_C(\omega)$ is the power spectral densities of the noise records at C, $S_X(\omega,r,\theta)$ is the power spectral densities of the microtremors at X, and $S_{CX}(\omega,r,\theta)$ is the cross-spectrum between the ground motions at these two locations.

The SPAC coefficients can be obtained by averaging the normalized coherence function of the cross-spectrum between points C and X in the direction of θ. The phase velocity for every frequency is estimated from the Bessel function in Equation 4.4. Finally, the velocity model can be inverted.

The SPAC analysis adopted in the present study is the modified version introduced by Bettig *et al*. (2001), which facilitates the computation of average SPAC coefficients for any irregular array configurations. This modification to SPAC uses a similar assumption to that adopted by the Aki (1957) version of SPAC, where the stochastic ambient noise wavefield is stationary in both time and space. The modification proposes that the computation of the averaged SPAC coefficients of the station pairs may be obtained from rings of finite radiuses $r_1 \leq r \leq r_2$, instead of using a fixed radius, r. The modified, averaged SPAC coefficient as defined by Bettig *et al*. (2001) is:

$$\bar{\rho}(r_1, r_2, \omega) = \frac{2}{r_2^2 - r_1^2} \int_{r_1}^{r_2} r \cdot J_0\left(\frac{\omega_r}{c(\omega)}\right) dr = \frac{2}{r_2^2 - r_1^2} \frac{c(\omega)}{\omega_r} \left[r \cdot J_1\left(\frac{\omega_r}{c(\omega)}\right)\right]_{r_1}^{r_2} \text{.....(4.6)}$$

In practice, r_1 and r_2 are, respectively, the minimum and maximum sensor distance (radius) obtained from the co-array configuration and selecting station pairs with similar interstation distances (Bonnefoy-Claudet *et al*., 2005). The application of the modified version of SPAC in the present study affects both the resolution limit parameter (k_{min}) and the depth of the investigation. These issues are discussed in detail later.

4.3.4 Bedrock estimation

Bedrock estimation using generic function (GF)

A generic function to estimate the bedrock level was presented by Kramer (1996). The function is based on the model of a damped linear elastic layer. A simple sedimentary basin, which consists of a soft layer overlying a rigid hard rock basement, is analyzed by providing n natural frequencies of the soft soil deposit as follows:

$$\omega_n = \frac{V_s}{h}\left(\frac{\pi}{2} + n\pi\right) \quad \text{for } n = 0,1,2,...,\infty \text{ .....(4.7)}$$

where ω_n is the circular frequency of ground shaking of the nth natural frequency (Hz), V_s is the shear wave velocity (m/s), and h is the thickness of the layer (m). Generally, the peak amplification ratio occurs near the lowest natural frequency, which is known as the fundamental frequency. The vibration period, corresponding to the fundamental frequency, is known as the site period (T_0) and the corresponding frequency is known as the fundamental resonant frequency (f_s). The relations are given as follows:

$$f_0 = \frac{V_s}{4h} \quad \text{.....(4.8)}$$

Bedrock estimation using shear wave velocity profile of SPAC method

a. Dispersion curve (DC) retrieval

In this study, evaluation of the dispersion curves is carried out using the spatial autocorrelation (SPAC) techniques implemented in the Geopsy software package (Geopsy, 2015). The dispersion curve is evaluated based only on the vertical components of the microtremor data. The sole use of the vertical component of the seismometer data is motivated by the objective of analysing Raleigh waves and excluding Love waves. The fundamental Raleigh mode generally provides sophisticated interpretation tools in SPAC, provided the energy is confined to this single mode (Asten et. al., 2004). Pre-processing is carried out using a classical procedure for signal synchronization and mean and trend elimination. The seismic analysis code (SAC) algorithms of Goldstein *et al*. (2003) are used for this pre-processing. In this study, the use of several tests at each array location allows investigating the consistency of the evaluated dispersion curves.

In order to evaluate the dispersion curves (DCs), two important features to consider are the resolution (k_{min}) and aliasing (k_{max}) limits characterizing the array configuration, estimated through the array transfer function (ATF: see Di Giulio, 2006). The parameter k_{min} refers to the width of the central peak of ATF and k_{max} refers to the limit to avoid alias effects. The values of k_{min} and k_{max} depend on the adopted array size (i.e. the minimum, D_{min}, and maximum, D_{max}, sensor spacing). Empirically Tokimatsu, (1997) defined the range of k_{min} and k_{max} within the following limits:

$$\frac{2\pi}{3D_{max}} < k_{min} < k_{max} < \frac{\pi}{D_{min}} \quad \text{.....} \quad (4.11)$$

In the case of the 50 m radius, circular hexagonal array adopted in this study, k_{min} and k_{max} lie in the range of $0.0209 < k_{min} < k_{max} < 0.0628$. These range values of k_{min} and k_{max} are used in this study to constrain the resolution limits.

The dispersion curves obtained from each location are presented in Figure 4.4. Four curves from each location are computed to confirm the reliability of the deduced dispersion curve. The results suggest good consistency at all locations, as shown by the black circles in Figure 4.4. The experimental dispersion curves can be as low as ~2.2 Hz. All of these dispersion curves, which correspond to the autocorrelation curves, are used to invert the shear wave velocity profiles for estimating the bedrock depth.

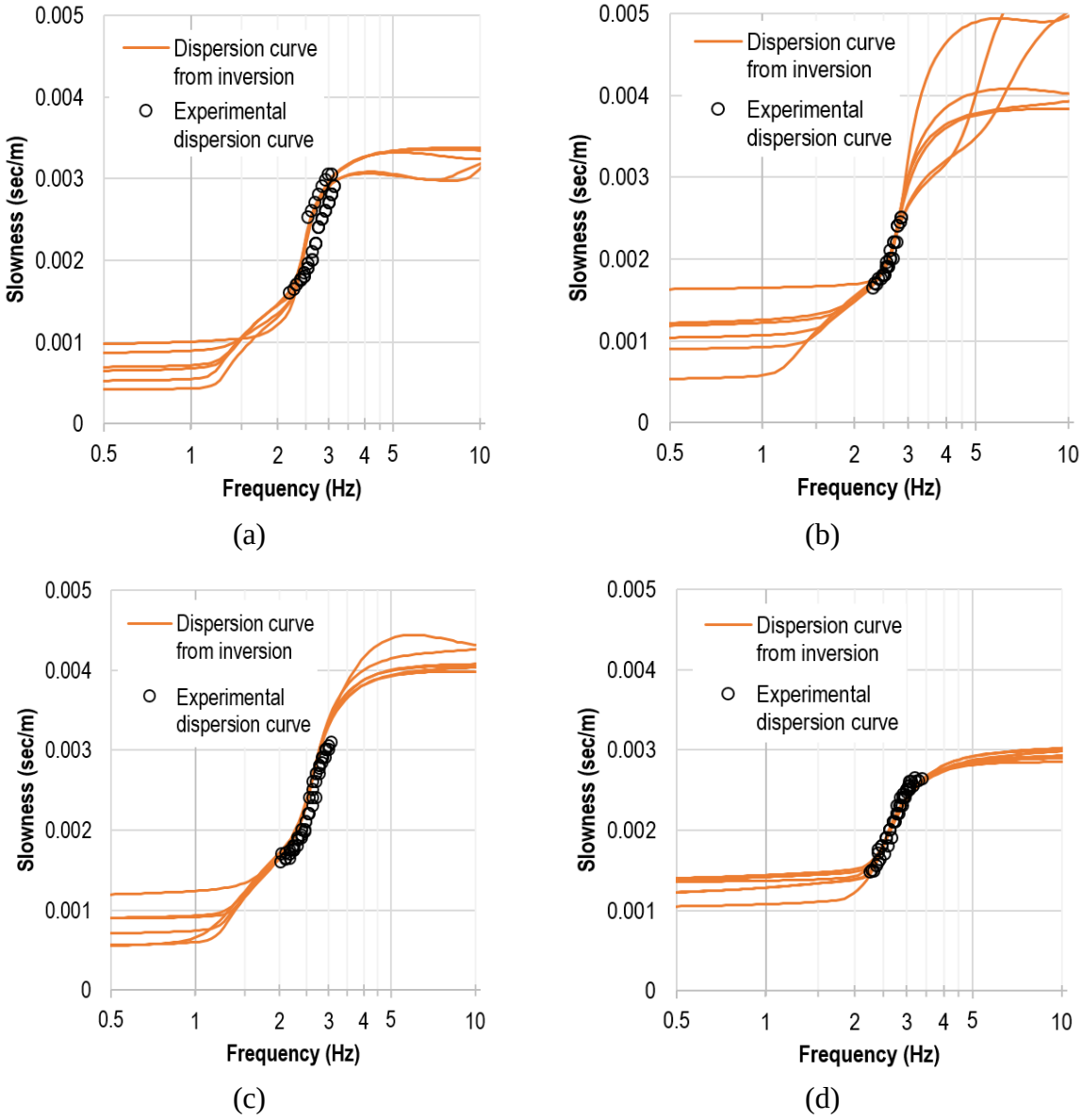

Figure 4.4 Selected dispersion curves for the best 20 models comparing inversion and experimental results from selected tests at Locations (a) #01, (b) #02, (c) #04, and (d) #05.

The dispersion curves computed during the inversion process for all models are examined to explore the appropriateness of the model. The selected computed dispersion curves are incorporated in Figure 4.4. It can be readily observed that the computed dispersion curves agree well with the experimental models. This confirms the appropriateness of the results obtained for the frequency range applicable to the experimental dispersion curves. Significant errors are observed at low frequencies beyond the aperture of the array. This large discrepancy at low frequencies can be attributed to the increasing uncertainty associated with the estimated shear wave velocity at the greater depths. However, for the study site, which is associated with bedrock depths up to approximately 118 m, the maximum sensor spacing of 100 m should be sufficient, as the penetration of surface waves is in the order of half of the wavelength (Xia *et al*., 2000). The longest wavelength that can be reliably analyzed is approximately 3 times the maximum sensor spacing (Tokitmatsu, 1997). Thus, the maximum depth for reliably measuring shear wave velocity is approximately 1.5 times the maximum sensor spacing.

b. Shear wave structure inversion (inversion technique)

The present study uses the neighborhood algorithm (NA) of Sambridge (1999) to infer the shear wave profile using the SPAC autocorrelation curve. This NA was implemented by Wathelet *et al*. (2005) in the Geopsy computer program. The NA is a stochastic direct-search method to identify an acceptable model inside a multidimensional parameter space. As with other direct-search methods, the NA generates pseudo-random samples in the parameter space using the dispersion curves constraint (Wathelet *et al*., 2005). Each sample corresponds to a set of parameters associated with a ground model. A misfit value is introduced to compare the computation results to the measured dispersion curve. This misfit value indicates how far the generated model deviates from the targeted solution. With poorly constrained parameters, inversion using the NA may result in different ground models, therefore it is recommended that several trials be undertaken using different random seeds (Sambridge, 1999). In this present paper, the shear wave velocity model is generated using the Geopsy program (Geopsy, 2015). The depth of bedrock is validated using the generated shear wave velocity profile.

The U.S. National Earthquake Hazards Reduction Program (NEHRP) classified rock Class B (Rock) and A (Hard rock) as materials with shear wave velocities greater than 760 m/s and 1,500 m/s, respectively (Building Seismic Safety Council (BSSC), 2001).

Moreover, McPherson & Hall (2007), in their development of the Australian National Regolith Site Classification Map, classified bedrock as materials with shear wave velocities greater than 760 m/s. The present study adopts these values of 760 m/s and 1,500 m/s shear wave values to indicate bedrock level. A shear wave velocity of 760 m/s is the most commonly adopted criterion for defining engineering bedrock (Estrada, 2010). However, several measurements in Australia have shown that such a shear wave velocity is associated with extremely weathered rock. Therefore, the NEHRP classification of Rock Class A, with a minimum shear wave velocity of 1,500 m/s, is also incorporated in the present study, which has been shown in Australia to be associated with bedrock of at least moderate strength (McPherson & Hall, 2007).

4.4 RESULTS

4.4.1 Bedrock estimation using generic function (GF)

Site fundamental frequency

HVSR analysis by means of Geopsy (2015) is carried out to obtain the site fundamental frequency. The results of this HVSR analysis, for all tests at all measured sites, are included in Setiawan *et al*. (2018a) which is attached in Appendix H. Several tentative window lengths (i.e. 25, 30. 35 and 40 s) have been undertaken to obtain as many reliable HVSR curves as possible. The 40 s window length was selected as it provides the most reliable HVSR curves. The reliability of the HVSR curves is based on the SESAME (2004) criteria, which found that many more HVSR curves satisfied the SESAME criteria when using a 40 s window length than when adopting other window lengths. This 40 s window length is also used to explore HVSR curves to frequencies as low as 0.25 Hz. The fundamental frequency at most of the sites in the study area is estimated to be around 1 Hz, whereas the remainder of the sites (#07, #08, #09 and #10) are below 1 Hz. A clear peak fundamental frequency of all deployed instruments was found at Locations #01, #02, #03, #04, #07, #08 and #09, whereas at Locations #05, #06 and #10 this peak was not well defined for some measurements due to unfavorable noise conditions. Instrument #A was unable to provide a distinct and reliable peak at Locations #05 and #06. Instruments #A and #B were also unable to produce a clear and reliable HVSR peak at Location #10. This may be due to some disturbances during the measurement period or some

inconsistencies during instrument setup, such as installation on a slightly unstable surface that caused a slight and gradual tilting during the measurement process. These unreliable data are excluded from the bedrock depth estimation.

A secondary peak at frequencies of 4-6 Hz, whose amplitude is between 2 and 4 is detected at Locations #01, #02, #03, #08 and #09. The possibility that the second peak corresponds to the higher mode of vibration is investigated using Equation 6, for $n > 0$. The results suggest that the ratio of 5-6, between the frequencies of the secondary peak and the fundamental mode of the HVSR analysis, is inconsistent with the expected ratio of 3. This inconsistency was found at all detected locations (i.e. Locations #01, #02, #03, #08 and #09). Therefore, the secondary peak appears not to be associated with higher modes of vibration. The two-peak structure, evident at Locations #01, #02, #03, #08 and #09, suggests that there are two different impedance contrasts at two different scales: the first peak relates to a thick structure and the second to a shallow structure (*cf* Gueguen *et al*., 1998; SESAME, 2004). Furthermore, since the greatest amplification occurs at approximately the lowest natural frequency, known as the fundamental frequency (Kramer, 1996), further analysis, in the present study, to deduce bedrock depth is carried out using only this fundamental frequency.

SESAME (2004) outlined a process by which the reliability of the HVSR curve can be assessed. Hence, further reliability assessment of the HVSR curves is undertaken using the SESAME (2004) criteria, as follows: (i) for the peak to be significant, f_0 should be greater than 10 divided by the window length (I_w), which in this study is 40 seconds; (ii) the number of significant cycles should be greater than 200; and (iii) the standard deviation of the amplitude of the HVSR curve, at frequencies between $0.5f_0$ and $2f_0$, should be less than two when $f_0 > 0.5$ Hz, or less than 3 when $f_0 < 0.5$ Hz. All three HVSR reliable criteria must be satisfied to consider a curve reliable for further analysis. Furthermore, SESAME (2004) also outlined the criteria for identifying a clear HVSR peak, which consists of 6 conditions. At least 5 out of the 6 criteria must be met to define a clear HVSR peak. Only the values of f_0 that pass the SESAME (2004) reliability and clear peak criteria were used for further analysis in the bedrock estimation at the measured sites, as shown in Figure 4.5(a). The tests that failed were removed. Figure 4.5(b) presents the amplitudes at f_0 of all tests that passed the SESAME (2004) criteria at all locations.

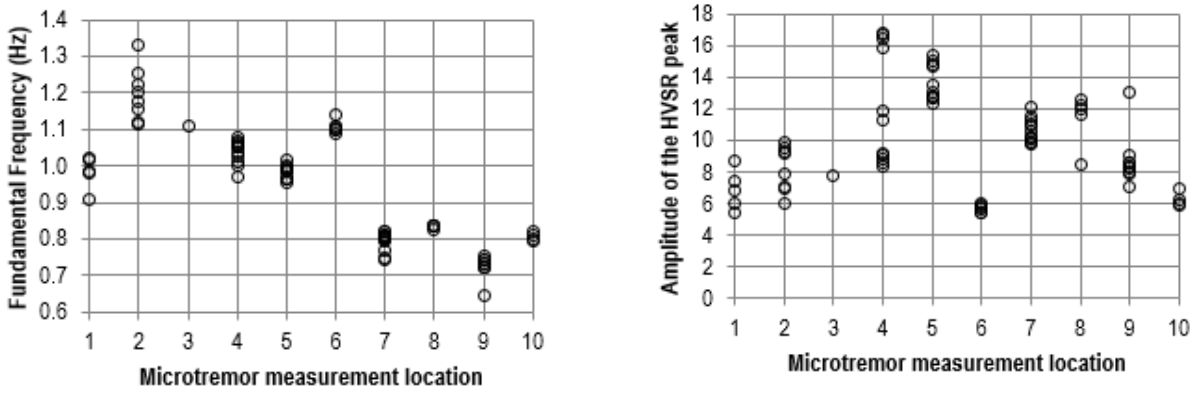

(a) **(b)**

Figure 4.5 Results of HVSR reliability and clear peak assessments of tests that pass the SESAME (2004) criteria at all locations: (a) fundamental frequencies, and (b) amplitudes at f_0.

Shear wave velocity profile

The average value of the shear wave velocity of the layers above bedrock must be defined to obtain the thickness of the overburden layer using the generic function suggested by Kramer (1996). The shear wave velocity profile of the present study is obtained by inverting the HVSR ellipticity curve. The 20 best models extracted from the results of the inversion are analyzed to obtain the arithmetic mean and median values of layer velocities. The appropriateness of the adopted shear wave velocity models was validated using forward computation, as suggested by Garcia-Jerez *et al*. (2016). The fundamental Raleigh wave, herein termed the 'calculated HVSR', is computed based on the adopted mean shear wave velocity and compared to the observed HVSR. Figure 4.6 presents a comparison of the mean observed and calculated HVSRs plotted using a logarithmic scale. As indicated in the plots, comparable results are observed at all measured sites for the bedrock depth estimation using GF. It is worth mentioning that comparisons between the experimental/observed and calculated HVSRs to validate the appropriateness of the inverted shear wave velocities have been carried out previously in many studies, such as by Apostolidis *et al*. (2004), Asten *et al*. (2004), Wathelet *et al*. (2004), Arai & Tokimatsu (2005), Garcia-Jerez *et al*. (2006), and Di Guilio *et al*. (2006, 2014).

A summary of the average shear wave velocities for all layers above bedrock, including the fundamental frequencies and estimated bedrock depths for all sites in the present study, are given in Table 4.2. In this study, it is preferable to use the mean shear wave velocity rather than the median shear wave velocity for estimating bedrock depth by means of the generic function as the forward computation suggests that the computed

ellipticity of the fundamental mode Rayleigh waves (calc. HVSR) for the inversion of the mean shear wave velocity profile aligns better with the observed HVSR microtremor array data (observed HVSR) than the inversion of the median shear wave velocity profile. Therefore, in the present study, bedrock depth is estimated using the mean shear wave velocity. Figure 4.7 presents the results of the estimated bedrock depths compared against the nearest boreholes. All bedrock depth estimations using this generic function (GF) are provided in Appendix I

.

Table 4.2 Estimated bedrock levels using the generic function (GF) for all measured sites.

Location	Average shear wave velocity of overlying layer (m/s)	Fundamental frequency (Hz)	Estimated bedrock level using generic function (m)	Bedrock depth from borehole data (m)
#01	406	0.91 – 1.07	95 – 112	59
#02	422	1.12 – 1.33	79 – 94	64
#03	304	1.06 – 1.11	68 – 72	44
#04	339	0.97 – 1.08	78 – 87	54
#05	268	0.96 – 1.02	65 – 70	50
#06	385	1.05 – 1.14	84 – 92	88.4
#07	311	0.74 – 0.82	95 – 105	96
#08	403	0.83 – 0.84	120 – 122	98
#09	451	0.65 – 0.76	149 – 174	107
#10	428	0.79 – 0.82	131 – 135	118

Table 4.3 Adopted inversion parameters.

Layer	Depth	Compression wave velocity (m/s)	Poisson's ratio	Shear wave velocity (m/s)	Density kg/m^3	Remarks
Upper Layer	1 – 30	200 – 2,000	0.2 – 0.5	150 – 1,000	18 – 20	$V_{p1} < V_{p2} < V_{p3}$ $N_{u1} < N_{u2} < N_{u3}$ $V_{s1} < V_{s2} < V_{s3}$ $Rho_1 < Rho_2 < Rho_3$
Transition Layer 1	15 – 60	200 – 4,000	0.2 – 0.5	150 – 2,000	18 – 20	
Transition Layer 2	50 – 150	200 – 5,000	0.2 – 0.5	150 – 3,500	18 – 20	
Bedrock	>150	200 – 5,000	0.2 – 0.5	150 – 3,500	20 – 24	

V_{p1}, V_{p2}, & V_{p3}: Compression wave velocity of the upper layer, transition layer 1 & transition layer 2, respectively.
N_{u1}, N_{u2}, & N_{u3}: Poisson's ratio of the upper layer, transition layer 1 & transition layer 2, respectively.
V_{s1}, V_{s2}, & V_{s3}: Shear wave velocity of the upper layer, transition layer 1 & transition layer 2, respectively.
Rho_1, Rho_2, & Rho_3: Density of the upper layer, transition layer 1 and transition layer 2, respectively.

4.4.2 Bedrock estimation using shear wave velocity profile of SPAC method

In the surface wave inversion of the SPAC autocorrelation curve, Wathelet *et al*. (2005) adopted 4 main parameters associated with each layer: the compression wave velocity, Poisson's ratio, shear wave velocity and the density. The layer can be assigned a specific thickness or over a reasonable range depending on the geological information available at the study site. In the present study, the profile of the site is assumed to be generally soft in the upper part (1-30 m depth), followed by gradually harder (15-60 m depth for Transition Layer 1 and 50-150 m depth for Transition Layer 2) before encountering hard bedrock (below 150 m depth). These layer depths are assigned to permit the neighborhood algorithm (NA) to search for the model that best fits the autocorrelation curve provided. The detailed parameter model adopted in the present study is summarized in Table 4.3.

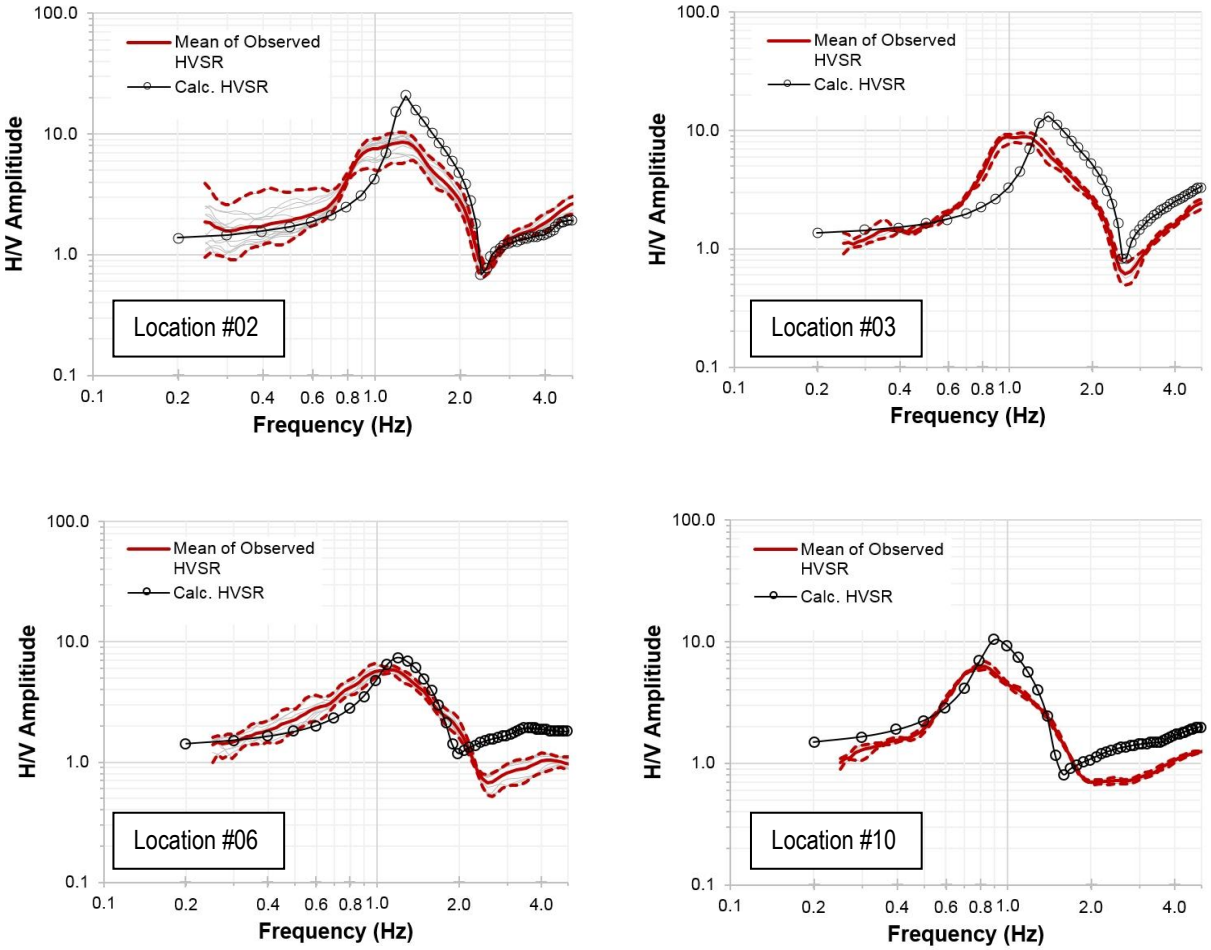

Figure 4.6 Comparison of the observed mean HVSR of the microtremor data (solid red line) ± one standard deviation (dashed red line) with the computed HVSR of the fundamental-mode Raleigh waves (black line) for bedrock estimation using GF.

For the bedrock depth estimation using the shear wave velocity profile of the SPAC method, 3 runs were carried out. At least 12,500 models were generated in each run, from which the 20 best models were extracted and analyzed. Typical results are provided in Figures 4.8 to 4.15. A summary of the interpreted bedrock depths using the SPAC method is shown in Figure 4.16.

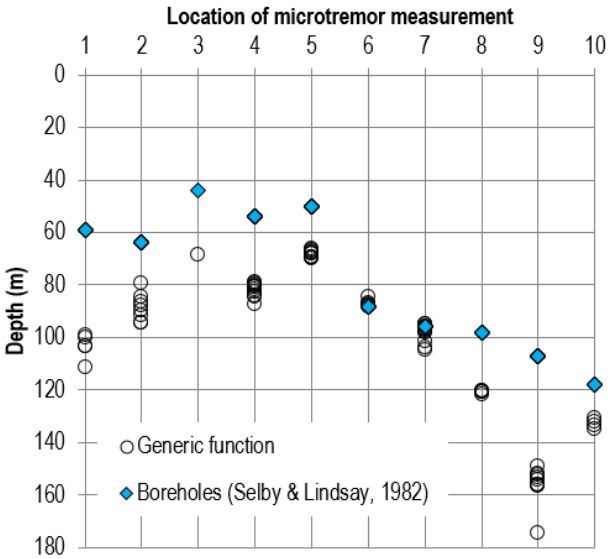

Figure 4.7 Interpreted bedrock depth (m) using the generic function at all locations compared against data from the nearest boreholes (Selby & Lindsay, 1982).

4.5 DISCUSSION

Correlations between the fundamental resonance periods at different sites and the bedrock depths estimated from (GF) and SPAC methods are examined. Figure 4.17 shows the analysis results from the various measurements acquired at the different sites investigated. The results obtained using the generic function (GF), in general, suggest an over-estimate when compared to the bedrock depths resulting from the boreholes, as shown in Figure 4.17(a). The largest error occurred at Location #09 (see Figure 4.7). Despite a rather large scatter, as shown in Figure 4.7, good agreement is obtained at two locations (Locations #06 and #07) using this method. The discrepancy between the bedrock estimates derived from the application of the GF and borehole data can be associated with the over- and under-estimation of the V_s of the overburden from the HVSR ellipticity curve.

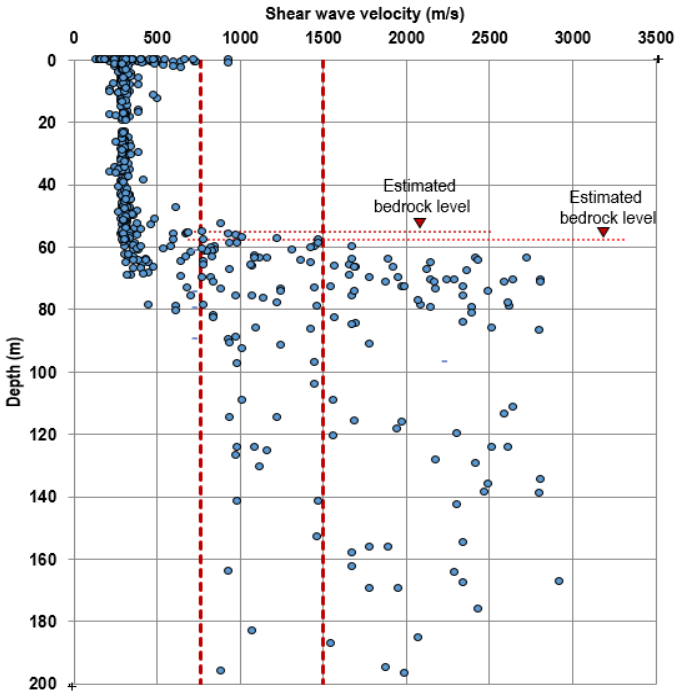

Figure 4.8 Typical interpreted bedrock depth using the SPAC method at Location #01. The dashed red lines represent the V_s bedrock threshold of 760 m/s and 1,500 m/s. The dotted red lines represent the level of estimated bedrock depths.

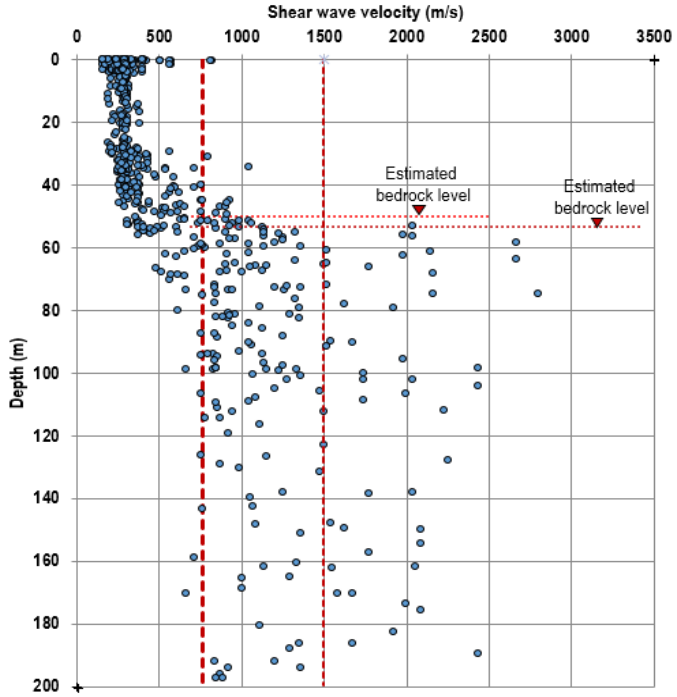

Figure 4.9 Typical interpreted bedrock depth using the SPAC method at Location #02. The dashed red lines represent the V_s bedrock threshold of 760 m/s and 1,500 m/s. The dotted red lines represent the level of estimated bedrock depths.

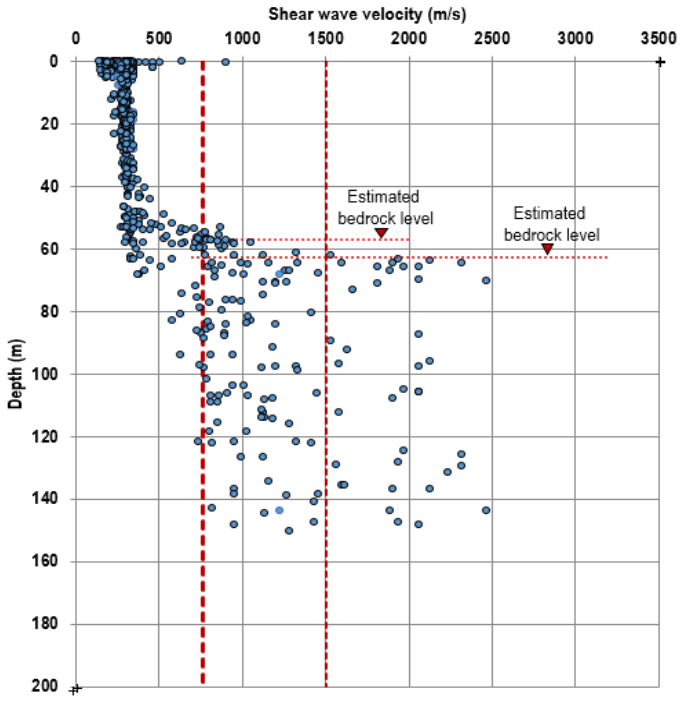

Figure 4.10 Typical interpreted bedrock depth using the SPAC method at Location #04. The dashed red lines represent the V_s bedrock threshold of 760 m/s and 1,500 m/s. The dotted red lines represent the level of estimated bedrock depths.

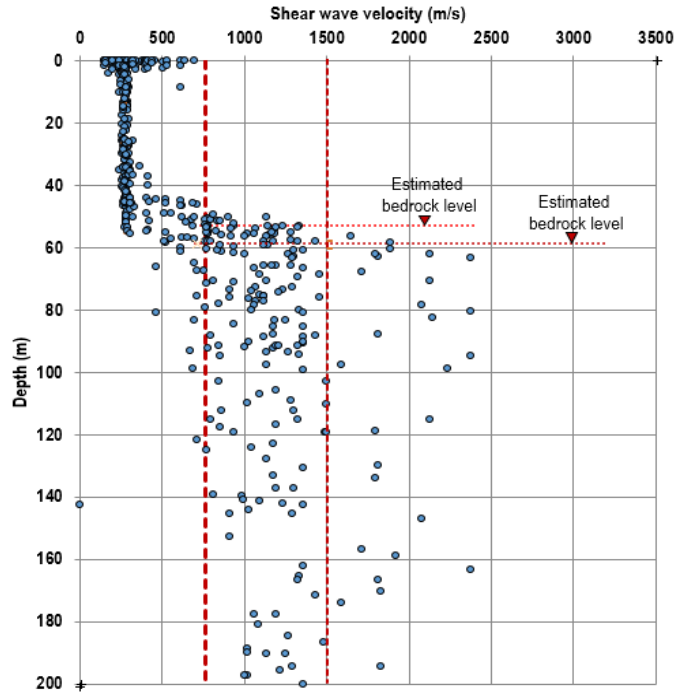

Figure 4.11 Typical interpreted bedrock depth using the SPAC method at Location #05. The dashed red lines represent the V_s bedrock threshold of 760 m/s and 1,500 m/s. The dotted red lines represent the level of estimated bedrock depths.

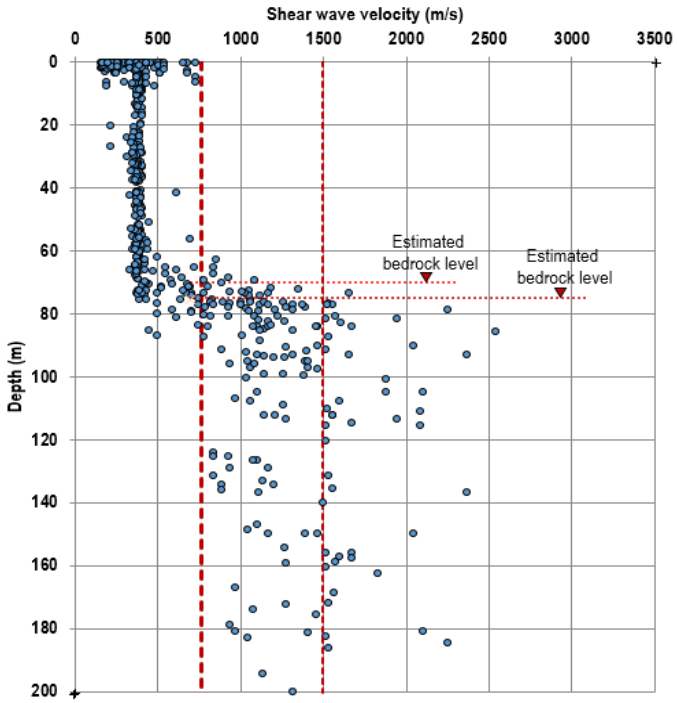

Figure 4.12 Typical interpreted bedrock depth using the SPAC method at Location #06. The dashed red lines represent the V_s bedrock threshold of 760 m/s and 1,500 m/s. The dotted red lines represent the level of estimated bedrock depths.

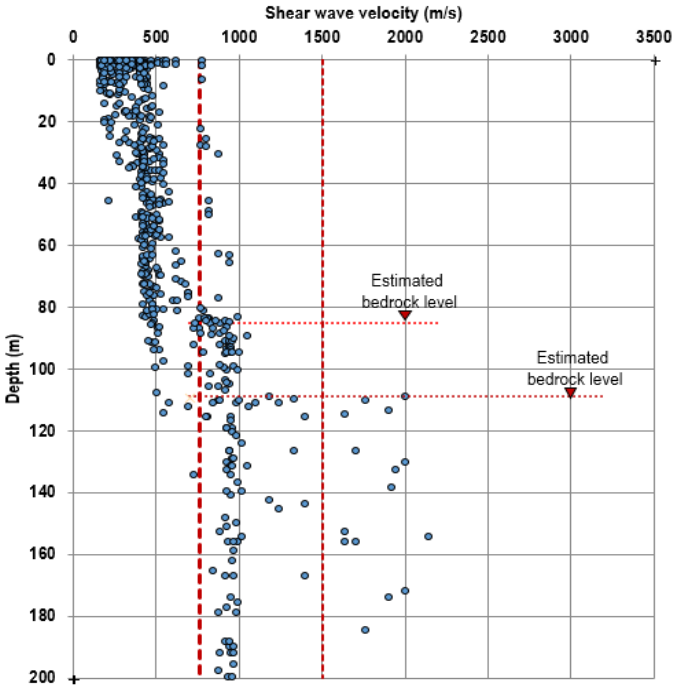

Figure 4.13 Typical interpreted bedrock depth using the SPAC method at Location #07. The dashed red lines represent the V_s bedrock threshold of 760 m/s and 1,500 m/s. The dotted red lines represent the level of estimated bedrock depths.

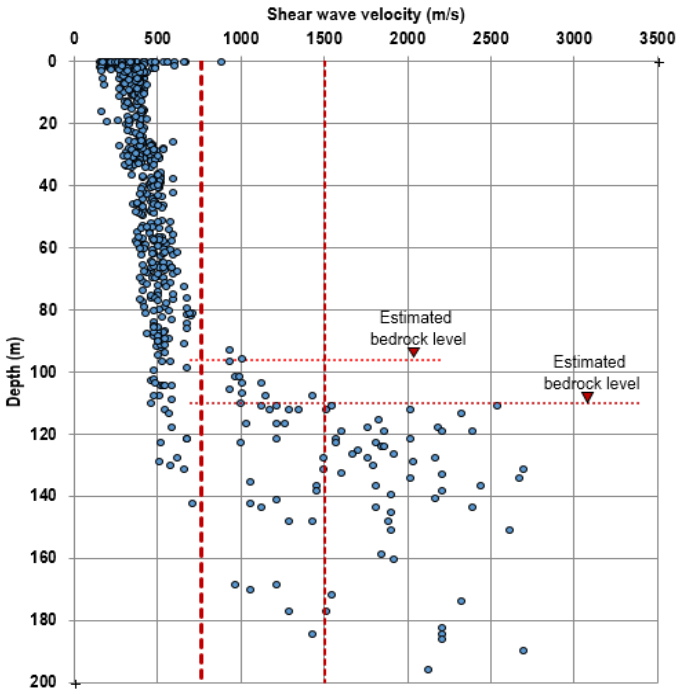

Figure 4.14 Typical interpreted bedrock depth using the SPAC method at Location #09. The dashed red lines represent the V_s bedrock threshold of 760 m/s and 1,500 m/s. The dotted red lines represent the level of estimated bedrock depths.

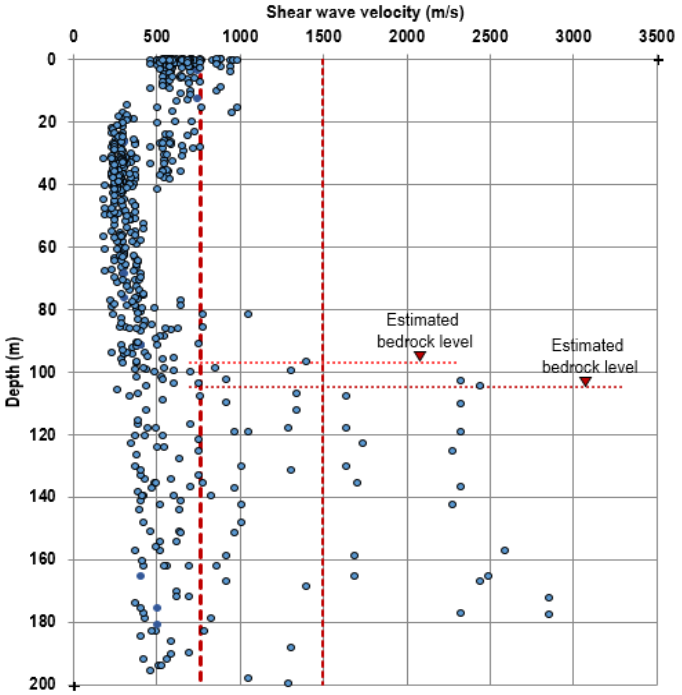

Figure 4.15 Typical interpreted bedrock depth using the SPAC method at Location #10. The dashed red lines represent the V_s bedrock threshold of 760 m/s and 1,500 m/s. The dotted red lines represent the level of estimated bedrock depths.

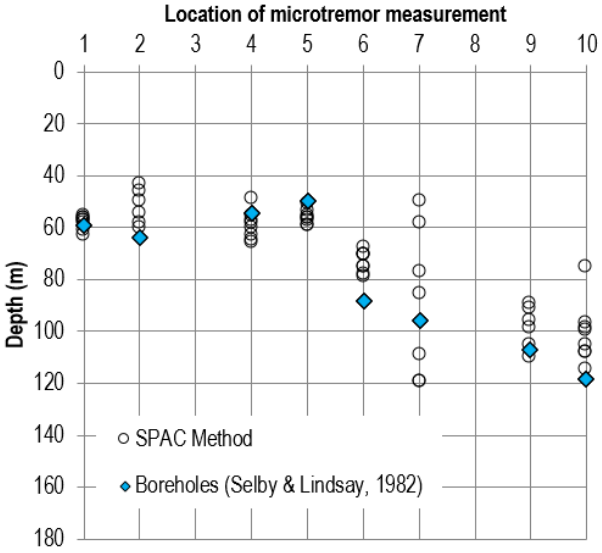

Figure 4.16 Summary of interpreted bedrock depths using the SPAC method.

In contrast to the previous method, the SPAC method provided bedrock depth values slightly under-estimated when compared with those derived from the boreholes, as shown in Figure 4.17(b), but in any case, better approximated to the real values in comparison to the GF results. As shown in Figure 4.16, most of the bedrock depth estimates from SPAC are within 6 m or less of the borehole data, except for Locations #06 and #07, where the maximum offset is 9 m and 13 m, respectively. This better accuracy of the SPAC estimates is further confirmed by plotting them with respect to the fundamental periods of the sites investigated, as shown in Figure 4.17(b). The regression line of best fit of the SPAC results is almost coincident with that of the borehole data.

Furthermore, the observed HVSR microtremor array data (observed HVSR) are compared with the computed ellipticity of the fundamental mode Rayleigh waves (calc. HVSR) for the inverted 1D simplified SPAC shear wave velocity profiles. The comparison is made to investigate the appropriateness of the inversion, even though the overburden shear wave velocity has no direct influence on the evaluation of bedrock depth using the SPAC method. Forward computing using Geopsy (2015) [calc. HVSR (Geopsy)], and Garcia-Jerez *et al*. (2016) [calc. HVSR (HVInv)] are employed to compute the calculated HVSR (calc. HVSR). The comparison of the observed and calculated HVSR curves, using logarithmic plots at all SPAC measured sites, is presented in Figure 4.18. Generally, the results of calculated HVSR using both Geopsy (2015) and Garcia-Jerez *et al*. (2016) are in good agreement. The comparison of the observed and calculated HVSR curves at all

SPAC measured sites suggests comparable results. At two sites (Locations #6 and #10) one of the theoretical curves shows good agreement with the observed HVSR curves. The remainder of the sites, in general, show over- or under-estimation of the experimental HVSR curves.

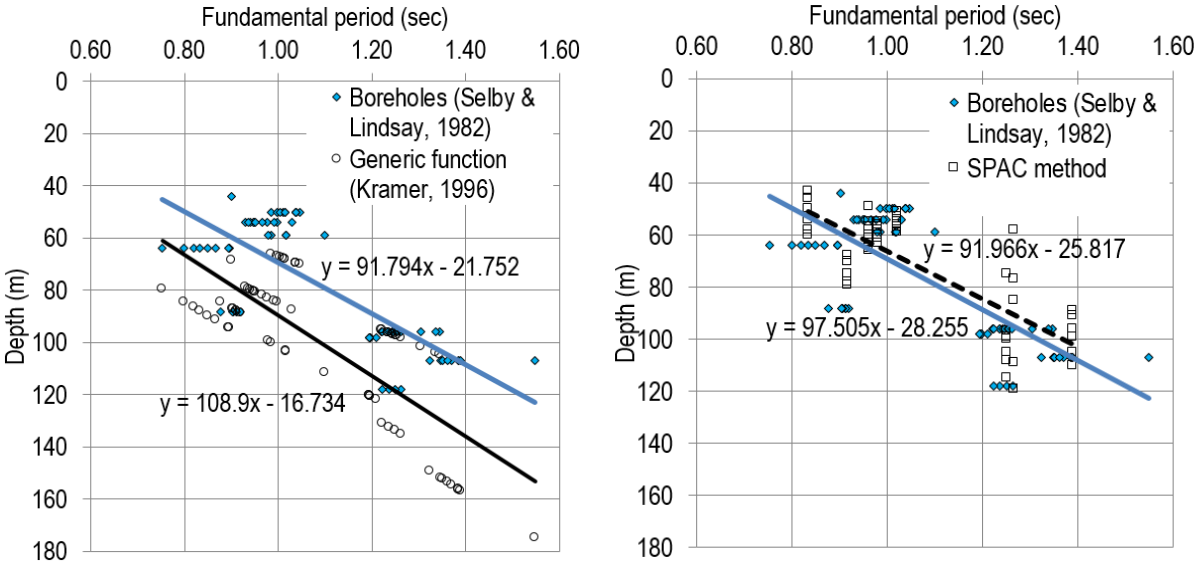

Figure 4.17 (a) Interpreted bedrock depths using the generic function method (Kramer, 1996) and (b) interpreted bedrock depths using the SPAC method.

In terms of the resonance frequency, the calculated HVSR of the SPAC V_s profile suggests a higher resonance frequency at all SPAC measured sites than the observed HVSR. This discrepancy may be attributed to the inclusion of other wave types in the Raleigh waves of the recorded noise. Thus, the observed HVSR should be treated with caution, as this observed HVSR is assumed to consist predominantly of fundamental Rayleigh waves. The inclusion of different waves with Raleigh waves can produce different HVSR curves (Bonnefoy-Claudet *et al*., 2006a; 2006b; Castellaro & Mulargia, 2009). Ideally, the other waves in this wavefield should be separated from the Raleigh waves. However, this task is difficult and contains many debatable issues (Bonnefoy-Claudet *et al*., 2006a; Poggi & Fah, 2010). Currently, there is very little information on the quantitative proportions of the different waves in ambient noise. Bonnefoy-Claudet *et al*. (2006a) suggested that low frequency ambient noise consists predominantly of fundamental Rayleigh waves, but this remains a topic for discussion at higher frequencies (f > 1 Hz). Furthermore, the HVSR curves obtained from Geopsy and HV-Inv, as shown in Figure 4.18, seem often to show stronger peaks for Geopsy than the HV-Inv ones. As

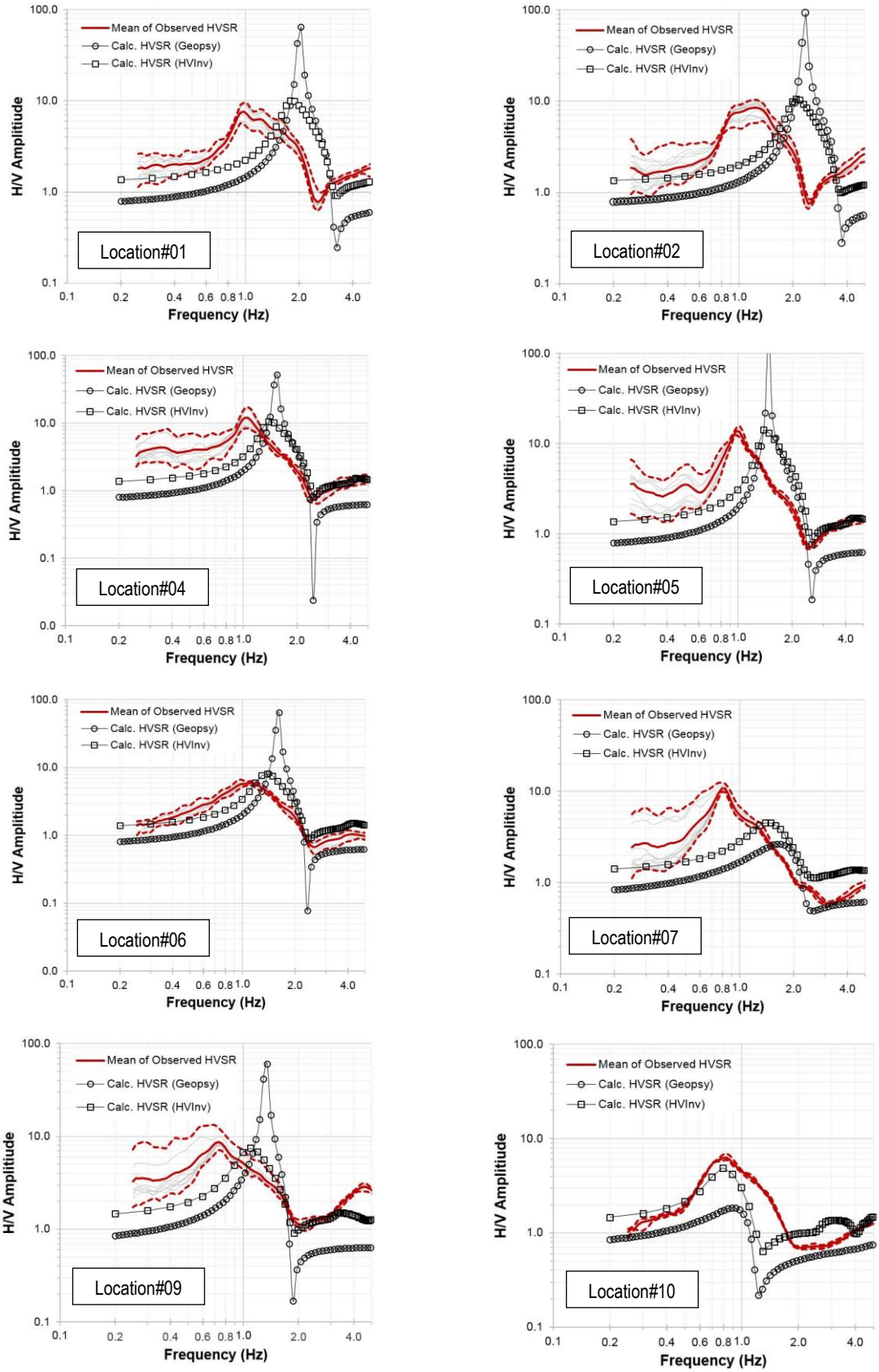

Figure 4.18 Comparison between the observed and calculated HVSRs at all SPAC measured sites.

the basic assumption of the calculated HVSR of the Geopsy model is that the HVSR corresponds to the ellipticity of Raleigh waves. Therefore, the stronger peak for Geopsy's HVSR curves is mostly due to singularities of Rayleigh wave ellipticity at the resonance frequency, whereas the Rayleigh vertical component tends to lose vertical-motion energy (*cf* Asten, 2004). Such sharp peaks in the HV-Inv's HVSR curves are smoothed by the contribution of other types of waves (i.e. body, Love) to the vertical component of the motion (*cf* Arai & Tokimatsu, 2004; Garcia-Jerez *et al*., 2016).

Both the GF and SPAC methods are compared directly to the bedrock depths obtained from the boreholes. Regression analysis is used for this purpose and the results are shown in Table 4.4, and Figure 4.19. As can be seen, good agreement is obtained between the bedrock depths predicted by ambient noise analysis and those physically observed from the boreholes. Furthermore, all the methods adopted in the present study are statistically analyzed to assess the accuracy of each method and to compare them. Here, the coefficient of correlation, *r*, the root mean squared error, RMSE, and the mean absolute error, MAE, are used to evaluate the methods. These three coefficients quantify the relative correlation and the goodness-of-fit between the estimated bedrock depth using the GF and SPAC methods and the actual bedrock level observed from the nearest boreholes. General guidelines, in relation to the absolute value of *r*, are suggested by Smith (1986) as follows: (a) $r \leq 0.2$ is an indication of weak correlation; (b) absolute of *r* between $0.2 < r < 0.8$ suggests moderate correlation; and (c) $r \geq 0.8$ is an indication of strong correlation.

The coefficient of correlation of *r*, RMSE, and MAE are calculated using:

$$r = \frac{n\sum y_j d_j - \left(\sum y_j\right)\left(\sum d_j\right)}{\sqrt{n\left(\sum y_j^2\right) - \left(\sum y_j\right)^2}\sqrt{n\left(\sum d_j^2\right) - \left(\sum d_j\right)^2}} \quad \text{.....(4.13)}$$

$$RMSE = \left\{\frac{1}{n}\sum_{j=1}^{n}\left(y_j - d_j\right)^2\right\}^{\frac{1}{2}} \quad \text{..... (4.14)}$$

$$MAE = \frac{1}{n}\sum_{j=1}^{n}\left|y_j - d_j\right| \quad \text{..... (4.15)}$$

where:

y_j = model (estimated) output, $y_j = y_1, y_2, y_3, ..., y_n$; d_j = desired (actual) output, $d_j = d_1, d_2, d_3, ..., d_n$; and n = the number of pairs of data.

Comparisons of the results of the validation set obtained using all the methods are presented in Table 4.4. Here it is observed that the SPAC method performs better than the GF method for all three performance measures considered. The coefficient of correlation, *r*, the RMSE, and MAE obtained using the SPAC model are: 0.83, 15.0 m and 11.5 m, respectively. In contrast, these measures are 0.80, 27.4 m and 22.3 m, respectively, for the GF method examined.

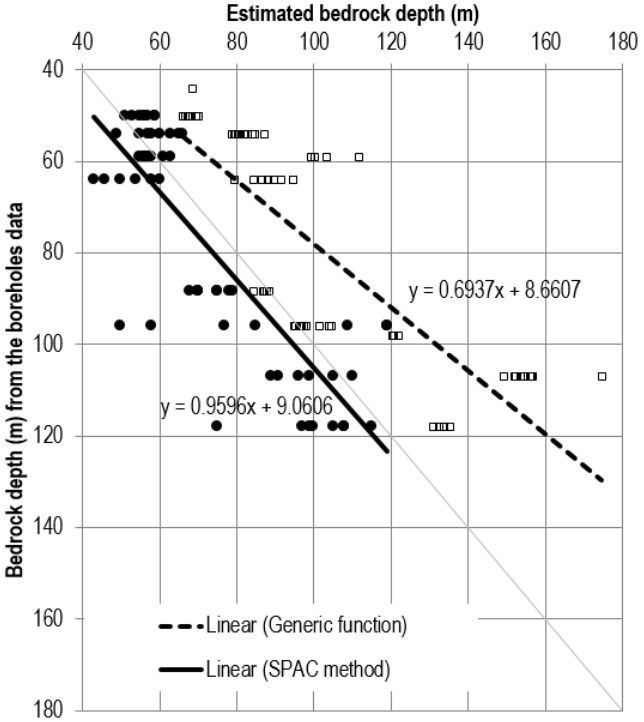

Figure 4.19 Comparison of results from both the GF and SPAC methods with bedrock depths from the boreholes using regression analysis.

Table 4.4 Statistical analysis of bedrock depth estimation using the GF and SPAC methods.

Performance measure	Generic function (Kramer, 1996)	SPAC		
		760 m/s	1,500 m/s	All
r	0.80	0.89	0.86	0.83
RMSE	27.4 m	16.8 m	12.9 m	15.0 m
MAE	22.3 m	13.4 m	9.6 m	11.5 m
Regression function	y = 0.6939*x* + 7.0522 for Generic function (Kramer, 1996); and y = 0.9596*x* + 9.0606 for SPAC			

The SPAC method is divided into the two different criteria for bedrock (i.e. shear wave velocities of 760 m/s and 1,500 m/s [BSSC, 2001]). The coefficient of correlation, *r*, RMSE, and MAE obtained using the 760 m/s criterion are 0.89, 16.6 m and 13.4 m, respectively and, for the 1,500 m/s criterion, these measures are: 0.86, 12.9 m and 9.6 m, respectively. This suggests that the 1,500 m/s criterion yields more accurate predictions of bedrock level than the 760 m/s criterion.

4.6 CONCLUSIONS

Local site effects need to be accounted for in seismic hazard assessment, as earthquake motions can be significantly amplified on soil sites and cause more severe structural damage, such as has occurred in many historical earthquakes around the world. The bedrock profile contributes to the amplification and de-amplification at the ground surface, as shown by the damage pattern of the Northridge, Sherman Oaks and Santa Monica earthquakes, for example. Therefore, information regarding bedrock depth is crucial in seismic hazard studies.

Considering the advantages of ambient noise analysis, this technique has been used in the investigation of bedrock level at many sites around the world, with most of these applications being for relatively thick homogenous, uniformly layered systems and strong impedance contrast sites, such as at the Lower Rhine Embayment and Cologne areas in Germany, Bangalore, India and Kathmandu, Nepal. Estimating the bedrock level using ambient noise analysis at regolith sites subjected to impedance contrasts in the low to high range is under-represented in the literature and, hence, requires further attention. This study seeks to address this need by investigating suitable methods to estimate the basement topography of regolith sites using microtremor observation. The case of Adelaide, the capital and largest city in South Australia, which exhibits site amplification and is founded on regolith, is investigated in the present paper. Ten microtremor measurements were obtained at various locations across Adelaide's central business district. At 8 locations a sensory array was used and at the remaining two, a single sensor was employed.

In order to estimate bedrock level, the paper presents analyses adopting the generic function (GF) and spatial autocorrelation (SPAC) method using the neighborhood algorithm (NA) inversion. The estimates are compared with boreholes drilled in close

proximity to the measurement locations and the results of the analyses suggest that the SPAC method outperforms the GF approach. This confirms that the microtremor SPAC method is an effective tool for estimating the bedrock depth at regolith sites.

INTENTIONALLY BLANK

Chapter Five

ESTIMATING NEAR SURFACE SHEAR WAVE VELOCITY USING THE SPAC METHOD AT A SITE EXHIBITING LOW TO HIGH IMPEDANCE CONTRAST

INTENTIONALLY BLANK

Statement of Authorship

Title of Paper	Estimating near surface shear wave velocity using SPAC method at a site exhibiting low to high impedance contrast
Publication Status	☐ Published ☐ Accepted for Publication ☑ Submitted for Publication ☐ Unpublished and Unsubmitted work written in manuscript style
Publication Details	Setiawan, B., Jaksa, M., Griffith, M., and Love, D., 2018. Estimating near surface shear wave velocity using the SPAC method at a site exhibiting low to high impedance contrast. Soil Dynamics and Earthquake Engineering, Under Review.

Principal Author

Name of Principal Author (Candidate)	Bambang Setiawan		
Contribution to the Paper	Performed field data collection, carried out analysis on all field data, interpreted the results, wrote the manuscript and acted as corresponding author.		
Overall percentage (%)	80%		
Certification:	This paper reports on original research I conducted during the period of my Higher Degree by Research candidature and is not subject to any obligations or contractual agreements with a third party that would constrain its inclusion in this thesis. I am the primary author of this paper.		
Signature		Date	14 June 2017

Co-Author Contributions

By signing the Statement of Authorship, each author certifies that:

i. the candidate's stated contribution to the publication is accurate (as detailed above);

ii. permission is granted for the candidate in include the publication in the thesis; and

iii. the sum of all co-author contributions is equal to 100% less the candidate's stated contribution.

Name of Co-Author	Mark Jaksa		
Contribution to the Paper	Overall percentage - 10% Supervised the development of work, helped in data interpretation and manuscript preparation. He also reviewed this manuscript rigorously.		
Signature		Date	14/6/17

Name of Co-Author	Michael Griffith		
Contribution to the Paper	Overall percentage - 5% Provided some valuable comments on the manuscript contents.		
Signature		Date	14/6/17

Name of Co-Author	David Love		
Contribution to the Paper	*Overall percentage - 5%* Helped the field data collection, evaluated and edit the manuscript.		
Signature		Date	14 June 2017

Please cut and paste additional co-author panels here as required.

5.1 INTRODUCTION

In areas of high seismic hazard risk, the reliable assessment of site amplification effects is crucial in the accurate prediction of ground accelerations of future, unexpected earthquakes. Such an assessment can be deduced from the damage characteristics resulting from historical seismic events. However, in low to moderate seismic regions, recorded historical events, which cover medium to high seismic magnitudes, are often unavailable. An alternative approach to quantify the effects of site amplification is based on the upper 30 meters of the shear wave velocity ($V_{s,30}$) ground profile. Such an approach is recommended by many national standards, such as the National Earthquake Hazards Reduction Program (NEHRP) (BSSC, 2001), European Standards (Eurocode 8, 2003), Standards New Zealand (Standards New Zealand, 2004) and Standards Australia (Standards Australia, 2007).

Several different techniques have been proposed to obtain subsurface shear wave velocity profiles. One approach adopted in practice is to use geological characteristics to estimate the mean shear wave velocity profile (e.g. Fumal, 1978; Bauer, 2004; Holser *et al.*, 2005). However, this technique requires detailed knowledge of the subsurface geology. An alternative approach, also used extensively in practice, makes use of conventional soil investigation techniques (e.g. standard penetration test [SPT] and cone penetration test [CPT]). Such penetration-based shear wave correlations have been used since 1966. A detailed overview of penetration-based shear wave velocity correlations is presented by Wair *et al*. (2012). More recently, an advanced seismic technique has been proposed, by making use of direct downhole or crosshole measurements (Lau, 2000; Luna & Jadi, 2000). However, these downhole and crosshole techniques require highly specialized and sophisticated equipment, which are generally costly and require significant amounts of time to perform the required tests.

In recent years, the application of surface waves has been demonstrated to produce reliable shear wave velocity profiles, relatively affordably and within a reasonable time frame (Bard, 1998; Puech *et al.*, 2004; Bonnefoy-Claudet *et al*., 2006). This surface wave technique is based on the assumption that, in heterogeneous, layered ground, surface waves are dispersive, or in the other words, the surface wave velocity depends on the

frequency of the induced waves (Aki & Richards, 2002). In essence, there are two main techniques which use surface wave dispersion to define the shear wave velocity profile and these are the active seismic source method – e.g. spectral analysis of surface wave (SASW) (Nazarian *et al*., 1983) and multi-channel analysis of surface waves (MASW) (Park *et al*., 1999) – and the passive source method (Aki, 1957; Nakamura, 1989; Bettig *et al.*, 2003; Asten, 2004; Picozzi *et al*., 2009; Asten *et al*., 2014; Garofalo *et. al*., 2016). These surface wave methods have been shown to be useful, efficient, non-invasive and relatively inexpensive. In urban areas, the passive source method has a further advantage in that it does not require a specific trigger (i.e. a hammer, blast or other controlled disturbance) to conduct the test. This passive source method uses ambient vibrations, which are present in a wide range of frequencies. Furthermore, the passive noise method can investigate the ground to greater depths than the active approach (Tokimatsu, 1997).

Recent developments in enhancing the passive source method to record surface waves in an array have been proposed by many researchers (e.g. Haubrich, 1968; Woods & Lintz, 1973; Harjes, 1990; Asten & Dhu, 1998; Kind, 2002; Ohori *et al*., 2002; Rost & Thomas, 2002; Kind *et al*., 2005; Schweitzer *et al*., 2011). Major advantages of the array passive source technique are: (1) the method can be used to define the source of the waves, and (2) the estimation of the shear wave velocity profile is more reliable than using a single station. Spatial autocorrelation (SPAC), introduced by Aki (1957), is one of the more reliable and more promising of the ambient vibration array techniques currently available (Roberts & Asten, 2008; Di Giulio *et al*., 2014; Asten *et al*. 2014). The basic assumption of this technique is that surface waves resulting from ambient noise can be regarded as the sum of waves propagating in a horizontal plane in different directions with different powers, but with the same phase velocity for a given frequency (Aki, 1965). Therefore, the phase velocity of these waves can be computed by estimating the spatial-correlation function for a fixed frequency without knowledge of the directionality of the waves. By varying the frequency, the phase velocity can be determined as a function of frequency. To capture the surface waves from all directions, as originally proposed, the microtremor SPAC method for phase-velocity determination requires measurement of noise data using sensors placed in a circular array, with an additional one located in the center of the array (Claprood, 2012). In many cases in urban areas, such a sensor layout is difficult to achieve. This constraint has hence led to a number of studies that have modified the

original SPAC method (e.g. Bettig *et al*., 2001; Cho *et al*., 2004; Cho *et al*., 2006; Tada *et al*., 2006).

This paper aims to: (1) investigate the applicability of the microtremor SPAC method to obtain the near surface shear wave velocity of a low to high impedance contrast site (≈ 3–5) (see Chapters 3 and 4), and (2) propose a new near surface shear wave velocity profile for Adelaide, South Australia. The improved subsurface shear wave velocity profile will provide more accurate site response analysis, including peak ground acceleration and peak ground velocity, at various sites across the city, which will also result in more resilient infrastructure and enhanced emergency response in the event of future earthquakes.

This paper presents the results of a series of measurements obtained from various sites located in the central business district of Adelaide, which was chosen because it is one of the Australian capital cities with the highest seismic risk in Australia (Leonard *et al*., 2013). Furthermore, Adelaide is the only Australian capital city that has experienced a seismic event in close proximity, which occurred on 1 March 1954. Known as the Adelaide Earthquake (Richter magnitude of 5.5 and at the depth of 4 km), this event injured three people, damaged many buildings in the city and the surrounding suburbs, cracked many houses, resulting in the collapse of many heavy parapets (Dyster, 1992), and at least 30,000 insurance claims were filed (McCue, 1975). Figure 5.1 presents a simplified geological map of the study site and the surrounding area, and includes the location of the 1954 Adelaide Earthquake.

In the present study, the methodology associated with the original SPAC method is adopted. A circular array, consisting of 6 identical seismometers, with an additional and identical seismometer placed in the center of the array, was deployed at all microtremor array measurement (MAM) sites. This hexagonal circular arrangement provided a better dispersion than the triangular one (Asten, 2006). For site characterization of the study area, the acquired data are analyzed using both the single-station (Nakamura, 1989; Lermo & Cha'vez-Garcia, 1993; Konno & Omachi, 1998) and array techniques (Aki, 1957; Wathelet *et al*., 2004).

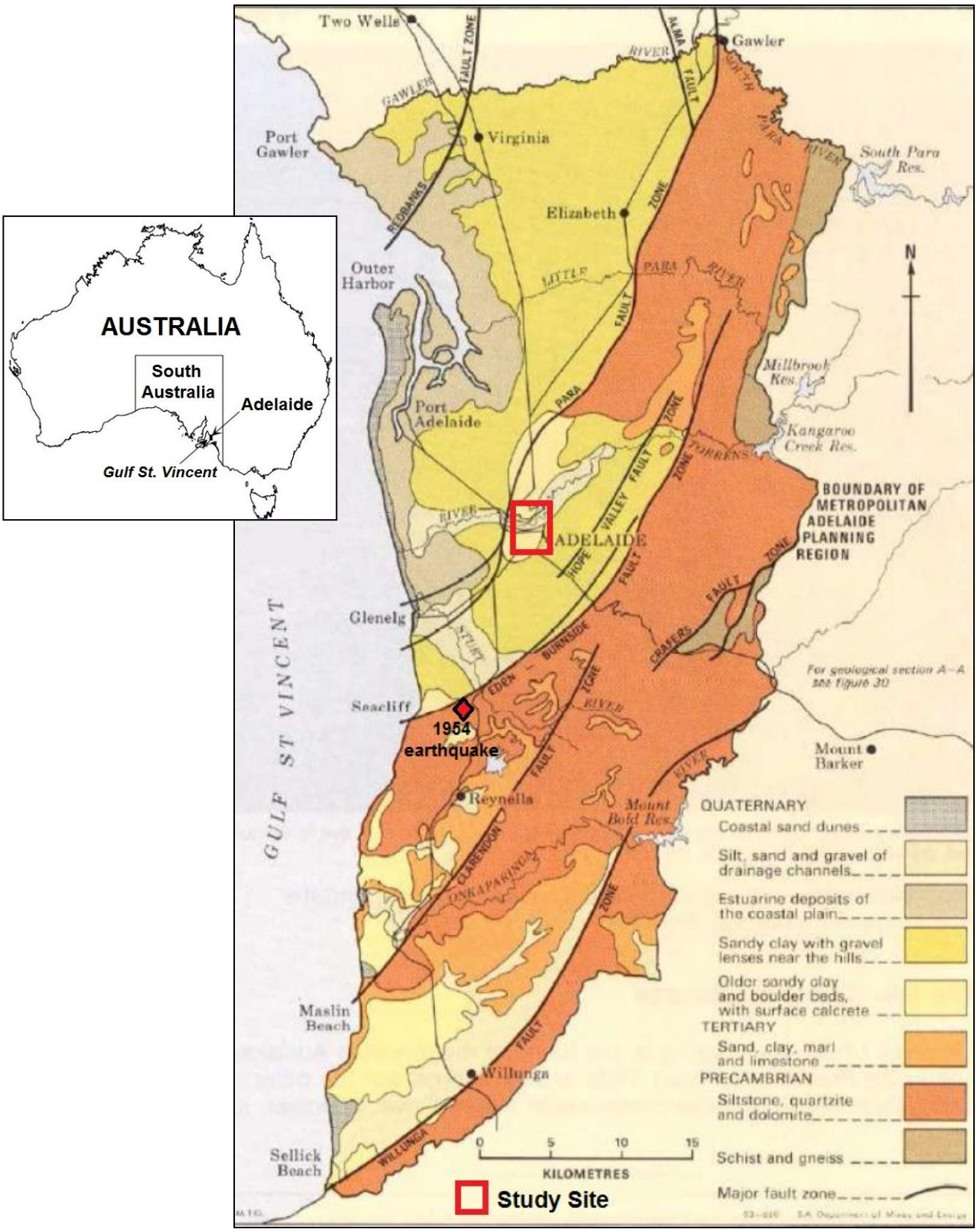

Figure 5.1 Locality of the study site and simplified geological map of the study site and the surrounding area (Selby, 1984).

5.2 SEISMICITY AND GEOLOGICAL FRAMEWORK

In terms of seismicity, Johnston (1996a), Celerier *et al*. (2005), and Hillis *et al*. (2008) categorized the Australian continent as a stable continent region (SCR). Furthermore, Veevers, (1984) classified the seismic activity in the Australian continent as low to moderate. The deformation rate of this region is higher than other SCRs (Hillis *et al*., 2008) and, hence historically, every five years or so the Australian continent is shaken by a seismic event of magnitude 6 or greater (McCue, 1990) (e.g. Meeberrie earthquake [1941; M_L 6.8], Meckering earthquake [1986; MS 6.8], Cadoux earthquake [1979; MS 6.4], Tennant Creek earthquake [1988; MS 6.3], and in Alice Springs [2016; MS 6.1]) (Johnston, 1996b; Crone *et al*., 1997; Sandiford *et al*., 2004; Boominathan *et al*., 2008; Geoscience Australia, 2016).

In the Australian SCR, Adelaide is within the most seismically active area (Sandiford *et al*., 2004; Quigley *et al*., 2006; Quigley *et al*., 2007). This prompted Malpas (1991) to carry out a comprehensive historical study of Adelaide by exploring seismically related historical records published in the local press, newspapers, meteorological records, and reports prior to the establishment of Adelaide's seismometer network, which is known as the 'pre-instrumental period.' This work identified at least 42 significant earthquakes in the Adelaide region. After the seismometer network was established in the Adelaide region in 1962, additional seismic events have been recorded. Furthermore, in South Australia there are at least 300 earthquakes (>ML 3.0) recorded annually and 15 seismic events of magnitude 5 or greater that have occurred in the last 150 years (Greenhalgh, 1994). Most of these contemporary seismic events have occurred in the Adelaide Geosyncline (Malpas, 1991; Celerier *et al*. 2005).

In terms of the geological framework, the structural geology of the Adelaide region is characterized by a series of faults oriented in the north-east to south-west direction. Several earthquakes associated with these faults have been documented (Selby, 1984). The most significant seismic event in recorded history is the Adelaide Earthquake which occurred on 1 March 1954, as mentioned above. It was associated with intra-plate activity along the Burnside-Eden Fault and exhibited a Richter magnitude of 5.5 (Selby, 1984; Love, 1996).

As shown in Figure 5.1, the city of Adelaide is bounded by the Para Fault to the west and the Eden-Burnside Fault to the east. These faults predominantly control the morphology of the city in the present day, as shown in Figure 5.2(a). The general morphology of the study site consists mainly of two plateaus in the north and south of the city, an upper outwash plain to the east of the city and lower an outwash plain to the west. The River Torrens, as shown, bisects the city from east to west.

Adelaide is located in the eastern part of the St. Vincent Basin. Most of the upper surface of the ground in the study area, below the surficial and fill layer, generally consists of Holocene stratigraphic units of the Callabonna Clay and the Pooraka Formation. A relatively narrow channel of another Holocene unit of alluvium occurs along the River Torrens, which traverses from east to west and may be up to 21 m thick (Selby & Lindsay, 1982; Sheard & Bowman, 1996). Below this is the Keswick Clay and, in some limited areas, the Hindmarsh Clay. Underlying these are units of either Carisbrooke Sand, Burnham Limestone or Hallett Cove Sandstone. Beneath these are either the Gull Rock member of the Blanche Point Formation, the sand unit of the Port Willunga Formation or the Tandanya Sand Member of the Chinaman Gully Formation (Selby & Lindsay, 1982). Underlying these, most of the sites in the Adelaide city area, encounter the South Maslin Sand and Clinton Formation, beneath which is Precambrian bedrock situated approximately 64 m or less below ground, to the north of the city, and up to 118 m or more to the south of the city (Selby & Lindsay, 1982). Furthermore, Selby & Lindsay (1982) also suggested more highly variable stratigraphic units to the south of the city than to the north. Further details of the geological units underlying the Adelaide City are given in Table 5.1 (after Selby & Lindsay, 1982).

5.3 HORIZONTAL TO VERTICAL SPECTRAL RATIO (HVSR) AND SPATIAL AUROCORRELATION (SPAC) ANALYSES

Generally, the analysis of HVSR is used to quantify the site fundamental frequency and single seismometer data can be used in this analysis. On the other hand, the SPAC method requires data obtained from multiple seismometers set out in an array. The following sections briefly describe these two analyses that are adopted in this study.

Table 5.1 A summary of the underlying stratigraphic units of Adelaide city (Selby & Lindsay, 1982; Sheard & Bowman, 1996).

Era, Periods, *Epoch*	Age in Millions of years	Geological Classification Name	Maximum Thickness (m)	Description
Cenozoic Quaternary *Holocene*	10,000 years	Alluvium of Torrens River	21	Red brown Silty CLAY; grades downwards to SAND and GRAVEL (SP-GP)
		Callabonna Clay		Red brown CLAY (CH)
		Pooraka Formation		Light brown Silty CLAY (CL-ML), calcareous with layers of calcrete GRAVEL (GM)
Cenozoic Quaternary *Pleistocene*	1.5	Keswick Clay	7	Grey-green CLAY (CH) with red and brown mottling, stiff to hard, fissured
		Hindmarsh Clay	16	Grey-green CLAY (CH) with yellow and red mottling with overlying SAND (SC)
		Carisbrooke Sand	13	Yellow, orange brown and grey, fine to medium Clayey and Silty SAND (SC/SM)
		Burnham Limestone	1 – 2	White Clayey, Sandy and rubbly LIMESTONE
Cenozoic Quaternary *Pliocene*	3	Hallett Cove Sandstone	12	Pale grey to brown calcareous SANDSTONE with layers of SAND (SP)
Cenozoic Quaternary *Eocene*	30 – 38	Port Willunga Formation	39	Sandy SILT and CLAY with strong CHERT nodules (GC-GP, ML, SM)
		Chinaman Gully Formation	12	Dark grey to black SILT and CLAY (ML-CL) with layer of Gravelly Clayey SAND (SC-GW)
		Blanche Point Formation	25	Alternating bands of cherty Siltstone and grey SILT (SM) overlying green to dark grey Clayey SAND (SC) and LIMESTONE
		South Maslin Sand	12	Grey to brown or yellow Silty SAND (SM) with pyrite lumps
	40	Clinton Formation	27	Dark grey CLAY (CL) with lignite; irregular Clayey SAND zones (SC)
Proterozoic		Pre-Cambrian bedrock		Brown, pink, grey to white weathered SILSTONE with quartz veinlets

5.3.1 Single station analysis of horizontal to vertical spectral ratio (HVSR)

The horizontal-to-vertical spectral ratio (HVSR) seismic method was first introduced by Nogoshi & Igarashi (1971) and was based on the initial studies of Kanay & Tanaka (1961). The method was extensively used and popularized by Professor Yutaka Nakamura, and hence the method has become well known as the Nakamura technique (Nakamura, 1989). The HVSR method is an experimental technique to evaluate the dynamic characteristics of the ground surface due to seismic vibrations. The method is based on the analysis of the spectral ratio between the Fourier amplitude spectrum of the horizontal (H) and vertical (V) components of the recorded ambient vibration (SESAME, 2004).

The HVSR technique (Nakamura, 1989) has been widely used in seismic hazard assessment because the method is straightforward, convenient and reliable, particularly in urban areas. Studies by Picozzi *et al*. (2009) and Mokhberi *et al*. (2010) have successfully implemented the HVSR technique in Turkey and Iran, respectively, for estimating the site resonance frequency. Despite some of the limitations inherent in this method, Di Stefano *et al*. (2014) and Wotherspoon *et al*. (2015) found that the HVSR method is quite robust for studies examining site effects, provided that the subsurface geological data of the targeted measurement are well defined.

5.3.2 Array station analysis of spatial autocorrelation (SPAC)

The basic premise of ambient noise array methods, used for the inversion of shear wave velocity profiles, is that the ambient noise wave field is composed mainly of surface waves (Tokamitsu, 1997; Bard, 1998). In the ambient noise vertical motion field, Rayleigh waves are assumed to be more dominant than body waves (Fah *et al*., 2003). This array method is widely used to obtain the site shear wave velocity profiles (i.e. Horike, 1985; Yamanaka *et al*., 1994; Horike, 1996; Tokimatsu, 1997; Chouet *et al*., 1998; Ishida *et al*., 1998; Miyakoshi *et al*., 1998; Satoh *et al*., 2001; Bettig *et al*., 2001; Scherbaum *et al*., 2003; Asten & Dhu, 2004). Given the assumptions that the site substructure is horizontally stratified and the ambient noise field is predominantly comprised of surface waves, the analysis of array measurement facilitates the generation of the autocorrelation and dispersion curves of the surface waves (Tokimatsu, 1997).

In the spatial autocorrelation analysis (SPAC) method, ambient vibration noise is considered as a temporal and spatial stochastic process. With these basic assumptions, the coherency spectra between all pairs of sensors in the array are evaluated. The coherency spectra are a measure of the similitude of ambient noise records from specific sensors for the frequency bandwidth investigated. The coherency spectra generated between all pairs of sensors in the array are azimuthally averaged over several inter-station separations (Henstridge, 1979; Cho *et al*., 2004) to determine spatially averaged coherency spectra, which have the shape of Bessel functions with respect to the shear wave profile (Aki, 1957). The principles of the method are described in detail by Okada (2003). Typical arrays used in practice are the centered triangular and hexagonal arrays (Claprood, 2012).

In the present study, a noise field measurement in a circular array is adopted for the SPAC method (Aki, 1957). In such a case, the spatial autocorrelation function is defined as:

$$\phi(r,\theta,\omega) = \overline{u(0,0,\omega,t)\cdot u(r,\theta,\omega,t)} \quad \text{..... (5.1)}$$

where ω is the frequency of the ambient noise harmonic waves, with the velocity wave forms of $u(0,0,\omega,t)$ and $u(r,\theta,\omega,t)$ observed simultaneously at $C(0,0)$ [the center of the array] and at $X(r,\theta)$ [a point in the array], respectively. The parameter $\overline{u(t)}$ is the average velocity of the wave forms in the time domain. The average of the autocorrelation function, ϕ, in all directions over the circular array is manifested as the spatial autocorrelation coefficient, ρ:

$$\rho(r,\omega) = \frac{1}{2\pi\cdot\phi(0,\omega)}\int_0^{2\pi}\phi(r,\theta,\omega)d\theta \quad \text{.....(5.2)}$$

where $\phi(0,\omega)$ is the SPAC function at the center $C(0,0)$ of the circular array. Re-writing Equation (5.2) by integrating Equation (5.1) yields:

$$\rho(r,\omega) = J_0\left(\frac{\omega r}{c(\omega)}\right) \quad \text{..... (5.3)}$$

where $J_0(x)$ is the zero-order Bessel function of the first kind of X and $c(\omega)$ is the phase velocity at frequency, ω. The computation of the spatial autocorrelation coefficient, $\rho(r,\omega)$, is calculated using the vertical component of the ambient noise (Di Giulio *et al.*, 2006); therefore $c(\omega)$ is assumed to be the phase velocity of the dispersion of the Rayleigh waves. Once the spatial autocorrelation coefficient of $\rho(r,\omega)$ at several frequencies is justified, then the velocity profile can be inverted using the inversion method.

5.3.3 SPAC array geometry, depth, and resolution and aliasing limits

Currently, there is no general consensus in terms of aperture size, shape and the number of sensors in the array measurement of ambient noise. Assuming that there is no particular ambient noise source to be captured at the targeted location, a circular array is suggested (Jongmans *et al.*, 2005). Asten & Henstridge (1984) recommended that the diameter of the array should be no less than the longest wavelength of interest and the station spacing should be less than half the shortest wavelength of interest. Furthermore, Asten & Henstridge (1984) also proposed the relationships between the minimum and maximum sensor spacing *(D_{min}* and *D_{max}*, respectively*)* and the minimum and maximum wavelengths (λ_{min} and λ_{max}, respectively) to achieve reliable measurements, as shown in the Equations (5.4) and (5.5).

$$\lambda_{\max} = 3D_{\max} \quad \text{(5.4)}$$

$$\lambda_{\min} = 2D_{\min} \quad \text{(5.5)}$$

Equation (5.4) was established from linear array, active source methods and is also applicable to ambient vibration arrays (Tokimatsu, 1997). This relationship is in good agreement with that suggested by Mokhberi *et al*. (2010), who proposed the maximum wavelength to be in the order of 2–4 times the maximum sensor spacing. Equation (5.5) was derived theoretically from the Nyquist wave-number. In the case of an irregular array geometry, Gaffet (1998) stressed that the λ_{min} limit obtained from the minimum sensor spacing may be inappropriate, as a minimum of two points per wavelength is difficult to achieve over the entire array.

The estimated depth of the investigation, d_{max}, that can be achieved using the array method is obtained from the λ/3 criterion of Tokimatsu (1997). The theoretical depth of investigation for an array is thus:

$$d_{max} = \frac{\lambda_{max}}{3} \quad \text{.....(5.6)}$$

The depth of penetration using the array method was also suggested by Xia *et al*. (2000) who estimated, for surface waves, penetration in the order of half of the maximum wavelength, λ_{max}. As a result, the maximum depth that a shear wave velocity, V_s, can be inferred from both the autocorrelation and dispersion curves is about $1.5D_{max}$. These empirical correlations suggest that a theoretical depth of at least 100 m is achievable using the largest aperture array in the present study.

Two additional and important aspects to consider when deducing the autocorrelation and dispersion curves are the resolution and aliasing limits. The resolution limit, k_{min}, is the minimum width of the central peak, whereas the aliasing limit, k_{max}, specifies the maximum radius of the concentric search region that is iterated until the amplitude exceeds 0.5 (Di Giulio *et al*., 2006). These limits are relevant for all processing techniques and define the limits of spatial aliasing. The actual numerical values of k_{min} and k_{max} depend on both the array size and its geometry. Theoretically, an estimate can be obtained using the array transfer function or theoretical beam pattern. Empirically Tokimatsu, (1997) defined the range of k_{min} and k_{max} to be within:

$$\frac{2\pi}{3D_{max}} < k_{min} < k_{max} < \frac{\pi}{D_{min}} \quad \text{.....(5.7)}$$

These two limits are considered to be reliable to evaluate both the autocorrelation and dispersion curves for array processing (Tokimatsu, 1997). In the case of a 50 m radius, for the circular hexagonal array used in the present study, as shown later, k_{min} and k_{max} are in the range of:

$$\frac{2\times 3.14}{3\times 100} < k_{min} < k_{max} = \frac{3.14}{50} \quad \text{.....(5.8)}$$

$$0.0209 < k_{\min} < k_{\max} = 0.0628 \quad (5.9)$$

The value of $k_{\min}$ was used in this study to constrain the resolution limits and the value of $k_{\max}$ was determined as high as possible to cover the upper 30 meters of the shear wave velocity ($V_{s,30}$) ground profile. Table 5.2 shows the values obtained for each of the trials for all microtremor array measurement (MAM) locations. As shown in Table 5.2, the constraint limit of $k_{\min}$ is within the range suggested by Tokimatsu (1997).

Table 5.2 Values of $k_{\min}$ and $k_{\max}$ adopted at each of the MAM locations.

Array name and location	Test	k_{min}	k_{max}
MAM#01 (Barton Tce W)	a	0.040	0.060
	b	0.025	0.060
	c	0.021	0.060
	d	0.025	0.055
MAM#02 (Lefevre Tce)	a	0.021	0.045
	b	0.024	0.035
	c	0.022	0.045
	d	0.025	0.045
MAM#03 (Finniss St)	a	0.030	0.062
	b	0.025	0.062
	c	0.025	0.062
	d	0.025	0.062
MAM#04 (Frome Rd/ War Mem. Dr)	a	0.021	0.060
	b	0.021	0.055
	c	0.021	0.060
	d	0.021	0.057
MAM#05 (West Tce/ Port Rd)	a	0.021	0.057
	b	0.021	0.055
	c	0.026	0.050
	d	0.026	0.050
MAM#06 (Bartels Rd)	a	0.021	0.062
	b	0.021	0.062
	c	0.021	0.057
	d	0.021	0.057
MAM#07 (South Tce/ West Tce)	a	–	–
	b	0.021	0.035
	c	0.021	0.050
	d	0.021	0.050
MAM#08 (Hutt Rd/ South Tce)	a	0.021	0.062
	b	0.021	0.062
	c	0.021	0.062
	d	0.021	0.062
Notes: *: One of the seismometers was unable to record data.			

5.4 METHODOLOGY

The following sections describe the acquisition of the ambient noise data, estimation of the site fundamental frequency using the HVSR method and the development of the subsurface shear wave velocity profile.

5.4.1 Array ambient noise data acquisition

The ambient vibration array data were acquired using 7 identical seismometers. A hexagonal layout, with a radius of 50 m and an additional seismometer in the center, was used as shown in Figure 2(b). This hexagonal configuration was selected to obtain surface waves from all directions; therefore, the stations were each arranged at an angle of 60° from one another to obtain the widest azimuthal coverage. This hexagonal geometry was also selected due to the unknown nature of the specific source zones around the measured sites. The data were collected over a minimum period of two hours, as indicated in Table 5.3. The geographical coordinates (latitude and longitude) of the array center, site characteristics and the conditions during measurement are also given in Table 5.3. The instrumentation consisted of 7 portable digital Kelunji stations equipped with 1 Hz Le3Dlite seismometers, as shown in Figure 5.2(c). The adopted sampling rate was 100 Hz and filtering was applied. All of the seismometers were protected by a plastic container and oriented to geographic North. A total of 8 microtremor array measurements were obtained, as shown in Figure 5.2(a). An example of the recorded ambient vibration array data is shown in Figure 5.3. Field survey data sheets are provided in Appendix E.

5.4.2 Site fundamental frequency assessment

As mentioned above, the site fundamental frequency is computed using HVSR analysis. Initially, single station processing of the horizontal vertical spectral ratio (HVSR) technique is carried out on the recorded ambient vibration data, using 3 of the 7 stations used in the present study. These stations were selected randomly in a triangular configuration. The HVSR analysis was undertaken using the Geopsy software, which is part of the SESAME project (Geopsy, 2018). This method allows the identification of the fundamental resonance frequency at each site. In general, the resonance frequency obtained using Geopsy, within the study site using this method, lies in the range between 0.79 to 1.1 Hz.

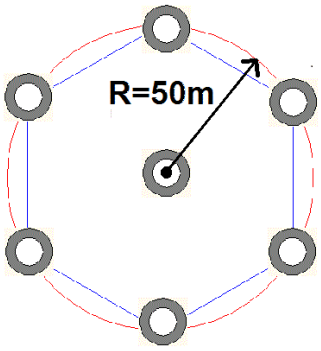

(a)

(b)

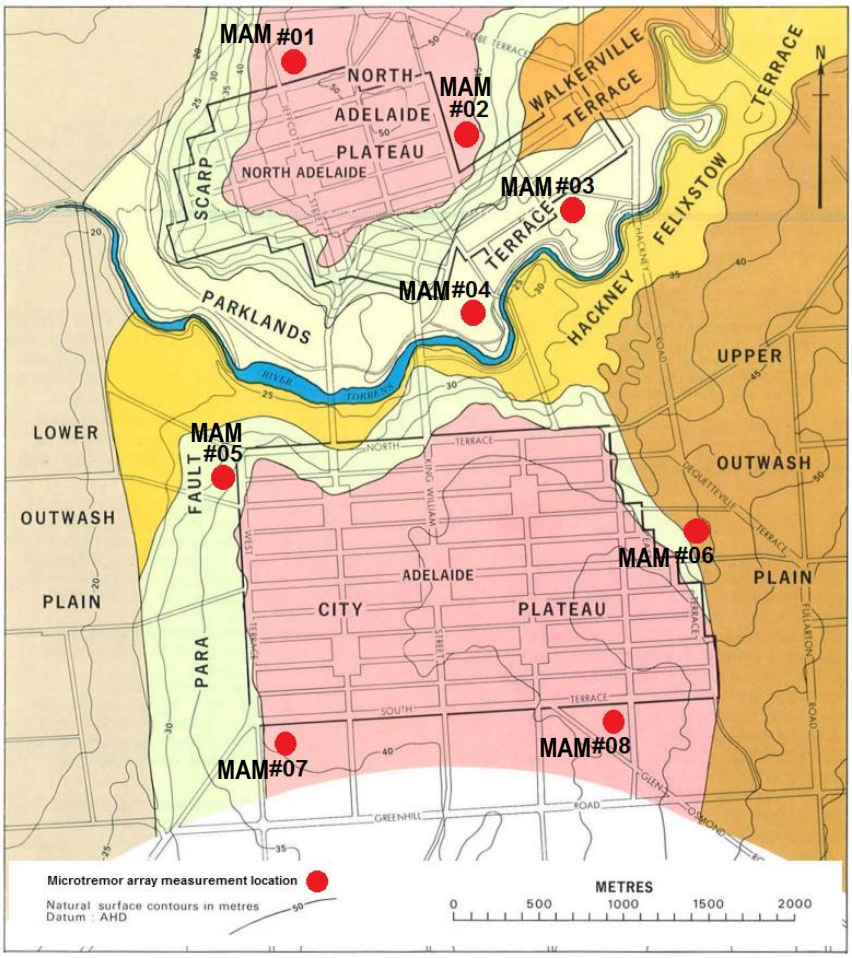

(c)

Figure 5.2 Details of microtremor array measurement (MAM): (a) Array layout; (b) LE3DLite Lennartz seismometer Kelunji Data Recorder; and (c) Location plan incorporating morphology of the study area (Selby & Lindsay, 1982).

According to the SESAME (2004) recommendations, the initial step in computing the spectral ratios is to divide the time series of each HVSR component into windows. The objective of this initial step is to select and retain stationary parts of the ambient vibration excluding transient waves, which are usually associated with unnecessary specific sources, such as nearby human and vehicular traffic. In each selected window, the time series of each HVSR component is smoothed using a filter and SESAME (2004) suggests constant bandwidth smoothing is inappropriate for low frequencies and, hence, should be avoided. Subsequently, the HVSR spectral ratio is computed using the merged horizontal components for each selected time window. In doing so, SESAME (2004) recommends using the geometric mean to combine the two smoothed horizontal components of the surface waves. Finally, the obtained HVSR spectral ratios are averaged and the standard deviations computed.

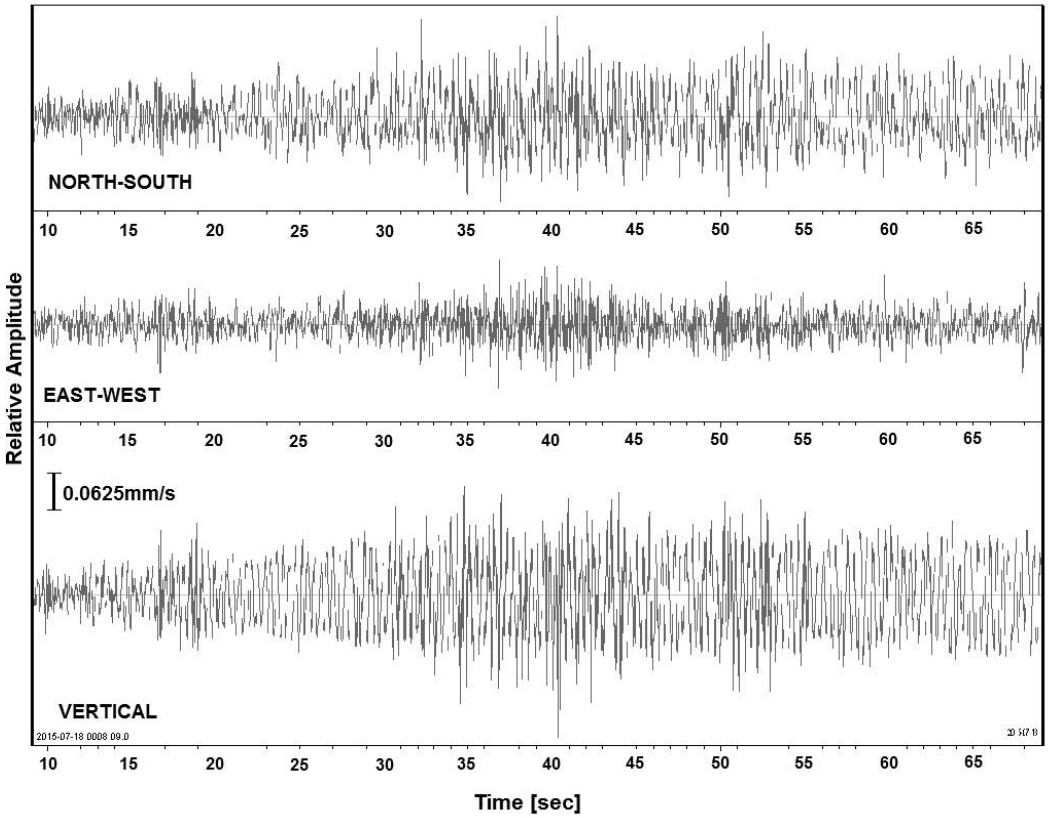

Figure 5.3 Example of seismic vibration component data acquired at each array station for the North-South (top), East-West (center) and vertical directions (bottom).

5.4.3 Evaluation of SPAC dispersion curve

The analysis of the array measurements can facilitate the evaluation of the dispersion curves of the surface waves provided that the site subsurface stratigraphy is horizontally stratified and the ambient vibration field is comprised predominantly of surface waves (Tokimatsu, 1997; Okada, 2003). In the present study the evaluation of the dispersion curve is carried out using the SPAC technique (Aki, 1957). SPAC is based on both the measurement of spatial coherence of the steady waveforms and non-correlated sources, randomly distributed in space and time (Bettig *et al*., 2001). In the present study the dispersion or autocorrelation curves for each array are developed based only on the vertical components of the acquired microtremor data using Geopsy (Geopsy, 2018). The data are pre-processed using a classical procedure for signal synchronization and the mean and trend elimination, which is implemented in seismic analysis code (SAC) algorithms (Goldstein *et al*., 2003). The dispersion curve was selected by using resolution

and aliasing limits, as mentioned above. The use of several trials at each array location in the present study allows investigation of the variability and consistency of each test. Figures 5.4 and 5.5 show the dispersion curves obtained for all trials, which are subsequently used to compute the shear wave velocity profiles. The "trials" indicated in Figures 5.4 and 5.5 correspond to a different dataset collected at the same location. These are discussed in detail later in this thesis.

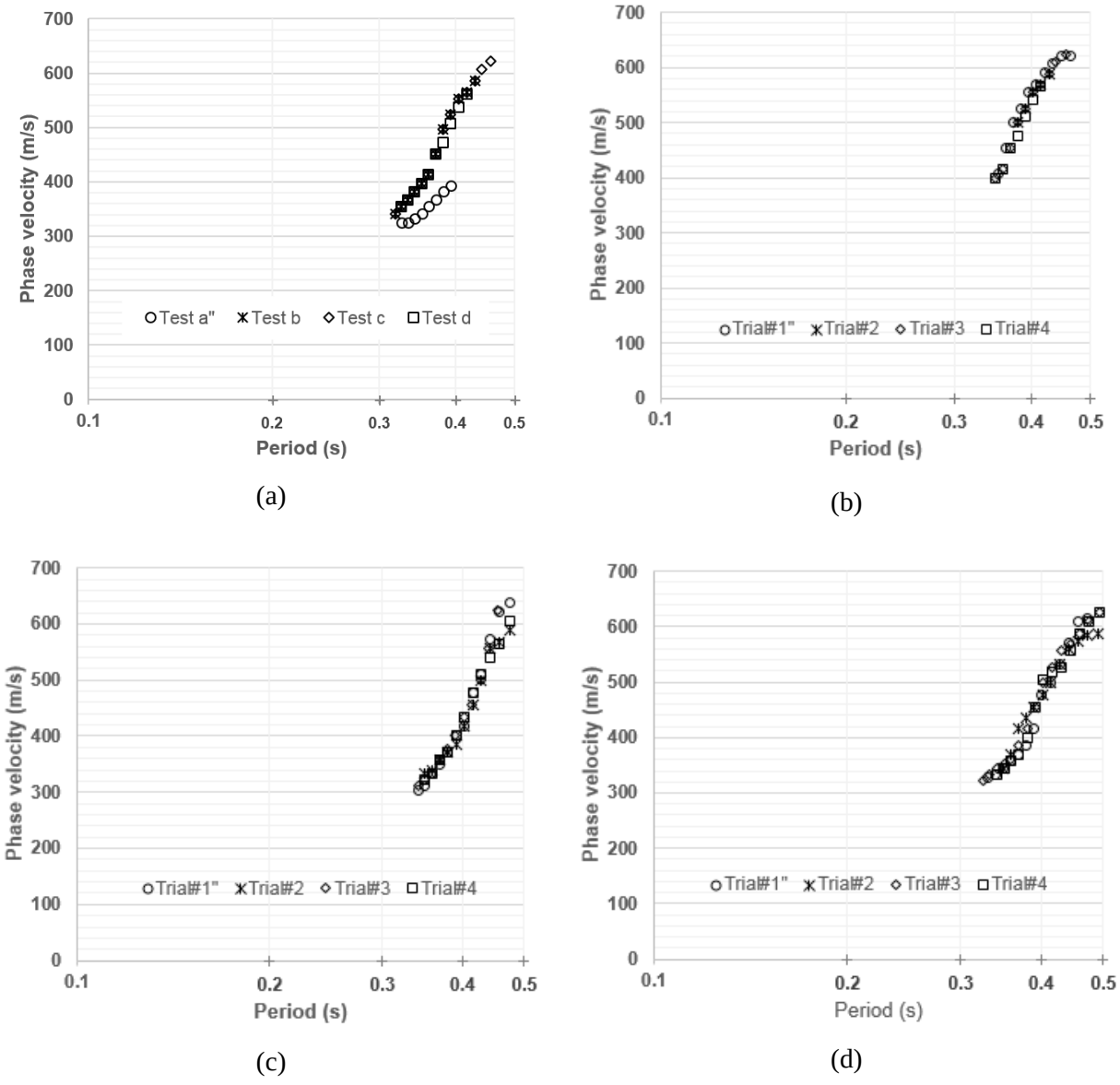

Figure 5.4 Dispersion curves obtained from all tests at Locations (a) #01, (b) #02, (c) #03, and (d) #04.

Table 5.3 Timetable and field records of all microtremor array measurement (MAM) locations.

Array location name with the center coordinates	Starting	Ending	Remarks
MAM#01 Lat/Long -34.936/138.612	2015-06-16 02:00AM	2015-06-16 04:30AM	No wind, no rain, temperature about 16 degrees, hard dry earth ground with short grass, situated on a flat parkland with mostly a single storey housing nearby at the south and aquatic center at the north-west sides. All seismometers were set on the open area with relatively far from any structures including tall trees.
MAM#02 Lat/Long -34.936/138.612	2015-07-02 03:30AM	2015-07-02 05:43AM	Weak wind, no rain, temperature about 17 degrees, hard dry earth ground with short grass, situated on a relatively flat parkland with some tall trees and nearby mostly a single storey housing on the south and west sides. Five of seven seismometers were set relatively close to tall trees (about 3 meters away).
MAM#03 Lat/Long -34.936/138.612	2015-07-01 01:10AM	2015-07-01 03:30AM	Weak wind, weak rain, temperature about 16 degrees, hard dry earth ground with short grass, situated on a flat parkland with mostly two storey housing nearby at the north side.
MAM#04 Lat/Long -34.936/138.612	2015-06-18 04:00AM	2015-06-18 05:59AM	No wind, no rain, temperature about 14 degrees, hard dry earth ground with short grass, situated on a flat parkland with single storey structures nearby at the north and Torrens River at the south sides.
MAM#05 Lat/Long -34.936/138.612	2015-06-30 01:36AM	2015-06-30 03:42AM	No wind, no rain, temperature about 16 degrees, hard dry earth ground with short grass, situated on a relatively flat parkland with a 6-7 storey under construction new hospital building nearby on the north side and three storey buildings at east sides.
MAM#06 Lat/Long -34.936/138.612	2015-07-08 03:00AM	2015-07-08 05:00AM	Weak wind, no rain, temperature about 16 degrees, hard dry earth ground with short grass, situated on a relatively flat parkland with a single storey shed at the north side.
MAM#07 Lat/Long -34.936/138.612	2015-06-25 02:00AM	2015-06-25 03:39AM	No wind, no rain, temperature about 16 degrees, hard dry earth ground with short grass, situated on a flat parkland. Seismometer Box 6 was set nearby a tree (about 10 meters).
MAM#08 Lat/Long -34.936/138.612	2015-06-15 04:38AM	2015-06-15 06:24AM	No wind, weak rain, temperature about 16 degrees, hard dry earth ground with short grass, situated on a flat parkland with mostly 2-3 storey buildings nearby at the north side.

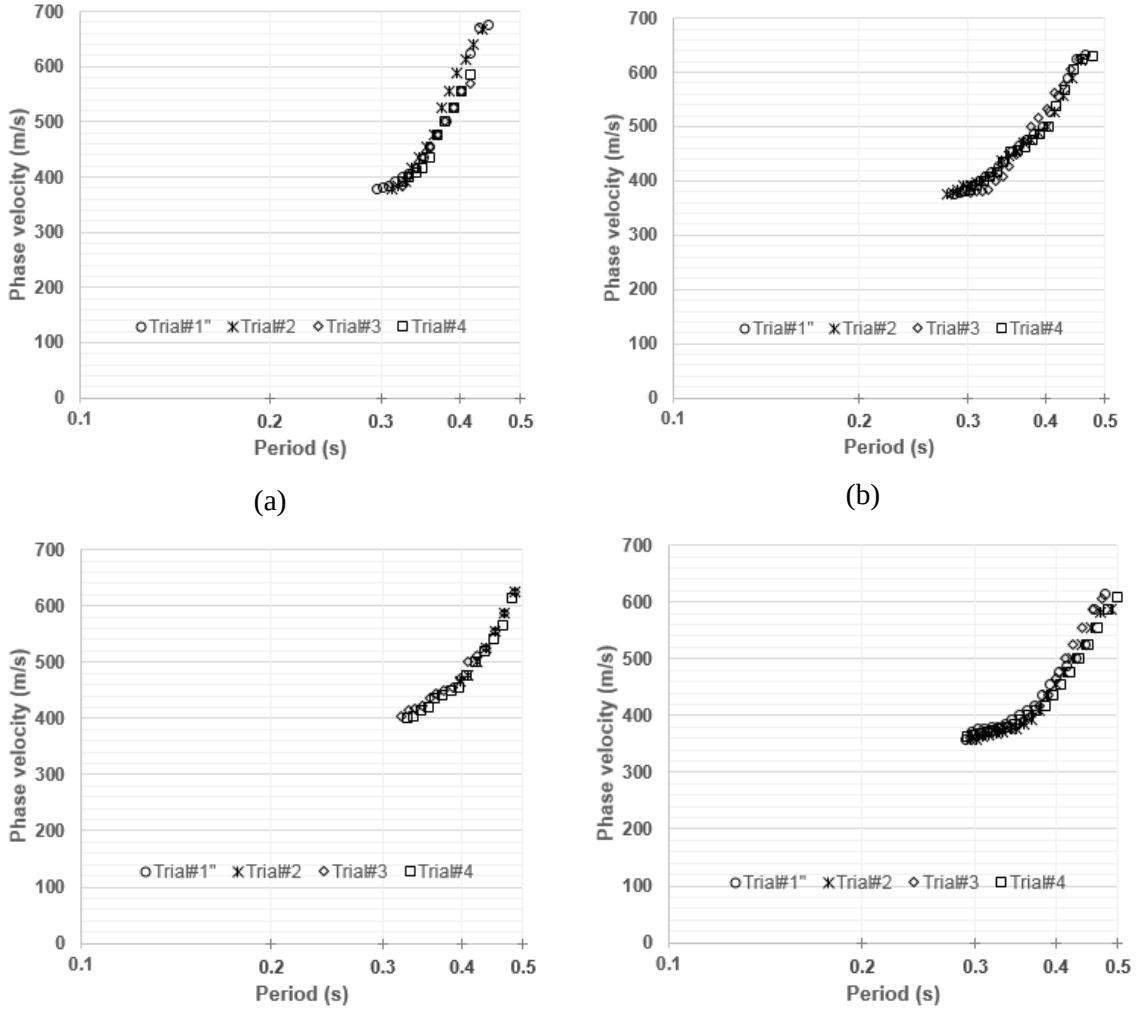

Figure 5.5 Dispersion curves obtained from all tests at Locations (a) #05, (b) #06, (c) #07, and (d) #08.

5.4.4 Shear wave velocity inversion

The neighborhood algorithm of Sambridge (1999), implemented by Wathelet (2005) and Wathelet *et al*. (2005, 2008), is employed to invert the surface wave dispersion (or autocorrelation) curves and obtain the shear wave velocity profiles associated with the test area. This implementation allows the generation of random velocity models for computing the theoretical dispersion curves. To identify the best shear wave velocity model, the theoretical dispersion curves are compared to the measurements. This comparison facilitates the computation of the misfit to justify the offset of the theoretical model to that measured, as follows:

$$misfit = \sqrt{\sum_{i-1}^{n_F} \frac{\left(x_{di} - x_{ci}\right)^2}{\sigma_i^2 n_F}} \quad \text{.....(5.10)}$$

where x_{di} is the experimental velocity at frequency f_i; x_{ci} is the theoretical velocity at frequency f_i; σ_i is the uncertainty of the frequency samples considered; and n_F is the number of frequency samples. The selection of the inversion, i.e. the final shear wave velocity model, should ideally be the model with the lowest misfit value.

As with all classical inversion procedures, one needs to define the data to invert and the parameters to evaluate. In the present case, the data are represented by the dispersion curves (Figures 5.4 and 5.5) of the vertical component of the ambient vibration. The input parameters are the limit estimates of the P-wave and S-wave velocities, the Poisson's ratio and the density. In the present study, each of these parameters is related to soil layers of fixed thickness, as the subsurface stratigraphy model is relatively well documented (Selby & Lindsay, 1982). The parameters are hence based on studies by Selby & Lindsay (1982), Jaksa, (1995), McPherson & Hall, (2007) and McBean, (2010), as summarized in Table 5.4.

By adopting these data, and to investigate the robustness of the inversion, at least three inversion processes are carried out using different seeds (i.e. starting models). At least 12,500 models are explored for each run. The best 20 models are extracted from each run and then combined, from which the mean and median shear wave velocities are deduced for each layer. The best 20 models are associated with the 20 lowest misfits from the obtained dispersion curves. Further inversion of the mean best 20 models is carried out based on the mean observed HVSR curve for the measured site. ModelHVSR of Herak (2008) was employed to perform this inversion.

5.5 RESULTS AND DISCUSSION

This section examines the results of the site fundamental frequency, which are obtained from the single station HVSR analysis, the dispersion curves and shear wave velocity profiles.

Table 5.4 Input parameters adopted for the constrained modelling.

Formation ***Epoch***	**Code**	**Compression wave velocity (m/s)**	**Shear wave velocity (m/s)**	**Poisson's ratio**	**Density (kg/m^3)**
Quaternary Alluvium, Pooraka Formation, *Holocene*	A	200–1000	150–500	0.3–0.5	18–20
Keswick Clay, *Pleistocene*	A1	200–1000	150–500	0.3–0.5	18.5–20
Hindmarsh Clay, *Pleistocene*	A2	200–1000	150–500	0.3–0.5	18.5–20
Carisbrooke Sand, *Pleistocene*	B	200–1000	150–500	0.2–0.3	18–20
Burnham Limestone and Hallett Cove Sandstone, *Pleistocene–Pliocene*	C	200–1000	150–500	0.2–0.3	18–20
Sand unit of Port Willunga Formation, *Eocene*	D	200–1000	150–500	0.2–0.3	18–20
Tandanya Sand Member of Chinaman Gully Formation, *Eocene*	E	200–1000	150–500	0.2–0.3	18–20
Gull Rock Member of Blanche point Formation, *Eocene*	F	200–1000	150–500	0.3–0.4	18–20
Undifferentiated basal Blanche Point Formation and Tortachilla Limestone, *Eocene*	G	200–1000	150–500	0.2–0.3	18–20
South Maslin Sand, *Eocene*	H	200–1000	150–500	0.2–0.4	18–20
Clinton Formation, *Eocene*	J	200–2000	150–1000	0.2–0.3	18–20
Precambrian bedrock, *Precambrian*	K	700–5000	500–3500	0.2–0.25	20–24

5.5.1 Site fundamental frequency

As mentioned above, estimation of the site fundamental frequency is carried out using HVSR analysis of 3 of the 7 stations in each array. At least 4 sets of ambient vibration data from each station are used in the HVSR analysis. Hence, at least 12 HVSR analyses are undertaken for each array. Reliability analyses are then performed using the SESAME (2004) guidelines. Only those HVSR curves that satisfy the reliability criteria are used to define the measured site fundamental frequency. A summary of the results for all array locations is presented in Table 5.5. In general, the measured site fundamental frequency of between 0.7 and 1.2 Hz, obtained from single station analysis of data from the MAM

stations, is in good agreement with the fundamental site frequency of 1 Hz suggested by McCue & Love (1997) for most of the Adelaide city.

The site fundamental frequency is also estimated by forward modeling of the shear wave velocity profiles, as shown later. This site fundamental frequency is herein referred to as the 'calculated site fundamental frequency.' Three forward modeling methods (i.e. Bardet *et al*., 2000; Herak, 2008; and Geopsy, 2018) are used for estimating this fundamental frequency, as shown in Table 5.5. A comparison of all calculated fundamental frequencies is given in Figure 5.6, which shows that the fundamental frequency obtained using forward modeling is appropriate for estimating the site fundamental frequency. These calculated site fundamental frequencies are used to validate the measured site fundamental frequencies. It can be observed that the measured fundamental frequencies for the study site are comparable to the results for all array sites.

Table 5.5 Measured and calculated site fundamental frequency of all MAM locations.

Array name and location	Fundamental frequency Hz)			
	Measured	Calculated		
		Ref. A	Ref. B	Ref. C
MAM#01 (Barton Tce W)	1.02	1.0	0.97	1.03
MAM#02 (Lefevre Tce)	1.20	1.2	1.12	1.21
MAM#03 (Finniss St)	1.04	1.0	1.02	1.06
MAM#04 (Frome Rd/ War Mem. Dr)	0.98	1.0	0.97	0.97
MAM#05 (West Tce/ Port Rd)	1.09	1.0	1.07	1.12
MAM#06 (Bartels Rd)	0.79	0.8	0.81	0.82
MAM#07 (South Tce/ West Tce)	0.72	0.6	0.74	0.73
MAM#08 (Hutt Rd/ South Tce)	0.80	0.8	0.77	0.85
Note: Ref. A is Bardet *et al*. (2000), Ref. B is Geopsy (2018), and Ref. C is Herak (2008).				

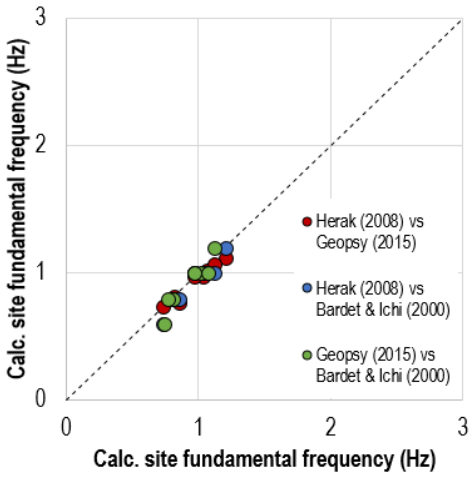

Figure 5.6 Comparison of calculated site fundamental frequency for all approaches.

5.5.2 Dispersion curve

As mentioned above, the dispersion curves obtained from each of the MAM locations tested were presented in Figures 5.4 and 5.5. Four trials at each MAM site are computed to confirm the reliability of the deduced dispersion curve. The results suggest good consistency in all trials at all MAM locations, except for Trial#4 at MAM#01, as shown in Figures 5.4 and 5.5. Therefore, Trial#4 of MAM#01 was exempted from further analysis as some technical abnormalities during field measurement contributed to this discrepancy. All of these dispersion curves, which correspond to the autocorrelation curves, are used to invert the shear wave velocity profiles.

Figures 5.7 and 5.8 show the fundamental Rayleigh-wave dispersion curves derived from the inversion process, for all of the models, in order to assess the appropriateness of the model. These dispersion curves are compared against the experimental model, which are identified by black circles. It is clear that the theoretical dispersion curves, which are the derived dispersion curves of the best 20 inverted models, agree well with the experimental dispersion curves, which confirms the robustness of the results obtained. However, due to limitations associated with the measured frequency range, the error is larger at frequencies beyond the array aperture, particularly at low frequencies, which can be related to the increasing uncertainty of the estimated shear wave velocities at greater depths.

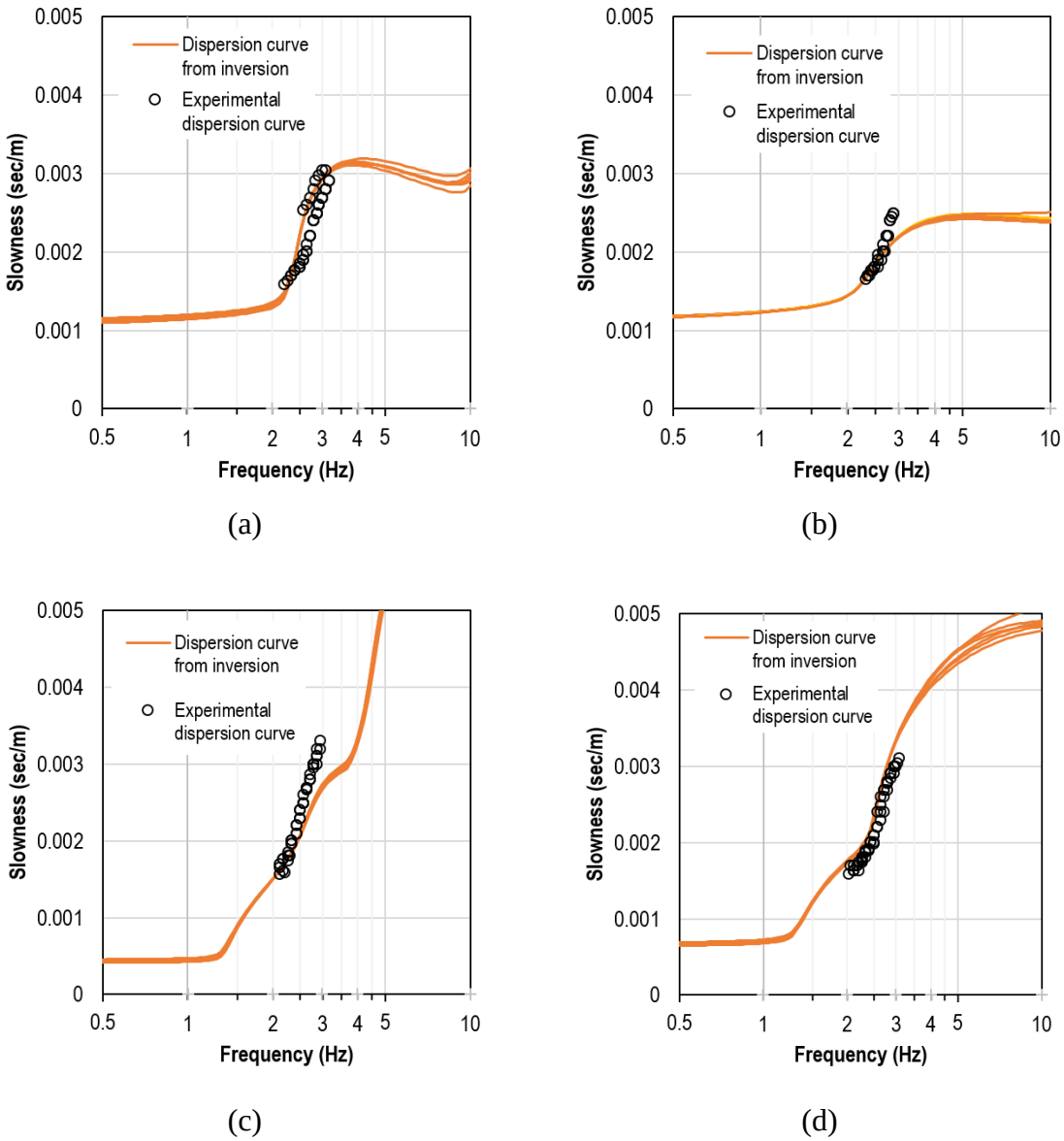

Figure 5.7 Dispersion curves of the best 20 models for the inversion compared to the experimental dispersion curve in black circle for some selected tests at (a) MAM#01, and (b) MAM#02, (a) MAM#03, and (b) MAM#04.

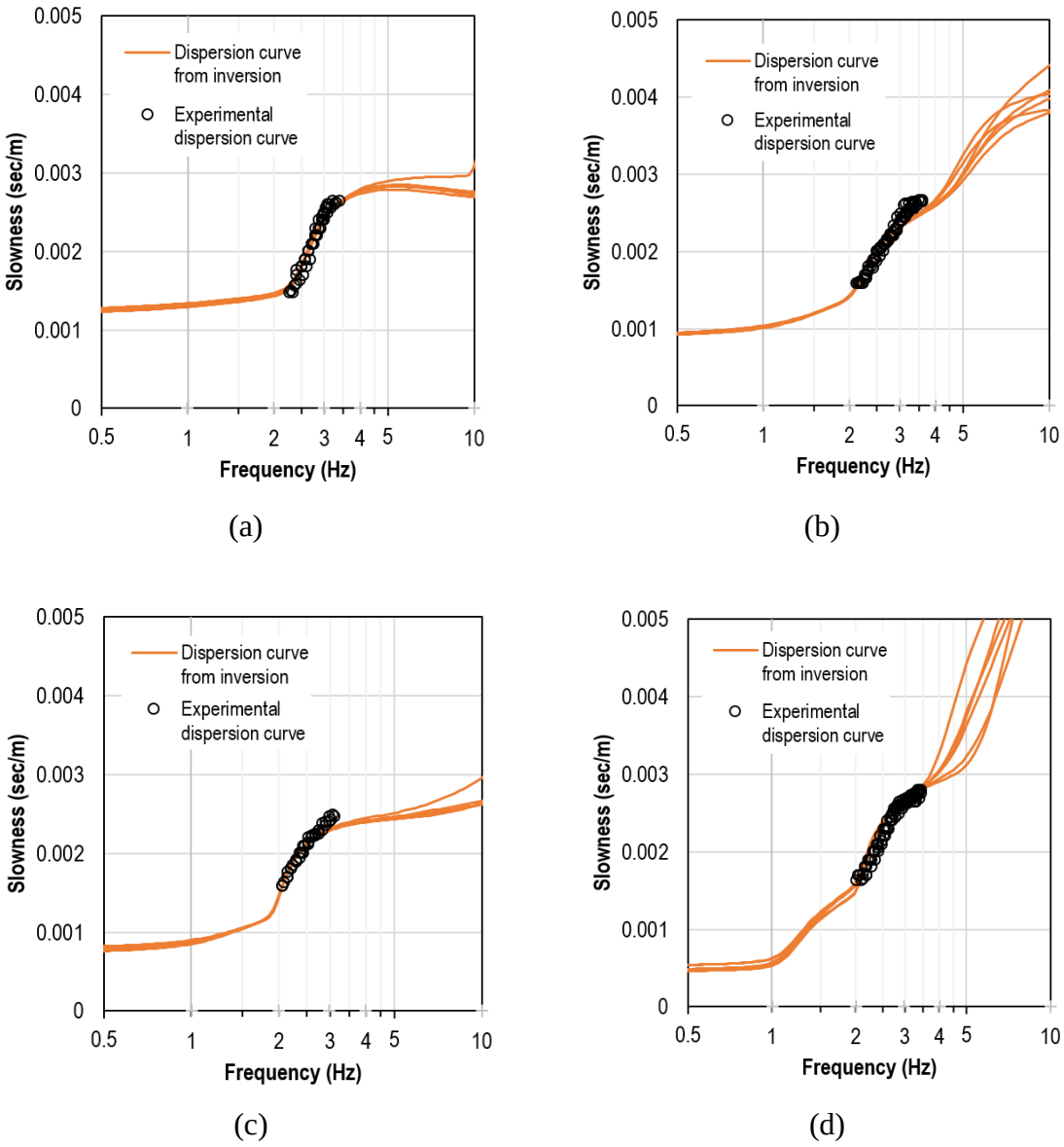

Figure 5.8 Dispersion curves of the best 20 models for the inversion compared to the experimental dispersion curve in black circle for some selected tests at (a) MAM#05, (b) MAM#06, (c) MAM#057, and (d) MAM#08.

5.5.3 Shear wave velocity

The Dinver code, which is part of the Geopsy software (Geopsy, 2018), is employed to obtain the shear wave velocity profiles from the dispersion curves at each of the measured sites. For each dispersion curve, in each run, a minimum of 12,500 models are generated, with each run repeated 3 times, using a different seed and the best 20 models are identified. The mean best model, at each MAM location, is obtained by combining each of the best 20 models from all runs and trials. The subsequent results are presented in Figures 5.9 to 5.12. Furthermore, the mean best shear wave velocity profiles obtained for

all MAM locations were adjusted based on the measured HVSR ellipticity curve, as mentioned previously. The results are also incorporated in Figures 5.9 to 5.12. Additional relationships between the obtained shear wave velocity profiles and the seismic site classification, as well as the site amplification factor, are examined in the following sections.

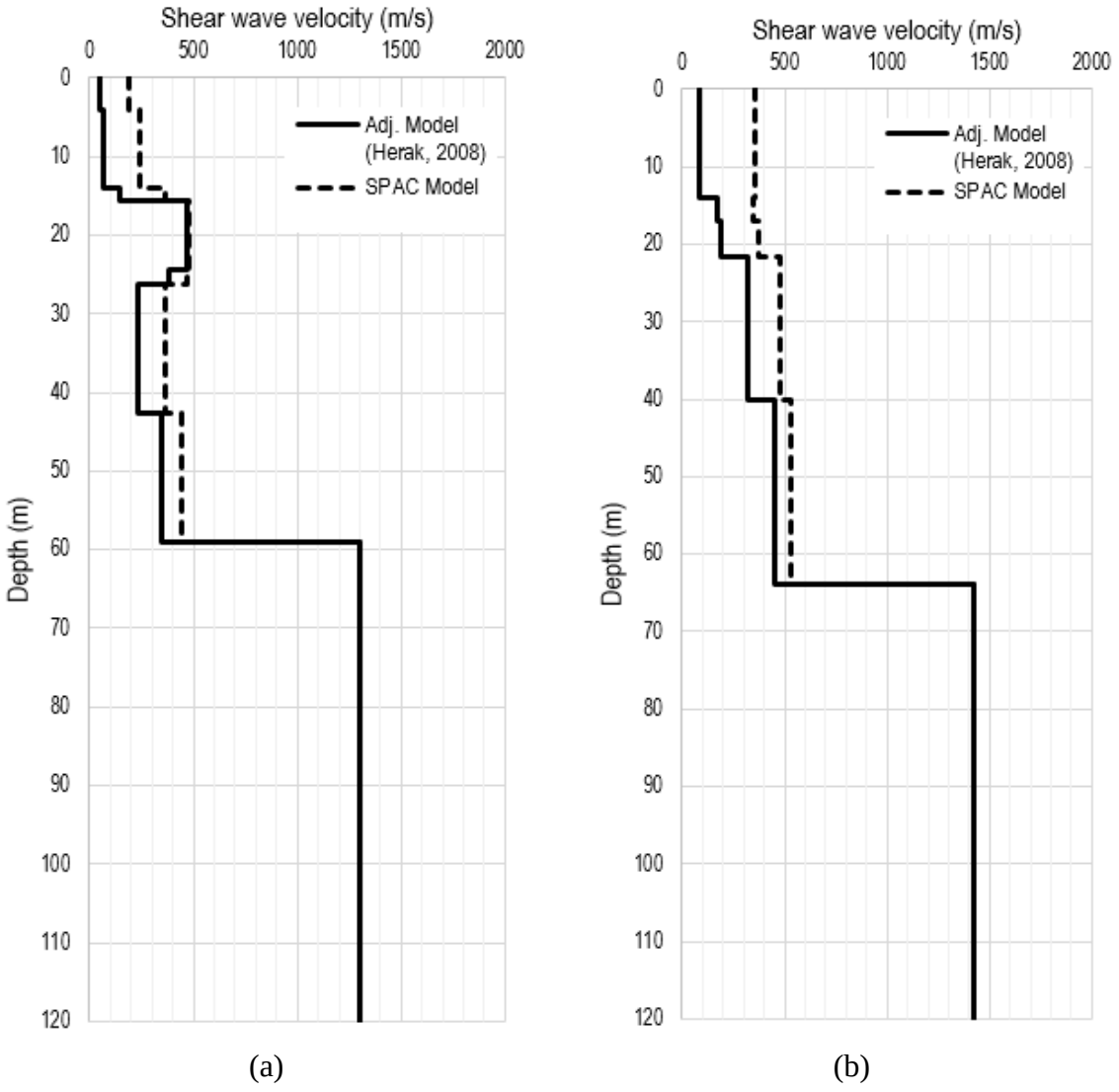

Figure 5.9 Shear wave velocity profiles at (a) MAM#01 and (b) MAM #02.

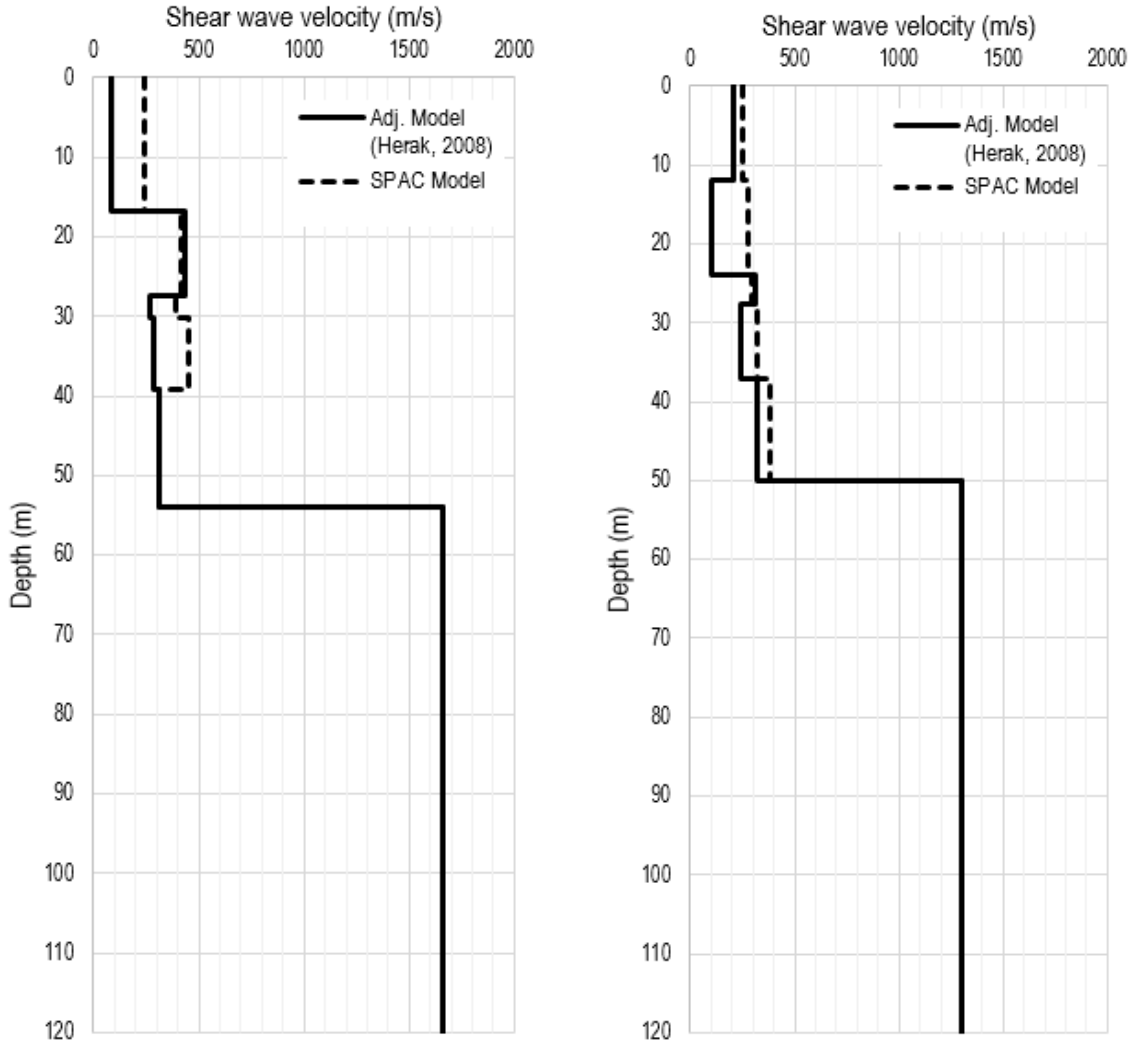

Figure 5.10 Shear wave velocity profiles at (a) MAM#03 and (b) MAM#04.

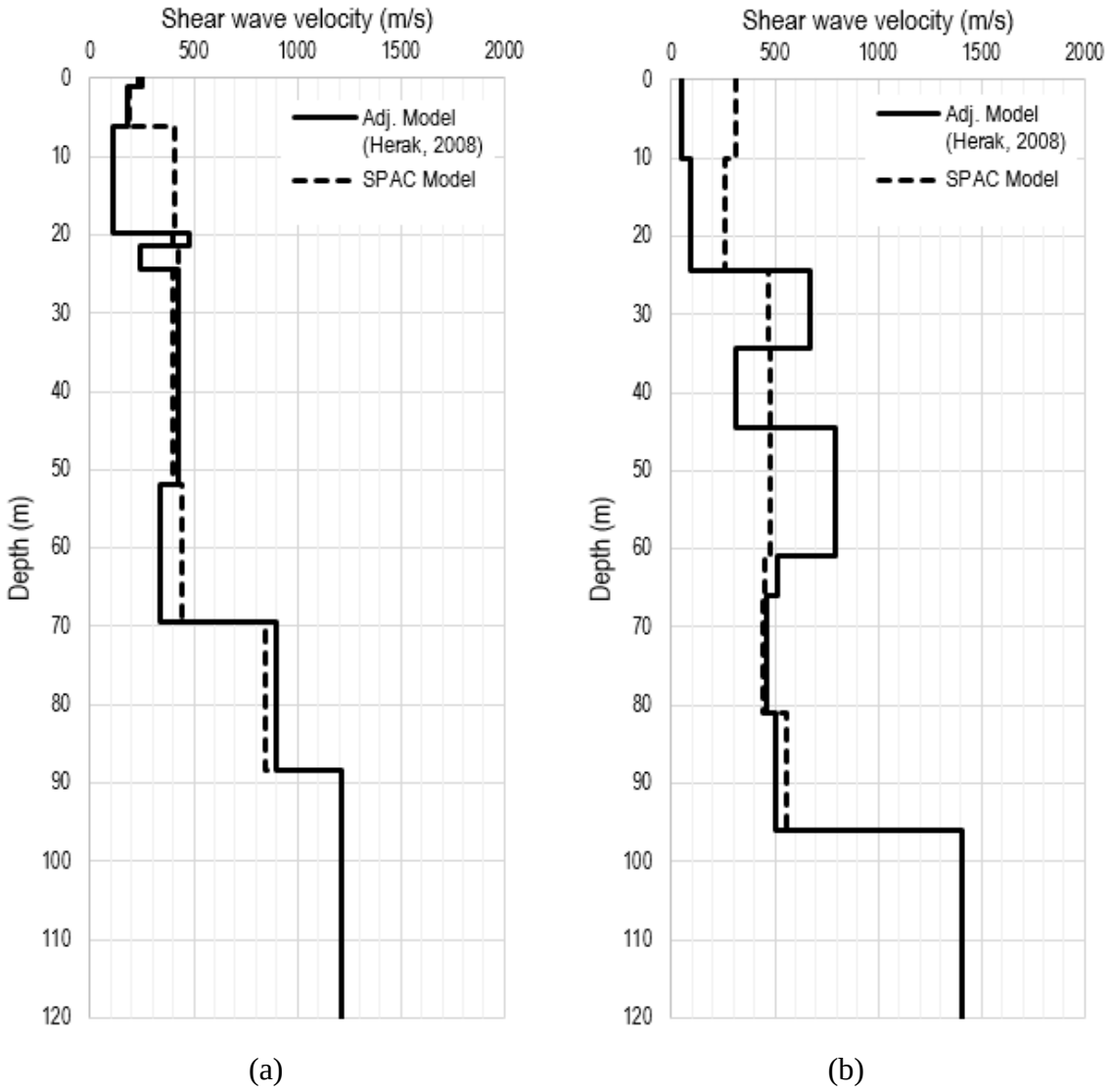

Figure 5.11 Shear wave velocity profiles at (a) MAM#05 and (b) MAM#06.

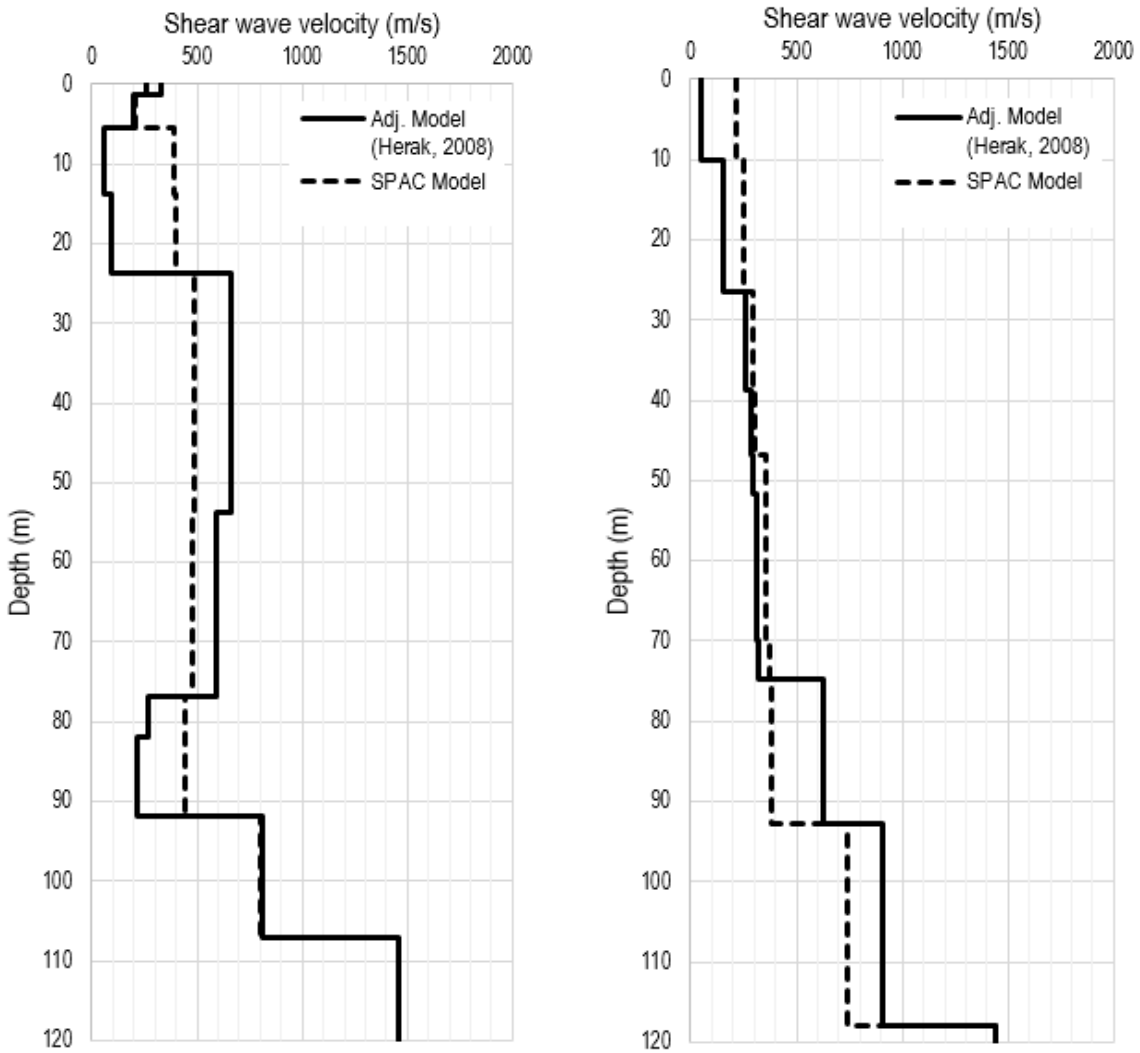

Figure 5.12 Shear wave velocity profiles at (a) MAM#07 and (b) MAM#08.

5.5.4 Site classification

The seismic site classification system, based on the mean shear wave velocity of the uppermost 30 m of the subsurface layers, $V_{s,30}$, which was proposed by the National Earthquake Hazards Reduction Program (NEHRP) [BSSC, 2001], is the most widely used such system for seismic hazard assessment (Volti *et al.*, 2016). The parameter $V_{s,30}$ can be calculated from:

$$V_{s,30} = \frac{\sum_{i=1}^{n} Z_i}{\sum_{i=1}^{n} \left(\frac{Z_i}{V_{si}} \right)} \quad \text{..... (5.11)}$$

where Z is the thickness (in meters); V_{si} is shear wave velocity of the ith layer; and n is a total number of layers in the uppermost 30 m. In the present study, several seismic site classifications are examined, as shown in Table 5.6. These include the methods proposed by NEHRP (BSSC, 2001), AS 1170.4 (Standards Australia, 2007) and McPherson & Hall (2007).

The NEHRP classification system classifies 5 subsoil classes from subsoil class A (hard rock) to subsoil class E (thick medium-soft soils). The Australian Standard (Standards Australia, 2007) seismic classification system adopts the following categories: (1) subsoil class B (rock) is used for $V_{s,30}$ > 360 m/s in contrast to the NEHRP system subsoil class C (very dense soil and soft rock); (2) a site fundamental period of surface-to-rock of 0.6 s is used to justify either subsoil Class C or Class D; and (3) subsoil Class E is used for very thick sites (> 10 m) with a shear wave velocity of 150 m/s or below, as shown in Table 5.6. With regards to the NEHRP seismic classification system, McPherson & Hall (2007) proposed a general seismic site classification for regolith sites. Two parameters are associated with this classification system, namely $V_{s,30}$ and a description of the lithology. McPherson & Hall (2007) adopt 7 sub classes (B, BC, C, CD, D, DE, and E).

Using the NEHRP system, all of the measured sites in the present study are classified as being between subsoil seismic class C and D; three sites (MAM#02, #05 and #07) are classified as subsoil class C; and the remainder as subsoil class D. A broad range of subclasses are specified by the Australian Standard, from subclass B to D. Subclass B is associated with a lower $V_{s,30}$ threshold (i.e. 360 m/s), and the inclusion of site periods (0.6s) in this classification system, shift MAM#02 to subsoil class B. Based on the McPherson & Hall (2007) classification system, the study area can be classified as between subsoil class D and C. As there is overlap in the shear wave velocity threshold in this system, most of the sites in the present study fall into two subsoil classes.

Table 5.6 Seismic site classifications.

Site class	Generalized soil description	NEHRP (BSSC, 2001)	AS 1170.4 (Standard Australia, 2007)	Australian National Regolith Site Classification Map (McPherson & Hall, 2007)	
		$V_{s,30}$ (m/s)			Description
A	Hard rock	> 1500	> 1500	–	–
B	Rock	760 – 1500	> 360	> 760	Fresh to moderately weathered hard rock units (plutonic & metamorphic rocks, most volcanic rocks, coarse-grained sedimentary rocks, Cretaceous & older)
BC	–	–	–	555 – 1000	Highly weathered hard rock; some Tertiary volcanics
C	Very dense soil & soft rock	360 – 760	≤ 0.6 s (surface to rock)	360 – 760	Sedimentary rocks of Oligocene age; coarse-grained sedimentary rocks of younger age; extremely weathered hard rock units
CD	–	–	–	270 – 555	Sedimentary rocks of Miocene and younger age, unless formation is notably coarse-grained; Plio-Pleistocene alluvial units; older (Pleistocene) alluvium; some areas of coarse younger alluvium
D	Dense to medium	180 – 360	> 0.6 s (surface to rock)	180 – 360	Young (Holocene to Late Pleistocene) alluvium
DE	–	–	–	90 – 270	Fine-grained alluvial, deltaic, lacustrine and estuarine deposits
E	Medium to soft soils	< 180	>10 m soil depth with $V_s \leq 150$	< 180	Intertidal and back-barrier swamp deposits

Using the NEHRP seismic site classification system, Collins *et al*. (2006) assigned the Government House site to Class D ($V_{s,30}$ = 257 m/s). However, this study involved only a single test location in the Adelaide city. The selection of subsoil class D by Collins *et al*. (2006) agrees well with the observation of McCue & Love (1997), who identified a fundamental site period for much of the Adelaide city of 1 s. Furthermore, subsoil class D was also suggested by McBean (2010). It is well accepted that the subsurface profile of Adelaide is highly variable (Selby & Lindsay, 1982; Jaksa, 1995) and this study seeks to recognize this by providing higher resolution of Adelaide's seismic site classification, as shown in Table 5.7.

Further analysis is undertaken by calculating the mean upper 30, 20 and 10 m shear wave velocities, V_{s30}, V_{s20} and V_{s10} respectively, at all locations. These shear wave velocities are used to estimate the seismic site classes and site amplification using a number of approaches, as shown earlier in Table 5.7. A further relationship between the seismic site classification based on V_{s30}, V_{s20} and V_{s10}, and site amplification factor is examined for the study site. The values of V_{s20} and V_{s10} are calculated, in addition to $V_{s,30}$ and the site periods, because of the difficulty in estimating the seismic site classes for MAMs #01, #02, #03, #04, #05 and #06. Zaineh *et al*. (2012) observed a similar challenge with

adopting $V_{s,30}$ for seismic assessment. The authors conducted a study in Damascus, Syria and found that using $V_{s,10}$ provided better agreement with the average amplification than using $V_{s,30}$. Similarly, implementing $V_{s,20}$ and $V_{s,10}$, in conjunction with all seismic classification systems is undertaken and the results are summarized in Table 5.7. As shown, the uppermost 20 m and 10 m shear wave velocities are estimated in the ranges between 73 and 163 m/s for $V_{s,20}$ and 50 to 203 m/s for $V_{s,10}$. In the NEHRP classification system, the use of $V_{s,20}$ and $V_{s,10}$ produce inconclusive results to support the $V_{s,30}$ results. In the AS 1170.4–2007, the results suggest subsoil class D for both MAM#04 and MAM#05, with the remainder falling into subsoil class E. The introduction of site periods into the classification system plays an important role in distinguishing between these classes. Finally, in McPherson & Hall (2007) classification system, the adopted sub-surface description suggests a subsoil class D for all investigated sites.

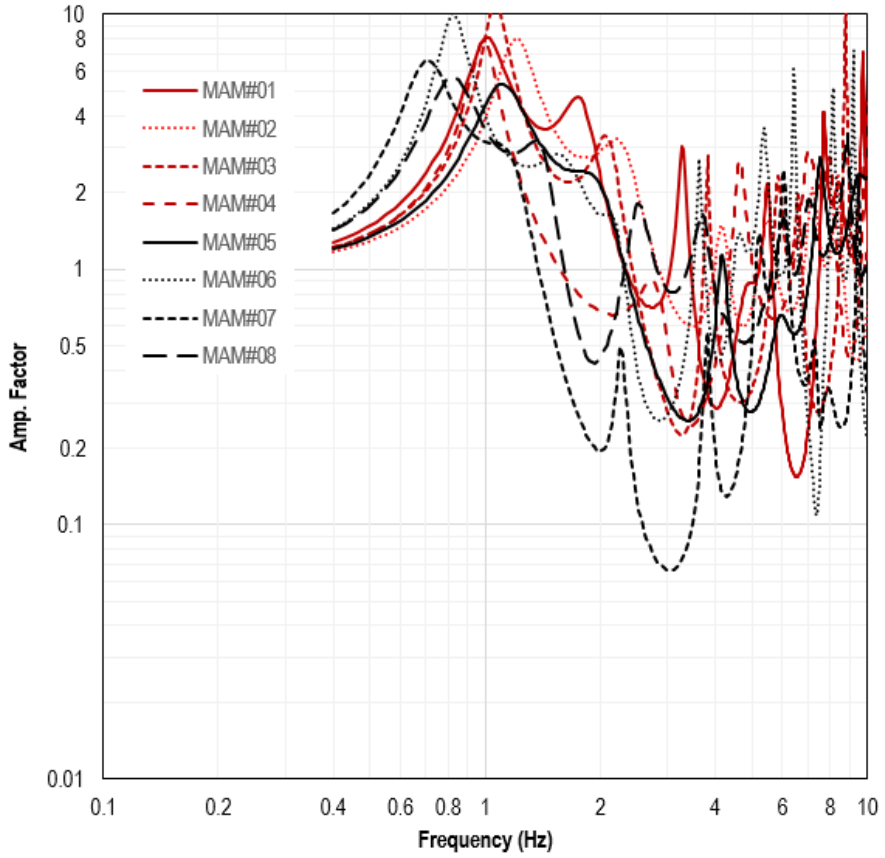

Figure 5.13 Average amplification factors plotted against frequency for each array.

Table 5.7 Seismic site classification for all MAM locations and site impedance contrast category.

Array name and location	Shear wave velocity			Site fundamental period (s)*	Seismic site classification (V_{s30}; V_{s20}; V_{s10})			Estimated impedance contrast	Category**
	V_{s30} (m/s)	V_{s20} (m/s)	V_{s10} (m/s)		NEHRP	Standards Australia	McPherson & Hall (2007)		
MAM#01 (Barton Tce W)	227	160	61	0.98	D; E; E	D; D; D	D; D; D	5.6	H
MAM#02 (Lefevre Tce)	177	115	86	0.83	D/E; E; E	D; D; D	D; D; D	4.3	H
MAM#03 (Finniss St)	224	140	84	0.96	D; E; E	D; D; D	D; D; D	8.3	H
MAM#04 (Frome Rd/ War Mem. Dr)	180	163	203	1.02	D/E; E; D	D; D; D	D; D; D	6.8	H
MAM#05 (West Tce/ Port Rd)	215	135	157	0.92	D; E; E	D; D; D	D; D; D	1.6	L
MAM#06 (Bartels Rd)	189	73	50	1.27	D; E; E	D; D; D	D; D; D	2.3	L
MAM#07 (South Tce/ West Tce)	222	112	149	1.39	D; E; E	D; D; D	D; D; D	1.7	L
MAM#08 (Hutt Rd/ South Tce)	131	102	50	1.25	E; E; E	D; D; D	D; D; D	1.7	L

*: Site fundamental period is based on the average calculated site periods using all models.

**: L = low impedance contrast; H = high impedance contrast, based on SESAME (2004), where impedance contrast is > 4–5.

5.5.5 Site amplification

Site amplification factors are estimated to understand better the seismic motion behavior in the study area, by means of the method proposed by Herak (2008). The site amplification factor defines the ratio of the ground motion at the surface to that at the bedrock level. The compression wave, shear wave and density models obtained in the present study are used to quantify the amplification factor. The quality factors, Q_p and Q_s,

are estimated using the methods suggested by Zhang & Stewart (2007) and Olsen *et al*. (2003), respectively. These quality factor estimations are deduced from the compression and shear waves in each layer. The calculated site amplification factors, Amp-HVSR, are presented in Figure 5.13. As can be seen, in general, a site amplification of approximately 3 is obtained for the study area. Averaging the amplification factor over a range of frequencies, from 0.4 to 2 Hz at each site, suggests that it varies between 2.2 and 3.9.

By using the identical subsurface models, dynamic amplification factors (DAFs) are also evaluated for all array sites, also using the method proposed by Herak (2008). In contrast to the evaluation of Amp-HVSR, DAF uses parameters associated with the most likely seismic event. In the present study, an earthquake of magnitude 7, with an epicenter lateral distance of 30 km and a focal depth of 10 km is adopted, as suggested by Malpas (1991). The results are presented in Table 5.8 and, in general, it is observed that DAF is slightly larger than Amp-HVSR, with DAF varying between 2.2 and 4.8.

As stated by Herak (2008) the amplification factors of both Amp-HVSR and DAF do not account for the non-linear behavior of the subsurface material, hence, one should be cautious when adopting these estimates in practice. A non–linear site response analysis would assist in this regard; however, is beyond the scope of the present study.

Table 5.8 Average amplification factor using HVSR analysis (Amp-HVSR) and dynamic amplification factor (DAF).

Array name and location	$V_{s,30}$ (m/s)	Site fundamental periods*	Amp-HVSR**	DAF
MAM#01 (Barton Tce W)	227	0.98	3.9	4.3
MAM#02 (Lefevre Tce)	177	0.83	3.5	4.1
MAM#03 (Finniss St)	224	0.96	3.5	4.3
MAM#04 (Frome Rd/ War Mem. Dr)	180	1.02	2.3	2.6
MAM#05 (West Tce/ Port Rd)	215	0.92	2.8	2.6
MAM#06 (Bartels Rd)	189	1.27	3.3	4.8
MAM#07 (South Tce/ West Tce)	222	1.39	2.2	2.2
MAM#08 (Hutt Rd/ South Tce)	131	1.25	2.5	4.7

*: Site fundamental period is based on the mean of the calculated approaches.
**: Amp-HVSR is the average amplification factor for 0.4–2 Hz.

5.5.6 Average shear wave velocities $V_{s,30}$, $V_{s,20}$, $V_{s,10}$ and site amplification relationships

The relationship between the amplification factors and the shear wave velocities of $V_{s,30}$, $V_{s,20}$ and $V_{s,10}$ are examined. The relationships for both the average amplification factor, at frequencies between 0.4 and 2 Hz, using the HVSR method (Amp-HVSR) and the dynamic amplification factor (DAF) for all array sites, as shown in Table 5.8, are presented in Figure 5.14. The correlation between Amp-HVSR and the amplification factor of the site is unclear; however, the correlations with respect to DAF suggest that an increase in the shear wave velocity at the top of the subsurface profile reduces the amplification factor of the site. Furthermore, each of the relationships between $V_{s,30}$, $V_{s,20}$, $V_{s,10}$ and the amplification factors (DAF) are presented in Figures 5.14(b), 5.14(d) and 5.14(f), respectively. The results clearly show a slightly higher slope for the relationships between the average shear wave velocities of $V_{s,10}$ and DAF than those for the others. As suggested above, the average amplifications with respect to $V_{s,10}$ and DAF indicate, from the regression line, slightly higher values than those associated with $V_{s,30}$ and $V_{s,20}$ and DAF. Furthermore, as indicated by the values of the coefficient of determination (R^2), superior correlation is obtained for the relationship between the amplification factor and $V_{s,10}$ than for $V_{s,30}$ and $V_{s,20.}$

5.5.7 Validation of HVSR site fundamental frequency and SPAC shear wave velocity profile

This section seeks to validate the site fundamental frequency and the shear wave velocity results using previous site effect studies and forward computational modeling.

Validation using the previous site effect studies in Adelaide region

In 1996, a seismic hazard and microzonation study was undertaken of the Adelaide metropolitan area by Love (1996) using site response analysis and single microtremor measurement. Of particular note were the results of a profile developed for the Adelaide central business district. In terms of site-specific peak ground accelerations (PGAs), the average calculated PGA for this site was found to be 0.4 g and an acceleration response spectra of approximately 1.0 g, with a period between 0.2 and 0.3 s and 5% damping. This study also predicted an average ratio of the surface-to-bedrock acceleration response spectra of approximately 2.3. This prediction is in good agreement with the estimation for

seismic site class D (AS 1170.4-2007) in the present study, which is as high as 2.8. However, the Love (1996) prediction is slightly lower than that estimated for subsoil class E in the present study, which is as high as 3.9. This discrepancy is likely due to differences in the analysis method and input data. The amplification in this study is deduced using forward modeling and specific seismic input, as shown above, whereas Love (1996) used site response analysis and scaling the seismic input motions to 0.1 g. In addition, the differences may reflect the complexity of quantifying seismic site amplification, which involves both the analysis method and the input data.

McCue & Love (1997) also indicated that amplification will occur at frequencies of 1 Hz at most of the sites in the Adelaide city. Generally, a fundamental frequency of 1 Hz is also suggested by the field microtremor results obtained in the present study. In particular, the field measurements indicate that the north of the city is associated with amplification in the frequency range of 1.0 to 1.2 Hz, whereas south of the city exhibits a range between 0.7 and 1.1 Hz. This larger variability in the south is due to the increasing thickness of soil overlying bedrock in this area. Forward modeling calculation in the present study suggests the fundamental frequency is approximately 1.0 Hz for most of the sites. The results of the forward modeling estimations indicate that the dominant frequencies in Adelaide are in good agreement with those proposed by previous researchers (Table 5.5). Most of the sites located in the north of Adelaide exhibit predominant frequencies of about 1.0 Hz. In the south of Adelaide, the predominant frequency varies between 0.6 and 1.1 Hz.

More recently, Leonard (2015) [Personal communication] conducted shear wave velocity mapping across the major cities in Australia. Preliminary results from this study (Leonard, 2015) suggested $V_{s,30}$ varies between 315 to 460 m/s for most of the sites in Adelaide. This study also suggested $V_{s,30}$ = 225 to 315 m/s for the area along the River Torrens. The estimate for $V_{s,30}$ in the present study of between 131 and 227 m/s is very much lower than the value proposed by Leonard (2015). This discrepancy may be attributed to the different resolution adopted by Leonard (2015). The present study covers only the city of Adelaide, whereas Leonard (2015) included the entire Adelaide metropolitan and the surrounding areas (Setiawan *et al.*, 2018b). As a result, a low resolution study tends to be unable to capture some minor, local variations.

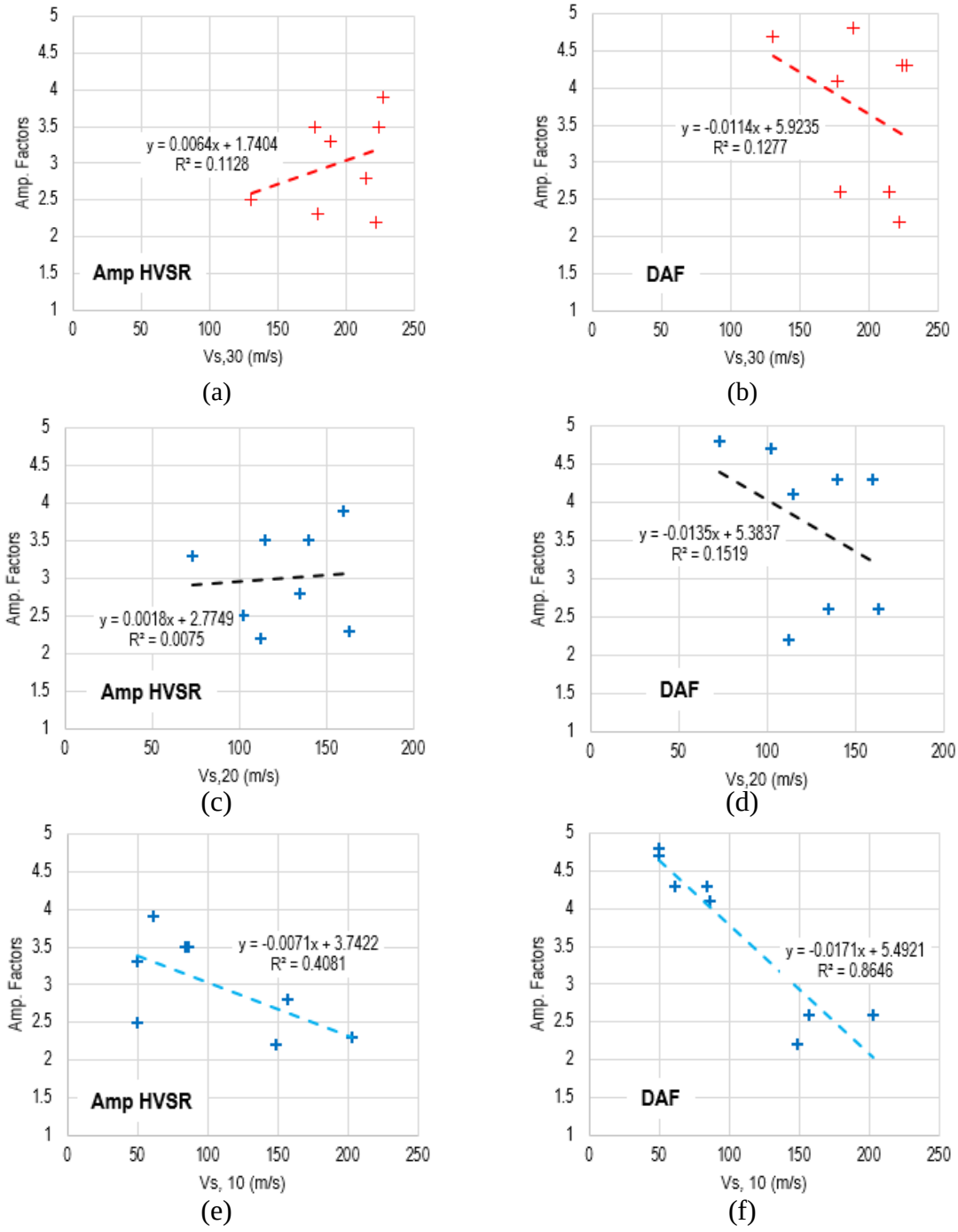

Figure 5.14 Relationships between amplification factor and shear wave velocity for all array sites: (a) Amp-HVSR for $V_{s,30}$; (b) DAF for $V_{s,30}$; (c) Amp-HVSR for $V_{s,20}$; (d) DAF for $V_{s,20}$; (e) Amp-HVSR for $V_{s,10}$; and (f) DAF for $V_{s,10}$.

Validation using single HVSR analysis of the array data

The spectral ratios between the horizontal and vertical components of the observed microtremor array data (referred to here as the 'observed HVSR') are compared with the computed ellipticity of the fundamental mode Rayleigh waves for the inverted 1D soil profiles. This comparison is undertaken to assess the appropriateness of the inversion.

Forward modeling, as proposed by Geopsy (2018), is employed to compute the ellipticity of the fundamental mode Rayleigh waves of the MAM sites, referred to here as the 'calculated HVSR.' The compression wave (V_p), shear wave (V_s), density (ρ) and thickness parameters used in the forward modelling were based on the mean of best 20 inverted profiles. The estimated quality factors of Q_p and Q_s were based on the Zhang & Stewart (2007) and Olsen *et al.* (2003) approaches, respectively. The comparison of the complete mean, measured and calculated HVSR curves are presented in Figures 5.15 and 5.16 in the form of logarithmic plots. In general, it can be concluded that the measured and calculated HVSR curves at all sites exhibit comparable results.

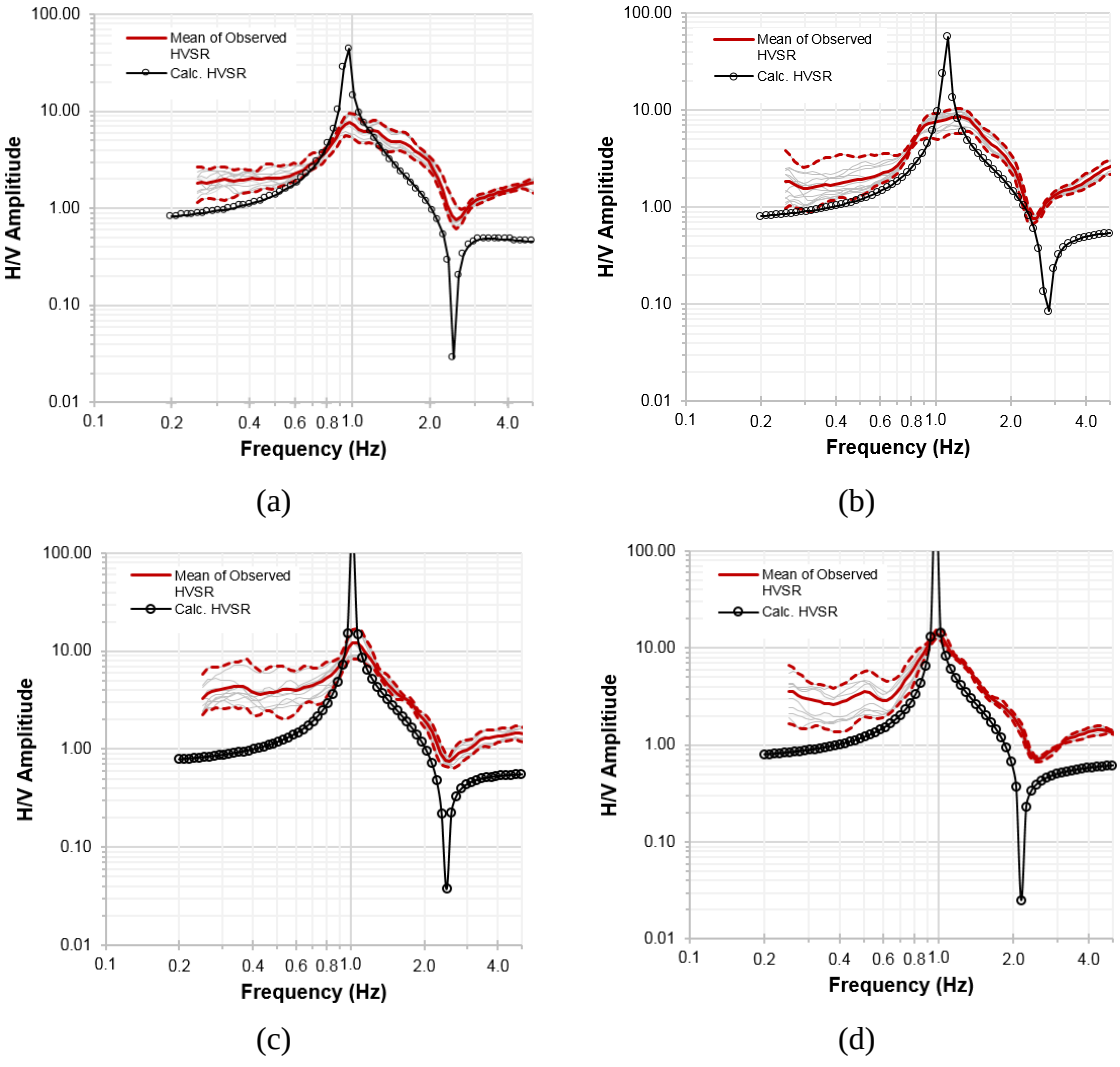

Figure 5.15 Comparison between the mean of observed and calculated HVSRs using Geopsy (2018) approach at: (a) MAM#01, (b) MAM#02, (c) MAM#03, and (d) MAM#04.

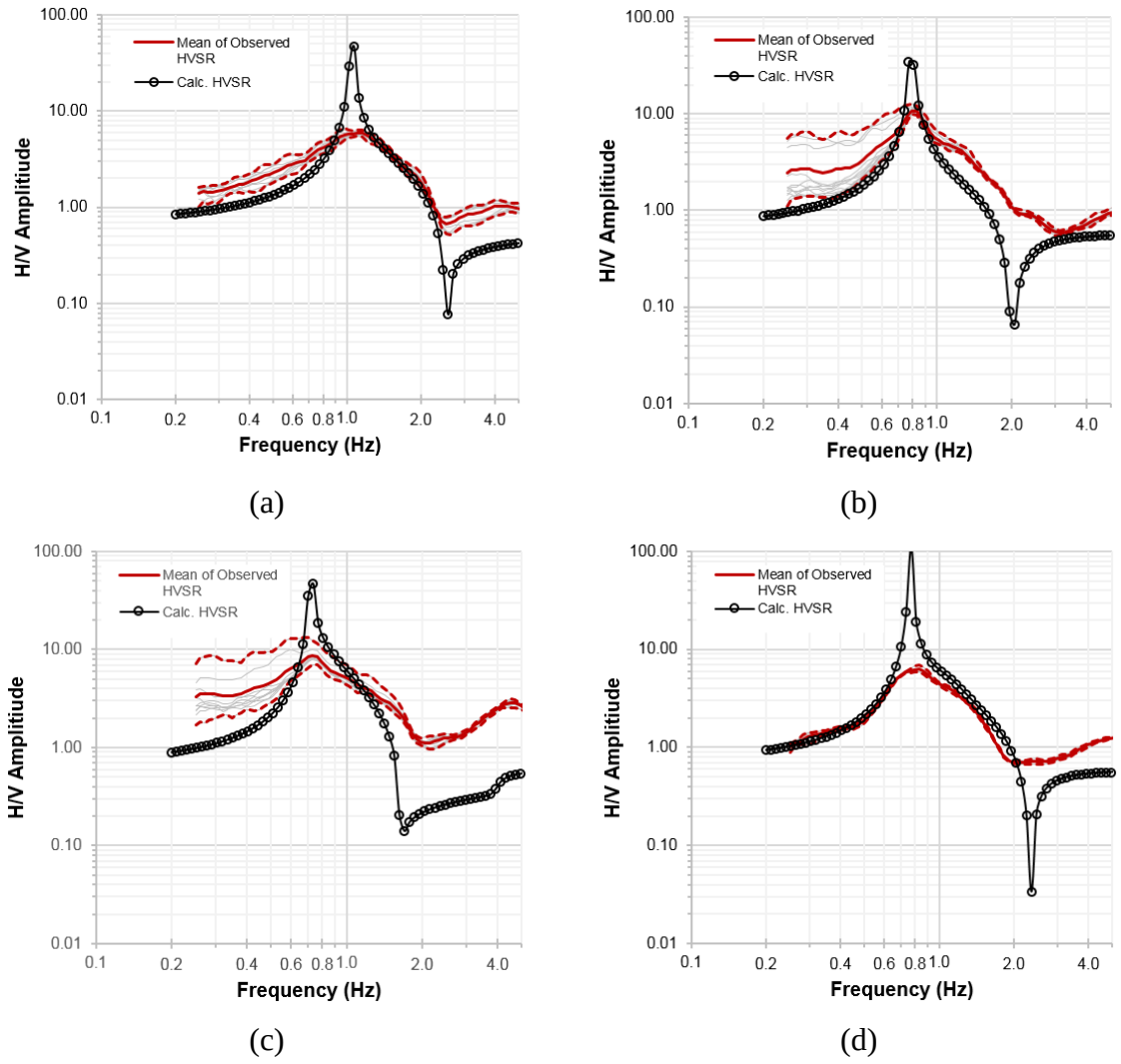

Figure 5.16 Comparison between the mean of observed and calculated HVSRs using Geopsy (2018) approach at: (a) MAM#05, (b) MAM#06, (c) MAM#07, and (d) MAM#08.

Validation using actual soil profile at the measured sites

An examination of the shear wave profiles, as shown in Figures 5.9 to 5.12, based on the actual soil profile at the measured sites, is carried out using conventional soil investigation data. Selby & Lindsay (1962) compiled at least 58 standard penetration test (SPT) data at various depths within the Hindmarsh CLAY from which the shear wave velocity of this layer was deduced using the approaches given by Dikman (2009) and Tsiambaos & Sabatakakis (2010). The Hindmarsh CLAY layer is indicated as the second layer at MAM#1, MAM#5, MAM#6, MAM#7, and MAM#8, as shown in Figures 5.17 to 5.19. This validation suggests that the shear wave velocity profiles for the Hindmarsh CLAY using the SPAC model provide better estimates than the shear wave velocity using the Adjustment model (Adj. Model) of Herak (2008).

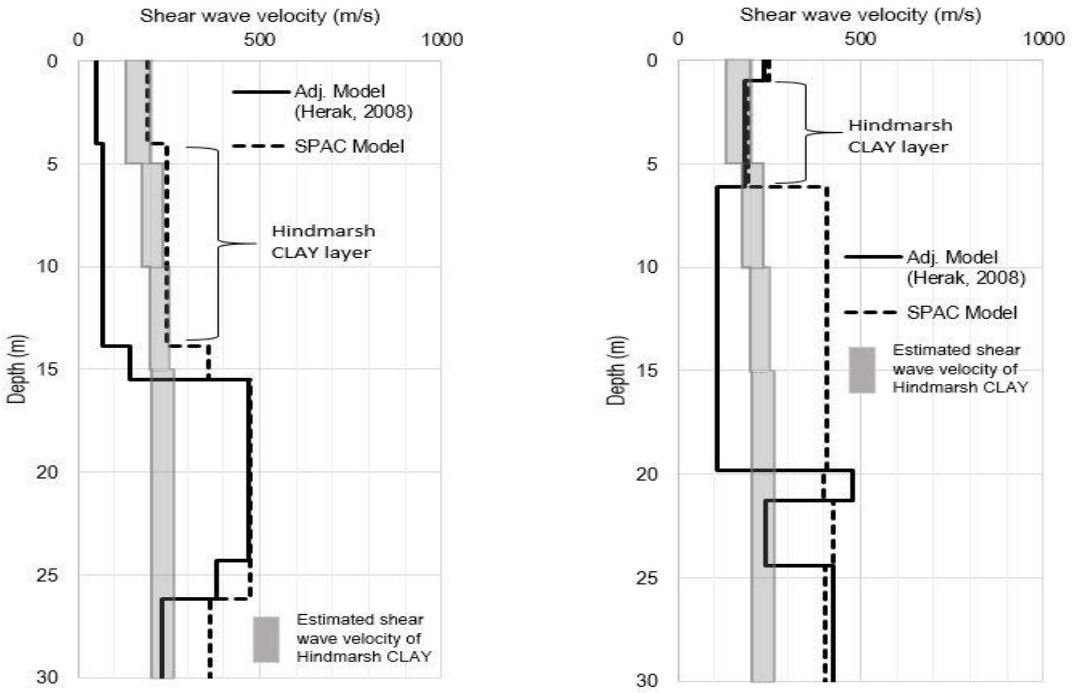

Figure 5.17 Examination of the shear wave profile based on the actual soil profile at (a) MAM#1, and (b) MAM#5

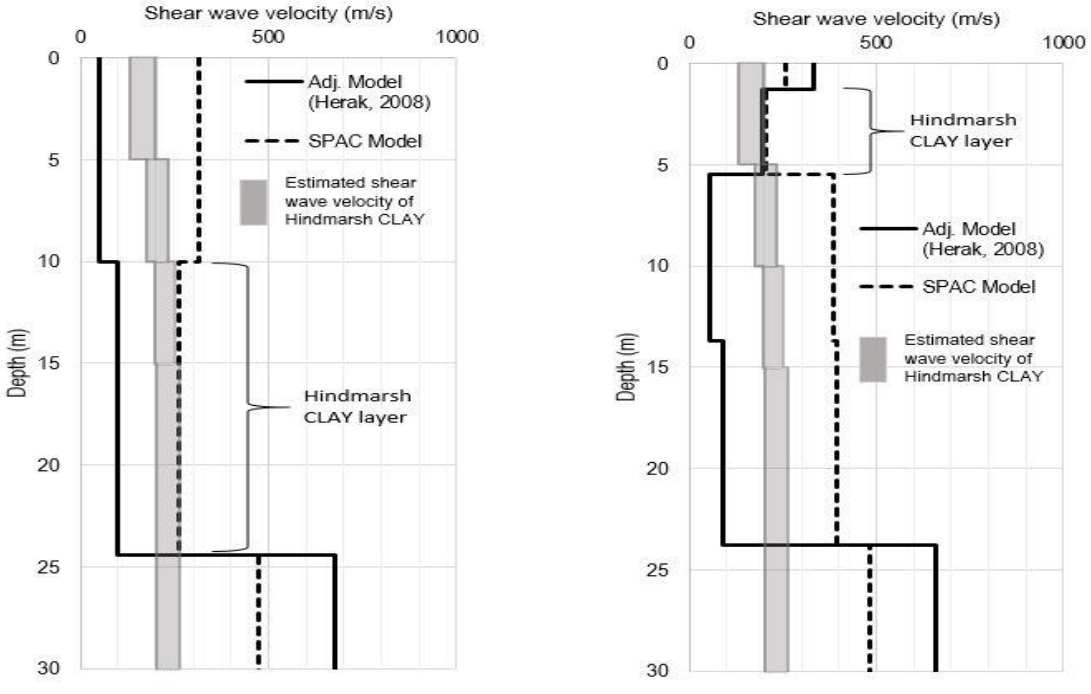

Figure 5.18 Examination of the shear wave profile based on the actual soil profile at (a) MAM#6, and (b) MAM#7

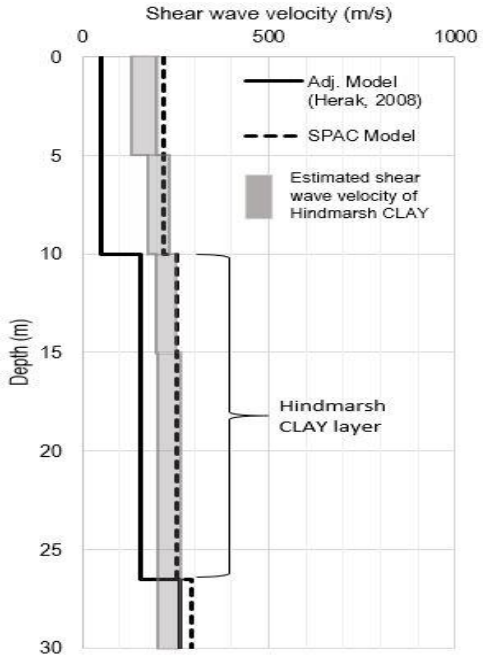

Figure 5.19 Examination of the shear wave profile based on the actual soil profile at MAM#8

5.6 CONCLUSIONS

In the general framework of seismic hazard analysis for quantifying site amplification in a highly seismic risk region, the information regarding the shear wave velocity profile is crucial. In low-to-moderate seismic regions and urban areas, where recorded strong-motion historical seismic events are usually quite sparse, array ambient noise analysis is particularly suitable for estimating shear wave velocity profiles, due to its non-invasive nature and its relatively low-cost. To date, several studies have been carried out to facilitate seismic hazard analysis using this technique. The primary objective of the present study is to investigate the accuracy of shear wave velocity profiles obtained by means of array ambient noise analysis SPAC method at various impedance contrast sites. A case study is examined, involving the city of the Adelaide, South Australia, which exhibits the highest earthquake risk of any capital city in Australia. The city is founded on a regolith which generally exhibits low-to-high impedance contrast. Eight array ambient noise measurements were recorded at a range of locations across the city. The acquired data were used to invert the shear wave velocity profiles through analysis of the dispersion characteristics of the surface waves. Eight 1D shear wave velocity profiles were subsequently developed. The results were compared and validated against previous

site effect studies and forward modeling of the 1D shear wave profile techniques, and the results of the present study are in good agreement with the previous research investigations. Furthermore, relatively low variability and consistent dispersion curves are produced in the measured frequency band. Consistent shear wave velocities are also obtained between depths of 20 to 90 m, despite moderate to high variations at shallower and greater depths (Setiawan *et al*., 2016). Consequently, adjusting the radius of the array to capture higher frequencies in order to resolve the shallow layers, presents an opportunity for future study. Another possibility to quantify the near surface shear wave velocity profile in detail is to adopt a combination of active and passive sources (Boore & Asten, 2008). On the basis of these results, the present study demonstrates the applicability of the array SPAC method at a regolith site, which is subject to various (low-high) impedance contrast.

INTENTIONALLY BLANK

Chapter Six

SUMMARY AND CONCLUSIONS

6.1 SUMMARY

This study has investigated the quantification of seismic site amplification at regolith sites in Adelaide, South Australia. The study applied single and array ambient noise analyses to quantify the amplification. The study involved a huddle test of all the deployed equipment sets, for more than two continuous days. This established the repeatability of all the deployed seismometers, the temporal variability at the study site, and the appropriate duration of the ambient noise measurement. Following this, in situ ambient noise measurements were carried out across the city of Adelaide in order to explore the relevance of this approach. The study examined 10 locations: Five to the north and five to the south of the city. In both the northern and southern locations, four sites were measured using array sets of equipment while one site in each region was measured using a single device. Detailed summaries of the main chapters are given below.

Chapter 2 presented an investigation of three historical seismic events that have damaged the Old Exchange Building which was graced by the Britannia statue on top of the building in Pirie St, Adelaide. The statue lost her arm during the 1897 Beachport earthquake, bowed her helmeted head in the 1902 Warooka seismic event, and was removed after the 1954 Adelaide earthquake (Dyster, 1992). Synthetic ground motion time histories of these past three seismic events (1897 Beachport, 1902 Warooka and 1954 Adelaide) were generated using EXSIM and validated using seismic time histories of the 1997 Burra earthquake. Representative 1D soil profiles were developed from the borehole data and validated using the forward modelling method. The chapter also presented a site response analysis that was carried out at the Old Exchange Building site.

The main outcomes of the site-specific ground response analysis were as follows:

- The analysis based on Model A, as presented in pages 23 to 25, showed that the investigated site PGA varies from 0.01 to 0.3*g*, with fundamental frequency of 0.8 Hz. Spectral accelerations with a 5% ratio of critical damping vary between 0.06 and 0.92*g*. The spectral displacement ranged from 0.6 to 2.7 cm.

- The analysis based on the Model B data, as shown in pages 23 to 25, revealed that the maximum acceleration at the ground surface level varies from 0.02 to 0.32*g*, with fundamental frequency of 0.8 Hz. Spectral acceleration is estimated to vary between 0.05 and 0.96*g* by assuming a 5% damping ratio. The spectral displacement ranged from 0.6 to 1.2 cm.

- A significant site amplification factor of up to 3.4, which is likely to have caused the observed damage to the Britannia statue.

Chapter 3 presented a case study involving the measurement of ambient noise in the central business district of Adelaide, South Australia, which is founded on a regolith. The case study incorporated 10 in situ ambient noise measurements carried out across the city. These measurements were used to estimate the site predominant period, and to infer the site shear wave profile, of the area. The chapter used seismic site classification to quantify site effects associated with seismic hazards.

The key findings of this study, presented in Chapter 3, were as follows:

- The predominant fundamental period for the city of Adelaide is 0.8 seconds or higher, which suggests sub-soil class D according to the Australian Standard.

- The upper 30 m shear wave velocities of Adelaide's regolith varies from 194 m/s to 418 m/s, which are related to classes D to C (NEHRP classification system), classes D to B (Australian Standard classification system) and classes D/DE to C (regolith case classification system).

- A comparison between the results of this study with several previous seismic site classification studies are in good agreement. The chapter demonstrated a promising application of HVSR analysis for seismic assessment of regolith sites.

Chapter 4 estimated the bedrock depth in the city of Adelaide. The depth of the bedrock has been shown to play an important role in altering seismic waves (Graves *et al*., 1998;

Bakir et al., 2002; Narayan & Rao, 2003; Narayan, 2005). Both the generic function (GF) of the classic horizontal-to-vertical spectral ratio (HVSR) method, and the spatial autocorrelation (SPAC), techniques were used to analyse the ambient noise data. The chapter compared bedrock depth predictions from the seismic methods of this study with boreholes drilled in close proximity to the measured sites. The comparison demonstrated that the SPAC method provides superior estimates to those of the GF method.

Chapter 5 demonstrated that, in the general framework of seismic hazard analysis for quantifying seismic site amplification, knowledge of the near-surface shear wave velocity profile is crucial. An investigation was carried out to examine the robustness of shear wave velocity profiles by means of array ambient noise analysis at regolith sites. Eight array ambient noise measurements were carried out across the city of Adelaide. The acquired data were used to invert the shear wave velocity profiles, which, prior to the present study were very limited, through the analysis of the dispersion characteristics of the surface waves. This was completed using the spatial autocorrelation (SPAC) method. New constraints, by means of the shear wave velocity for the study case site of all 8 investigated sites, were developed and proposed in this chapter. Following this, a rigorous validation of the proposed shear wave velocity models was carried out by means of previous studies data and forward modelling techniques. Finally, the applicability of the array SPAC method at regolith sites, subjected to various (low to high) impedance contrasts, was established.

6.2 LIMITATIONS AND RECOMMENDATIONS FOR FURTHER STUDY

Due the limited availability of instruments, this study was limited to the ambient noise analysis of 10 sites. While the results of this study have made important contributions to the state of knowledge of seismic hazard assessment in Adelaide and more broadly, they are applicable to limited locations, such as the Adelaide CBD and sites with similar impedance contrast characteristics. More representative results for the entire Adelaide metropolitan area would be obtained by conducting the assessment over a much larger area. However, such a study is beyond the scope of this research and would require significant equipment and personnel resources and time.

As discussed in Chapters 3 and 5, the site resonance frequency, f_0, is an important parameter in seismic site amplification assessment. For the study site, f_0 can be

deduced from the in-situ noise measurements, and from the forward modelling, as suggested in this study. However, this approach may not yield reliable results for a number of reasons, including the seismometers used, and the data processing application adopted. Thus, further investigation of the value of f_0 using different specifications of seismometer sets and processes is recommended.

In order to understand how the amplified seismic waves are likely to affect structures founded on Adelaide's regolith, soil-structure interaction analysis is desirable. The soil-structure interaction analysis can be undertaken using both the most affected structures in Adelaide city during strong seismic events and the most representative geotechnical dynamic characteristics of Adelaide's regolith, as developed in this study.

Additional suggestions for further work, that may help to improve this study include: (i) the use of noise interferometry to measure dispersion at a higher frequency range; (ii) perform a joint inversion of the HVSR (or ellipticity curve) and dispersion curves to better constrain the V_s profiles down to bedrock; and (iii) obtain in-situ measurements of the typical building resonance frequency by using ambient noise methods to validate whether the 10/N approximation for the resonance frequency of buildings is suitable for typical Australian buildings.

6.3 CONCLUSIONS

This study has demonstrated that ambient noise analysis is very useful for the evaluation of seismic site amplification at regolith sites, provided that its limitations and range of application are recognised and not exceeded. From the analyses presented in this thesis, it can be concluded that:

1) a significant site amplification factor of up to 3.4 in Adelaide's regolith is justified;

2) the Adelaide CBD can be classified into the Australian Standard seismic site classes D to B;

3) the SPAC method with a slight adjustment is a reliable tool for estimating bedrock depth;

4) site resonance frequency, which is important in seismic microzonation, in regolith sites is about 1.0 Hz at the north of Adelaide city and between 0.7 to 1.1 Hz at the south of Adelaide city; and

5) shear wave velocity profiles have been developed at all 8 investigated sites which can facilitate site response and dynamic soil-structure interaction analyses of any critical infrastructure founded on Adelaide's regolith.

INTENTIONALLY BLANK

References

Aitchison, G., Sprigg, R., & Cochrane, G. (1954). *The soils and geology of Adelaide and suburbs*. Adelaide: Department of Mines.

Aki, K. & Richards, P. (2002). *Quantitative Seismology*. 2nd Ed., University Science Books, Sausalito, California.

Aki, K. (1957). Space and time spectra of stationary stochastic waves, with special reference to microtremors. *Bull. Earthq. Res. Inst*. 35:415–456.

Aki, K. (1965). A note on the use of microseisms in determining the hallow structures of the Earth's crust. *Geophysics*, 30 (4):665-666.

Allen, T. (2012). Stochastic ground-motion prediction equations for southeastern Australian earthquakes using updated source and attenuation parameters. *Record 2012/69*, Geoscience Australia: Canberra, p. 66.

Anbazhagan, P., Sheikh, N., & Parihar, A. (2013). Influence of rock depth on seismic site classification for shallow bedrock regions. *Natural Hazards Review*, 14 (2):108-121, DOI:10.1061/(ASCE)NH.1527-6996.0000088.

Anbazhagan, P., Sheikh, N., & Tsang, H. (2010). Seismic site classification practice in Australia, China and India: suitability. In *R. Abraham, S. Latheswary & N. Unnikrishnan (Eds.), International Conference on Materials Mechanics and Management*. New Delhi: Excel India Publishers, pp. 189-197.

Arai, H. & Tokimatsu, K. (2004). S-wave velocity profiling by inversion of microtremor H/V spectrum. *Bull. Seismol. Soc. Am*. 94(1):53–63.

Asten, M. & Dhu, T. (1998). Enhanced interpretation of microtremor spectral ratios using multimode Rayleigh-wave particle-motion computations. In *Proceedings of Total*

Risk Management in the Privatised Era, Adelaide, Australia. Australian Earthquake Engineering Society Conference.

Asten, M. & Dhu, T. (2004). Site response in the Botany area, Sydney, using microtremor array methods and equivalent linear site response modelling. Australian Earthquake Engineering in the New Millennium, Proceedings of a conference of the Australian Earthquake Engineering Soc., Mt Gambier South Australia, Paper 33.

Asten, M. & Henstridge, J. (1984). Array estimators and the use of microseims for reconnaissance of sedimentary basins, *Geophysics*, 49(11):1828–1837.

Asten, M. (2004a). Passive seismic methods using the microtremor wave field for engineering and earthquake site zonation. In *SEG 74th Annual Meeting*, Denver, USA.

Asten, M. (2004b). Comment on ‘‘Microtremor observations of deep sediment resonance in metropolitan Memphis, Tennessee’’ by Paul Bodin, Kevin Smith, Steve Horton and Howard Hwang. *Eng. Geol.* 72: 343–349. DOI: 10.1016/j.enggeo.2003.09.001

Asten, M. (2006). On bias and noise in passive seismic data from finite circular array data processed using SPAC methods. *Geophysics*, 71(6): 153–162.

Asten, M., Askan, A., Ekincioglu, E., Sisman, F., & Ugurhan, B. (2014). Site characterization in north-western Turkey based on SPAC and HVSR analysis of microtremor noise. *Exploration Geophysics*, 45: 74–85, DOI:10.1071/EG12026.

Asten, M., Dhu, T., & Lam, N. (2004). Optimised array design for microtremor array studies applied to site classification; comparison of results with SCPT logs. In *13th World Conf. on Earthquake Engineering*, Vancouver, BC, Canada, 1-6 August 2004, Paper No. 2903.

ASTM D1586-11 (2011). Standard Test Method for Standard Penetration Test (SPT) and Split-Barrel Sampling of Soils. *ASTM International*, West Conshohocken, PA, www.astm.org.

Atkinson, G. & Macias, M. (2009). Predicted ground motions for great interface earthquakes in the Cascadia subduction zone. *Bull. Seism. Soc. Am.* 99(3): 1552–1578. DOI: 10.1785/0120080147.

Bakir, B., Ozkan, M., & Ciliz, S. (2002). Effects of basin edge on the distribution of damage in 1995 Dinar, Turkey earthquake. *Soil Dyn. Earthq. Eng*. 22:335–345.

Bard, P-Y. (1998). Microtremor measurements: a tool for site effect estimation. In *Second International Symposium on the Effects of Surface Geology on Seismic Motion*, 3: 125 - 1279, Yokohama, Japan.

Bardet J., Ichii K., & Lin C. (2000). *EERA a computer program for Equivalent-linear Earthquake site Response Analyses of layered soil deposits*. Department of Civil Engineering, University of Southern California.

Bauer, R. (2004). Shear wave velocity determination of unlithified geologic materials and production of soil amplification maps for project impact community areas in the Cusec region. In *Final Technical Report March 2004*, Illinois State Geological Survey, Champaign, Illinois, USA.

Beresnev, I. & Atkinson, G. (1998). FINSIM-a FORTRAN program for simulating stochastic acceleration time histories from finite faults. *Seismol. Res. Lett*., 69 (1): 27-32.

Bettig. B., Bard, P-Y., Scherbaum, F., Riepl, J., Cotton, F., Cornou, C., & Hatzfeld, D. (2001). Analysis of dense array noise measurements using the modified spatial auto-correlation method (SPAC): Application to the Grenoble area. *Boll. Geof. Teor. Appl.* 42 (3-4):281–304.

Bindi, D., Castro, R., Franceschina, G., Luzi, L. & Pacor, F. (2004). The 1997-1998 Umbria. Marche sequence (central Italy): source, path and site effects estimated from strong motion data recorded in the epicentral area. *J. Geophys. Res*. 109, B04312, DOI: 10.1029/2003JB002857.

Bodin, P., Smith, K., Horton, S., & Hwang, H. (2001). Microtremor observations of deep sediment resonance in metropolitan Memphis, Tennessee. *Eng. Geol*. 62:159–168.

Bonnefoy-Claudet, S., Cornou, C., Bard, P-Y., Cotton, F., Moczo, P., Kristek, J., & Fah, D. (2006). H/V ratio: a tool for site effects evaluation. Results from 1-D noise simulations. *Geophys. J. Int.* 167: 827–837.

Bonnefoy-Claudet, S., Cornou, C., Di Giuglio, G., Guiller, B., Jongmans, D., Kohler, A., Ohrnberger, M., Savvaidis, A., Roten, D., Scherbaum, F., Schissele, E., Vollmer, D., & Wathelet, M. (2005). Report on FK/SPAC capabilities and limitations. *Deliverable WP06-D19.06*, University of Potsdam, Germany, 43 pp.

Bonnefoy-Claudet, S., Cotton, F., & Bard, P-Y. (2006). The nature of noise wavefield and its applications for site effects studies. A literature review. *Earth-Science Reviews*, 79:205 – 227.

Boominathan, A., Dodagoudar, G., Suganthi, A., & Maheswari, R. (2008). Seismic hazard assessment of Chennai city considering local site effects. *J. Earth Syst. Sci*. 117 (S2): 853–863.

Boore, D. & Asten, M. (2008). Comparisons of shear-wave slowness in the Santa Clara Valley, California, using blind interpretations of data from invasive and non-invasive methods. *Bull. Seismol. Soc. Am.* 98: 1983–2003, DOI: 10.1785/0120070277.

Booth, E., Pappin, J., Mills, J., Degg, M., & Steedman, R. (1986). The Mexican earthquake of 19th September 1985. *A field report by EEFIT*, Institution of Structural Engineers.

Borcherdt, R., Wentworth, C., Janssen, A., Fumal, T. & Gibbs, J. (1991). Methodology for predictive GIS mapping of special study zones for strong ground motion in the San Francisco bay region, CA, In *4th International Conference on Seismic Zonation*, (Stanford, California, August 25-29, 1991), Earthquake Engineering Research Institute, III, pp. 545-552.

Borja, R., Lin, C-H., Sama, K., & Masada, G. (2000). Modelling non-linear ground response of non-liquefiable soils. *Earthq. Eng. Struct. Dyn.* 29: 63-83.

Brebbia, C., Beskos, D., & Kausel, E. (1996). The Kobe earthquake: geodynamical aspects. *Computational Mechanics Publications*, Southampton, p. 165.

Building Seismic Safety Council [BSSC] (2001). NEHRP recommended provisions for seismic regulations for new buildings and other structures 2000 edition, part 1: Provisions. Report no. FEMA 368, Building seismic safety council for the federal emergency management agency, Washington, DC, USA.

Castellaro, S. & Mulargia, F. (2009). Vs30 estimates using constrained H/V measurements. *Bull. Seismol. Soc. Am.* 99(2A): 761–773. DOI:10.1785/0120080179.

Castro, R., Pacor, F., Bindi, D., Franceschina, G., & Luzi, L. (2004). Site response of strong motion stations in the Umbria region, Central Italy. *Bull. Seism. Soc. Am.*, 94: 576-590.

Celerier, J., Sandiford, M., Hansen, D., & Quigley, M. (2005). Modes of active intraplate deformation, Flinders Ranges, Australia. *Tectonics*, 24 (TC6006): 1-17. DOI:10.1029/2004TC001679.

Cho, I., Tada, T., & Shinozaki, Y. (2004). A new method to determine phase velocities of Rayleigh waves from microseisms. *Geophysics*, 69:1535– 1551.

Cho, I., Tada, T., & Shinozaki, Y. (2006). Centerless circular array method: inferring phase velocity of Rayleigh waves in broad wavelength ranges using microtremor records. *J. Geophys. Res*. 111, B09315; DOI: 10.1029/2005JB004235.

Chouet, B., Luca, G., Milana, G., Dawson, P., Martini, M. & Scarpa, R. (1998). Shallow velocity of Stromboli volcano, Italy, derived from small-aperture array measurements of Strombolian tremor. *Bull. Seismol. Soc. Am*. 88(3): 653–666.

Claprood, M. (2012). Spatially averaged coherency spectrum (SPAC) ambient noise array method. In Shear Wave Velocity Measurement Guidelines for Canadian Seismic Site Characterization. In Soil and Rock, Ed. J. A. Hunter & H. L. Crow, Geological Survey of Canada, *Open File 7078*, 94-102.

Collins, C., Kayen, R., Carkin, B., Allen, T., Cummins, P., & McPherson, A. (2006). Shear wave velocity measurement at Australian ground motion seismometer sites by the spectral analysis of surface waves (SASW) method. In *Proceedings of Earthquake Engineering in Australia*, Canberra, pp. 173-178.

Cox, J. (1970). A review of the geotechnical characteristics of the soils in the Adelaide City area. In *Proceedings of Symposium on Soils and Earth Structures in Arid Climates*, Institute of Engineers Australia and Australian Geomechanics Society, Adelaide, pp. 72–86.

Crone, A., Machette, M., & Bowman, J. (1997). Episodic nature of earthquake activity in stable continental regions revealed by palaeoseismicity studies of Australian and North American quaternary faults. Australian Journal of Earth Sciences: *An International Geoscience Journal of the Geological Society of Australia*, 44(2): 203-214, DOI: 10.1080/08120099708728304.

D'Amico, V., Picozzi, M., Albarello, D., Naso, G., & Tropenscovino, S. (2004). Quick estimates of soft sediment thicknesses from ambient noise horizontal to vertical spectral ratios: a case study in southern Italy. *J. Earthq. Eng*. 8(6):895–908.

Del Gaudio, V., Muscillo, S., & Wasowski, J. (2014). What we learn about slope response to earthquakes from ambient noise analysis: An overview. *Eng. Geol*. 182:182-200. DOI: 10.1016/j.enggeo.2014.05.010.

Delgado, J., Casado, C., Giner, J., Estevez, A., Cuenca, A., Molina, S. (2000). Microtremors as a Geophysical Exploration Tool: Application and Limitations. *Pure and Appl. Geophys*. 157:1445-1462.

Department of Manufacturing, Innovation, Trade, Resources and Energy Official Website [DMITRE Minerals] (2013). Urban Monitoring. http://www.pir.sa.gov.au/minerals/earthquakes/urban_monitoring accessed on 2 November 2013.

Di Giulio, G., Cornou, C., Ohrnberger, M., Wathelet, M., & Rovelli, A. (2006). Deriving wavefield characteristics and shear-velocity profiles from two-dimensional small-aperture arrays analysis of ambient vibrations in a small-size alluvial basin, Colfiorito, Italy. *Bull. Seismol. Soc. Am.* 96:1915–1933.

Di Giulio, G., Gaudiosi, I., Cara, F., Milana, G., & Tallini, M. (2014). Shear-wave velocity profile and seismic input derived from ambient vibration array

measurements: the case study of downtown L'Aquila. *Geophys. J. Int.* 198:848-866, DOI: 10.1093/gji/ggu162.

Di Stefano, P., Luzio, D., Renda, P., Martorana, R., Capizzi, P., D'Alessandro, A., Messina, N., Napoli, G., Todaro, S.& Zarcone, G. (2014). Integration of HVSR measures and stratigraphic constraints for seismic microzonation studies: the case of Oliveri (ME). *Nat. Hazards Earth Syst. Sciences*, 2: 2597-2637, DOI:10.5194/nhessd-2-2597-2014.

Di Stefano, P., Luzio, D., Renda, P., Martorana, R., Capizzi, P., D'Alessandro, A., Messina, N., Napoli, G., Todaro, S., & Zarcone, G. (2014). Integration of HVSR measures and stratigraphic constraints for seismic microzonation studies: the case of Oliveri (ME). *Nat. Hazards Earth Syst. Sci.* 2: 2597–2637. DOI: 10.5194/nhessd-2-2597-2014.

Dikmen, U. (2009). Statistical correlations of shear wave velocity and penetration resistance for soils. *J. Geophys. Eng.* 6(1):61–72, DOI:10.1088/1742-2132/6/1/007.

Dinesh, B., Nair, G., Prasad, A., Nakkeeran, P., & Radhakrishna, M. (2010). Estimation of sedimentary layers shear wave velocity using micro-tremor H/V ratio measurements for Bangalore city. *Soil Dyn. Earthq. Eng.* 30:1377–1382.

Dyster, T. (1992). Strong shock of earthquake: the story of the four greatest earthquakes in the history of South Australia. Department of Mines and Energy South Australia. *Report No. SR 126/A/86,* Vol. 3. 77 pp.

Dyster, T. (1996). Strong shock of earthquake: the strong of the four greatest earthquakes in the history of South Australia. *Report Book 95/47*, Department of Mines and Energy, Geology Survey of South Australia.

Endrun, B., Ohrnberger, M., Savvaidis, A. (2010). On the repeatability and consistency of three-component ambient vibration array measurements. *Bull. Earthq. Eng.* 8:535-570. DOI: 10.1007/s10518-009-9159-9

Environmental systems & services [ES&S] (2013). *eqWave 3 – seismic waveform analysis: product user manual*. Environmental Systems & Services, 28 pp.

Erdik, M. (2017). Earthquake risk assessment. *Bull. Earthq. Eng.* 15:5055-5092. DOI: 10.1007/s10518-017-0235-2

Estrada, G. (2010). Analysis of Earthquake Site Response and Site Classification for Seismic Design Practices. In *5th Int. Conf. on Recent Advances in Geotechnical Earthquake Engineering and Soil Dynamics and Symposium in Honor of Professor I. M. Idriss*, San Diego, California, http://scholarsmine.mst.edu/icrageesd/05icrageesd/session06b/4

Eurocode 8 (2003). Design of Structures for Earthquake Resistance, Part I: General Rules, Seismic Actions and Rules for Buildings. In European Committee for Standardization, *Doc CEN/TC250/ SC8/N335*, Draft No. 6.

Everingham, I., McEwin, A., & Denham, D. (1982). Atlas of isoseismal maps of Australian earthquakes. Bureau of Mineral Resources, *Geology and Geophys. Bull.* 214, p. 184.

Fah, D., Wathelet, M., Kristekova, M., Havenith, H., Endrun, B., Stamm, G., Poggi, V., Burjanek, J., & Cornou, C. (2003). Using ellipticity information for site characterisation. Report for Network of Research Infrastructures for European Seismology, Sixth Framework Program, *EC Project Number: 026130*, 54 pp.

Finn, W. & Wightman, A. (2003). *Ground motion amplification factors for the proposed 2005 edition of the National Building Code of Canada*. The National Research Council Canada (NRC) Research Press Web.

Fumal, T. (1978). Correlations between seismic wave velocities and physical properties of near-surface geologic materials in the Southern San Francisco Bay Region, California, in U.S. *Geological Survey Open-File Report 78-1067*, http://pubs.usgs.gov/of/1978/1067/.

Gaffet, F. (1998). A dense array experiment for the observation of waveform perturbations. *Soil Dyn. Earthq. Eng.* 17:475 – 484.

García-Jerez, A., Piña-Flores, J., Sánchez-Sesma, F., Luzón, F., & Perton, M. (2016). A computer code for forward computation and inversion of the HVSR spectral ratio under the diffuse field assumption. *Comput. Geosci.* 97:67-78.

Garofalo, F., Foti, S., Hollender, F., Bard, P-Y., Cornou, C., Cox, B., Ohrnberger, M., Sicilia, D., Asten, M., Di Giulio, G., Forbriger, T., Guillier, B., Hayashi, K., Martin, A., Matsushima, S., Mercerat, D., Poggi, V., & Yamanaka, H. (2016). InterPACIFIC project: Comparison of invasive and non-invasive methods for seismic site characterization. Part I: Intra-comparison of surface wave methods. *Soil Dyn. Earthq. Eng*. 82: 222–240. DOI: 10.1016/j.soildyn.2015.12.010

Geopsy (2015). Geopsy home: software applications for ambient vibration. http://www.geopsy.org, accessed 1/12/2015.

Geopsy., 2018. *Geopsy home: software applications for ambient vibration*. http://www.geopsy.org, accessed 1/06/2018.

Geoscience Australia. (2016). *Geoscience Australia earthquakes*. http://www.ga.gov.au/earthquakes/list.do?isRegionSelected=true&region=NT, accessed 1/12/2016.

Goldstein, P., Dodge, D., Firpo, M., & Minner, L. (2003). SAC2000: Signal processing and analysis tools for seismologists and engineers. *Int. Geophysics*, 81(2):1613-1614.

Gosar, A. (2007). Microtremor HVSR study for assessing site effects in the Bovec basin (NW Slovenia) related to 1998 Mw5.6 and 2004 Mw5.2 earthquakes. *Eng. Geol*. 91:178–193.

Graves, R., Pitarka, A., & Somerville, P. (1998). Ground motion amplification in the Santa Monica area: Effects of shallow basin edge structure. *Bull. Seismol. Soc. Am.* 88:1224–1242.

Greenhalgh, S. & Parham, R. (1986). The Richter earthquake magnitude scale in South Australia. *Australian J. Earth Sciences*, 33:519-528.

Greenhalgh, S., Love, D., Malpas, K., & McDougall, R. (1994). South Australian earthquakes, 1980-92. *Australian J. Earth Sciences*, 41(5):483-495. DOI: 10.1080/08120099408728158.

Gueguen, P., Chatelain, J-L., Guilier, B., Yepes, H., & Egred, J. (1998). Site effect and damage distribution in Pujili (Ecuador) after the 28 March Earthquake. *Soil Dyn. Earthq. Eng*. 17:329-334.

Guo, A., Aydin, A., & Kuszmaul, J. (2014). Microtremor recordings in Northern Mississippi. *Eng. Geol*. 179:146–157.

Guo, Z. & Aydin, A. (2016). A modified HVSR method to evaluate site effect in Northern Mississippi considering ocean wave climate. *Eng. Geol*. 200:104–113.

Hamedi, F. & Tehranizadeh, M. (2000). Influence of effective duration of strong motion on elastic response spectra. In *12th World Conference on Earthquake Engineering*, Auckland, New Zealand, January 30 – February 4, 2000, 7pp

Harjes, H. (1990). Design and siting of a new regional array in Central Europe. *Bull. Seismol. Soc. Am*. 80:1801–1817.

Hartzell, S. (1978). Earthquake aftershocks as Green's functions. *Geophys. Res. Lett*. 5: 1–14.

Harutoonian, P., Leo, C., Doanh, T., Castellaro, S., Zou, J., Liyanapathirana, D., Wong, H., & Tokeshi, K. (2012). Microtremor meansurements of rolling compacted ground. *Soil Dyn. Earthq. Eng*. (special publication): pp. 23-31, DOI: 10.1016/j.soildyn.2012.05.006.

Haubrich, R. (1968). Array design. *Bull. Seismol. Soc. Am.* 58:977–991.

Henstridge, J. (1979). A signal processing method for circular arrays. *Geophysics*, 44: 179–184.

Herak, M. (2008). ModelHVSR-a Matlab tool to model horizontal-to-vertical spectral ratio of ambient noise. *Comp. & Geosciences*, 34:1514 – 1526, DOI: 10.16/j.cageo.2007.07.009.

Herak, M., Allegretti, I., Herak, D., Kuk, K., Kuk, V., Maric, K., Markusic, S., & Stipcevic J. (2010). HVSR of ambient noise in Ston (Croatia): comparison with theoretical spectra and with the damage distribution after the 1996 Ston-Slano earthquake. *Bull. Earthq. Eng*. 8: 483-499.

Herald Sun News Official Website (2014). *Before-and-after interactive photos from the Christchurch quake*. http://www.heraldsun.com.au/news/special-features/christchurch-cathedral-before-and-after/story-fn7z04co-1226010885907 accessed on 5th January 2014.

Hillis, R., Sandiford, M., Reynolds, S., & Quigley, M. (2008). Present-day stresses, seismicity and Neogene-to-Recent tectonics of Australia's 'passive' margins: intraplate deformation controlled by plate boundary forces, In: *Johnson, H., Dore', A., Gatliff, R., Holdsworth, R., Lundin, E., & Ritchie, J., (Eds), The Nature and Origin of Compression in Passive Margins*. Geological Society, London, Special Publications, 306, 71–90. DOI: 10.1144/SP306.3.

Hinzen, K., Weber, B., & Scherbaum, F. (2004). On the resolution of H/V measurements to determine sediment thickness, a case study across a normal fault in the Lower Rhine Embayment. Germany. *J. Earthq. Eng*. 8 (6):909–926.

Holser, T., Bennett, M., Noce, T., & Tinsley, J. (2005). Shear-wave velocity of surficial geologic sediments in Northern California: statistical distributions and depth dependence. *Earthq. Spectra*. 21(1):161–177.

Horike, M. (1985). Inversion of phase velocity of long-period microtremors to the S-wave-velocity structure down to the basement in urbanized areas. *J. Physics of the Earth*. 33:59–69.

Horike, M. (1996). Geophysical exploration using microtremor measurements. In Proc. of 11th World Conference on Earthquake Engineering, Acapulco, Mexico, *Paper No. 2033*.

Humire, F., Saez, E., Leyton, F., & Yanez, G. (2015). Combining active and passive multi-channel analysis of surface waves to improve reliability of Vs,30 estimation using standard equipment. *Bull. Earthq. Eng.* 13:1303-1321. DOI: 10.1007/s10518-014-9662-5

Ibs-von Seht, M. & Wohlenberg, J. (1999). Microtremor measurements used to map thickness of soft sediments. *Bull. Seismol. Soc. Am*. 89:250–259.

Idriss, I. & Sun J. (1992). *User's manual for SHAKE91 (a computer program for conducting equivalent linear seismic response analyses of horizontally layered soil deposits*. Center for Geotechnical Modeling, Department of Civil & Environmental Engineering, University of California, Davis, California.

Idriss, I. (1990). *Response of soft soil sites during earthquakes*. H. Bolton Seed Memorial Symposium, Vancouver.

Iervolino, I. & Cornell, C. (2008). Probability of occurrence of velocity pulses in near-source ground motions. *Bull. Seismol. Soc. Am.* 98 (5), 2262–2277.

Ishida, H., Nozawa, T. & Niwa, M. (1998). Estimation of deep surface structure based on phase velocities and spectral ratios of long period microtremors. In *2nd Int. Symp. on the Effects of Surface Geology on Seismic Motion*, Yokohama, Japan, (2):697–704.

Jaksa, M. (1995). The influence of spatial variability on the geotechnical design properties of a stiff, overconsolidated clay. *Ph.D. thesis*, University of Adelaide, Australia.

Johnston, A. (1996a). Seismic moment assessment of earthquakes in stable continental regions-I. Instrumental seismicity. *Geophys. J. Int*. 124:381-414.

Johnston, A. (1996b). Seismic moment assessment of earthquakes in stable continental regions-III. New Madrid 181 1-1812, Charleston 1886 and Lisbon 1755. *Geophys. J. Int*. 126:314–344.

Jongmans, D., Ohrnberger, M. & Wathelet, M. (2005). Recommendations for array measurements and processing. SESAME European Research Project, *WP12 – Deliverable D24.13* European Commission – Research General Directorate, Project No. EVG1-CT-200-00026.

Joyner, W. & Boore, D. (1986). On simulating large earthquakes by Green's-function addition of smaller earthquakes. In Proceedings of the Fifth Maurice Ewing Symposium on Earthquake Source Mechanics, *Am. Geophys. Union*, 269–274.

Kanay, K. & Tanaka, T. (1961). On microtremors VIII. *Bull Earthq Res Inst*. 97 – 114

Kerr-Grant, C. (1956). The Adelaide earthquake of 1st March 1954. *Transactions of the Royal Society of South Australia*, 59:177-185.

Kind, F. (2002). Development of microzonation methods: application to Basle, Switzerland. *Ph.D. thesis*, Swiss Federal Institute of Technology, Switzerland, Dissertation ETH No. 14548.

Kind, F., Fah, D. & Giardini, D. (2005). Array measurements of S-wave velocities from ambient vibrations. *Geophys. J. Int*. 160:114–126.

Konno, K. & Omachi, T. (1998). Ground motion characteristics estimated from spectral ratio between horizontal and vertical components of microtemors. *Bull. Seismol. Soc. Am*. 88(1):228-241.

Kramer, S. (1996). *Geotechnical earthquake engineering*. Prentice Hall, Upper Saddle River, New Jersey.

Lane, J., White, E., Steele, G., & Cannia, J. (2008). Estimation of bedrock depth using the horizontal-to-vertical (H/V) ambient-noise seismic method. *Proceedings of Symposium on the Application of Geophysics to Engineering and Environmental Problems*, April 6-10, 2008, Philadelphia, Pennsylvania.

Lau, K. (2000). A review of downhole geophysical methods for ground investigation. In *Geo report No. 99*, Geotechnical Engineering Office, Civil Engineering Department, The Government of the Hong Kong Special Administrative Region.

Leonard, M. (2015). Personal communication: preliminary results of Vs30 for the Adelaide region, South Australia.

Leonard, M., Burbidge, D., & Edwards, M. (2013). Atlas of seismic hazard maps of Australia: seismic hazard maps, hazard curves and hazard spectra. *Record 2013/41*. Geoscience Australia: Canberra, p. 39.

Lermo, J. & Cha'vez-Garcia, F. (1993). Site effect evaluation using spectral ratios with only one station. *Bull. Seismol. Soc. Am*. 83:1574 – 1594.

Linkimer, L. (2008). Relationship between peak ground acceleration and modified Mercalli intensity in Costa Rica. *Revista Geologica de America Central*, 38:81–94.

Love, D. (1996). *Seismic hazard and microzonation of the Adelaide metropolitan area*. Adelaide: Sutton Earthquake Centre, Department of Mines and Energy, South Australia.

Luna, R. & Jadi, H. (2000). Determination of dynamic soil properties using geophysical methods. In *Proc. 1st International Conference on the Application of Geophysical and NDT Methodologies to Transportation Facilities and Infrastructure*, St Louis, MO.

Lunedei, E. & Albarello, D. (2015). Horizontal-to-vertical spectral ratios from a full-wavefield model of ambient vibrations generated by a distribution of spatially correlated surface sources. *Geophys. J. Int.* 201:1140-1153.

Luzi L., Bindi D., Franceschina G., Pacor F., & Castro R. (2005). Geotechnical site characterisation in the Umbria Marche area and evaluation of earthquake site-response. *Pure Appl. Geophys.* 162:2133-2161, DOI: 10.1007/s00024-005-2707-6.

Macau, A., Benjumea, B., Gabàs, A., Figueras, S. & Vilà, M. (2014). The effect of shallow Quaternary deposits on the shape of the H/V spectral ratio, *Surv. Geophys*. 36(1): 185–208. DOI: 10.1007/s10712-014-9305-z.

Malpas, K. (1991). Seismic risk of South Australia. *Master Thesis*, School of Earth Sciences Flinders University of South Australia, p. 179.

Mavroeidis, G. & Papageorgiou, A. (2003). A mathematical representation of near-fault ground motions. *Bull. Seism. Soc. Am.* 93 (3), 1099–1131.

McBean, P. (2010). Design implications for structures within the Adelaide CBD arising from changes to the subsoil classification system in AS 1170.4. *Australian Geomechanics*, 45(3): 93–100.

McCue, K. & Love, D. (1997). *Earthquake microzonation Adelaide, South Australia*. Australian Geological Survey Organisation (AGSO), Primary Industries and Resources South Australia, Final Report.

McCue, K. (1975). Seismicity and seismic risk in South Australia. *Report ADP 137*, Department of Physics, University of Adelaide, South Australia.

McCue, K. (1990). Australia's large earthquakes and recent fault scarps, *J. Structural Geology*, 12 (5/6):761-766.

McCue, K., Gregson, P., Sinadinovski, C., & Hodgson, L. (2001). Australian seismological report 1997. *AGSO Record 2001/28*, AGSO – Geoscience Australia, Dept. of Industry, Science & Resources, Canberra, 68 pp.

McPherson, A. & Hall, L. (2007). Development of the Australian National Regolith Site Classification Map. *Geoscience Australia Record 2007/07*, Canberra ACT, Australia, 37 pp. Available at: https://www.ga.gov.au/products/servlet/controller?event=GEOCAT_DETAILS&catno=65240

McVerry, G., Zhao, J., Abrahamson, N., & Somerville, G. (2000). Crustal and subduction zone attenuation relations for New Zealand earthquakes. In *Proceedings 12th World Conference on Earthquake Engineering*, Auckland, New Zealand, Paper No. 1834.

McVerry, G., Zhao, J., Abrahamson, N., & Somerville, G. (2006). New Zealand acceleration response spectrum attenuation relations for crustal and subduction zone earthquake. *Bull. New Zealand Soc. Earthq. Eng.* 39(1), March 2006, 58 pp.

Mimoglou, P., Psycharis, I., & Taflampas, I. (2017). Determination of the parameters of the directivity pulse embedded in near-fault ground motions and its effect on structural response, In: *Papadrakakis M., Plevris V. and Lagaros N.D. (eds), Computational methods in earthquake engineering*, Springer, DOI:10.1007/978-3-319-47798-5_2.

Miyakoshi, K., Kagawa, T., & Kinoshita, T. (1998). Estimation of geological structures under the Kobe area using the array recordings of microtremors. In *2nd*

International Symposium on the Effects of Surface Geology on Seismic Motion, Yokohama, Japan, 691–696.

Mokhberi, M., Davoodi, M., & Haghshenas, E. (2010). The Application of the H/V Spectral Ratio Technique for Estimating the Site Characterization in the South of Iran. *Soil Dyn. Earthq. Eng*. pp. 300-308. DOI: 10.1061/41102(375)37.

Motazedian, D. & Atkinson, G. (2005). Stochastic finite fault modeling based on a dynamic corner frequency. *Bull. Seism. Soc. Am*. 95:995-1010.

Motazedian, D. & Moinfar, A. (2006). Hybrid stochastic finite fault modeling of 2003, M6.5, Bam earthquake (Iran). *J. Seism.* 10: 91–103, DOI: 10.1007/s10950-005-9003-x.

Nakamura, Y. (1989). A method for dynamic characteristics estimation of subsurface using microtremor on the ground surface. In *Railway Tech. Res. Inst. Quarterly Rep.* 30 (1):25-33.

Narayan, J. & Rao, P. (2003). Two and half dimensional simulation of ridge effects on the ground motion characteristics. *Pure and Appl. Geophys*. 160:1557–1571.

Narayan, J. (2005). Study of Basin-edge effects on the ground motion characteristics using 2.5-D modeling. *Pure and Appl. Geophys*. 162:273–289.

National Committee on Soil and Terrain [NCCST] (2009). Australian soil and land survey field handbook. *Australian Soil and Land Survey Handbook*, Series; No. 1, 3rd ed. CSIRO Publishing, Collingwood, Victoria.

Nazarian, S., Stokoe, K., & Hudson, W. (1983). Use of spectral analysis of surface waves method for determination of moduli and thicknesses of pavement systems. *Transportation Research Record,* 930:38-45.

Nogoshi, M. & Igarashi, T. (1971). On the amplitude characteristics of microtremor (part 2). *J. Seismol. Soc. Japan*, 26-40.

Ohori, M., Nobat, A., & Wakamatsu K. (2002). A comparison of ESAC and FK methods of estimating phase velocity using arbitrarily shaped microtremor analysis. *Bull. Seismol. Soc. Am*. 92:2323–2332.

Okada, H. (2003). The microseismic survey method. Geophysical Monograph Series No. 12. Society of exploration geophysicists with the cooperation of Society of exploration geophysicists of Japan and Australian Society of Exploration Geophysicists. Translated by Koya Suto, ISBN: 1-56080-120-4, 135 pp.

Olsen, K., Day, S., & Bradley, C. (2003). Estimation of Q for Long-Period (>2 sec) waves in the Los Angeles Basin. *Bull. Seism. Soc. Am.* 93(2):627-638.

Orchant, C., Kulhawy, F., & Trautmann, C. (1988). Critical Evaluation of In-Situ Test Methods and their Variability. *Report EL-5507*, Vol. 2, Electric Power Research Institute, Palo Alto.

Panagiotou, M. (2008). Seismic design, testing and analysis of reinforced concrete wall buildings. *Ph.D. Dissertation*, University of California, San Diego.

Pantulin, M., Moratto, L., Sarao, A., & Slejko, D. (2012). Ground motion modelling including finite fault and 1D site effects in north-eastern Italy. *Boll. Geof. Teor. Appl.* 53 (3):313-330, DOI 10.4430/bgta0071.

Papadopoulos, I., Papazachos, C., Saccaidis, A., Theodoulidis, N., & Vallianatos, F. (2017). Seismic microzonation of the broader Chania basin area (Southern Greece) from the joint evaluation of ambient noise and earthquake recordings. *Bull. Earthq. Eng.* 15:861-888. DOI: 10.1007/s10518-016-0019-0

Park, C., Miller, R., & Xia, J. (1999). Multi-channel analysis of surface waves. *Geophysics*, 64:800-808.

Parolai, S., Bormann, P., & Milkereit, C. (2002). New relationship between vs, thickness of sediments, and resonance frequency calculated by the H/V ratio of seismic noise for the Cologne area (Germany). *Bull. Seismol. Soc. Am*. 92 (6):2521–2527.

Parolai, S., Richwalski, S., Milkereit, C., & Fah, D. (2006). S-wave velocity profiles for earthquake engineering purposes for the Cologne area (Germany). *Bull. Earthq. Eng.* 4:65-94. DOI: 10.1007/s10518-005-5758-2

Paudyal, Y., Bhandary, N., & Yatabe, R., (2012b). Seismic Microzonation of densely populated area of Kathmandu Valley of Nepal using microtremor observations. *J. Earthq. Eng*. 16 (8):1208–1229.

Paudyal, Y., Yatabe, R., Bhandary, N., & Dahal, R., (2012a). A study of local amplification effect of soil layers on ground motion in the Katmandu Valley using microtremor analysis. *J. Earthq. Eng. and Eng. Vib.* 11 (2):257–268.

Picozzi, M., Strollo, A., Paraloi, S., Durukal, E., Ozel, O., Karabulut, S., Zschau, J., & Erdik, M. (2009). Site characterization by seismic noise in Istanbul, turkey. *Soil Dyn. Earthq. Eng*. pp. 469-482. DOI: 10.1016/j.soildyn.2008.05.07.

Poggi, V. & Fah, D. (2010). Estimating Rayleigh wave particle motion from three-component. *Geophys. J. Int.* 180: 251–267. DOI: 10.1111/j.1365-246X.2009.04402.x

Priolo, E., Poli, M., Laurenzano, G., Vuan, A., & Barnaba, C. (2008). Site response estimation in the Vittorio Veneto area (NE Italy), Part 2: mapping the local seismic effects in the urban settlement. *Boll. Geof. Teor. Appl*. 49 (3-4): 387-400.

Professor Keith Woodford Personal Website (2014). *Understanding the Christchurch earthquake: building damage*. http://keithwoodford.wordpress.com/2011/02/27/understanding-the-christchurch-earthquake-building-damage/ accessed on 6th January 2014.

Puech, A., Rivoallan, X., & Cherel, L. (2004). The use of surface waves in the characterisation of seabed sediments: development of a MASW system for offshore applications. In *Colloque "Caracterisation in situ des fonds marins*," Seatechweek, Brest, France.

Quigley, M., Sandiford, M., Fifield, K., & Alimanovic, A. (2006). Bedrock erosion and relief production in the northern Flinders Ranges, Australia. *Earth Surf. Processes & Landforms*, 32:929-944, DOI: 10.1002/esp. 1459.

Quigley, M., Sandiford, M., Fifield, K., & Alimanovic, A. (2007). Landscape responses to intraplate tectonism: Quantitative constraints from 10Be nuclide abundances. *Earth and Planetary Science Lett.* 261:120–133.

Roberts, J. & Asten, M. (2008). A study of near source effects in array-based (SPAC) microtremor surveys. *Geophys. J. Int.* 174:159-177, DOI: 10.1111/j.1365-246X.2008.03729.x.

Rost, S. & Thomas, C. (2002). Array seismology: methods and applications. *Review of Geophysics,* 40(3), 27 pp.

Sambridge, M. (1999). Geophysical inversion with a neighborhood algorithm I. Searching a parameter space. *J. Geophysical Res*. 103:4839-4878.

Sandiford, M. (2003). Neotectonics of southeastern Australia: linking the Quaternary faulting record with seismicity and in situ stress. In: *Hillis, R.R., Muller, D. (Eds.), Evolution and Dynamics of the Australian Plate*, Geological Society of Australia Special Publication, 22:101–113.

Sandiford, M., Wallace, M., & Coblentz, D. (2004). Origin of the in situ stress field in south-eastern Australia. *Basin Research*, 16:325–338, DOI: 10.1111/j.1365-2117.2004.00235.x.

Santulin, M., Moratto, L., Sarao, A., & Slejko, D. (2012). Ground motion modelling including finite fault and 1D site effects in north-eastern Italy. *Boll. Geof. Teor. Appl*. 53 (3), 313-330, DOI: 10.4430/bgta0071.

Satoh, T., Kawase, H., & Shin'Ichi, M. (2001). Estimation of S-wave velocity structures in and around the Sendai Basin, Japan, using arrays records of microtremors. *Bull. Seismol. Soc. Am.* 91(2):206 – 218.

Scherbaum, F., Hinzen, K., & Ohrnberger, M. (2003). Determination of shallow shear wave velocity profiles in the Cologne, Germany area using ambient vibrations, *Geophys. J. Int.* 152 (3):597 – 612.

Schnabel, P., Lysmer, J., & Seed, H. (1972). SHAKE: A computer program for earthquake response analysis of horizontally layered sites. *EERC Report 72-12*, Earthquake Engineering Research Center, Berkeley, California: University of California, 102pp.

Schweitzer, S., Fyen, J., Mykkeltveit, S., Gibbons, S., Pirli, M., Kuhn, D., & Kvaerna, T. (2011). Chapter 9: Seismic arrays. In *IASPEI New Manual of Seismological Observatory Practice*. p. 79, ed. Bormann, P., Geo Forschungs Zentrum, Potsdam.

Seed, H. & Idriss, I. (1970). Soil Moduli and Damping Factors for Dynamic Response Analysis. *Report No. UCB/EERC-70/10*, Earthquake Engineering Research Center, University of California, Berkeley, California, 48pp.

Seed, H. & Sun, J. (1989). Implication of site effects in the Mexico City earthquake of September 19, 1985 for earthquake-resistance-design criteria in the San Francisco Bay Area of California. *Report No. UCB/EERC-89/03*, Earthquake Engineering Research Center, University of California, Berkeley, California, 140pp.

Selby, J. & Lindsay, J. (1982). Engineering geology of the Adelaide City area. Department of Mines and Energy, Geological Survey of South Australia, D. J. Woolman, Government Printer, *Bulletin 51*, 94 pp.

Selby, J. (1984). Geology and the Adelaide Environment. Department of Mines and Energy, South Australia, D.J. Woolman, Government Printer, Adelaide, ISSN: 0726 1519, 168 pp.

SESAME (2004). Guidelines for the implementation of the H/V spectral ratio technique on ambient vibrations Measurements, processing and interpretation. In: *SESAME European Research Project Wp12 – Deliverable d23.12*, European Commission – Research General Directorate, Project No. EVG1-CT-2000-00026. <http://sesame-fp5.obs.ujf-grenoble.fr>.

Setiawan, B., Jaksa, M., Griffith, M., & Love, D. (2015). HVSR recording duration for regolith sites: an experimental approach. *Proceedings of the Tenth Pacific Conference on Earthquake Engineering*, "Building an Earthquake-Resilient Pacific" 6-8 November 2015, Sydney, Australia.

Setiawan, B., Jaksa, M., Griffith, M., & Love, D. (2016). Analysis of microtremor array measurement using the spatial autocorrelation (SPAC) method across the Adelaide City. *Research Report No. 196*, School of Civil, Environmental, and Mining Engineering, the University of Adelaide, 36 pp.

Setiawan, B., Jaksa, M., Griffith, M., & Love, D. (2018a). Passive noise datasets at regolith sites. *Data in Brief*. (In print).

Setiawan, B., Jaksa, M., Griffith, M., & Love, D. (2018b). Seismic site classification based on constrained modeling of measured HVSR curve in regolith sites. *Soil Dyn. Earthq. Eng.* 110: 244–261, DOI: 10.1016/j.soildyn.2017.08.006.

Shapiro, N. & Campillo, M. (2004). Emergence of broadband Rayleigh waves from correlations of the ambient seismic noise. *Geophys. Res. Lett.* 31(7).

Sheard, M. & Bowman, G. (1987a). Definition of the Keswick Clay: Adelaide/Golden Grove Embayment, Para and Eden Blocks, South Australia. *Q. geol. Notes, geol. Surv. S. Aust*. 103, 4–9.

Sheard, M. & Bowman, G. (1987b). Redefinition of the Upper Boundary of the Hindmarsh Clay: Adelaide Plains Sub-Basin and Adelaide/Golden Grove Embayment. *Q. geol. Notes, geol. Surv. S. Aust.* 103, 9–16.

Sheard, M. & Bowman, G. (1996). *Soils, stratigraphy and engineering geology of near surface materials of the Adelaide Plains*. Adelaide: Department of Mines and Energy, South Australia.

Smith, G. (1986). *Probability and statistics in civil engineering: An introduction*. Collins, London.

Somerville, P. & Graves, R. (1996). Site effects in the Los Angeles area during the 1994 Northridge earthquake. In Eleventh World Conference on Earthquake Engineering, *Paper No. 2030*.

Standards Australia (2004). AS 1289.6.3.1–2004 Methods of testing soils for engineering purposes. Method 6.3.1: Soil strength and consolidation tests – Determination of the penetration resistance of a soil – Standard penetration test (SPT), in *Standards Australia*.

Standards Australia (2007). AS 1170.4-2007 Australian Standard of Structural Design Actions Part 4: Earthquake Actions in Australia, in *Standards Australia*.

Standards New Zealand (2004). NZS 1170.5:2004 Structural design actions Part 5 Earthquake actions – New Zealand, in *New Zealand Standards*.

Street, R., Woolery, E., Wang, Z., & Harris, J. (2001). NEHRP soil classifications for estimating site-dependent seismic coefficients in the Upper Mississippi Embayment. *Eng. Geol.* 62:123–135.

Sykora, D. & Davis, J. (1993). *Site-specific earthquake response analysis for Paducah Gaseous Diffusion Plant, Paducah, Kentucky*. Vicksburg, MS: U.S. Department of Energy.

Tada, T., Cho, I., & Shinozaki, Y. (2006). A two-radius circular array method: inferring phase velocities of Love waves using microtremor records. *Geophys. Res. Lett.* 33, L10303; DOI: 10.1029/2006GL025722.

Taflampas, I. & Psycharis, I. (2008). Investigation of the effect of the ground motion characteristics on the Ry−l relation for the inelastic response of SDOF structures. In *14th World Conference on Earthquake Engineering*, Beijing, China, 12–17 October 2008.

Tokimatsu, K. (1997). Geotechnical site characterization using surface waves. In *Proceeding of the First International Conference on Earthquake Geotechnical Engineering*, 3:1333 – 1368.

Toshinawa, T., Taber, J. J., & Berril, J. (1997). Distribution of ground motion intensity inferred from questionnaire survey earthquake recordings and microtremors measurements – a case study in Christchurch New Zealand during the Arthurs Pass Earthquake. *Bull. Seismol. Soc Am.* 87: 356-369.

Tsiambaos, G. & Sabatakakis, N. (2010). Empirical estimation of shear wave velocity from in situ tests on soil formations in Greece. *Bull. Eng. Geology & Environ.*, 70:291–297, DOI 10.1007/s10064-010-0324-9.

Uthayakumar, U. & Naesgaard, E. (2004). Ground response analysis for seismic design in Fraser River Delta, British Columbia. In *13th World Conference on Earthquake Engineering*.

Van der Baan, M. (2009). The origin of SH-wave resonance frequencies in sedimentary layers. *Geophys. J. Int.* 178:1587-1596.

Veevers, J. (1984). Phanerozoic Earth History of Australia. Oxford University Press, New York, 418 pp.

Volti, T., Burbidge, D., Collins, C., Asten, M., Odum, J., Stephenson, W., Pascal, C. & Holzschuh, J. (2016). Comparisons between Vs30 and spectral response for 30 sites in Newcastle, Australia, from collocated seismic cone penetrometer, active- and passive-source VS data. *Bull. Seismol. Soc. Am.* 106, (4): 1690–1709, DOI: 10.1785/0120150073.

Wair, B, DeJong, J., & Shantz, T. (2012). Guidelines for estimation of shear wave velocity profiles. In *PEER Report 2012/08*, Pacific Earthquake Engineering Research Center.

Wald, D., Quintoriano, V., Heaton, T., & Kanamori, H. (1999). Relationship between peak ground acceleration, peak ground velocity and modified Mercalli intensity in California. *Earthq. Spectra*, 15:557 – 564.

Wathelet, M. (2005). Array recordings of ambient vibrations: surface-waves inversion, *PhD thesis*, University of Liege, Belgium.

Wathelet, M., Jongmans, D., & Ohrnberger, M. (2004). Surface-wave inversion using direct search algorithm and its application to ambient vibration measurements, *Near Surf. Geophysics.* 2:211-221.

Wathelet, M., Jongmans, D., Ohrnberger, M., & Bonnefoy-Claudet, S. (2008). Array performances for ambient vibrations on a shallow structure and consequences over Vs inversion. *J. Seismol.* 12: 1 - 19.

Wathelet, M., Jongmas, D., & Ohremberg, M. (2005). Direct inversion of spatial autocorrelation curves with the neighborhood algorithm. *Bull. Seismol. Soc Am.* 95(5): 1787 - 1800.

Wilford, J. & Thomas, M. (2013). Predicting regolith thickness in the complex weathering setting of the central Mt Lofty Ranges, South Australia. *Geoderma*, 206:1-13. DOI: 10.1016/j.geoderma.2013.04.002.

Woods, J. & Lintz, P. (1973). Plane waves at small arrays. *Geophysics*, 38:1023–1041.

Wotherspoon, L., Bradley, B., Van Houtte, C., & Larkin, T. (2015). Horizontal to vertical spectral ratio: applications and limitations. NZ Geomechanics News, *Bull. New Zealand Geotech. Soc. Inc.* 89: 136-139, ISSN 0111-6851.

Xia, J., Miller, R., Park, C., & Ivanov, J., (2000). Construction of 2D vertical shear-wave velocity field by the multi channels analysis of surface waves technique. In *Proceedings of the Symposium on the Application of Geophysics to Engineering and Environmental Problems*, 1197 - 1206, Arlington, VA., USA.

Yamamoto, H. (2000). Estimation of shallow S-wave velocity structures from phase velocities of love and Rayleigh-waves in microtremors. In *Proceedings of the 12th World Conference on Earthquake Engineering*, Auckland, New Zealand.

Yamanaka, H., Takemura, M., Hyshida, H., & Niwa, M. (1994). Characteristics of long-period microtremors and their applicability in exploration of deep sedimentary layers. *Bull. Seismol. Soc Am.* 84(6): 1831–1841.

Zaineh, H., Yamanaka, H., Dakkak, R., Khalil, A., & Daoud, M. (2012). Estimation of shallow S-wave velocity structure in Damascus city Syria, using microtremor exploration. *Soil Dyn. Earthq. Eng*. 39: 88 – 99.

Zhang, Z. & Stewart, R. (2007). Seismic attenuation and rock property analysis in a heavy oilfield: Ross Lake, Saskatchewan. University of Calgary, CREWES *Research Report Volume 19*.

Appendix A:

AN INTERNATIONAL PEER REVIEWED CONFERENCE PAPER

INTENTIONALLY BLANK

Proceedings of the Tenth Pacific Conference on Earthquake Engineering
Building an Earthquake-Resilient Pacific
6-8 November 2015, Sydney, Australia

HVSR recording duration for regolith sites: an experimental approach

B. Setiawan

School of Civil, Environmental & Mining Engineering, University of Adelaide, Australia and Faculty of Engineering, Syiah Kuala University, Indonesia

M. B. Jaksa

School of Civil, Environmental & Mining Engineering, University of Adelaide, Australia

M. C. Griffith

School of Civil, Environmental & Mining Engineering, University of Adelaide, Australia

D. Love

Department of State Development, Government of South Australia, Australia

ABSTRACT: The application of the horizontal vertical spectral ratio (HVSR) technique using microtremor measurement to quantify the natural period of sites in urban areas is widely used around the world. However, this technique is still under development in regions with low impedance contrast between the top layer and the underlying bedrock, such as regolith. This paper investigates the recording duration of the aforementioned method for quantifying the site fundamental frequency in regolith environments. An experimental study has been carried out at a regolith site where two days of continuous data acquisition are used to investigate the HVSR technique measurement duration. A series of reliability tests were applied to the HVSR analysis results. The analyses suggest that at least 20 minutes duration is required for more reliable HVSR analysis results at regolith sites.

1 INTRODUCTION

The geophysical community is in agreement that the horizontal vertical spectral ratio (HVSR) technique provides valuable results in seismic hazard assessment in urban areas (Bard, 2002). However, guidelines for the minimum recording duration in a region with low impedance contrast between the top layer and the underlying bedrock, such as regolith sites, is still under development. Therefore, an experimental study has been carried out in accordance with the SESAME European project (Site EffectS assessment using AMbient Excitations) guidelines (SESAME 2004) at such a site in metropolitan Adelaide (Payneham), South Australia. The study aims to measure the fundamental frequency of the site and assess the reliability of various ambient noise measurement durations.

2 HVSR TECHNIQUE

2.1 *Equipment and data acquisition*

The equipment and data acquisition adopted in the present study utilised an LE-3DLite Lennartz seismometer with a Kelunji EchoPro digital data recorder, as shown in Figure 1. In order to reduce extraneous noise generated primarily by the wind, the seismometer was placed on a concrete slab, to provide a firm foundation, and a bucket and brick were used to shield the instrument (Figure 1).

Figure 1. HVSR technique main equipment and data acquisition setup

Horizontal vertical spectral ratio (HVSR) processing was carried out using the Geopsy software (Geopsy Project 2015) developed within the framework of the SESAME Project. This open source software processes the microtremor data in the following steps:

- Select as many as possible most-stationary windows (N) within the recorded data;
- Compute Fourier spectra amplitudes and carry out smoothing for the N most-stationary windows;
- Average of horizontal components for the N most-stationary windows;
- Compute N HVSRs for the N most-stationary windows; and
- Compute the average HVSR and the estimation error.

In the present study, default parameters and auto window selection are employed in the HVSR analysis.

2.2 *Recording duration*

In accordance with the SESAME guidelines (SESAME 2004), the recommended minimum recording duration for the HVSR technique is 30 minutes. However, when the expected fundamental frequency (f_0) is known, the recording duration can be less than that. Details of the SESAME recommendations are given in the Table 1.

Table 1. SESAME Recommendation for recording duration (SESAME 2004)

Minimum expected f_0 (Hz)	Recommended minimum recording duration (minutes)
0.2	30
0.5	20
1	10
2	5
5	3
10	2

2.3 *Reliability of HVSR technique curve*

The SESAME guidelines (SESAME 2004) outline a process by which the reliability of the HVSR curve can be assessed. The following criteria are suggested:

a. Criterion 1: So that the peak is significant, the fundamental frequency, f_0, should be greater than 10 divided by the window length (I_w), which in this study is 40 seconds;
b. Criterion 2: The analysis requires that a large number of windows and cycles is needed. Hence, the number of significant cycles should be greater than 200; and
c. Criterion 3: The level of scatter should be low. Hence, the standard deviation of the amplitude of the HVSR curve, at frequencies between $0.5f_0$ and $2f_0$, should be less than two when $f_0 >$ 0.5 Hz, or less than 3 when $f_0 <$ 0.5 Hz.

3 METHODOLOGY

The methodology adopted in the present study is outlined as follows:

- Collect continuous microtremor data over a duration of two days;
- Select and arrange the two-day measured ambient noise data into a series of 5, 10, 20, 30 and 60 minute recordings;
- Process each of the 5, 10, 20, 30 and 60 minute record subsets using the HVSR technique, in accordance with the SESAME guidelines (SESAME 2004); and
- Apply the reliability criteria to each of the HVSR results, as outlined in §2.3 above.

4 RESULTS OF HVSR AND RELIABILITY ANALYSES

4.1 HVSR analysis

A summary of the HVSR results for the 5, 10, 20, 30 and 60 minute subsets is given in Table 2. Detailed plots of the HVSR results are presented in Figures 2 to 4.

Table 2. Summary of all HVSR results

Recording duration (minutes)	Average f_0 (Hz) with the standard deviation	Median f_0 (Hz)
5	0.97±0.14	1.00
10	0.97±0.13	1.00
20	0.98±0.10	1.01
30	0.98±0.01	1.01
60	0.99±0.02	1.01

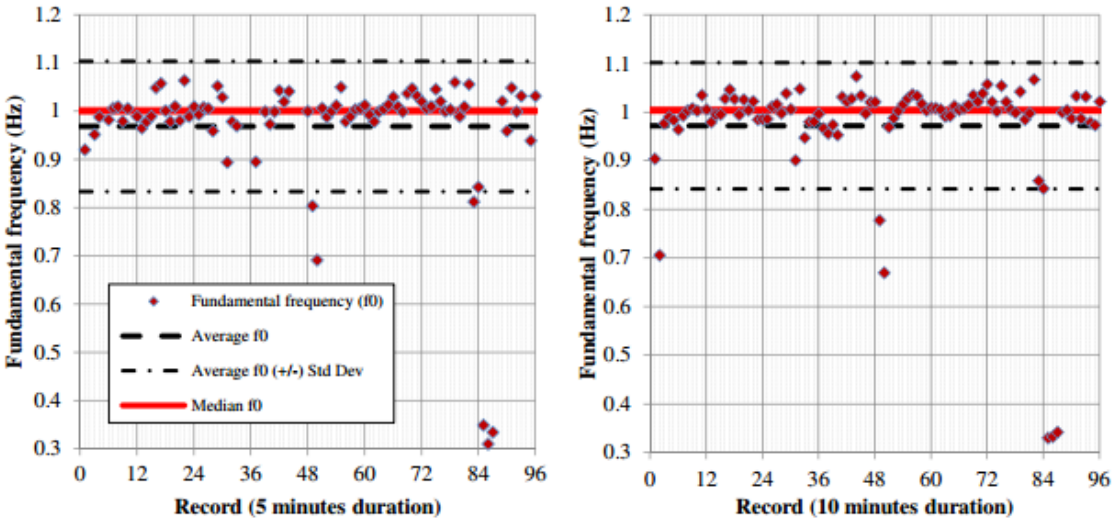

Figure 2. Results of HVSR technique for (a) 5 and (b) 10 minute recording duration

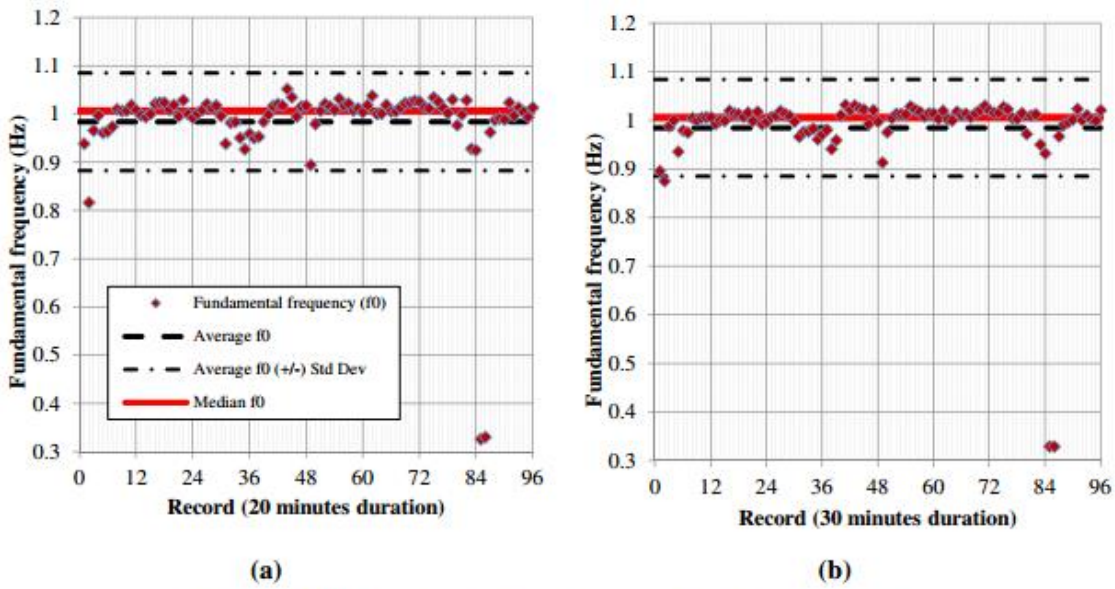

Figure 3. Results of HVSR technique for (a) 20 and (b) 30 minute recording duration

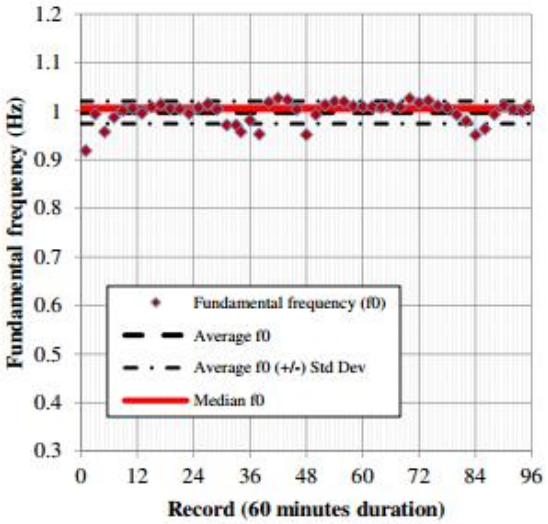

Figure 4. Results of HVSR technique for 60 minute recording duration

4.2 Reliability analysis

In accordance with the SESAME guidelines (SESAME 2004) the three reliability criteria have been applied to the HVSR results and these are summarised in Table 2. The reliability analysis results show that the 5 and 10 minute records produce only 14% and 64% records respectively pass the three criteria. Good results, however, are obtained for the 20, 30 and 60 minute duration records. These produce 86% to 89% of the records which pass the criteria.

Analysis of the reliable records show that all the durations yield estimates of f_0 = 1 Hz with a maximum standard deviation of ±0.03. Furthermore, the median f_0 of the reliable records is about 1.0 Hz as well. Detailed results are given in Table 3 and Figure 5.

Table 2. Summary of reliability test of HVSR results

Recording duration (minutes)	Criterion 1		Criterion 2		Criterion 3		Remarks
	Pass	Fail	Pass	Fail	Pass	Fail	
5	84	12	14	82	68	28	12 records do not produce a f_0. 13 of 96 records pass the reliability criteria (14%).
10	96	0	70	26	78	18	62 of 96 records pass the reliability criteria (64%).
20	96	0	93	3	84	12	83 of 96 records pass the reliability criteria (86%).
30	96	0	95	1	86	10	86 of 96 records pass the reliability criteria (89%).
60	96	0	96	0	91	5	44 of 49 records pass the reliability criteria (89%).

Table 3. Average and median f_0 for reliable records

Recording duration (minutes)	Average f_0 for only the reliable measurement with the standard deviation (Hz)	Median f_0 for only the reliable measurement (Hz)	Remarks
5	1.03±0.02	1.03	14% pass
10	1.01±0.03	1.01	64% pass
20	1.00±0.03	1.01	86% pass
30	1.00±0.02	1.01	89% pass
60	1.00±0.02	1.01	89% pass

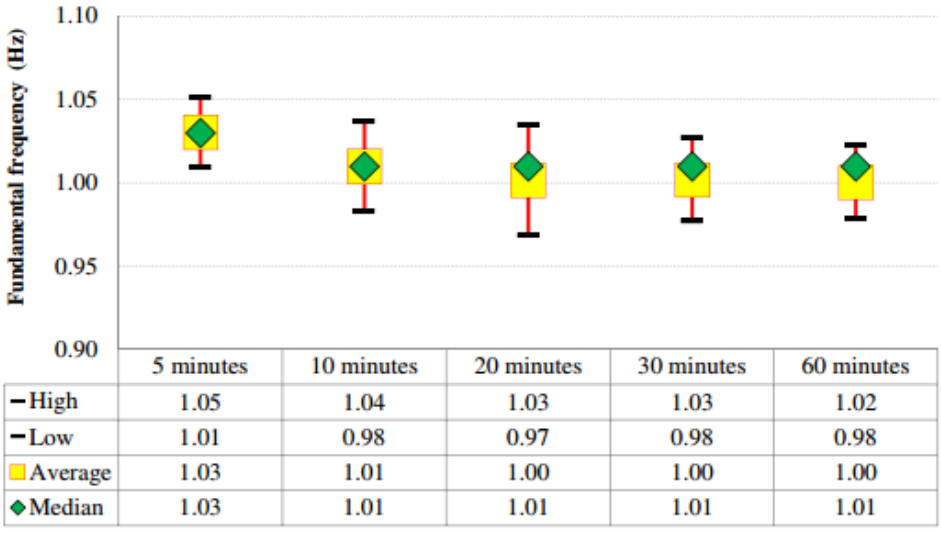

	5 minutes	10 minutes	20 minutes	30 minutes	60 minutes
High	1.05	1.04	1.03	1.03	1.02
Low	1.01	0.98	0.97	0.98	0.98
Average	1.03	1.01	1.00	1.00	1.00
Median	1.03	1.01	1.01	1.01	1.01

Figure 5. Plot of average and median f_0 for reliable records for all record durations

5 CONCLUSIONS

The HVSR technique has been applied to data obtained from a regolith site in metropolitan Adelaide. Two days of continuous ambient noise data were used to examine the reliability of the HVSR technique over a range of measurement durations. The analyses consistently yielded a site frequency, f_0, of

1 Hz and, based on 96 recordings, the results demonstrated that a duration of 20, 30 and 60 minutes duration provided more reliable HVSR results than records obtained over a 5 and 10 minute duration. This conclusion is in contrast with the guidelines provided by the SESAME Project, which recommend a recording duration of 10 minutes.

6 REFERENCES

Bard P. Y. 2002. Extracting information from ambient seismic noise: The SESAME project (Site EffectS assessment using AMbient Excitations). European Project No. EVG1-CT-2000-00026 SESAME. http://sesame-fp5.obs.ujf-grenoble.fr/index.htm Review meeting. Brussels, Belgium.

Geopsy Project. 2015. Geopsy home: software applications for ambient vibration techniques, (accessed August 2015), http://www.geopsy.org

SESAME 2004. Guidelines for the implementation of the H/V spectral ratio technique on ambient vibrations. SESAME European Research Project, WP12- Deliverable D23.12.

Appendix B:

AN INTERNATIONAL PEER REVIEWED JOURNAL PAPER 1

(COPY OF PAPER FROM CHAPTER 2)

SETIAWAN, B., JAKSA, M., GRIFFITH, M., AND LOVE, D. (2018). AN INVESTIGATION OF LOCAL SITE EFFECTS IN ADELAIDE-SOUTH AUSTRALIA: LEARNING FROM THE PAST. BOLLETTINO DI GEOFISICA TEORICA ED APPLICATA, 59(1): 27–46, DOI: 10.4430/BGTA0218.

INTENTIONALLY BLANK

Bollettino di Geofisica Teorica ed Applicata Vol. 59, n. 1, pp. 27-46; March 2018
DOI 10.4430/bgta0218

An investigation of local site effects in Adelaide, south Australia: learning from the past

B. Setiawan[1, 2], M. Jaksa[1], M. Griffith[1] and D. Love[3]

[1] *School of Civil, Environmental and Mining Engineering, the University of Adelaide, Australia*
[2] *Faculty of Engineering, Syiah Kuala University, Darussalam, Banda Aceh, Indonesia*
[3] *Department of State Development, the Government of South Australia, Adelaide, Australia*

(Received: June 20, 2017; accepted: December 20, 2017)

ABSTRACT Three major seismic events have damaged the Old Exchange Building, Adelaide, southern Australia. The building was graced by the Britannia statue on the parapet of the building. The statue lost its arm during the 1897 Beachport earthquake and bowed its helmeted head during the 1902 Warooka seismic event. It was removed after the 1954 Adelaide earthquake. Local site effects contributed significantly to the destruction of the Britannia statue. This paper investigates and presents the historical local site effects with respect to the Old Exchange Building. Synthetic ground motion time histories of the past three seismic events are generated and confirm the suitability of the method. Representative 1D soil profiles are developed and validated. Site response analysis was then carried out at the Old Exchange Building site to obtain the seismic parameters at the investigated site. The results are compared against historical intensity maps of the events, which are assumed as the actual spectral accelerations during the events. Hazard spectra and amplification triggered by the seismic events are deduced. This study reveals the significance of local site effects by an amplification factor of up to 3.4 that led to the destruction of the Britannia statue.

Key words: seismic, site effect, amplification, Adelaide, southern Australia.

1. Introduction

Of all Australia's cities, Adelaide is the most at risk of a severe earthquake (Standards Australia, 2007). In the last 150 years, the city has experienced more medium-sized earthquakes than any other Australian city. Three significant events include the 1897 Beachport earthquake, the 1902 Warooka earthquake, and the 1954 Adelaide earthquake (the 'three historical seismic events'), (McCue, 1990; Malpas, 1991; Dyster, 1996; Love, 1996). These three historical seismic events caused damage to the Old Exchange Building at Pirie St., Adelaide, southern Australia (Fig. 1). The damage was manifested in the Britannia statue located on the parapet of the building. The statue lost its arm during the 1897 Beachport earthquake [Modified Mercalli Intensity (MMI) IV-V], and its helmeted head was bent over in the 1902 Warooka seismic event (MMI V-VI). Due to heavy damage, the statue was finally removed after the 1954 Adelaide earthquake (MMI VI-VII) (Malpas, 1991; Dyster, 1996). Local site effects for the particular case of the Old Exchange Building have never been investigated.

Fig. 1 - The Old Exchange Building with the Britannia Statue on the parapet.

This study investigates the local site effects with respect to the Old Exchange Building, which is situated on a regolith site. The investigation is based on past seismic events.

Synthetic bedrock time histories of the three historic seismic events have been generated using EXSIM (Motazedian and Atkinson, 2005). The time histories are used in the 1D site response analyses to estimate the peak ground acceleration (PGA), and other seismic parameters (i.e. response spectral acceleration, velocity and displacement) at the Old Exchange Building site. The results are examined alongside the historical experiences and the intensity maps associated with the seismic events that are assumed the actual spectral accelerations during these events. The MMIs of the 1897 Beachport, 1902 Warooka, and 1954 Adelaide earthquakes were of IV-V, V-VI, and VI-VII, respectively (Malpas, 1991; Dyster, 1996). The comparison reveals the significance of local site effects in the damage manifested in the building. The findings from this study may form a basis for further comprehensive and systematic analyses of site effects and seismic-related studies in Adelaide, southern Australia.

2. The characteristics of the past seismic and geological setting of the investigated site (the Old Exchange Building site) and surrounding areas

As mentioned above, this study examines the impact of just three historical seismic events. These seismic events were estimated at 6.5, 6.0 and 5.3 on the Richter local magnitude scale (M_L) for the 1897 Beachport, 1902 Warooka and 1954 Adelaide earthquakes, respectively (Everingham *et al*., 1982). Both the 1897 Beachport and 1902 Warooka events caused extensive damage (MMI IX-VII) in the areas near the epicentre. These events were also felt at distances of hundreds of kilometres from the epicentres, including the city of Adelaide (Malpas, 1991). After about a half century, Kerr-Grant (1956) and McCue (1975) reported that Adelaide was shaken on March 1, 1954. This seismic event is the strongest earthquake in Adelaide's recorded history. Due to this

event, at least 30,000 insurance claims were made. Each of these three past seismic events testify to the need for estimating ground surface motion in the city, which includes site effects. The location of Adelaide, as well as the epicentres of the three major historical earthquakes (after Everingham *et al*., 1982), are shown in Fig. 2. The Old Exchange Building is located in the middle of the central business district (CBD) of Adelaide, as shown in Fig. 3.

The major geological structures of the Adelaide city and its surrounding region are fault segments that develop in a NE to SW direction. Most of the faults can be characterised by lithological disposition. There were several past seismic events associated with these faults as documented and presented by Selby (1984). The most significant event was associated with intra-plate activity along the Burnside-Eden Fault zone. This occurred on March 1, 1954, and is known as the 'Adelaide earthquake'. This seismic event was estimated at a magnitude of 5.3 (Selby, 1984; Love, 1996). Two main faults delimit the city of Adelaide to the west (Para Fault) and east (Eden-Burnside Fault). Both the Para and Eden-Burnside faults predominantly control the ground surface morphology of the city and its adjacent areas.

Most of the upper ground layer of Adelaide is made up of fill material and other surficial covers. Below the top fill and surficial cover, the subsurface profile is composed of Holocene deposits of Callabonna Clay and the Pooraka Formation. Beneath these Holocene deposits is the Hindmarsh Clay formation. Sheard and Bowman (1987a, 1987b) separated Keswick Clay from the Hindmarsh Clay formation below the Holocene deposits. Below these Quaternary deposits there is an unconformity beneath which are the Burnham Limestone and Hallett Cove Sandstone

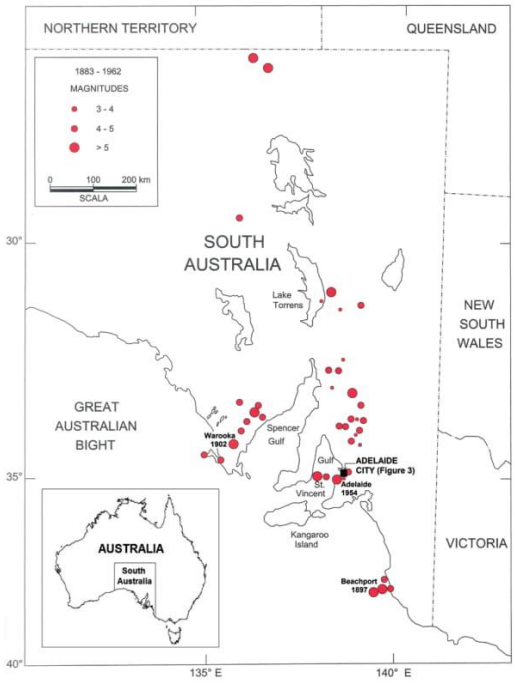

Fig. 2 - Locations of the epicentres of the South Australian historical seismic events, including the three events that damaged the Old Exchange Building (after Malpas, 1991).

Boll. Geof. Teor. Appl., **59**, 27-46 Setiawan *et al.*

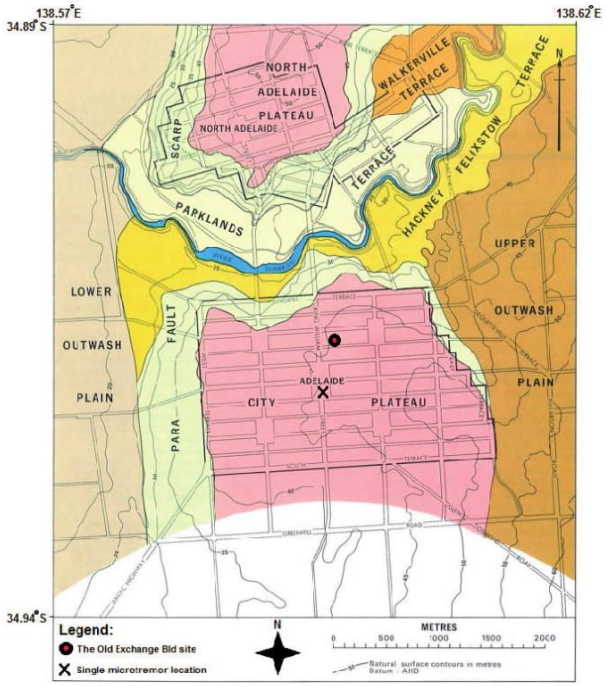

Fig. 3 - Morphology of the Adelaide city, with the location of the Old Exchange Building site.

Formation. Below this lies another unconformity followed by the sand unit of the Port Willunga Formation and the Tandanya Sand Member of the Chinaman Gully Formation. These units were deposited between the Pleistocene and Eocene (Selby and Lindsay, 1982). They are followed by the Undifferentiated Basal Blanche Point Formation and Tortachilla Limestone, South Maslin Sand and Clinton Formation, prior to the Precambrian bedrock. The reduced level of the bedrock is believed to be approximately 88.5 m or less to the north of the city, and can be up to 94.3 m or more below ground to the south of the city (Selby and Lindsay, 1982).

As shown in Fig. 3, much of the commercial development of the Adelaide city is founded on two morphological plateaus; one to the north and the other to the south of the city. The remaining morphologies, i.e. the upper outwash plain, lower outwash plain, terrace and fault scarps, are associated with either parklands or residential developments. Selby and Lindsay (1982) suggested that faults predominantly control the morphology of the city in the present day.

3. Methodology of this study

In this study, as there were no actual ground motions recorded for the three major historical seismic events, synthetic seismic motions are considered to represent the ground motions of these earthquakes. The generation of the synthetic seismic motions, as well as other parameters and site response analysis adopted in this study, are described below.

3.1. Generating input seismic motions

Table 1 details the main data associated with the seismic events of the 1987 Beachport, 1902 Warooka, and 1954 Adelaide earthquakes that were used to generate the seismic motions. This study uses a stochastic finite-fault model, EXSIM (Motazedian and Atkinson, 2005), to simulate the time histories of the 1897 Beachport, 1902 Warooka, and 1954 Adelaide earthquakes. There are some salient features of the adopted approach (EXSIM). Firstly, the model has been validated using a minimum of 300 strong motion stations at distances of 40 to 500 km (Motazedian and Atkinson, 2005; Atkinson and Macias, 2009). For the case of the close distance seismic event (i.e. 1954 Adelaide earthquake), an analytical model proposed by Mavroeidis and Papageorgiou (2003) is included in EXSIM. Secondly, the model was based on FINSIM (Beresnez and Atkinson, 1998) with ground motions generated by ruptures along faults. Thirdly, this finite-source model is appropriate for large earthquakes at relatively close distances (Hartzell, 1978; Joyner and Boore, 1986). Santulin *et al*. (2012) employed EXSIM for generating two historical earthquakes (the 1936 Cansiglio and 1976 Friuli earthquakes) in Italy. In the present study, additional parameters are needed to produce the synthetic ground motions as shown in Table 2. Most of the input parameters are adopted from Allen (2012). Additional parameters for analytical modelling proposed by Mavroeidis and Papageorgiou (2003) were employed in the case of the close distance seismic event. These additional parameters, shown in Table 2, have been validated by Motazedian and Moinfar (2006) against the 2003 Bam earthquake in SE Iran.

Four different input motions are considered. The first is a synthetic seismic motion generated for the 1897 Beachport event (earthquake of M_L 6.5 at a distance, R, of 260 km from the city of Adelaide). The second is a synthetic seismic motion produced for the 1902 Warooka event (earthquake of M_L 6.0 at R = 60 km from Adelaide). The third is a synthetic seismic motion calculated for the 1954 Adelaide event, considered the worst near-field seismic scenario for the city (earthquake of M_L 5.3 at R = 12 km from Adelaide). The fourth is a synthetic seismic motion calculated for the 1997 Burra event (earthquake of M_L 5.1 at R = 130 km from Adelaide). The first three synthetic ground motion time histories are shown in Fig. 4. These synthetic time histories are used for a site-specific ground response analysis of the site of interest, to estimate the PGA and validate site amplification during the 1897 Beachport, 1902 Warooka and 1954 Adelaide earthquakes. The fourth synthetic seismic motion for the 1997 Burra earthquake is generated to examine the suitability of the stochastic finite-fault model in this study. The application of this 1997 Burra synthetic seismic motion into the site response analysis of the investigated site is compared to the application of the actual recorded seismic motions at the Government House site (GHS) Adelaide, which is a similar model (Fig. 5). The GHS is a soil site and is located

Table 1 - Three historical seismic events contributed to the damage of the Old Exchange Building.

Event	Magnitude (M_L)	Depth (km)	Estimated distance (km)	Intensity at the investigated site	
				MMI	Reference
1897 Beachport earthquake	6.5	14	260	IV-V	McCue (1975)
1902 Warooka earthquake	6.0	4	60	V	McCue (1975)
				VI	Malpas (1991)
1954 Adelaide earthquake	5.3	4	12	VI-VII	After Malpas (1991)

Boll. Geof. Teor. Appl., **59**, 27-46 Setiawan *et al.*

Table 2 - Parameters for ground motion simulations using EXSIM (after Allen, 2012).

Input Parameter	Value	Remarks
Shear-wave velocity, β	3,600 m/s (Wesson, 1988)	Beta
Density, ρ	2,800 kg/m^3	Rho
Rupture propagation speed	0.8 β	Vrup
Brune stress drop, Δσ	23 MPa	Stress
Pulsing percentage	25%	Pulsing Percent
Geometrical attenuation R^b, b	–1.33 (0-90 km) +0.32 (90-150 km) –1.66 (> 150 km)	Gsprd
κ_0	0.006 s	Kappa
Distance-dependent duration	0.00 (0-10 km) +0.14 (10-70 km) –0.04 (70-160 km) +0.07 (> 160 km)	Trilinier duration and properties
Fault dip	35°	Dip
Earthquake magnitude (M)	6.5, 6.0 and 5.3	1898 Beachport, 1902 Warooka, and 1954 Adelaide earthquakes
Earthquake distance	260, 60 and 12 km	Distance from the epicentre of each earthquake to Adelaide CBD
Prevailing frequency ($f_p = 1/T_p$)	Log T_p = -2.2+0.4M	Parameters for the 1954 Adelaide earthquake only.
Phase angle	10°	
Oscillatory character	1.5	

approximately 0.5 km from the Old Exchange Building. A deconvolution of the generated time histories at bedrock level using EXSIM was carried out. This deconvolution of the time histories was compared to the actual time histories at the GHS site.

3.2. Developing a one-dimensional (1D) profile

Detailed knowledge of the subsurface characteristics of the investigated site contributed to generating a 1D profile for the investigated site. The subsurface lithology profiles of the investigated site are developed based on the work of Selby and Lindsay (1982). They examined an extensive amount of geotechnical borehole, groundwater and deep excavation data from which stratigraphic profiles and cross-sections of Adelaide were developed. Two boreholes (BH 42 and BH 83) were drilled by Selby and Lindsay (1982) near the Old Exchange Building site, and two sections (C-C and G-G) were developed by Selby and Lindsay (1982) from these boreholes.

From these two sections, two subsurface models are established in this study. The first model is based mainly on Section C-C, hereafter referred to as Model A. The second is established primarily from Section G-G, hereafter referred to as Model B. The total depth of both models A and B is up to the Pre-Cambrian bedrock. Both models A and B share similar geological formations from the ground surface down to the Pre-Cambrian bedrock. Slight differences in the thicknesses of the formations are observed due to the modest lateral heterogeneity of the geological formations.

In addition to the stratigraphic profile, in situ, ambient-noise single station and array measurements were conducted in order to quantify the shear wave velocity profiles in the Adelaide city (Setiawan *et al.*, 2016).

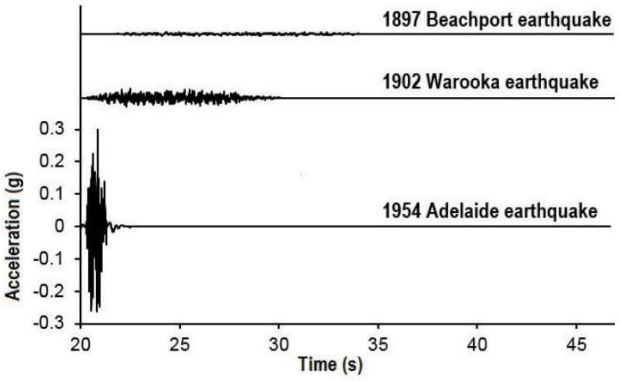

Fig. 4 - Synthetic acceleration time histories of the three past earthquakes.

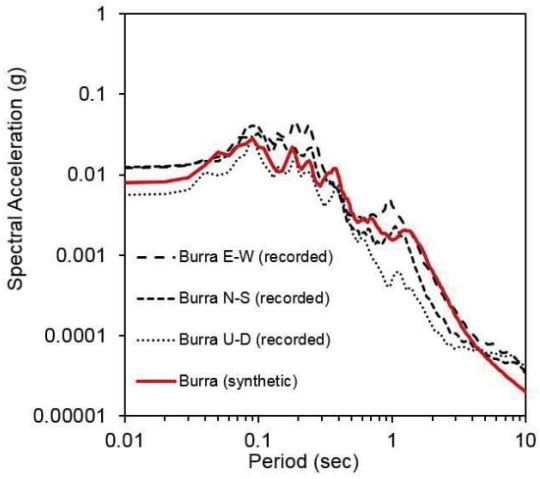

Fig. 5 - Response spectral acceleration validation of the synthetic time histories generated using the 1997 Burra seismic event.

A shear wave velocity profile at a location of approximately 200 m from the investigated site was developed by the authors (Setiawan *et al*., 2016). This shear wave velocity profile is incorporated into the 1D profile for the site response analysis at the investigated site. To validate the appropriateness of the shear wave velocity model deduced by Setiawan *et al*. (2016), a forward-computation of the model proposed by Garcia-Jerez *et al*. (2016) is employed to obtain a spectral ratio between the horizontal and vertical components (HVSR). The computed HVSR for the inverted 1D soil profiles is compared with the observed HVSR of the measured microtremor. The comparison of the mean HVSR observed by McCue and Love (1997), the mean HVSR observed by Setiawan *et al*. (2016), and the computed HVSR in this study, are presented in Fig. 6. Generally, the comparison between the observed and calculated HVSR curves show comparable results. Both the observed and calculated HVSRs suggest two-peak frequency characteristics at frequencies of about 0.8-0.9 and 4.0-5.0 Hz. The subsequent developed 1D profiles for the Old Exchange Building site are presented in Table 3.

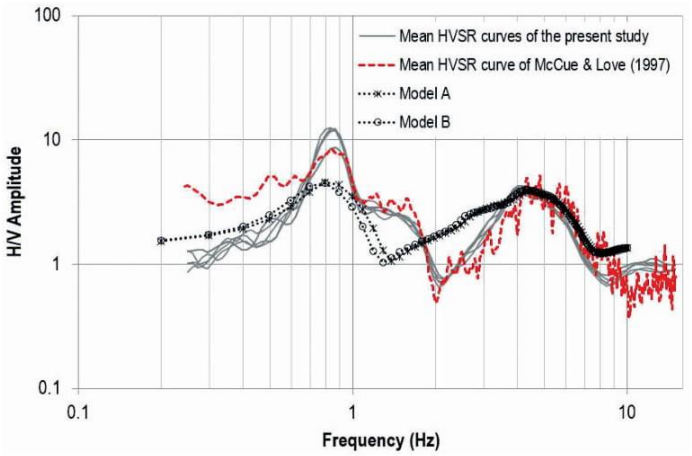

Fig. 6 - Comparison between the mean of the observed and calculated HVSR curves from the best fit models.

Table 3 - Developed 1D profiles for the investigated site.

Formation	Description	Thickness or (Depth)		Estimated mean shear wave (m/s)
		Model A	Model B	
Quaternary alluvium, Pooraka Formation [HOLOCENE]	Red brown silty CLAY (CH), grades downwards to SAND and GRAVEL (SP-GP)	2.4	2.3	137
Keswick CLAY [PLEISTOCENE]	Grey-green CLAY (CH) with red and brown mottling, stiff to hard, fissured	6.1	6.3	159
Hindmarsh CLAY [PLEISTOCENE]	Grey-green CLAY (CH) with yellow and red mottling with overlying SAND (SC)	6.1	6.3	354
Bunham Limestone and Hallett Cove Sandstone [PLEISTOCENE TO PLIOCENE]	White clayey, sandy and rubbly LIMESTONE; Pale grey to yellow brown calcareous SANDSTONE with layers of sand (SP)	7.9	9.1	433
Sand unit of Port Willunga Formation [EOCENE]	Fine silty SAND (SM)	5.5	4.0	330
Tandanya Sand Member of Chinaman Gully Formation [EOCENE]	Gravelly, clayey SAND (SC-GW)	9.7	12.6	333
Gull Rock Member of Blanche point Formation [EOCENE]	Alternating bands of cherty siltstone and grey SILT (ML)	21.8	22.9	317
Undifferentiated basal Blanche Point Formation and Tortachilla Limestone [EOCENE]	Green to dark grey clayey SAND (SC) with LIMESTONE	4.8	5.1	283
South Maslin Sand [EOCENE]	Dark grey, brown at depth, but weathering to red brown or yellow, silty SAND (SM) with pyrite lumps	10.3	11.4	261
Clinton Formation [EOCENE]	Dark grey CLAY (CL) with LIGNITE; irregular clayey SAND zones (SC)	13.9	14.3	269
Precambrian bedrock	White, pink, brown, purple, blue-grey and greenish grey with thin sandy bands, decomposed quartzite or quartz veins, high plasticity SILT slightly sandy, very stiff to hard with a moisture content well below the plastic limit > 480 kPa	(88.5)	(94.3)	926

3.3. Modulus reduction and damping curves

Ideally, for a site-specific ground response analysis, the modulus reduction and damping curves are developed in accordance with the samples obtained from the soil profile. However, as the default curves provided by SHAKE91 (Idriss and Sun, 1992) or EERA (Equivalent-linear Earthquake Response Analysis) (Bardet *et al.*, 2000) have proven to work well in most applications for site response analysis (Sykora and Davis, 1993; Uthayakumar and Naesgaard, 2004): this study has also adopted these curves (Fig. 7). Each curve represents a unique, typical

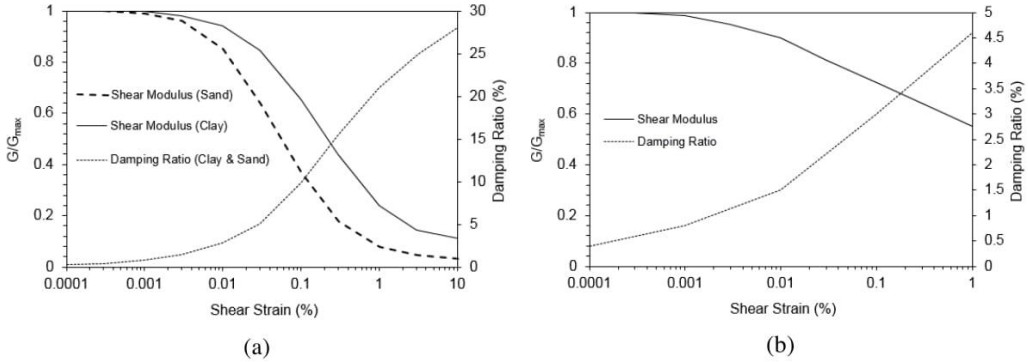

Fig. 7 - Shear modulus, shear strain and damping ratios for: a) clay (upper range) (Seed and Sun, 1989), sand (Seed and Idriss, 1970) and clay and sand damping ratio [Idriss (1990) cited by Bardet *et al.* (2000)], b) rock [Schnabel *et al.* (1972) cited by Bardet *et al.* (2000)].

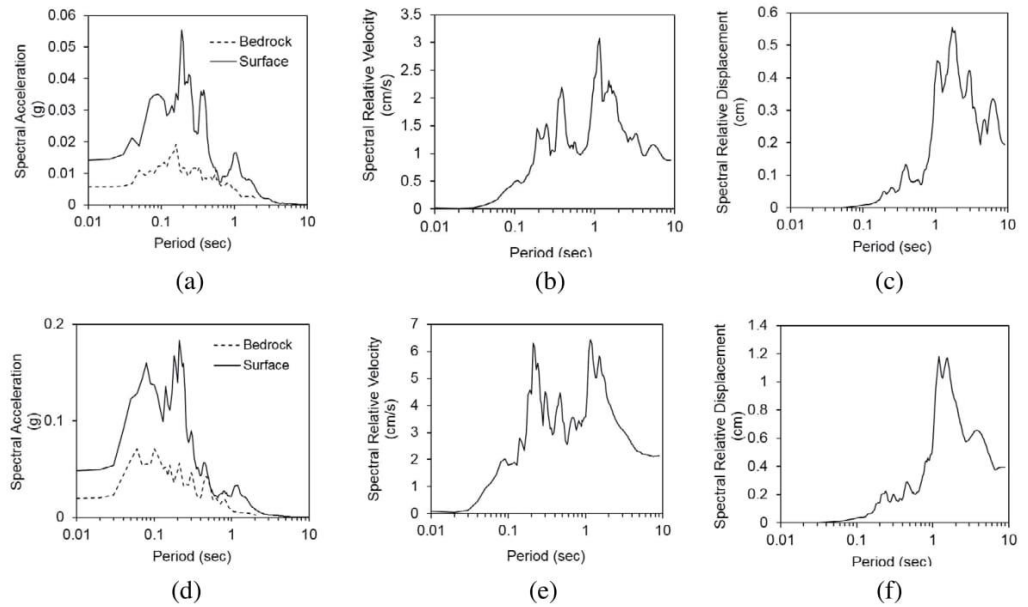

Fig. 8 - Model A input motion of 1897 Beachport earthquake: a) response spectral acceleration, b) velocity, and c) displacement outputs; and Model A input motion of 1902 Warooka earthquake: d) response spectral acceleration, e) velocity, and f) displacement outputs.

Boll. Geof. Teor. Appl., **59**, 27-46 Setiawan *et al.*

material behaviour during strain. The shear modulus reduction and damping ratio curves (Fig. 7a) were proposed by Seed and Sun (1989). The curves were developed from the upper bound shear modulus curve for clay (Seed and Sun, 1989). The shear modulus curve for sand (Fig. 7a) was by Seed and Idriss (1970). This was developed from the upper bound shear modulus curve of sand. The damping curves for clay and sand were proposed by Idriss (1990) cited by Bardet et al. (2000) (Fig. 7a), and for rocks by Schnabel *et al.* (1972) (Fig. 7b). In the present site response analysis, these curves are accordingly assigned to each layer of the subsurface model.

3.4. Conducting equivalent-linear site response analysis

Standard practice for the dynamic analysis of soils in geotechnical earthquake engineering is the equivalent-linear site response analysis (Borja *et al.*, 2000). This method assumes that soil stiffness and damping are consistent for a certain level of maximum shear-strain. It has been demonstrated that this analysis is able to reliably simulate soil behaviour due to dynamic loading (Priolo *et al*., 2008). This equivalent-linear site response analysis has been implemented in the SHAKE (Schnabel *et al*., 1972) computer program, which has been one of the most widely used tools for site response analysis for decades. The advantages of SHAKE are that it is simple and compact. Another equivalent-linear site response analysis program, EERA (Bardet *et al*., 2000), was developed by taking advantage of the most recent developments of FORTRAN 90 and the Windows operating system at the time. The EERA program was developed from the basic principles of SHAKE. Unlike SHAKE, EERA is an add-on program embedded in Microsoft Excel. Good agreement is obtained between the results of SHAKE and those of EERA for use in site-specific ground response analysis, as demonstrated by Bardet *et al*. (2000). As a result, EERA has been adopted here.

4. Results and discussions

Several outputs of the site-response analysis at the Old Exchange Building site, using the synthetic ground motions, are presented in Figs. 8a to 9c, for Model A, and in Figs. 9d to 10f, for Model B. The results are summarised in Tables 4 and 5 for Models A and B, respectively.

For Model A, the PGA results are 0.01, 0.06 and 0.30 g for the 1897 Beachport, 1902 Warooka and 1954 Adelaide seismic events, respectively. The estimated fundamental frequency of the site is estimated about 0.8 Hz. The response spectrum analysis, with a critical damping ratio of 5%, shows maximum spectral accelerations (SAs) for these events to be 0.06, 0.18 and 0.92 g for the 1987 Beachport, 1902 Warooka, and 1954 Adelaide earthquakes, respectively. The maximum spectral relative velocities (SVs) are estimated as equal to 3.1 cm/s for the 1897 Beachport event, 6.4 cm/s for 1902 Warooka event, and 36.8 cm/s for the 1954 Adelaide event. By considering the PGA, SA, and SV, the analysis here determines that the 1954 Adelaide earthquake presented the highest threat of all three to damage the Old Exchange Building. As expected, in terms of spectral displacement (SD), the highest displacement of the Old Exchange Building appears to have also resulted from the 1954 Adelaide earthquake. That earthquake generated a displacement of approximately 2.7 cm. The 1897 Beachport earthquake

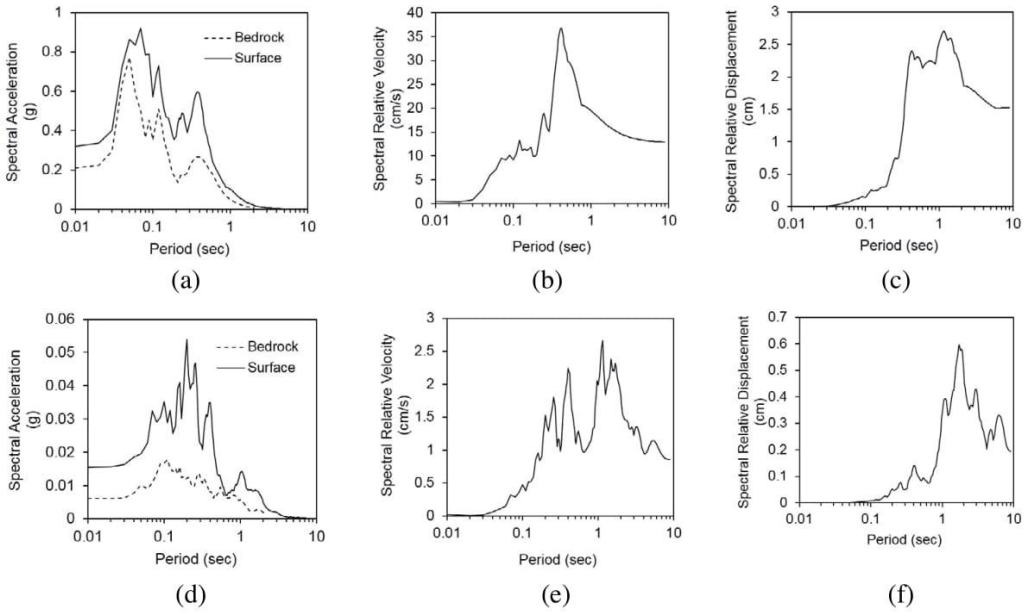

Fig. 9 - Model A input motion of 1954 Adelaide earthquake: a) response spectral acceleration, b) velocity, and c) displacement outputs; and Model B input motion of 1897 Beachport earthquake: d) response spectral acceleration, e) velocity, and f) displacement outputs.

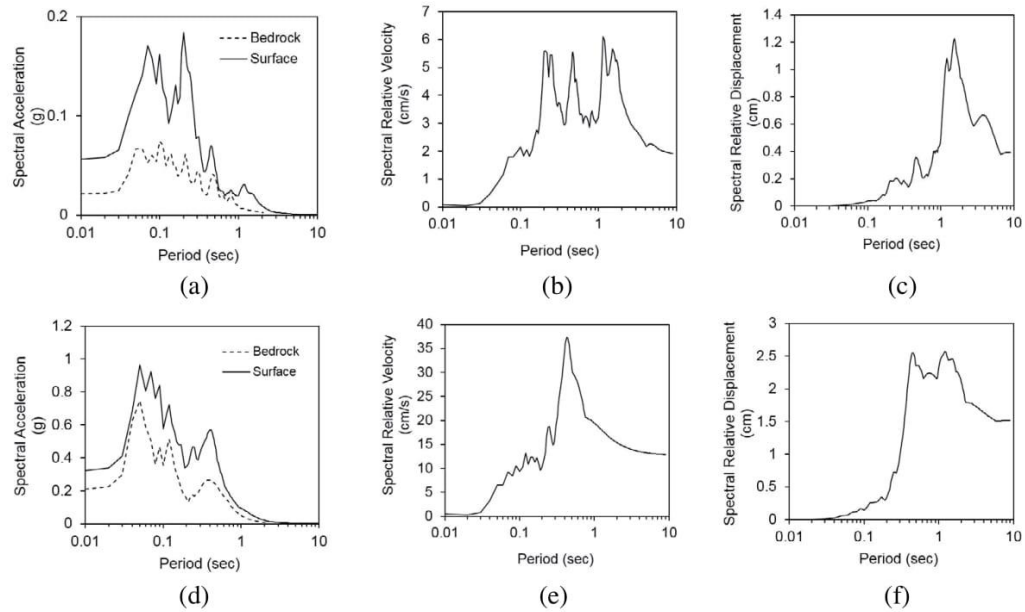

Fig. 10 - Model B input motion of 1902 Warooka earthquake: a) response spectral acceleration, b) velocity, and c) displacement outputs; and Model B input motion of 1954 Adelaide earthquake: d) response spectral acceleration, e) velocity, and f) displacement outputs.

Boll. Geof. Teor. Appl., **59**, 27-46 Setiawan *et al.*

Table 4 - Results of site-specific ground response analysis using EERA for Model A.

Parameters	1897 Beachport	1902 Warooka	1954 Adelaide
PGA (g)	0.014	0.049	0.321
Fundamental frequency (Hz)	0.800	0.800	0.800
Max spectral relative acceleration (g)	0.060	0.180	0.920
Max spectral relative velocity (cm/s)	3.080	6.430	36.800
Max spectral relative displacement (cm)	0.550	1.170	2.680

Table 5 - Results of site-specific ground response analysis using EERA for Model B.

Parameters	1897 Beachport	1902 Warooka	1954 Adelaide
PGA (g)	0.016	0.056	0.322
Fundamental frequency (Hz)	0.800	0.800	0.800
Max spectral relative acceleration (g)	0.050	0.180	0.960
Max spectral relative velocity (cm/s)	2.660	6.100	37.360
Max spectral relative displacement (cm)	0.580	1.210	2.560

caused a displacement of 0.55 cm, and the 1902 Warooka earthquake was estimated to cause a displacement of about 1.2 cm.

For Model B, the PGA results are 0.02, 0.06 and 0.32 g for the 1897 Beachport, 1902 Warooka, and 1954 Adelaide seismic events, respectively. Model B results in an estimated fundamental frequency at the Old Exchange Building site of 0.8 Hz. The maximum amplification for this model occurs at a frequency of 2.4 or 4.0 Hz. The response spectrum analysis, using a critical damping ratio of 5%, produces a maximum SA of 0.05, 0.18 and 0.96 g for the 1987 Beachport, 1902 Warooka, and 1954 Adelaide earthquakes, respectively. The maximum SV is 2.66 cm/s for the 1897 Beachport event, 6.1 cm/s for the 1902 Warooka event, and 37.4 cm/s for the 1954 Adelaide event. Among these three historical seismic events, Model B, again by considering the PGA, SA and SV, indicates that the 1954 Adelaide earthquake presented the highest threat of the three events. As with Model A, in terms of SD of the Old Exchange Building, the most critical value resulted from the 1954 Adelaide earthquake. This event again produced a displacement approximately 2.6 cm. The 1897 Beachport and 1902 Warooka earthquakes are estimated to cause displacements of approximately 0.58 and 1.20 cm, respectively.

The use of the analytical approach by Mavroeidis and Papageorgiou (2003) in the generation of the near source seismic event (i.e. Adelaide earthquake) in this study has several consequences on the results of the site response analysis. It estimates the PGA of up to 0.3 g, which generally provides better estimation than without the Mavroeidis and Papageorgiou (2003) analytical approach. This 0.3 g PGA for the 1954 Adelaide seismic event slightly overestimates the actual damage for this MMI of VI-VII event (see the later discussion). Furthermore, the analytical approach by Mavroeidis and Papageorgiou (2003) in the Adelaide earthquake case allows EXSIM to generate the long-period velocity pulses (Motazedian and Atkinson, 2005). This extension will

simulate low frequency or long period ground motion components. An amplification of the long period of the ground motion coherent components (i.e. velocity and displacement) is unavoidable in such near-source seismic events (Mimoglou *et al.*, 2017). The application of the analytical approach by Mavroeidis and Papageorgiou (2003) has increased the maximum SV up to 36.8 cm/s in Model A and up to 37.4 cm/s in Model B. The maximum spectral displacement of the Adelaide earthquake has also increased up to 2.7 cm in Model A and up to 2.6 cm in Model B. By contrast, the site response analyses without the application of the Mavroeidis and Papageorgiou (2003) analytical approach suggest the maximum spectral velocity of 20.9 cm/s for Model A, 23.4 cm/s for Model B and the maximum SD of 0.9 cm for both Models A and B (not shown in this paper). The effect of the seismic duration on the velocity component of ground motion was also suggested by Tehranizadeh and Hamedi (2000). The SV and displacement amplification on the inelastic response of structures due to near seismic sources is also reported by Panagiotou (2008), Iervolino and Cornell (2008), and Taflampas and Psycharis (2008). Therefore, the site response analysis results of the spectral relative velocity and displacement of the Adelaide earthquake must be carefully examined.

The PGA outputs from our study are compared with the empirical attenuation function by Wald *et al*. (1999) and Linkimer (2008), as shown in Table 6. The PGA calculations, using the empirical attenuation functions, are based on the seismic MMIs of IV-V, V-VI, and VI-VII for the 1897 Beachport, 1902 Warooka, and 1954 Adelaide earthquakes, respectively. The comparison suggests good agreement with the results of both the 1897 Beachport and 1902 Warooka earthquakes. However, this study suggests a slightly higher seismic intensity resulting from the 1954 Adelaide earthquake.

5. Hazard spectra

Log-log plots of the spectral accelerations for both Models A and B for the three historical seismic events are shown in Fig. 11. As mentioned above, the 1954 Adelaide earthquake is estimated to result in higher spectral accelerations than others, particularly below a period of 0.4 s.

Seismic event	Estimated MMI at Old Exchange Building site	Estimated PGA (g)		
		Wald *et al.* (1999)	Linkimer (2008)	Present study
1897 Beachport	IV-V (McCue, 1975; Dyster, 1996)	0.020 to 0.070	0.020 to 0.060	0.014 to 0.016
1902 Warooka	V-VI (McCue, 1975; Malpas, 1991)	0.070 to 0.130	0.060 to 0.110	0.049 to 0.056
1954 Adelaide	VI-VII (Malpas, 1991)	0.130 to 0.240	0.110 to 0.200	0.320

Table 6 - Comparison PGA estimation at the Old Exchange Building site.

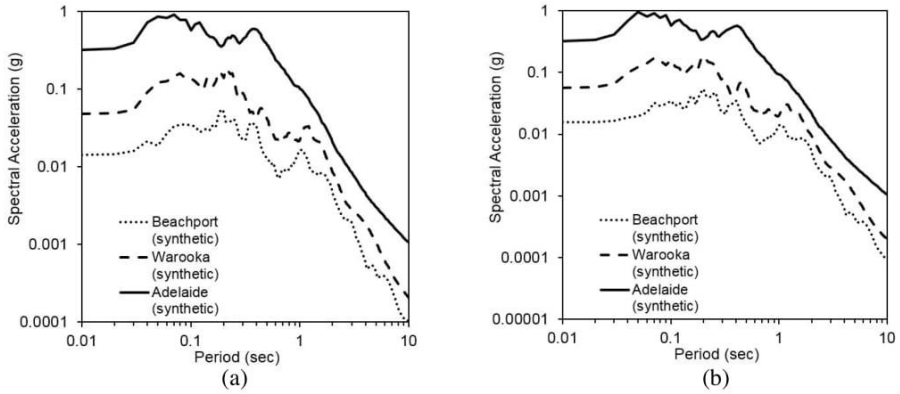

Fig. 11 - Response spectral accelerations of site response analysis for: a) Model A; b) Model B.

The spectral acceleration outputs are compared with the results of Love (1996) and Leonard *et al*. (2013). The maximum SA obtained is 0.92 g, which is associated with the 1954 Adelaide earthquake. Love (1996) suggested a maximum SA of 0.76 g and Leonard *et al*. (2013) estimated a value of approximately 0.30 g for a 2,500-year return period. Hence, our study has obtained slightly larger estimated SAs than those proposed by Love (1996). Furthermore, this work suggests a maximum SA three times larger than that suggested by Leonard *et al.* (2013). This large discrepancy is likely to be caused by the adopted shear wave velocity profile, modulus reduction and damping curves, and input ground motion. Our study adopts shear wave velocity profiles based on forward modelling of the measured HVSR curves with an average of the top 30 m shear wave velocity (V_{s30}) between 315 and 320 m/s, whereas Leonard *et al.* (2013) most likely employed an empirical shear wave profile with V_{s30} between 315 and 460 m/s. The study here employs the generic modulus reduction and damping curves, whereas Leonard *et al.* (2013) likely used different modulus reduction and damping curves. In terms of input ground motions, we selected the ground motions based on past seismic events (i.e. 1897 Beachport, 1902 Warooka, and 1954 Adelaide earthquakes), whereas the seismic event adopted by Leonard *et al.* (2013) is based on a probabilistic analysis. The paucity of strong motion events in the low-moderate seismic region of southern Australia, influences the results of such probabilistic analysis, as the seismic source zone is difficult to define.

6. Site amplification

Site amplification can be estimated using a comparison between the maximum acceleration of the ground surface layer and the maximum acceleration at bedrock level. Site response analysis results of the maximum acceleration profile at the Old Exchange Building site for models A and B are shown in Figs. 12a and 12b. These maximum acceleration profiles are used to deduce the amplification factor at the investigated site. The results are shown in Figs. 12c and 12d, which indicate an amplification factor at the ground surface level for Model A of between 1.5 to 2.5 and Model B of 1.5 to 2.6.

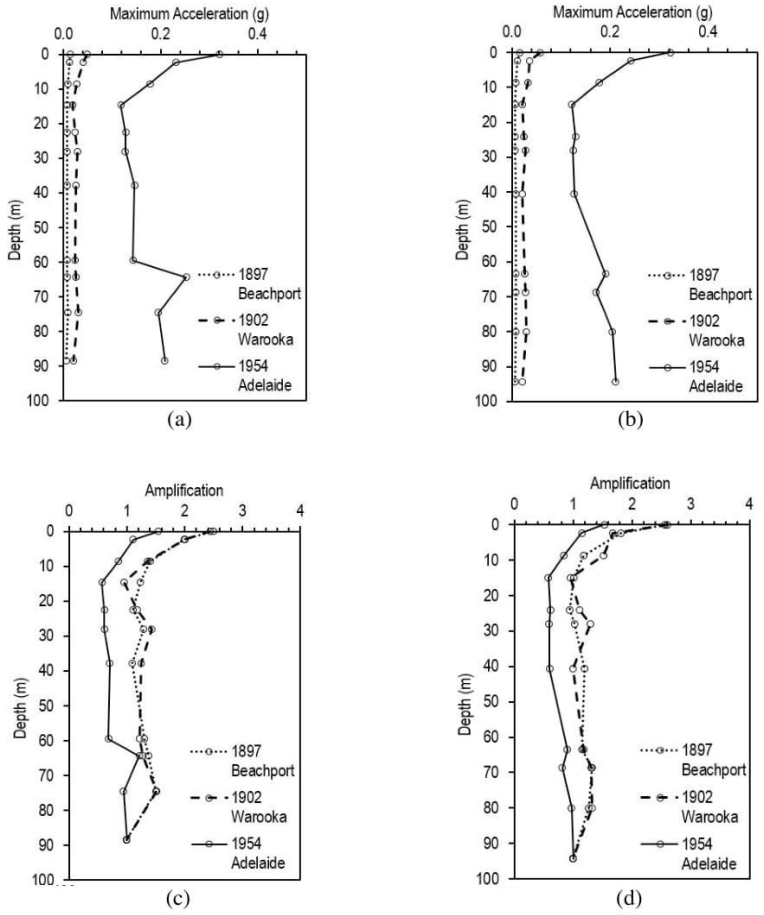

Fig. 12 - Site response analysis results: maximum acceleration profiles for Model A (a), and Model B (b), and amplification profiles for Model A (c) and Model B (d).

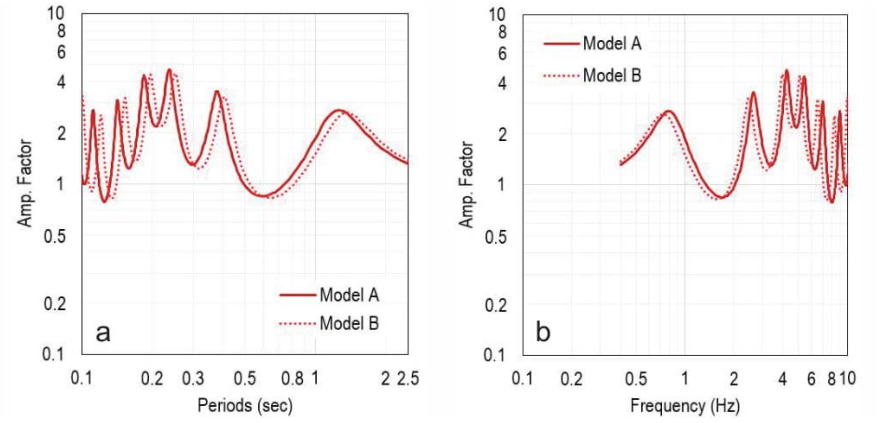

Fig. 13 - Amplification factors plotted against period (a) and frequency (b) at the Old Exchange Building site.

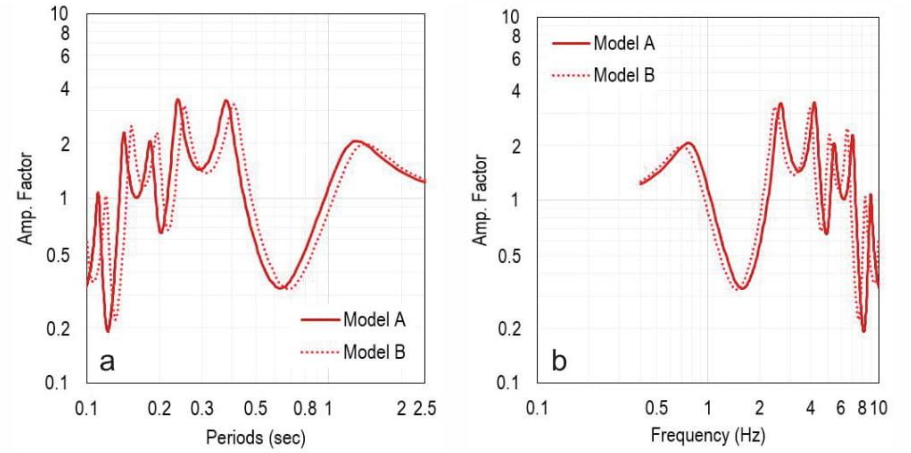

Fig. 14 - DAFs plotted against period (a) and frequency (b) at the Old Exchange Building site.

Site amplification factors are used to understand the seismic motion behavior in the study area by means of the method proposed by Herak (2008), which has been shown to yield reliable results (Herak *et al.*, 2010; Lunedei and Albarello, 2015). The mean compression wave, shear wave and density models obtained here are used to quantify the amplification factors. The quality factors of Q_p and Q_s, for the compression and shear waves, respectively, are estimated using the approaches suggested by Olsen *et al.* (2003) and Zhang and Stewart (2007), respectively, which represent a linear estimate of amplification.

The results of the site amplification factors (Amp-HVSR) are presented in Fig. 13. Generally, a site amplification of up to 3.4 is suggested. Averaging the amplification from 0.4 to 10 Hz at each site implies that the amplification factor is only 1.2. By using identical subsurface models, a dynamic amplification factor (DAF) for the investigated site is also calculated. The method proposed by Herak (2008) is employed to calculate DAF. Unlike the Amp-HVSR, the DAF uses the most likely seismic event in the calculation. Generally, the result of this study shows that the estimated DAF slightly overestimates the amplification analysis using the Amp-HVSR method. As shown in Fig. 14, the obtained value of DAF is 1.9.

As stated by Herak (2008), the amplification factors of both Amp-HVSR and DAF do not consider the non-linear behavior of the subsurface material. Therefore, these estimates need to be judiciously applied in practice. Whilst a non-linear site response analysis could potentially yield more reliable estimates, this is beyond the scope of the work here.

Additional evidence of site amplification in Adelaide is obtained from the recorded ground motions that occurred during the 1997 Burra earthquake. The recorded earthquake ground accelerations in Adelaide's regolith have been shown to be very much stronger than those recorded on bedrock just outside the city during this seismic event (DMITRE Minerals, 2013). Ground response analyses using historical ground motions also confirm site amplification. Thus, site amplification contributed to the damage experienced by the Old Exchange Building, as has been demonstrated to occur to similar buildings, such as in Mexico (Booth *et al.*, 1986; Finn and Wightman, 2003), Kobe (Brebbia, 1996), and Umbria-Marche-Italy (Bindi *et al.*, 2004; Castro *et al.*, 2004; Luzi *et al.*, 2005).

7. Site fundamental frequency

For the Old Exchange Building site, observed HVSR curves by McCue and Love (1997) and Setiawan *et al*. (2016), have indicated a site fundamental frequency of 0.7-0.8 Hz (as shown in Fig. 6) and first mode frequency of 4.0-4.5 Hz. Good agreement between both the observed HVSR curves of McCue and Love (1997) and Setiawan *et al*. (2016) highlight the consistency of the HVSR method with respect to time, as the measurement of the first reference was carried out in 1997, whereas the HVSR data of the later reference were obtained in 2015. This temporal stability of the HVSR analysis was also suggested by Okada (2003). The obtained site frequencies are also correlated to the Old Exchange Building frequency to analyze the possibility of resonance effects which will occur when the ground frequency is equal or close to the natural frequency of the building. In terms of the number of stories (N), the Old Exchange Building was a low-rise (3 story) building. By adopting the building fundamental frequency approximation of Kramer (1996), which is approximated by 10/N (Hz), the Old Exchange Building frequency is estimated to be between 3.0 and 3.5 Hz. As mentioned above, the observed site fundamental frequency at the Old Exchange Building site is 0.8-0.9 Hz, which is three times lower than the Old Exchange Building's natural frequency. However, the first mode site frequency (4.0-4.5 Hz) is relatively close to the Old Exchange Building's natural frequency. This implies that the first mode of site frequency is likely to have increased the Old Exchange Building's vibration and enhanced the prospect of structural collapse.

8. Study limitations and future work

While this study has provided useful information relating to site effects, the analysis is limited. Firstly, the study is confined to a specific case at a single site (i.e. the Old Exchange Building case). Clearly, extending the study to incorporate several sites across the city of Adelaide is desirable to obtain a more reliable prediction of the dynamic characteristics of Adelaide's sub-surface. However, given the limited data currently available, such additional analyses are not possible at this time. Secondly, the sub-surface shear wave velocity models were developed from forward modelling of a measurement obtained at a distance of approximately 200 m from the site. Again, it is preferable for the direct shear wave velocity measurement to be obtained at the site of interest. However, this was not possible due to access constraints. Finally, soil-structure interaction effects were not considered here and are beyond the scope of this study. Future improvements include extending the use of ambient vibration measurements for site characterisation in regolith environments and enhancing geophysical methods to investigate the basin structure of the investigated site.

9. Conclusion

Three historical seismic events, the 1897 Beachport (MMI IV-V), 1902 Warooka (MMI V-VI), 1954 Adelaide (MMI VI-VII) earthquakes, caused damage to the Old Exchange Building located

in Pirie St., Adelaide. As there were no recorded time histories of the three events, generated time histories are required. Time histories of the three events have been generated using a method that was validated using recorded ground motions of the 1997 Burra earthquake. Two representative models for the Old Exchange Building site were developed and validated using a single microtremor measurement at the nearby site.

The results of both the synthetic time histories of historical seismic events and the development of 1D profiles of the Old Exchange Building site, were used for investigating site effects. Analytical models used in this study for a site-specific ground response analysis proved to simulate the ground behaviour reasonably well. The results of the ground response analyses clearly indicate that, for the case of Old Exchange Building site, the input parameters are influenced by local site effects by an amplification factor of up to 3.4.

Acknowledgments. The authors wish to acknowledge the University of Adelaide for providing a research scholarship for the first author. In addition, the first author is grateful to the Faculty of Engineering of Syiah Kuala University for their support. The authors also acknowledge the editorial assistance of Leticia Mooney.

REFERENCES

Allen T.I.; 2012: *Stochastic ground-motion prediction equations for southeastern Australian earthquakes using updated source and attenuation parameters*. Geosci. Australia, Canberra, Australia, Record 2012/69, 76 pp.

Atkinson G.M. and Macias M.; 2009: *Predicted ground motions for great interface earthquakes in the Cascadia subduction zone.* Bull. Seismol. Soc. Am., **99**, 1552-1578, doi:10.1785/0120080147.

Bardet J.P., Ichii K. and Lin C.H.; 2000: *EERA a computer program for equivalent-linear earthquake site response analyses of layered soil deposits*. Dept. of Civil Eng., Univ. of Southern California, Los Angeles, CA, USA, 38 pp.

Beresnev I.A. and Atkinson G.M.; 1998: *FINSIM-a FORTRAN program for simulating stochastic acceleration time histories from finite faults*. Seismol. Res. Lett., **69**, 27-32.

Bindi D., Castro R.R., Franceschina G., Luzi L. and Pacor F.; 2004: *The 1997-1998 Umbria- Marche sequence (central Italy): source, path and site effects estimated from strong motion data recorded in the epicentral area*. J. Geophys. Res., **109**, B04312, doi:10.1029/2003JB002857.

Booth E.D., Pappin J.W., Mills J.H., Degg M.R. and Steedman R.S.; 1986: *The Mexican earthquake of 19th September 1985*. Earthquake Eng. Field Invest. Team (EEFIT), Soc. Earthquakes Civ. Eng. Dyn., London, U.K., 146 pp.

Borja R.I., Lin C-H., Sama K.M. and Masada G.M.; 2000: *Modelling non-linear ground response of non-liquefiable soils*. Earthquake Eng. Struct. Dyn., **29**, 63-83.

Brebbia C.A. (ed); 1996: *The Kobe earthquake: geodynamical aspects*. Comput. Mech. Publ., Southampton, U.K., 145 pp.

Castro R.R., Pacor F., Bindi D., Franceschina G. and Luzi L.; 2004: *Site response of strong motion stations in the Umbria region, central Italy*. Bull. Seismol. Soc. Am., **94**, 576-590.

DMITRE Minerals (Department of Manufacturing, Innovation, Trade, Resources and Energy Official Website); 2013: *Urban monitoring*. <www.pir.sa.gov.au/minerals/earthquakes/urban_monitoring accessed on 2 November 2013>.

Dyster T.; 1996: *Strong shock of earthquake: the strong of the four greatest earthquakes in the history of South Australia*. Dept. Mines and Energy, Geol. Surv. South Australia, Report Book 95/47.

Everingham I.B., McEwin A.J. and Denham D.; 1982: *Atlas of isoseismal maps of Australian earthquakes*. Dept. National Dev. & Energ., Bur. of Min. Resour., Geol. and Geophys., Canberra, Australia, Bull. 214, 184 pp.

Finn W.D.L. and Wightman A.; 2003: *Ground motion amplification factors for the proposed 2005 edition of the national building code of Canada*. Can. J. Civ. Eng., **30**, 272-278, doi:10.1139/l02-081.

García-Jerez A., Piña-Flores J., Sánchez-Sesma F.J., Luzón F. and Perton M.; 2016: *A computer code for forward computation and inversion of the HVSR spectral ratio under the diffuse field assumption.* Comput. Geosci., **97**, 67-78.

Hartzell S.; 1978: *Earthquake aftershocks as Green's functions.* Geophys. Res. Lett., **5**, 1-14.

Herak M.; 2008: *ModelHVSR-a Matlab tool to model horizontal-to-vertical spectral ratio of ambient noise*. Comput. Geosci., **34**, 1514-1526, doi:10.16/j.cageo.2007.07.009.

Herak M., Allegretti I., Herak D., Kuk K., Kuk V., Maric K., Markusic S. and Stipcevic J.; 2010: *HVSR of ambient noise in Ston (Croatia): comparison with theoretical spectra and with the damage distribution after the 1996 Ston-Slano earthquake*. Bull. Earthquake Eng., **8**, 483-499.

Idriss I.M.; 1990: *Response of soft soil sites during earthquakes*. In: Proc. H. Bolton Seed Memorial Symposium, Duncan J.M. (ed), BiTech Publishers, Vancouver, BC, Canada, pp. 273-289.

Idriss I.M. and Sun J.I.; 1992: *User's manual for SHAKE91 (a computer program for conducting equivalent linear seismic response analyses of horizontally layered soil deposits*. Centre Geotech. Model., Dept. Civ. and Environ. Eng., Univ. of California, Davis, CA, USA, 12 pp.

Iervolino I. and Cornell C.A.; 2008: *Probability of occurrence of velocity pulses in near-source ground motions*. Bull. Seismol. Soc. Am., **98**, 2262-2277.

Joyner W. and Boore D.; 1986: *On simulating large earthquakes by Green's-function addition of smaller earthquakes*. In: Proc. 5th Maurice Ewing Symp. Earthquake Source Mech., S. Das, J. Boatwright and C. Scholz (eds), Am. Geophys. Union, Washington, DC, USA, pp. 269-274.

Kerr-Grant C.; 1956: *The Adelaide earthquake of 1st March 1954*. Trans. Royal Soc. South Australia, **59**, 177-185.

Kramer S.L.; 1996: *Geotechnical earthquake engineering*. Prentice Hall, Upper Saddle River, NJ, USA, 673 pp.

Leonard M., Burbidge D. and Edwards M.; 2013: *Atlas of seismic hazard maps of Australia: seismic hazard maps, hazard curves and hazard spectra*. Geosci. Australia, Canberra, Australia, Record 2013/41, 39 pp.

Linkimer L.; 2008: *Relationship between peak ground acceleration and modified Mercalli intensity in Costa Rica.* Rev. Geol. America Central, **38**, 81-94.

Love D.; 1996: *Seismic hazard and microzonation of the Adelaide metropolitan area*. Sutton Earthquake Centre, Dept. of Mines and Energy South Australia, Adelaide, Australia, Report 27, 104 pp.

Lunedei E. and Albarello D.; 2015: *Horizontal-to-vertical spectral ratios from a full-wavefield model of ambient vibrations generated by a distribution of spatially correlated surface sources*. Geophys. J. Int., **201**, 1140-1153.

Luzi L., Bindi D., Franceschina G., Pacor F. and Castro R.; 2005: *Geotechnical site characterisation in the Umbria Marche area and evaluation of earthquake site-response*. Pure Appl. Geophys., **162**, 2133-2161, doi:10.1007/s00024-005-2707-6.

Malpas K.L.; 1991: *Seismic risk of South Australia*. Master Thesis, School of Earth Sci., Flinders Univ., Adelaide, South Australia, 179 pp.

Mavroeidis G.P. and Papageorgiou A.S.; 2003: *A mathematical representation of near-fault ground motions*. Bull. Seismol. Soc. Am., **93**, 1099-1131.

McCue K.; 1975: *Seismicity and seismic risk in South Australia*. Dept. of Phys., Univ. of Adelaide, South Australia, Report ADP 137.

McCue K.; 1990: *Australia's large earthquakes and recent fault scarps*. J. Struct. Geol., **12**, 761-766.

McCue K. and Love D.; 1997: *Earthquake microzonation Adelaide, South Australia*. Australian Geol. Surv. Organ. (AGSO), Final Report, 22 pp.

Mimoglou P., Psycharis I.N. and Taflampas I.; 2017: *Determination of the parameters of the directivity pulse embedded in near-fault ground motions and its effect on structural response*, In: Papadrakakis M., Plevris V. and Lagaros N.D. (eds), Computational methods in earthquake engineering, Springer, DOI:10.1007/978-3-319-47798-5_2.

Motazedian D. and Atkinson G.M.; 2005: *Stochastic finite fault modeling based on a dynamic corner frequency*. Bull. Seismol. Soc. Am., **95**, 995-1010.

Motazedian D. and Moinfar A.; 2006: *Hybrid stochastic finite fault modeling of 2003, M6.5, Bam earthquake (Iran)*. J. Seismol., **10**, 91-103, doi:10.1007/s10950-005-9003-x.

Okada H.; 2003: *The microtremor survey method*. Soc. of Explor. Geophys., Geophys. Monogr. Ser. No. 12, 150 pp., doi:10.1190/1.9781560801740, (Translated by Koya Suto).

Olsen K.B., Day S.M. and Bradley C.R.; 2003: *Estimation of Q for Long-Period (>2 sec) waves in the Los Angeles Basin*. Bull. Seismol. Soc. Am., **93**, 627-638.

Panagiotou M.; 2008: *Seismic design, testing and analysis of reinforced concrete wall buildings*. Ph.D. Dissertation in Struct. Eng., Univ. of California, San Diego, CA, USA, 289 pp.

Priolo E., Poli M.E., Laurenzano G., Vuan A. and Barnaba C.; 2008: *Site response estimation in the Vittorio Veneto area (NE Italy), Part 2: mapping the local seismic effects in the urban settlement*. Boll. Geof. Teor. Appl., **49**, 387-400.

Santulin M., Moratto L., Sarao A. and Slejko D.; 2012: *Ground motion modelling including finite fault and 1D site effects in north-eastern Italy*. Boll. Geof. Teor. Appl., **53**, 313-330, doi:10.4430/bgta0071.

Schnabel P.B., Lysmer J. and Seed H.B.; 1972: *SHAKE: A computer program for earthquake response analysis of horizontally layered sites*. Report 72-12, Earthquake Engineering Research Center, University of California, Berkeley, California, 102 pp.

Seed H.B. and Idriss I.M.; 1970: *Soil moduli and damping factors for dynamic response analysis*. Report No. UCB/EERC-70/10, Earthquake Engineering Research Center, University of California, Berkeley, California, 48 pp.

Seed H.B. and Sun J.H.; 1989: *Implication of site effects in the Mexico City earthquake of September 19, 1985 for earthquake-resistance-design criteria in the San Francisco Bay Area of California*. Report No. UCB/EERC-89/03, Earthquake Engineering Research Center, University of California, Berkeley, California, 140 pp.

Selby J.; 1984: *Geology and the Adelaide environment*. South Australian Dept. of Mines and Energy, Adelaide, Australia, 168 pp.

Selby J. and Lindsay J.M.; 1982: *Engineering geology of the Adelaide city area*. Dept. of Mines and Energy, Geol. Surv. of South Australia, 91 pp.

Setiawan B., Jaksa M., Griffith M. and Love D.; 2016: *Analysis of microtremor array measurement using the spatial autocorrelation (SPAC) method across the Adelaide city*. School of Civil, Environ. and Mining Eng., Univ. of Adelaide, Australia, Research Report No. R196, 36 pp.

Sheard M.J. and Bowman G.M.; 1987a: *Definition of the Keswick Clay: Adelaide/Golden Grove embayment, para and eden blocks, South Australia*. Quarterly Geol. Notes of the Geol. Surv. of South Australia, **103**, 4-8.

Sheard M.J. and Bowman G.M.; 1987b: *Redefinition of the upper boundary of the Hindmarsh Clay: Adelaide Plains Sub-Basin and Adelaide/Golden Grove embayment*. Quarterly Geol. Notes of the Geol. Surv. of South Australia, **103**, 9-16.

Standards Australia; 2007: *AS 1170.4-2007 Australian standard of structural design actions Part 4: earthquake actions in Australia.* Standards, Australia, 48 pp., <www.standards.org.au>.

Sykora D.W. and Davis J.J.; 1993: *Site-specific earthquake response analysis for Paducah gaseous diffusion plant, Paducah, Kentucky*. U.S. Dept. of Energy, Vicksburg, MS, USA, 266 pp.

Taflampas I. and Psycharis I.N.; 2008: *Investigation of the effect of the ground motion characteristics on the Ry-l relation for the inelastic response of SDOF structures*. In: Proc. 14th World Conf. Earthquake Eng., Beijing, China, 8 pp.

Tehranizadeh M. and Hamedi F.; 2000: *Influence of effective duration of strong motion on elastic response spectra*. In: Proc. 12th World Conf. Earthquake Eng., Auckland, New Zealand, 7 pp.

Uthayakumar U.M. and Naesgaard E.; 2004: *Ground response analysis for seismic design in Fraser River Delta, British Columbia*. In: Proc. 13th World Conf. Earthquake Eng., Vancouver, Canada, 10 pp.

Wald D.J., Quintoriano V., Heaton T.H. and Kanamori H.; 1999: *Relationship between peak ground acceleration, peak ground velocity and modified Mercalli intensity in California*. Earthquake Spectra, **15**, 557-564.

Zhang Z. and Stewart R.R.; 2007: *Seismic attenuation and rock property analysis in a heavy oilfield: Ross Lake, Saskatchewan*. CREWES Res. Report, Univ. of Calgary, Canada, Vol. 19, 16 pp.

Corresponding author: Bambang Setiawan
Faculty of Engineering, Syiah Kuala University
Jl. Tgk. Syech Abdurrauf 7, Darussalam, Banda Aceh, 23111, Indonesia
Phone: +62 821 78501824; e-mail: bambang.setiawan@unsyiah.ac.id

Appendix C:

AN INTERNATIONAL PEER REVIEWED JOURNAL PAPER 2

(COPY OF PAPER FROM CHAPTER 3)

SETIAWAN, B., JAKSA, M., GRIFFITH, M., AND LOVE, D. (2018). SEISMIC SITE CLASSIFICATION BASED ON CONSTRAINED MODELING OF MEASURED HVSR CURVE IN REGOLITH SITES. SOIL DYNAMICS AND EARTHQUAKE ENGINEERING, 110: 244–261, DOI: 10.1016/J.SOILDYN.2017.08.006.

INTENTIONALLY BLANK

Soil Dynamics and Earthquake Engineering 110 (2018) 244–261

Contents lists available at ScienceDirect

Soil Dynamics and Earthquake Engineering

journal homepage: www.elsevier.com/locate/soildyn

Seismic site classification based on constrained modeling of measured HVSR curve in regolith sites

Bambang Setiawan[a,b,*], Mark Jaksa[a], Michael Griffith[a], David Love[c]

[a] School of Civil, Environmental and Mining Engineering, the University of Adelaide, North Terrace Campus, the University of Adelaide, SA 5005, Australia
[b] Faculty of Engineering, Syiah Kuala University, Jl. Tgk. Syech Abdurrauf 7, Darussalam, Banda Aceh 23111, Indonesia
[c] Department of State Development, Government of South Australia, 101 Grenfell Street, Adelaide, SA 5000, Australia

ARTICLE INFO

Keywords:
Seismic site classes
HVSR
Ambient noise
Regolith

ABSTRACT

Seismic site classification is the most widely accepted practical method in the design of seismic resistant infrastructure. The horizontal vertical spectral ratio (HVSR) technique for analyzing ambient noise data has been successfully applied to quantify site effects in the estimation of seismic site classes associated with seismic hazards. This successful application was mainly carried out in high impedance contrast sites. The present paper focuses on the application of the HVSR technique to regolith sites which were suggested by previous studies to be low in impedance contrast between the upper and underlying bedrock layers (< 4–5). A case study is examined which explores the central business district of Adelaide, South Australia and incorporates 10 in situ ambient noise measurements carried out across the city. Adelaide experienced more medium-sized earthquakes than any other capital city in Australia in the past half of the last century. Site amplification was also observed to occur in Adelaide. Ambient noise data were used to estimate the site predominant period and to infer the site shear wave profile, after establishing that the data were free from noises from an industrial source, checking the reliability of the HVSR ellipticity curve and validating the appropriateness of the adopted method and resulting shear wave models. The results show that the predominant fundamental period for Adelaide is 0.8 s or higher, which suggests a subsoil class D according to the Australian Standard. Results of the inversion for the upper 30 m shear wave velocities of Adelaide's subsoil layers varies from 194 m/s to 418 m/s, which are related to classes D to C (NEHRP classification system), classes D to B (Australian Standard classification system) or classes D/DE to C (regolith case classification system). These results are in a good agreement with several previous studies. This suggests a promising application of the HVSR analysis for seismic assessment at regolith sites.

1. Introduction

Seismic site classification is widely accepted in the design of seismic resistant infrastructure. Currently, the majority of seismic site classifications are carried out based on recommendations provided by the National Earthquake Hazards Reduction Program (NEHRP) [1]. However, the application of the NEHRP classification system in regolith sites is the subject significant research effort (e.g. [2,3]), including in Adelaide, South Australia. The National Committee on Soil and Terrain [4] characterized regolith as unique geological materials which generally have low impedance contrast comparable to that of bedrock. Regoliths are formed or altered by land surface processes, whereas bedrock is formed or altered by deep-seated crustal processes. The characterization of regoliths and bedrock is by their formation processes, rather than by their material type [5]. These different formation processes result in distinctive characteristics of regolith masses when compared to bedrock. Generally, the density, strength, and cohesion of regolith masses are lower than bedrock masses [4]. Anbazhagan et al. [3] addressed the difficulties in the application of NEHRP seismic site classification in such sites, including ones in Australia. McPherson and Hall [2] suggested a modification to the NEHRP seismic classification system for the application to regolith sites.

The horizontal vertical spectral ratio (HVSR) technique [6] has been widely used in seismic hazard assessment since it is relatively straightforward, convenient and reliable in urban areas. Separate studies by [7] and [8] successfully implemented the HVSR technique in Turkey and Iran, respectively, to calculate the site predominant frequency and [9,10] and [11] enhanced the HVSR technique to infer the subsurface shear wave profile. To date, the application of the HVSR technique in regolith regions for site seismic classification is still under

* Corresponding author at: Faculty of Engineering, Syiah Kuala University, Jl. Tgk. Syech Abdurrauf 7, Darussalam, Banda Aceh 23111, Indonesia.
E-mail addresses: bambang.setiawan@unsyiah.ac.id, bambangsetiawan@adelaide.edu.au (B. Setiawan), mark.jaksa@adelaide.edu.au (M. Jaksa), michael.griffith@adelaide.edu.au (M. Griffith), david.love@sa.gov.au (D. Love).

http://dx.doi.org/10.1016/j.soildyn.2017.08.006
Received 18 November 2016; Received in revised form 2 May 2017; Accepted 6 August 2017
Available online 19 October 2017

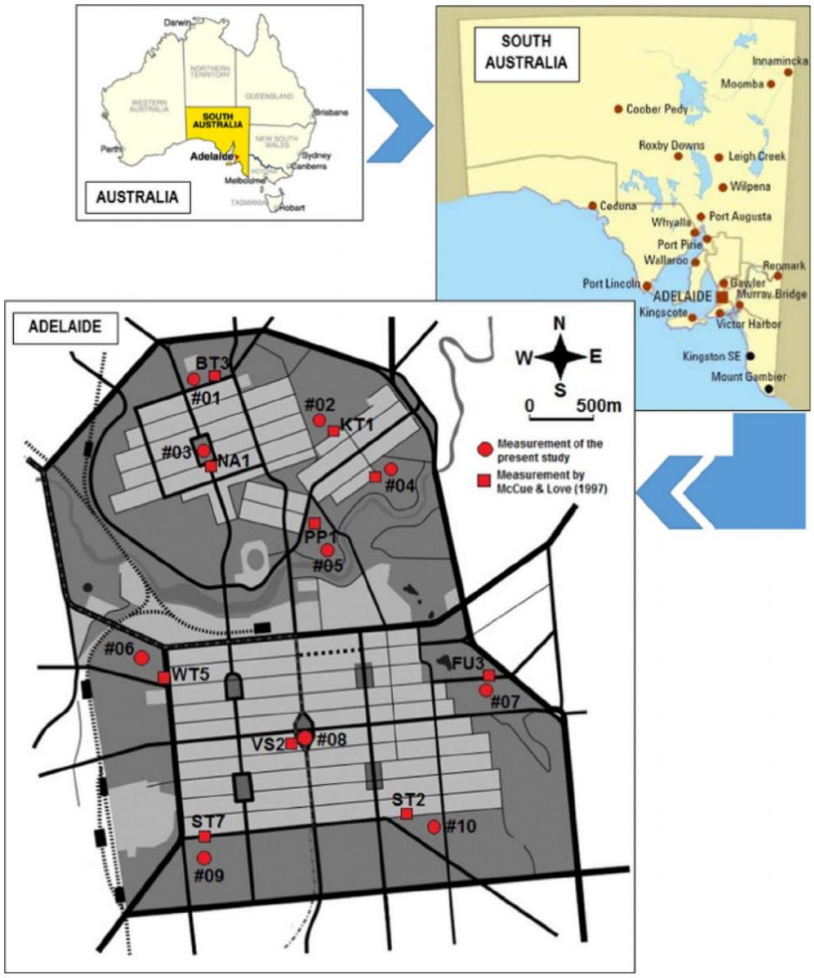

Fig. 1. Site locations of microtremor measurements of the present study (red circles) and [41] (red squares). (For interpretation of the references to color in this figure legend, the reader is referred to the web version of this article.)

development [2]. Regardless of some limitations of this method, [11] and [12] observed that the HVSR method is reasonably robust in seismic hazard assessment, provided the geological setting at the target location is well defined.

The present study aims to investigate the HVSR method for seismic site classification at regolith and Adelaide, the capital and largest city in South Australia, which is founded on a regolith, is selected as a case study in the present work. Previous investigations (*cf* [13] and [14]) suggested low impedance contrast of the regolith of Adelaide (assuming that large impedance contrast is > 4–5 as suggested by [15]). Shear wave velocity measurement at the Government House Site (GHS), using the spectral analysis of surface waves (SASW) method [13], suggested an average of about 420 m/s and 810 m/s for Adelaide's overlying layer and bedrock shear wave velocities, respectively. By assuming densities of 1900 kg/m^3 and 2100 kg/m^3 for the top layer and the bedrock, respectively, measurements by [13] suggested an impedance contrast of only 2.1 (i.e. a low impedance contrast). Preliminary results from a site investigation by [14] suggested a shear wave velocity of at least 315 m/s for the upper 30 m for most of the Adelaide city. Only the areas along the River Torrens were expected to have a shear wave velocity of at least 225 m/s. Thus, a raw estimation of the impedance contrast of most of the Adelaide city sites, based on the recommendations of [14], will be approximately 3.5 by assuming the shear wave velocity of the top layer and bedrock are 315 m/s and 1000 m/s, respectively. Densities of 1900 kg/m^3 and 2100 kg/m^3 for the top layer and the bedrock, respectively, are used for this raw impedance contrast calculation. This impedance contrast of 3.5 is also below that suggested by [15], where values > 4–5 are considered as large impedance contrast.

Adelaide is within the most seismically active region on the Australian continent ([16–18]). Although this continent is classified as a stable continent region (SCR) ([19–21]) with low to moderate [22] seismic activity, the Australian continent deformation rate is higher than other stable intraplate regions [21]. The continent experiences a magnitude ≥ 6.0 earthquake approximately every 5 years [23] and historically, the continent has experienced some major devastating earthquakes, such as those that occurred at Meeberrie (1941; ML 6.8), Meckering (1986; MS 6.8), Cadoux (1979; MS 6.4) and Tennant Creek (1988; MS 6.3) ([24–26]). The seismic activity of the Adelaide region was also investigated by [27] and [28]. Greenhalgh et al. [28] found at least 300 earthquakes are recorded by instruments each year in South Australia and in the last 150 years, 15 events were of magnitude 5 or greater. McCue [23] found that the Adelaide city experienced more medium-sized earthquakes than any other capital city in Australia in the past half of the last century. Furthermore, the site amplification

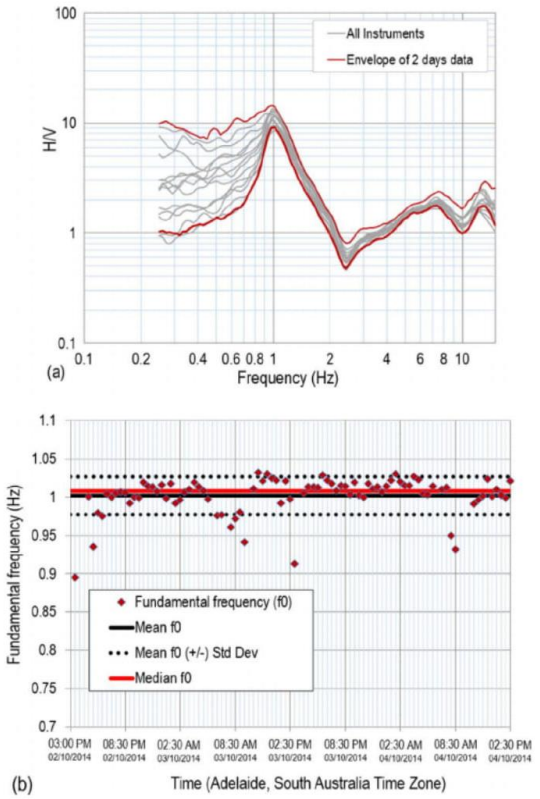

Fig. 2. (a) The envelope of HVSR test results of continous 2 days of data in lengths of 30 min for one of equipment sets used in the present study, (this figure, also, HVSR test results for all used equipment sets used in the present study), and (b) Fundamental frequency of HVSR test results of continous 2 days of data in lengths of 30 min for one of equipment sets used in the present study.

phenomenon also occurs in Adelaide, which is observed by comparing the ground motion recording on Adelaide's regolith to that on a rock site just outside the city during the 1997 Burra earthquake. The recorded motions on the regolith are very much stronger than those recorded on rock [29]. Thus, an in-depth seismic hazard study of the Adelaide region is highly desirable.

A group of seismometer sets has been deployed across the Adelaide city to measure the ambient noise at a range of regolith sites. The data are used to obtain the seismic hazard parameters, such as site periods and shear wave profiles, from which the seismic site classification of Adelaide is quantified. The results of the present study are valuable, not only to the seismic site classification of Adelaide, but also to the seismic assessment of regolith sites with a similar geological context.

1.1. Seismic site classification in Australia

The most widely used seismic site classification system is based on the mean shear wave velocity of the uppermost 30 m of the subsurface layers, $V_{s,30}$, which was proposed by the National Earthquake Hazards Reduction Program (NEHRP) [3,13], and [30] and can be calculated by:

$$V_{s30} = \frac{\sum_{i=1}^{n} Z_i}{\sum_{i=1}^{n} \left(\frac{Z_i}{V_{si}}\right)}$$

where:

Z = thickness (in meters);
V_{si} = shear wave velocity of ith layer; and
n = a total number of layers in the top 30 m.

This classification system categorizes the subsoil into 5 subsoil classes from hard rock (subsoil class A) to thick medium-soft soils (subsoil class E). Standards Australia [31] (AS 1170.4–2007) modified the NEHRP seismic classification system in the following manner: (1) rock (subsoil class B) applies to $V_{s,30}$ above 360 m/s instead of 760 m/s in the NEHRP system; (2) a site fundamental period is introduced to separate subsoil Class D from Class C; and (3) subsoil Class E applies to sites with greater than 10 m thickness of soil with a shear wave velocity less than 150 m/s. The amendment to AS 1170.4 Standards Australia followed Standards New Zealand [32] at a stage when the two countries were attempting to produce a unified earthquake code. The work, principally performed by [33] and [34], showed that deep stiff soils produced amplification similar to soft shallow soils, thus producing a departure from the standard NEHRP method. An alternative and applicable classification system was suggested by [2], which clusters the system into 7 classes and includes a physical description and age associated with each.

1.2. Geological setting of Adelaide

The structural geology of the Adelaide city is characterized by faults oriented in the north-east to south-west directions. Earthquakes related to the faults in Adelaide were documented and presented by [35]. The most significant seismic event in Adelaide was the 1954 Adelaide Earthquake which was associated with intra-plate activity along the Burnside-Eden Fault to the east of the city ([35,36]). Adelaide is situated in the eastern part of the St. Vincent Basin and the morphology of the city is predominantly controlled by the bounding faults to the west (Para Fault) and east (Eden-Burnside Fault) of the city [37]. Below the fill and surficial layer, most of the natural immediate surface consists of Holocene stratigraphic units of either red brown clay (Callabonna Clay) or light brown silty clay with calcareous with layers of calcrete gravel (Pooraka Formation). In addition, a relatively narrow channel along the River Torrens, crossing from east to west within the Adelaide city, has eroded these layers and deposited alluvium. The combined thickness of these Holocene units may up to 21 m thick ([37] and [38]). Below the Holocene units is a layer of Keswick Clay, Hindmarsh Clay, or a combination of both, for the majority of the southern part of the city [39]. These layers are highly plastic, over-consolidated clays which exhibit properties remarkably similar to those of the London Clay [40]. These layers are underlain by either the Carisbrooke Sand, Burnham Limestone and Hallett Cove Sandstone or the Gull Rock member of the Blanche Point Formation. In some areas these are underlain by a sand unit of the Port Willunga Formation or the Tandanya Sand Member of the Chinaman Gully Formation. The age of these stratigraphic units varies from Pleistocene to Eocene [37]. Most areas in the city of Adelaide are further underlain by the South Maslin Sand and Clinton Formation, before Precambrian bedrock is encountered at about 64 m or less to the north of the city and up to 118 m or more to the south [37]. Moreover, Selby & Lindsay [37] suggested a higher stratigraphic variability to the south of the city than to the north.

1.3. Adelaide seismic hazard study

Adelaide, with a population in excess of 1.3 million people, is the only capital city in Australia that has recorded a medium or higher seismic event with an epicenter in very close proximity to the city, with an earthquake of a magnitude of 5.4 ML which struck the city on 28 February 1954. This has been responsible for the city being assigned the highest seismic exposure of all capital cities in Australia. Despite several

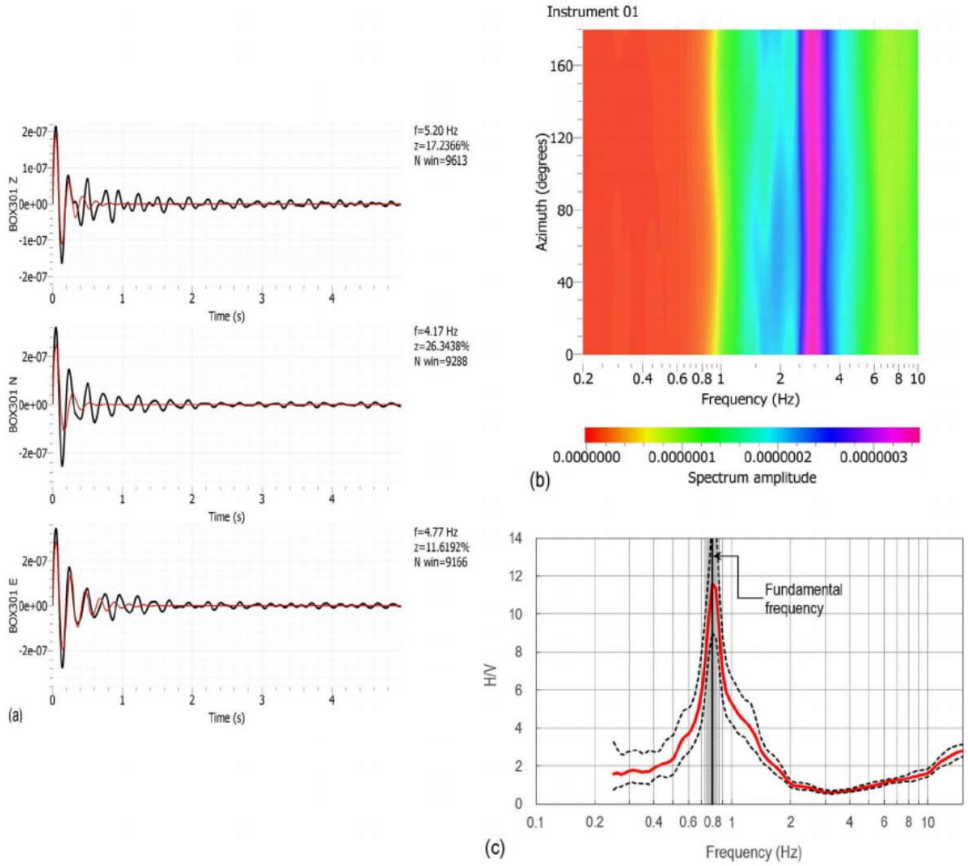

Fig. 3. (a) Typical results of identification of data from an industrial source, (b) Typical results of frequency of noise sources in the recorded ambient noise data, and (c) Examples of HVSR curves.

changes in seismic hazard exposure among Australian capital cities in 2012, the seismic hazard for Adelaide remains under development. To date, several studies examining local site effects related to Adelaide have been undertaken ([2,13,14,41]). McPherson and Hall [2] undertook a further seismic assessment which resulted in a general seismic site classification for South Australia at low resolution. McCue and Love [41] identified a fundamental site frequency of 1 Hz for most of the Adelaide city. A study by [13], using the NEHRP seismic site classification system, assigned Adelaide a Class D, which corresponds to a $V_{s,30}$ of 257 m/s. However, their measurement was limited to only a single location, namely the Government House site. These studies combined, suggest that the applicable soil model for Adelaide lies in the subsoil range between Classes C and D.

This broad seismic classification has a number of ramifications from an earthquake structural design perspective and [42] investigated the consequences of these two different seismic classes and concluded that the Adelaide CBD can be represented as Class D. However, it is widely appreciated that the subsurface of the City of Adelaide is highly variable ([37,39]).

2. Site location, data acquisition and processing

In order to undertake the HVSR technique, microtremor measurements were carried out across the Adelaide city. Ten locations were examined, 5 to the north and 5 to the south of the city, as indicated by the red circles in Fig. 1. Three sets of equipment were deployed at 4 sites (#01, #02, #04 and #05) to the north of Adelaide and one site (#03) was measured using a single device. Similarly, to the south of the city, 3 sets of equipment were deployed at 4 sites (#06, #07, #09 and #10) and location #08 was measured using a single device. The recorded noise data were separated into 30-min duration datasets using the Eqwave application [43] as suggested by [44]. Each dataset includes noise measurement in 3 orthogonal directions (two horizontal and one vertical). Fig. 1 also shows (with red squares) the locations of selected tests undertaken by [41], which will be discussed in a later section. A typical subset of the acquired 30 min waveform data, saved as standard ASCII (*. SAF) files, as recommended by the Site Effects Assessment using Ambient Excitation (SESAME) [15], along with the field data sheets, are included in Appendix A of the Supplementary Data associated with the present paper.

The equipment used to acquire the data consisted of a seismometer with two horizontal and one vertical sensor, an analog-to-digital recorder, a GPS antenna and a laptop computer which was used for initial setup and checking. A battery was used to power the system. Ambient noise data were acquired continuously for at least two hours using a LE-3Dlite Lennartz seismometer and Kelunji digital data recorder. The seismometer was set on top of a 20 mm thick circular concrete slab over a generally firm to stiff ground surface. The location, where the seismometer was fixed, was cleared of any tall grass and leveled so as to minimize any instability to the seismometer during recording. The

Table 1
Site fundamental frequencies of all instruments.

Location	Fundamental frequency (Hz)														
	Instrument #1					Instrument #2					Instrument #3				
	#1	#2	#3	#4	#5	#1	#2	#3	#4	#5	#1	#2	#3	#4	#5
#01 (Barton Tce W)	1.01	0.98	1.04	1.03	1.04	F	0.91	F	0.98	F	1.02	1.07	F	1.05	1.04
	1.02 (average)					0.95 (average)					1.05 (average)				
#02 (Lefevre Tce)	1.19	1.22	1.22	1.18	1.19	1.33	1.12	1.25	1.20	1.25	1.19	1.12	1.18	1.15	NA
	1.2 (average)					1.23 (average)					1.16 (average)				
#03 (Wellington Sq)	1.11	1.08	1.09	1.06	NA										
	1.09 (average)														
#04 (Finniss St)	F	1.00	F	0.97	NA	1.02	1.05	1.06	1.06	1.01	1.04	1.08	1.07	1.05	NA
	0.99 (average)					1.04 (average)					1.06 (average)				
#05 (Frome Rd/ War Mem. Dr)	F	F	F	F	F	1.02	1.00	0.99	0.99	1.00	0.96	0.99	0.96	0.96	0.96
	F					1 (average)					0.97 (average)				
#06 (West Tce/ Port Rd)	F	F	F	F	F	1.10	1.09	1.10	1.10	1.14	1.05	1.11	1.08	1.07	NA
	F					1.11 (average)					1.08 (average)				
#07 (Bartels Rd)	0.82	0.81	0.81	0.80	0.82	0.80	0.80	0.80	0.79	NA	0.77	0.74	0.75	F	NA
	0.81 (average)					0.80 (average)					0.75 (average)				
#08 (Victoria Sq)	0.84	0.84	0.84	0.83	0.84										
	0.84 (average)														
#09 (South Tce/ West Tce)	F	F	0.65	F	0.67	0.72	0.72	F	0.74	NA	0.74	0.72	0.73	0.76	0.73
	0.66 (average)					0.73 (average)					0.74 (average)				
#10 (South Tce/ Hutt Rd)	F	F	F	F	NA	F	F	F	F	NA	0.79	0.80	0.81	0.82	NA
	F					F					0.81 (average)				

Note:
NA is ambient noise no data available.
F is FAIL to comply SESAME (2004) criteria.

seismometer was oriented to North and protected from the wind with a plastic bucket and stabilized with a masonry brick.

In the present study, two hours of noise data are considered sufficient for appropriately representing the measured site, as temporal variability has been examined by recording more than two days of continuous ambient noise data in the Adelaide city. After examining the reliability of the recorded noise data, as well as exploring whether any of the data originated from an industrial source over 96 datasets (each set involves a 30 min noise record, as suggested by [44]), an HVSR analysis using Geopsy [45] is carried out and the results are shown in Fig. 2. The HVSR analysis using Geopsy is explained in detail later. As shown in Fig. 2(a), the envelope of the results of the HVSR analysis demonstrate very similar curve patterns, particularly from about 0.8–10.0 Hz. A high curve pattern dispersion, from a frequency of 0.8 Hz downward to 0.25 Hz, suggests a low noise source intensity over this frequency interval, as shown later in the paper. Further investigation is undertaken to validate whether or not two hours of noise data are sufficient by arranging the fundamental frequency of all the HVSR analyses, with respect to the time and date of the measurement, the results of which are shown in Fig. 2(b). This is undertaken because 4 consecutive fundamental frequencies, beyond the mean fundamental frequency ± one standard deviation, are unavailable. The analysis also suggests a fundamental frequency of 1.0 Hz with a discrepancy of approximately 0.025 Hz. In other words, the analysis confirms that two hours of continuously recorded data are sufficient to detect any spurious measurements. Moreover, Fig. 2(b) also demonstrates that the time of measurement has no appreciable effect on the results. Furthermore, all of the equipment sets deployed in the present study are examined for their repeatability. Whilst conducting the testing described above, all other deployed equipment sets were also run at the same location, with a separation distance of approximately 0.5 m from one another. The HVSR analysis curves of all deployed

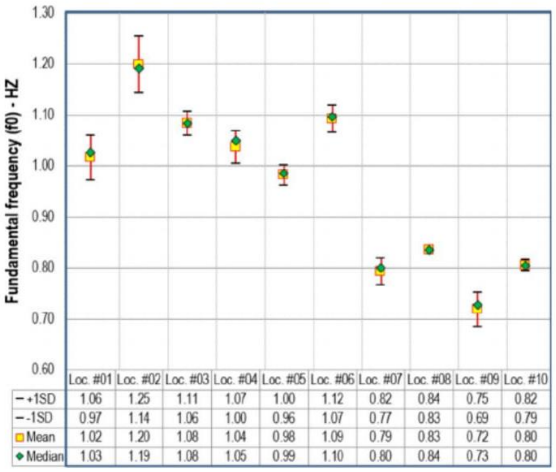

	Loc. #01	Loc. #02	Loc. #03	Loc. #04	Loc. #05	Loc. #06	Loc. #07	Loc. #08	Loc. #09	Loc. #10
+1SD	1.06	1.25	1.11	1.07	1.00	1.12	0.82	0.84	0.75	0.82
-1SD	0.97	1.14	1.06	1.00	0.96	1.07	0.77	0.83	0.69	0.79
Mean	1.02	1.20	1.08	1.04	0.98	1.09	0.79	0.83	0.72	0.80
Median	1.03	1.19	1.08	1.05	0.99	1.10	0.80	0.84	0.73	0.80

Fig. 4. Fundamental frequencies of each site location from the ambient noise measurements.

equipment sets are presented in Fig. 2(a). These results confirm the repeatability of the equipment.

As mentioned above, 30-min datasets were post-processed to obtain the horizontal vertical spectral ratio (HVSR), which is necessary to determine the site periods and to infer the shear wave velocity profile. HVSR processing was carried out using the Geopsy software [45] developed within the framework of the Site Effects Assessment using Ambient Excitation (SESAME) Project. In the present study, the default parameters and auto window selection were adopted. Prior to conducting the HVSR analysis, the Geopsy damping toolbox is adopted to detect the presence of any data originating from an industrial source. An industrial origin is concluded if the damping is much lower than 1% and the frequency is sustained. This detection is important to justify the validity of the recorded ambient noise data used in the HVSR analysis. Some typical results from the detection of any data originating from an industrial source are shown in Fig. 3(a). Further details of all such analyses are included in Appendix B of the Supplementary Data associated with the paper.

2.1. Sources of recorded ambient noise data

In the investigation of the subsurface structure the frequency of the ambient noise sources is found to range between 0.005 and 10 Hz. A threshold of 1 Hz is widely accepted to delineate natural sources of noise from anthropogenic sources [15]. The frequency range of the natural noise, known as microseisms and triggered by natural processes such as ocean waves, tides and wind, is between 0.005 Hz and 1 Hz, whereas the frequency range of anthropogenic noise, known as microtremor and is associated with human activities, ranges between 1 and 10 Hz [15]. In the present study, ambient noise data sources, recorded at all the measured sites, ranged between 0.4 and 15 Hz. However, greater intensity is captured from at least 0.8 Hz. Spectral analysis of the ambient noise data recorded in the present study suggests the highest intensity, manifested by strong amplitude, occurs at a range of 2–6 Hz, a typical example of which is shown in Fig. 3(b). These observations suggest that the sources of the recorded ambient noise data are related mainly to human activities. This frequency range has been found to be useful in investigating the near-surface geology, which is mainly concerned with site effects for seismic hazard assessment ([46,47] and [48]). Fig. 3(b) also shows that the anthropogenic noise sources in the present study originate from all directions. This suggests that noise originating from industrial sources is not present in any of the recorded data used in this study.

2.2. Calculation of the HVSR curve

The HVSR method is based on the spectral ratio analysis between the Fourier amplitude spectrum of the horizontal (H) and vertical (V) components of the recorded ambient vibration. Initially, selecting the most stationary parts of the ambient vibration to exclude transient waves, such as footsteps and close distance traffic, was carried out by dividing the time series of each component into windows. Several parameters i.e. window length, a threshold of the short-time average/long-time average (STA/LTA) and the lengths of STA/LTA were employed in this process. Each selected window is then smoothed using a filter. The present study adopts the Konno and Omachi [49] smoothing approach with a smoothing constant of 40. Subsequently, the HVSR is computed with the merged horizontal (H) components for each selected time window using the geometric mean. Finally, evaluation and averaging of the HVSR are carried out. The Geopsy software implemented within the SESAME project [15] is used to carry out the HVSR analysis. The HVSR method is undertaken at three stations at each of the sites. This method allows the generation of an HVSR ellipticity curve for each site from which the fundamental resonance frequency is identified. The HVSR ellipticity curve is also used to obtain the shear wave velocity profile for each site.

2.3. Inversion of the HVSR ellipticity curve

As discussed above, the HVSR ellipticity curves are inverted to a 1D shear wave velocity profile. A stratigraphic constraint is also incorporated in the inversion process by fixing the layer depths, including the level of the bedrock, in the inversion code. A comprehensive subsurface analysis of the study site, developed by [37], is adopted in the present study to establish the stratigraphic parameters at the measurement sites. Additional data by [2,38,39] and [42] are also incorporated in the development of the parametric limit search.

The inversion of the HVSR ellipticity curves is carried out using the Dinver inversion code in the Geopsy software ([50,51] and [52]). The neighborhood algorithm of [53] was implemented by [50] in the Dinver inversion code. The neighborhood algorithm offers a simple interpolation of an irregular distribution of points in space by using Voronoi geometry to detect the most promising parts of the parameter space. Hence, Wathelet et al. [50] suggested checking the robustness of the final results by running the same inversion several times using different random seeds. As such, in the present study, at least three runs using different seeds (i.e. starting models) were carried out in the inversion process. At least 28,050 models for each run were generated, from which the best 20 models are extracted. The best 20 shear wave profiles represent the lowest 20 misfit inversions from the measured HVSR ellipticity curves. Finally, the ground shear wave velocity models are developed from each run of each ellipticity curve inversion and the mean and median shear wave velocities are subsequently evaluated.

3. HVSR technique results

This section presents the results of the HVSR technique and examines the site fundamental frequency and shear wave velocity profiles.

3.1. Site fundamental frequency

The site fundamental frequencies obtained from the HVSR analyses are shown in Table 1. All HVSR analysis curves of the present study are attached in Appendix C of the Supplementary Data. Typical examples of these are shown in Fig. 3(c). Most of the sites in Adelaide are estimated to yield a fundamental frequency of approximately 1 Hz. Only 3 sites

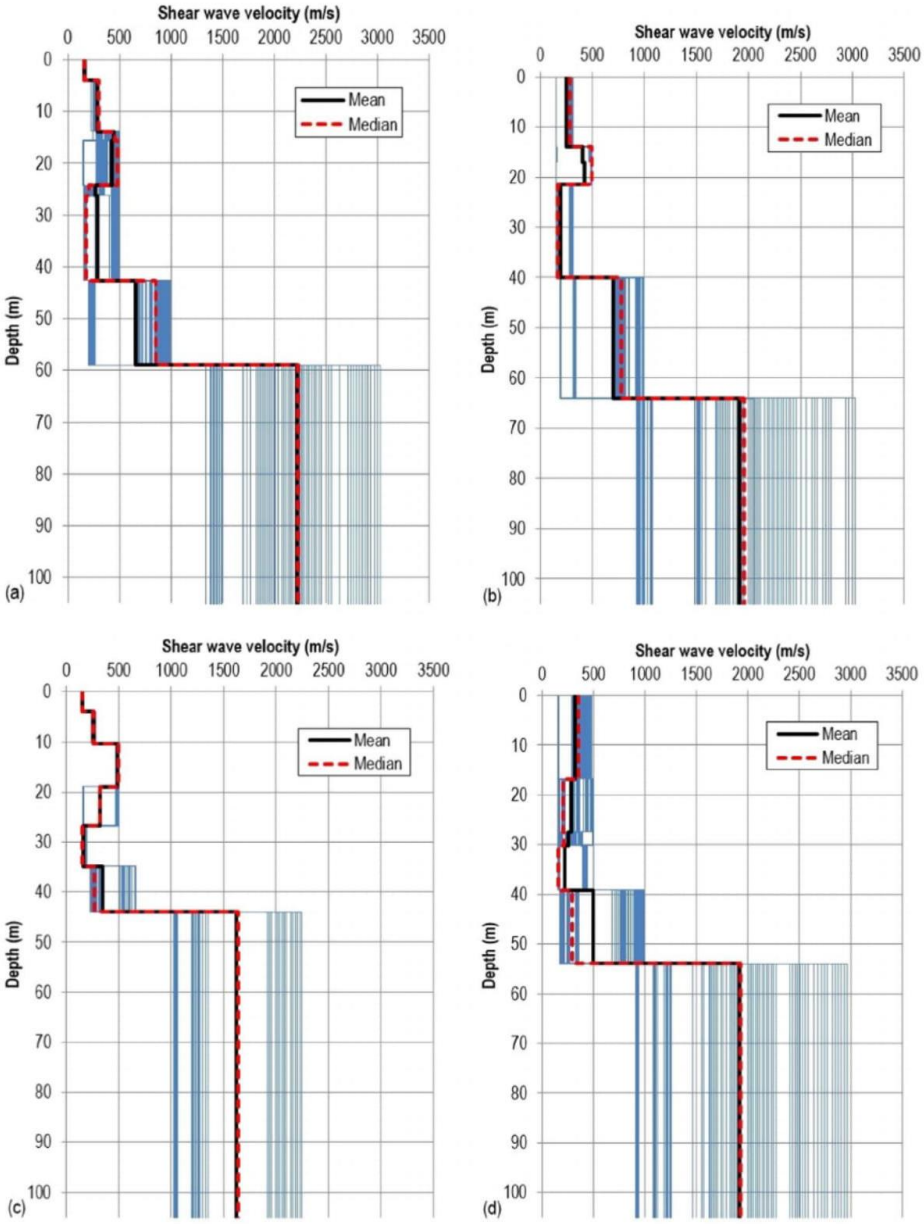

Fig. 5. Shear wave velocity profiles at (a) Location #01, (b) Location #02, (c) Location #03 and (d) Location #04.

(#07, #8, #10) exhibit fundamental frequencies below 1 Hz. A clear fundamental frequency peak can be observed at Locations #01, #02, #03, #04, #07, #08 and #09, whereas #05, #06 and #10 indicate otherwise. At Location #05 and #06, Instrument #1 was unable to capture a distinct and reliable peak. Two instruments at Location #10 (Instruments #1 and #2), were unable to obtain a clear and reliable HVSR peak curve. This suggests a high lateral variability of the subsurface conditions at Locations #05, #06 and #10. Location #05 is adjacent to the River Torrens, which is underlain by recent fluvial deposits ([37] and [38]). On the other hand, Location #06 is adjacent to the Para Fault zone [54] which is also expected to exhibit high lateral variability due to sediment tilting. Furthermore, stresses along the faults also may contribute to the complexity of the dynamic parameter, i.e. the shear wave velocity of the subsurface profile at this site. At Location #10 the deepest bedrock level was encountered. Another factor which contributes to the unclear and unreliable nature of the

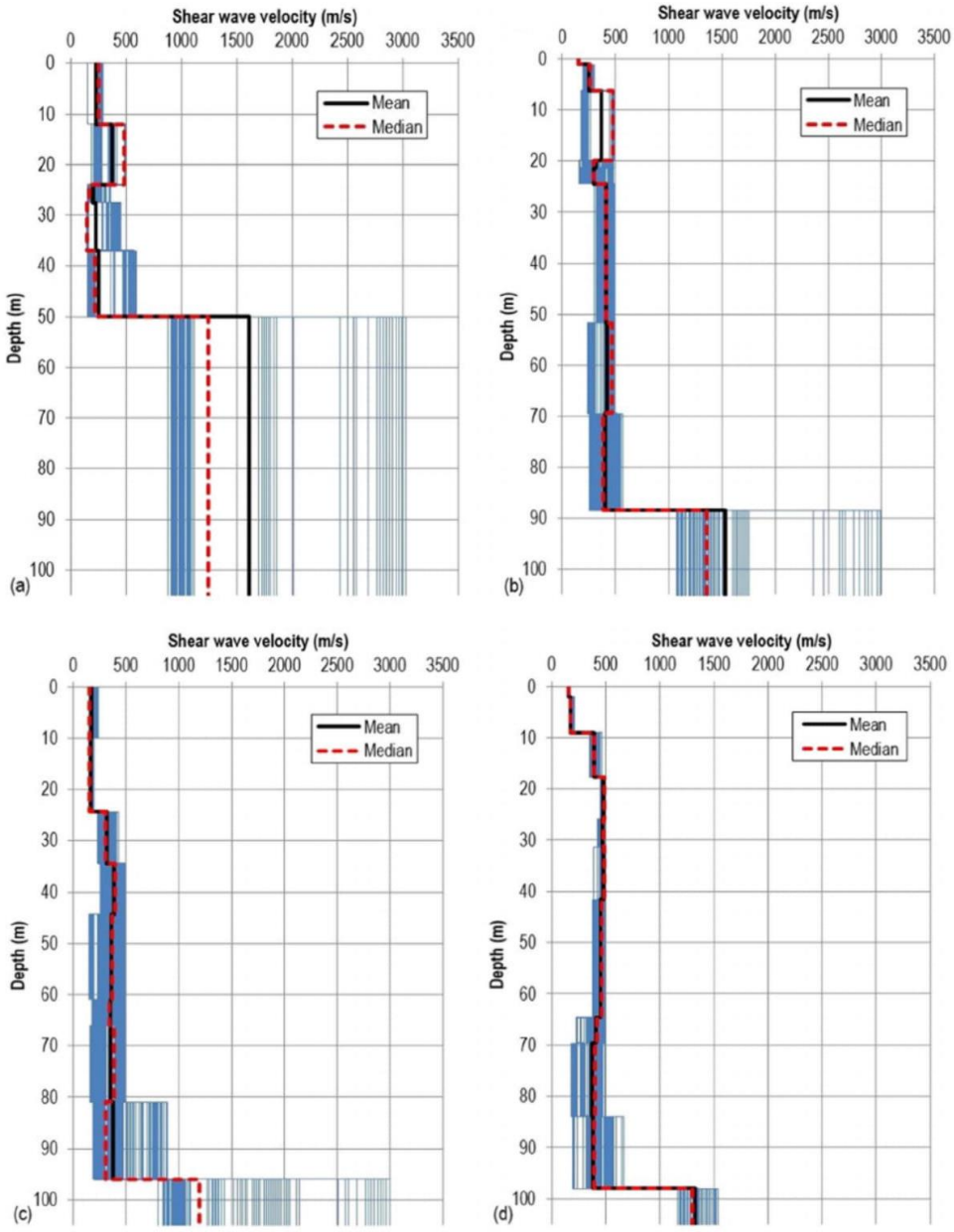

Fig. 6. Shear wave velocity profiles at (a) Location #05, (b) Location #06 (c) Location #07, and (d) Location #08.

HVSR curve is the source of the ambient noise during the measurement. The amplitude of the noise sources was not strong enough to be captured during site measurement.

Another interesting observation associated with the HVSR curves is the presence of secondary peaks, even at low amplitudes (less than 4), at Locations #01, #02, #03, #08 and #09. The secondary peak frequency is between 4 and 6 Hz. The two-peak HVSR curves suggest that there are two different impedance contrasts at two different scales: the first peak relates to a deep structure and the second a shallow structure ([15,55] and [56]).

The primary fundamental frequencies of all sites in Table 1 are plotted in Fig. 4, which also presents the mean and median of the fundamental frequencies. As shown in Fig. 4, generally the amount of data variation, expressed by the standard deviation (SD), is low. The highest SD of the fundamental frequency in the present study is 0.06 Hz at Location #02. The remaining SDs from the measured sites vary between 0.004 and 0.004 Hz. Furthermore, the mean and the median of the fundamental frequency at the measured sites are generally similar, with only a discrepancy of as little as 0.013 Hz.

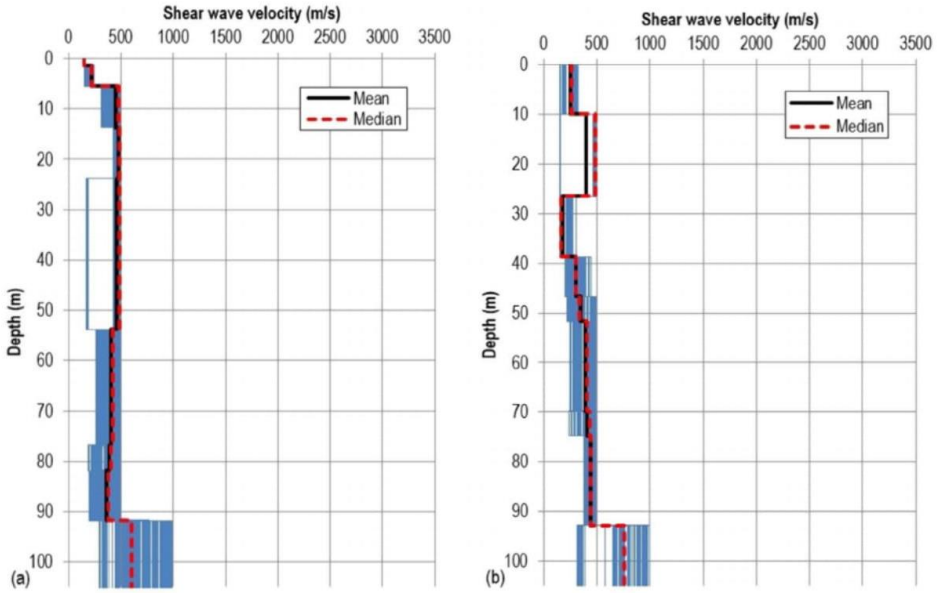

Fig. 7. Shear wave velocity profile at (a) Location #09 and (b) Location #10.

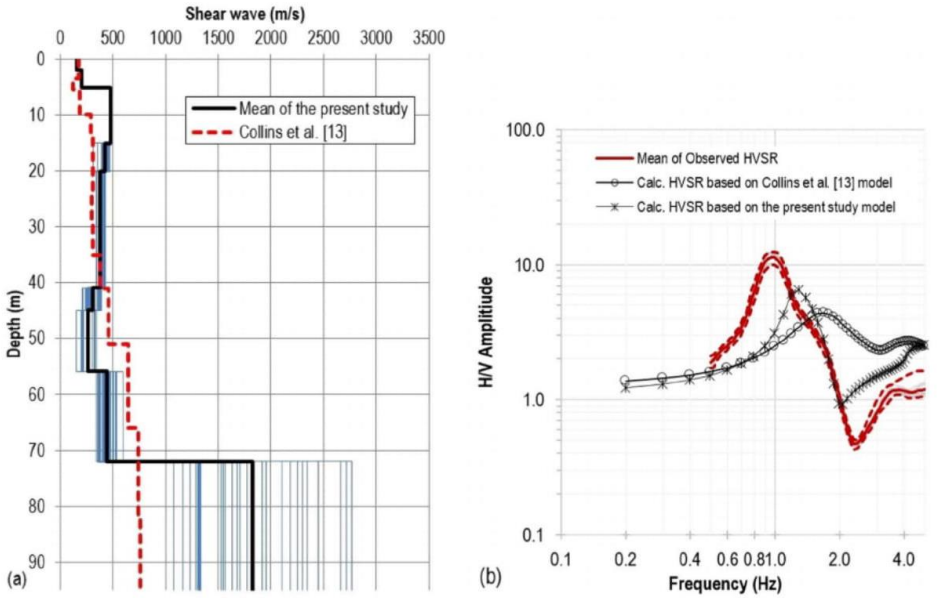

Fig. 8. (a) A comparison of the shear wave velocity profile of the present study to the shear wave velocity profile using the SASW method by [13] at Government House and (b) The observed mean HVSR of the microtremor data (solid red line) ± one standard deviation (dashed red line) with the computed HVSR of the fundamental-mode Raleigh waves of the present study (black line with circle) and the present study (black line with crossline) at Government House. (For interpretation of the references to color in this figure legend, the reader is referred to the web version of this article.)

3.2. Site shear wave profiles

In the present study, the shear wave profiles were obtained by using constrained modeling of the measured HVSR curves. This method has been successfully applied by [10] and [11]. A slight adjustment is introduced in the present study by using a group of 3 seismometers to measure the identical noise source. The distance between each seismometer is approximately 50 m. The reason for using 3 seismometers in the present study is to ensure the consistency of the microtremor data.

As discussed above, input parameters from some previous studies

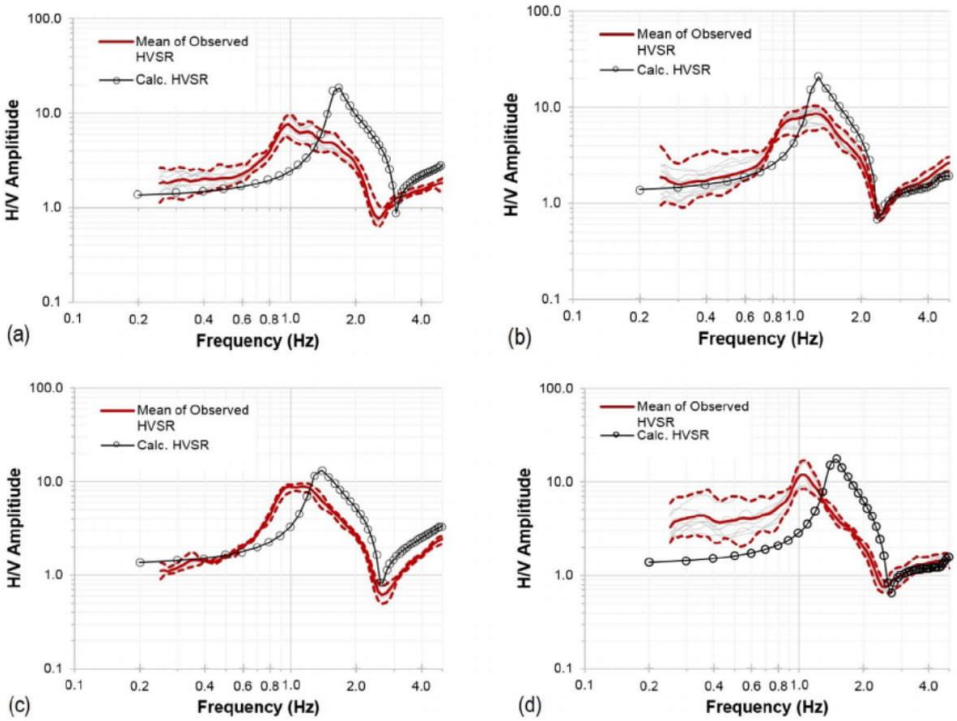

Fig. 9. Comparison of the observed mean HVSR of the microtremor data (solid red line) ± one standard deviation (dashed red line) with the computed HVSR of the fundamental-mode Raleigh waves (black line with circle) for (a) Location #01, (b) Location #02, (c) Location #03, and (d) Location #04. (For interpretation of the references to color in this figure legend, the reader is referred to the web version of this article.)

were adopted for the constrained modeling in the present study. The site specific parameters are developed and estimated based on studies by [2,37–39] and [42]. The number of layers in the parameterization models is determined from the nearest subsurface data available (i.e. boreholes and cross sections). The main data are provided by Selby & Lindsay [37]. Additional subsurface data associated with the study sites have also been incorporated from other references ([38,39] and [42]). The main reason for adopting the available stratigraphic data is to simplify the inversion process and to minimize subjectivity. These site specific input parameters are used to generate at least 28,050 shear wave profile models based on the elliptical nature of the HVSR curves in each 30-min dataset. The best 20 models are extracted and selected from the generated profiles of each HVSR curve. In the present study, only the HVSR curve, which satisfies the reliability criteria of SESAME [15], is used in estimating the shear wave profile; the remainder is discarded. Generally, each set of instruments is expected to obtain 5 HVSR curves. The following sections present the results which are divided into two main sections. The first section elaborates the results of all locations to the north of the River Torrens (North Adelaide) and another presents the results of all locations to the south of the River Torrens (South Adelaide).

3.2.1. Shear wave profiles at North Adelaide

Five locations were measured in North Adelaide: #01 (Barton West Terrace); #02 (Lefevre Terrace); #03 (Wellington Square); #04 (Finniss Street) and #05 (Frome Road/War Memorial Drive). The ground surface profiles at the North Adelaide sites consist of 5–6 formations above bedrock [37]. These upper layer formations suggest mean shear wave velocities varying between 152 and 703 m/s. The bedrock levels at these locations are estimated to vary between 50 and 64 m below ground level, which suggests shear wave velocity of at least 1610 m/s. The detailed mean and median shear wave velocity profiles for these North Adelaide locations are shown in Figs. 5(a) to 6(a). Appendix D of the Supplementary Data includes a detailed tabulation of shear wave velocity profiles. For Location #05, which is situated near the River Torrens the HVSR analysis of instrument Set#1 at this location is unable to satisfy the reliability criteria as outlined in [15]. Therefore, the present study excludes the inversion of the ellipticity curve for this instrument from further analysis, as indicated by “FAIL”.

3.2.2. Shear wave profile at South Adelaide

In South Adelaide ambient noise was measured at 5 sites: #06 (West Terrace/Port Road), #07 (Bartels Road), #08 (Victoria Square), #09 (South Terrace/West Terrace) and #10 (Hutt Road/South Terrace). Despite some difficulties to justify the bedrock level at the south-eastern of Adelaide City, the South Adelaide, generally, are founded on 8–10 formations overlying Precambrian bedrock [37]. Mean shear wave velocities of these formations vary between 153 and 711 m/s. The South Adelaide sites suggest gradually deeper bedrock levels toward the southeast, which is estimated to be encountered between 88 and 118 m below ground level [37]. The estimated shear wave velocity of this bedrock is at least 1191 m/s (as shown in inverted shear wave velocity profile at Location #07 in Fig. 6(c). Detailed estimated mean and median shear wave velocity profiles associated with these sites are shown in Figs. 6(b) to 7(b). Appendix D of the Supplementary Data includes a detailed tabulation of the estimated mean and median shear wave velocity profiles associated with these sites. The HVSR analyses that were unable to satisfy the reliability criteria, as outlined in [15], are excluded from further analysis and are indicated by “FAIL”. For Location #06, the discarded shear wave profile is the inferred profile

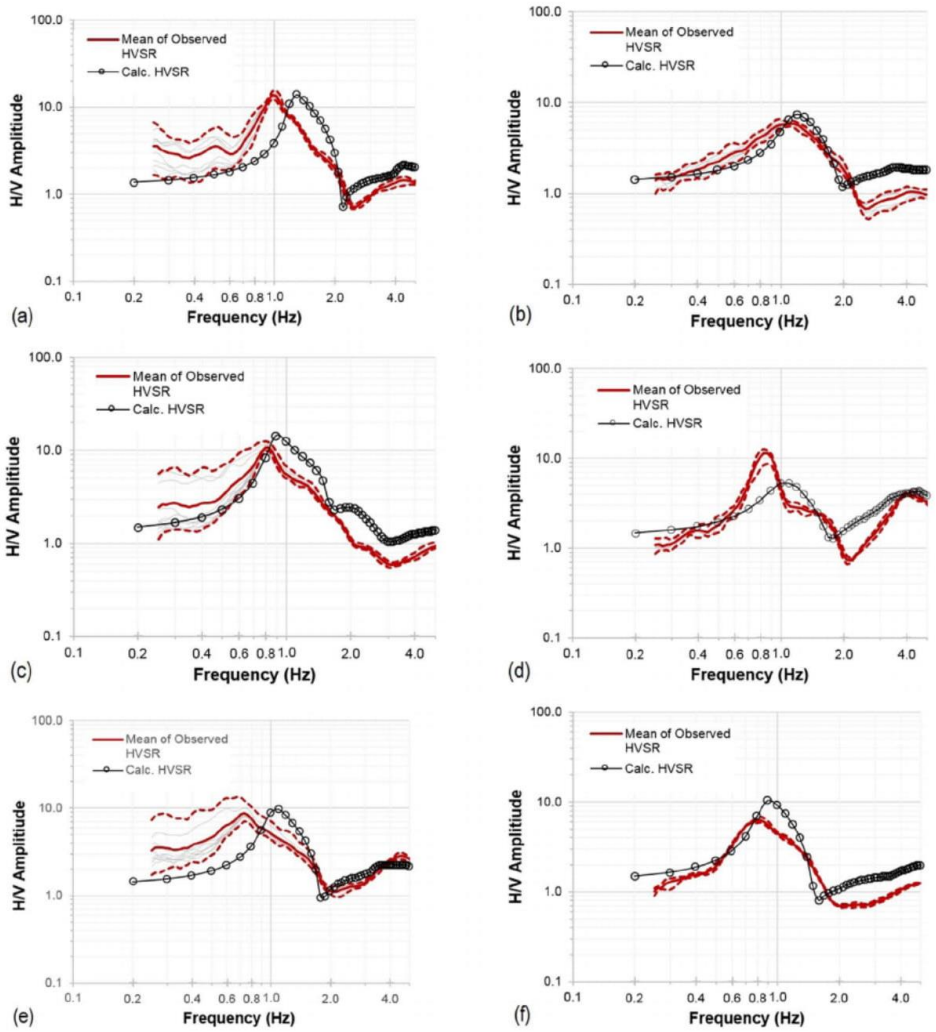

Fig. 10. Comparison of the observed mean HVSR of the microtremor data (solid red line) ± one standard deviation (dashed red line) with the computed HVSR of the fundamental-mode Raleigh waves (black line with circle) for (a) Location #05, (b) Location #06, (c) Location #07, (d) Location #08, (e) Location #09, and (f) Location #10. (For interpretation of the references to color in this figure legend, the reader is referred to the web version of this article.)

from HVSR analyses of instrument Set #1 and for Location #10 is Set #1 and Set #2.

3.2.3. Validation of the obtained shear wave velocity profiles

In order to validate the results of shear wave velocity profiles obtained in the present study and the appropriateness of the inversion results the spectral analysis of surface waves (SASW) method is adopted in addition to forward computation. These are discussed below.

3.2.3.1. Shear wave velocity validation using a comparison with SASW method. As discussed above, Collins et al. [13] obtained shear wave measurements using the SASW method at Government House (GHS) in Adelaide (34°55′142.2″S, 138°36′00.6″E). The results of this study are compared with those from the present study using the method discussed above. More than 12 h of single microtremor measurement was recorded at the location 34°55′08.4″S, 138°36′03.6″E. Unfortunately, it is approximately 200 m from the location where the SASW measurements were obtained due to unforeseen factors. After assessing the possibility of noise originating from an industrial source, generating the HVSR ellipticity curve, checking the reliability of the HVSR ellipticity curve using the SESAME [15] criteria, inverting the "passed" curve using the Dinver code, extracting and averaging the best 20 models and combining all the shear wave velocity models from 24 datasets with 30 min of noise record in each, the results of the analysis are shown in Fig. 8(a). In general, as can be seen, the results of the present study are comparable with the results using the SASW method by [13]. The lateral and vertical variability of the site could be the main reason for the discrepancies in the results due to the 200 m separation distance as mentioned earlier. The results show that the present model is in good agreement for the top 5 m depth and from 15 to 40 m depth.

A forward computation of the fundamental Raleigh wave of the

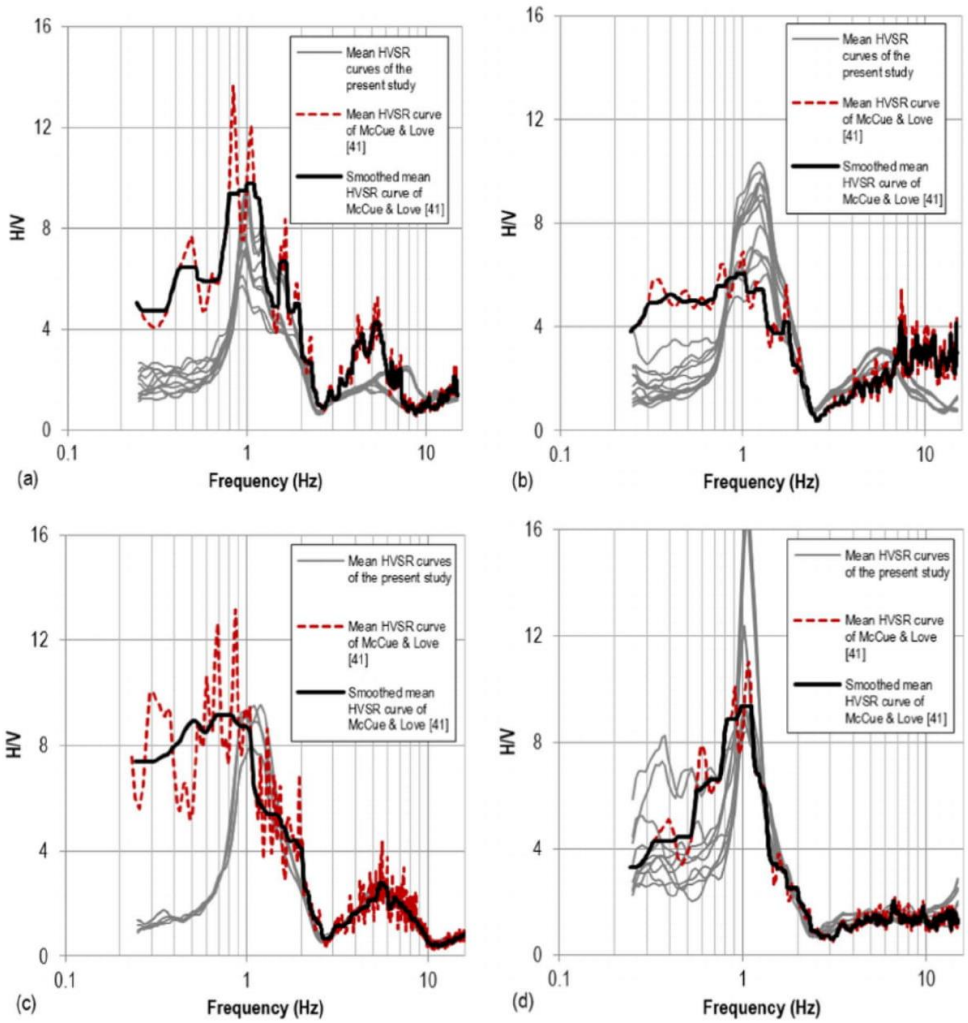

Fig. 11. HVSR curve comparison at (a) Location #01, (b) Location #02, (c) Location #03 and (d) Location #04.

measured site [57] is also carried out to explore the appropriateness of the shear wave velocity model by comparing it to the observed HVSR. Forward computation modeling is also carried out for the SASW model. The comparison of the observed HVSR and the calculated HVSR is shown in Fig. 8(b). The calculated HVSR from the present study and the observed HVSR is in good agreement. Furthermore, Fig. 8(b) suggests better agreement between the calculated HVSR from the present study to the observed than the calculated HVSR from the SASW measurements. Again, the lateral and vertical variability of the shear wave velocity profiles are likely to be the main for the disparity.

3.2.3.2. Shear wave velocity validation using forward computation. The shear wave velocity model validation using forward computation into the fundamental Raleigh wave, herein termed 'calculated HVSR', is carried out for all developed models of the present study to explore the appropriateness of the developed model. Forward modeling proposed by [55] is employed in the present study. The horizontal to vertical spectral ratios of the calculated HVSR is compared to the observed HVSR. The comparison of the mean observed and calculated HVSR, plotted as logarithmic graphs, are given in Figs. 9 and 10. The observed and calculated HVSR peak frequency lies between 0.7 and 1.3 Hz. Overall, all measured sites exhibit comparable HVSR curves.

4. Discussion of the results

This section examines and discusses the results of the HVSR measurements with respect to the site fundamental frequency and seismicity site classes.

4.1. Site fundamental frequency

In order to provide context to the present study, this section compares the HVSR results from the present study with the extensive HVSR measurements obtained across Adelaide by [41]. The comparison is undertaken using the nearest locations adopted by [41], as shown in Fig. 1 above. The results of the comparison are presented in Figs. 11–13. As can be observed, the mean HVSR curves of [41] fluctuate sharply, as indicated by the dashed red line, and hence a smoothing algorithm is

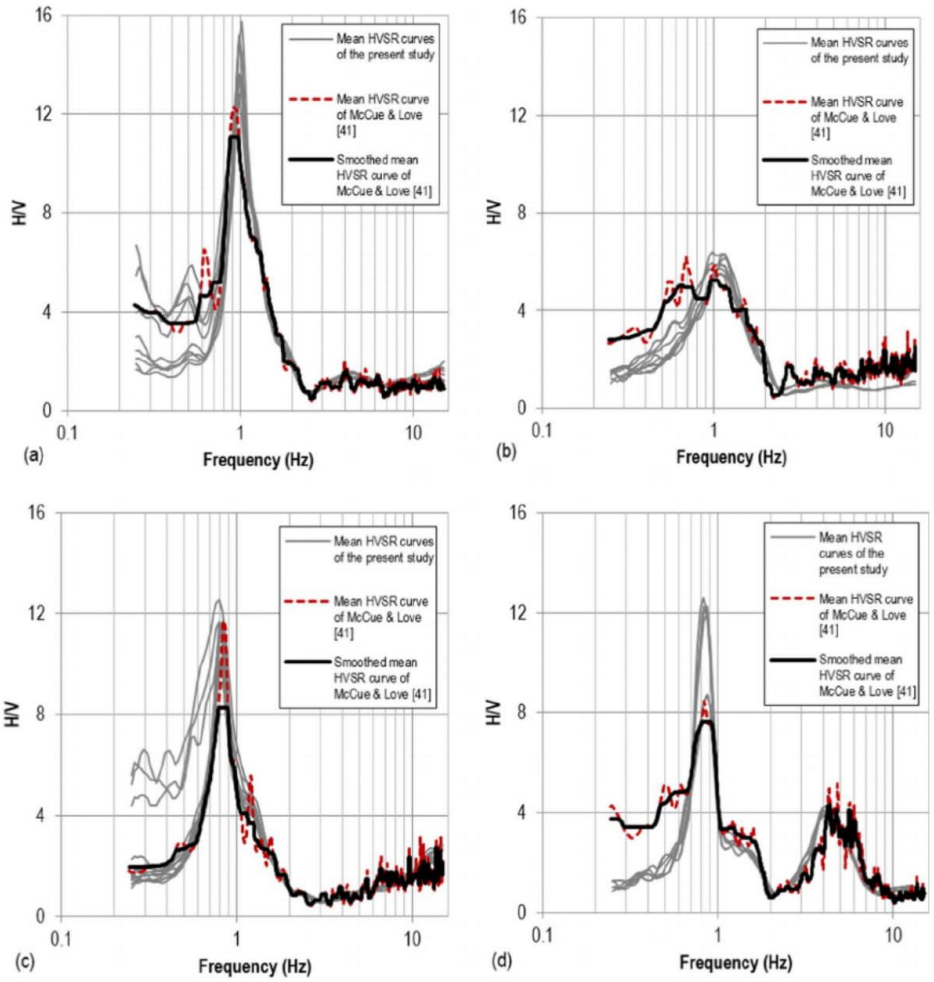

Fig. 12. HVSR curve comparison at (a) Location #05, (b) Location #06 (c) Location #07 and (d) Location #08.

applied to these curves and the outcomes are presented by the thick black line in the comparison figures.

As shown in the figures, most of the mean HVSR curves of the present study are in very good agreement with those obtained by [41], including all of the frequencies of the HVSR curve-peaks, except for Location #03. Furthermore, there is a clear, large-amplitude, HVSR peak at Locations #04, #05 and #07, which is likely to be the resulting of relatively high impedance contrast between the upper layers and the underlying bedrock, with estimated site frequencies ranging from 0.7 to 1.0 Hz. As mentioned above, Locations #04 and #05 are near the River Torrens, and Location #07 is close to a small creek leading to the River Torrens. Double HVSR curve peaks are encountered at Locations #01, #02, #03, #08 and #09, which highlight more complex sub-surface dynamic characteristics.

The good agreement between the mean HVSR curves of the present study and those obtained by [40], as shown in Figs. 11–13, suggest the consistency of the HVSR method with respect to time, as McCue and Love [41] carried out their measurement in 1997, whereas the present study data were obtained in 2015. In particular, this temporal reliability of the HVSR analysis in the present study is also corroborated by the continuous 96 sets of ambient noise analysis from 3:00 p.m. on 02/10/2014 to 2:30 p.m. on 04/10/2014 (see Fig. 2(b)]. This temporal stability of the analysis of microtremor data was also demonstrated by [58].

The Adelaide CBD incorporates a variety of building types and building materials. In terms of the number of stories (N), most of the north and southeast of Adelaide consists of low-rise (1–5 story) buildings. Only the city center includes medium-rise (6–10 stories) to high-rise (> 10 story) buildings. By adopting the building fundamental frequency approximation suggested by [59], which is approximated by 10/N (Hz), the Adelaide building frequency in the north and southeast of Adelaide is between 2 and 10 Hz, whereas in the city center, it is between 1 (or below) and 1.7 Hz. Resonance effects will occur when the building frequency is equal to or close to the ground frequency. This will lead to enhanced building vibration and increase the prospect of structural collapse and hence human injury and fatalities.

Overall, the results suggest a fundamental frequency of 1 Hz for much of the Adelaide City, which suggests significant seismic

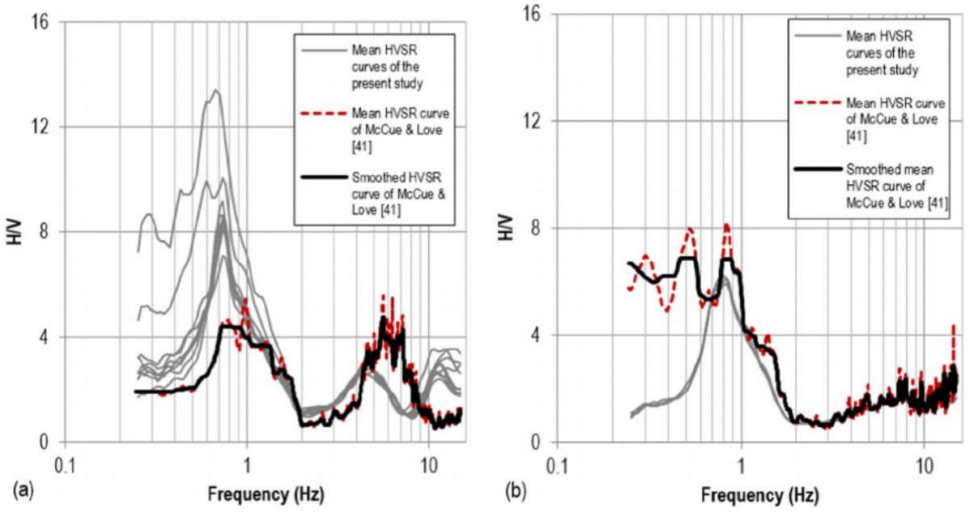

Fig. 13. HVSR curve comparison at (a) Location #09 and (b) Location #10.

Table 2
Adelaide CBD seismic site classes for all instruments at Locations #01 – #10.

Site/Location												
North Adelaide												
#01			**#02**			**#03**	**#04**			**#05**		
INS#1	**INS#2**	**INS#3**	**INS#1**	**INS#2**	**INS#3**	**INS#1**	**INS#1**	**INS#2**	**INS#3**	**INS#1**	**INS#2**	**INS#3**
304	305	342	305	259	254	315	297	340	280	NA	278	289
D	D	D	D	D	D	D	D	D	D	NA	D	D
NEHRP [1]												
D	D	D	D	D	D	D	D	D	D	NA	D	D
AS 1170.4 [31]												
D	D	D	D	CD/D	CD/D	CD/D	CD/D	CD	CD/D	NA	CD/D	CD/D
Ref. [2]												
318			274			315	299			284		
D			D			D	D			D		
NEHRP [1]												
D			D			D	D			D		
AS 1170.4 [31]												
D			D			D	D			D		
Ref. [2]												
SOUTH ADELAIDE												
#06			**#07**			**#08**	**#09**			**#10**		
INS#1	**INS#2**	**INS#3**	**INS#1**	**INS#2**	**INS#3**	**INS#1**	**INS#1**	**INS#2**	**INS#3**	**INS#1**	**INS#2**	**INS#3**
NA	412	243	194	203	184	361	384	427	425	NA	NA	326
NA	C	C	D	D	D	C	C	C	C	NA	NA	D
NEHRP [1]												
NA	B	B	D	D	D	B	B	B	B	NA	NA	D
AS 1170.4 [31]												
NA	C	CD/D	DE	D	DE	C	C	C	C	NA	NA	CD/D
Ref. [2]												
337			194			361	418			326		
C			D			C	C			D		
NEHRP [1]												
B			D			B	B			D		
AS 1170.4 [31]												
D			D/DE			C	C			D		
Ref. [2]												

Note: .
INS#1 is Instrument #1.
INS#2 is Instrument #2.
INS#3 is Instrument #3.

Table 3
Summary of Adelaide seismic site classes and comparison of V constrained using the ellipticity of the HVSR and SPAC curves.

Location	Seismic site classes based on Vs,30 and		constrained using the ellipticity of the HVSR and SPAC curves			Remarks
	NEHRP[1]	AS 1170.4[31]	Ref. [2]	Classic HVSR	SPAC	
#01 (Barton Tce W)	D	D	D	318	340	North Adelaide
#02 (Lefevre Tce)	D	D	D	274	390	
#03 (Wellington Sq)	D	D	D	-	-	
#04 (Finniss St)	D	D	D	299	390	
#05 (Frome Rd/ War Memorial Dr)	D	D	D	284	317	
#06 (West Tce/ Port Rd)	C	B	D	337	272	South Adelaide
#07 (Bartels Rd)	D	D	D/DE	194	366	
#08 (Victoria Sq)	C	B	C	–	–	
#09 (South Tce/ West Tce)	C	B	C	418	378	
#10 (Hutt Rd/ South Tce)	D	D	D	326	245	

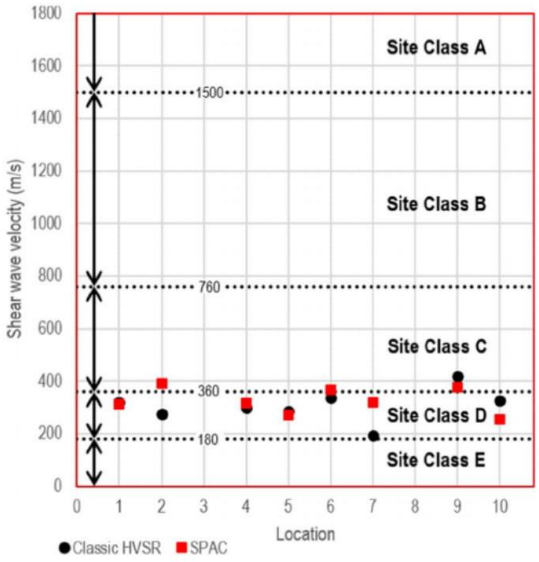

Fig. 14. Results of shear wave velocity of the top 30 m constrained by the ellipticity of the classic HVSR and SPAC curves plotted relative to NEHRP seismic site classifications.

amplification for medium-rise buildings throughout the city. The fundamental frequency at several locations (#07, #08, #09 and #10) is expected to be about 0.7–0.8 Hz, which suggests high vibration of high-rise structures around these locations during a seismic event. Furthermore, an additional second fundamental frequency of between 4 and 6 Hz is suggested for Locations #01, #02, #03, #08 and #09, which also indicates resonance of low-rise structures at these locations.

4.2. Adelaide seismic site classes

The seismic site class across all of North Adelaide sites is consistent for all classification systems adopted in the present study. All locations in this area can be classified as subsoil Class D by NEHRP, AS 1170.4 and [2], as shown in Table 2. The estimated uppermost 30 m shear wave velocity ranges between 274 and 318 m/s. This uniform seismic site classification is likely the result of a relatively consistent and shallow bedrock level in this area, which is 64 m below ground or less. In the north of Adelaide a high shear wave velocity, which is typically close to that of bedrock (> 760 m/s), is suggested at both Locations #01 and #02 (see Figs. 5(a) and 5(b)), at depths shallower than those indicated by the borehole data. The nearest borehole to Locations #01 and #02 indicates respective bedrock depths of 59 m and 64 m, whereas the present study suggests the bedrock surface is at 43 m and 40 m, respectively. This discrepancy highlights the difficulty estimating bedrock level utilizing HVSR analysis in low impedance contrast sites, such as regoliths.

In contrast, the area to the south of the Adelaide CBD suggests much more variable subsoil classification. In the present of study, the south of Adelaide is estimated to relate to an upper 30 m shear wave velocity between 194 m/s and 418 m/s, as shown in Appendix D of the Supplementary Data. This suggests a complex subsoil classification ranging from subsoil Class C to D, in the NEHRP classification system, or subsoil Class B to D in the AS 1170.4 classification system, or subsoil Class C to DE in the classification system by [2]. Generally, the AS 1170.4 classification system is more conservative than the others, as shown at Locations #06, #08 and #09. The AS 1170.4 method classifies subsoil class B for all Locations #06, #08 and #09, whereas the others classify these as subsoil classes C or D. This variable subsoil classification in the southern part of Adelaide is likely the result of highly variable stratigraphy and the increasing bedrock depth, which is approximately 100 m below ground level. Summary of Adelaide seismic site classes of the present study is shown in Table 3.

Another ambient noise analysis by means of spatial autocorrelation (SPAC) method to infer the shear profile is also carried out by [60] for 8 of the 10 locations in the present study. A comparison by means of the SPAC method with respect to the $V_{s,30}$ results is included to confirm the reliability of the inversion from the HVSR curve incorporating the stratigraphic constraints at regolith sites. The resulting values of $V_{s,30}$ from this study are in good agreement with the present study for Locations #01, #04, #05, #06, #09 and #10, as shown in Table 3 and Fig. 14. By adjusting the $V_{s,30}$ at Locations #02 and #07 to follow the SPAC results, and constraining the areas along the Torrens River, the $V_{s,30}$ of the present study is plotted and compared against the most recent $V_{s,30}$ mapping by [14], as shown in Fig. 15. Generally, the region corresponding to $V_{s,30}$ values less than 315 m/s is wider in the present study than that proposed by [14]. The preliminary result of the present study suggests that at least half of the Adelaide CBD areas to the north and south of the River Torrens has a $V_{s,30}$ value less than 315 m/s.

5. Conclusions

Currently, seismic site classification is widely accepted in the design of seismic resilient infrastructure. Many researchers have successfully implemented the HVSR technique for seismic site classification because it is relatively straightforward, convenient and reliable in urban areas. However, the application of the HVSR technique in regions with various impedance contrast between the upper layer and bedrock, such as regoliths, for site seismic classification is uncertain and requires attention. The present study seeks to add to the body of knowledge associated with various impedance contrasts sites. Adelaide, the capital of and largest city in South Australia, is founded on a regolith site and is selected for the study case area. Ambient noise across the study case site is

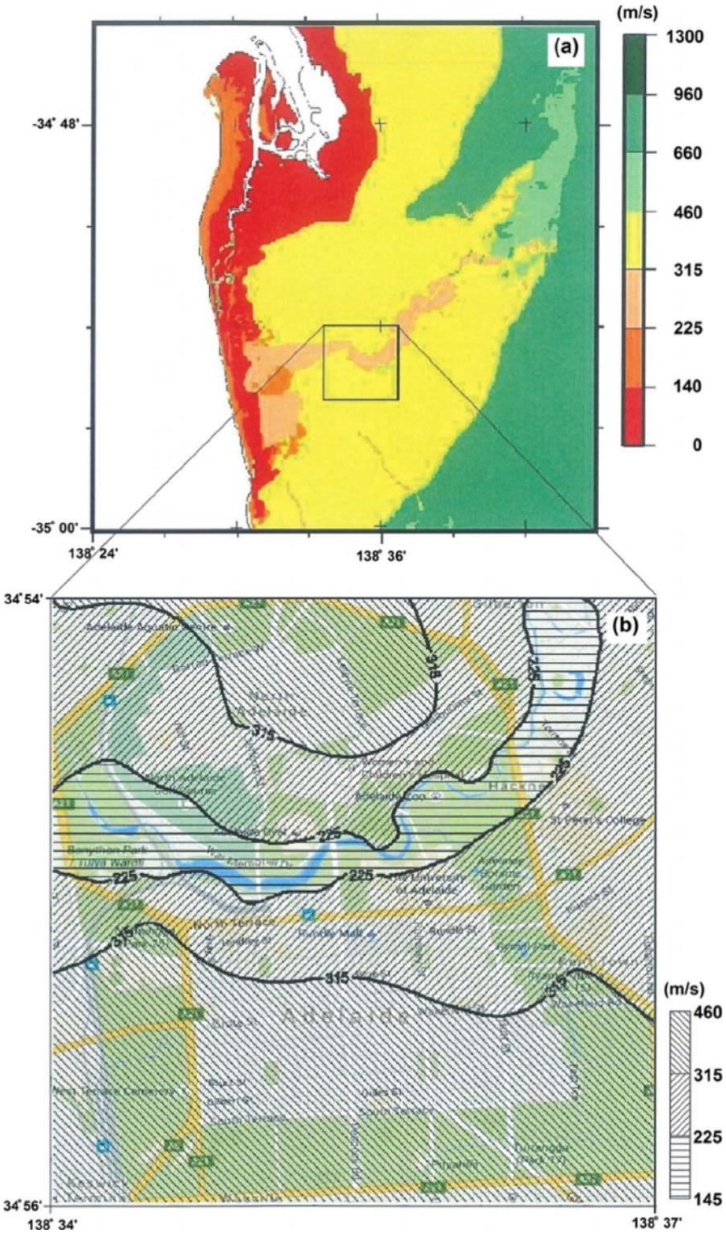

Fig. 15. (a) Preliminary map of $V_{S,30}$ of the Adelaide CBD and the surrounding areas by Leonard [14] and (b) map of $V_{S,30}$ of the Adelaide CBD based on constrained modeling of the measured HVSR curve of the present study.

measured from which the seismic hazard parameters, i.e. site periods and shear wave profiles, are quantified using HVSR analysis and constrained modeling of measured HVSR ellipticity curves.

In the case of the Adelaide regolith, the majority of the locations are likely to have a site period greater than 0.8 s, and hence the site subsoil class D (NEHRP and Australian Standard) or class CD/D [2] is the appropriate classification for seismic design purposes for locations in the northern part of the Adelaide CBD, whereas more complex seismic site classes from subsoil classes B to DE are identified in southern part of the CBD. Based on the 3 classification systems mentioned above, this southern part of the city can be classified as follows: subclasses D to C (NEHRP) or subclasses D to B (AS 1170.4) or DE to C [2]. These results are in reasonably good agreement with several previous studies.

A preliminary upper 30 m shear wave map of the study case site is proposed. A slightly wider area of shear wave velocities below 315 m/s is identified. This result can be used to increase the resolution of map proposed by [14].

Finally, this study presents a promising application of HVSR analysis for seismic assessment of regolith sites. In this case, the ambient noise analysis is relatively straightforward, convenient and reliable.

Acknowledgements

The authors would like to acknowledge the University of Adelaide for providing a research scholarship for the first author. In addition, the first author is grateful to the Faculty of Engineering of Syiah Kuala University for their support. The authors also wish to acknowledge the anonymous reviewers for their valuable comments, which have improved the paper.

Appendix A. Supporting information

Supplementary data associated with this article can be found in the online version at http://dx.doi.org/10.1016/j.soildyn.2017.08.006.

References

[1] Building Seismic Safety Council [BSSC]. NEHRP recommended provisions for seismic regulations for new buildings and other structures2000 edition, part 1: Provisions, Report no. FEMA368, Building seismic safety council for the federal emergency management agency, Washington, DC, USA; 2001.
[2] McPherson A, Hall L. Development of the Australian National Regolith Site Classification Map. Geoscience Australia Record2007/07, 37 p.
[3] Anbazhagan P, Sheikh N, Parihar A. Influence of rock depth on seismic site classification for shallow bedrock regions. Nat Hazards Rev 2013;14(2):108–21. http://dx.doi.org/10.1061/(ASCE)NH.1527-6996.0000088.
[4] National Committee on Soil and Terrain. Australian soil and land survey field handbook, Series no 1. 3rd ed Collingwood, Victoria: CSIRO Publishing; 2009.
[5] Wilford J, Thomas M. Predicting regolith thickness in the complex weathering setting of the central Mt Lofty Ranges, South Australia. Geoderma 2013. http://dx.doi.org/10.1016/j.geoderma.2013.04.002.
[6] Nakamura Y. A method for dynamic characteristics estimation of subsurface using microtremor on the ground surface. Q Report Railw Tech Res Inst 1989;30(1):25–30.
[7] Picozzi M, Strollo A, Paraloi S, Durukal E, Ozel O, Karabulut S, Zschau J, Erdik M. Site characterization by seismic noise in Istanbul, turkey. Soil Dyn Earthq Eng 2009:469–82. http://dx.doi.org/10.1016/j.soildyn.2008.05.07.
[8] Mokhberi M, Davoodi M, Haghshenas E. The application of the H/V spectral ratio technique for estimating the site characterization in the south of Iran. Soil Dyn Earthq Eng 2010:300–8. http://dx.doi.org/10.1061/41102(375)37.
[9] Fah D, Wathelet M, Kristekova M, Havenith H, Endrun B, Stamm G, Poggi V, Burjanek J, Cornou C. Using ellipticity information for site characterisation. Report for Network of Research Infrastructures for European Seismology, Sixth Framework Program, EC Project Number: 026130, 54 pp; 2003.
[10] Harutoonian P, Leo C, Doanh T, Castellaro S, Zou J, Liyanapathirana D, Wong H, Tokeshi K. Microtremor measurements of rolling compacted ground. Soil Dyn Earthq Eng 2012:23–31. http://dx.doi.org/10.1016/j.soildyn.2012.05.006.
[11] Di Stefano P, Luzio D, Renda P, Martorana R, Capizzi P, D'Alessandro A, Messina N, Napoli G, Todaro S, Zarcone G. Integration of HVSR measures and stratigraphic constraints for seismic microzonation studies: the case of Oliveri (ME). Nat Hazards Earth Syst Sci 2014;2:2597–637. http://dx.doi.org/10.5194/nhessd-2-2597-2014.
[12] Wotherspoon L, Bradley B, Van Houtte C, Larkin T. Horizontal to vertical spectral ratio: applications and limitations. NZ Geomech News, Bull NZ Geotech Soc Inc 2015;89:136–9 issn:0111-6851 .
[13] Collins C, Kayen R, Carkin B, Allen T, Cummins P, McPherson A. Shear wave velocity measurement at Australian ground motion seismometer sites by the spectral analysis of surface waves (SASW) method. In: Proceedings of earthquake engineering in Australia, Canberra, 2006, p. 173–8.
[14] Leonard M. Personal communication: preliminary results of Vs30 for the Adelaide region, South Australia; 2015.
[15] SESAME. Guidelines for the implementation of the H/V spectral ratio technique on ambient vibrations measurements processing and interpretation. SESAME European Research Project, WP12 –Deliverable D23.12 European Commission – Research General Directorate, Project No. EVG1-CT-200-00026; 2004.
[16] Sandiford M. Neotectonics of southeastern Australia: linking the quaternary faulting record with seismicity and in situ stress. Evolution and Dynamics of the Australian Plate, 22. **Australia**: Geological Society of Australia Special Publication; 2003. p. 101–13.
[17] Quigley M, Sandiford M, Fifield K, Alimanovic A. Bedrock erosion and relief production in the Northern Flinders Ranges, Australia. Earth Surf Process Landf 2006;32:929–44. http://dx.doi.org/10.1002/esp.1459.
[18] Quigley M, Sandiford M, Fifield K, Alimanovic A. Landscape responses to intraplate tectonism: quantitative constraints from 10Be nuclide abundances. Earth Planet Sci Lett 2007;261:120–33.
[19] Johnston AC. Seismic moment assessment of earthquakes in stable continental regions-I. Instrumental seismicity. Geophys J Int 1996;124(381–414):382.
[20] Celerier J, Sandiford M, Hansen DL, Quigley M. Modes of active intraplate deformation, Flinders Ranges, Australia. Tectonics 2005;24(TC6006):17. http://dx.doi.org/10.1029/2004TC001679.
[21] Hillis RR, Sandiford M, Reynolds SD, Quigley MC. Present-day stresses, seismicity and neogene-to-recent tectonics of Australia's 'passive' margins: intraplate deformation controlled by plate boundary forces. In: JOHNSON H, DORE´ AG, GATLIFF RW, HOLDSWORTH R, LUNDIN ER, RITCHIE JD, editors. The Nature and Origin of Compression in Passive Margins, 306. London: Geological Society; 2008. p. 71–90. http://dx.doi.org/10.1144/SP306.3.
[22] Veevers JJ. Phanerozoic earth history of Australia. New York: Oxford University Press; 1984. p. 418.
[23] McCue K. Australia's large earthquakes and recent fault scarps. J Struct Geol 1990;12(5/6):761–6.
[24] Johnston AC. Seismic moment assessment of earthquakes in stable continental regions-111. New Madrid 181 1-1812, Charleston 1886 and Lisbon 1755. Geophys J Int 1996;126:314–44.
[25] Crone AJ, Machette MN, Bowman JR. Episodic nature of earthquake activity in stable continental regions revealed by palaeoseismicity studies of Australian and North American quaternary faults. Aust J Earth Sci: Int Geosci J Geol Soc Aust 1997;44(2):203–14. http://dx.doi.org/10.1080/08120099708728304.
[26] Sandiford M, Wallace M, Coblentz D. Origin of the in situ stress field in south-eastern Australia. Basin Res 2004;16:325–38. http://dx.doi.org/10.1111/j.1365-2117.2004.00235.x.
[27] Greenhalgh SA, Parham RT. The Richter earthquake magnitude scale in South Australia. Aust J Earth Sci 1986;33:519–28.
[28] Greenhalgh SA, Love D, Malpas K, McDougall R. South Australian earthquakes, 1980–92. Aust J Earth Sci 1994;41(5):483–95. http://dx.doi.org/10.1080/08120099408728158.
[29] Department of Manufacturing, Innovation, Trade, Resources and Energy Official Website (DMITRE Minerals). Urban Monitoring; 2013. http://www.pir.sa.gov.au/minerals/earthquakes/urban_monitoring [accessed on 2 November 2013].
[30] Anbazhagan P, Sheikh N, Tsang H. Seismic site classification practice in Australia, China and India: suitability. In: Abraham R, Latheswary S, Unnikrishnan N, editors. International Conference on Materials Mechanics and Management. New Delhi: Excel India Publishers; 2010.
[31] Standards Australia. AS 1170.4-2007 Australian Standard of Structural Design Actions Part 4: Earthquake Actions in Australia. Standards Australia; 2007.
[32] Standards New Zealand. NZS 1170.5:2004 Structural design actions Part 5 Earthquake actions – New Zealand. New Zealand Standards; 2004.
[33] McVerry G, Zhao J, Abrahamson N, Somerville G. Crustal and subduction zone attenuation relations for New Zealand earthquakes. In: Proceedings 12th world conference on earthquake engineering, Auckland, New Zealand, Paper no. 1834.
[34] McVerry G, Zhao J, Abrahamson N, Somerville G. New Zealand acceleration response spectrum attenuation relations for crustal and subduction zone earthquake. Bull NZ Soc Earthq Eng 2006;39(1):58. [March 2006].
[35] Selby J. Geology and the AdelaideEnvironment. *Department of Mines and Energy, South Australia*, D.J. Woolman, Government Printer, Adelaide, ISSN: 0726 1519; 1984. 168 pp.
[36] Love D. Seismic hazard and microzonation of the Adelaide metropolitan area. Adelaide: Sutton Earthquake Centre, Department of Mines and Energy, South Australia; 1996.
[37] Selby J, Lindsay J. Engineering geology of the Adelaide City area. Department of Mines and Energy, Geological Survey of South Australia, D. J. Woolman, Government Printer, Bulletin 51, 94 pp; 1982.
[38] Sheard M, Bowman G. Soils, stratigraphy and engineering geology of near surface materials of the Adelaide Plains. Adelaide: Department of Mines and Energy, South Australia.; 1996.
[39] Jaksa MB. The influence of spatial variability on the geotechnical design properties of a stiff, overconsolidated clay (Ph.D.thesis). **Australia**: The University of Adelaide; 1995.
[40] Cox JB. A review of the geotechnical characteristics of the soils in the Adelaide City Area. In: Proceedings of symposium on soils and earth structures in arid climates. Institution of Engineers Australia and Australian Geomechanics Society, Adelaide; 1970 p. 72–86.
[41] McCue K, Love D. Earthquake microzonation Adelaide, South Australia. Australian Geological Survey Organisation, Final Report; 1997.
[42] McBean P. Design implications for structures within the Adelaide CBD arising from changes to the subsoil classification system in AS 1170.4. Aust Geomech 2010;3:45.
[43] Environmental systems & services [ES & S]. eqWave 3 – seismic waveform analysis: product user manual. Environmental Systems & Services; 2013. 28 p.
[44] Setiawan B, Jaksa M, Griffith M, Love D. HVSR recording duration for regolith sites: an experimental approach. In: Proceedings of the tenth pacific conference on earthquake engineering, building an earthquake-resilient pacific; 6–8 November 2015, Sydney, Australia.
[45] Geopsy. Geopsy home: software applications for ambient vibration; 2015. http://www.geopsy.org , [accessed 1 December 2015].
[46] Bard P.-Y. Microtremor measurements: a tool for site effect estimation. In: Proceedings of the second international symposium on the effects of surface geology on seismic motion, Yokohama, Japan. Irikura, Kudo, & Satani 3; 1998. p. 125 – 1279.
[47] Shapiro N, Campillo M. Emergence of broadband Rayleigh waves from correlations of the ambient seismic noise. Geophys Res Lett 2004;31:7.
[48] Bonnefoy-Claudet S, Cotton F, Bard P-Y. The nature of noise wavefield and its applications for site effects studies. A literature review. Earth-Sci Rev 2006;79:205–27.
[49] Konno K, Omachi T. Ground motion characteristics estimated from spectral ratio between horizontal and vertical components of microtremors. Bull Seismol Soc Am 1998;88(1):228–41.
[50] Wathelet M, Jongmans D, Ohrnberger M. Surface-wave inversion using direct search algorithm and its application to ambient vibration measurements. Surf Geophys 2004;2:211–21.
[51] Wathelet M, Jongmans D, Ohrnberger M, Bonnefoy-Claudet S. Array performances

for ambient vibrations on a shallow structure and consequences over Vs inversion. J Seismol 2008;12:1–19.
[52] Wathelet M, Jongmas D, Ohremberg M. Direct inversion of spatial autocorrelation curves with the neighborhood algorithm. Bull Seismol Soc Am 2005;95:1787–800.
[53] Sambridge M. Geophysical inversion with a neighborhood algorithm I. Searching a parameter space. J Geophys Res 1999;103:4839–78.
[54] Aitchison G, Sprigg R, Cochrane G. The soils and geology of Adelaide and suburbs. Adelaide: Department of Mines; 1954.
[55] Toshinawa T, Taber JJ, Berril J. Distribution of ground motion intensity inferred from questionnaire survey earthquake recordings and microtremors measurements – a case study in Christchurch new Zealand during the Arthurs pass Earthquake. Bull Seismol Soc Am 1997;87:356–69.
[56] Gueguen P, Chatelain J-L, Guilier B, Yepes H, Egred J. Site effect and damage distribution in Pujili (Ecuador) after the 28 March earthquake. Soil Dyn Earthq Eng 1998;17:329–34.
[57] García-Jerez A, Piña-Flores J, Sánchez-Sesma FJ, Luzón F, Perton M. A computer code for forward computation and inversion of the H/V spectral ratio under the diffuse field assumption. Comput Geosci 2017:2016. Accepted for publication.
[58] Okada H. The microseismic survey method. Geophysical Monograph Series No. 12. Society of exploration geophysicists with the cooperation of Society of exploration geophysicists of Japan and Australian Society of Exploration Geophysicists. Translated by Koya Suto, ISBN: 2003 1-56080-120-4, 135 pp.
[59] Kramer S. Geotechnical earthquake engineering 80. Upper Saddle River, New Jersey: Prentice Hall; 1996.
[60] Setiawan B, Jaksa M, Griffith M, Love D. Analysis of microtremor array measurement using the spatial autocorrelation (SPAC) method across the Adelaide City. Research Report No. 196, School of Civil, Environmental, and Mining Engineering, the University of Adelaide; 2016. 36 p.

Appendix D:

AN INTERNATIONAL PEER REVIEWED JOURNAL PAPER 3

(COPY OF PAPER FROM CHAPTER 4)

SETIAWAN, B., JAKSA, M., GRIFFITH, M., AND LOVE, D. (2018). ESTIMATING BEDROCK DEPTH IN THE CASE OF REGOLITH SITES USING AMBIENT NOISE ANALYSIS. ENGINEERING GEOLOGY, 243: 145–159, DOI: 10.1016/J.ENGGEO.2018.06.022.

INTENTIONALLY BLANK

Engineering Geology 243 (2018) 145–159

Contents lists available at ScienceDirect

Engineering Geology

journal homepage: www.elsevier.com/locate/enggeo

Estimating bedrock depth in the case of regolith sites using ambient noise analysis

Bambang Setiawan[a,*], Mark Jaksa[b], Michael Griffith[c], David Love[d]

[a] Faculty of Engineering, Syiah Kuala University, Jl. Tgk. Syech Abdurrauf 7, Darussalam, Banda Aceh 23111, Indonesia
[b] School of Civil, Environmental and Mining Engineering, The University of Adelaide, North Terrace Campus, SA 5005, Australia
[c] School of Civil, Environmental and Mining Engineering, The University of Adelaide, North Terrace Campus, SA 5005, Australia
[d] Department of State Development, Government of South Australia, 101 Grenfell Street, Adelaide, SA 5000, Australia

ARTICLE INFO

Keywords:
Bedrock depth
Ambient noise
Regolith
Impedance contrasts

ABSTRACT

Subsurface geometry, particularly the depth of bedrock, is crucial in seismic hazard studies because the basin geometry has been shown to play an important role in the altering of seismic waves. Estimating the bedrock surface using ambient seismic noise analysis has been undertaken by many researchers, with most studies focusing on sites with a strong impedance contrast between the bedrock and the overlying materials. The application of this technique at regolith sites, which is subjected to impedance contrasts in the low to high range is underdeveloped and requires further attention. This study seeks to address this need and is focused on the city of Adelaide in South Australia, which exhibits site amplification and is associated with various impedance contrasts. Analyses of ambient noise data are carried out using the generic function (GF) of the classic horizontal vertical spectral ratio (HVSR) method and the spatial autocorrelation (SPAC) technique to estimate the depth to bedrock. Comparison of the bedrock depth predictions from the seismic methods with boreholes drilled in close proximity to the measured sites demonstrate that the SPAC method provides superior estimates especially to those obtained from the other approach. This work demonstrates that the microtremor SPAC method is an effective tool for estimating bedrock structure at regolith sites.

1. Introduction

Local site effects need to be considered when conducting seismic hazard assessments (Booth et al., 1986; Brebbia et al., 1996; Street et al., 2001) as earthquake motion can be significantly amplified at vulnerable soil sites and cause severe structural damage, such as that which occurred in the 1985 Mexico, 1988 Armenian, 1989 Loma Prieta, 1989 Newcastle, and 1995 Kobe earthquakes. The bedrock profile and overburden sedimentary deposits contribute to site amplification effects (Graves et al., 1998; Bakir et al., 2002; Narayan and Rao, 2003; Narayan, 2005). Irregular sub-surface profiles, subjected to incident body waves, can result in focusing and defocusing of the seismic wave field manifested at ground level. The basin interface may change the velocity and direction of the waves. In certain circumstances, the focusing and defocusing phenomenon may cause amplification and de-amplification at the ground surface. The effect of the basin bedrock profile is revealed by the damage patterns of the Northridge, Sherman Oaks, and Santa Monica, California earthquakes (Somerville and Graves, 1996; Graves et al., 1998).

Single station ambient noise measurements are useful for investigating the depth of bedrock. Ibs-von Seht and Wohlenberg (1999) developed an empirical relationship between fundamental resonance frequencies and overburden thickness for the Lower Rhine Embayment in Germany and suggested good agreement between the horizontal to vertical spectral ratio (HVSR) peak frequency with the overall overburden thickness, ranging from tens to > 1000 m. These developments have provided a practical means of estimating overburden thickness using ambient noise data. Subsequently, many studies have used similar approaches for estimating the thickness of sediments overlying bedrock (e.g. Bodin et al., 2001; Parolai et al., 2002; Gosar, 2007; D'Amico et al., 2004; Hinzen et al., 2004; Lane et al., 2008; Dinesh et al., 2010; Paudyal et al., 2012a & b; Guo et al., 2014; Guo and Aydin, 2016). All of these studies were carried out essentially in relatively thick, homogenous and uniformly layered systems and in high impedance contrast sites. Estimating the bedrock surface using ambient noise analysis at regolith sites subjected to a complex layered system and various (low to high) impedance contrasts is the subject of ongoing research.

The present study is focused on bedrock depth estimation in

* Corresponding author.
E-mail addresses: bambang.setiawan@unsyiah.ac.id (B. Setiawan), mark.jaksa@adelaide.edu.au (M. Jaksa), michael.griffith@adelaide.edu.au (M. Griffith), david.love@sa.gov.au (D. Love).

https://doi.org/10.1016/j.enggeo.2018.06.022
Received 22 May 2017; Received in revised form 25 June 2018; Accepted 25 June 2018
Available online 30 June 2018

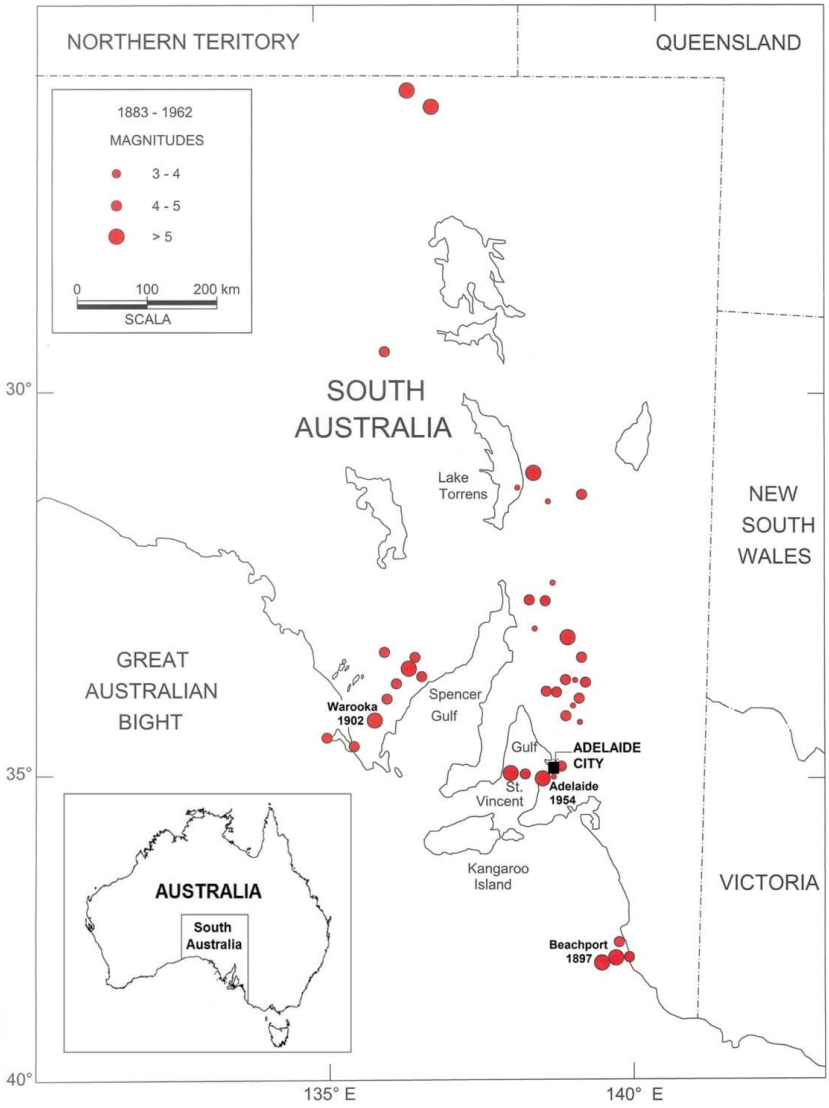

Fig. 1. Epicenters of the historical earthquakes (Malpas, 1991) including Adelaide city study area (Black Square).

presence of a complex subsurface profile and various impedance contrast sites, which is manifested in Adelaide's regolith. Regoliths include all weathered materials in the zone between the ground surface and the underlying bedrock (Wilford and Thomas, 2013). The Australian National Committee on Soil and Terrain (NCST) (2009) characterizes the regolith as the mantle of earth and rock altered or formed by land surface processes, whereas bedrock is the zone formed or altered by deep-seated crustal processes. The NCST characterized regolith and bedrock by different processes, rather than grouping them into different classes of material. Thus, characterizing earth layers as either regolith or bedrock is a task which involves many parameters including mineralogy and structure; climate, particularly rainfall and temperature; aeolian inputs; topography; biota, including vegetation and organisms; age, and soil-landscape history (Wilford and Thomas, 2013). The unique processes and parameters that control the development of a regolith when compared to bedrock result in different characteristics of masses within the regolith zone to those within the bedrock zone. Generally, the regolith tends to have lower density, strength, and cohesion than bedrock (NCST, 2009). Two previous investigations, namely Leonard (2015) and Collins et al. (2006), suggested various (~2.1 to ~3.5) impedance contrasts for the regolith at the investigated sites. Collins et al. (2006) measured the shear wave velocity at the Government House Site (GHS) in Adelaide, South Australia, using the spectral analysis of surface waves (SASW) method. Collins et al. (2006)

Table 1
Descriptions of the formations of the Adelaide City (Selby and Lindsay, 1982).

Code	Formation	Description
A	Quaternary alluvium, Pooraka Formation [HOLOCENE]	Red brown silty CLAY (CH), grades downwards to SAND and GRAVEL (SP-GP)
A1	Keswick CLAY [PLEISTOCENE]	Grey-green CLAY (CH) with red and brown mottling, stiff to hard, fissured
A2	Hindmarsh CLAY [PLEISTOCENE]	Grey-green CLAY (CH) with yellow and red mottling with overlying SAND (SC)
B	Carisbrooke Sand [PLEISTOCENE]	Yellow, orange brown and grey, fine to medium clayey and silty SAND (SC-SM)
C	Bunham Limestone and Hallet Cove Sandstone [PLEISTOCENE TO PLIOCENE]	White clayey, sandy and rubbly LIMESTONE; Pale grey to yellow brown calcareous SANDSTONE with layers of sand (SP)
D	Sand unit of Port Willunga Formation [EOCENE]	Fine silty SAND (SM)
E	Tandanya Sand Member of Chinaman Gully Formation [EOCENE]	Gravelly, clayey SAND (SC-GW)
F	Gull Rock Member of Blanche point Formation [EOCENE]	Alternating bands of cherty siltstone and grey SILT (ML)
G	Undifferentiated basal Blanche Point Formation and Tortachilla Limestone [EOCENE]	Green to dark grey clayey SAND (SC) with LIMESTONE
H	South Maslin Sand [EOCENE]	Dark grey, brown at depth, but weathering to red brown or yellow, silty SAND (SM) with pyrite lumps
J	Clinton Formation [EOCENE]	Dark grey CLAY (CL) with LIGNITE; irregular clayey SAND zones (SC)
K	Precambrian bedrock	White, pink, brown, purple, blue-grey and greenish grey with thin sandy bands, decomposed quartzite or quartz veins, high plasticity SILT slightly sandy, very stiff to hard with a moisture content well below the plastic limit > 480 kPa

suggested an average shear wave velocity of about 420 m/s for Adelaide's overlying layer and 810 m/s for Adelaide's bedrock. By assuming densities of 1900 kg/m^3 for the overlying layer and 2100 kg/m^3 for the bedrock, the SASW measurements by Collins et al. (2006) suggested an impedance contrast of ~2.1. A near surface seismic site classification by Leonard (2015) suggested a shear wave velocity of 315 m/s for the upper 30 m for most of the Adelaide city. Thus, the impedance contrast raw estimation for much of the city is ~3.5, by assuming the shear wave velocities of the overlying layer and bedrock are 315 and 1000 m/s, respectively, assuming respective densities of 1900 and 2100 kg/m^3. This study, also, suggested various impedance contrasts for the regolith at the study sites, as shown by the shear wave velocity profiles presented later in the paper. The uniqueness of the regolith in Australia has been highlighted by McPherson and Hall (2007) who suggested a modification to the seismic classification system in the widely adopted National Earthquake Hazard Reduction Program (NEHRP) for Australian National Regolith Site Classification Map. The main objective of this paper is to investigate the reliability of various ambient noise data analysis methods for engineering assessment of bedrock depth for such sites.

Adelaide, South Australia, the case study area of this paper, is considered the most seismically active of the Australian capital cities. Adelaide has suffered great losses from earthquakes (Dyster, 1996; McCue, 1975). Observations of seismic recordings obtained during the 1997 Burra earthquake suggest significant ground amplification at Adelaide (McCue et al., 2001). Therefore, this study is relevant for enhancing understanding of the seismic hazards of Adelaide.

2. Seismicity and geology of the case study area

The Australian continent is classified as a stable continent region (SCR) (Johnston, 1996a; Celerier et al., 2005; Hillis et al., 2008). Seismic activity in this region is categorized as low to moderate (Veevers, 1984). However, the deformation rate of the Australian continent is faster than other stable intraplate regions (Hillis et al., 2008). The continent experiences magnitude ≥6.0 earthquake every 5 years (McCue, 1990). Furthermore, several major devastating earthquakes have occurred in such 'stable' continents such as at Meeberrie (1941; ML 6.8), Meckering (1986; MS 6.8), Cadoux (1979; MS 6.4) and Tennant Creek (1988; MS 6.3) (cf. Johnston, 1996b; Crone et al., 1997; Sandiford et al., 2004; Boominathan et al., 2008).

Adelaide lies within the most seismically active region in the Australian continent (Sandiford, 2003; Quigley et al., 2006; Quigley et al., 2007). A comprehensive study of the historical seismicity in the Adelaide region was conducted by Malpas (1991). This author extended the seismic data by exploring historical records, local newspapers, meteorological records and other reports and at least 42 significant events ranging from 4 to 7 on the modified Mercalli intensity scale (MM) earthquakes were identified in the Adelaide region since 1837. In this pre-instrumental period, two moderate seismic events occurred at Beachport in 1897, with Richter local magnitude (ML) of 6.3, and at Warooka in 1902 (ML 5.9) (Malpas, 1991). Both the 1897 and 1902 events caused extensive damage in the epicenter area and were felt strongly hundreds of kilometers (Malpas, 1991) from the epicenters. The epicenters of these historical earthquakes are shown in Fig. 1. The Malpas (1991) study suggests the importance of seismic hazard investigations in the case study area. The findings of Malpas (1991) are supported by Greenhalgh et al. (1994), who concluded that at least 300 earthquakes are recorded by seismic instruments each year in South Australia, with 15 events of magnitude 5 or greater in the last 150 years.

The Adelaide case study area lies within the Adelaide Plains (Selby and Lindsay, 1982). The field sites are separated into two main plateaus, on the north and south sides of the Torrens River. In the north plateau area, geological profiles consist of 5 to 6 formations above the bedrock, which are predominantly Quaternary alluvium-Pooraka Formation, Gull Rock Member of the Blanche Point Formation, Undifferentiated basal Blanche Point Formation and Tortachilla Limestone, South Maslin Sand, and Clinton Formation (see Table 1). The bedrock depth of the north plateau area is estimated to range from 50 to 64 m below ground surface (BGS) (Selby and Lindsay, 1982). The situation is more complex in the south plateau area. In this area, 8 to 10 formations (most of the formations indicated in Table 1) overlie Precambrian bedrock. Available information on the South Adelaide site suggests bedrock deepens towards the southeast, ranging from 88 to 118 m BGS, as shown in Fig. 2 (Selby and Lindsay, 1982). General descriptions of the formations are given in Table 1. A typical high variability sub surface setting beneath the Adelaide city center is suggested by Selby and Lindsay (1982). Furthermore, the Keswick and Hindmarsh Clays underlying Adelaide have attracted some research attention. Both the Keswick and Hindmarsh clays are very similar in nature, characterized as stiff to hard, fissured, overconsolidated clays of high plasticity. Cox (1970) studied the physical properties of these clays and concluded that their geotechnical characteristics are remarkably similar to those of the London Clay. Sheard and Bowman (1996) indicated that a disconformable erosion surface exists between the Keswick and Hindmarsh clays.

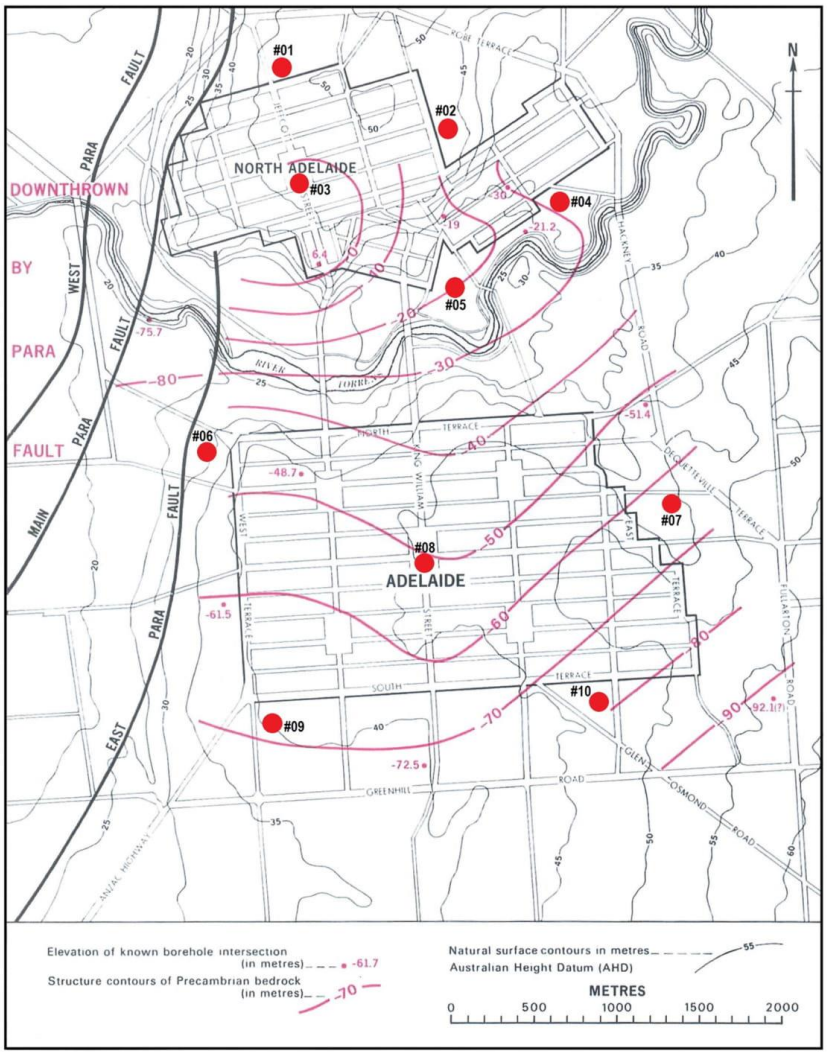

Fig. 2. Map of the study area showing isobaths of the Precambrian bedrock (Selby and Lindsay, 1982) including locations of microtremor measurements (red circles). (For interpretation of the references to colour in this figure legend, the reader is referred to the web version of this article.)

3. Methodology

3.1. Field noise measurements

Ambient noise field measurements were conducted at 8 sites in the parklands that surround the Adelaide city area (Fig. 2) using 7 sets of 3-component seismometers and at two sites using a single 3-component seismometer. Sites #01, #02, #04, #05, #06, #07, #09 and #10 used 7 sets, whereas the remainder of the sites (#03 and #08) used a single seismometer. These seismometers record the 3 orthogonal components of vibration: two horizontals (i.e. east–west and north–south) and one vertical. The data were recorded and saved to internal memory storage in each instrument. At each survey location, noise measurements were conducted for at least 2 h at a sampling frequency of 100 Hz. Field data were filtered with a cutoff frequency of 50 Hz. A hexagonal array with a radius of 50 m (R = 50 m) was used for the array field noise measurement. Only recordings on 3 instruments (in a triangular arrangement) were used for the horizontal to vertical spectral ratio (HVSR) analysis and the vertical seismometer readings from all instruments were used to analyze the spatial autocorrelation (SPAC). At each of the 8 sites, four tests with a duration of 30 min were conducted at a different time using all instruments.

All the equipment used for the noise data acquisition consisted of 3 component (3C) LE-3Dlite Lennartz seismometers with an eigen-frequency of 1 Hz. These 3C seismometers were equipped with an analog-to-digital recorder (Kelunji digital data recorder), a global

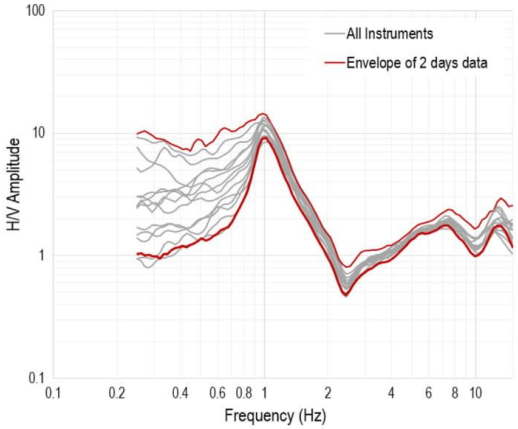

Fig. 3. HVSR test results for all deployed equipment sets in this study incorporating the envelope of the HVSR analysis of 2 days of continuously recorded data at a station outsite the investigated sites ~3 km at the north-east of Adelaide city.

positioning system (GPS), antenna and a battery. A laptop computer was used for initial setup and checking. The seismometers were placed on a 20 mm thick circular concrete slab over a generally firm to a stiff ground surface, which was previously cleared of vegetation. The seismometers were leveled so as to minimize any instability during recording. The seismometers were also oriented to magnetic North and protected from wind-induced vibrations by means of a plastic container and stabilized with a masonry brick on top. All of the equipment sets deployed in this study were examined for their repeatability. All equipment sets were run simultaneously at the same location, with a separation distance of approximately 0.5 m from one another. The HVSR analysis was carried out on all recorded data from all deployed equipment sets. The HVSR analysis curves for all equipment sets are presented in Fig. 3, which suggests similar curve patterns, particularly between about 0.8 and 10.0 Hz. This result confirms the repeatability of the equipment. The details of the HVSR and SPAC methods are presented below.

3.2. Horizontal to vertical spectral ratio (HVSR) analysis

The horizontal to vertical spectral ratio (HVSR) ambient noise method, herein referred to as HVSR, was introduced by Nogoshi and Igarashi (1971) based on the work of Kanay and Tanaka (1961). HVSR was popularized by Nakamura (1989) and has been used extensively since. Analysis of the spectral ratio between the Fourier amplitude spectrum of the horizontal (H) and vertical (V) components of the recorded ambient noise record is the key to HVSR. In accordance with the recommendations of the project "Site Effects Assessment Using Ambient Excitation" (SESAME, 2004), the selection of the windows with the most stationary wave forms to exclude the transient noises is a crucial initial step in computing HVSR spectral ratios. The Fourier spectra of each HVSR component are smoothed in each selected window and then merged by adopting the geometric mean. Finally, the obtained HVSR is computed and averaged.

The HVSR is calculated by taking the root mean square of the Fourier amplitude spectra of the horizontal components (F_{NS} for the Fourier amplitude spectra in the north-south and F_{EW} for the Fourier amplitude spectra in the east-west directions) divided by the vertical component spectrum (F_{UD}), as shown in Eq. (1) (Delgado et al., 2000):

$$\frac{H}{V} = \sqrt{\frac{(F_{NS}^2 + F_{EW}^2)}{(2F_{UD}^2)}} \tag{1}$$

The ellipticity curve indicated by HVSR analysis has been used to constrain successfully the generation of the shear wave velocity model by Arai and Tokimatsu (2004), Castellaro and Mulargia (2009), Di Stefano et al. (2014) and Del Gaudio et al. (2014). In this study, the HVSR approach is used to estimate the shear wave velocities of layers above bedrock at the instrumented sites.

The frequency corresponding to the first dominant peak of the HVSR spectrum plot is referred to as the site fundamental resonance frequency (SESAME, 2004). Once the fundamental resonance frequency of the site is obtained, it can be used to estimate bedrock depth, as suggested by Kramer (1996), provided the shear wave velocity of the overlying layer is known. This approach is herein referred to as the generic function (GF). Further explanation of this approach is provided later.

3.3. Spatial autocorrelation (SPAC) analysis

The spatial autocorrelation (SPAC) method (Aki, 1957) requires simultaneous recording of ambient noise at a minimum of 3 microtremor stations to conform to an appropriate instrumental array (Claprood, 2012). In the present study, 7 instruments were deployed in a hexagonal array. Following the process described below, the Rayleigh wave dispersion curve is obtained and used to determine the shear wave velocity profile.

In the SPAC method, Aki (1957) considered a circular array of stations for the noise field observation. Given, for harmonic waves of frequency ω, the time series of ground velocity $u(0,0,\omega,t)$ and $u(r,\theta,\omega,t)$, recorded at the center $C(0,0)$ and at a point $X(r,\theta)$ of the array, respectively, the spatial autocorrelation function can be defined as:

$$\varnothing(r,\theta,\omega) = \overline{u(0,0,\omega,t).\ u(r,\theta,\omega,t)} \tag{2}$$

where the right-hand-side of Eq. (2) represents the average of the products of simultaneous samples of the two time series. The spatial autocorrelation coefficient ρ is defined as the average of the normalized autocorrelation function in all directions over the circular array:

$$\rho(r,\omega) = \frac{1}{2\pi.\ \varnothing(0,\omega)} \int_0^{2\pi} \varnothing(r,\theta,\omega)d\theta \tag{3}$$

where $\phi(0,\omega)$ is the SPAC function at the center, $C(0,0)$, of the circular array. Assuming that waves are stochastic and stationary in space and time, the integration of Eq. (3) yields:

$$\rho(r,\omega) = J_0\left(\frac{\omega r}{c(\omega)}\right) \tag{4}$$

where $J_0(x)$ is the zero-order Bessel function of the first kind of x, and $c(\omega)$ is the phase velocity at the frequency ω. Using the Fourier Transform of the observed noise recording, the SPAC coefficient $\rho(r,\omega)$ can be obtained in the frequency domain as follows:

$$\rho(r,\omega) = \frac{1}{2\pi} \int_0^{2\pi} \frac{Re[S_{CX}(\omega,r,\theta)]}{\sqrt{S_C(\omega).\ S_X(\omega,r,\theta)}} d\theta \tag{5}$$

where $S_C(\omega)$ is the power spectral densities of the noise records at C, $S_X(\omega,r,\theta)$ is the power spectral densities of the microtremors at X, and $S_{CX}(\omega,r,\theta)$ is the cross-spectrum between the ground motions at these two locations.

The SPAC coefficients can be obtained by averaging the normalized coherence function of the cross-spectrum between points C and X in the direction of θ. The phase velocity for every frequency is estimated from the Bessel function in Eq. (4). Finally, the velocity model can be inverted.

The SPAC analysis adopted in the present study is the modified version introduced by Bettig et al. (2001), which facilitates the computation of average SPAC coefficients for any irregular array

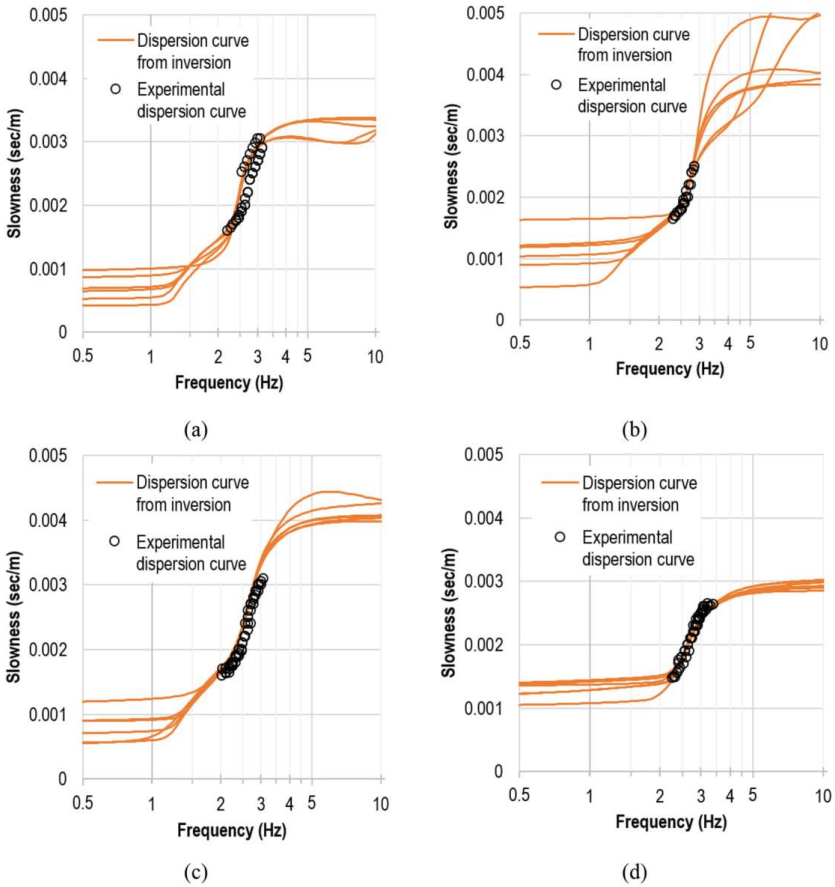

Fig. 4. Selected dispersion curves for the best 20 models comparing inversion and experimental results from selected tests at Locations (a) #01, (b) #02, (c) #04, and (d) #05.

configurations. This modification to SPAC uses a similar assumption to that adopted by the Aki (1957) version of SPAC, where the stochastic ambient noise wavefield is stationary in both time and space. The modification proposes that the computation of the averaged SPAC coefficients of the station pairs may be obtained from rings of finite radiuses $r_1 \le r \le r_2$, instead of using a fixed radius, r. The modified, averaged SPAC coefficient as defined by Bettig et al. (2001) is:

$$\bar{\rho}(r_1, r_2, \omega) = \frac{2}{r_2^2 - r_1^2} \int_{r_1}^{r_2} r \bullet J_0\left(\frac{\omega_r}{c(\omega)}\right) dr = \frac{2}{r_2^2 - r_1^2} \frac{c(\omega)}{\omega_r} \left[r \bullet J_1\left(\frac{\omega_r}{c(\omega)}\right) \right]_{r_1}^{r_2} \tag{6}$$

In practice, r_1 and r_2 are, respectively, the minimum and maximum sensor distance (radius) obtained from the co-array configuration and selecting station pairs with similar interstation distances (Bonnefoy-Claudet et al., 2005). The application of the modified version of SPAC in the present study affects both the resolution limit parameter (k_{min}) and the depth of the investigation. These issues are discussed in detail later.

4. Bedrock estimation

4.1. Bedrock estimation using generic function (GF)

A generic function to estimate the bedrock level was presented by Kramer (1996). The function is based on the model of a damped linear elastic layer. A simple sedimentary basin, which consists of a soft layer overlying a rigid hard rock basement, is analyzed by providing n natural frequencies of the soft soil deposit as follows:

$$\omega_n = \frac{V_S}{h}\left(\frac{\pi}{2} + n\pi\right) for\ n = 0,\ 1,\ 2,\ \ldots, \infty \tag{7}$$

where ω_n is the circular frequency of ground shaking of the nth natural frequency (Hz), V_s is the shear wave velocity (m/s), and h is the thickness of the layer (m). Generally, the peak amplification ratio occurs near the lowest natural frequency, which is known as the fundamental frequency. The vibration period, corresponding to the fundamental frequency, is known as the site period (T_0) and the corresponding frequency is known as the fundamental resonant frequency (f_s). The relations are given as follows:

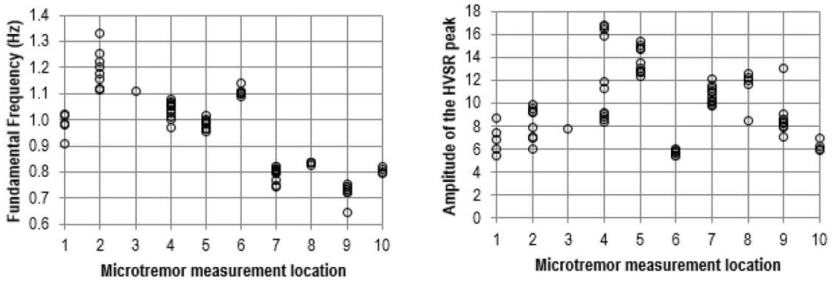

Fig. 5. Results of measurements that pass the SESAME (2004) test criteria for HVSR reliability and clear peak assessments at all locations: (a) fundamental frequencies, and
(b) amplitudes at f_0.

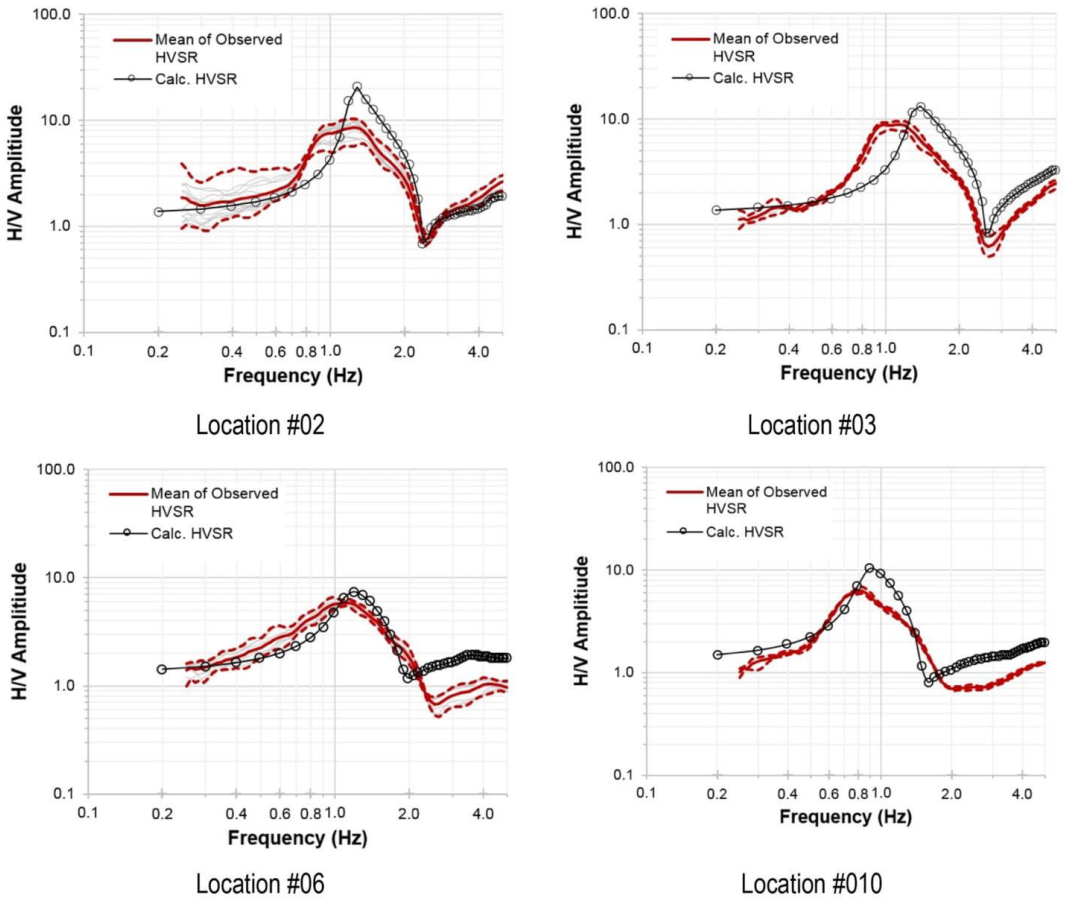

Fig. 6. Comparison of the observed mean HVSR of the microtremor data (solid red line) ± one standard deviation (dashed red line) with the computed HVSR of the fundamental-mode Raleigh waves (black line) for bedrock estimation using GF. (For interpretation of the references to colour in this figure legend, the reader is referred to the web version of this article.)

$$f_0 = \frac{V_s}{4h} \tag{8}$$

4.2. Bedrock estimation using shear wave profile of SPAC method

4.2.1. Dispersion curve (DC) retrieval

In this study, evaluation of the dispersion curves is carried out using the spatial autocorrelation (SPAC) techniques implemented in the Geopsy software package (Geopsy, 2015). The dispersion curve is evaluated based only on the vertical components of the microtremor data. The sole use of the vertical component of the seismometer data is motivated by the objective of analysing Raleigh waves and excluding Love waves. The fundamental Raleigh mode generally provides sophisticated interpretation tools in SPAC, provided the energy is confined to this single mode (Asten et al., 2004). Pre-processing is carried out using a classical procedure for signal synchronization and mean and trend elimination. The seismic analysis code (SAC) algorithms of Goldstein et al. (2003) are used for this pre-processing. In this study, the use of several tests at each array location allows investigating the consistency of the evaluated dispersion curves.

In order to evaluate the dispersion curves (DCs), two important features to consider are the resolution (k_{min}) and aliasing (k_{max}) limits characterizing the array configuration, estimated through the array transfer function (ATF: see Di Giulio et al., 2006). The parameter k_{min} refers to the width of the central peak of ATF and k_{max} refers to the limit to avoid alias effects. The values of k_{min} and k_{max} depend on the adopted array size (i.e. the minimum, D_{min}, and maximum, D_{max}, sensor spacing). Empirically Tokimatsu (1997) defined the range of k_{min} and k_{max} within the following limits:

$$\frac{2\pi}{3D_{max}} < k_{min} < k_{max} < \frac{\pi}{D_{min}} \tag{9}$$

In the case of the 50 m radius, circular hexagonal array adopted in this study, k_{min} and k_{max} lie in the range of $0.0209 < k_{min} < k_{max} < 0.0628$. These range values of k_{min} and k_{max} are used in this study to constrain the resolution limits.

The dispersion curves obtained from each location are presented in Fig. 4. Four curves from each location are computed to confirm the reliability of the deduced dispersion curve. The results suggest good consistency at all locations, as shown by the black circles in Fig. 4. The experimental dispersion curves can be as low as ~2.2 Hz. All of these dispersion curves, which correspond to the autocorrelation curves, are used to invert the shear wave velocity profiles for estimating the bedrock depth.

The dispersion curves computed during the inversion process for all models are examined to explore the appropriateness of the model. The selected computed dispersion curves are incorporated in Fig. 4. It can be readily observed that the computed dispersion curves agree well with the experimental models. This confirms the appropriateness of the results obtained for the frequency range applicable to the experimental dispersion curves. Significant errors are observed at low frequencies beyond the aperture of the array. This large discrepancy at low frequencies can be attributed to the increasing uncertainty associated with the estimated shear wave velocity at the greater depths. However, for the study site, which is associated with bedrock depths up to approximately 118 m, the maximum sensor spacing of 100 m should be sufficient, as the penetration of surface waves is in the order of half of the wavelength (Xia et al., 2000). The longest wavelength that can be reliably analyzed is approximately 3 times the maximum sensor spacing (Tokimatsu, 1997). Thus, the maximum depth for reliably measuring shear wave velocity is approximately 1.5 times the maximum sensor spacing.

4.2.2. Shear wave structure inversion (inversion technique)

The present study uses the neighborhood algorithm (NA) of Sambridge (1999) to infer the shear wave profile using the SPAC autocorrelation curve. This NA was implemented by Wathelet et al. (2005) in the Geopsy computer program. The NA is a stochastic direct-search method to identify an acceptable model inside a multi-dimensional parameter space. As with other direct-search methods, the NA generates pseudo-random samples in the parameter space using the dispersion curves constraint (Wathelet et al., 2005). Each sample corresponds to a set of parameters associated with a ground model. A misfit value is introduced to compare the computation results to the measured dispersion curve. This misfit value indicates how far the generated model deviates from the targeted solution. With poorly constrained parameters, inversion using the NA may result in different ground models, therefore it is recommended that several trials be undertaken using different random seeds (Sambridge, 1999). In this present paper, the shear wave velocity model is generated using the Geopsy program (Geopsy, 2015). The depth of bedrock is validated using the generated shear wave velocity profile.

The U.S. National Earthquake Hazards Reduction Program (NEHRP) classified rock Class B (Rock) and A (Hard rock) as materials with shear wave velocities > 760 m/s and 1500 m/s, respectively (Building Seismic Safety Council (BSSC), 2001). Moreover, McPherson and Hall (2007), in their development of the Australian National Regolith Site Classification Map, classified bedrock as materials with shear wave velocities > 760 m/s. The present study adopts these values of 760 m/s and 1500 m/s shear wave values to indicate bedrock level. A shear wave velocity of 760 m/s is the most commonly adopted criterion for defining engineering bedrock (Estrada, 2010). However, several measurements in Australia have shown that such a shear wave velocity is associated with extremely weathered rock. Therefore, the NEHRP classification of Rock Class A, with a minimum shear wave velocity of 1500 m/s, is also incorporated in the present study, which has been shown in Australia to be associated with bedrock of at least moderate strength (McPherson and Hall, 2007).

5. Results

5.1. Bedrock estimation using generic function (GF)

5.1.1. Site fundamental frequency

HVSR analysis by means of Geopsy (2015) is carried out to obtain the site fundamental frequency. The results of this HVSR analysis, for all tests at all measured sites, are included in a companion paper (Setiawan et al., 2018). Several tentative window lengths (i.e. 25, 30. 35 and 40 s) have been undertaken to obtain as many reliable HVSR curves as possible. The 40 s window length was selected as it provides the most reliable HVSR curves. The reliability of the HVSR curves is based on the SESAME (2004) criteria, which found that many more HVSR curves satisfied the SESAME criteria when using a 40 s window length than when adopting other window lengths. This 40 s window length is also used to explore HVSR curves to frequencies as low as 0.25 Hz. The fundamental frequency at most of the sites in the study area is estimated to be around 1 Hz, whereas the remainder of the sites (#07, #08, #09 and #10) are below 1 Hz. A clear peak fundamental frequency of all deployed instruments was found at Locations #01, #02, #03, #04, #07, #08 and #09, whereas at Locations #05, #06 and #10 this peak was not well defined for some measurements due to unfavorable noise conditions. Instrument #A was unable to provide a distinct and reliable peak at Locations #05 and #06. Instruments #A and #B were also unable to produce a clear and reliable HVSR peak at Location #10. This may be due to some disturbances during the measurement period or some inconsistencies during instrument setup, such as installation on a slightly unstable surface that caused a slight and gradual tilting during the measurement process. These unreliable data were excluded from the bedrock depth estimation.

A secondary peak at frequencies of 4–6 Hz, whose amplitude is between 2 and 4 is detected at Locations #01, #02, #03, #08 and #09.

Table 2
Estimated bedrock levels using the generic function (GF) for all measured sites.

Location	Average shear wave velocity of overlying layer (m/s)	Fundamental frequency (Hz)	Estimated bedrock level using generic function (m)	Bedrock depth from borehole data (m)
#01	406	0.91–1.07	95–112	59
#02	422	1.12–1.33	79–94	64
#03	304	1.06–1.11	68–72	44
#04	339	0.97–1.08	78–87	54
#05	268	0.96–1.02	65–70	50
#06	385	1.05–1.14	84–92	88.4
#07	311	0.74–0.82	95–105	96
#08	403	0.83–0.84	120–122	98
#09	451	0.65–0.76	149–174	107
#10	428	0.79–0.82	131–135	118

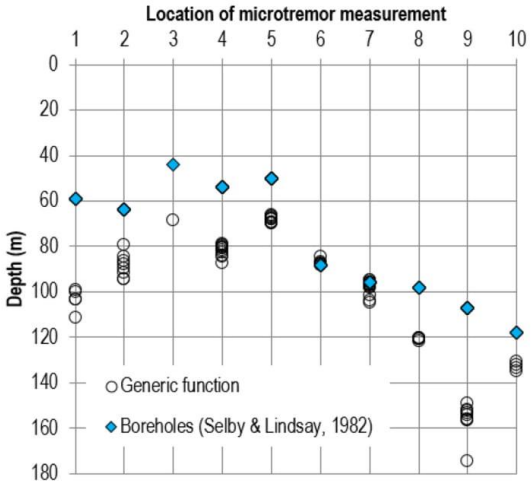

Fig. 7. Interpreted bedrock depth (m) using the generic function at all locations compared against data from the nearest boreholes (Selby and Lindsay, 1982).

The possibility that the second peak corresponds to the higher mode of vibration is investigated using Eq. (6), for $n > 0$. The results suggest that the ratio of 5–6, between the frequencies of the secondary peak and the fundamental mode of the HVSR analysis, is inconsistent with the expected ratio of 3. This inconsistency was found at all detected locations (i.e. Locations #01, #02, #03, #08 and #09). Therefore, the secondary peak appears not to be associated with higher modes of vibration. The two-peak structure, evident at Locations #01, #02, #03, #08 and #09, suggests that there are two different impedance contrasts at two different scales: the first peak relates to a thick structure and the second to a shallow structure (cf Gueguen et al., 1998; SESAME, 2004).

Furthermore, since the greatest amplification occurs at approximately the lowest natural frequency, known as the fundamental frequency (Kramer, 1996), further analysis, in the present study, to deduce bedrock depth is carried out using only this fundamental frequency.

SESAME (2004) outlined a process by which the reliability of the HVSR curve can be assessed from the following criteria: (i) for the peak to be significant, f_0 should be > 10 divided by the window length (I_w), which in this study is 40 s; (ii) the number of significant cycles should be > 200; and (iii) the standard deviation of the amplitude of the HVSR curve, at frequencies between $0.5f_0$ and $2f_0$, should be less than two when $f_0 > 0.5$ Hz, or < 3 when $f_0 < 0.5$ Hz. All three HVSR reliable criteria must be satisfied to consider a curve reliable for further analysis. Furthermore, SESAME (2004) also outlined the criteria for identifying a clear HVSR peak, which consists of 6 conditions. At least 5 out of the 6 criteria must be met to define a clear HVSR peak. Only the values of f_0 that pass the SESAME (2004) reliability and clear peak criteria were used for further analysis in the bedrock estimation at the measured sites, as shown in Fig. 5(a). The measurements that failed to pass the test were removed. Fig. 5(b) presents the amplitudes at f_0 of all tests that passed the SESAME (2004) criteria at all locations.

5.1.2. Shear wave velocity profile

The average value of the shear wave velocity of the layers above bedrock must be defined to obtain the thickness of the overburden layer using the generic function suggested by Kramer (1996). The shear wave velocity profile of the present study is obtained by inverting the HVSR ellipticity curve. The 20 best models extracted from the results of the inversion are analyzed to obtain the arithmetic mean and median values of layer velocities. The appropriateness of the adopted shear wave velocity models was validated using forward computation, as suggested by García-Jerez et al. (2016). The fundamental Raleigh wave ellipticity, herein termed the 'calculated HVSR', is computed based on the adopted mean shear wave velocity and compared to the observed HVSR. Fig. 6 presents a comparison of the mean observed and calculated HVSRs plotted using a logarithmic scale. As indicated in the plots, comparable results are observed at all measured sites for the bedrock depth estimation using GF. It is worth mentioning that comparisons between the experimental/observed and calculated HVSRs to validate the appropriateness of the inverted shear wave velocities have been carried out previously in many studies, such as by Apostolidis et al. (2004), Asten et al. (2004), Wathelet et al. (2004), Arai and Tokimatsu (2004), Di Giulio et al. (2006, 2014) and García-Jerez et al. (2016).

A summary of the average shear wave velocities for all layers above bedrock, including the fundamental frequencies and estimated bedrock depths for all sites in the present study, are given in Table 2. In this study, it was found that it is preferable to use the mean rather than the median of the shear wave velocity for estimating bedrock depth by means of the generic function as the forward computation suggests that this choice provides the best fitting of the computed ellipticity of the Rayleigh wave fundamental mode with the HVSR observed from microtremor array data. Fig. 7 presents the results of the estimated bedrock depths compared against the nearest boreholes. All bedrock depth estimations using GF are provided in Appendix A of the Supplementary

Table 3
Adopted inversion parameters.

Layer	Depth	Compression wave velocity (m/s)	Poisson's ratio	Shear wave velocity (m/s)	Density kg/m^3	Remarks
Upper Layer	1–30	200–2000	0.2–0.5	150–1000	18–20	$V_{p1} < V_{p2} < V_{p3}$
Transition Layer 1	15–60	200–4000	0.2–0.5	150–2000	18–20	$N_{u1} < N_{u2} < N_{u3}$
Transition Layer 2	50–150	200–5000	0.2–0.5	150–3500	18–20	$V_{s1} < V_{s2} < V_{s3}$
Bedrock	> 150	200–5000	0.2–0.5	150–3500	20–24	$Rho_1 < Rho_2 < Rho_3$

V_{p1}, V_{p2}, & V_{p3}: Compression wave velocity of the upper layer, transition layer 1 & transition layer 2, respectively.
N_{u1}, N_{u2}, & N_{u3}: Poisson's ratio of the upper layer, transition layer 1 & transition layer 2, respectively.
V_{s1}, V_{s2}, & V_{s3}: Shear wave velocity of the upper layer, transition layer 1 & transition layer 2, respectively.
Rho_1, Rho_2, & Rho_3: Density of the upper layer, transition layer 1 and transition layer 2, respectively.

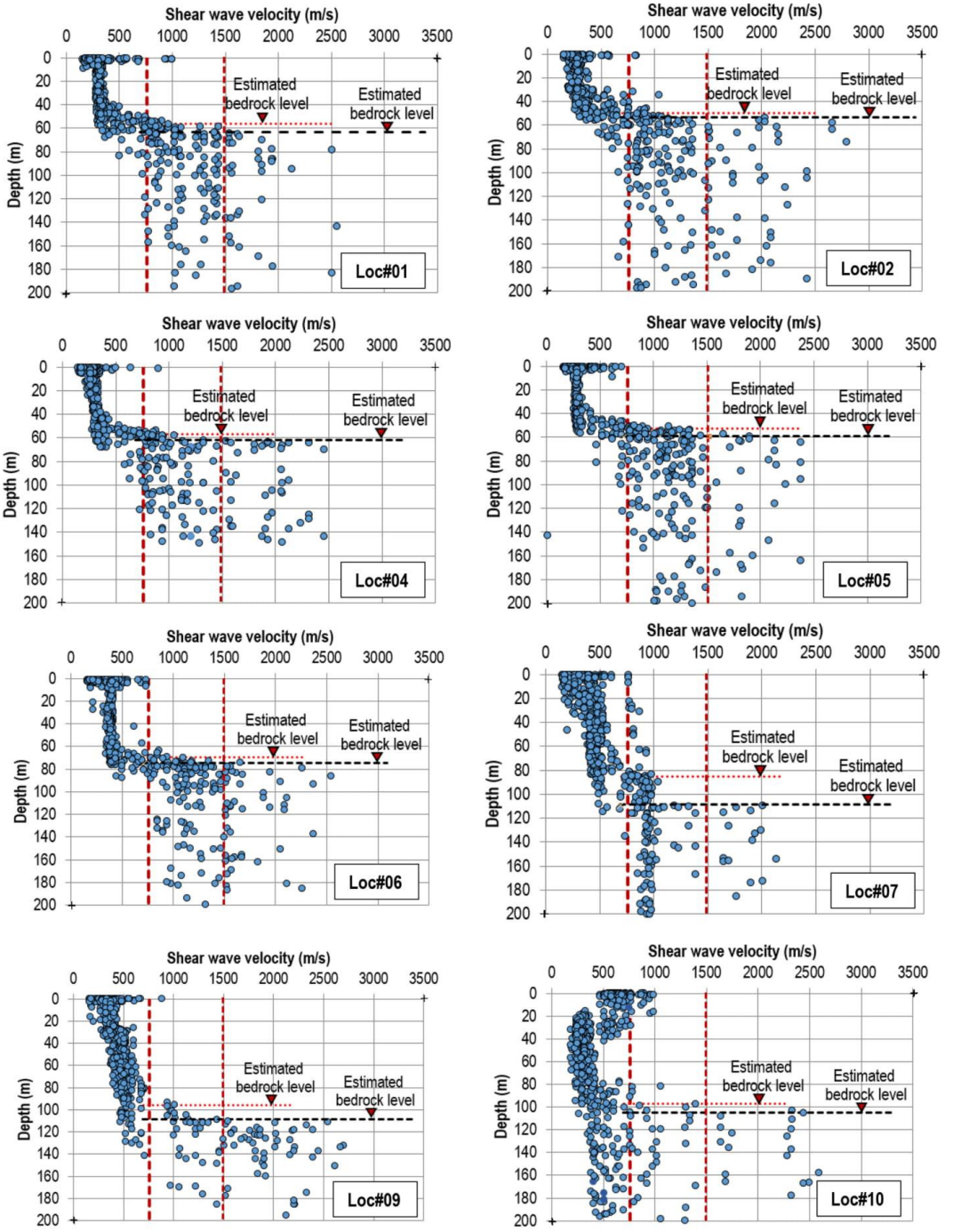

(caption on next page)

Fig. 8. Typical interpreted bedrock depth using the SPAC method at all locations. The dashed red vertical lines represent the V_s bedrock threshold of 760 m/s and 1500 m/s. The dotted red and dashed black horizontal lines represent the level of estimated bedrock depths of 760 m/s and 1500 m/s criteria, respectively. (For interpretation of the references to colour in this figure legend, the reader is referred to the web version of this article.)

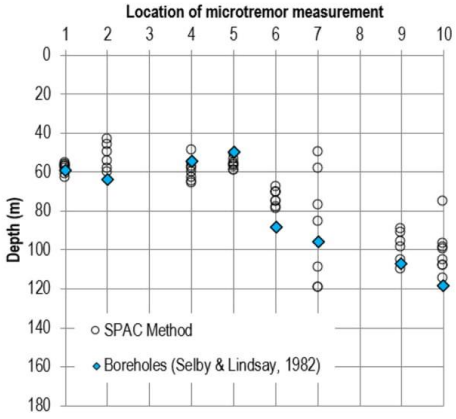

Fig. 9. Summary of interpreted bedrock depths using the SPAC method.

Data.

5.2. Bedrock estimation using shear wave profile of SPAC method

In the inversion of the SPAC-derived surface wave curves, Wathelet et al. (2005) adopted 4 main parameters associated with each layer: the compression wave velocity, Poisson's ratio, shear wave velocity and the density. The layer can be assigned a fixed thickness or a reasonable range depending on the geological information available at the study site. In the present study, the profile of the site is assumed to be generally soft in the upper part (1–30 m depth), followed by gradually harder (15–60 m depth for Transition Layer 1 and 50–150 m depth for Transition Layer 2) before encountering hard bedrock (below 150 m depth). These layer depths are assigned to permit the neighborhood algorithm (NA) to search for the model that best fits the autocorrelation curve provided. The detailed parameter model adopted is summarized in Table 3.

For the bedrock depth estimation using the shear wave velocity profile of the SPAC method, 3 runs were carried out. At least 12,500 models were generated in each run, from which the 20 best models were extracted and analyzed. Typical results are provided in Fig. 8. A summary of the interpreted bedrock depths using the SPAC method is shown in Fig. 9.

6. Discussion

Correlations between the fundamental resonance periods at different sites and the bedrock depths estimated from (GF) and SPAC methods are examined. Fig. 10 shows the analysis results from the various measurements acquired at the different sites investigated. As shown in Fig. 10(a), the results obtained using the generic function (GF), in general, suggest an over-estimate when compared to the bedrock depths resulting from the boreholes, except for sites #06 and #07, with the largest error occurring at Location #09 (see Fig. 7). These discrepancies can be associated with the local over- or under-estimation of the overburden V_s inferred from the HVSR ellipticity curves.

In contrast to the previous method, the SPAC method provided slight under-estimations for bedrock depths, as shown in Fig. 10(b), but in any case, better approximated to the real values in comparison to the GF results. As shown in Fig. 9, most of the bedrock depth estimates from SPAC are within 6 m or less of the borehole data, except for Locations #06 and #07, where the maximum offset is 9 m and 13 m, respectively. This better accuracy of the SPAC estimates is further confirmed by plotting them with respect to the fundamental periods of the sites investigated, as shown in Fig. 10(b). The best fit regression line of SPAC results is almost coincident with that of the borehole data.

Furthermore, the HVSR derived from microtremor array data (observed HVSR) are compared with the Rayleigh wave fundamental mode ellipticity (calc. HVSR) computed from the shear wave velocity profiles derived through simplified 1D inversion of SPAC data. The comparison is made to investigate the appropriateness of the inversion, even though the overburden shear wave velocity has no direct influence on the evaluation of bedrock depth using the SPAC method. Forward computing using Geopsy (2015) [calc. HVSR (Geopsy)], and García-Jerez et al. (2016) [calc. HVSR (HVInv)] are employed to compute the

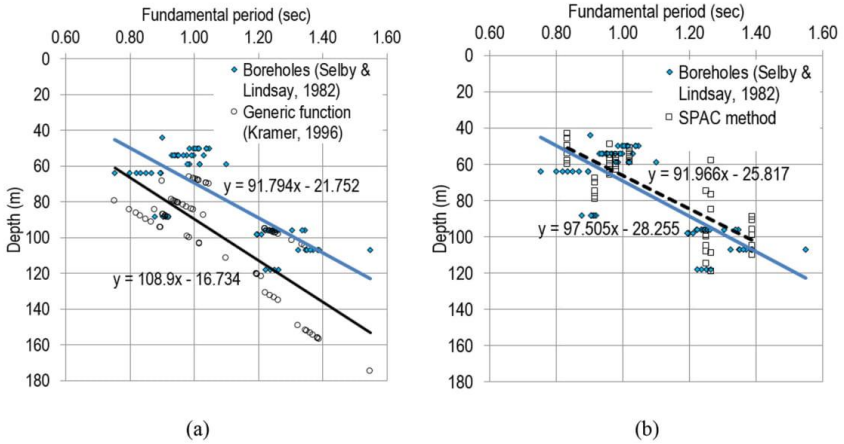

Fig. 10. Bedrock depths estimated using (a) the generic function method (Kramer, 1996) and (b) the SPAC method.

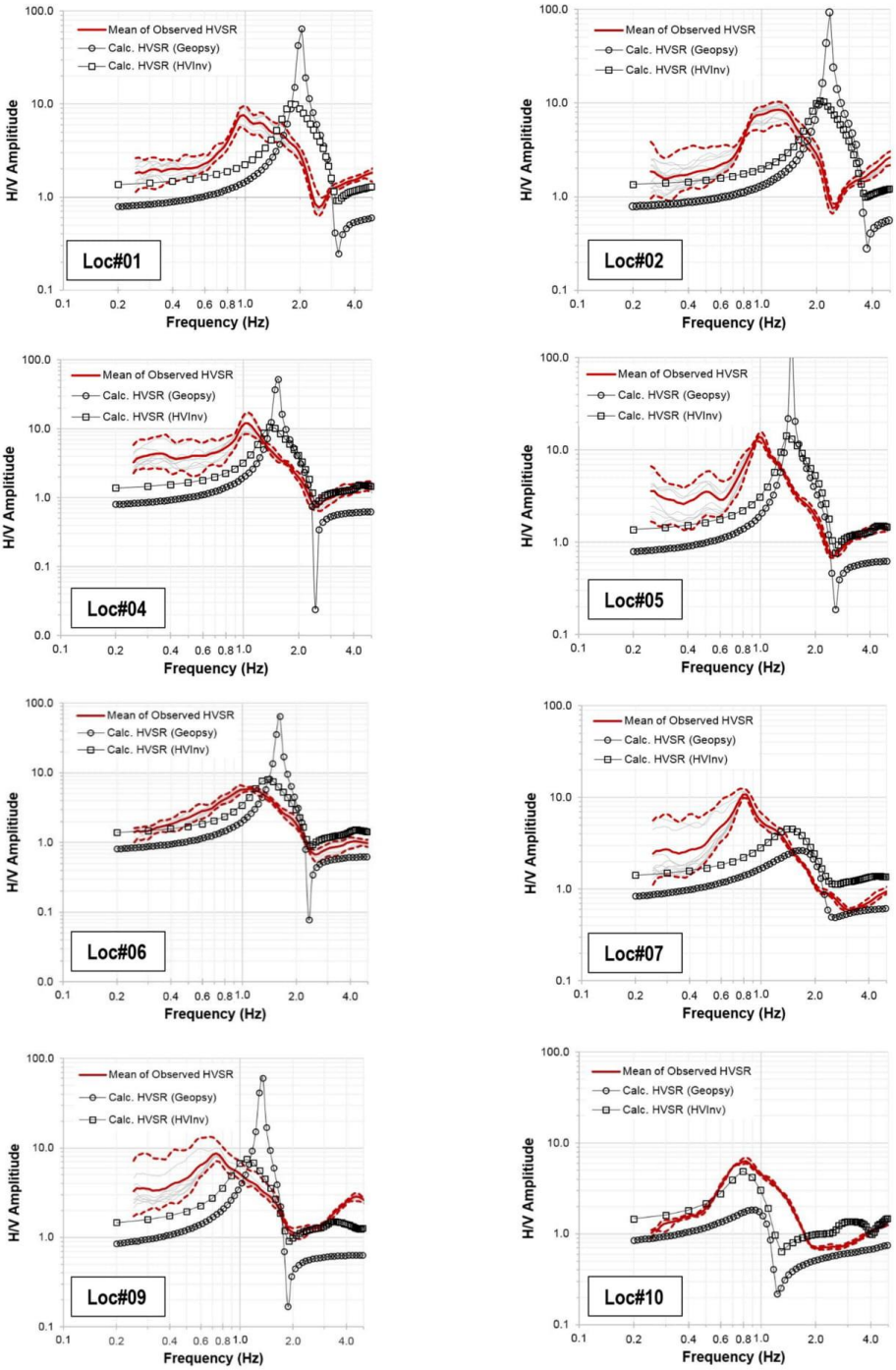

Fig. 11. Comparison between the observed and calculated HVSRs at all SPAC measured sites.

Table 4
Statistical analysis of bedrock depth estimation using the GF and SPAC methods.

Performance measure	Generic function (Kramer, 1996)	SPAC		
		760 m/s	1500 m/s	All
r	0.80	0.89	0.86	0.83
RMSE	27.4 m	16.8 m	12.9 m	15.0 m
MAE	22.3 m	13.4 m	9.6 m	11.5 m
Regression function	$y = 0.6939\times + 7.0522$ for Generic function; and $y = 0.9596\times + 9.0606$ for SPAC			

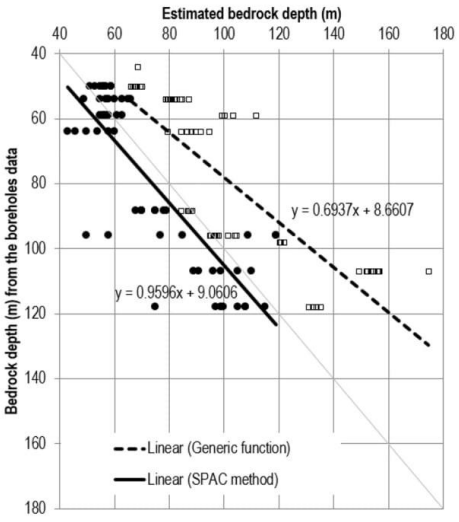

Fig. 12. Comparison of results from both the GF and SPAC methods with bedrock depths from the boreholes using regression analysis.

calculated HVSR. The comparison of the observed and calculated HVSR curves, using logarithmic plots at all SPAC measured sites, is presented in Fig. 11. Generally, the results of calculated HVSR using both Geopsy (2015) and García-Jerez et al. (2016) are in good agreement. The observed and calculated HVSR curves at all SPAC measured sites appear in general quite comparable. At two sites (Locations #6 and #10), [calc. HVSR (HVInv)] shows good agreement with the observed HVSR curves, whereas discrepancies are observed in the frequency and/or peak amplitudes for the remainder of the sites. These discrepancies may be attributed to the inclusion of other wave types in the Raleigh waves of the recorded noise. Actually, some caution is needed when interpreting the observed HVSR as consisting predominantly of fundamental Rayleigh waves. The inclusion of different waves with Raleigh waves can produce different HVSR curves (Bonnefoy-Claudet et al., 2006a, 2006b; Castellaro and Mulargia, 2009). Ideally, the other waves in this wavefield should be separated from the Raleigh waves. However, this task is difficult and contains many debatable issues (Bonnefoy-Claudet et al., 2006a; Poggi and Fah, 2010). Currently, there is very little information on the quantitative proportions of the different waves in ambient noise, notwithstanding a new technique which was recently proposed to extract Rayleigh/Love wave properties from ambient noise recordings (Del Gaudio, 2017). Bonnefoy-Claudet et al. (2006a) suggested that low frequency ambient noise consists predominantly of fundamental Rayleigh waves, but this remains a topic for discussion at higher frequencies ($f > 1$ Hz). Furthermore, the HVSR curves obtained from Geopsy and HV-Inv, as shown in Fig. 11, seem often to show stronger peaks for Geopsy than the HV-Inv ones. As the basic assumption of the calculated HVSR of the Geopsy model is that the HVSR corresponds to the ellipticity of Raleigh waves, the stronger peaks it provides is mostly due to singularities of Rayleigh wave ellipticity at the resonance frequency, where the Rayleigh vertical component tends to lose vertical-motion energy (cf Asten, 2004). Such sharp peaks in the HV-Inv's HVSR curves are smoothed by the contribution of other types of waves (i.e. body, Love) to the vertical component of the motion (cf Arai and Tokimatsu, 2004; García-Jerez et al., 2016).

Both the GF and SPAC methods are compared directly to the bedrock depths obtained from the boreholes. Regression analysis is used for this purpose and the results are shown in Table 4 and Fig. 12. Improved agreement is obtained between the bedrock depths predicted by the outcome of the SPAC method and those physically observed from the boreholes, in comparison to the results obtained from GF-based estimations. This is confirmed by the calculation of the coefficient of correlation, *r*, the root mean squared error, RMSE, and the mean absolute error, MAE, according to the following relationships:

$$r = \frac{n\sum y_j d_j - (\sum y_j)(\sum d_j)}{\sqrt{n\left(\sum y_j^2\right) - (\sum y_j)^2}\ \sqrt{n(\sum d_j^2) - (\sum d_j)^2}} \tag{10}$$

$$RMSE = \left\{\frac{1}{n}\sum_{j=1}^{n}(y_j - d_j)^2\right\}^{\frac{1}{2}} \tag{11}$$

$$MAE = \frac{1}{n}\sum_{j=1}^{n}|y_j - d_j| \tag{12}$$

where:

y_j = model (estimated) output, $y_j = y_1, y_2, y_3, \ldots, y_n$;
d_j = desired (actual) output, $d_j = d_1, d_2, d_3, \ldots, d_n$; and
n = the number of pairs of data.

These three coefficients were used to quantify the relative correlation and the goodness-of-fit between the estimated and observed values of bedrock depth. General guidelines, in relation to the absolute value of *r*, are suggested by Smith (1986) as follows: (a) $r \leq 0.2$ is an indication of weak correlation; (b) absolute of *r* between $0.2 < r < 0.8$ suggests moderate correlation; and (c) $r \geq 0.8$ is an indication of strong correlation.

Results are presented in Table 4, which shows that the SPAC method performs better than the GF. The coefficient of correlation, *r*, the RMSE, and MAE obtained using the SPAC model are: 0.83, 15.0 m and 11.5 m, respectively. In contrast, these measures are 0.80, 27.4 m and 22.3 m, respectively, for the GF method examined.

Applying the SPAC method, two different criteria were used for bedrock definition (i.e. shear wave velocities of 760 m/s and 1500 m/s [BSSC, 2001]). The coefficient of correlation, *r*, RMSE, and MAE obtained using the 760 m/s criterion are 0.89, 16.6 m and 13.4 m, respectively, whereas, for the 1500 m/s criterion, these measures are: 0.86, 12.9 m and 9.6 m, respectively. This suggests that the 1500 m/s criterion yields more accurate predictions of bedrock level than the 760 m/s criterion.

7. Conclusions

Local site effects need to be accounted for in seismic hazard assessment, as earthquake motions can be significantly amplified on soil sites and cause more severe structural damage, such as has occurred in many historical earthquakes around the world. The bedrock profile contributes to the amplification and de-amplification at the ground surface, as shown by the damage pattern of the Northridge, Sherman Oaks and Santa Monica earthquakes, for example. Therefore, information regarding bedrock depth is crucial in seismic hazard studies.

Considering the advantages of ambient noise analysis, this technique has been used in the investigation of bedrock level at many sites

around the world, with most of these applications being for relatively thick homogenous, uniformly layered systems and strong impedance contrast sites, such as at the Lower Rhine Embayment and Cologne areas in Germany, Bangalore, India and Kathmandu, Nepal. Estimating the bedrock level using ambient noise analysis at regolith sites subjected to impedance contrasts in the low to high range is under-represented in the literature and, hence, requires further attention. This study seeks to address this need by investigating suitable methods to estimate the basement topography of regolith sites using microtremor observation. The case of Adelaide, the capital and largest city in South Australia, which exhibits site amplification and is founded on regolith, is investigated in the present paper. Ten microtremor measurements were obtained at various locations across Adelaide's central business district. At 8 locations a sensory array was used and at the remaining two, a single sensor was employed.

In order to estimate bedrock level, the paper presents analyses adopting the generic function (GF) and spatial autocorrelation (SPAC) method using the neighborhood algorithm (NA) inversion. The estimates are compared with boreholes drilled in close proximity to the measurement locations and the results of the analyses suggest that the SPAC method outperforms the GF approach. This confirms that the microtremor SPAC method is an effective tool for estimating the bedrock depth at regolith sites.

Acknowledgements

The first author is grateful to the University of Adelaide's Graduate Centre for providing scholarship funding (1188687 BAMBANG SETIAWAN - AGRS 2013) and the Faculty of Engineering, Syiah Kuala University, Banda Aceh, Indonesia for their support. The authors also acknowledge the reviewers of the paper for their helpful feedback.

Notation

c	phase velocity
D_{max}	maximum spacing sensor distance
D_{min}	minimum spacing sensor distance
d_j	desired (actual) output, $d_j = d_1, d_2, d_3, \ldots, d_n$
F_{EW}	Fourier amplitude spectra in east-west direction
F_{NS}	Fourier amplitude spectra in north-south direction
F_{UD}	Fourier amplitude of vertical component
f_0	fundamental frequency
J_0	zero-order Bessel function of first kind
h	thickness of the layer
k_{max}	aliasing limit
k_{min}	resolution limit
MAE	mean absolute error
n	number of pairs of data
r	coefficient of correlation
RMSE	root mean squared error
S	power spectral density
T_0	Fundamental site period
u	wave forms velocity
V_s	shear wave velocity
y_j	model (estimated) output, $y_j = y_1, y_2, y_3, \ldots, y_n$
Z	depth
ρ	spatial autocorrelation coefficient
ϕ	directions
ω	angular frequency

Appendix A. Supplementary data

Supplementary data to this article can be found online at https://doi.org/10.1016/j.enggeo.2018.06.022.

References

Aki, K., 1957. Space and time spectra of stationary stochastic waves, with special reference to microtremors. Bull. Earthq. Res. Inst. 35, 415–456.
Apostolidis, P., Raptakis, D., Pitilakis, K., 2004. The use of microtremors for the definition of soil properties and bedrock depth in an urban area. In: 13th World Conf. on Earthquake Engineering, Vancouver, BC, Canada, 1-6 August 2004, Paper No. 2770.
Arai, H., Tokimatsu, K., 2004. S-wave velocity profiling by inversion of microtremor H/V spectrum. Bull. Seismol. Soc. Am. 94 (1), 53–63.
Asten, M., 2004. Comment on "microtremor observations of deep sediment resonance in metropolitan Memphis, Tennessee" by Paul Bodin, Kevin smith, Steve Horton and Howard Hwang. Eng. Geol. 72, 343–349. http://dx.doi.org/10.1016/j.enggeo.2003.09.001.
Asten, M., Dhu, T., Lam, N., 2004. Optimised array design for microtremor array studies applied to site classification; comparison of results with SCPT logs. In: 13th World Conf. on Earthquake Engineering, Vancouver, BC, Canada, 1-6 August 2004, Paper No. 2903.
Bakir, B., Ozkan, M., Ciliz, S., 2002. Effects of basin edge on the distribution of damage in 1995 Dinar, Turkey earthquake. Soil Dyn. Earthq. Eng. 22, 335–345.
Bettig, B., Bard, P.-Y., Scherbaum, F., Riepl, J., Cotton, F., Cornou, C., Hatzfeld, D., 2001. Analysis of dense array measurements using the modified spatial auto-correlation method (SPAC). Application to Grenoble area. Boll. Geof. Teor. Appl. 42 (3–4), 281–304.
Bodin, P., Smith, K., Horton, S., Hwang, H., 2001. Microtremor observations of deep sediment resonance in metropolitan Memphis, Tennessee. Eng. Geol. 62, 159–168.
Bonnefoy-Claudet, S., Cornou, C., Di Giuglio, G., Guiller, B., Jongmans, D., Kohler, A., Ohrnberger, M., Savvaidis, A., Roten, D., Scherbaum, F., Schissele, E., Vollmer, D., Wathelet, M., 2005. Report on FK/SPAC capabilities and limitations. In: Deliverable WP06-D19.06. University of Potsdam, Germany (43 pp).
Bonnefoy-Claudet, S., Cotton, F., Bard, P.-Y., 2006a. The nature of noise wavefield and its applications for site effects studies (a literature review). Earth-Science Rev. 79, 205–227.
Bonnefoy-Claudet, S., Cornou, C., Bard, P.-Y., Cotton, F., Moczo, P., Kristek, J., Fah, D., 2006b. H/V ratio: a tool for site effects evaluation. Results from 1-D noise simulations. Geophys. J. Int. 167, 827–837.
Boominathan, A., Dodagoudar, G., Suganthi, A., Maheswari, R., 2008. Seismic hazard assessment of Chennai city considering local site effects. J. Earth Syst. Sci. 117, 853–863.
Booth, E., Pappin, J., Mills, J., Degg, M., Steedman, R., 1986. The Mexican earthquake of 19th September 1985. In: A field report by EEFIT. Institution of Structural Engineers.
Brebbia, C., Beskos, D., Kausel, E., 1996. The Kobe Earthquake: Geodynamical Aspects. Computational Mechanics Publications, Southampton.
Building Seismic Safety Council, 2001. NEHRP recommended provisions for seismic regulations for new buildings and other structures 2000 edition, part 1: provisions. In: Report no. FEMA 368. Building seismic safety council for the federal emergency management agency, Washington, DC, USA.
Castellaro, S., Mulargia, F., 2009. Vs30 estimates using constrained H/V measurements. Bull. Seismol. Soc. Am. 99 (2A), 761–773. http://dx.doi.org/10.1785/0120080179.
Celerier, J., Sandiford, M., Hansen, D., Quigley, M., 2005. Modes of active intraplate deformation, flinders ranges, Australia. Tectonics 24 (TC6006), 1–17.
Claprood, M., 2012. Spatially averaged coherency spectrum (SPAC) ambient noise array method. In: Hunter, J.A., Crow, H.L. (Eds.), Shear Wave Velocity Measurement Guidelines for Canadian Seismic Site Characterization in Soil and Rock. 7078. Geological Survey of Canada, pp. 94–102 Open File.
Collins, C., Kayen, R., Carkin, B., Allen, T., Cummins, P., McPherson, A., 2006. Shear wave velocity measurement at Australian ground motion seismometer sites by the spectral analysis of surface waves (SASW) method. In: Proc. Earthquake Engineering in Australia, Canberra, pp. 173–178.
Cox, J., 1970. A review of the geotechnical characteristics of the soils in the Adelaide City area. In: Proc. of Symp. on Soils and Earth Structures in Arid Climates. Inst. of Engineers Australia and Australian Geomechanics Society, Adelaide, pp. 72–86.
Crone, A., Machette, M., Bowman, J., 1997. Episodic nature of earthquake activity in stable continental regions revealed by palaeoseismicity studies of Australian and north American quaternary faults. Aust. J. Earth Sci. 44 (2), 203–214.
D'Amico, V., Picozzi, M., Albarello, D., Naso, G., Tropenscovino, S., 2004. Quick estimates of soft sediment thicknesses from ambient noise horizontal to vertical spectral ratios: a case study in southern Italy. J. Earthq. Eng. 8 (6), 895–908.
Del Gaudio, V., 2017. Instantaneous polarization analysis of ambient noise recordings in site response investigations. Geophys. J. Int. 210, 443–464. http://dx.doi.org/10.1093/gji/ggx175.
Del Gaudio, V., Muscillo, S., Wasowski, J., 2014. What we can learn about slope response to earthquakes from ambient noise analysis: an overview. Eng. Geol. 182, 182–200. http://dx.doi.org/10.1016/j.enggeo.2014.05.010.
Delgado, J., Casado, C., Giner, J., Estevez, A., Cuenca, A., Molina, S., 2000. Microtremors as a geophysical exploration tool: application and limitations. Pure and Appl. Geophys. 157, 1445–1462.
Di Giulio, G., Cornou, C., Ohrnberger, M., Wathelet, M., Rovelli, A., 2006. Deriving wavefield characteristics and shear-velocity profiles from two-dimensional small-aperture arrays analysis of ambient vibrations in a small-size alluvial basin, Colfiorito. Italy. Bull. Seismol. Soc. Am. 96, 1915–1933.
Di Giulio, G., Gaudiosi, I., Cara, F., Milana, G., Tallini, M., 2014. Shear-wave velocity profile and seismic input derived from ambient vibration array measurements: the case study of downtown L'Aquila. Geophys. J. Int. 198, 848–866. http://dx.doi.org/10.1093/gji/ggu162.
Di Stefano, P., Luzio, D., Renda, P., Martorana, R., Capizzi, P., D'Alessandro, A., Messina,

N., Napoli, G., Todaro, S., Zarcone, G., 2014. Integration of HVSR measures and stratigraphic constraints for seismic microzonation studies: the case of Oliveri (ME). Nat. Hazards Earth Syst. Sci. 2, 2597–2637.
Dinesh, B., Nair, G., Prasad, A., Nakkeeran, P., Radhakrishna, M., 2010. Estimation of sedimentary layers shear wave velocity using micro-tremor H/V ratio measurements for Bangalore city. Soil Dyn. Earthq. Eng. 30, 1377–1382.
Dyster, T., 1996. Strong shock of earthquake: the strong of the four greatest earthquakes in the history of South Australia. In: Report Book 95/47. Department of Mines and Energy, Geology Survey of South Australia.
Estrada, G., 2010. Analysis of earthquake site response and site classification for seismic design practices. In: 5th Int. Conf. on Recent Advances in Geotechnical Earthquake Engineering and Soil Dynamics and Symposium in Honor of Professor I. M. Idriss, (San Diego, California). http://scholarsmine.mst.edu/icrageesd/05icrageesd/session06b/4.
García-Jerez, A., Piña-Flores, J., Sánchez-Sesma, F.J., Luzón, F., Perton, M., 2016. A computer code for forward calculation and inversion of the HVSR spectral ratio under the diffuse field assumption. Comput. Geosci. 97, 67–78.
Geopsy, 2015. Geopsy Home: Software Applications for Ambient Vibration. http://www.geopsy.org (accessed 1/12/2015).
Goldstein, P., Dodge, D., Firpo, M., Minner, L., 2003. SAC2000: signal processing and analysis tools for seismologists and engineers. Int. Geophysics 81 (2), 1613–1614.
Gosar, A., 2007. Microtremor HVSR study for assessing site effects in the Bovec basin (NW Slovenia) related to 1998 Mw5.6 and 2004 Mw5.2 earthquakes. Eng. Geol. 91, 178–193.
Graves, R., Pitarka, A., Somerville, P., 1998. Ground motion amplification in the Santa Monica area: effects of shallow basin edge structure. Bull. Seismol. Soc. Am. 88, 1224–1242.
Greenhalgh, S., Love, D., Malpas, K., McDougall, R., 1994. South Australian earthquakes, 1980-92. Aust. J. Earth Sci. 41 (5), 483–495.
Gueguen, P., Chatelain, J.-L., Guilier, B., Yepes, H., Egred, J., 1998. Site effect and damage distribution in Pujili (Ecuador) after the 28 March earthquake. Soil Dyn. Earthq. Eng. 17, 329–334.
Guo, Z., Aydin, A., 2016. A modified HVSR method to evaluate site effect in Northern Mississippi considering ocean wave climate. Eng. Geol. 200, 104–113.
Guo, A., Aydin, A., Kuszmaul, J., 2014. Microtremor recordings in Northern Mississippi. Eng. Geol. 179, 146–157.
Hillis, R., Sandiford, M., Reynolds, S., Quigley, M., 2008. Present-day stresses, seismicity and Neogene-to-recent tectonics of Australia's 'passive' margins: intraplate deformation controlled by plate boundary forces. In: Johnson, H., Dore, A., Gatliff, R., Holdsworth, R., Lundin, E., Ritchie, J. (Eds.), The Nature and Origin of Compression in Passive Margins. 306. Geological Society, London, Special Publications, pp. 71–90.
Hinzen, K., Weber, B., Scherbaum, F., 2004. On the resolution of H/V measurements to determine sediment thickness, a case study across a normal fault in the Lower Rhine embayment, Germany. J. Earthq. Eng. 8 (6), 909–926.
Ibs-Von Seht, M., Wohlenberg, J., 1999. Microtremor measurements used to map thickness of soft sediments. Bull. Seismol. Soc. Am. 89, 250–259.
Johnston, A., 1996a. Seismic moment assessment of earthquakes in stable continental regions-I. Instrumental seismicity. Geophys. J. Int. 124, 381–414.
Johnston, A., 1996b. Seismic moment assessment of earthquakes in stable continental regions-III. New Madrid 181 1-1812, Charleston 1886 and Lisbon 1755. Geophys. J. Int. 126, 314–344.
Kanay, K., Tanaka, T., 1961. On microtremors VIII. Bul. Earthquake Res. Inst. 97–114.
Kramer, S., 1996. Geotechnical Earthquake Engineering. Prentice Hall, Upper Saddle River, New Jersey.
Lane, J., White, E., Steele, G., Cannia, J., 2008. Estimation of bedrock depth using the horizontal-to-vertical (H/V) ambient-noise seismic method. In: Proc. of Symp. on the Application of Geophysics to Engineering and Environmental Problems, April 6–10, 2008, Philadelphia, Pennsylvania.
Leonard, M., 2015. Personal Communication: Preliminary Results of V_{s30} for the Adelaide Region, South Australia.
Malpas, K., 1991. Seismic Risk of South Australia. School of Earth Sciences Flinders University of South Australia.
McCue, K., 1975. Seismicity and Seismic Risk in South Australia. In: Report ADP 137. Department of Physics, University of Adelaide, South Australia.
McCue, K., 1990. Australia's large earthquakes and recent fault scarps. J. Structural Geol. 12, 761–766.
McCue, K., Gregson, P., Sinadinovski, C., Hodgson, L., 2001. Australian seismological report. In: AGSO Record 2001/28, AGSO – Geoscience Australia. Dept. of Industry, Science & Resources, Canberra (68 pp).
McPherson, A., Hall, L., 2007. Development of the Australian national regolith site classification map. In: Geoscience Australia Record 2007/07. Canberra ACT, Australia Available at: https://www.ga.gov.au/products/servlet/controller?event=GEOCAT_DETAILS&catno=65240.
Nakamura, Y., 1989. A method for dynamic characteristics estimation of subsurface using microtremor on the ground surface. Quarterly Report of the Railway Tech. Res. Inst. 30, 25–33.
Narayan, J., 2005. Study of basin-edge effects on the ground motion characteristics using 2.5-D modeling. Pure and Appl. Geophys. 162, 273–289.
Narayan, J., Rao, P., 2003. Two and half dimensional simulation of ridge effects on the ground motion characteristics. Pure and Appl. Geophys. 160, 1557–1571.
National Committee on Soil and Terrain, 2009. Australian soil and land survey field handbook. In: Australian Soil and Land Survey Handbook, Series; No. 1, 3rd ed. CSIRO Publishing, Collingwood, Victoria.
Nogoshi, M., Igarashi, T., 1971. On the amplitude characteristics of microtremor (part 2). J. Seismol. Soc. Japan 26–40.
Parolai, S., Bormann, P., Milkereit, C., 2002. New relationship between vs, thickness of sediments, and resonance frequency calculated by the H/V ratio of seismic noise for the cologne area (Germany). Bull. Seismol. Soc. Am. 92 (6), 2521–2527.
Paudyal, Y., Yatabe, R., Bhandary, N., Dahal, R., 2012a. A study of local amplification effect of soil layers on ground motion in the Katmandu Valley using microtremor analysis. J. Earthq. Eng. and Eng. Vib. 11 (2), 257–268.
Paudyal, Y., Bhandary, N., Yatabe, R., 2012b. Seismic microzonation of densely populated area of Kathmandu Valley of Nepal using microtremor observations. J. Earthq. Eng. 16 (8), 1208–1229.
Poggi, V., Fah, D., 2010. Estimating Rayleigh wave particle motion from three-component. Geophys. J. Int. 180, 251–267. http://dx.doi.org/10.1111/j.1365-246X.2009.04402.x.
Quigley, M., Sandiford, M., Fifield, K., Alimanovic, A., 2006. Bedrock erosion and relief production in the northern flinders ranges, Australia. Earth Surf. Processes and Landforms 32, 929–944.
Quigley, M., Sandiford, M., Fifield, K., Alimanovic, A., 2007. Landscape responses to intraplate tectonism: quantitative constraints from 10Be nuclide abundances. Earth Planet. Sci. Lett. 261, 120–133.
Sambridge, M., 1999. Geophysical inversion with a neighbourhood algorithm I. Searching a parameter space. Geophys. J. Int. 138, 479–494.
Sandiford, M., 2003. Neotectonics of southeastern Australia: linking the Quaternary faulting record with seismicity and in situ stress. In: Hillis, R.R., Muller, D. (Eds.), Evolution and Dynamics of the Australian Plate. 22. Geological Society of Australia Special Publication, pp. 101–113.
Sandiford, M., Wallace, M., Coblentz, D., 2004. Origin of the in situ stress field in south-eastern Australia. Basin Res. 16, 325–338.
Selby, J., Lindsay, J., 1982. Engineering geology of the Adelaide City area. Department of Mines and Energy, Geological Survey of South Australia, D. J. Woolman, (Government Printer, Bulletin 51).
SESAME, 2004. Guidelines for the implementation of the H/V spectral ratio technique on ambient vibrations Measurements, processing and interpretation. In: SESAME European Research Project Wp12 – Deliverable d23.12, European Commission – Research General Directorate, Project No. EVG1-CT-2000-00026, . http://sesame-fp5.obs.ujf-grenoble.fr.
Setiawan, B., Jaksa, M., Griffith, M., Love, D., 2018. Passive noise datasets at regolith sites. In: Data in Brief, (In print).
Sheard, M., Bowman, G., 1996. Soils, Stratigraphy and Engineering Geology of near Surface Materials of the Adelaide Plains. Department of Mines and Energy, South Australia, Adelaide.
Smith, G., 1986. Probability and Statistics in Civil Engineering: An Introduction. Collins, London.
Somerville, P., Graves, R., 1996. Site effects in the Los Angeles area during the 1994 Northridge earthquake. In: 11th World Conf. on Earthquake Engineering, Paper No. 2030.
Street, R., Woolery, E., Wang, Z., Harris, J., 2001. NEHRP soil classifications for estimating site-dependent seismic coefficients in the upper Mississippi embayment. Eng. Geol. 62, 123–135.
Tokimatsu, K., 1997. Geotechnical site characterization using surface waves. In: Proc. of 1st Int. Conf. on Earthquake Geotechnical Engineering. 3. pp. 1333–1368.
Veevers, J., 1984. Phanerozoic Earth History of Australia. Oxford University Press, New York.
Wathelet, M., Jongmans, D., Ohrnberger, M., 2004. Surface-wave inversion using direct search algorithm and its application to ambient vibration measurements. Near Surf. Geophysics 2, 211–221.
Wathelet, M., Jongmas, D., Ohremberg, M., 2005. Direct inversion of spatial autocorrelation curves with the neighborhood algorithm. Bull. Seismol. Soc. Am. 95, 1787–1800.
Wilford, J., Thomas, M., 2013. Predicting regolith thickness in the complex weathering setting of the central Mt lofty ranges, South Australia. Geoderma 206, 1–13.
Xia, J., Miller, R., Park, C., Ivanov, J., 2000. Construction of 2D vertical shear-wave velocity field by the multichannels analysis of surface waves technique. In: Proc. of Symp. on the Application of Geophysics to Engineering and Environmental Problems, 1197–1206, Arlington, VA., USA.

INTENTIONALLY BLANK

Appendix E:

FIELD SURVEY DATA SHEETS

INTENTIONALLY BLANK

PROJECT NAME: **Quantyfying the seismic and site amplification characteristics of Adelaide's regolith**

LOCATION: **Adelaide, South Australia**

DATE : **16/06/2015**	HOUR: **11:45 AM**	PLACE : **Adelaide, South Australia**	
OPERATOR : **D. Love & B. Setiawan**		GPS TYPE and # **Digital Satellite GPS**	
LATITUDE: **-34.902**	LONGITUDE: **138.592**	ALTITUDE: **-**	

STATION TYPE: **TEMPORAL STATION**	SENSOR TYPE: **SEISMOMETER LE-3Dlite LENNARTZ**
STATION#: **LOCATION #01**	SENSOR#: **BOX 3, BOX 6 & BOX 7** DISK#: **BOX 3, BOX 6 & BOX 7**
FILE NAME: **BOX 3, BOX 6 & BOX 7**	POINT# **near Barton Terrace West**
GAIN: **-** SAMPLE FREQ.: **100Hz Filltered**	REC. DURATION: **At least 2 hours**

WEATHER CONDITIONS

WIND [X] none [ ] weak [ ] medium [ ] strong Measurement (if any): _____

RAIN [X] none [ ] weak [ ] medium [ ] strong Measurement (if any): _____

TEMPERATURE (APPROX) **16** °C Remarks _____

GROUND TYPE

[X] earth (HARD / ~~SOFT~~) [ ] gravel [ ] sand [X] grass (SHORT / ~~TALL~~)

[ ] asphalt [ ] cement [ ] concrete [ ] paved [ ] other _____

[X] dry soil [ ] wet soil Remarks: _____

ARTIFICIAL GROUND-SENSOR COUPLING [X] no [ ] yes, type: _____

BUILDING DENSITY [X] none [ ] scattered [ ] dense [ ] other, type: **Park Land**

TRANSIENTS

	none	few	moderate	many	very dense	distance
cars			X			~80m
trucks		X				~80m
pedestrians	X					
other						
-type of other:						

MONOCROMATIC NOISE SOURCES
(factories, works, pumps, rivers,…)
[ ] no [X] yes, type: **water pump**

NEARBY STRUCTURES (trees, polls,builings, bridges underground structures, …)
(description, height, distance)
BOX 7 is about 80 m from Aquatic centre (pump station???)

OBSERVATIONS:

N W E S

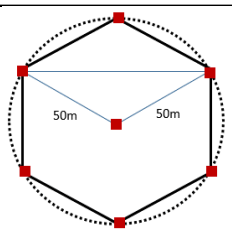

FREQUENCY: - Hz
(if computed in the field)

PROJECT NAME: **Quantyfying the seismic and site amplification characteristics of Adelaide's regolith**

LOCATION: **Adelaide, South Australia**

DATE :	**02/07/2015**	HOUR: **13:00 PM**	PLACE : **Adelaide, South Australia**
OPERATOR :	**D. Love & B. Setiawan**		GPS TYPE and # **Digital Satellite GPS**
LATITUDE:	**-34.906**	LONGITUDE: **138.602**	ALTITUDE: **-**

STATION TYPE: **TEMPORAL STATION**	SENSOR TYPE: **SEISMOMETER LE-3Dlite LENNARTZ**
STATION#: **LOCATION #02**	SENSOR#: **BOX 3, BOX 6 & WOM 3** DISK#: **BOX 3, BOX 6 & WOM 3**
FILE NAME: **BOX 3, BOX 6 & WOM 3**	POINT# **near Lefevre Terrace**
GAIN: **-** SAMPLE FREQ.: **100Hz Filltered**	REC. DURATION: **At least 2 hours**

WEATHER CONDITIONS

WIND [X] none [X] weak [ ] medium [ ] strong Measurement (if any): _____

RAIN [X] none [ ] weak [ ] medium [ ] strong Measurement (if any): _____

TEMPERATURE (APPROX) **17** °C Remarks _____

GROUND TYPE

[X] earth (HARD / ~~SOFT~~) [ ] gravel [ ] sand [X] grass (SHORT / ~~TALL~~)

[ ] asphalt [ ] cement [ ] concrete [ ] paved [ ] other _____

[X] dry soil [ ] wet soil Remarks: _____

ARTIFICIAL GROUND-SENSOR COUPLING [X] no [ ] yes, type: _____

BUILDING DENSITY [X] none [ ] scattered [ ] dense [ ] other, type: **Park Land**

TRANSIENTS

	none	few	moderate	many	very dense	distance
cars			X			~50m
trucks		X				~50m
pedestrians	X	X				~10m
other						
-type of other:						

MONOCROMATIC NOISE SOURCES
(factories, works, pumps, rivers,…)
[X] no [ ] yes, type: _____

NEARBY STRUCTURES (trees, polls,builings, bridges underground structures, …)
(description, height, distance)
BOX 3 & WOM 3 are about 3-5 m from tall trees.

OBSERVATIONS:

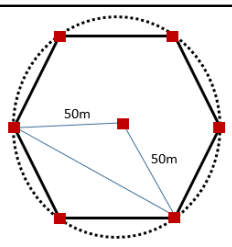

FREQUENCY: **-** Hz
(if computed in the field)

PROJECT NAME: **Quantyfying the seismic and site amplification characteristics of Adelaide's regolith**

LOCATION: **Adelaide, South Australia**

DATE : **18/07/2015**	HOUR: **09:10 AM**	PLACE : **Adelaide, South Australia**	
OPERATOR : **B. Setiawan**		GPS TYPE and # **Digital Satellite GPS**	
LATITUDE: **-34.907**	LONGITUDE: **138.592**	ALTITUDE: **-**	
STATION TYPE: **TEMPORAL STATION**		SENSOR TYPE: **SEISMOMETER LE-3Dlite LENNARTZ**	
STATION#: **LOCATION #03**		SENSOR#: **BOX 3** DISK#: **BOX 3**	
FILE NAME: **BOX 3**		POINT# **Wellington Square**	
GAIN: **-**	SAMPLE FREQ.: **100Hz Filltered**	REC. DURATION: **At least 2 hours**	

WEATHER CONDITIONS

WIND [X] none [ ] weak [ ] medium [ ] strong Measurement (if any): _____

RAIN [X] none [ ] weak [ ] medium [ ] strong Measurement (if any): _____

TEMPERATURE (APPROX) **10** °C Remarks _____

GROUND TYPE

[ ] earth (HARD / ~~SOFT~~) [ ] gravel [ ] sand [ ] grass (SHORT / ~~TALL~~)

[X] asphalt [ ] cement [ ] concrete [ ] paved [ ] other _____

[ ] dry soil [ ] wet soil Remarks: _____

ARTIFICIAL GROUND-SENSOR COUPLING [X] no [ ] yes, type: _____

BUILDING DENSITY [X] none [ ] scattered [ ] dense [ ] other, type: **Park Land**

TRANSIENTS

	none	few	moderate	many	very dense	distance
cars			X			~50m
trucks		X				~50m
pedestrians	X	X				~5m
other						
-type of other:						

MONOCROMATIC NOISE SOURCES
(factories, works, pumps, rivers,…)
[X] no [ ] yes, type: _____

NEARBY STRUCTURES (trees, polls,builings, bridges underground structures, …)
(description, height, distance)

OBSERVATIONS:

FREQUENCY: **-** Hz
(if computed in the field)

PROJECT NAME: **Quantyfying the seismic and site amplification characteristics of Adelaide's regolith**

LOCATION: **Adelaide, South Australia**

DATE :	**18/06/2015**	HOUR: **13:30 PM**	PLACE : **Adelaide, South Australia**
OPERATOR :	**D. Love & B. Setiawan**		GPS TYPE and # **Digital Satellite GPS**
LATITUDE:	**-34.909**	LONGITUDE: **138.608**	ALTITUDE: **-**

STATION TYPE: **TEMPORAL STATION**	SENSOR TYPE: **SEISMOMETER LE-3Dlite LENNARTZ**
STATION#: **LOCATION #04**	SENSOR#: **BOX 3, BOX 6 & WOM 4** DISK#: **BOX 3, BOX 6 & WOM 4**
FILE NAME: **BOX 3, BOX 6 & WOM 4**	POINT# **near Finnis Street**
GAIN: **-** SAMPLE FREQ.: **100Hz Filltered**	REC. DURATION: **At least 2 hours**

WEATHER CONDITIONS

WIND [X] none [X] weak [ ] medium [ ] strong Measurement (if any): _____

RAIN [X] none [X] weak [ ] medium [ ] strong Measurement (if any): _____

TEMPERATURE (APPROX) **16** °C Remarks _____

GROUND TYPE

[X] earth (HARD / ~~SOFT~~) [ ] gravel [ ] sand [X] grass (SHORT / ~~TALL~~)

[ ] asphalt [ ] cement [ ] concrete [ ] paved [ ] other _____

[X] dry soil [ ] wet soil Remarks: _____

ARTIFICIAL GROUND-SENSOR COUPLING [X] no [ ] yes, type: _____

BUILDING DENSITY [X] none [ ] scattered [ ] dense [ ] other, type: **Park Land**

TRANSIENTS

	none	few	moderate	many	very dense	distance
cars			X			~40m
trucks	X					~40m
pedestrians	X	X				
other						
-type of other:						

MONOCROMATIC NOISE SOURCES
(factories, works, pumps, rivers,…)
[X] no [ ] yes, type: _____

NEARBY STRUCTURES (description, height, distance)
(trees, polls, builings, bridges underground structures, …)

OBSERVATIONS:

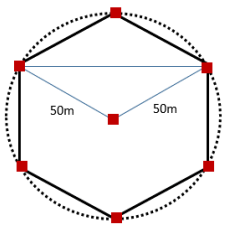

FREQUENCY: **-** Hz
(if computed in the field)

PROJECT NAME: **Quantyfying the seismic and site amplification characteristics of Adelaide's regolith**

LOCATION: **Adelaide, South Australia**

DATE : **01/07/2015**	HOUR: **11:00 AM**	PLACE : **Adelaide, South Australia**	
OPERATOR : **D. Love & B. Setiawan**		GPS TYPE and # **Digital Satellite GPS**	
LATITUDE: **-34.914**	LONGITUDE: **138.603**	ALTITUDE: **-**	
STATION TYPE: **TEMPORAL STATION**		SENSOR TYPE: **SEISMOMETER LE-3Dlite LENNARTZ**	
STATION#: **LOCATION #05**		SENSOR#: **BOX 3, BOX 6 & BOX 7** DISK#: **BOX 3, BOX 6 & BOX 7**	
FILE NAME: **BOX 3, BOX 6 & BOX 7**		POINT# **near Frome Road/ War Memorial Drive**	
GAIN: **-**	SAMPLE FREQ.: **100Hz Filltered**	REC. DURATION: **At least 2 hours**	

WEATHER CONDITIONS

WIND [X] none [ ] weak [ ] medium [ ] strong Measurement (if any): _____

RAIN [X] none [ ] weak [ ] medium [ ] strong Measurement (if any): _____

TEMPERATURE (APPROX) **14** °C Remarks _____

GROUND TYPE

[X] earth (HARD / ~~SOFT~~) [ ] gravel [ ] sand [X] grass (SHORT / ~~TALL~~)

[ ] asphalt [ ] cement [ ] concrete [ ] paved [ ] other _____

[X] dry soil [ ] wet soil Remarks: _____

ARTIFICIAL GROUND-SENSOR COUPLING [X] no [ ] yes, type: _____

BUILDING DENSITY [X] none [ ] scattered [ ] dense [ ] other, type: **Park Land**

TRANSIENTS

	none	few	moderate	many	very dense	distance
cars			X	X		~60m
trucks		X				~60m
pedestrians		X				
other						
-type of other:						

MONOCROMATIC NOISE SOURCES
(factories, works, pumps, rivers,...)
[X] no [ ] yes, type: _____

NEARBY STRUCTURES (trees, polls,builings, bridges underground structures, ...)
(description, height, distance)

OBSERVATIONS:

N
W E
S

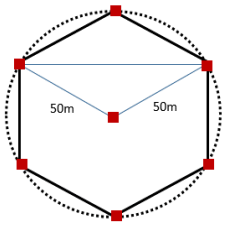

FREQUENCY: - Hz
(if computed in the field)

PROJECT NAME: **Quantyfying the seismic and site amplification characteristics of Adelaide's regolith**

LOCATION: **Adelaide, South Australia**

DATE :	**30/06/2015**	HOUR: **11:00 AM**	PLACE : **Adelaide, South Australia**
OPERATOR :	**D. Love & B. Setiawan**		GPS TYPE and # **Digital Satellite GPS**
LATITUDE:	**-34.923**	LONGITUDE: **138.585**	ALTITUDE: **-**

STATION TYPE: **TEMPORAL STATION**	SENSOR TYPE: **SEISMOMETER LE-3Dlite LENNARTZ**
STATION#: **LOCATION #06**	SENSOR#: **BOX 3, BOX 5 & BOX 7** DISK#: **BOX 3, BOX 5 & BOX 7**
FILE NAME: **BOX 3, BOX 5 & BOX 7**	POINT# **near West Terrace/ Port Road**
GAIN: **-** SAMPLE FREQ.: **100Hz Filltered**	REC. DURATION: **At least 2 hours**

WEATHER CONDITIONS

WIND [X] none [ ] weak [ ] medium [ ] strong Measurement (if any): _____

RAIN [X] none [ ] weak [ ] medium [ ] strong Measurement (if any): _____

TEMPERATURE (APPROX) **16** °C Remarks _____

GROUND TYPE

[X] earth (HARD / ~~SOFT~~) [ ] gravel [ ] sand [X] grass (SHORT / ~~TALL~~)

[ ] asphalt [ ] cement [ ] concrete [ ] paved [ ] other _____

[X] dry soil [ ] wet soil Remarks: _____

ARTIFICIAL GROUND-SENSOR COUPLING [X] no [ ] yes, type: _____

BUILDING DENSITY [X] none [ ] scattered [ ] dense [ ] other, type: **Park Land**

TRANSIENTS

	none	few	moderate	many	very dense	distance
cars				X		~60m
trucks		X	X			~60m
pedestrians	X					
other						
-type of other:						

MONOCROMATIC NOISE SOURCES
(factories, works, pumps, rivers,…)
[X] no [ ] yes, type: _____

NEARBY STRUCTURES (trees, polls,builings, bridges underground structures, …)
(description, height, distance)
New RAH Hospical was under construction. There was excavator in used during the measurement.

OBSERVATIONS:

N W E S

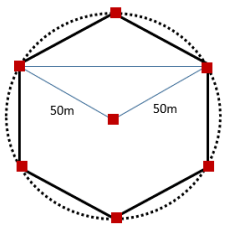

FREQUENCY: **-** Hz
(if computed in the field)

PROJECT NAME: **Quantyfying the seismic and site amplification characteristics of Adelaide's regolith**

LOCATION: **Adelaide, South Australia**

DATE :	**08/06/2015**	HOUR: **12:45 AM**	PLACE : **Adelaide, South Australia**
OPERATOR :	**D. Love & B. Setiawan**		GPS TYPE and # **Digital Satellite GPS**
LATITUDE:	**-34.926**	LONGITUDE: **138.616**	ALTITUDE: **-**

STATION TYPE: **TEMPORAL STATION**	SENSOR TYPE: **SEISMOMETER LE-3Dlite LENNARTZ**
STATION#: **LOCATION #07**	SENSOR#: **BOX 3, BOX 6 & BOX 8** DISK#: **BOX 3, BOX 6 & BOX 8**
FILE NAME: **BOX 3, BOX 6 & BOX 8**	POINT# **near Bartels Road**
GAIN: **-** SAMPLE FREQ.: **100Hz Filltered**	REC. DURATION: **At least 2 hours**

WEATHER CONDITIONS

WIND [X] none [X] weak [ ] medium [ ] strong Measurement (if any): _____

RAIN [X] none [ ] weak [ ] medium [ ] strong Measurement (if any): _____

TEMPERATURE (APPROX) **16** °C Remarks _____

GROUND TYPE

[X] earth (HARD / ~~SOFT~~) [ ] gravel [ ] sand [X] grass (SHORT / ~~TALL~~)

[ ] asphalt [ ] cement [ ] concrete [ ] paved [ ] other _____

[X] dry soil [ ] wet soil Remarks: _____

ARTIFICIAL GROUND-SENSOR COUPLING [X] no [ ] yes, type: _____

BUILDING DENSITY [X] none [ ] scattered [ ] dense [ ] other, type: **Park Land**

TRANSIENTS

	none	few	moderate	many	very dense	distance
cars				X		~50m
trucks		X				~50m
pedestrians	X	X				
other						
-type of other:						

MONOCROMATIC NOISE SOURCES
(factories, works, pumps, rivers,...)
[X] no [ ] yes, type: _____

NEARBY STRUCTURES (trees, polls,builings, bridges underground structures, ...)
(description, height, distance)
Grass cutting vehicle was working around at 1:10 pm and 1:15 pm.

OBSERVATIONS:

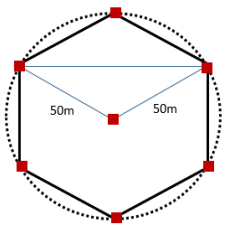

FREQUENCY: - Hz
(if computed in the field)

PROJECT NAME: **Quantyfying the seismic and site amplification characteristics of Adelaide's regolith**

LOCATION: **Adelaide, South Australia**

DATE : **19/07/2015**	HOUR: **07:10 AM**	PLACE : **Adelaide, South Australia**	
OPERATOR : **B. Setiawan**		GPS TYPE and # **Digital Satellite GPS**	
LATITUDE: **-34.929**	LONGITUDE: **138.600**	ALTITUDE: **-**	
STATION TYPE: **TEMPORAL STATION**		SENSOR TYPE: **SEISMOMETER LE-3Dlite LENNARTZ**	
STATION#: **LOCATION #08**		SENSOR#: **BOX 3** DISK#: **BOX 3**	
FILE NAME: **BOX 3**		POINT# **Victoria Square**	
GAIN: **-**	SAMPLE FREQ.: **100Hz Filltered**	REC. DURATION: **At least 2 hours**	

WEATHER CONDITIONS

WIND [X] none [ ] weak [ ] medium [ ] strong Measurement (if any): _____

RAIN [X] none [ ] weak [ ] medium [ ] strong Measurement (if any): _____

TEMPERATURE (APPROX) **5** °C Remarks _____

GROUND TYPE

[X] earth (HARD / ~~SOFT~~) [ ] gravel [ ] sand [X] grass (SHORT / ~~TALL~~)

[ ] asphalt [ ] cement [ ] concrete [ ] paved [ ] other _____

[X] dry soil [ ] wet soil Remarks: _____

ARTIFICIAL GROUND-SENSOR COUPLING [X] no [ ] yes, type: _____

BUILDING DENSITY [X] none [ ] scattered [ ] dense [ ] other, type: **Park Land**

TRANSIENTS

	none	few	moderate	many	very dense	distance
cars			X			~20m
trucks		X				~20m
pedestrians	X	X				~10m
other						
-type of other:						

MONOCROMATIC NOISE SOURCES
(factories, works, pumps, rivers,…)
[ ] no [X] yes, type: **water fountain**

NEARBY STRUCTURES (trees, polls,builings, bridges underground structures, …)
(description, height, distance)
There are a water faountain in about 15 m away.

OBSERVATIONS:

FREQUENCY: **-** Hz
(if computed in the field)

PROJECT NAME: **Quantyfying the seismic and site amplification characteristics of Adelaide's regolith**

LOCATION: **Adelaide, South Australia**

DATE : **25/06/2015**	HOUR: **11:00 AM**	PLACE : **Adelaide, South Australia**	
OPERATOR : **D. Love & B. Setiawan**		GPS TYPE and # **Digital Satellite GPS**	
LATITUDE: **-34.938**	LONGITUDE: **138.590**	ALTITUDE: **-**	
STATION TYPE: **TEMPORAL STATION**		SENSOR TYPE: **SEISMOMETER LE-3Dlite LENNARTZ**	
STATION#: **LOCATION #09**		SENSOR#: **BOX 3, BOX 8 & WOM 4** DISK#: **BOX 3, BOX 8 & WOM 4**	
FILE NAME: **BOX 3, BOX 8 & WOM 4**		POINT# **near South Terrave / West Terrace**	
GAIN: **-**	SAMPLE FREQ.: **100Hz Filltered**	REC. DURATION: **At least 2 hours**	

WEATHER CONDITIONS

WIND [X] none [X] weak [ ] medium [ ] strong Measurement (if any): _____

RAIN [X] none [ ] weak [ ] medium [ ] strong Measurement (if any): _____

TEMPERATURE (APPROX) **10** °C Remarks _____

GROUND TYPE

[X] earth (HARD / ~~SOFT~~) [ ] gravel [ ] sand [X] grass (SHORT / ~~TALL~~)

[ ] asphalt [ ] cement [ ] concrete [ ] paved [ ] other _____

[X] dry soil [ ] wet soil Remarks: _____

ARTIFICIAL GROUND-SENSOR COUPLING [X] no [ ] yes, type: _____

BUILDING DENSITY [X] none [ ] scattered [ ] dense [ ] other, type: **Park Land**

TRANSIENTS

	none	few	moderate	many	very dense	distance
cars				X		~80m
trucks		X				~80m
pedestrians						
other		X				~10m
-type of other: Jogger						

MONOCROMATIC NOISE SOURCES
(factories, works, pumps, rivers,...)
[X] no [ ] yes, type: _____

NEARBY STRUCTURES (trees, polls,builings, bridges underground structures, ...)
(description, height, distance)

OBSERVATIONS:

N
W E
S

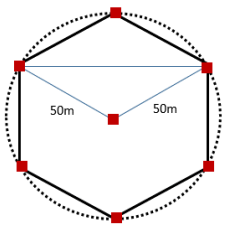

FREQUENCY: - Hz
(if computed in the field)

PROJECT NAME:	**Quantyfying the seismic and site amplification characteristics of Adelaide's regolith**		
LOCATION:	**Adelaide, South Australia**		
DATE :	**15/06/2015**	HOUR: **02:00 PM**	PLACE : **Adelaide, South Australia**
OPERATOR :	**D. Love & B. Setiawan**		GPS TYPE and # **Digital Satellite GPS**
LATITUDE:	**-34.936**	LONGITUDE: **138.612**	ALTITUDE: **-**
STATION TYPE: **TEMPORAL STATION**			SENSOR TYPE: **SEISMOMETER LE-3Dlite LENNARTZ**
STATION#: **LOCATION #10**			SENSOR#: **BOX 3, BOX 5 & Wom 3** DISK#: **BOX 3, BOX 5 & Wom 3**
FILE NAME: **BOX 3, BOX 5 & Wom 3**			POINT# **near Hutt Road / South Terrace**
GAIN: **-**	SAMPLE FREQ.: **100Hz Filltered**		REC. DURATION: **At least 2 hours**

WEATHER CONDITIONS	WIND	[X] none	[ ] weak	[ ] medium	[ ] strong	Measurement (if any):
	RAIN	[X] none	[X] weak	[ ] medium	[ ] strong	Measurement (if any):
	TEMPERATURE (APPROX) **16** °C			Remarks		
GROUND TYPE	[X] earth (HARD / ~~SOFT~~)	[ ] gravel	[ ] sand	[X] grass (SHORT / ~~TALL~~)		
	[ ] asphalt	[ ] cement	[ ] concrete	[ ] paved	[ ] other	
	[X] dry soil	[ ] wet soil	Remarks:			
ARTIFICIAL GROUND-SENSOR COUPLING	[X] no	[ ] yes, type:				
BUILDING DENSITY	[X] none	[ ] scattered	[ ] dense	[ ] other, type: **Park Land**		

TRANSIENTS	none	few	moderate	many	very dense	distance
cars				X		**~30m**
trucks		X				**~30m**
pedestrians	X					
other						
-type of other:						

MONOCROMATIC NOISE SOURCES
(factories, works, pumps, rivers,…)
[X] no [ ] yes, type:

NEARBY STRUCTURES (description, height, distance)
(trees, polls,builings, bridges underground structures, …)

OBSERVATIONS:

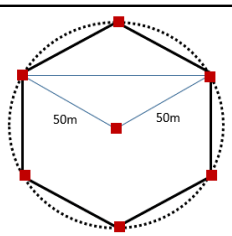

FREQUENCY: **-** Hz
(if computed in the field)

Appendix F:

INDUSTRIAL ORIGIN DETECTION RESULTS

INTENTIONALLY BLANK

<table>
<tr>
<td colspan="3"> 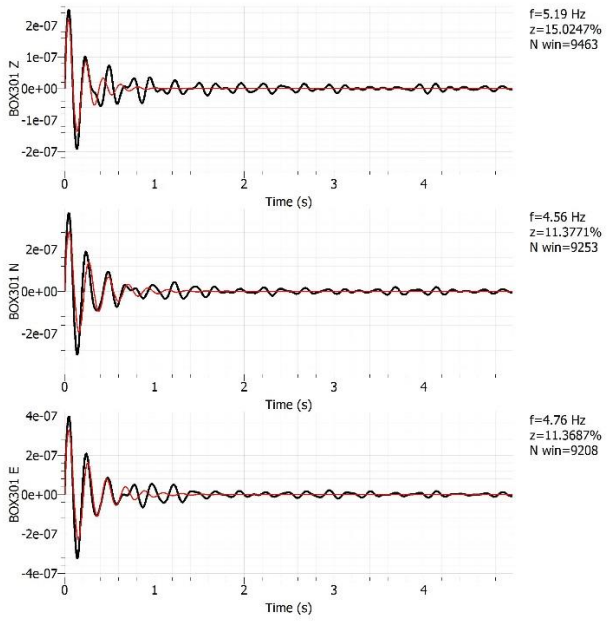
</td>
<td colspan="3"> 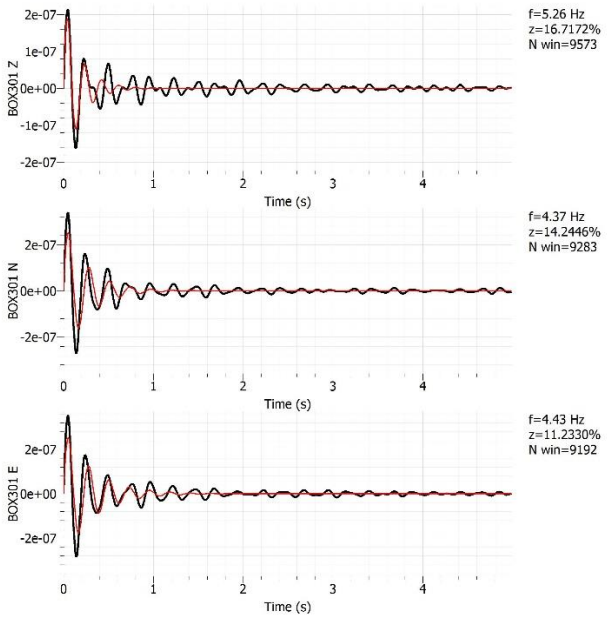
</td>
</tr>
<tr>
<td rowspan="3">Estimated damping</td><td>Up-Down</td><td>15%</td>
<td rowspan="3">Estimated damping</td><td>Up-Down</td><td>16%</td>
</tr>
<tr>
<td>North-</td><td>11%</td>
<td>North-</td><td>14%</td>
</tr>
<tr>
<td>East-West</td><td>11%</td>
<td>East-West</td><td>11%</td>
</tr>
<tr>
<td colspan="2">Sustained frequency?</td><td>No</td>
<td colspan="2">Sustained frequency?</td><td>No</td>
</tr>
<tr>
<td colspan="3">Test#a</td>
<td colspan="3">Test#b</td>
</tr>
<tr>
<td colspan="3"> 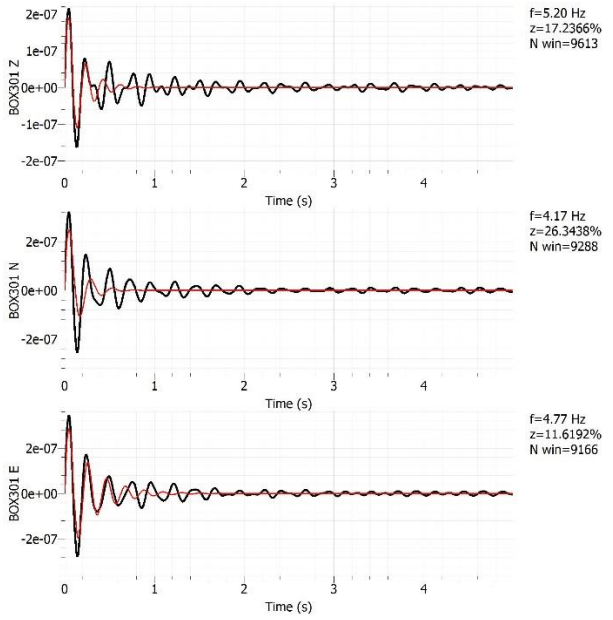
</td>
<td colspan="3"> 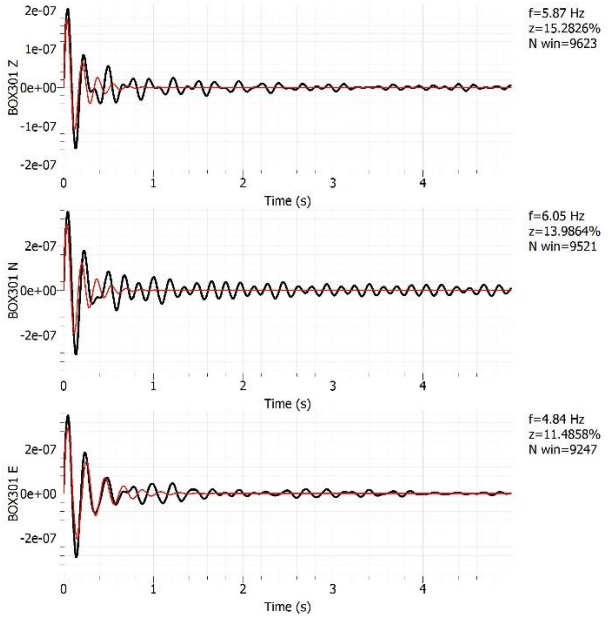
</td>
</tr>
<tr>
<td rowspan="3">Estimated damping</td><td>Up-Down</td><td>17%</td>
<td rowspan="3">Estimated damping</td><td>Up-Down</td><td>15%</td>
</tr>
<tr>
<td>North-</td><td>26%</td>
<td>North-</td><td>13%</td>
</tr>
<tr>
<td>East-West</td><td>11%</td>
<td>East-West</td><td>11%</td>
</tr>
<tr>
<td colspan="2">Sustained frequency?</td><td>No</td>
<td colspan="2">Sustained frequency?</td><td>No</td>
</tr>
<tr>
<td colspan="3">Test#c</td>
<td colspan="3">Test#d</td>
</tr>
<tr>
<td colspan="6">Industrial origin detection at Location #01</td>
</tr>
</table>

<table>
<tr>
<td> 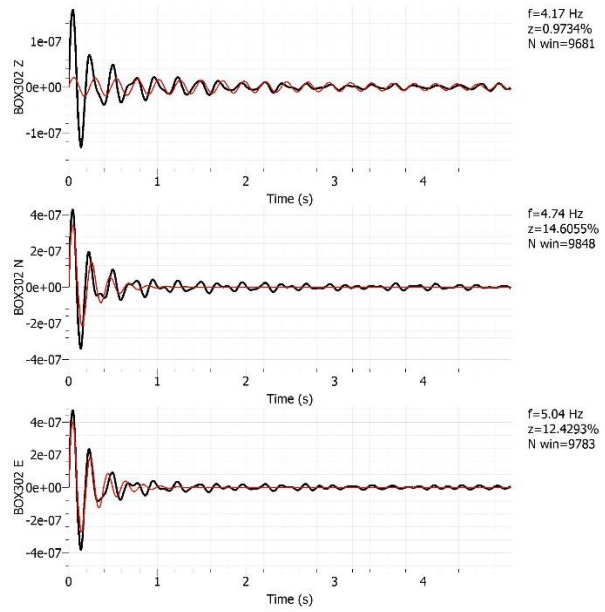
</td>
<td> 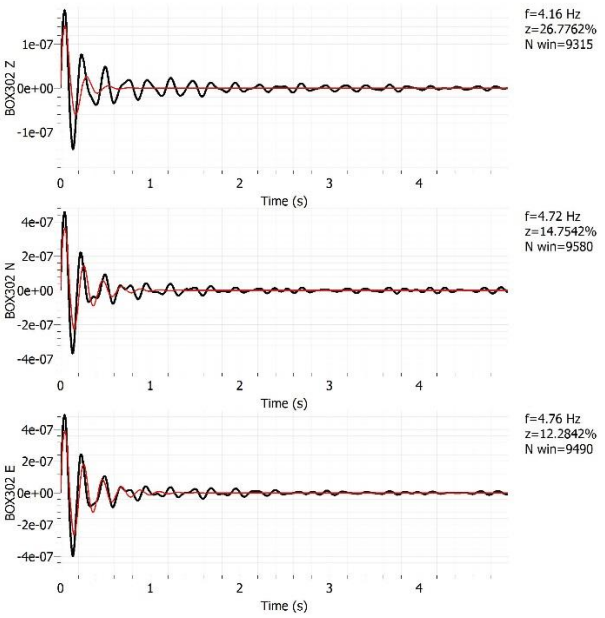
</td>
</tr>
<tr>
<td>
<table>
<tr><td rowspan="3">Estimated damping</td><td>Up-Down</td><td>0.97%</td></tr>
<tr><td>North-</td><td>15%</td></tr>
<tr><td>East-West</td><td>12%</td></tr>
<tr><td colspan="2">Sustained frequency?</td><td>No</td></tr>
</table>
</td>
<td>
<table>
<tr><td rowspan="3">Estimated damping</td><td>Up-Down</td><td>26%</td></tr>
<tr><td>North-</td><td>14%</td></tr>
<tr><td>East-West</td><td>12%</td></tr>
<tr><td colspan="2">Sustained frequency?</td><td>No</td></tr>
</table>
</td>
</tr>
<tr>
<td>Test#a</td>
<td>Test#b</td>
</tr>
<tr>
<td> 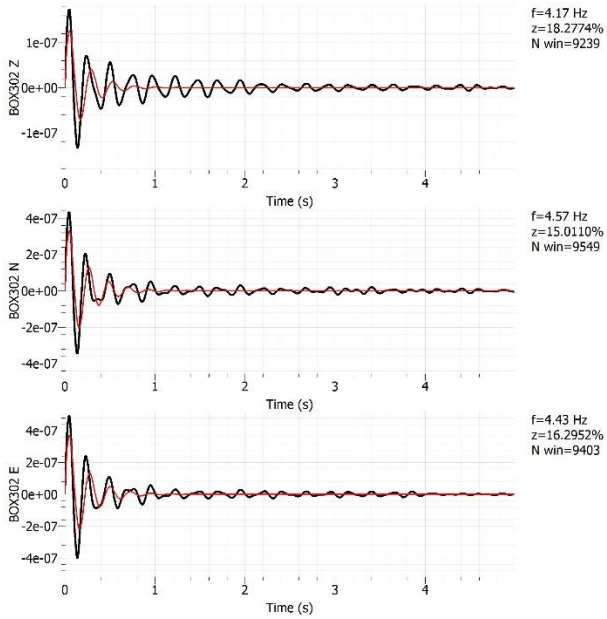
</td>
<td> 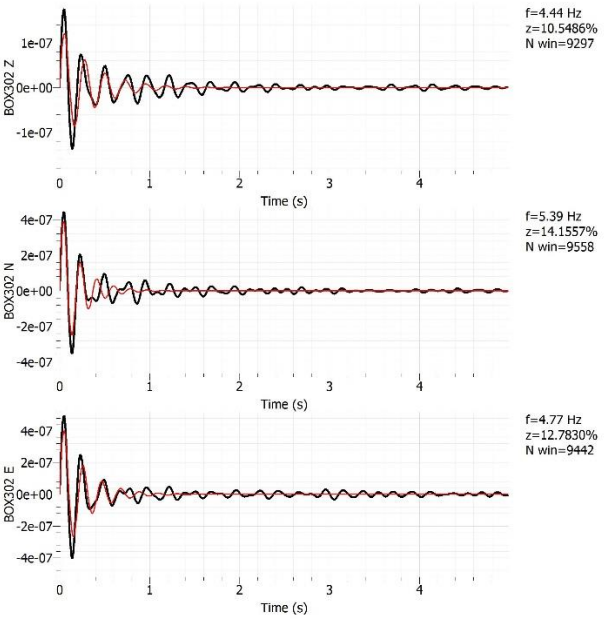
</td>
</tr>
<tr>
<td>
<table>
<tr><td rowspan="3">Estimated damping</td><td>Up-Down</td><td>18%</td></tr>
<tr><td>North-</td><td>15%</td></tr>
<tr><td>East-West</td><td>16%</td></tr>
<tr><td colspan="2">Sustained frequency?</td><td>No</td></tr>
</table>
</td>
<td>
<table>
<tr><td rowspan="3">Estimated damping</td><td>Up-Down</td><td>10%</td></tr>
<tr><td>North-</td><td>14%</td></tr>
<tr><td>East-West</td><td>12%</td></tr>
<tr><td colspan="2">Sustained frequency?</td><td>No</td></tr>
</table>
</td>
</tr>
<tr>
<td>Test#c</td>
<td>Test#d</td>
</tr>
<tr>
<td colspan="2">Industrial origin detection at Location #02</td>
</tr>
</table>

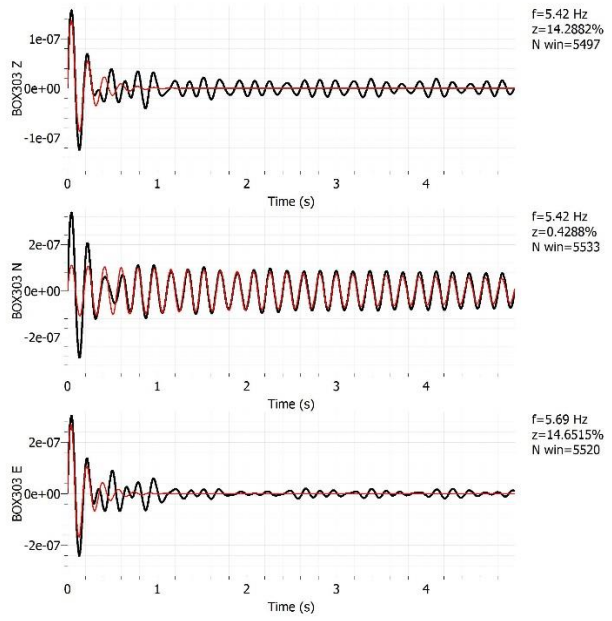

Estimated damping	Up-Down	14%
	North-	0.42%
	East-West	14%
Sustained frequency?		Yes for North-South data

Test#a

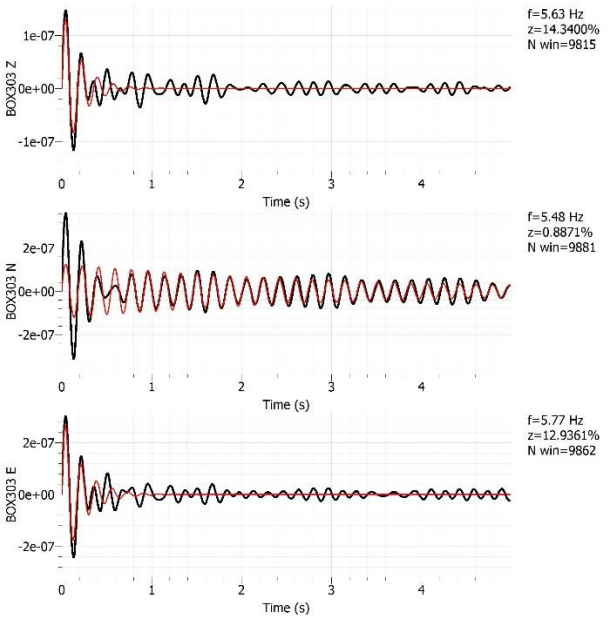

Estimated damping	Up-Down	14%
	North-	0.88%
	East-West	12%
Sustained frequency?		No

Test#b

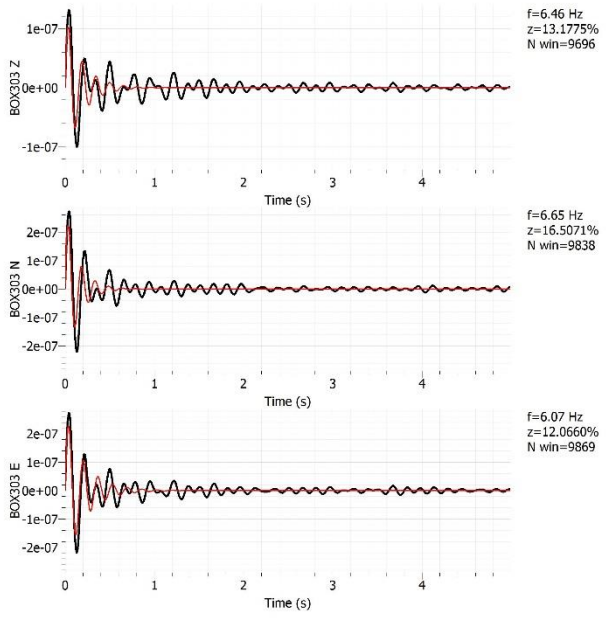

Estimated damping	Up-Down	13%
	North-	16%
	East-West	12%
Sustained frequency?		No

Test#c

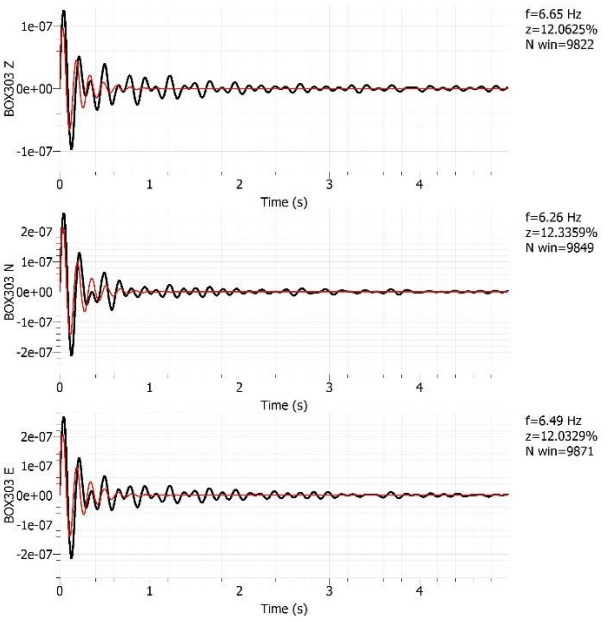

Estimated damping	Up-Down	12%
	North-	12%
	East-West	12%
Sustained frequency?		No

Test#d

Industrial origin detection at Location #03

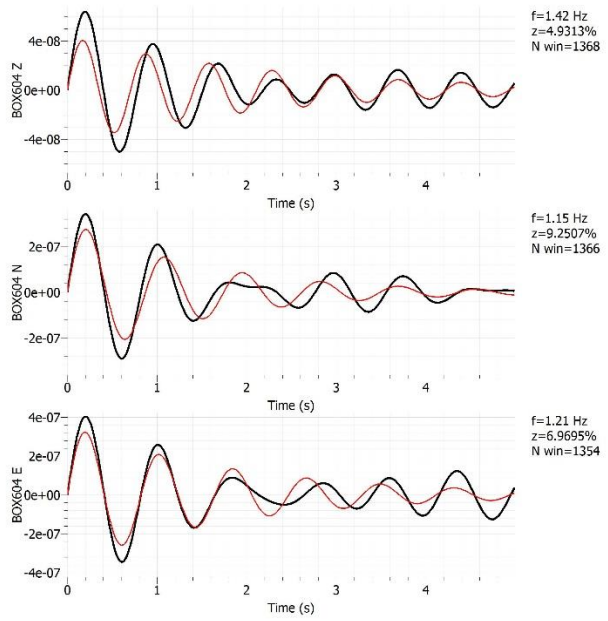

Estimated damping	Up-Down	4%
	North-	9%
	East-West	6%
Sustained frequency?		No

Test#a

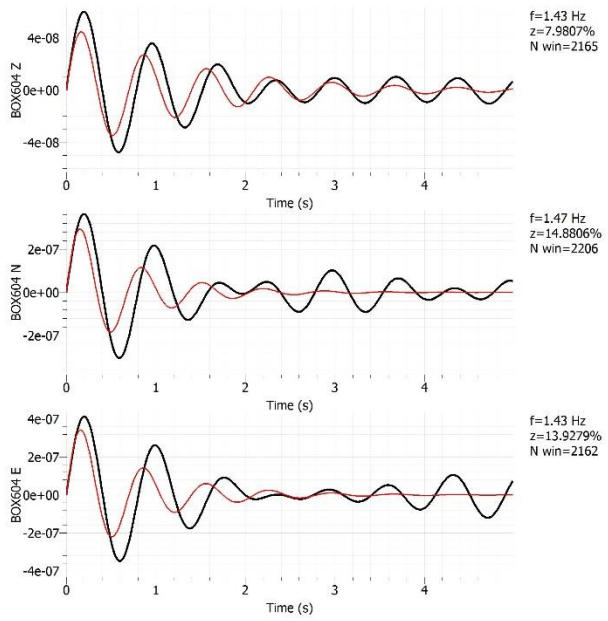

Estimated damping	Up-Down	7%
	North-	14%
	East-West	13%
Sustained frequency?		No

Test#b

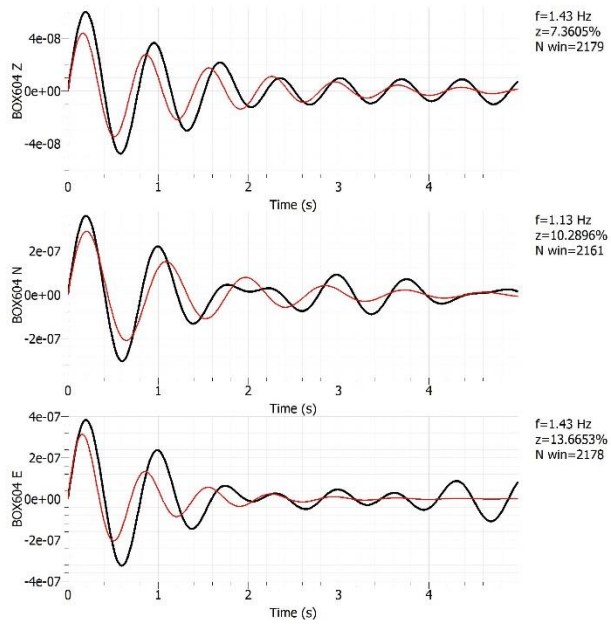

Estimated damping	Up-Down	7%
	North-	10%
	East-West	13%
Sustained frequency?		No

Test#c

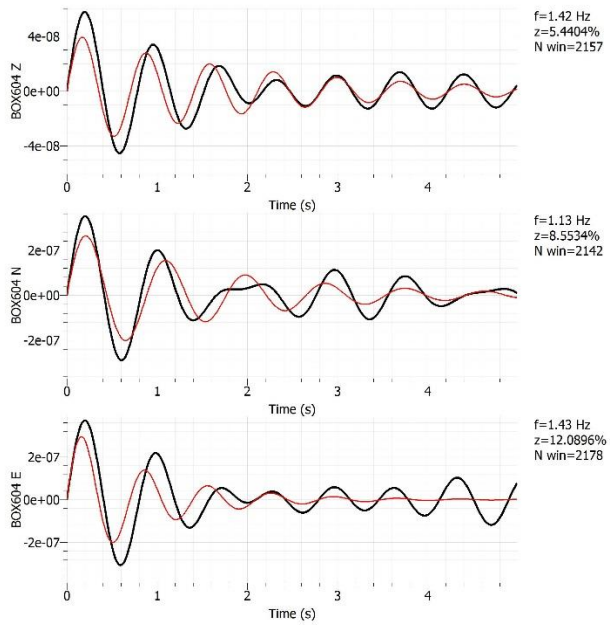

Estimated damping	Up-Down	5%
	North-	8%
	East-West	12%
Sustained frequency?		No

Test#d

Industrial origin detection at Location #04

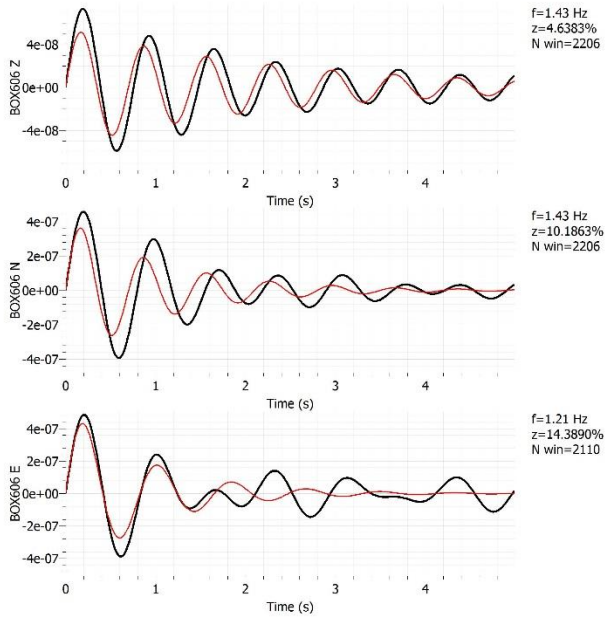

Estimated damping	Up-Down	4%
	North-	10%
	East-West	14%
Sustained frequency?		No

Test#a

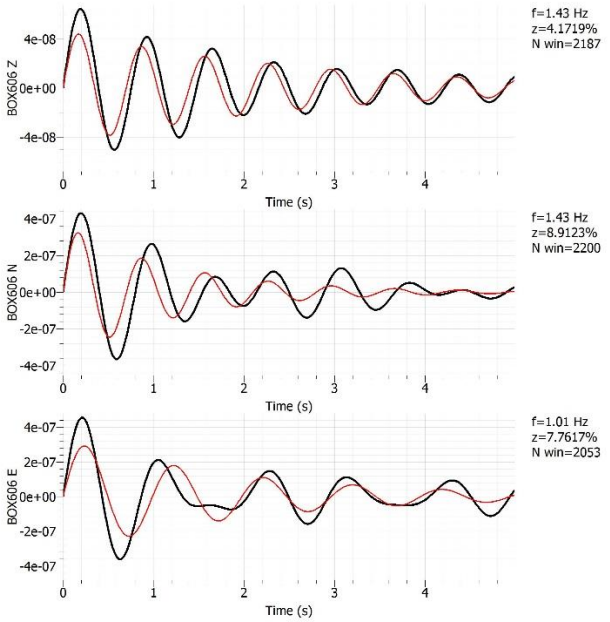

Estimated damping	Up-Down	4%
	North-	8%
	East-West	7%
Sustained frequency?		No

Test#b

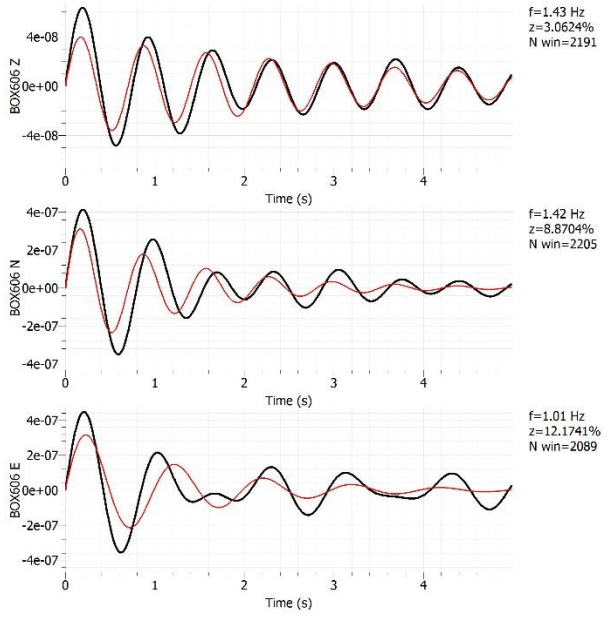

Estimated damping	Up-Down	3%
	North-	8%
	East-West	12%
Sustained frequency?		No

Test#c

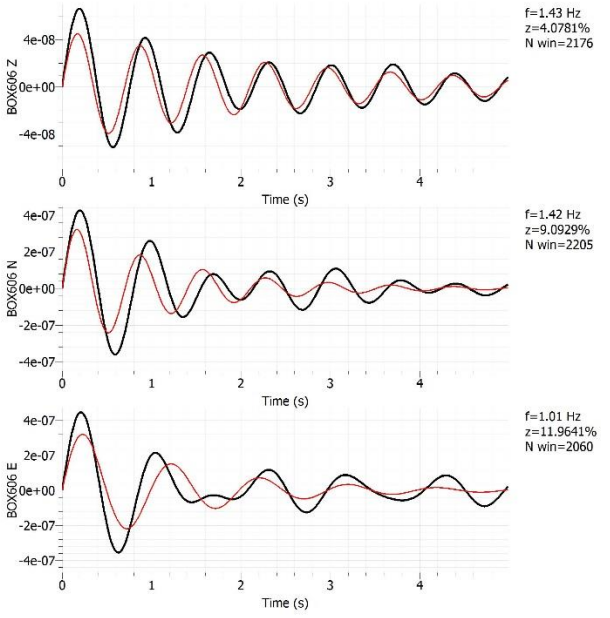

Estimated damping	Up-Down	4%
	North-	9%
	East-West	11%
Sustained frequency?		No

Test#d

Industrial origin detection at Location #05

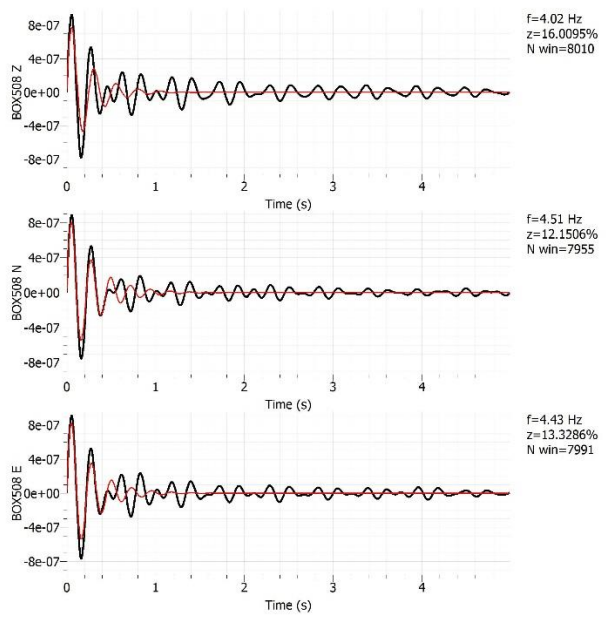

Estimated damping	Up-Down	16%
	North-	12%
	East-West	13%
Sustained frequency?		No

Test#a

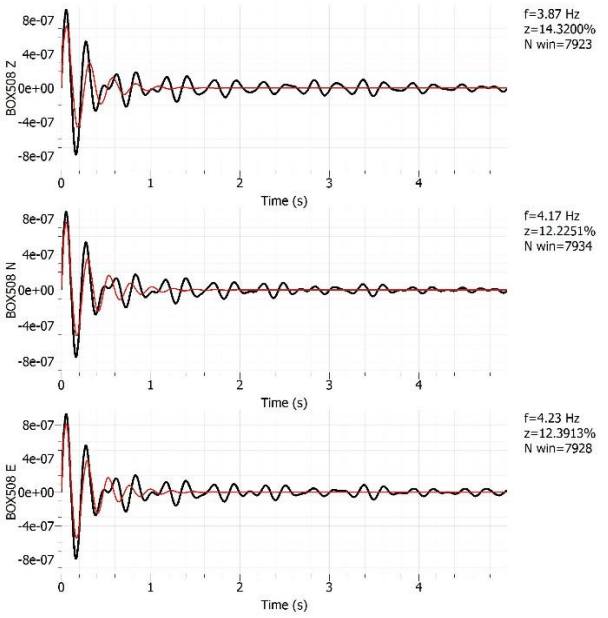

Estimated damping	Up-Down	14%
	North-	12%
	East-West	12%
Sustained frequency?		No

Test#b

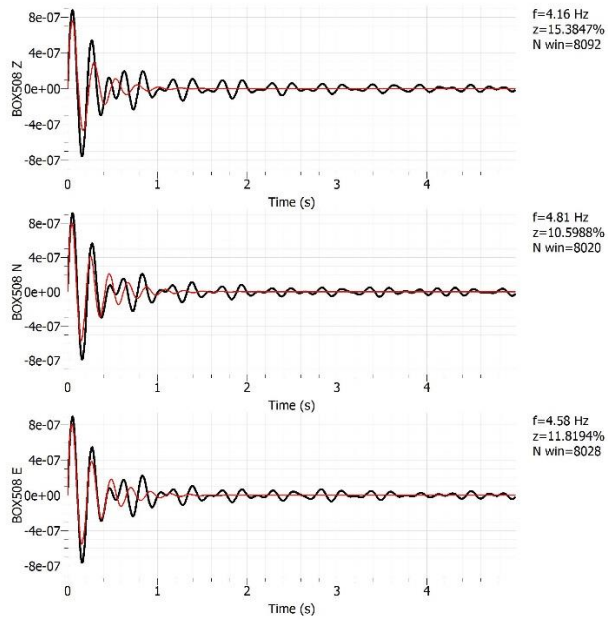

Estimated damping	Up-Down	15%
	North-	10%
	East-West	11%
Sustained frequency?		No

Test#c

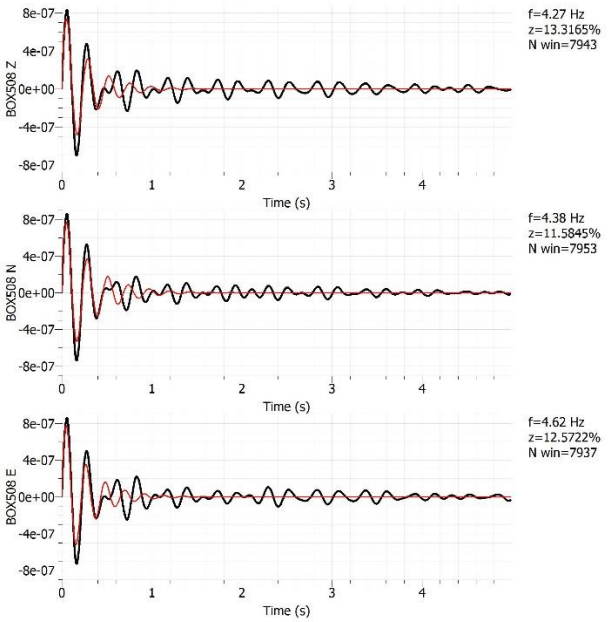

Estimated damping	Up-Down	13%
	North-	11%
	East-West	12%
Sustained frequency?		No

Test#d

Industrial origin detection at Location #06

<table>
<tr>
<td colspan="3"> 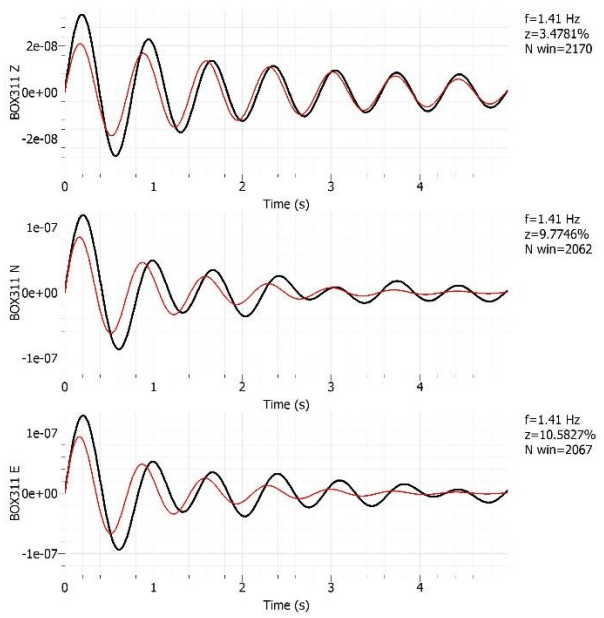
</td>
<td colspan="3"> 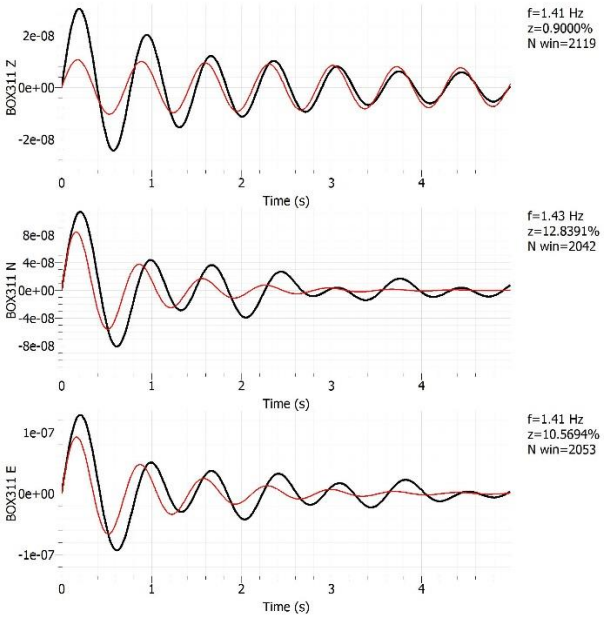
</td>
</tr>
<tr>
<td rowspan="3">Estimated damping</td><td>Up-Down</td><td>3%</td>
<td rowspan="3">Estimated damping</td><td>Up-Down</td><td>0.90%</td>
</tr>
<tr>
<td>North-</td><td>9%</td>
<td>North-</td><td>12%</td>
</tr>
<tr>
<td>East-West</td><td>10%</td>
<td>East-West</td><td>10%</td>
</tr>
<tr>
<td colspan="2">Sustained frequency?</td><td>No</td>
<td colspan="2">Sustained frequency?</td><td>No</td>
</tr>
<tr>
<td colspan="3">Test#a</td>
<td colspan="3">Test#b</td>
</tr>
<tr>
<td colspan="3"> 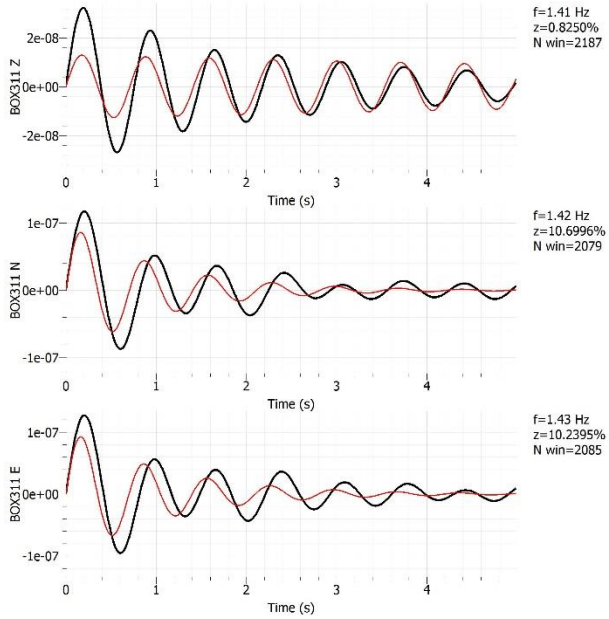
</td>
<td colspan="3"> 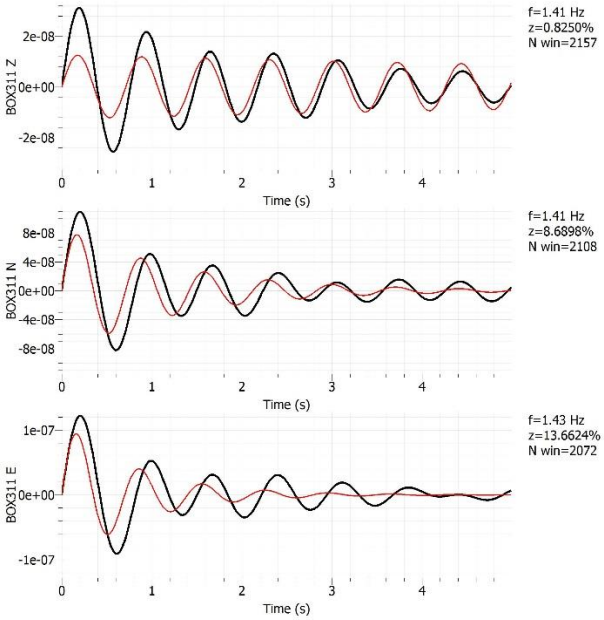
</td>
</tr>
<tr>
<td rowspan="3">Estimated damping</td><td>Up-Down</td><td>0.82%</td>
<td rowspan="3">Estimated damping</td><td>Up-Down</td><td>0.82%</td>
</tr>
<tr>
<td>North-</td><td>10%</td>
<td>North-</td><td>8%</td>
</tr>
<tr>
<td>East-West</td><td>10%</td>
<td>East-West</td><td>13%</td>
</tr>
<tr>
<td colspan="2">Sustained frequency?</td><td>No</td>
<td colspan="2">Sustained frequency?</td><td>No</td>
</tr>
<tr>
<td colspan="3">Test#c</td>
<td colspan="3">Test#d</td>
</tr>
<tr>
<td colspan="6">Industrial origin detection at Location #07</td>
</tr>
</table>

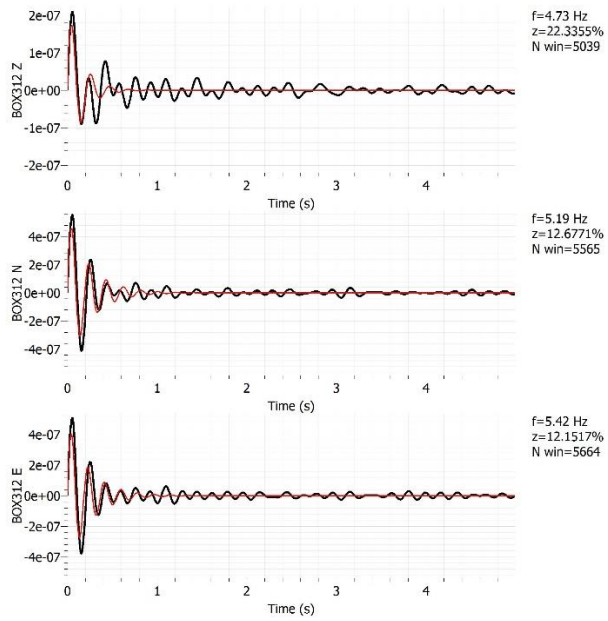

Estimated damping	Up-Down	22%
	North-	12%
	East-West	12%
Sustained frequency?		No

Test#a

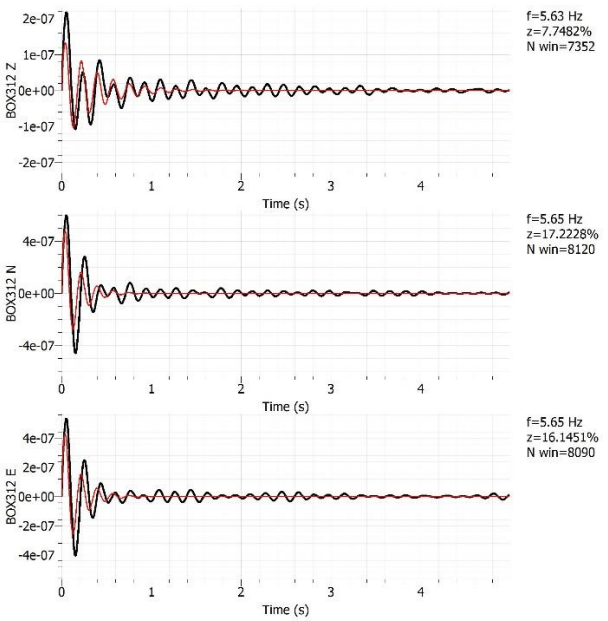

Estimated damping	Up-Down	7%
	North-	17%
	East-West	16%
Sustained frequency?		No

Test#b

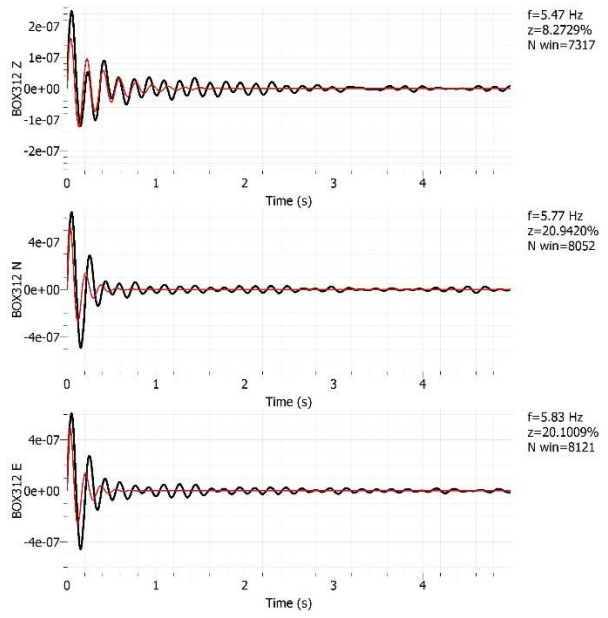

Estimated damping	Up-Down	8%
	North-	20%
	East-West	20%
Sustained frequency?		No

Test#c

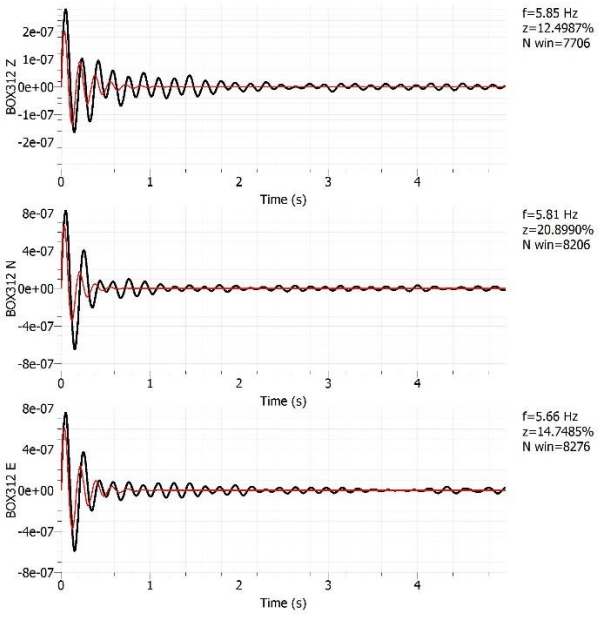

Estimated damping	Up-Down	12%
	North-	20%
	East-West	14%
Sustained frequency?		No

Test#d

Industrial origin detection at Location #08

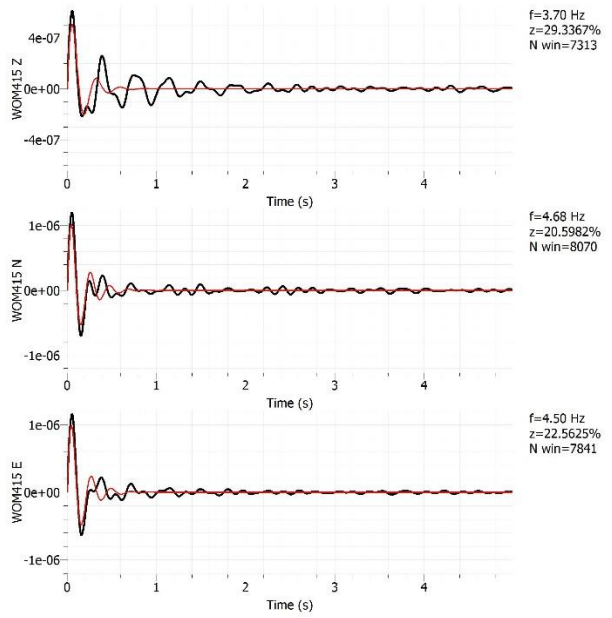

Estimated damping	Up-Down	29%
	North-	20%
	East-West	22%
Sustained frequency?		No

Test#a

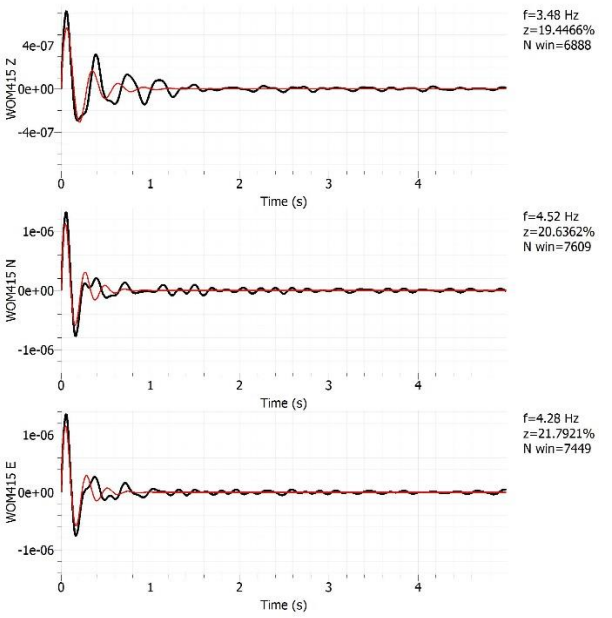

Estimated damping	Up-Down	19%
	North-	20%
	East-West	21%
Sustained frequency?		No

Test#b

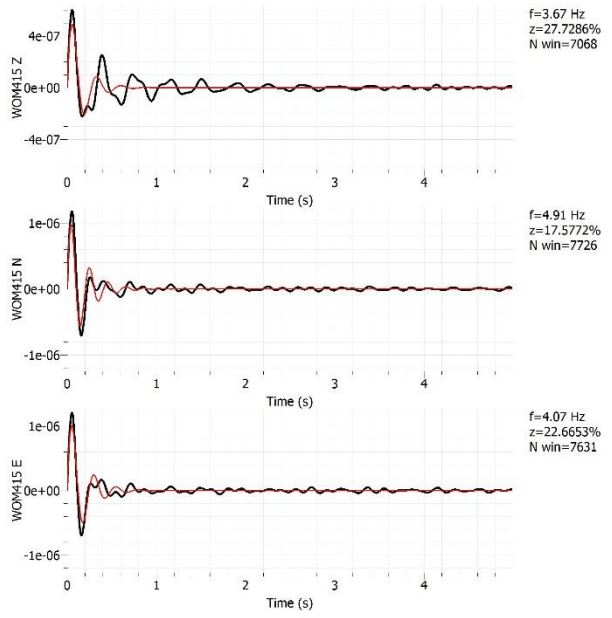

Estimated damping	Up-Down	27%
	North-	17%
	East-West	22%
Sustained frequency?		No

Test#c

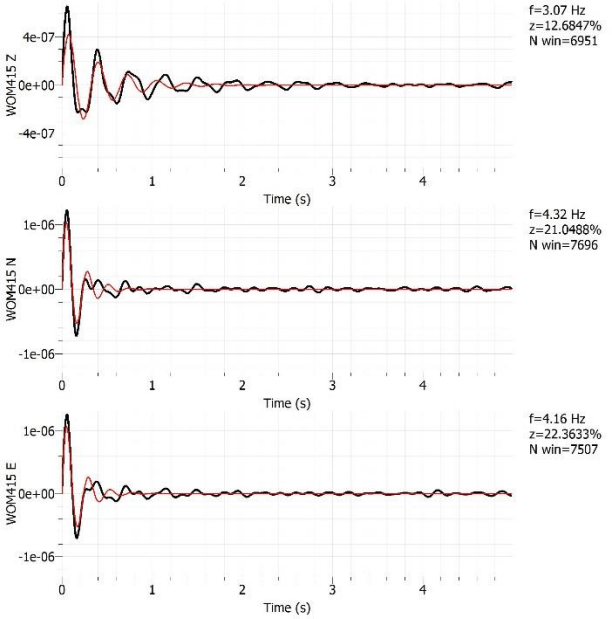

Estimated damping	Up-Down	12%
	North-	21%
	East-West	22%
Sustained frequency?		No

Test#d

Industrial origin detection at Location #09

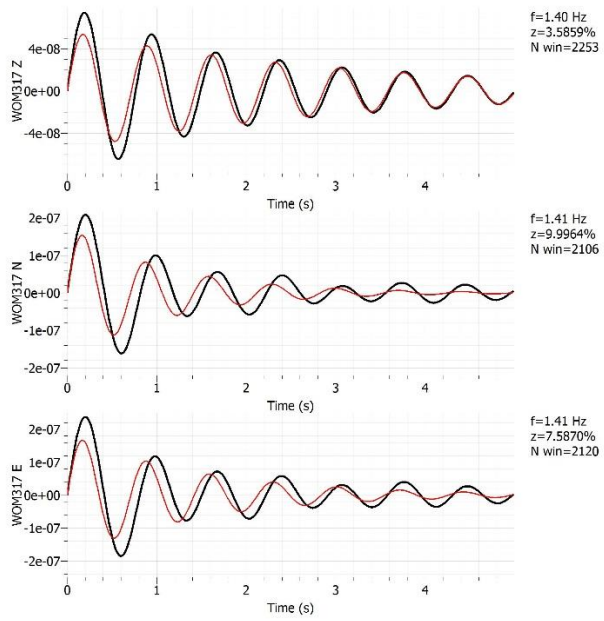

Estimated damping	Up-Down	3%
	North-	9%
	East-West	7%
Sustained frequency?		No

Test#a

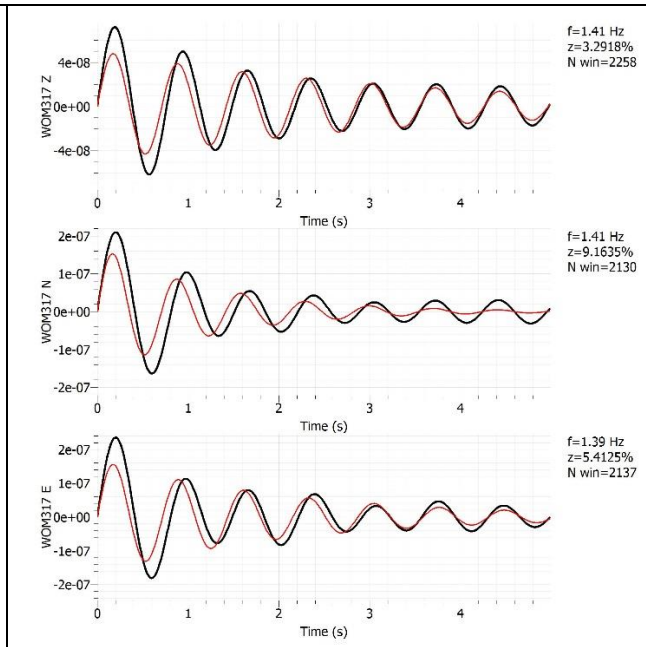

Estimated damping	Up-Down	3%
	North-	9%
	East-West	5%
Sustained frequency?		No

Test#b

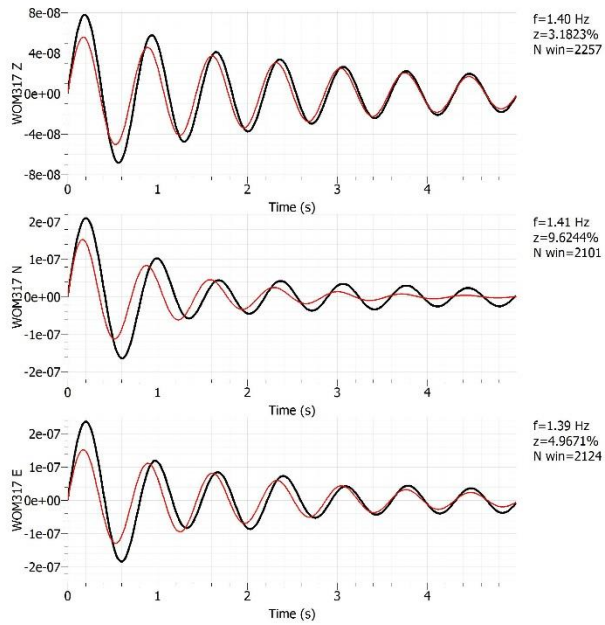

Estimated damping	Up-Down	3%
	North-	9%
	East-West	4%
Sustained frequency?		No

Test#c

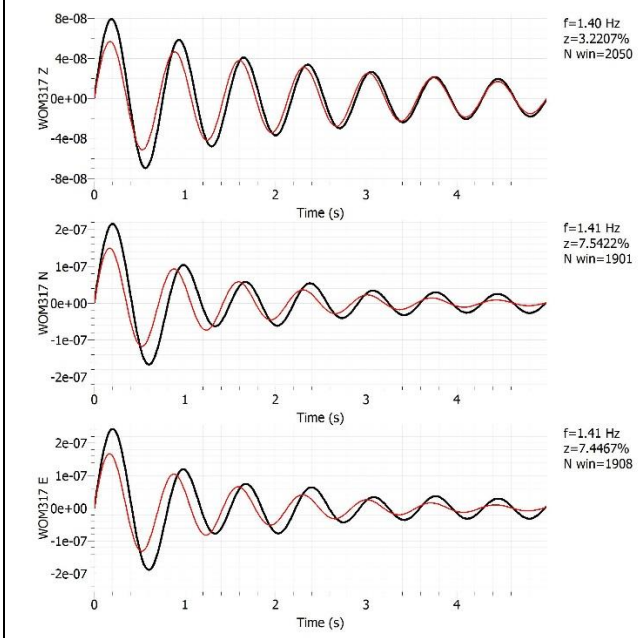

Estimated damping	Up-Down	3%
	North-	7%
	East-West	7%
Sustained frequency?		No

Test#d

Industrial origin detection at Location #10

Appendix G:

HVSR Analysis Curves

INTENTIONALLY BLANK

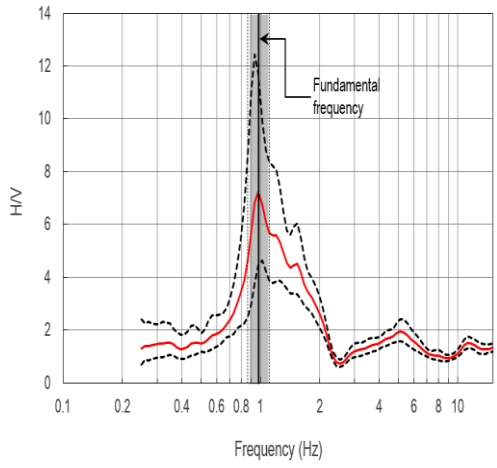

Fundamental frequency	0.970

Location #01 Instrument #A Test a

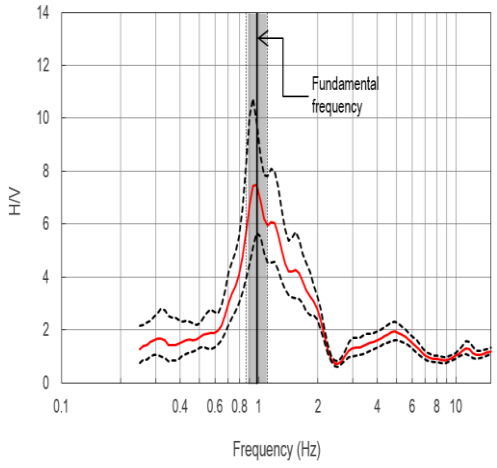

Fundamental frequency	0.979

Location #01 Instrument #A Test b

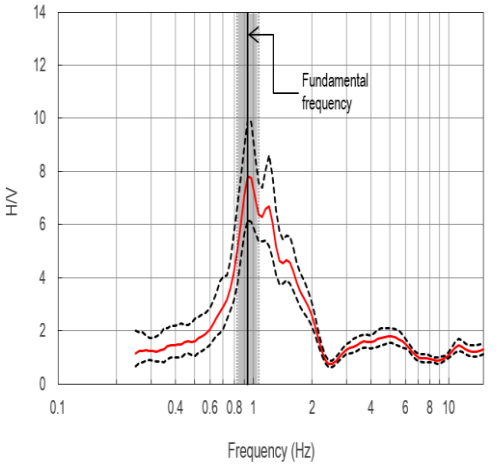

Fundamental frequency (Hz)	0.939

Location #01 Instrument #A Test c

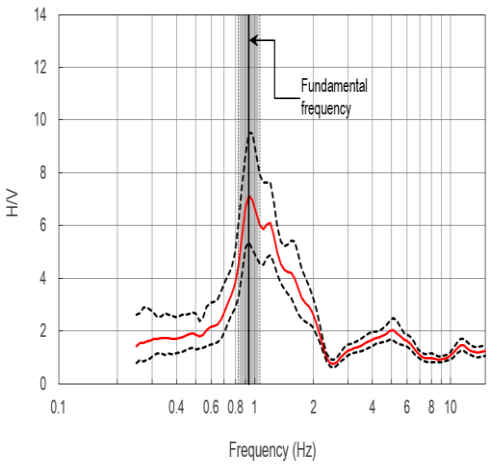

Fundamental frequency	0.939

Location #01 Instrument #A Test d

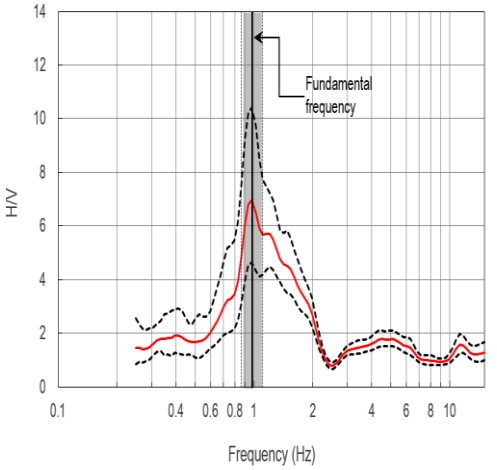

Fundamental frequency (Hz)	0.979

Location #01 Instrument #A Test e

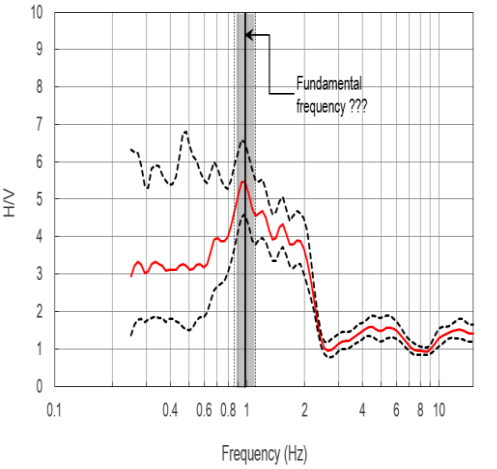

Fundamental frequency	0.979???

Location #01 Instrument #B Test a

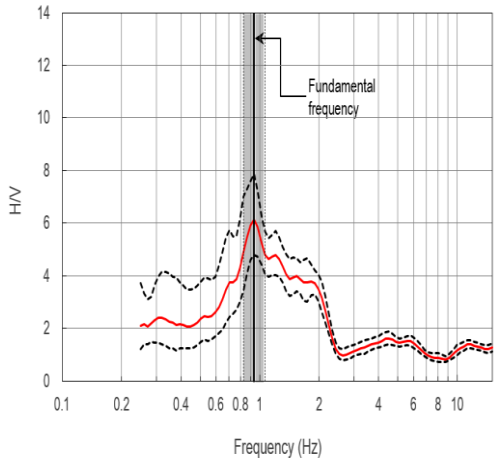

Fundamental frequency (Hz)	0.939

Location #01 Instrument #B Test b

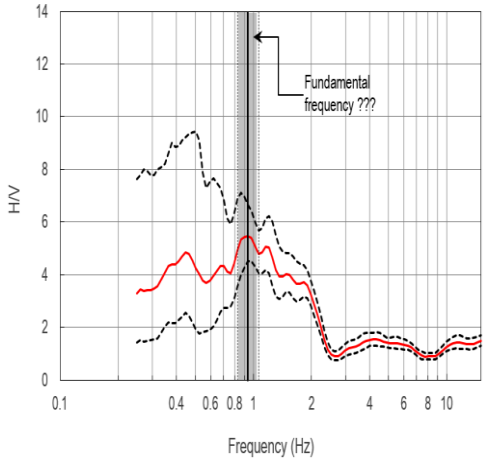

Fundamental frequency	0.939???

Location #01 Instrument #B Test c

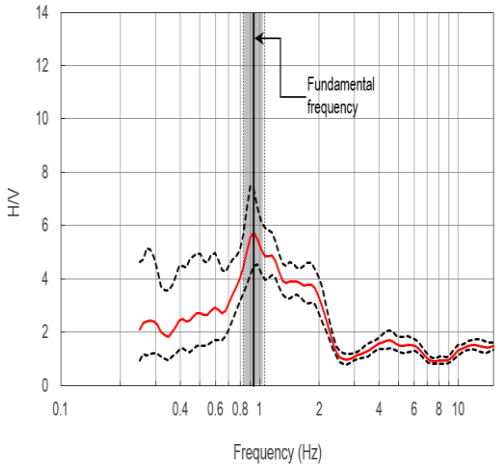

Fundamental frequency (Hz)	0.939

Location #01 Instrument #B Test d

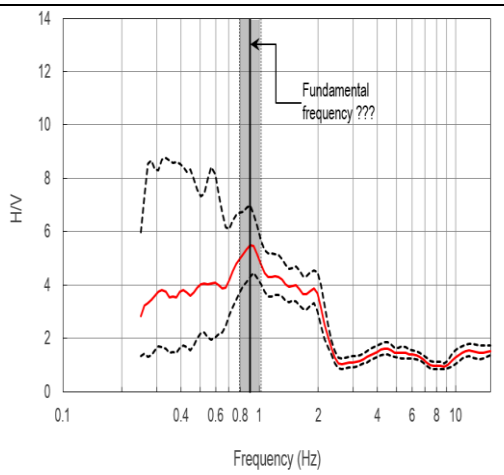

Fundamental frequency	0.901???

Location #01 Instrument #B Test e

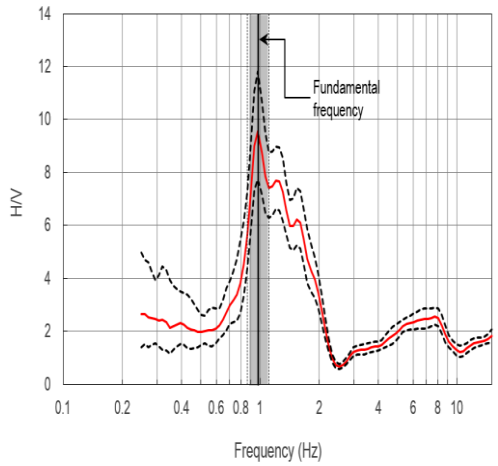

Fundamental frequency (Hz)	0.979

Location #01 Instrument #C Test a

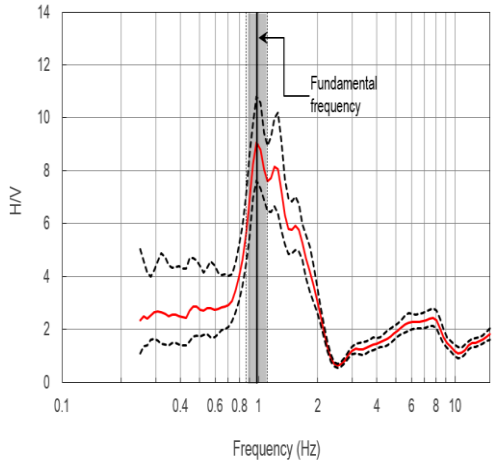

Fundamental frequency	0.979

Location #01 Instrument #C Test b

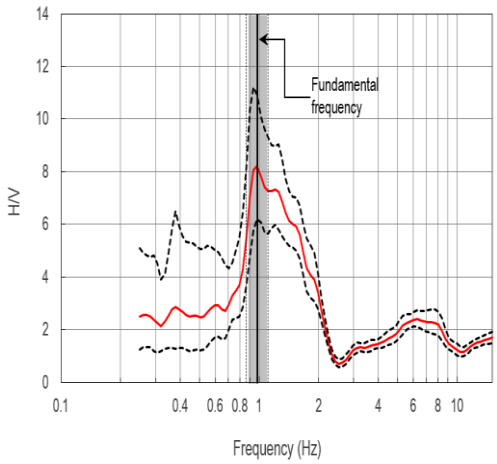

Fundamental frequency (Hz)	0.979

Location #01 Instrument #C Test c

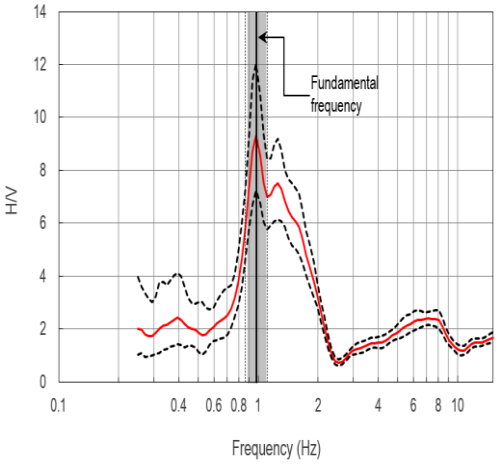

Fundamental frequency	0.979

Location #01 Instrument #C Test d

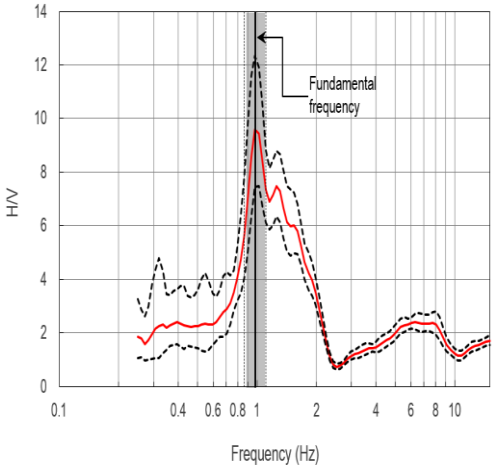

Fundamental frequency (Hz)	0.979

Location #01 Instrument #C Test e

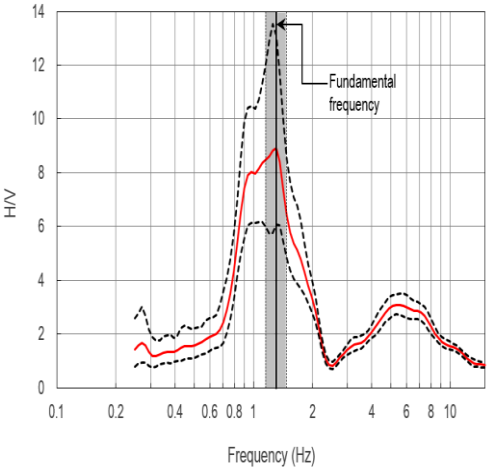

Fundamental frequency	1.307

Location #02 Instrument #A Test a

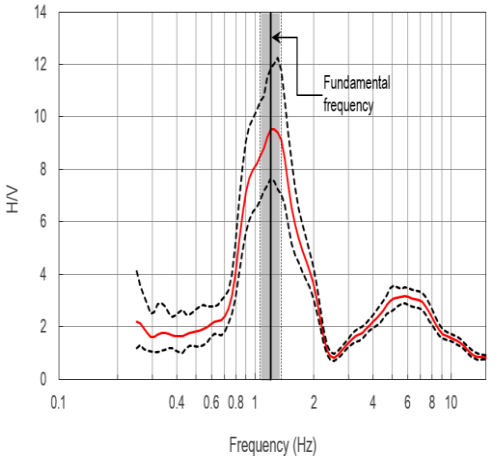

Fundamental frequency (Hz)	1.204

Location #02 Instrument #A Test b

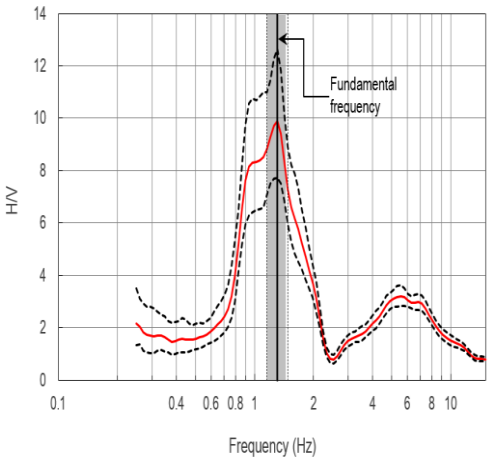

Fundamental frequency	1.307

Location #02 Instrument #A Test c

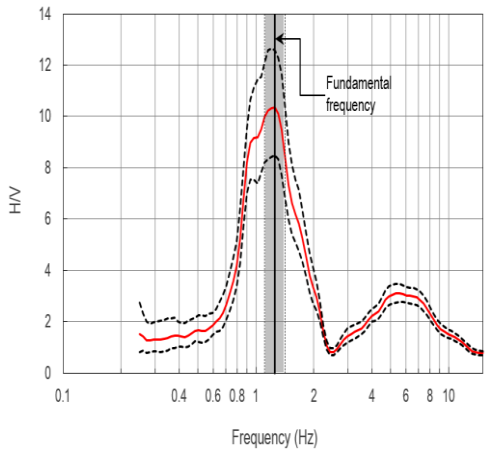

Fundamental frequency (Hz)	1.254

Location #02 Instrument #A Test d

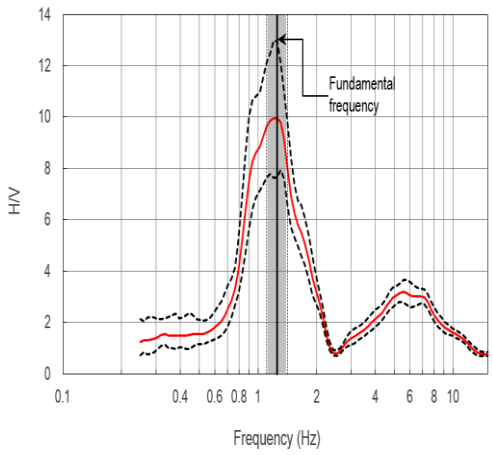

Fundamental frequency	1.254

Location #02 Instrument #A Test e

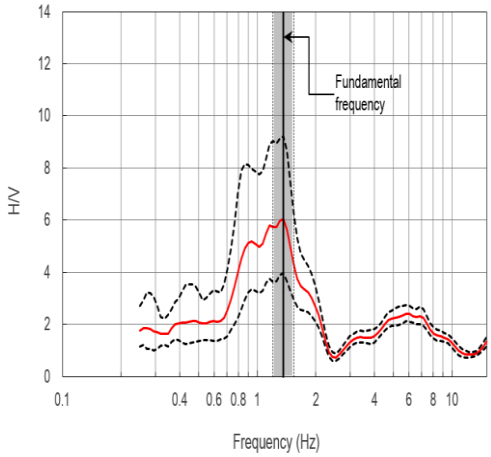

Fundamental frequency (Hz)	1.363

Location #02 Instrument #B Test a

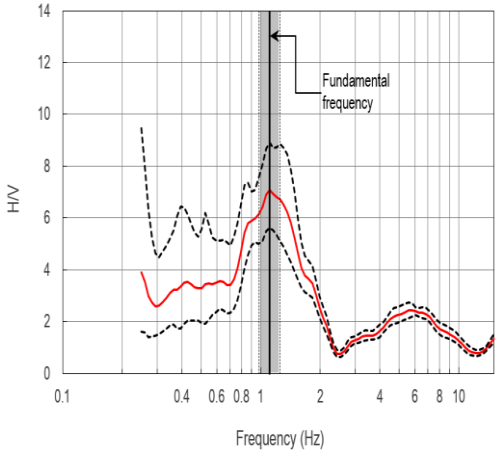

Fundamental frequency	1.108

Location #02 Instrument #B Test b

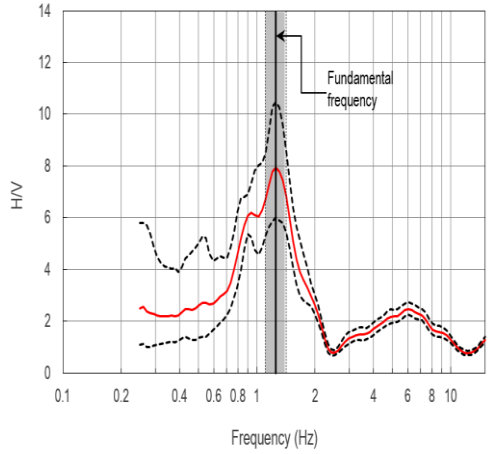

Fundamental frequency (Hz)	1.254

Location #02 Instrument #B Test c

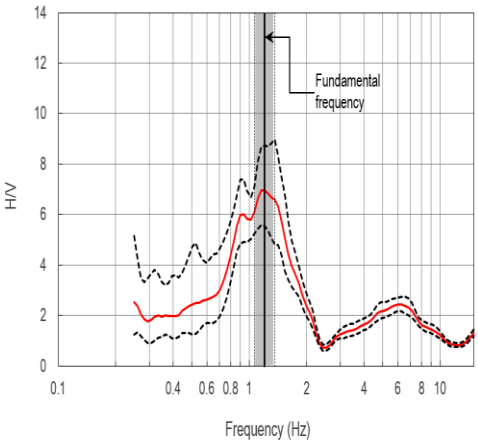

Fundamental frequency	1.204

Location #02 Instrument #B Test d

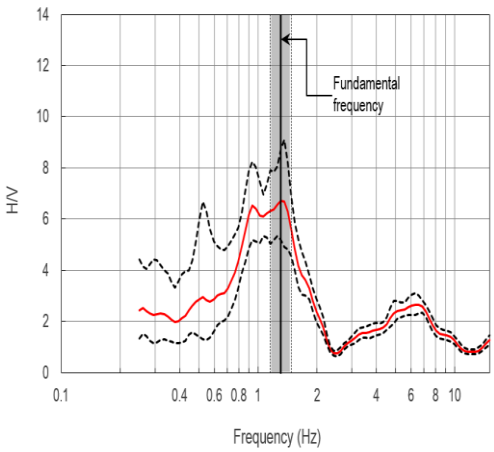

Fundamental frequency (Hz)	1.307

Location #02 Instrument #B Test e

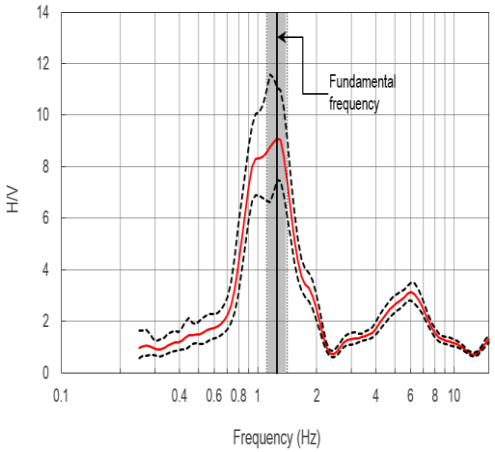

Fundamental frequency	1.254

Location #02 Instrument #C Test a

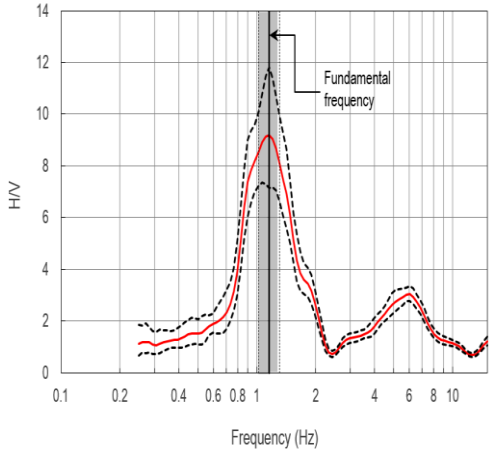

Fundamental frequency (Hz)	1.154

Location #02 Instrument #C Test b

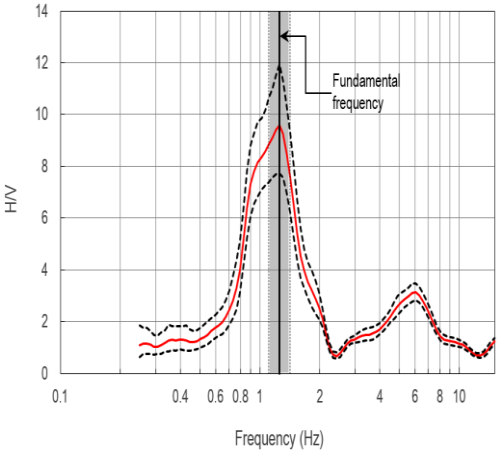

Fundamental frequency	1.254

Location #02 Instrument #C Test c

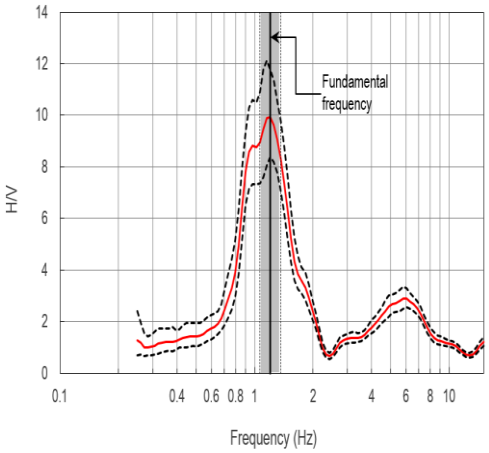

Fundamental frequency (Hz)	1.204

Location #02 Instrument #C Test d

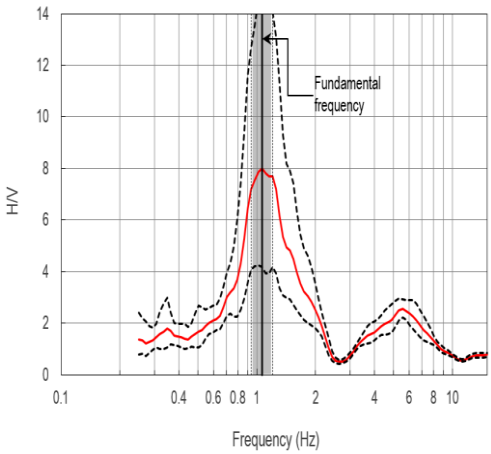

Fundamental frequency	1.063

Location #03 Instrument #A Test a

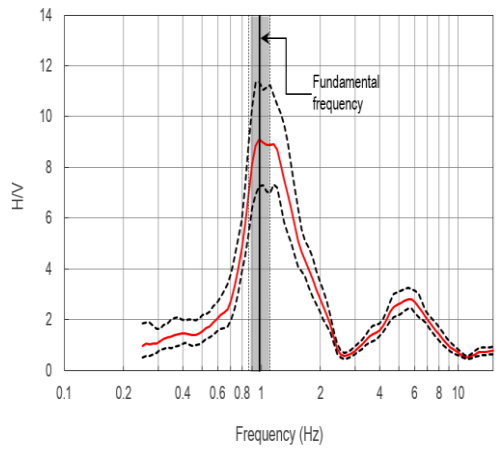

Fundamental frequency (Hz)	0.978

Location #03 Instrument #A Test b

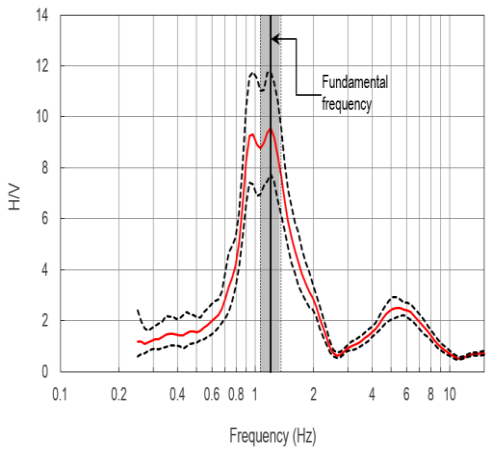

Fundamental frequency	1.204

Location #03 Instrument #A Test c

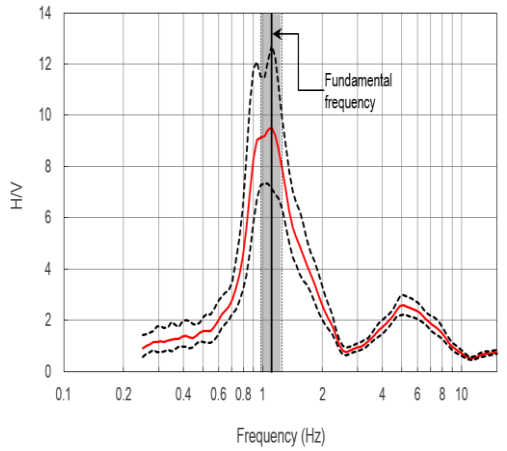

Fundamental frequency (Hz)	1.108

Location #03 Instrument #A Test d

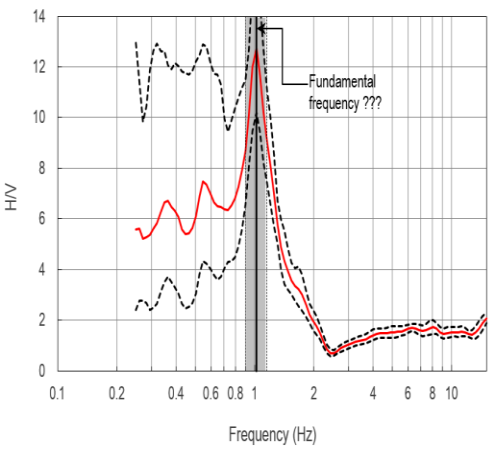

Fundamental frequency	1.020???

Location #04 Instrument #A Test a

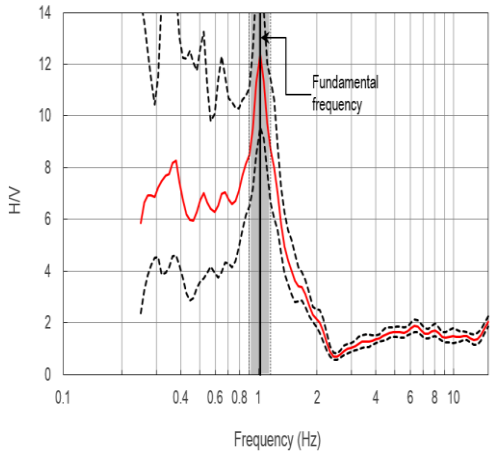

Fundamental frequency (Hz)	1.020

Location #04 Instrument #A Test b

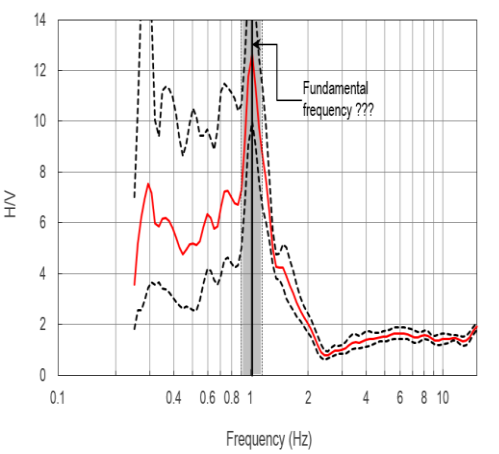

Fundamental frequency	1.020???

Location #04 Instrument #A Test c

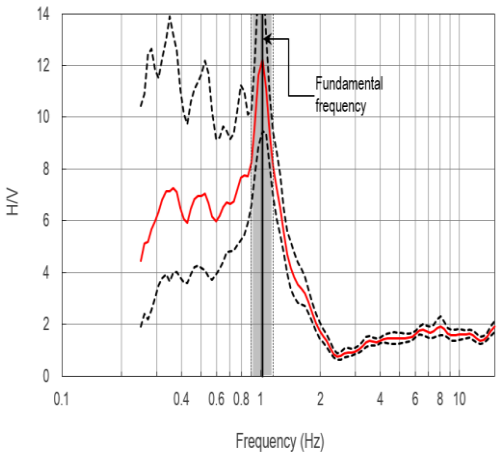

Fundamental frequency (Hz)	1.020

Location #04 Instrument #A Test d

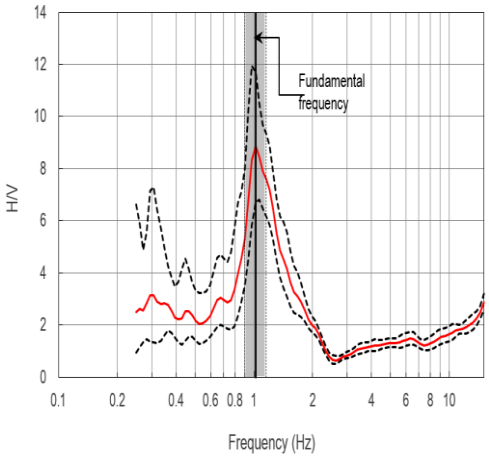

Fundamental frequency	1.020

Location #04 Instrument #B Test a

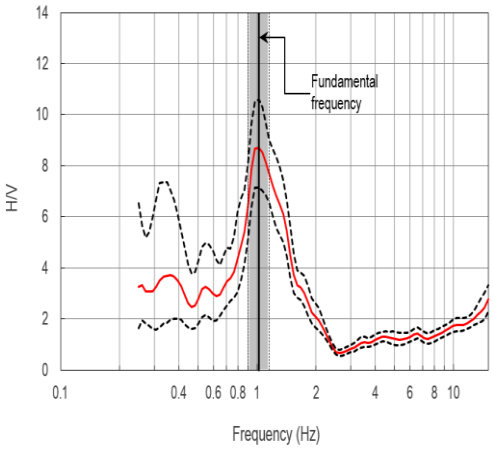

Fundamental frequency (Hz)	1.020

Location #04 Instrument #B Test b

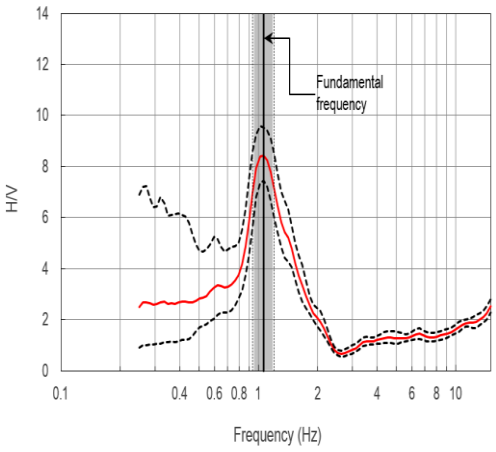

Fundamental frequency	1.063

Location #04 Instrument #B Test c

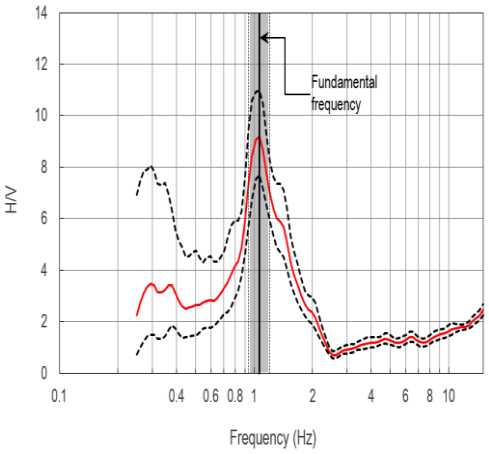

Fundamental frequency (Hz)	1.063

Location #04 Instrument #B Test d

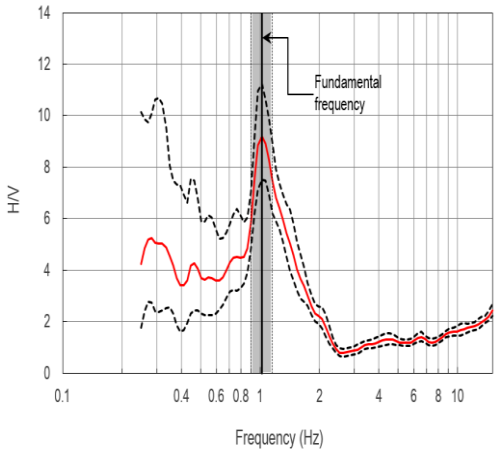

Fundamental frequency	1.020

Location #04 Instrument #B Test e

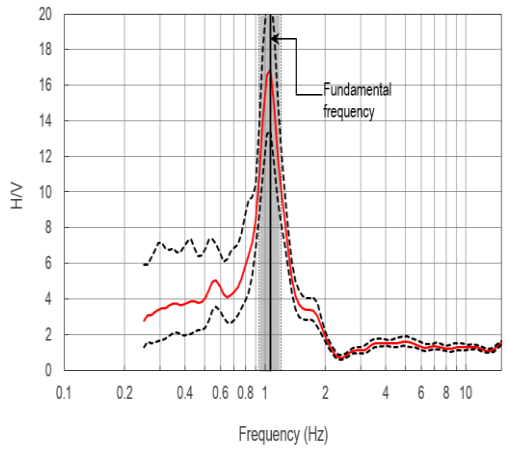

Fundamental frequency (Hz)	1.063

Location #04 Instrument #C Test a

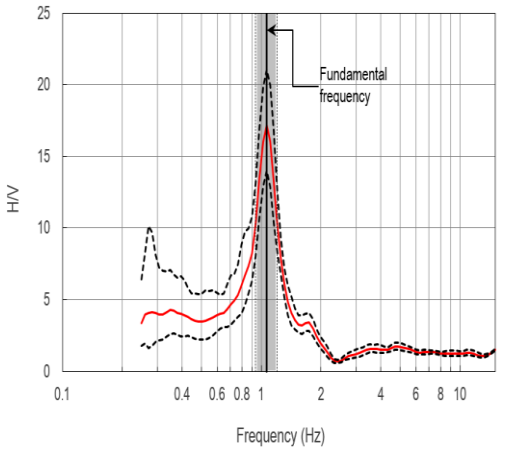

Fundamental frequency	1.063

Location #04 Instrument #C Test b

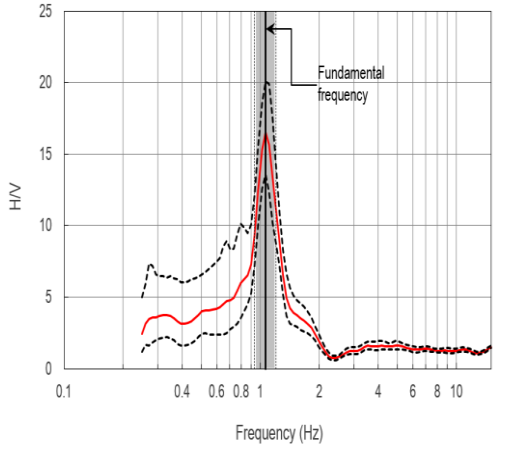

Fundamental frequency (Hz)	1.063

Location #04 Instrument #C Test c

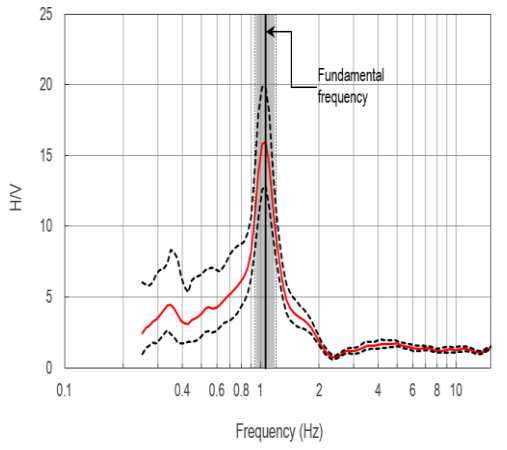

Fundamental frequency	1.063

Location #04 Instrument #C Test d

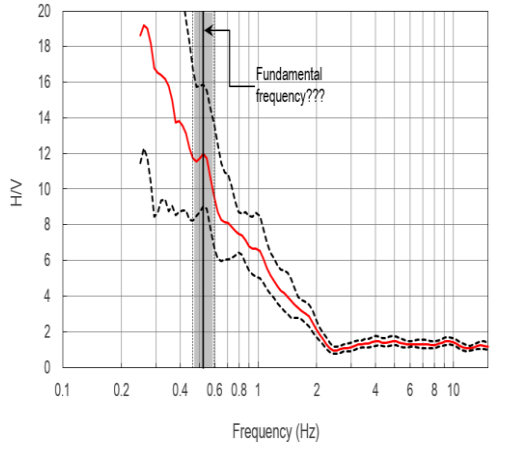

Fundamental frequency (Hz)	0.526???

Location #05 Instrument #A Test a

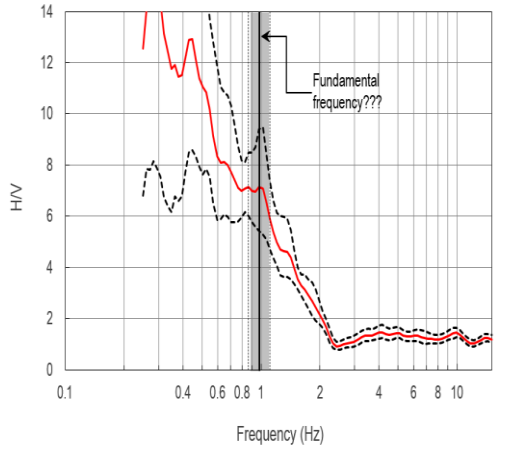

Fundamental frequency	0.978???

Location #05 Instrument #A Test b

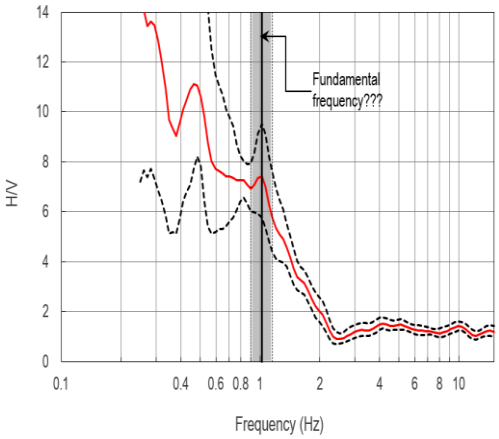

Fundamental frequency (Hz)	1.020???

Location #05 Instrument #A Test c

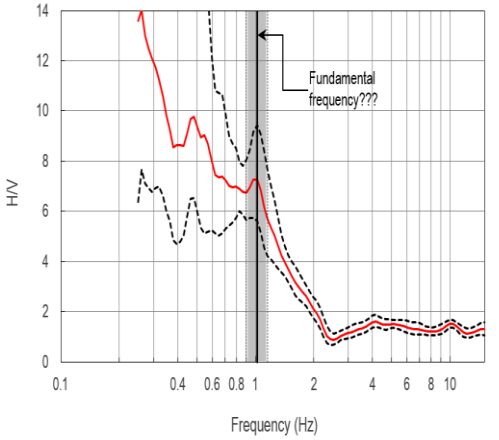

Fundamental frequency	1.020???

Location #05 Instrument #A Test d

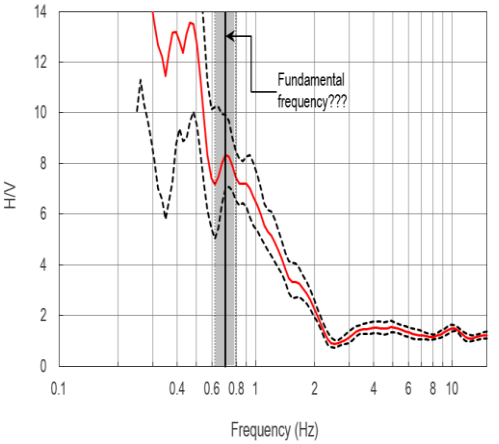

Fundamental frequency (Hz)	0.703???

Location #05 Instrument #A Test e

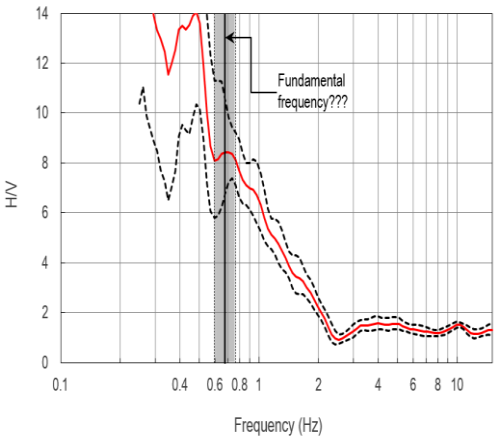

Fundamental frequency	0.675???

Location #05 Instrument #A Test f

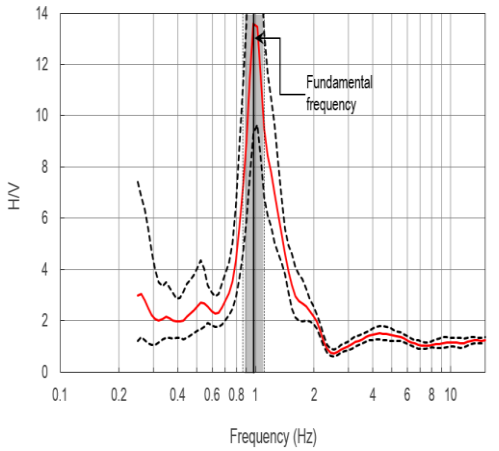

Fundamental frequency (Hz)	0.979

Location #05 Instrument #B Test a

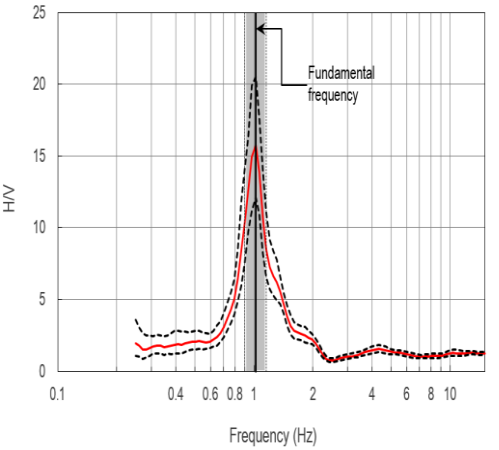

Fundamental frequency	1.020

Location #05 Instrument #B Test b

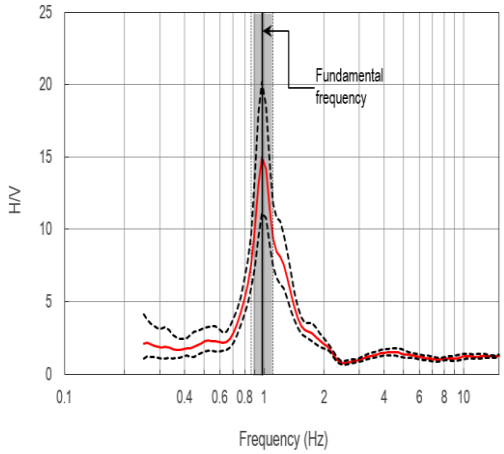

Fundamental frequency (Hz)	0.979

Location #05 Instrument #B Test c

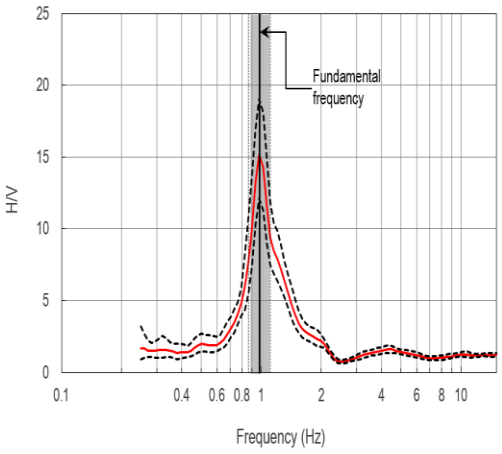

Fundamental frequency	0.979

Location #05 Instrument #B Test d

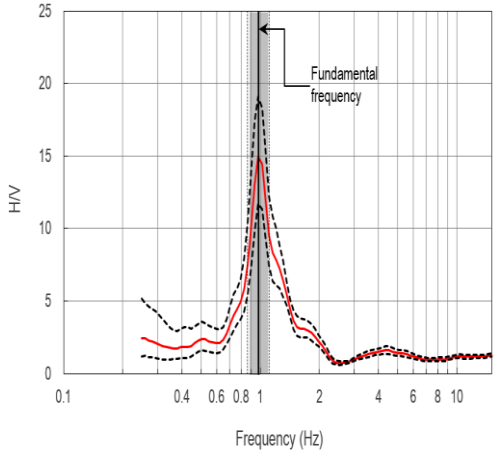

Fundamental frequency (Hz)	0.979

Location #05 Instrument #B Test e

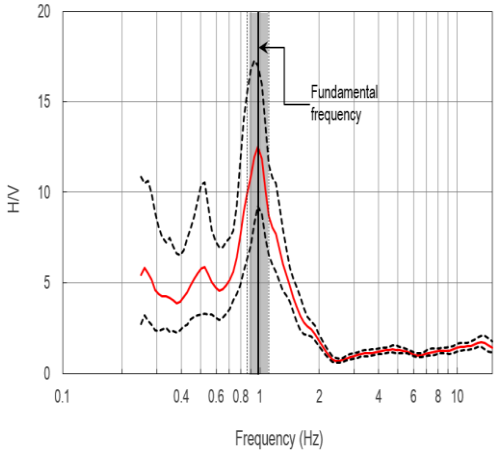

Fundamental frequency	0.979

Location #05 Instrument #C Test a

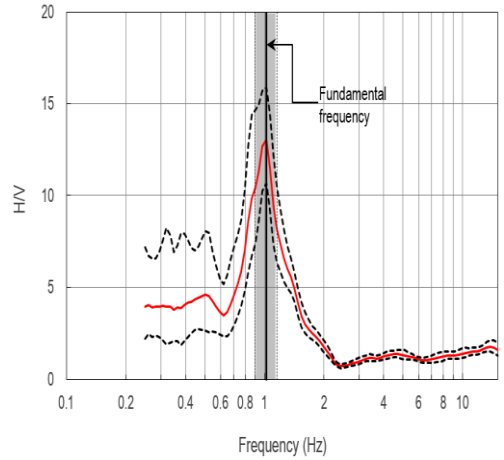

Fundamental frequency (Hz)	1.020

Location #05 Instrument #C Test b

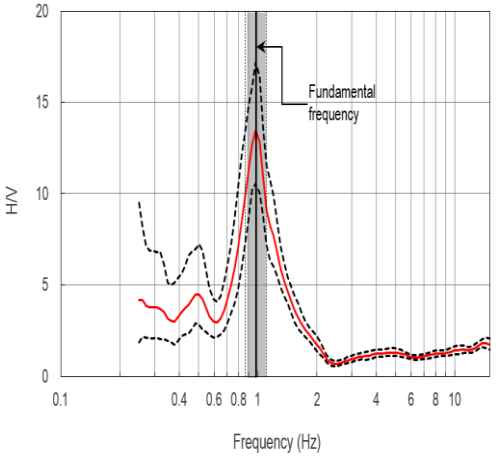

Fundamental frequency	0.979

Location #05 Instrument #C Test c

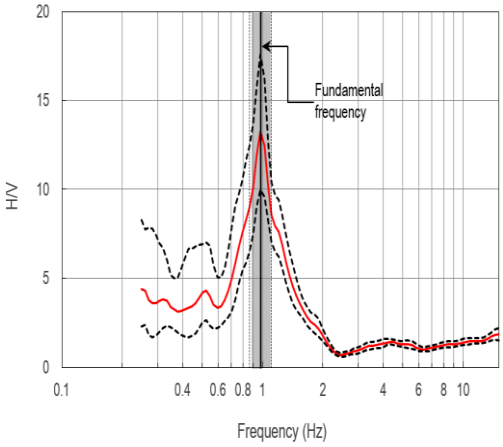

Fundamental frequency	0.979

Location #05 Instrument #C Test d

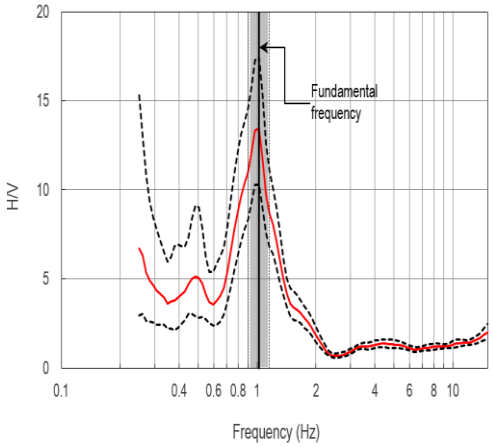

Fundamental frequency	1.020

Location #05 Instrument #C Test e

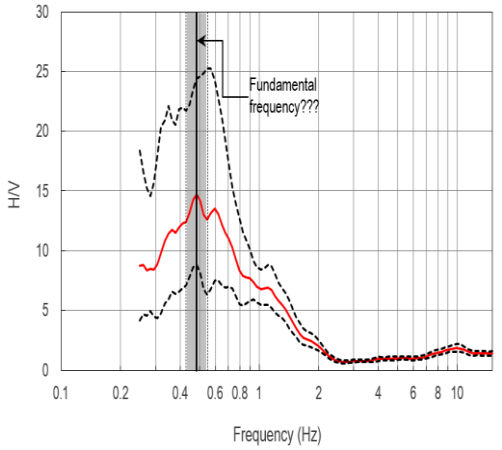

Fundamental frequency	0.485???

Location #06 Instrument #A Test a

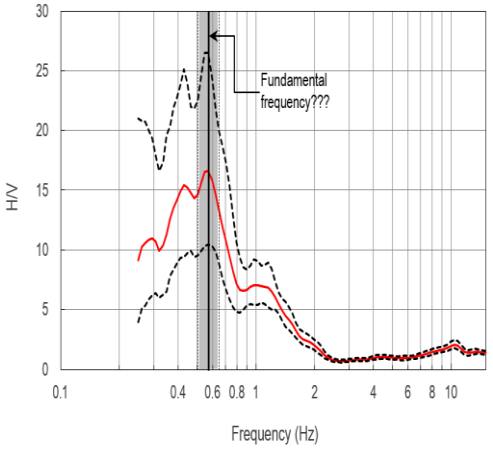

Fundamental frequency	0.572???

Location #06 Instrument #A Test b

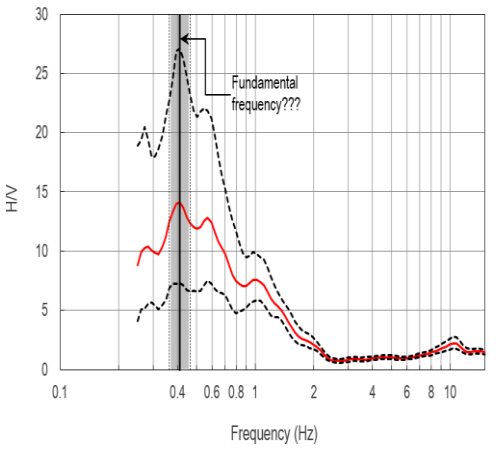

Fundamental frequency	0.411???

Location #06 Instrument #A Test c

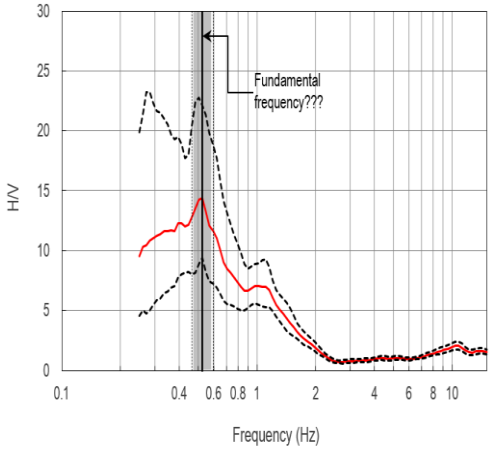

Fundamental frequency	0.526???

Location #06 Instrument #A Test d

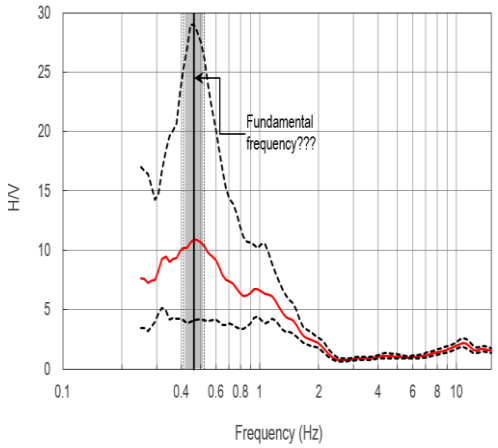

Fundamental frequency (Hz)	0.465???

Location #06 Instrument #A Test e

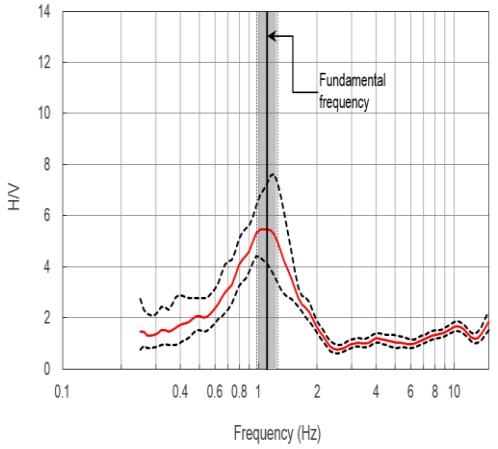

Fundamental frequency	1.108

Location #06 Instrument #B Test a

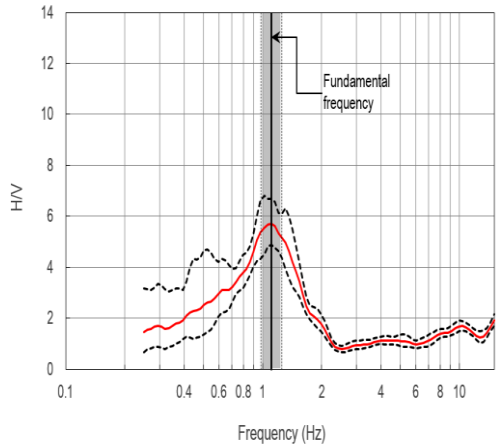

Fundamental frequency (Hz)	1.108

Location #06 Instrument #B Test b

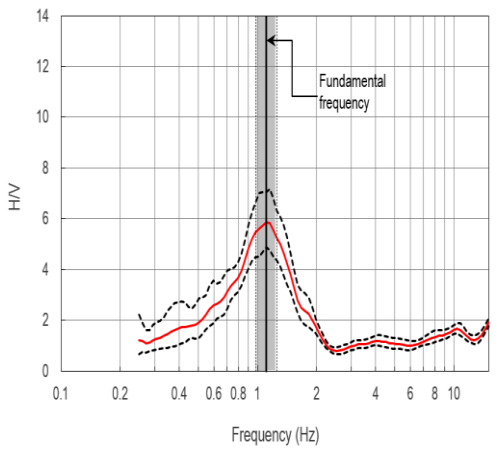

Fundamental frequency	1.108

Location #06 Instrument #B Test c

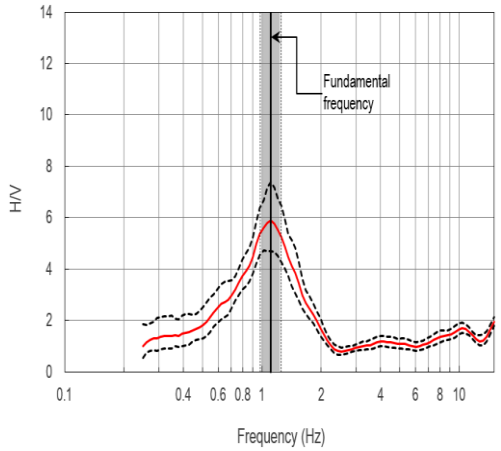

Fundamental frequency (Hz)	1.108

Location #06 Instrument #B Test d

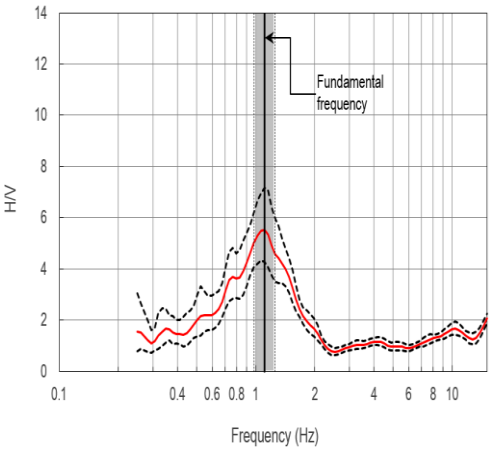

Fundamental frequency	1.108

Location #06 Instrument #B Test e

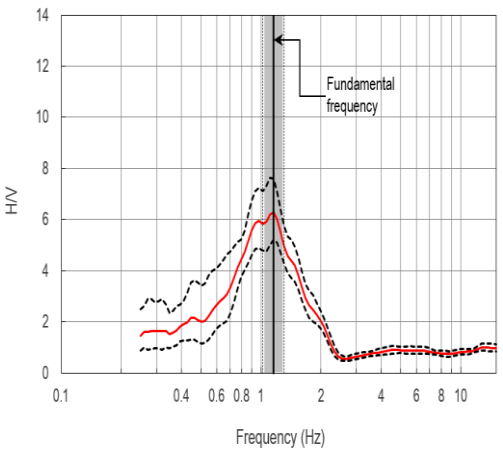

Fundamental frequency (Hz)	1.155

Location #06 Instrument #C Test a

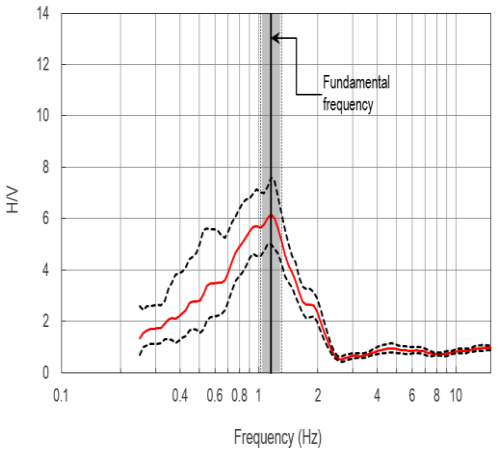

Fundamental frequency	1.155

Location #06 Instrument #C Test b

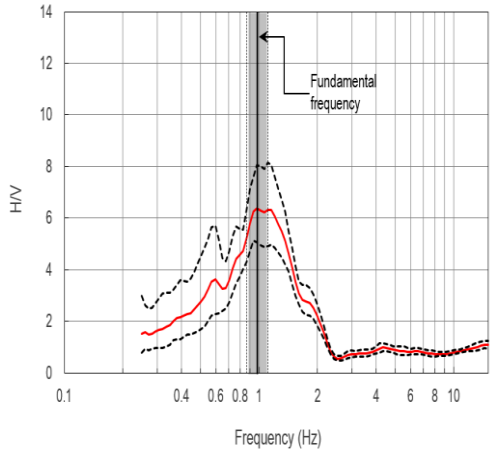

Fundamental frequency (Hz)	0.979

Location #06 Instrument #C Test c

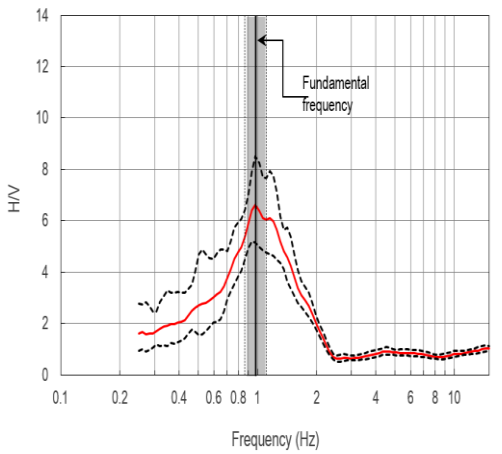

Fundamental frequency	0.979

Location #06 Instrument #C Test d

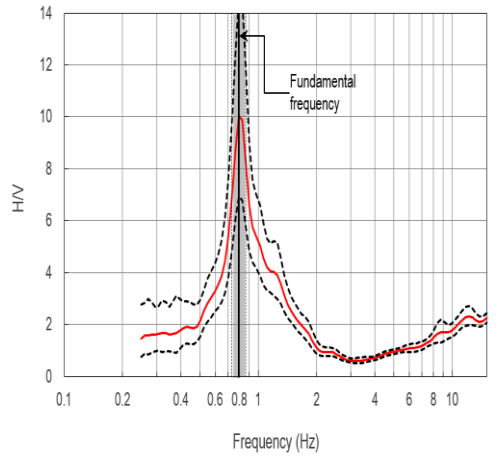

Fundamental frequency (Hz)	0.796

Location #07 Instrument #A Test a

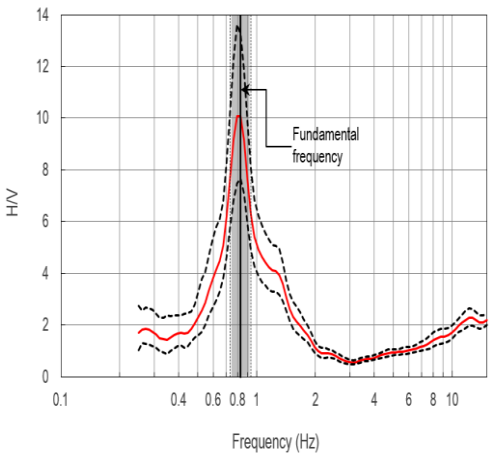

Fundamental frequency	0.829

Location #01 Instrument 07 Test b

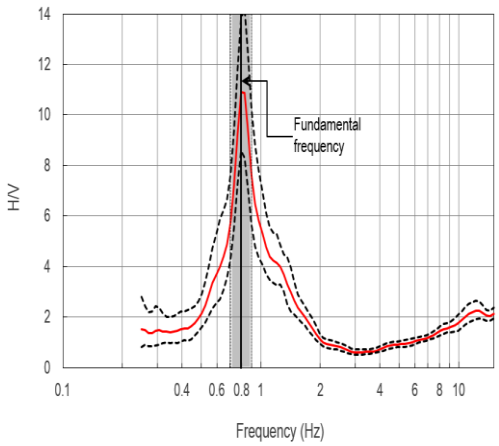

Fundamental frequency (Hz)	0.796

Location #07 Instrument #A Test c

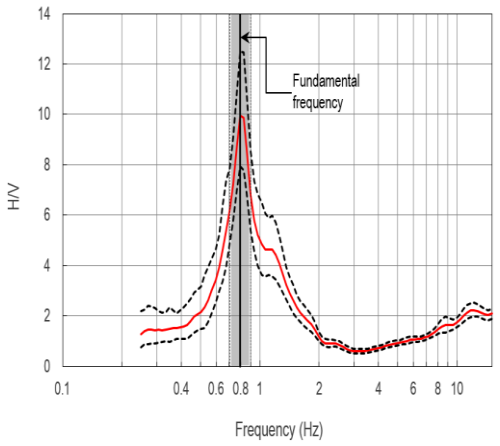

Fundamental frequency	0.796

Location #01 Instrument 07 Test d

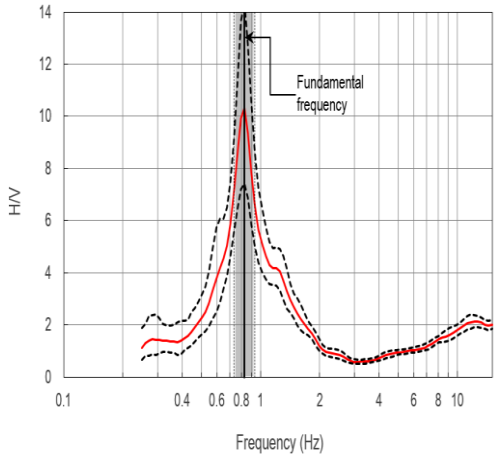

Fundamental frequency (Hz)	0.829

Location #07 Instrument #A Test e

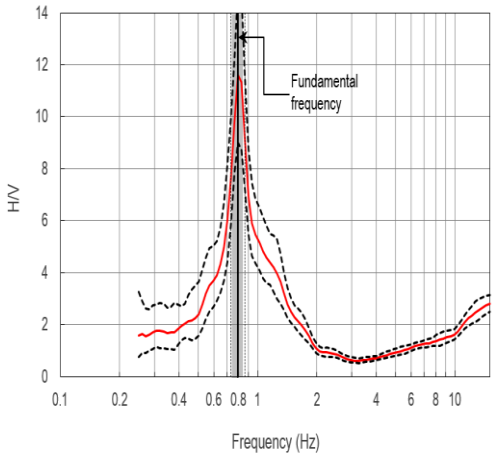

Fundamental frequency	0.796

Location #07 Instrument #B Test a

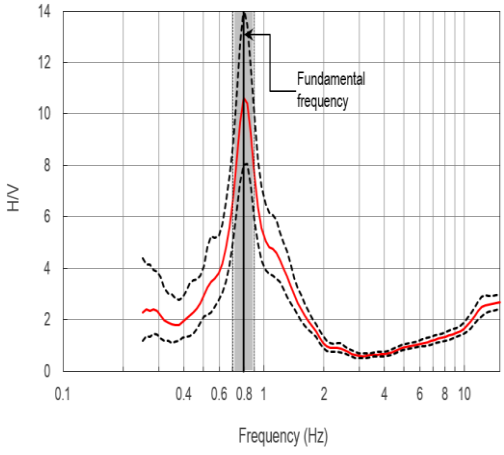

Fundamental frequency (Hz)	0.796

Location #07 Instrument #B Test b

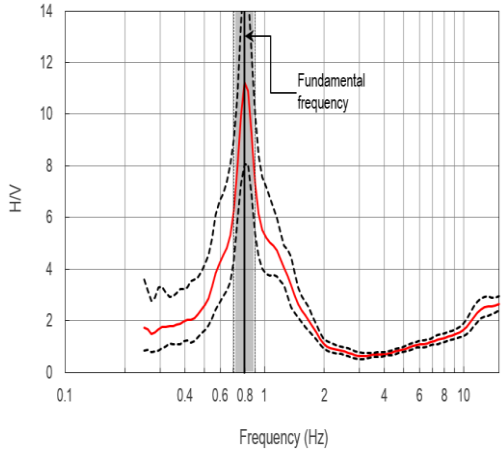

Fundamental frequency	0.796

Location #07 Instrument #B Test c

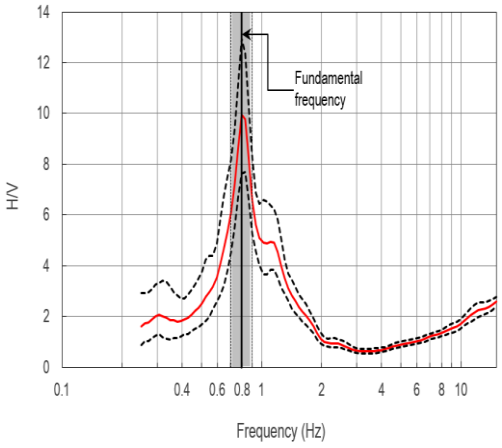

Fundamental frequency (Hz)	0.796

Location #07 Instrument #B Test d

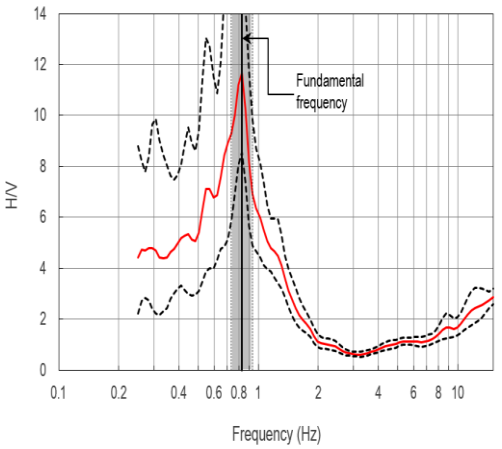

Fundamental frequency	0.829

Location #07 Instrument #C Test a

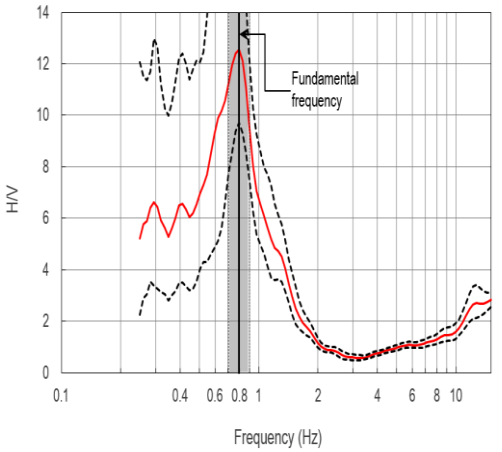

Fundamental frequency (Hz)	0.796

Location #07 Instrument #C Test b

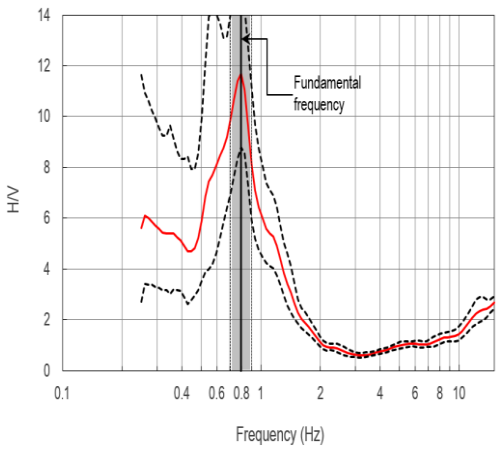

Fundamental frequency	0.796

Location #07 Instrument #C Test c

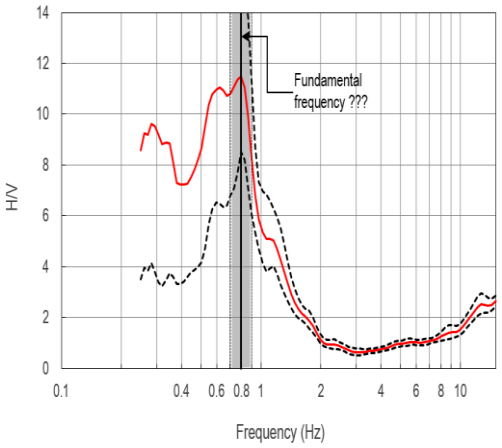

Fundamental frequency (Hz)	0.796???

Location #07 Instrument #C Test d

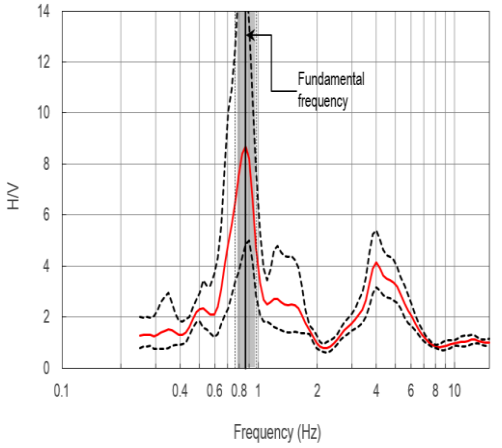

Fundamental frequency	0.865

Location #08 Instrument #A Test a

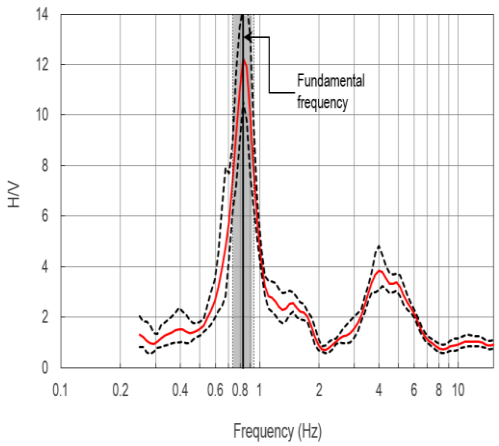

Fundamental frequency (Hz)	0.829

Location #08 Instrument #A Test b

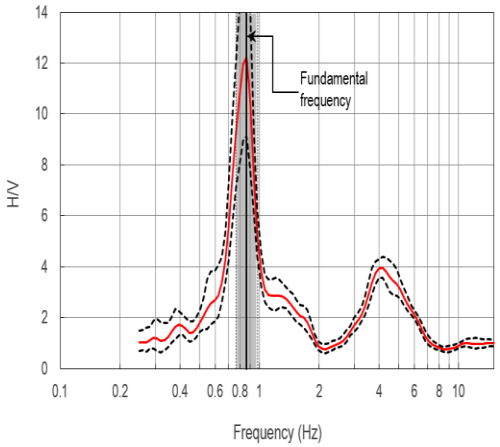

Fundamental frequency	0.865

Location #08 Instrument #A Test c

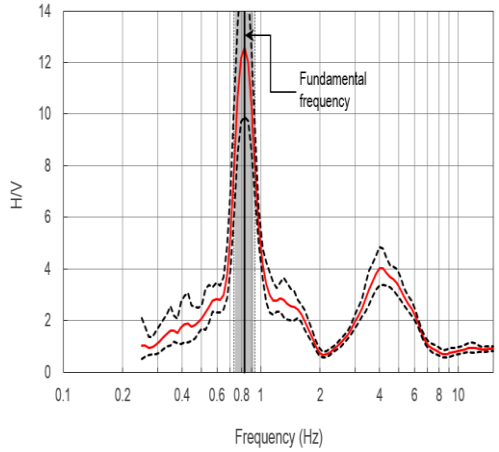

Fundamental frequency (Hz)	0.829

Location #08 Instrument #A Test d

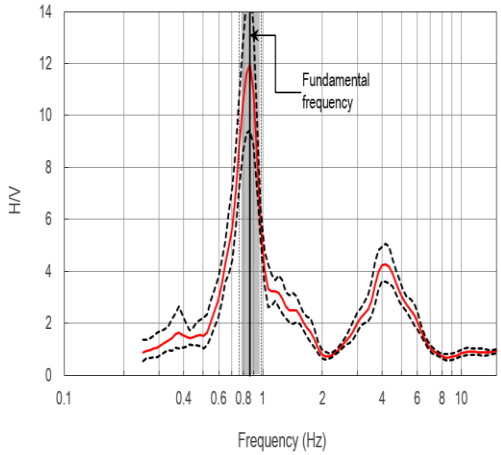

Fundamental frequency	0.865

Location #08 Instrument #A Test e

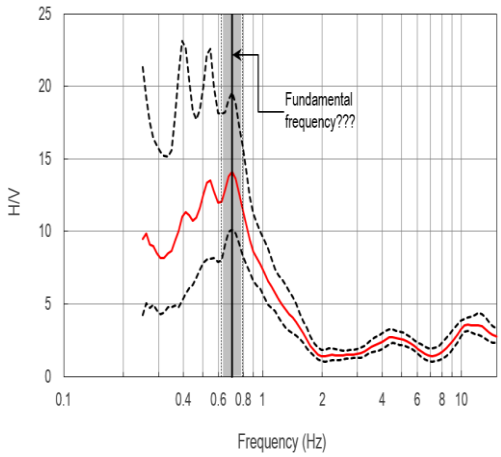

Fundamental frequency (Hz)	0.703???

Location #09 Instrument #A Test a

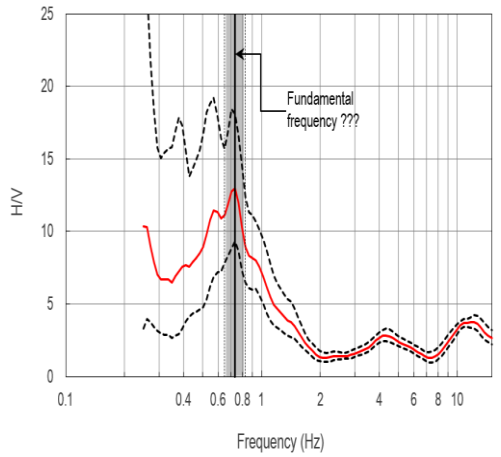

Fundamental frequency	0.733???

Location #09 Instrument #A Test b

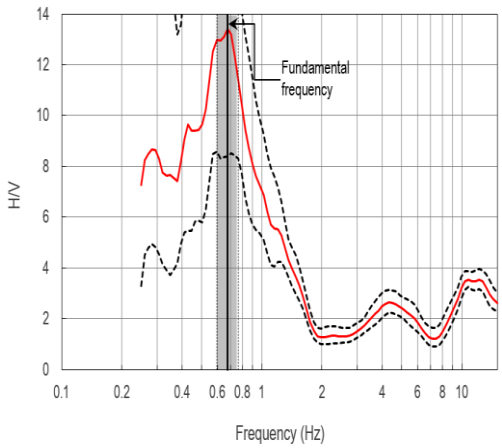

Fundamental frequency (Hz)	0.675

Location #09 Instrument #A Test c

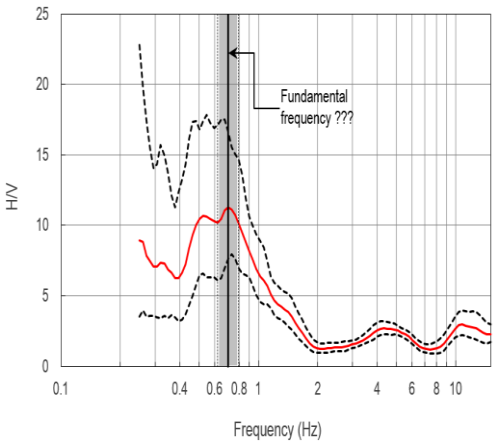

Fundamental frequency	0.703???

Location #09 Instrument #A Test d

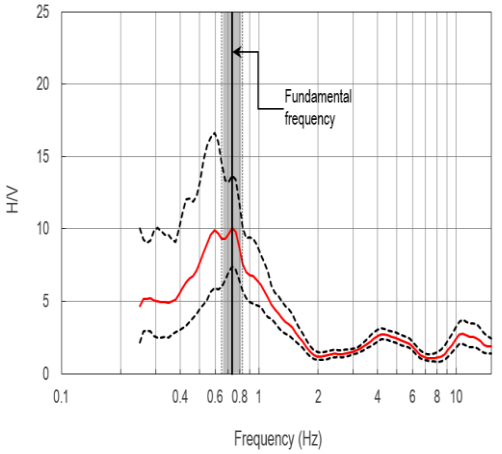

Fundamental frequency (Hz)	0.733

Location #09 Instrument #A Test e

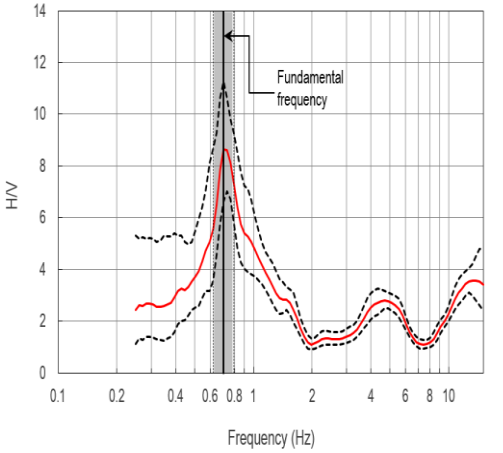

Fundamental frequency	0.703

Location #09 Instrument #B Test a

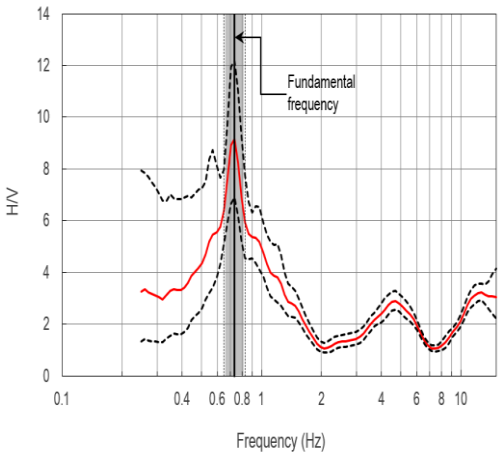

Fundamental frequency (Hz)	0.733

Location #09 Instrument #B Test b

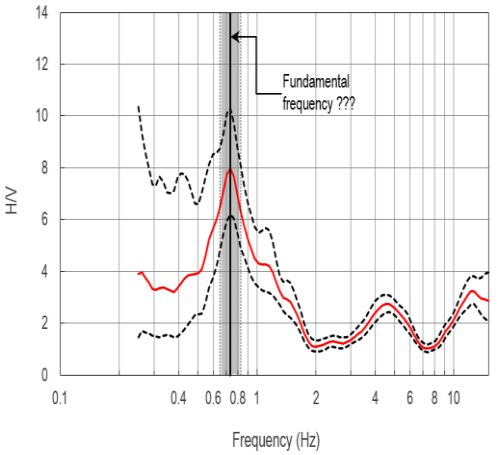

Fundamental frequency	0.733???

Location #09 Instrument #B Test c

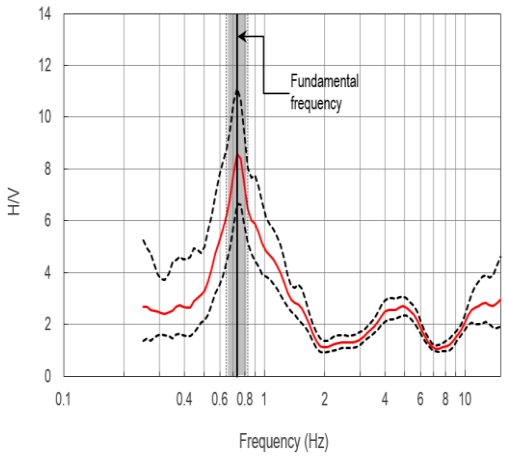

Fundamental frequency (Hz)	0.733

Location #09 Instrument #B Test d

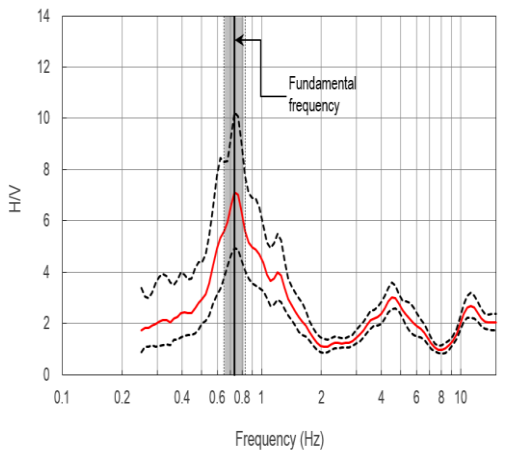

Fundamental frequency	0.733

Location #09 Instrument #C Test a

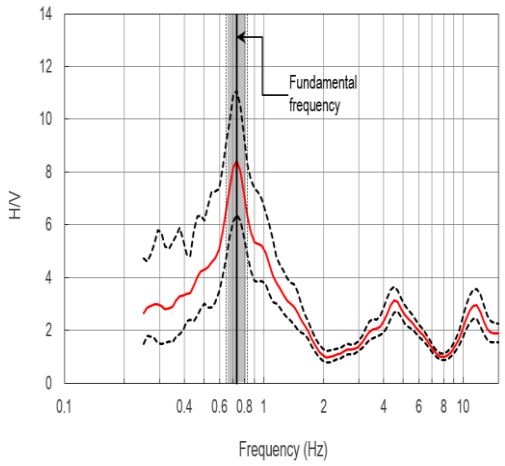

Fundamental frequency (Hz)	0.733

Location #09 Instrument #C Test b

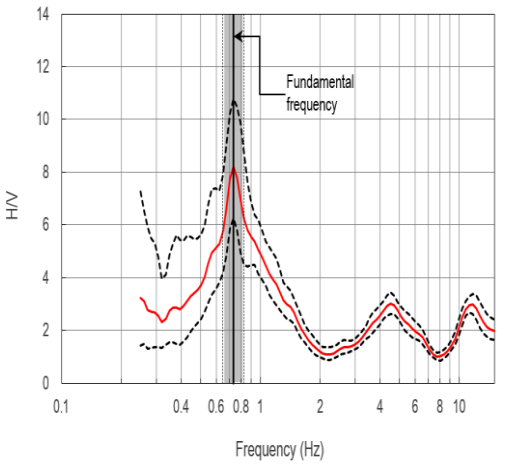

Fundamental frequency	0.733

Location #09 Instrument #C Test c

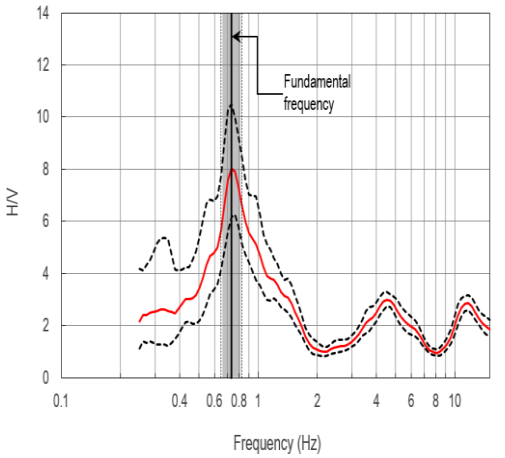

Fundamental frequency (Hz)	0.733

Location #09 Instrument #C Test d

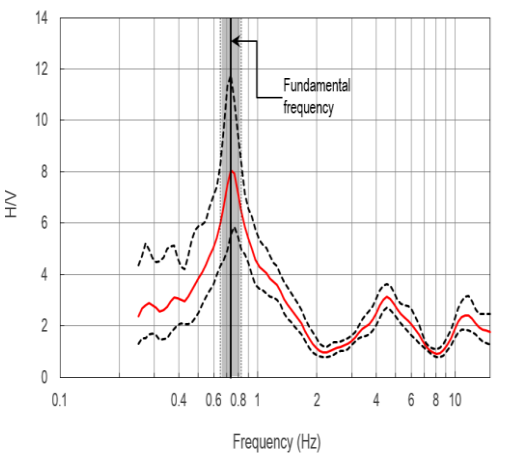

Fundamental frequency	0.733

Location #09 Instrument #C Test e

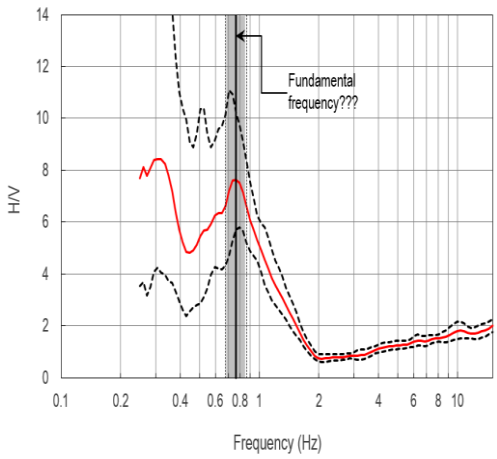

Fundamental frequency (Hz)	0.764???

Location #10 Instrument #A Test a

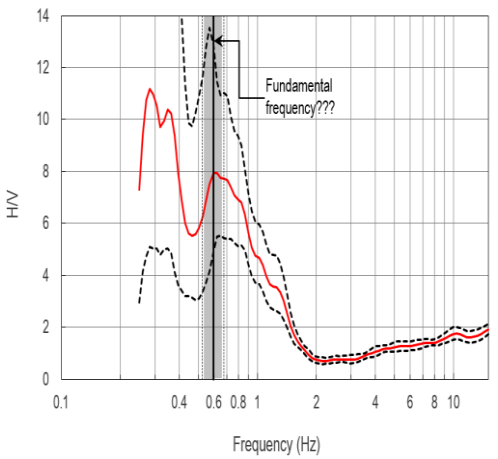

Fundamental frequency	0.596???

Location #10 Instrument #A Test b

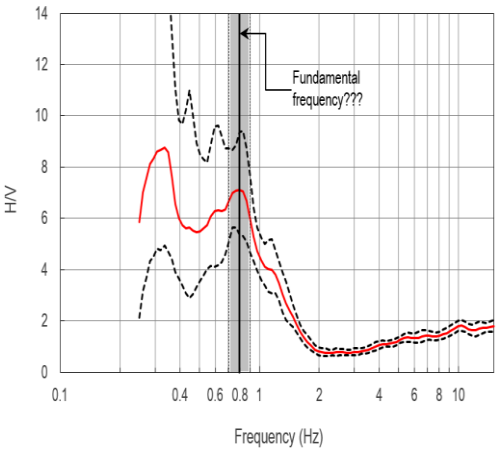

Fundamental frequency (Hz)	0.796???

Location #10 Instrument #A Test c

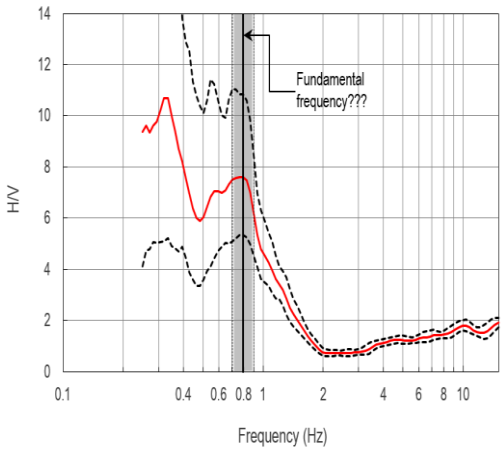

Fundamental frequency	0.796???

Location #10 Instrument #A Test d

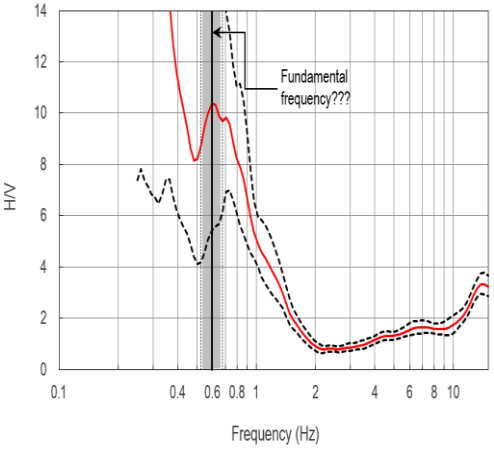

Fundamental frequency (Hz)	0.596???

Location #10 Instrument #B Test a

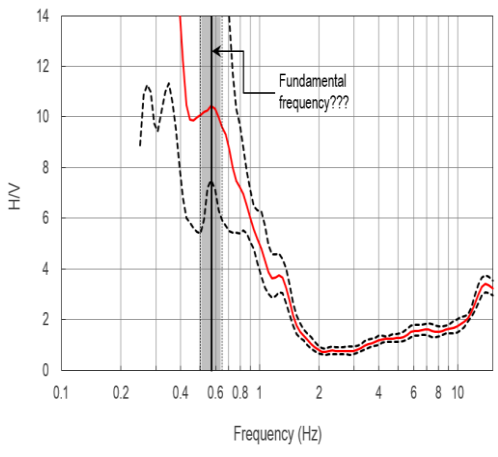

Fundamental frequency	0.572???

Location #10 Instrument #B Test b

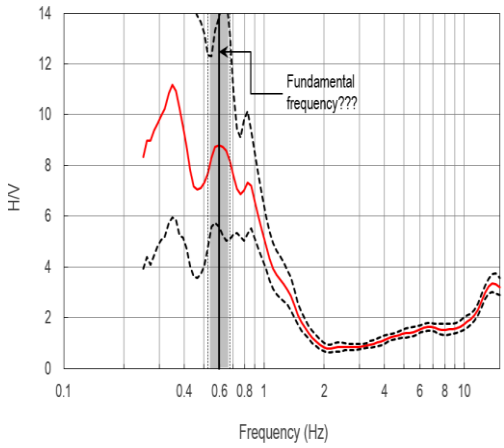

Fundamental frequency (Hz)	0.596???

Location #10 Instrument #B Test c

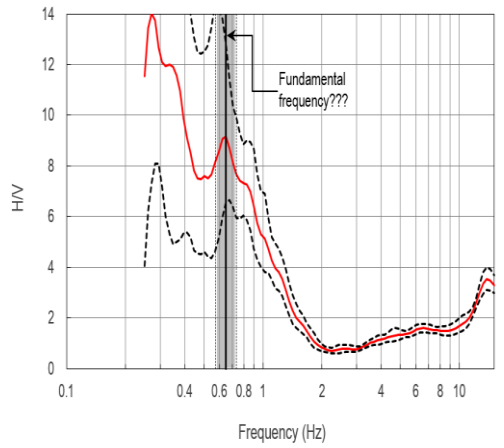

Fundamental frequency	0.647???

Location #10 Instrument #B Test d

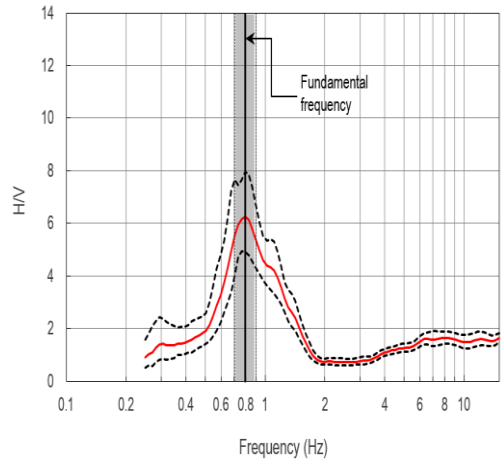

Fundamental frequency (Hz)	0.796

Location #10 Instrument #C Test a

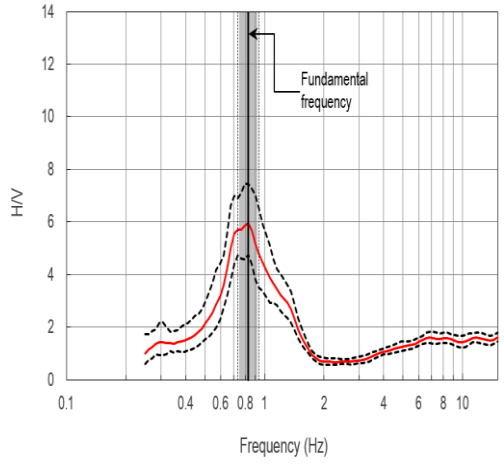

Fundamental frequency	0.829

Location #10 Instrument #C Test b

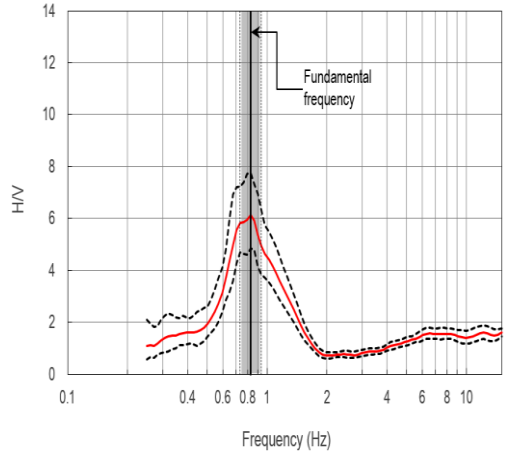

Fundamental frequency (Hz)	0.829

Location #10 Instrument #C Test c

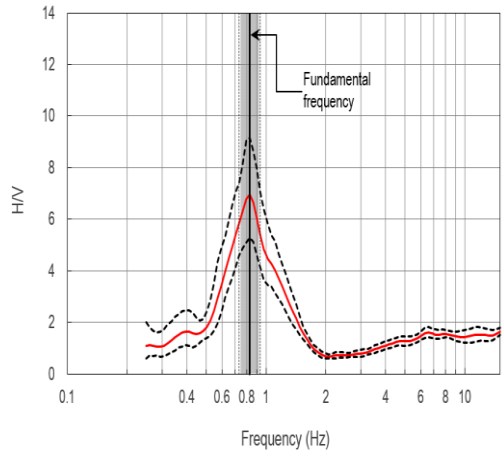

Fundamental frequency	0.829

Location #10 Instrument #C Test d

Appendix H:

AN INTERNATIONAL PEER REVIEWED JOURNAL PAPER 4

SETIAWAN, B., JAKSA, M., GRIFFITH, M., AND LOVE, D. (2018). PASSIVE NOISE DATASETS AT REGOLITH SITES. DATA IN BRIEF. 20: 735 - 747, DOI: 10.1016/J.DIB.2018.08.055.

INTENTIONALLY BLANK

Data in Brief 20 (2018) 735–747

Contents lists available at ScienceDirect

Data in Brief

journal homepage: www.elsevier.com/locate/dib

Data Article

Passive noise datasets at regolith sites

Bambang Setiawan [a,*], Mark Jaksa [b], Michael Griffith [b], David Love [c]

[a] *Faculty of Engineering, Syiah Kuala University, Jl. Tgk. Syech Abdurrauf 7, Darussalam, Banda Aceh 23111, Indonesia*
[b] *School of Civil, Environmental and Mining Engineering, the University of Adelaide, North Terrace Campus, SA 5005, Australia*
[c] *Department of State Development, Government of South Australia, 101 Grenfell Street, Adelaide, SA 5000, Australia*

ARTICLE INFO

Article history:
Received 19 July 2018
Received in revised form
10 August 2018
Accepted 21 August 2018
Available online 31 August 2018

Keywords:
Passive noise
Array
HVSR
SPAC
Regolith

ABSTRACT

The data presented in this article contain datasets of passive noise measurements at regolith sites in Adelaide, South Australia. The data were acquired using three component (3C) LE-3Dlite Lennartz seismometers with an eigenfrequency of 1 Hz. The data were acquired at eight sites across Adelaide's regolith in a hexagonal array layout. Four tests, each with a duration of 30 min, were conducted at different times. The ambient noise data can be used for both horizontal to vertical spectral ratio (HVSR) analysis and array analyses, which are essential to obtain the site fundamental frequency and the ellipticity of the fundamental mode Rayleigh waves at the measured site. The array analyses are useful to obtain the dispersion curves, which are needed to estimate the shear wave velocity profile.

Specifications Table

Subject area	*Geophysics*
More specific subject area	*Near surface geophysics*
Type of data	*Table, text file, and figure*

* Corresponding author.
E-mail address: bambang.setiawan@unsyiah.ac.id (B. Setiawan).

https://doi.org/10.1016/j.dib.2018.08.055

How data was acquired	*3 component (3C) LE-3Dlite Lennartz seismometers with an eigen-frequency of 1 Hz*
Data format	*Raw, filtered, analyzed*
Experimental factors	*The passive noise measurements were conducted for at least 2 h at a sampling frequency of 100 Hz*
Experimental features	*The 3C LE-3Dlite Lennartz seismometers were equipped with an analog-to-digital recorder & a global positioning system (GPS)*
Data source location	*Adelaide City, South Australia*
Data accessibility	*Data are included with this article*

Value of the data

- The ambient noise data can be used in the development of further experiments at other regolith sites
- The data can be compared to other measurements for provide greater insight
- The HVSR curves serve as a benchmark for other researchers
- The data are important to evaluate the reliability of ambient vibration data analysis and for comparison of other sites with similar or divergent geophysical characteristics.

1. Data

The data in this article contain a series of measurements of ambient noise (microtremor) at regolith sites in Adelaide, South Australia (Fig. 1). Eight sites across Adelaide's regolith were measured in a hexagonal array layout. The acquired data contains four continuous ambient noise tests, each with a duration of 30 min. The ambient noise data, which were acquired in arrays consisting of three instruments in a triangular arrangement, are important for horizontal to vertical spectral ratio (HVSR) analyses. The HVSR method was introduced by [1] based on the work of [2]. This HVSR method was popularized by [3]. Due to its simplicity this HVSR method has been used extensively since 1989. The data from all seismometers in the hexagonal array can be used to evaluate the dispersion curves in array analyses, such as spatial autocorrelation (SPAC) analysis [4]. HVSR analyses are carried out to

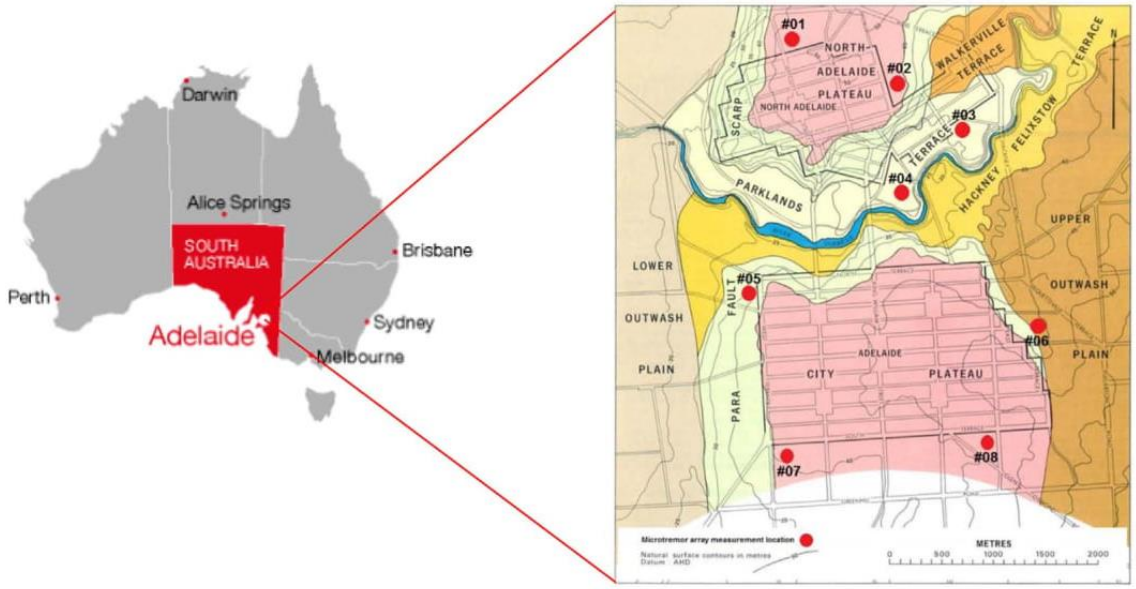

Fig. 1. Locality of the collected data sites [5].

obtain the site fundamental frequency and ellipticity of the fundamental mode Rayleigh waves at each of the measured sites. The use of the array analyses to evaluate the dispersion curve is motivated by the objective of analyzing Raleigh waves and excluding Love waves.

2. Experimental design, equipment and analyses

2.1. Experimental design

A hexagonal array with a radius of 50 m was used in the measurement process, as shown in Fig. 2*(a)*. Eight ambient noise field measurements were conducted in the parklands that surround the Adelaide city area (Fig. 1) using seven sets of 3-component seismometers. These seismometers record the three orthogonal components of vibration: two horizontals (i.e. east–west and north–south) and one vertical. The data were recorded and saved to the internal memory storage within each instrument.

2.2. Equipment

All the seismometers used for the noise data acquisition are three component (3C) LE-3Dlite Lennartz seismometers with an eigenfrequency of 1 Hz, as shown in Fig. 2(b). These 3C seismometers were connected to an analog-to-digital recorder [Kelunji digital data recorder, as shown in Fig. 2(b)], a global positioning system (GPS), antenna and a battery. The digital data recorder was equipped with a memory disk to store the acquired data. A laptop computer was used for initial setting up and checking the status of the recording process.

In order to be provide a stable measurement platform at each site, the seismometers were placed onto of a 20 mm thick circular concrete slab over a generally firm to a stiff ground surface, which was previously cleared of vegetation and any pebble-sized rubble. The seismometers were leveled by adjusting the legs so as to minimize any instability during recording. For consistency with the measured horizontal vibration, all the seismometers were also oriented to magnetic North. Furthermore, to maintain the stability of the seismometer during the data acquisition, all the seismometers were protected from wind-induced vibrations by means of a plastic container and stabilized with a paving block on top, as shown in Fig. 2(c).

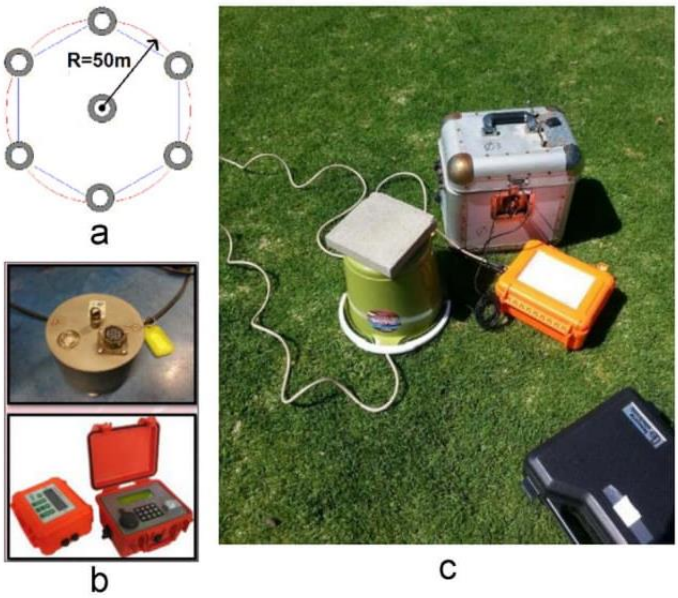

Fig. 2. (a) Array layout; (b) LE3DLite Lennartz seismometer Kelunji Data Recorder; and (c) field setting up of the equipment.

Table 1
Fundamental frequency, maximum horizontal vertical spectral ratio, number of stationary data and SESAME reliability criteria checks.

No.	Date		Hour		f_0	n	A_0	Check for reliability		
	GMT	Adelaide	GMT	Adelaide				i	ii	iii
1	2/10/2014	2/10/2014	6:31:00 a.m.	3:01:00 p.m.	0.90	13	12.82	PASS	PASS	PASS
2			7:00:00 a.m.	3:30:00 p.m.	0.88	12	9.92	PASS	PASS	FAIL
3			7:30:00 a.m.	4:00:00 p.m.	0.99	16	11.42	PASS	PASS	FAIL
4			8:00:00 a.m.	4:30:00 p.m.	1.00	20	11.68	PASS	PASS	PASS
5			8:30:00 a.m.	5:00:00 p.m.	0.94	22	11.18	PASS	PASS	PASS
6			9:00:00 a.m.	5:30:00 p.m.	0.98	23	12.63	PASS	PASS	PASS
7			9:30:00 a.m.	6:00:00 p.m.	0.98	25	13.31	PASS	PASS	PASS
8			10:00:00 a.m.	6:30:00 p.m.	1.00	18	11.37	PASS	PASS	PASS
9			10:30:00 a.m.	7:00:00 p.m.	1.00	22	11.01	PASS	PASS	PASS
10			11:00:00 a.m.	7:30:00 p.m.	1.00	24	10.85	PASS	PASS	PASS
11			11:30:00 a.m.	8:00:00 p.m.	1.01	23	11.99	PASS	PASS	PASS
12			12:00:00 p.m.	8:30:00 p.m.	1.01	25	10.49	PASS	PASS	PASS
13			12:30:00 p.m.	9:00:00 p.m.	0.99	26	10.88	PASS	PASS	PASS
14			1:00:00 p.m.	9:30:00 p.m.	1.00	26	11.28	PASS	PASS	PASS
15			1:30:00 p.m.	10:00:00 p.m.	1.00	23	11.53	PASS	PASS	PASS
16			2:00:00 p.m.	10:30:00 p.m.	1.02	23	11.43	PASS	PASS	PASS
17			2:30:00 p.m.	11:00:00 p.m.	1.01	23	11.20	PASS	PASS	PASS
18			3:00:00 p.m.	11:30:00 p.m.	1.01	27	11.60	PASS	PASS	PASS
19		3/10/2014	3:30:00 p.m.	12:00:00 a.m.	1.01	25	11.11	PASS	PASS	PASS
20			4:00:00 p.m.	12:30:00 a.m.	1.02	25	11.63	PASS	PASS	PASS
21			4:30:00 p.m.	1:00:00 a.m.	1.00	24	11.06	PASS	PASS	PASS
22			5:00:00 p.m.	1:30:00 a.m.	1.02	21	10.75	PASS	PASS	PASS
23			5:30:00 p.m.	2:00:00 a.m.	0.99	23	11.35	PASS	PASS	PASS
24			6:00:00 p.m.	2:30:00 a.m.	1.00	19	11.49	PASS	PASS	PASS
25			6:30:00 p.m.	3:00:00 a.m.	1.01	21	11.01	PASS	PASS	PASS
26			7:00:00 p.m.	3:30:00 a.m.	1.01	23	11.62	PASS	PASS	PASS
27			7:30:00 p.m.	4:00:00 a.m.	1.02	24	12.42	PASS	PASS	PASS
28			8:00:00 p.m.	4:30:00 a.m.	1.01	23	12.35	PASS	PASS	PASS
29			8:30:00 p.m.	5:00:00 a.m.	1.01	25	11.45	PASS	PASS	PASS
30			9:00:00 p.m.	5:30:00 a.m.	1.00	21	9.54	PASS	PASS	PASS
31			9:30:00 p.m.	6:00:00 a.m.	0.97	28	11.52	PASS	PASS	FAIL
32			10:00:00 p.m.	6:30:00 a.m.	0.98	29	12.92	PASS	PASS	PASS
33			10:30:00 p.m.	7:00:00 a.m.	0.98	24	14.42	PASS	PASS	PASS
34			11:00:00 p.m.	7:30:00 a.m.	0.98	9	13.93	PASS	PASS	FAIL
35			11:30:00 p.m.	8:00:00 a.m.	0.96	17	12.30	PASS	PASS	PASS
36	3/10/2014		12:00:00 a.m	8:30:00 a.m.	0.97	15	12.21	PASS	PASS	PASS
37			12:30:00 a.m	9:00:00 a.m.	0.98	23	12.54	PASS	PASS	PASS
38			1:00:00 a.m	9:30:00 a.m.	0.94	14	13.56	PASS	PASS	PASS
39			1:30:00 a.m	10:00:00 a.m.	0.96	19	12.22	PASS	PASS	FAIL
40			2:00:00 a.m	10:30:00 a.m.	1.01	22	12.80	PASS	PASS	PASS
41			2:30:00 a.m	11:00:00 a.m.	1.03	16	12.55	PASS	PASS	PASS
42			3:00:00 a.m	11:30:00 a.m.	1.02	12	12.36	PASS	PASS	PASS
43			3:30:00 a.m	12:00:00 p.m.	1.03	18	11.80	PASS	PASS	PASS
44			4:00:00 a.m	12:30:00 p.m.	1.02	13	12.42	PASS	PASS	PASS
45			4:30:00 a.m	1:00:00 p.m.	1.02	15	11.13	PASS	PASS	PASS
46			5:00:00 a.m	1:30:00 p.m.	0.99	22	12.18	PASS	PASS	PASS
47			5:30:00 a.m	2:00:00 p.m.	1.02	15	9.32	PASS	PASS	PASS
48			6:00:00 a.m	2:30:00 p.m.	1.00	18	12.27	PASS	PASS	PASS
49			6:30:00 a.m	3:00:00 p.m.	0.91	21	12.88	PASS	PASS	PAS
50			7:00:00 a.m	3:30:00 p.m.	0.98	17	13.08	PASS	PASS	FAIL
51			7:30:00 a.m	4:00:00 p.m.	1.00	22	12.79	PASS	PASS	PASS
52			8:00:00 a.m	4:30:00 p.m.	1.01	20	11.67	PASS	PASS	PASS
53			8:30:00 a.m	5:00:00 p.m.	1.01	28	11.85	PASS	PASS	PASS
54			9:00:00 a.m	5:30:00 p.m.	1.01	25	12.74	PASS	PASS	PASS
55			9:30:00 a.m	6:00:00 p.m.	1.03	23	11.71	PASS	PASS	PASS
56			10:00:00 a.m	6:30:00 p.m.	1.02	20	11.48	PASS	PASS	PASS
57			10:30:00 a.m	7:00:00 p.m.	1.02	22	10.47	PASS	PASS	PASS

Table 1 (*continued*)

No.	Date		Hour		f_0	n	A_0	Check for reliability		
	GMT	Adelaide	GMT	Adelaide				i	ii	iii
58			11:00:00 a.m	7:30:00 p.m.	1.01	27	11.27	PASS	PASS	PASS
59			11:30:00 a.m	8:00:00 p.m.	1.01	20	10.56	PASS	PASS	PASS
60			12:00:00 p.m.	8:30:00 p.m.	1.01	27	10.36	PASS	PASS	PASS
61			12:30:00 p.m.	9:00:00 p.m.	1.00	23	10.20	PASS	PASS	PASS
62			1:00:00 p.m.	9:30:00 p.m.	1.02	22	10.55	PASS	PASS	PASS
63			1:30:00 p.m.	10:00:00 p.m.	1.00	29	10.91	PASS	PASS	PASS
64			2:00:00 p.m.	10:30:00 p.m.	1.00	31	10.10	PASS	PASS	PASS
65			2:30:00 p.m.	11:00:00 p.m.	1.02	25	9.16	PASS	PASS	PASS
66			3:00:00 p.m.	11:30:00 p.m.	1.01	29	10.01	PASS	PASS	PASS
67		4/10/2014	3:30:00 p.m.	12:00:00 a.m.	1.01	29	9.22	PASS	PASS	PASS
68			4:00:00 p.m.	12:30:00 a.m.	1.01	23	9.82	PASS	PASS	PASS
69			4:30:00 p.m.	1:00:00 a.m.	1.01	29	10.52	PASS	PASS	PASS
70			5:00:00 p.m.	1:30:00 a.m.	1.02	28	10.60	PASS	PASS	PASS
71			5:30:00 p.m.	2:00:00 a.m.	1.03	29	9.97	PASS	PASS	PASS
72			6:00:00 p.m.	2:30:00 a.m.	1.02	18	10.68	PASS	PASS	PASS
73			6:30:00 p.m.	3:00:00 a.m.	1.02	29	11.89	PASS	PASS	PASS
74			7:00:00 p.m.	3:30:00 a.m.	1.02	22	10.69	PASS	PASS	PASS
75			7:30:00 p.m.	4:00:00 a.m.	1.03	28	11.98	PASS	PASS	PASS
76			8:00:00 p.m.	4:30:00 a.m.	1.02	26	11.26	PASS	PASS	PASS
77			8:30:00 p.m.	5:00:00 a.m.	1.00	30	12.11	PASS	PASS	PASS
78			9:00:00 p.m.	5:30:00 a.m.	1.00	29	11.86	PASS	PASS	PASS
79			9:30:00 p.m.	6:00:00 a.m.	1.01	30	12.40	PASS	PASS	PASS
80			10:00:00 p.m.	6:30:00 a.m.	0.97	19	13.45	PASS	PASS	FAIL
81			10:30:00 p.m.	7:00:00 a.m.	1.01	23	11.51	PASS	PASS	PASS
82			11:00:00 p.m.	7:30:00 a.m.	1.01	19	11.79	PASS	PASS	PASS
83			11:30:00 p.m.	8:00:00 a.m.	0.95	18	13.19	PASS	PASS	PASS
84	4/10/2014		12:00:00 a.m.	8:30:00 a.m.	0.93	16	11.51	PASS	PASS	PASS
85			12:30:00 a.m.	9:00:00 a.m.	0.33	16	13.58	PASS	PASS	FAIL
86			1:00:00 a.m.	9:30:00 a.m.	0.33	8	18.05	PASS	FAIL	FAIL
87			1:30:00 a.m.	10:00:00 a.m.	0.97	12	11.29	PASS	PASS	FAIL
88			2:00:00 a.m.	10:30:00 a.m.	0.99	14	12.12	PASS	PASS	PASS
89			2:30:00 a.m.	11:00:00 a.m.	1.00	15	12.65	PASS	PASS	PASS
90			3:00:00 a.m.	11:30:00 a.m.	1.00	19	11.55	PASS	PASS	PASS
91			3:30:00 a.m.	12:00:00 p.m.	1.02	17	11.99	PASS	PASS	PASS
92			4:00:00 a.m.	12:30:00 p.m.	1.00	22	11.91	PASS	PASS	PASS
93			4:30:00 a.m.	1:00:00 p.m.	1.01	16	12.84	PASS	PASS	PASS
94			5:00:00 a.m.	1:30:00 p.m.	1.00	16	13.72	PASS	PASS	PASS
95			5:30:00 a.m.	2:00:00 p.m.	1.00	23	13.18	PASS	PASS	PASS
96			6:00:00 a.m.	2:30:00 p.m.	1.02	17	13.12	PASS	PASS	PASS

2.3. Equipment repeatability

Prior to data acquisition, all of the equipment sets were examined to assess their repeatability. All equipment sets were run simultaneously at the same location, with a separation distance of approximately 0.5 m from one another for at least two days. The results of this huddle test are presented in Table 1 (where f_0 is the fundamental frequency; n is the number of windows selected for the average HVSR curve; A_0 is the HVSR peak amplitude at frequency f_0; and i, ii, and iii are the criteria suggested by [6] to assess the reliability of the HVSR curves. The HVSR curves from the huddle tests that passed the SESAME reliability criteria, were plotted with respect to HVSR amplitude and frequency. The results are presented in Fig. 3, which demonstrates very similar curves, particularly between 0.8 and 10.0 Hz. A high dispersion is shown from a frequency of 0.8 Hz, downward to 0.25 Hz, which suggests a low noise source intensity over this frequency interval. Further investigation of this huddle test is available in [7].

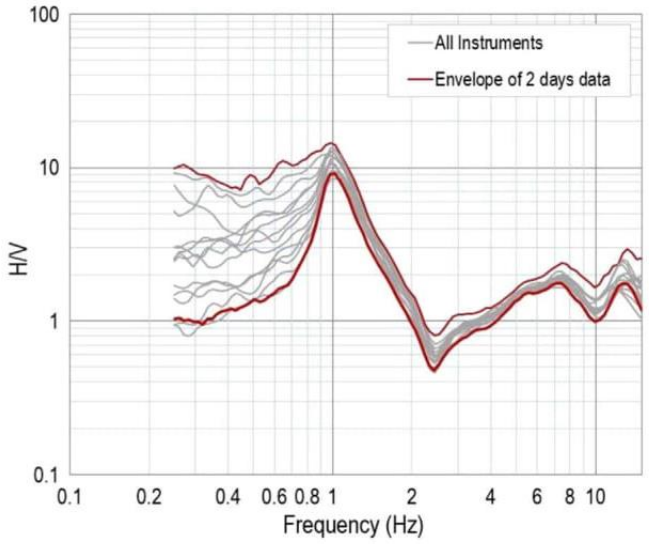

Fig. 3. HVSR curves of all adopted seismometers and the envelope of HVSR test results from two continuous days of measurement over 30-min time periods.

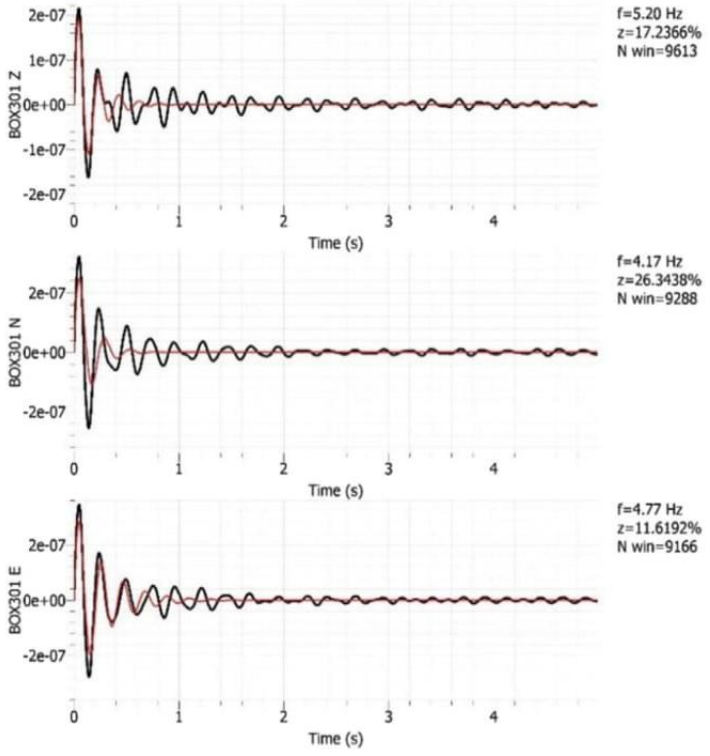

Fig. 4. Example results of identification of data from an industrial source.

2.4. Detection of industrial origin

The Geopsy [8] damping toolbox was used to detect the presence of any vibration originating from an industrial source. Data from an industrial origin is concluded if the damping is much lower than 1% and the frequency is sustained. This identification is important in the HVSR analysis. Example results are shown in Fig. 4. Further details of all such analyses are included in Appendix A of the Supplementary Data associated with this paper.

DATE :	16/06/2015	HOUR: 11:45 AM		PLACE : Adelaide, South Australia		
OPERATOR :	D. Love & B. Setiawan			GPS TYPE and # Digital Satellite GPS		
LATITUDE:	-34.902	LONGITUDE:	138.592	ALTITUDE: -		
STATION TYPE: TEMPORAL STATION				SENSOR TYPE: SEISMOMETER LE-3Dlite LENNARTZ		
STATION#: LOCATION #01				SENSOR#: BOX 3, BOX 6 & BOX 7 DISK#: BOX 3, BOX 6 & BOX 7		
FILE NAME: BOX 3, BOX 6 & BOX 7				POINT# near Barton Terrace West		
GAIN: -	SAMPLE FREQ.: 100Hz Filltered			REC. DURATION: At least 2 hours		
WEATHER CONDITIONS	WIND [X] none [ ] weak [ ] medium [ ] strong Measurement (if any):					
	RAIN [X] none [ ] weak [ ] medium [ ] strong Measurement (if any):					
	TEMPERATURE (APPROX) 16 °C Remarks					
GROUND TYPE	[X] earth (HARD / ~~SOFT~~) [ ] gravel [ ] sand [X] grass (SHORT / ~~TALL~~)					
	[ ] asphalt [ ] cement [ ] concrete [ ] paved [ ] other					
	[X] dry soil [ ] wet soil Remarks:					
ARTIFICIAL GROUND-SENSOR COUPLING	[X] no [ ] yes, type:					
BUILDING DENSITY	[X] none [ ] scattered [ ] dense [ ] other, type: Park Land					

TRANSIENTS	none	few	moderate	many	very dense	distance
cars			X			~80m
trucks		X				~80m
pedestrians	X					
other						
-type of other:						

MONOCROMATIC NOISE SOURCES
(factories, works, pumps, rivers,...)
[ ] no [X] yes, type: water pump

NEARBY STRUCTURES (trees, polls,builings, bridges underground structures, ...)
(description, height, distance)
BOX 7 is about 80 m from Aquatic centre (pump station???)

Fig. 5. Example of a field data sheet.

2.5. Field data and Analyses

2.5.1. Field data

At each survey location, noise measurements were conducted for at least 2 h, at a sampling frequency of 100 Hz. Field data were filtered using a cutoff frequency of 50 Hz. Only recordings on three instruments (in a triangular arrangement) were used for the horizontal to vertical spectral ratio (HVSR) analysis and the vertical seismometer readings from all instruments were used to analyze the spatial autocorrelation (SPAC). At each of the 8 sites, four tests, with a duration of 30 min, were conducted at different times using all instruments. An example of the field data sheet is shown in Fig. 5. All the field data sheets are included in [9].

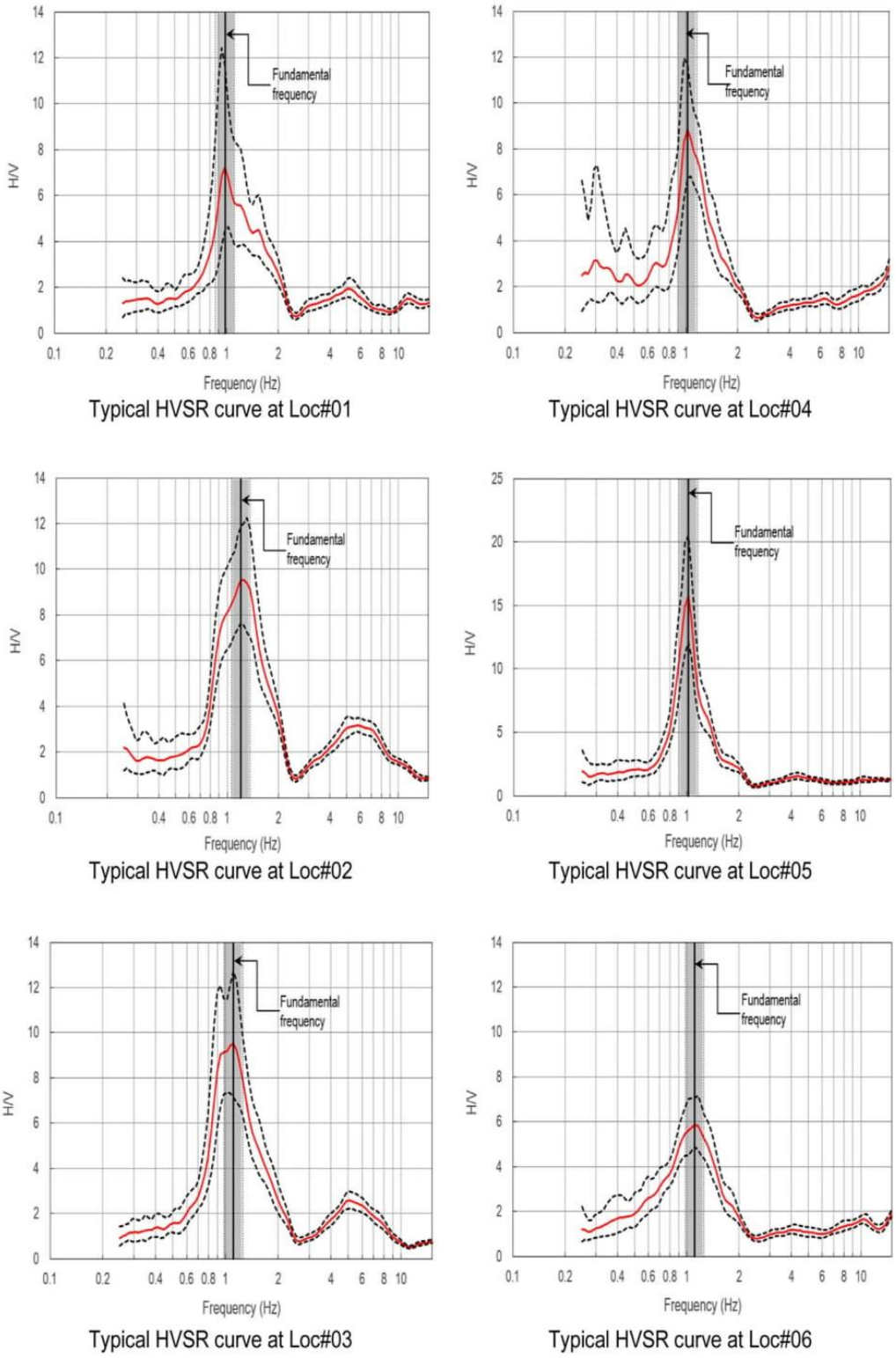

Fig. 6. Selected HVSR curves at Locations #01 to #06.

2.5.2. HVSR analysis

Analysis of the spectral ratio, between the Fourier amplitude spectrum of the horizontal (H) and vertical (V) components of the ambient noise, is fundamental to the horizontal to vertical spectral ratio (HVSR) method.

The selection of the windows with the most stationary wave forms is a crucial initial step in computing HVSR spectral ratios. This selection is used to exclude transient vibrations [6]. Subsequently, in each selected window, the Fourier spectra of each HVSR component are smoothed and merged by adopting the geometric mean.

The computation of HVSR is performed by taking the root mean square of the horizontal components of the Fourier amplitude spectra (F_{NS} and F_{EW}) divided by the vertical component frequency spectrum (F_{UD}) [10], as shown below.

$$\frac{H}{V} = \sqrt{\frac{\left(F_{NS}^2 + F_{EW}^2\right)}{\left(2F_{UD}^2\right)}} \tag{1}$$

In the process, several parameters (window length, threshold of the short-time average/long-time average (STA/LTA) and the lengths of STA/LTA) were employed. Each selected window was then smoothed using a smoothing constant of 40 [11].

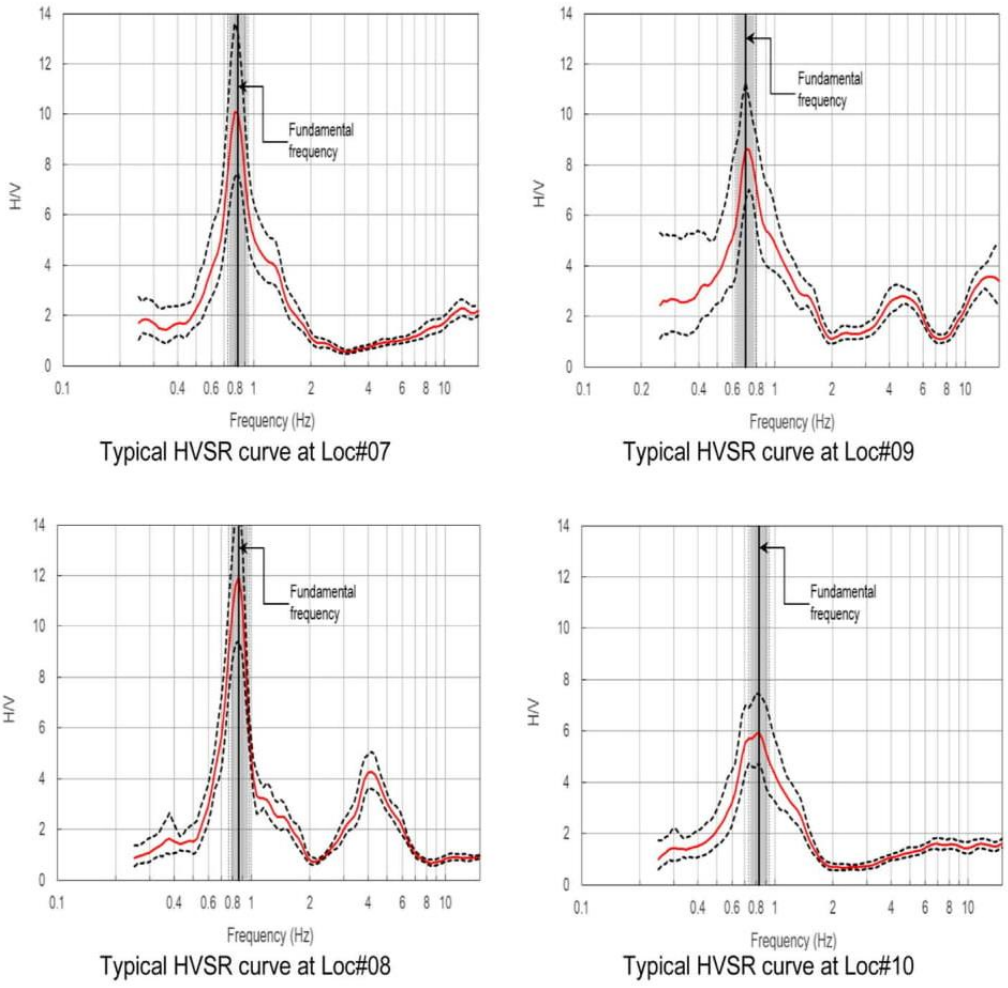

Fig. 7. Selected HVSR curves Locations #07 to #10.

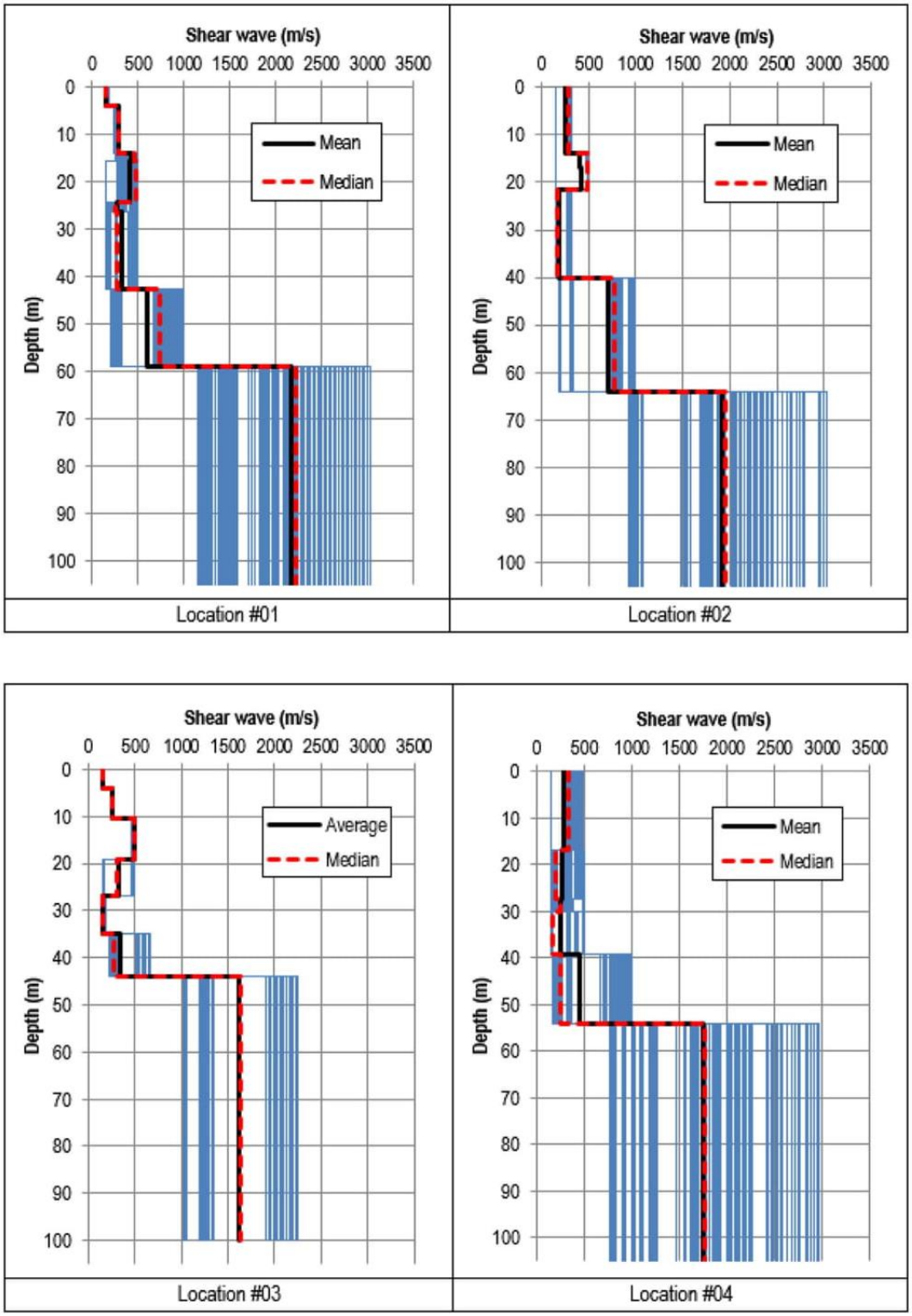

Fig. 8. Shear wave velocity profiles inverted using the classic HVSR ellipticity constraint at Locations #01 to #04.

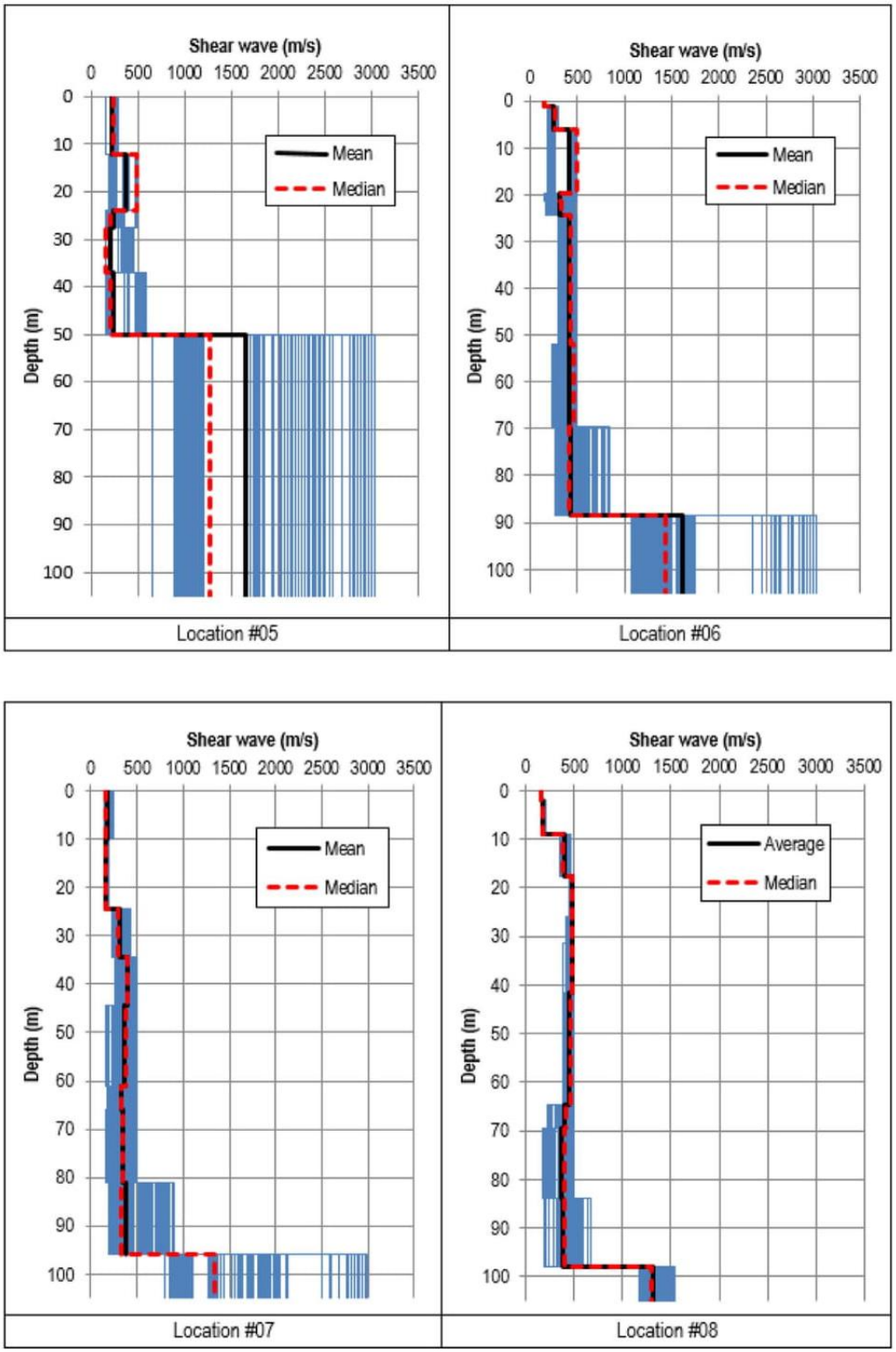

Fig. 9. Shear wave velocity profiles inverted using the classic HVSR ellipticity constraint at Locations #05 to #08.

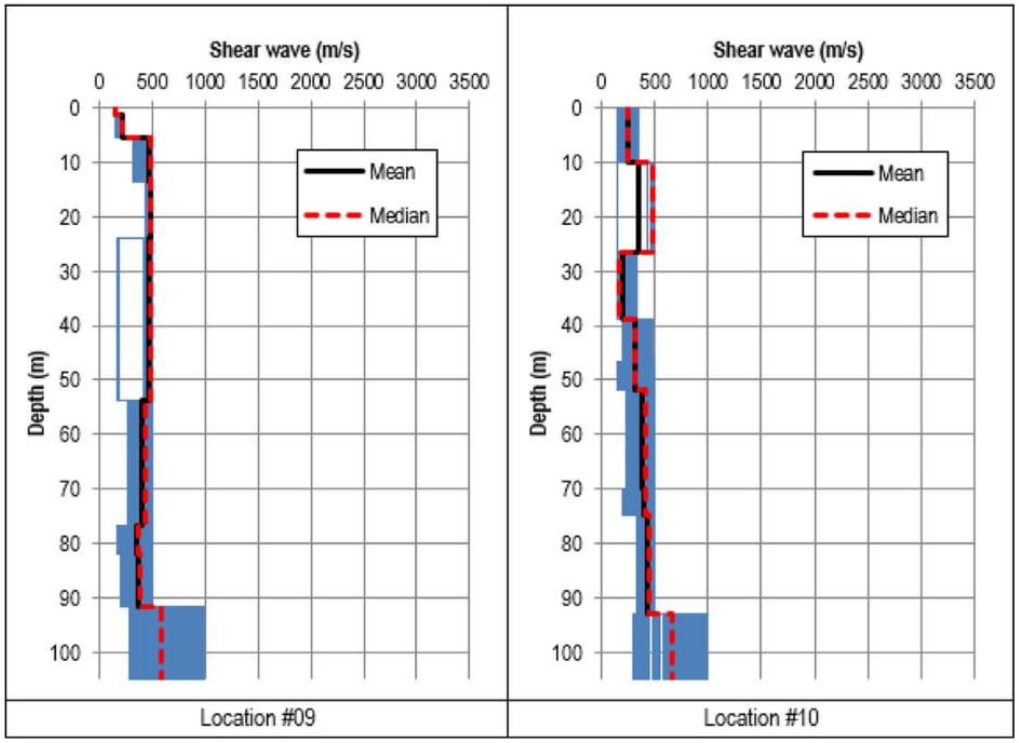

Fig. 10. Shear wave velocity profiles inverted using the classic HVSR ellipticity constraint at Locations #09 to #10.

HVSR analysis was carried out using the method proposed by [11] to obtain the HVSR ellipticity curves, from which the site fundamental frequency is obtained. The results of this HVSR analysis, at all measured sites, are included in Appendix B of the Supplementary Data associated with the present paper. Prior to the HVSR analysis, as presented in this paper, several tentative window lengths (i.e. 25, 30, 35 and 40 s) were trialed to obtain as many reliable HVSR curves as possible, as suggested by [8], and the 40 s window length was found to be the optimal. Selected HVSR curves from the study areas are shown in Figs. 6 and 7.

2.5.3. Shear wave velocity profile

Shear wave velocity profiles were obtained by inverting the HVSR ellipticity curves using the process recommended by [8] and 20 best shear wave velocity models were extracted from the results of the inversion. The profiles are presented in Figs. 8–10. From the 20 best models, arithmetic mean and median values of the shear wave velocity were calculated.

Acknowledgements

The authors would like to acknowledge the University of Adelaide for providing a research scholarship for the first author. In addition, the first author is grateful to the Faculty of Engineering of Syiah Kuala University for their support.

Transparency document. Supporting information

Transparency data associated with this article can be found in the online version at http://dx.doi.org/10.1016/j.dib.2018.08.055.

Appendix A. Supporting information

Supplementary data associated with this article can be found in the online version at http://dx.doi.org/10.1016/j.dib.2018.08.055.

References

[1] M. Nogoshi, T. Igarashi, On the amplitude characteristics of microtremor (part **2**), J. Seismol. Soc. Jpn. (1971) 26–40.
[2] K. Kanay, T. Tanaka, On microtremors VIII, Bull. Earthq. Res. Inst. (1961) 97–114.
[3] Y. Nakamura, A method for dynamic characteristics estimation of subsurface using microtremor on the ground surface, Q. Report. Railw. Tech. Res. Inst. 30 (1) (1989) 25–30.
[4] H. Okada, The microseismic survey method. Geophysical Monograph Series No. 12. Society of exploration geophysicists with the cooperation of Society of exploration geophysicists of Japan and Australian Society of Exploration Geophysicists. Translated by Koya Suto, ISBN: 1-56080-120-4135 pp, 2003.
[5] J. Selby, J. Lindsay, Engineering geology of the Adelaide City area, Department of Mines and Energy, Geological Survey of South Australia, 51, 1982, D. J. Woolman, Government Printer, Bulletin (94 pp).
[6] SESAME, Guidelines for the implementation of the H/V spectral ratio technique on ambient vibrations measurements processing and interpretation. SESAME European Research Project, WP12 –Deliverable D23.12 European Commission – Research General Directorate, Project No. EVG1-CT-200-00026 (2004).
[7] B. Setiawan, M.B. Jaksa, M.C. Griffith, D. Love, HVSR recording duration for regolith sites: an experimental approach. in: Proceedings of the Tenth Pacific Conference on Earthquake Engineering, "Building an Earthquake-Resilient Pacific" 6-8 November 2015, Sydney, Australia (2015).
[8] Geopsy, Geopsy home: software applications for ambient vibration (2015). ⟨http://www.geopsy.org⟩, (Accessed 1 December 2015) (2015).
[9] B. Setiawan, M.B. Jaksa, M.C. Griffith, D. Love, Analysis of microtremor array measurement using the spatial autocorrelation (SPAC) method across the Adelaide City, School of Civil, Environmental, and Mining Engineering, the University of Adelaide, Research Report No. R196 (2016).
[10] J. Delgado, C. Casado, J. Giner, A. Estevez, A. Cuenca, S. Molina, Microtremors as a geophysical exploration tool: application and limitations, Pure Appl. Geophys. 157 (2000) 1445–1462.
[11] K. Konno, T. Omachi, Ground motion characteristics estimated from spectral ratio between horizontal and vertical components of microtemors, Bull. Seismol. Soc. Am. 88 (1) (1998) 228–241.

INTENTIONALLY BLANK

Appendix I:

BEDROCK DEPTH ESTIMATION USING GENERIC FUNCTION

INTENTIONALLY BLANK

Locations #01 to #05:

Location (Mean f_0)	Instrument (mean f_0)	Test	f_0	Amplitude at f_0	Reliability criteria test (SESAME, 2004)			HVSR peak clear criteria test (SESAME, 2004)	Average V_s of the upper	Estimated bedrock depth (m)
					i	ii	iii			
		a	1.01	6.81	Pass	Pass	Pass	Clear Peak	406	100
	#A	b	0.98	7.41	Pass	Pass	Pass	Clear Peak	406	103
		c	1.04	6.67	Pass	Pass	Pass	Unclear peak		
		d	1.03	6.36	Pass	Pass	Pass	Unclear peak		
	(1.02 Hz)	e	1.04	6.24	Pass	Pass	Pass	Unclear peak		
		a	0.95	5.46	Pass	Pass	Fail	Unclear peak		
#01	#B	b	0.91	5.96	Pass	Pass	Pass	Clear Peak	406	111
		c	0.99	5.30	Pass	Pass	Fail	Unclear peak		
		d	0.98	5.46	Pass	Pass	Pass	Clear Peak	406	103
	(0.95 Hz)	e	0.90	5.45	Pass	Pass	Fail	Unclear peak		
		a	1.02	8.69	Pass	Pass	Pass	Clear Peak	406	99
	#C	b	1.07	8.00	Pass	Pass	Pass	Unclear peak		
		c	1.07	7.39	Pass	Pass	Fail	Unclear peak		
		d	1.05	7.85	Pass	Pass	Pass	Unclear Peak		
(1.01)	(1.05 Hz)	e	1.04	8.88	Pass	Pass	Pass	Unclear Peak		
		a	1.19	8.58	Pass	Pass	Pass	Unclear Peak		
	#A	b	1.22	9.53	Pass	Pass	Pass	Clear Peak	422	86
		c	1.22	9.43	Pass	Pass	Pass	Unclear Peak		
		d	1.18	10.28	Pass	Pass	Pass	Unclear Peak		
	(1.20 Hz)	e	1.19	9.91	Pass	Pass	Pass	Unclear Peak		
		a	1.33	6.00	Pass	Pass	Pass	Clear Peak	422	79
#02	#B	b	1.12	7.05	Pass	Pass	Pass	Clear Peak	422	94
		c	1.25	7.92	Pass	Pass	Pass	Clear Peak	422	84
		d	1.20	6.96	Pass	Pass	Pass	Clear Peak	422	88
	(1.23 Hz)	e	1.25	6.53	Pass	Pass	Pass	Unclear Peak		
		a	1.19	8.89	Pass	Pass	Pass	Unclear Peak		
	#C	b	1.12	9.14	Pass	Pass	Pass	Clear Peak	422	94
		c	1.18	9.25	Pass	Pass	Pass	Clear Peak	422	90
(1.20)	(1.16 Hz)	d	1.15	9.87	Pass	Pass	Pass	Clear Peak	422	91
		a	1.11	7.80	Pass	Pass	Pass	Clear peak	304	68
#03	#A	b	1.08	8.87	Pass	Pass	Pass	Unclear Peak		
		c	1.09	8.88	Pass	Pass	Pass	Unclear peak		
(1.07)	(1.07 Hz)	d	1.06	9.40	Pass	Pass	Pass	Unclear Peak		
		a	0.99	12.24	Pass	Pass	Fail	Unclear peak		
	#A	b	1.00	11.92	Pass	Pass	Pass	Clear Peak	339	84
		c	1.01	12.52	Pass	Pass	Fail	Unclear peak		
	(0.99 Hz)	d	0.97	11.28	Pass	Pass	Pass	Clear Peak	339	87
		a	1.02	8.82	Pass	Pass	Pass	Clear Peak	339	83
#04	#B	b	1.05	8.55	Pass	Pass	Pass	Clear Peak	339	81
		c	1.06	8.41	Pass	Pass	Pass	Clear Peak	339	80
		d	1.06	9.13	Pass	Pass	Pass	Clear Peak	339	80
	(1.04 Hz)	e	1.01	9.09	Pass	Pass	Pass	Clear Peak	339	84
		a	1.04	16.68	Pass	Pass	Pass	Clear Peak	339	82
	#C	b	1.08	16.83	Pass	Pass	Pass	Clear Peak	339	79
		c	1.07	16.41	Pass	Pass	Pass	Clear Peak	339	79
(1.04)	(1.06 Hz)	d	1.05	15.92	Pass	Pass	Pass	Clear Peak	339	80
		a	0.31	16.51	Pass	Pass	Fail	Unclear peak		
		b	0.31	13.99	Pass	Pass	Fail	Unclear peak		
	#A	c	0.43	10.59	Pass	Pass	Fail	Unclear peak		
		d	0.31	11.62	Pass	Pass	Fail	Unclear peak		
		e	0.32	12.64	Pass	Pass	Fail	Unclear peak		
	(-)	f	0.32	13.05	Pass	Pass	Fail	Unclear peak		
		a	1.02	13.49	Pass	Pass	Pass	Clear Peak	268	66
#05	#B	b	1.00	15.40	Pass	Pass	Pass	Clear Peak	268	67
		c	0.99	14.75	Pass	Pass	Pass	Clear Peak	268	68
		d	0.99	15.02	Pass	Pass	Pass	Clear Peak	268	68
	(1.00 Hz)	e	1.00	14.73	Pass	Pass	Pass	Clear Peak	268	67
		a	0.96	12.30	Pass	Pass	Pass	Clear Peak	268	70
	#C	b	0.99	12.74	Pass	Pass	Pass	Clear Peak	268	68
		c	0.96	13.03	Pass	Pass	Pass	Clear Peak	268	70
		d	0.96	12.72	Pass	Pass	Pass	Clear Peak	268	70
(0.98)	(0.97 Hz)	e	0.96	12.83	Pass	Pass	Pass	Clear Peak	268	70

Locations #06 to #10:

Location (Mean f_0)	Instrument (mean f_0)	Test	f_0	Amplitude at f_0	Reliability criteria test (SESAME, 2004)			HVSR peak clear criteria test (SESAME, 2004)	Average V_s of the upper layer	Estimated bedrock depth (m) GF
					i	ii	iii			
	#A	a	0.49	14.61	Pass	Pass	Fail	Unclear peak		
		b	0.52	15.15	Pass	Pass	Fail	Unclear peak		
		c	0.44	13.19	Pass	Pass	Fail	Unclear peak		
		d	0.50	13.91	Pass	Pass	Fail	Unclear peak		
	(-)	e	0.47	10.88	Pass	Pass	Fail	Unclear peak		
#06	#B	a	1.10	5.46	Pass	Pass	Pass	Clear Peak	385	88
		b	1.09	5.69	Pass	Pass	Pass	Clear Peak	385	88
		c	1.10	5.83	Pass	Pass	Pass	Clear Peak	385	88
		d	1.10	5.89	Pass	Pass	Pass	Clear Peak	385	87
	(1.11 Hz)	e	1.14	5.39	Pass	Pass	Pass	Clear Peak	385	84
	#C	a	1.05	5.88	Pass	Pass	Pass	Unclear peak		
		b	1.11	6.01	Pass	Pass	Pass	Clear Peak	385	87
		c	1.08	6.25	Pass	Pass	Pass	Unclear Peak		
(1.10)	(1.09 Hz)	d	1.07	6.08	Pass	Pass	Pass	Unclear Peak		
	#A	a	0.82	9.92	Pass	Pass	Pass	Clear Peak	311	95
		b	0.81	10.09	Pass	Pass	Pass	Clear Peak	311	96
		c	0.81	10.88	Pass	Pass	Pass	Clear Peak	311	96
		d	0.80	9.93	Pass	Pass	Pass	Clear Peak	311	97
	(0.81 Hz)	e	0.82	10.18	Pass	Pass	Pass	Clear Peak	311	95
#07	#B	a	0.80	11.54	Pass	Pass	Pass	Clear Peak	311	97
		b	0.80	10.61	Pass	Pass	Pass	Clear Peak	311	97
		c	0.80	11.23	Pass	Pass	Pass	Clear Peak	311	98
	(0.80 Hz)	d	0.79	9.80	Pass	Pass	Pass	Clear Peak	311	98
	#C	a	0.77	10.14	Pass	Pass	Pass	Clear Peak	311	101
		b	0.74	12.10	Pass	Pass	Pass	Clear Peak	311	104
		c	0.75	11.04	Pass	Pass	Pass	Clear Peak	311	104
(0.79)	(0.75 Hz)	d	0.71	10.86	Pass	Pass	Fail	Unclear peak		
	#A	a	0.84	8.45	Pass	Pass	Pass	Clear Peak	403	120
#08		b	0.84	12.18	Pass	Pass	Pass	Clear Peak	403	121
		c	0.84	11.99	Pass	Pass	Pass	Clear Peak	403	121
		d	0.83	12.56	Pass	Pass	Pass	Clear Peak	403	122
(0.83)	(0.83 Hz)	e	0.84	11.68	Pass	Pass	Pass	Clear Peak	403	120
	#A	a	0.64	12.72	Pass	Pass	Fail	Unclear peak		
		b	0.66	11.51	Pass	Pass	Fail	Unclear peak		
		c	0.65	13.10	Pass	Pass	Pass	Clear Peak	451	174
		d	0.65	10.45	Pass	Pass	Fail	Unclear peak		
	(0.66 Hz)	e	0.67	9.30	Pass	Pass	Pass	Unclear Peak		
#09	#B	a	0.72	8.62	Pass	Pass	Pass	Clear Peak	451	156
		b	0.72	9.07	Pass	Pass	Fail	Clear Peak	451	156
		c	0.69	7.49	Pass	Pass	Fail	Unclear peak		
	(0.73 Hz)	d	0.74	8.53	Pass	Pass	Pass	Clear Peak	451	152
	#C	a	0.74	7.07	Pass	Pass	Pass	Clear Peak	451	152
		b	0.72	8.31	Pass	Pass	Pass	Clear Peak	451	156
		c	0.73	8.18	Pass	Pass	Pass	Clear Peak	451	154
		d	0.76	7.94	Pass	Pass	Pass	Clear Peak	451	149
(0.72)	(0.74 Hz)	e	0.73	8.06	Pass	Pass	Pass	Clear Peak	451	153
	#A	a	0.33	8.25	Pass	Pass	Fail	Unclear peak		
		b	0.32	9.73	Pass	Pass	Fail	Unclear peak		
		c	0.34	8.74	Pass	Pass	Fail	Unclear peak		
	(-)	d	0.36	9.46	Pass	Pass	Fail	Unclear peak		
	#B	a	0.32	14.33	Pass	Pass	Fail	Unclear peak		
#10		b	0.35	18.66	Pass	Fail	Fail	Unclear peak		
		c	0.35	11.09	Pass	Pass	Fail	Unclear peak		
	(-)	d	0.33	11.97	Pass	Fail	Fail	Unclear peak		
	#C	a	0.79	6.24	Pass	Pass	Pass	Clear Peak	428	135
		b	0.80	5.86	Pass	Pass	Pass	Clear Peak	428	134
		c	0.81	6.02	Pass	Pass	Pass	Clear Peak	428	132
(0.80)	(0.80 Hz)	d	0.82	6.89	Pass	Pass	Pass	Clear Peak	428	131